# RESEARCH AND TECHNOLOGY 1993

National Aeronautics and Space Administration

Ames Research Center

# Foreword

Each year, brief summaries of selected achievements at Ames Research Center are compiled as a NASA Technical Memorandum.

This year's report, Research and Technology 1993, presents some of the challenging work recently accomplished in the areas of Aerospace Systems, Flight Operations and Research, Aerophysics, and Space Research. Here, you can sample the scope and diversity of the research that is now being conducted and obtain a view of the stimulating research challenges of the future.

If you would like further information on any of the Ames research and technology programs, please call the contact person(s) at the end of each article.

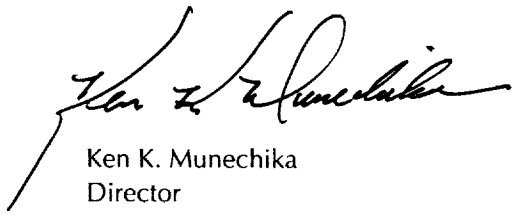

Ken K. Munechika
Director

# Aerospace Systems Directorate

## Aeronautical Projects Office



## Full-Scale Aerodynamics Research Division

## Aerospace Systems Directorate (continued)

### Full-Scale Aerodynamics Research Division (continued)



### Information Sciences Division

## Aerospace Systems Directorate (continued)

### Information Sciences Division (continued)



### Aerospace Human Factors Research Division

## Aerospace Systems Directorate (continued)

### Aerospace Human Factors Research Division (continued)

## Aerospace Systems Directorate (continued)

### Flight Systems and Simulation Research Division

# Aerophysics Directorate

## Aerodynamics Division



## Fluid Dynamics Division

## Aerophysics Directorate (continued)

### Fluid Dynamics Division (continued)



### Thermosciences Division

## Aerophysics Directorate (continued)

### Thermosciences Division (continued)

# Space Research Directorate

## Advanced Life Support Division



## Centrifuge Facility Project



## Space Projects Division



## Earth System Science Division

## Space Research Directorate (continued)

### Search for Extraterrestrial Intelligence Office



### Life Science Division

## Space Research Directorate (continued)

### Space Life Sciences Payloads Office



### Space Science Division

## Space Research Directorate (continued)

### Space Science Division (continued)

## Space Research Directorate (continued)

### Space Science Division (continued)

## Dryden Flight Research Facility Directorate

### Research Engineering Division



## Appendix

# Design Trade Study for High-Speed Proprotors

C. W. Acree

The Boeing Helicopter Company, under contract to NASA, carried out a design trade study for a proprotor suitable for a high-speed (400+ knots) civil tiltrotor. The goal was to achieve maximum cruise propulsive efficiency while maintaining acceptable hover efficiency (figure of merit) and low noise. The baseline aircraft was a 40-passenger tiltrotor cruising at 400 knots at 25,000 feet, with a hover disc loading of 20 pounds per square foot.

Many different aspects of rotor design and behavior for several candidate blade designs were investigated. The study focused on aerodynamic design, including chord, airfoil, and twist distributions, with close attention paid to the effects of blade sweep. Interactional aerodynamics—that is, wing/fuselage flow interference at the rotor—were studied to determine the effect on rotor loads and performance. Rotor noise trends were also calculated.

State-of-the-art analysis methods were used for the study, including CAMRAD/JA, TECH-01, VSAERO, FPR, and several others. A key objective was to determine weaknesses in existing design and analytical methods. A rigorous, detailed design optimization was not performed, hence the designs should be considered preliminary and subject to improvement.

The figure shows six of the blade designs studied. From top to bottom, blades with optimized nonlinear taper, a compromise semilinear taper, and an inverse-taper planform optimized for cruise only are shown. The unswept blades are on the left, and the swept versions are on the right. Propulsive efficiencies ($\eta_p$) at 400 knots are also shown. (The inverse-taper blade is not practical with current structural technology, but represents a limiting aerodynamic benchmark.) For all designs, the airfoils used were XN-18 (root), VR-12 (mid-span), and VR-15 (tip).

The study was extended to 420 knots with designs similar to the "B-U" and "B-S" planforms (see figure), but with more sweep and reoptimized twist. The critical limiting factor was excessive drag rise at the root, not the tip. This implies that root aerodynamics can be as important as the tip at very high speeds and should be given equal emphasis in future studies.

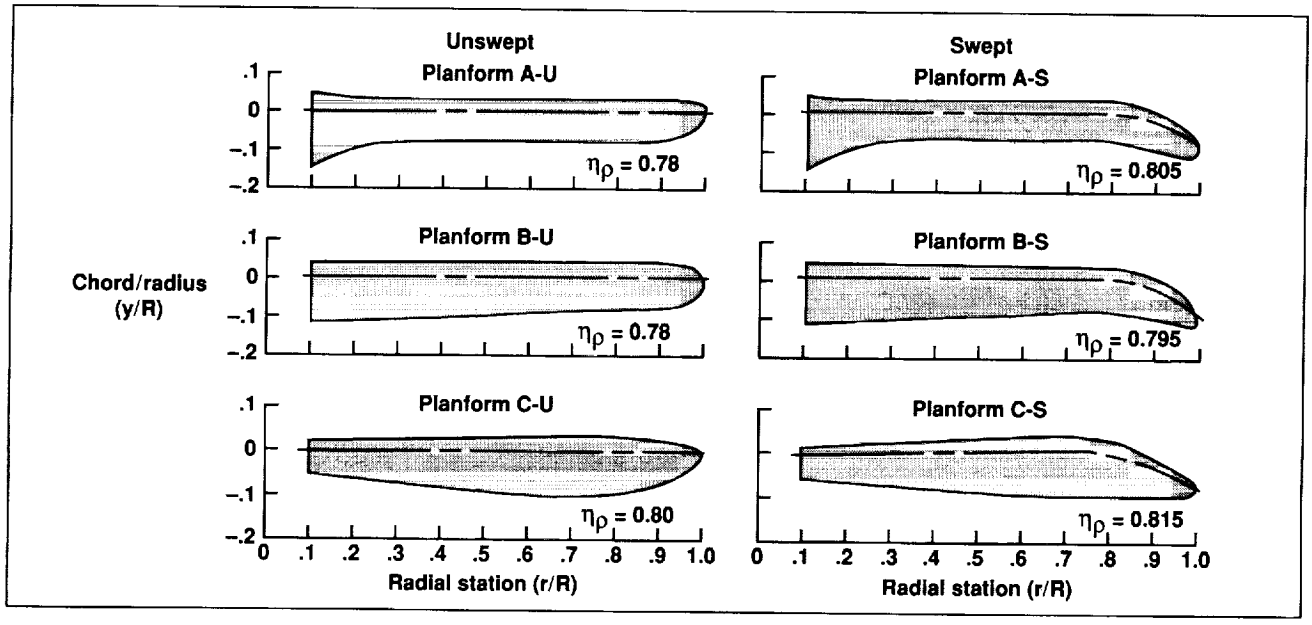


*Fig. 1. Candidate blade planforms.*

A key design goal was to fall below the Federal Aviation Administration noise limit by 5 decibels, which is achievable in all flight phases, assuming that blade–vortex interaction (BVI) can be avoided during approach. The study concluded that 400- to 420-knot blade designs are definitely feasible, but the trade-off between planform complexity and performance needs further study. Structural requirements at the blade root need detailed study before root airfoils and inboard sweep can be realistically defined and evaluated. The impact of wing and fuselage interference is potentially very large, as is the effect of nonaxial flow conditions. No significant problems were found with regard to conversion loads or whirl flutter.

**Ames-Moffett contact: C. Acree**
**(415) 604-5423**
**Headquarters program office: OA**

## UH-60 Airloads Program

**William G. Bousman, Robert M. Kufeld**

A UH-60A helicopter with a highly instrumented rotor has been successfully tested in flight at Ames Research Center. The primary goal of these tests is to obtain high-quality pressure measurements on the rotor blade during flight. A total of 221 pressure transducers have been installed on one blade at nine radial stations, and another 21 transducers are located near the blade leading edge between the radial arrays. Flight data have been obtained in level flight for a range of loading conditions, in maneuvers, and in conjunction with acoustic measurements both in flight and on the ground.

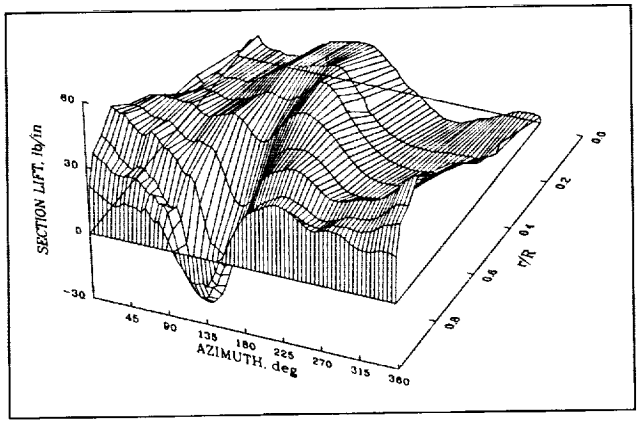


*Fig. 1. Measured section lift distribution for UH-60A aircraft at maximum level flight speed; advance ratio ($\mu$) = 0.37, weight coefficient/solidity ($C_W/\sigma$) = 0.079.*

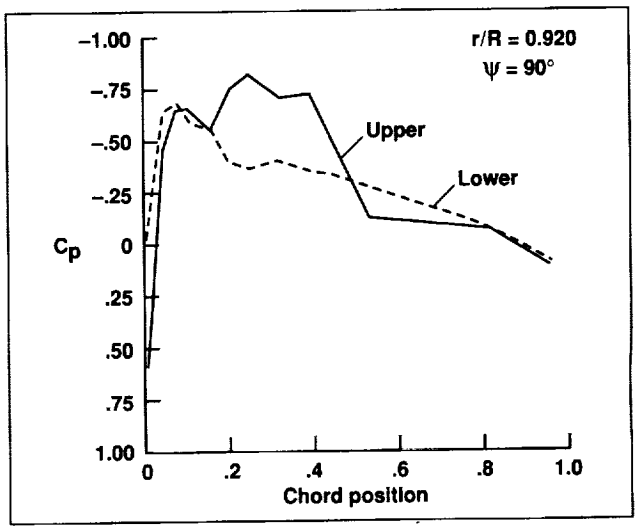


*Fig. 2. Measured chordwise pressure distribution on UH-60A aircraft at 0.92R and y = 90 degrees; $\mu$ = 0.37, $C_W/\sigma$ = 0.079.*

The first figure shows the measured distribution of lift on the pressure blade as a function of azimuth and radial station. These data were obtained at the maximum flight speed of the aircraft for this weight coefficient. At zero (or 360) degrees azimuth, with reference to the tail of the aircraft, the lift increases from a low value near the root of the blade to a peak at about three-fourths of the blade radius (R) with a

decrease as it approaches the tip where the lift must be zero. As the blade moves around the azimuth, the lift near the blade tip decreases and then becomes negative on the advancing side of the disk. This negative lift is a consequence of the need to maintain roll moment balance on the aircraft in forward flight. It is in this area where shocks are seen on both the upper and lower surfaces of the airfoil (see second figure). As the blades move around toward the nose of the aircraft, the lift at the tip is seen to increase, but the lift is far larger inboard on the blade as a consequence of strongly yawed flows at these radial stations and azimuths. As the blade reaches an azimuth of 270 degrees, a normal lift distribution is obtained except at the most inboard radial station where the flow is actually reversed at that blade section. In that case, the forward component of velocity is greater than the rotational component, and the "leading edge" of the airfoil is actually its trailing edge and the lift is negative.

Information obtained in this series of flight tests will provide new insights into rotor behavior and will provide a set of data that can be used to validate analytical methods and, hence, will enable rotor designers to design better helicopters at reduced risk.

**Ames-Moffett contact: W. Bousman**
**(415) 604-3748**
**Headquarters program office: OA**

## Space Launch Vehicle Concept Comparisons

**Jeffrey V. Bowles**

As part of the NASA Access-to-Space study, the Systems Analysis Branch has completed a comparative mission-performance analysis of three launch-vehicle concepts, including an all-rocket configuration and an air-breather/rocket-assist hybrid vehicle, both of which are single-stage-to-orbit (SSTO) designs, and a two-stage-to-orbit (TSTO) concept. The first stage of the TSTO system uses all air-breathing propulsion, whereas the second stage is an all-rocket design. Relative performance, including vehicle gross weight, empty weight, and overall life-cycle costs were compared.

Mission requirements for both SSTO concepts included SSTO launch to a 220-nautical-mile polar orbit inclined at 51.6 degrees, with both carrying the same payload weight and volume, which is representative of the Space Station Freedom mission. Technology levels for structural concept and material selection were commensurate with the Initial Operational Capability date of 2008. The all-rocket design is a wing-body vertical takeoff/horizontal landing concept. A lifting-body shape was selected for the air-breather/rocket hybrid design and both stages of the TSTO system. All concepts have horizontal-takeoff/horizontal-landing capability. The upper stage, or orbiter, of the TSTO system is carried submerged atop the first-stage vehicle to reduce the transonic drag of the TSTO system (first figure). The Ames hypersonic vehicle conceptual design code HAVOC was used to compute aerodynamic and propulsion system performance, and structural/weight characteristics to size each vehicle. The all-rocket vehicle flew a low-dynamic-pressure (≤200 pounds per square foot) trajectory. The ascent trajectory for the air-breather/rocket hybrid was optimized for dual-mode propulsion system performance. The TSTO stages the orbiter at Mach 5, the first stage flying a high-dynamic-pressure trajectory while the orbiter follows a low-dynamic-pressure ascent similar to that of the SSTO all-rocket design.

Aerodynamic analysis showed superior performance for the all-body shapes of the air-breather/rocket hybrid design and TSTO system, which have approximately one-third the zero-lift flat-plate drag area that the all-rocket configuration has. The optimized ascent trajectory for the air-breather hybrid resulted in an order-of-magnitude increase in flight dynamic pressure over that of the rocket. Higher aerodynamic loads and aerothermodynamic heating

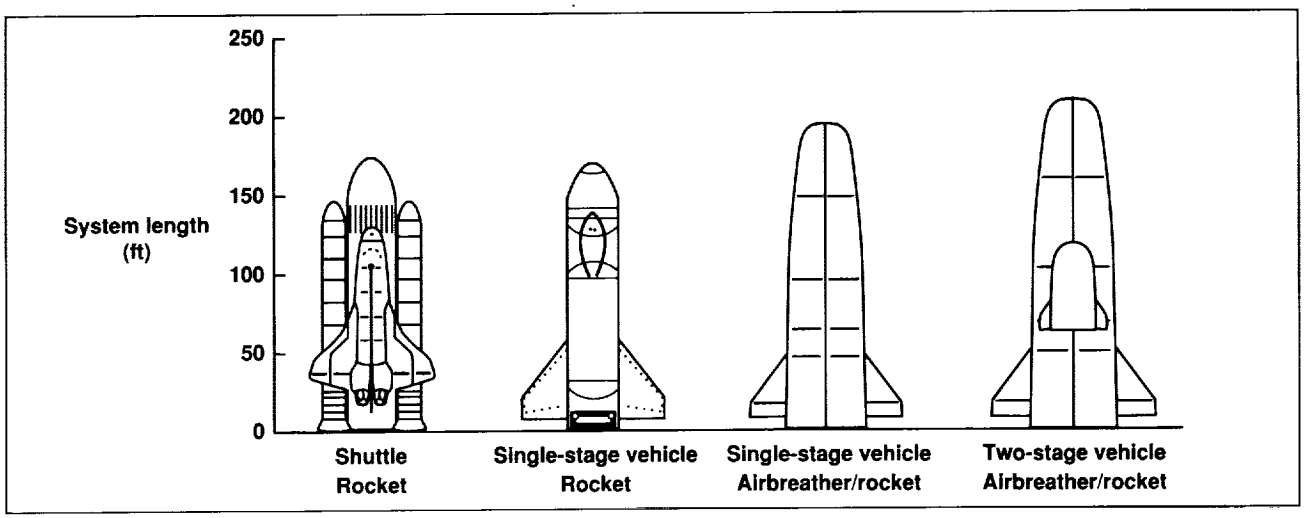


*Fig. 1. Candidate space launch systems.*

increase the unit structural weight for the SSTO air-breather hybrid. The heat loads for the Mach 5 first stage of the TSTO are significantly less than those for the SSTO hybrid, whereas the orbiter's aerothermal environment is the same as that of the all-rocket SSTO. The significantly better propulsion system performance of the SSTO hybrid requires about 60% of the mission propellant weight required for the all-rocket, and the propellant mass fraction of the air-breather hybrid is around 70%, versus 90% for the all-rocket. The TSTO system has a mission fuel fraction of 58%. The sized gross weights of the air-breather/rocket hybrid and the TSTO system are roughly one-third that of the all-rocket concept. The empty weight of the SSTO concepts are similar, whereas the TSTO has a total empty weight approximately 33% higher. Sensitivity studies show the TSTO concept to have the lowest vehicle weight sensitivities to variations in structural weight and propulsion system performance.

All-rocket and air-breather/rocket hybrid concepts are viable candidates for space launch missions, with empty weight characteristics traded off

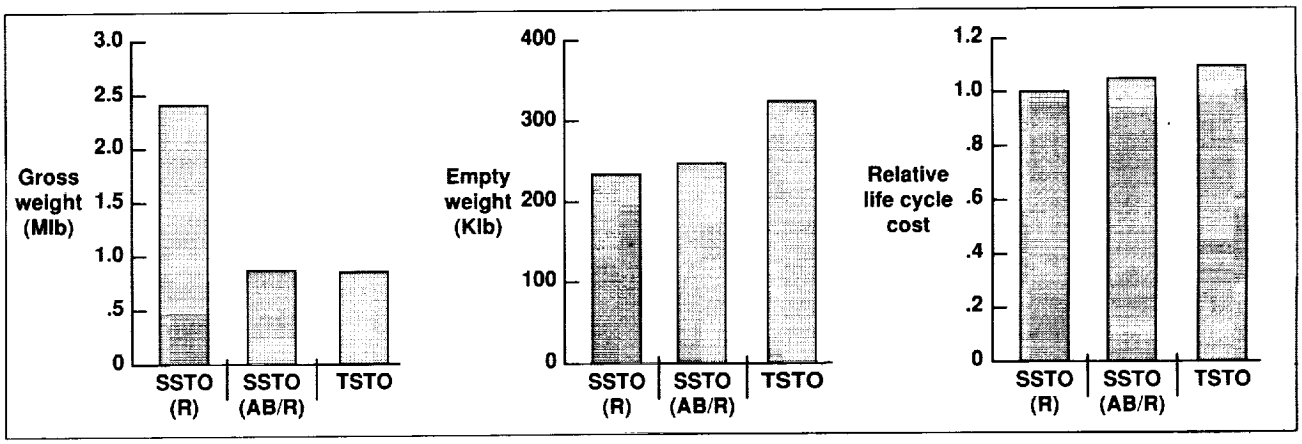


*Fig. 2. Gross weight, empty weight, and relative life cycle cost for the three candidate launch concepts.*

against mission fuel requirements. The air-breather/rocket hybrid and TSTO design have lower gross weight, but with RTD&E and acquisition costs a strong function of empty weight, the all-rocket has a somewhat lower life-cycle cost (second figure). The TSTO concept has the lowest risk, with potential for nearer-term operational capability than the SSTO hybrid design, and with more mission flexibility and growth potential than the SSTO all-rocket design.

**Ames-Moffett contact: J. Bowles**
**(415) 604-6651**
**Headquarters program office: OA**

## Reduced Takeoff Roll for Aircraft

**Joseph C. Eppel, Martin D. Maisel**

A flight investigation to evaluate the takeoff ground roll distance obtainable from a rapid extension of the nose gear strut (called the "jump strut") has demonstrated that reduced distances are achieved compared to unassisted (no jump strut) takeoffs. The flight tests, conducted under a joint NASA/Air Force program, used the NASA Ames quiet short-haul research aircraft (QSRA) because of its demonstrated safe low-speed flying qualities, which were required for safe operation during this activity.

A key feature of the jump strut is that it can be implemented with a lightweight, low-cost, and low-complexity modification to a standard nose gear assembly. The QSRA jump strut, illustrated in the first figure, consists of the standard nose gear modified to accept high pneumatic pressure for the extension, a control valve/timing system, and a pneumatic reservoir and supply system.

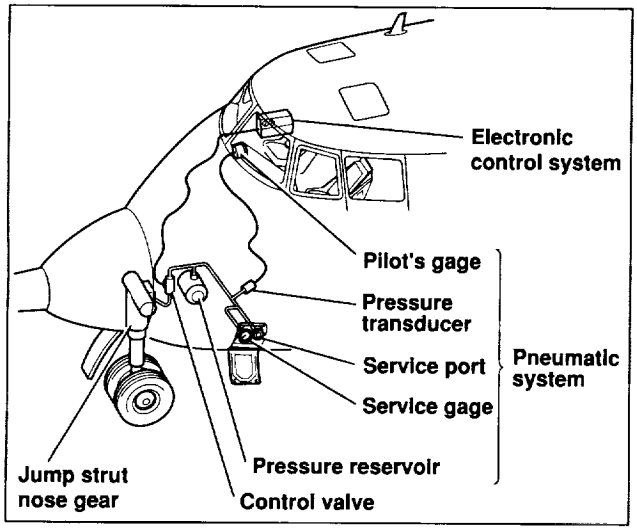


*Fig. 1. Jump strut installed in quiet short-haul research aircraft.*

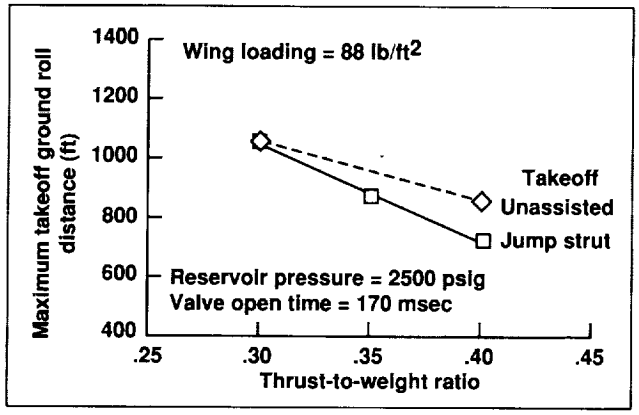


*Fig. 2. Effect of thrust-to-weight ratio on minimum ground roll distance for jump-strut-assisted and unassisted takeoffs.*

The flight-test program established the minimum takeoff ground roll distance without use of the jump strut for a fixed set of aircraft parameters (such as wing loading, thrust-to-weight ratio, and center of gravity) and for a specific pilot elevator technique. The same conditions and piloting technique were repeated with the crew activating the jump strut at the instant the control yoke was pulled aft to initiate rotation. The ground roll distance was determined in

each case from a ground-based laser tracking system and from on-board instrumentation which provided an indication of the full extension of the main landing-gear strut. During the tests, the initial pneumatic reservoir pressure and the duration of the opening of the control valve were varied. The brief test series showed that the use of the jump strut reduced the takeoff ground roll distance by 13% at a 0.4 thrust-to-weight ratio and a wing loading of 88 pounds per square foot (see second figure). This reduction diminished to a negligible amount at a thrust-to-weight ratio of 0.3. No significant effect of reservoir pressure or valve open time on the takeoff ground roll distance was observed.

**Ames-Moffett contact: J. Eppel**
**(415) 604-6276**
**Headquarters program office: OA**

## Improved Aerodynamic Predictions at High Angles of Attack for Conceptual Design

**Paul Gelhausen, Steven Brandt, J. R. Gloudemans**

A methodology was developed that provides improved accuracy and physical quality of high-angle-of-attack aerodynamics during conceptual design. Significant improvements in the prediction of lift, drag, and, more important, pitching moment is realized by applying a vortex-burst modeling method (VBM), which was originally developed for use with Euler methods, to a vortex lattice method (VLM). The figure shows the lift, drag, and pitching moment for a highly swept delta wing predicted by the VLM and the VBM/VLM analyses compared with wind-tunnel data.

The significance of this research is not only the improvement in accuracy but also the speed of the computation. Other methods, such as an Euler method, can provide better results and closer correlation with experiment but require very complex geometric models. The VBM/VLM method requires only simple geometric models that can be generated in minutes with conceptual design tools such as ACSYNT (Aircraft Synthesis) code. This method allows an aircraft designer to better understand the fundamental high-angle-of-attack problems for a particular configuration, and provides information for developing configurations that do not have major pitch-up problems and provide adequate control at high angles of attack. This type of analysis will be important in future multidisciplinary optimization of configurations that have a requirement for high-angle-of-attack maneuverability and agility.

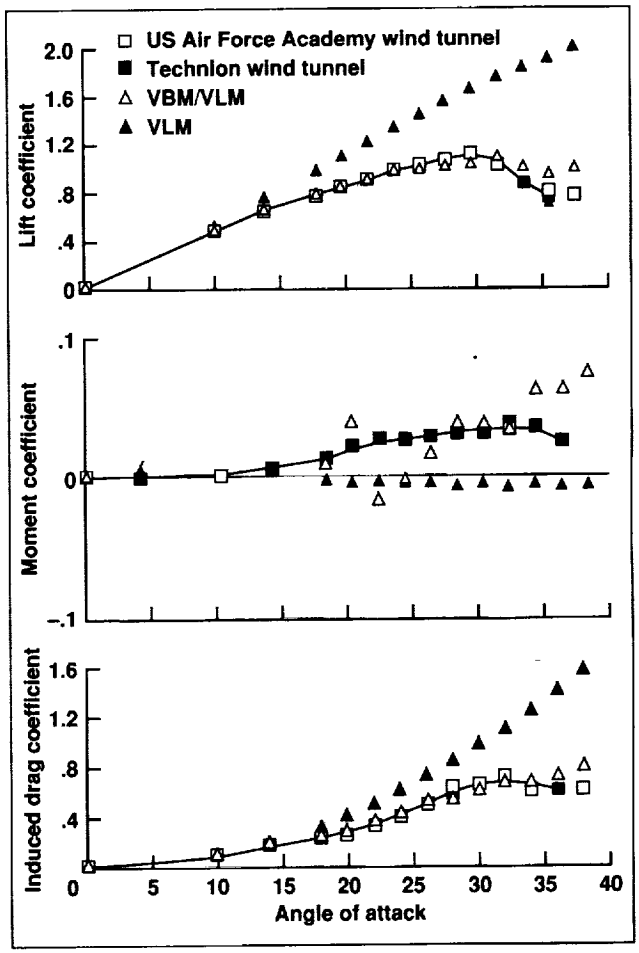


*Fig. 1. Lift, pitching-moment, and induced-drag curves for a 60-degree delta wing.*

**Ames-Moffett contact: P. Gelhausen**
**(415) 604-5701**
**Headquarters program office: OA**

# Advanced Tiltrotor Transport Technology Cost/Benefit/Risk Study

**David R. Schleicher, Martin D. Maisel**

An assessment of the influence of technology improvements on the implementation of civil tiltrotor transport aircraft in the air transportation system was conducted by the Helicopters Division of the Boeing Defense and Space Group under contract to NASA Ames Research Center. The study was triggered by an earlier evaluation which showed that a market-responsive tiltrotor transport aircraft is technically feasible and economically competitive, and provides complementary information for the recently initiated NASA Short Haul (Civil Tiltrotor) Program.

The current study examined an array of factors that could inhibit the successful introduction of a passenger-carrying tiltrotor transport. Of the technical inhibitors, safety, community noise, and economics of operation were seen to be most significant. These inhibitors were found to be dependent on a number of technology-specific areas which were subsequently evaluated to determine the effect of selected improvements on the viability of the civil tiltrotor aircraft. The technology areas included, for example, noise-reducing developments, safety- and weight-related programs such as powertrain development, and integrated cockpit design development.

These areas were evaluated using an analytic hierarchy process (a pairwise comparison method) to establish a weighting and ranking in terms of the overall benefits, cost, and probability of achieving the desired results. The technology items were the subject of detailed sensitivity studies to establish their value to the public (i.e., the user and neighbor communities) and private companies (i.e., development cost, operating cost, and return on investment). The resulting classification of the research and technology programs considered in this study is shown in the list that follows. These results reflect an emphasis on safety and community acceptance of the use of tiltrotor technology in the civil transport marketplace and are generally consistent with prior results of the NASA Aeronautics Advisory Committee Task Force Report on High-Speed Rotorcraft issued in August 1992.

Recommended research tasks for the advanced tiltrotor transport technology program

- Critical technologies
  - Advanced ultra-safe power train
  - Multiple quiet blades/acoustics
  - Contingency power for one-engine-inoperative (OEI) recovery
  - Advanced ergonomic cockpit
  - Concurrent health and use monitoring system (HUMS)/diagnostics development for each of the above
- Enhancing technologies
  - Improved configuration aerodynamics
  - Synthetic vision
  - Improved dynamics
  - Active control of internal noise
  - Composite fuselage
  - Engine cycle development
- Supporting engineering and technologies
  - Configuration layout and sizing studies
  - Icing protection systems

Selected critical high-risk technologies identified in this study are included in the NASA Short Haul (Civil Tiltrotor) Program. Investigations of costs, benefits, and risks are being continued to aid in the direction of resources available for the development of advanced tiltrotor transport technology.

**Ames-Moffett contact: M. Maisel**
**(415) 604-6372**
**Headquarters program office: OA**

## Variable-Diameter Tiltrotor Wind Tunnel Test

**Karen F. Studebaker**

A wind tunnel test of a 1/6-scale model of a variable-diameter tiltrotor (VDTR) was performed by Sikorsky Aircraft with the participation of NASA engineers.

The VDTR model, shown in the figure, is a semispan model mounted to a reflection ground plane in the United Technology Research Center wind tunnel. The model was remotely converted from helicopter mode to airplane mode by simultaneously tilting the nacelle down and retracting the rotor to 66% of the full diameter.

One objective of the test was to investigate the feasibility of the VDTR concept as a candidate rotor system for an advanced tiltrotor. Another objective was to measure blade loads in hover, conversion, and cruise to investigate the aeroelastic characteristics of the rotor. Hover and cruise performance measurements were also made.

This was the first wind tunnel test of the VDTR concept. The VDTR has the benefit of a large-diameter rotor for increased efficiency in helicopter mode and a small-diameter rotor in airplane mode to achieve high speeds (over 400 knots). The VDTR is one concept being investigated under the Short Haul (Civil Tiltrotor) Program as a candidate for an advanced civil tiltrotor to be used as a commuter aircraft operated from vertiports.

The VDTR model was successfully tested in hover, conversion, and cruise. In the complex conversion regime, the measured blade loads were low. As a result, it was shown that the VDTR is a viable concept that warrants larger- and Mach-scale tests. Further studies are being planned such as a study of an acoustically scaled model, piloted simulation, and computer analyses.

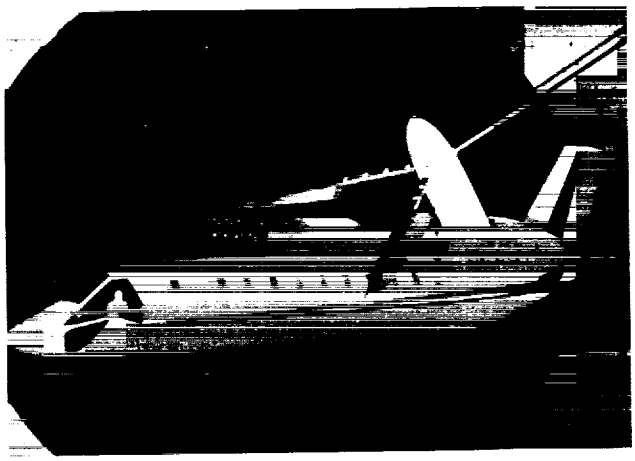

*Fig. 1. The 1/6-scale variable-diameter tiltrotor in conversion mode in the wind tunnel.*

**Ames-Moffett contact: K. Studebaker**
**(415) 604-4682**
**Headquarters program office: OA**

## Investigation of Maximum Normal Force Coefficients on Rotating Airfoils

**Peter D. Talbot, Mark Meyer**

The objective of this research is to confirm and measure the lift behavior of propeller airfoils under rotating conditions near maximum lift. Indirect physical evidence and existing literature have suggested that lift coefficients are higher or that stall is somehow delayed on rotating sections compared to the nonrotating (two-dimensional (2-D) test) case. The most recent accomplishment has been to obtain baseline data consisting of measurements of the pressure coefficients at the 50 percent radius station on a nonrotating propeller blade. Although the test

setup is not a true 2-D test condition, the measurements are of an airfoil that has been and will be used under rotating conditions.

The tests were conducted with the assistance of the U.S. Army in the Ames 7- by 10-Foot Wind Tunnel in August 1993. Pressure coefficients were measured as blade incidence angle was increased. The values of the pressure coefficients were integrated to yield normal force coefficients, Cn, and are plotted versus blade incidence angle in the first figure. At this time, comparisons with the original rotating measurements are inconclusive because the original rotating data set did not achieve true maximum normal force levels. When higher incidence angles are tested in the rotating system, either clear evidence of stall delay will appear or some other explanation of apparent delayed stall will be necessary. The pressure measurements were accompanied by simultaneous microtuft photographs of flow patterns on the upper surface of the blade. The tuft pattern for a condition close to the maximum normal force condition shown in the first figure is presented in the second figure.

Future plans include testing in the Army anechoic chamber hover test facility so that range of the data set from the former test can be extended

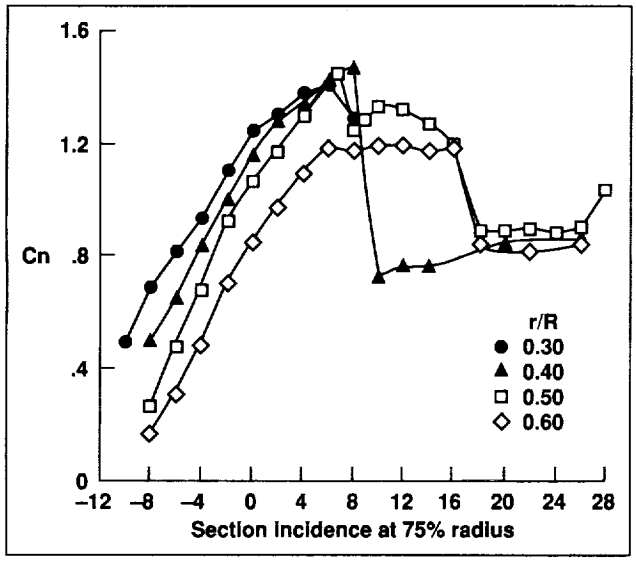


*Fig. 1. Normal force coefficients at adjacent spanwise blade stations (nonrotating propeller blade).*

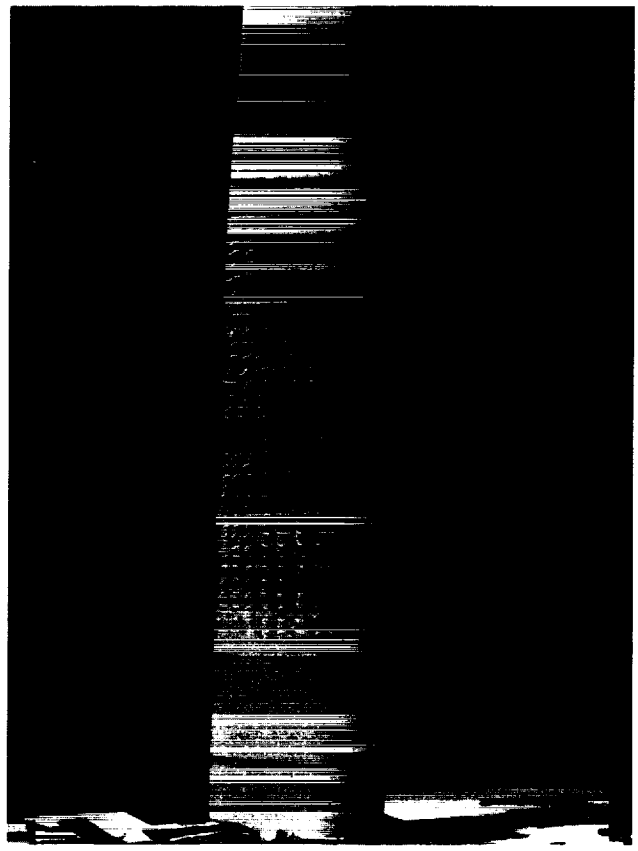

*Fig. 2. Tuft pattern near maximum normal condition.*

to higher blade pitch angles. The results of this research are valuable for a more precise prediction of the performance limits of tail rotors. Knowledge of maximum thrust is needed for handling-qualities purposes, and accurate knowledge of torque and thrust is needed for load and power considerations during design. Also, any rotor or propeller mathematical models that use two-dimensional test data for airfoil characteristics would give improper results at the highest thrust levels. The results may have application to windmill aerodynamics at high thrust levels. An understanding of the phenomenon of higher-than-predicted rotor thrust may lead to improved rotor designs.

**Ames-Moffett contact: W. Snyder**
**(415) 604-6570**
**Headquarters program office: OA**

# Laser Velocimeter for Large-Scale Wind Tunnel Testing

**Stephen E. Dunagan**

Laser velocimetry is widely used for measuring velocity at a specified point in a flow field without disrupting the flow with an invasive probe. Implementing this technique in large-scale wind tunnel testing requires large aperture optics and high optical power densities in the measurement region. For closed-test-section wind tunnels, a compact optical assembly must be placed inside the wind tunnel to avoid the need for very large, high-quality windows in the test section wall. A new instrument utilizing current laser velocimetry technology has been designed and built for the 40- by 80-Foot Wind Tunnel at the Ames Research Center National Full-Scale Aerodynamics Complex.

Facility characteristics constrain this instrument to a back-scatter mode of operation. A Schmidt–Cassegrain optical design has been chosen to simultaneously perform the separate optical functions of focusing the laser beams to a very small waist at the probe volume and collecting Doppler-shifted back-scattered light over a large solid angle. The figure represents a schematic of the optical layout for this instrument. This optical design permits excellent imaging of the small probe volume onto a spatial filter (pinhole) located in front of the photodetector and thereby permits the rejection of all extraneous light from the optical signal. The folded-path design is compact, and reflective (rather than refractive) optics permit multicolor operation without dispersion, which would degrade spatial filtering capability. Zoom focusing of the probe volume is easily and accurately achieved by translating the primary mirror.

This instrument also incorporates other new technology. Single-mode polarization-preserving fiber optics have been used to transfer the coherent radiation from the remotely located argon ion laser to the optical probe assembly. Multimode fiber is used to transfer the Doppler-shifted signal light from the probe assembly to a remotely located photodetector. These features permit the optical probe assembly to be relatively small, its size essentially limited by the required collector aperture, and therefore flow disturbance is minimal. The probe assembly is 75 inches long and has a 20 × 20 inch cross section.

The new instrument takes advantage of the best signal-processing technology available. Digital signal processing, including digital Fourier transform and digital auto-correlation techniques, permit the successful extraction of the fundamental Doppler-shift frequency from very noisy signals. While the optical design for this instrument successfully incorporates several noise reduction concepts, the long operating range still degrades signal power to a level where conventional counter processors are incapable of accurate signal processing. Additionally, the combined effects of small probe volume and low beam-convergence angle inherent to the design result in less that 10 fringes in the probe volume. Digital signal processing techniques are better suited for this condition than conventional counter processing.

The optical configuration has been tested in the optics lab and appears to work well. Design predictions for probe-volume size and collector spatial filtering efficiency have been verified. A wind tunnel prototype is being constructed and will be implemented on an upcoming jet-engine test in the 40- by 80-Foot Wind Tunnel.

**Ames-Moffett contact: S. Dunagan**
**(415) 604-4560**
**Headquarters program office: OA**

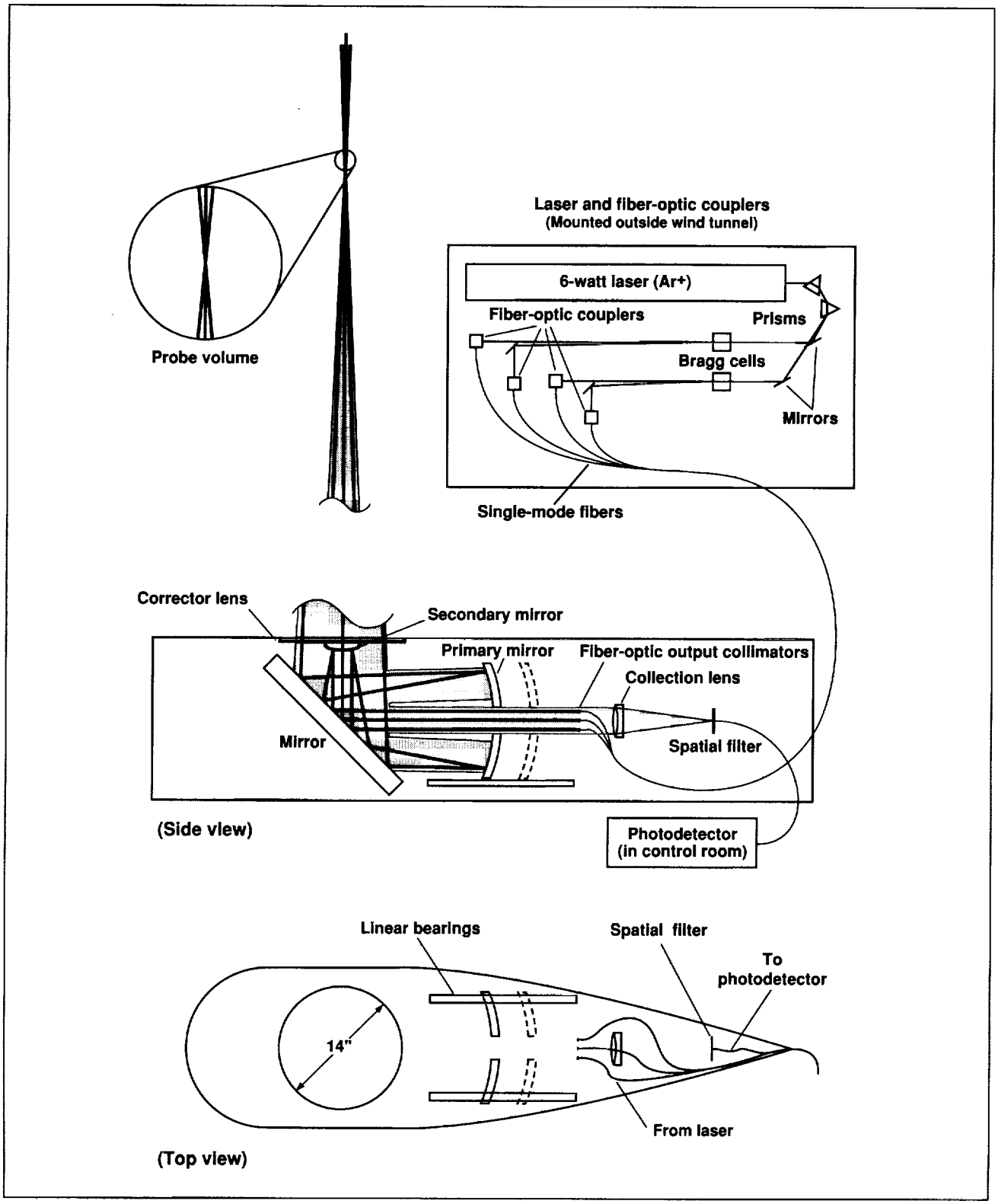


*Fig. 1. Optical layout for Schmidt–Cassegrain long-range laser velocimeter.*

## Accuracy of Tiltrotor Hover Performance Predictions

**Fort F. Felker**

The accuracy of various methods used to predict tiltrotor hover performance was established by comparing predictions with large-scale experimental data. A wide range of analytical approaches were examined. Blade lift was predicted with a lifting line analysis, two lifting surface analyses, and by using a finite-difference solution of the full-potential equation. Blade profile drag was predicted with two different types of airfoil tables and an integral boundary layer analysis. The inflow at the rotor was predicted using momentum theory, two prescribed wakes, and two free-wake analyses.

All of the analyses were accurate at moderate thrust coefficients. The accuracy of the analyses at high thrust coefficients was dependent upon their treatment of high sectional angles of attack on the inboard sections of the rotor blade. The analyses that allowed sectional lift coefficients on the inboard stations of the blade to exceed the maximum observed in two-dimensional wind tunnel tests provided better accuracy at high thrust coefficients than those that limited lift to the maximum two-dimensional value. For tiltrotor aircraft designers, these results provide guidance on which analytical approaches provide the best results and the level of accuracy that can be expected from the best analyses.

**Ames-Moffett contact: F. Felker**
**(415) 604-6096**
**Headquarters program office: OA**

## Advanced Ducted Propulsion Demonstrator Engine

**Clifton Horne, Paul Soderman**

Increasingly tough demands on fuel efficiency and noise reduction have prompted engine manufacturers to explore new propulsion technologies such as ultra-high bypass ratio and advanced blade design. Pratt & Whitney's Advanced Ducted Propulsion (ADP) demonstrator engine was tested in the Ames 40- by 80-Foot Wind Tunnel as part of a joint research program in concert with NASA's Advanced Subsonic Transport technology development effort.

The ADP engine is a production scale (50,000-pounds thrust) research propulsion system that incorporates a high-bypass-ratio variable-pitch fan that is driven through a reduction gear by the low-pressure turbine. The variable-pitch capability was provided to allow optimum blade-angle settings for takeoff, cruise, engine-out feather, and reverse-thrust modes. The gear reduction drive permits efficient turbine operation and reduces the fan-tip speed to minimize fan noise.

The objectives of the wind tunnel test were to (1) validate model-scale projections of reverse-thrust performance under simulated landing and rejected-takeoff conditions, (2) measure the engine-out windmill drag with different blade-angle settings, and (3) measure the acoustic field near the engine. The first figure shows a photograph of the ADP engine in the wind tunnel test section with fixed and traversing microphones used to map the sound field. Unsteady pressures in the fan duct were also measured in order to quantify the fan noise source regions.

Because of the large thrust levels of the ADP engine, the wind tunnel balance system was

modified to extend the thrust measuring capacity to 23,500 pounds to simulate landing approach thrust levels. Full thrust measurements of 50,000 pounds were planned for follow-on tests in the Ames 80- by 120-Foot Wind Tunnel.

The ADP engine operation was stable during all static and dynamic operations. Smooth transitions from forward to reverse thrust were demonstrated for a variety of engine and tunnel speeds, including simulated landing rollout operation. A laser-sheet flow-visualization system, shown in the second figure, was one of several experimental methods used to document the onset of engine reverse thrust. Steady-state fan-operating characteristics and engine-out loss measurements were acquired and will be used to validate the Pratt & Whitney design, scaling,

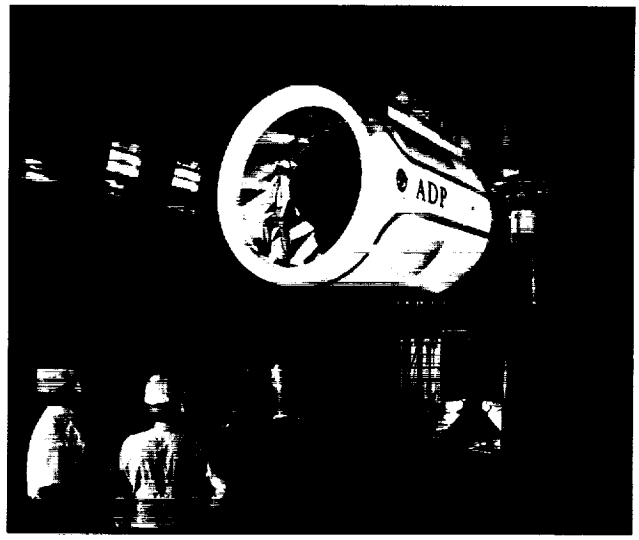


*Fig. 2. Laser-sheet flow-visualization system.*

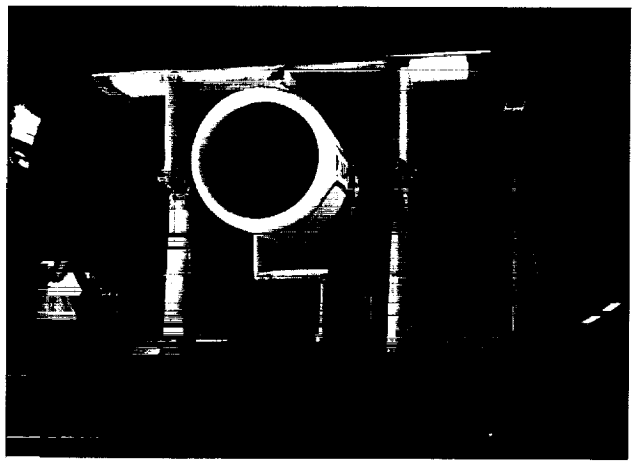

*Fig. 1. Noise measurement setup.*

and prediction methods. These techniques will be applied to ADP production engines that are forecast for introduction in the late 1990s. This test successfully demonstrated the capability for large-engine testing in the Ames full-scale wind tunnels.

**Ames-Moffett contact: C. Horne**
**(415) 604-4571**
**Headquarters program office: OA**

# Individual Blade Control Test

**Stephen Jacklin, Stephen Swanson**

A wind tunnel test was conducted with a full-scale helicopter rotor to evaluate the potential of open-loop individual blade control (IBC) to improve rotor performance, reduce blade–vortex interaction (BVI) noise, and alleviate vibrations. The wind tunnel test was a collaborative effort between the United States and Germany and was conducted in accordance with the United States/German memorandum of agreement on rotorcraft aeromechanics.

Helicopter control through the conventional swashplate, whether for trim or other objectives, is fundamentally limited for rotor systems with four or more blades. In these cases, specification of the pitch (or servo-flap) control of one blade predetermines the control for the other blades. This shortcoming limits the degrees of freedom available for reducing rotorcraft vibrations, loads, and acoustics because it is not possible to move one blade without moving all the rest.

Recently, a German company, Henschel Flugzeug-Werke (HFW), developed a set of high-frequency actuators that replace the rotating pitchlinks of the rotor system. This use of actuators represents a breakthrough in rotor-control technology. Low-amplitude flight testing using an HFW IBC system on a Messerschmidt-Bolkow-Blohm BO-105 helicopter was conducted in 1990 and 1991. Although the initial flight-test results indicated vibration and noise reductions with IBC, the limited thrust and speed of the aircraft, combined with the safety-imposed low amplitude of the actuators, prevented exploring the full potential of the IBC system. For this reason, a full-scale wind tunnel test program was proposed using the Ames 40- by 80-Foot Wind Tunnel.

To obtain the wind tunnel test data, the ordinary blade pitch control links of the rotor were replaced by servo-actuators so that the pitch of each blade could be controlled independently of the other blades. Though similar to the flight test hardware, the IBC system for the wind tunnel had much higher control amplitude and increased frequency response. The wind tunnel test was conducted with a full-scale BO-105 rotor system mounted on the Ames Rotor Test Apparatus.

The IBC test evaluated open-loop IBC controls at amplitudes up to ±1.2 degrees, with single-frequency harmonics of 2/rev–6/rev, multiharmonic combinations, pulses, wavelets, and doublet inputs. Inputs of 1/rev–12/rev were also tested without blades. Extensive measurement information was acquired for each IBC data point. This included rotor performance data, static and dynamic hub-force and moment data, rotor loads data, control loads data, inboard- and outboard-blade pitch-motion data, and microphone (BVI noise) data.

The effect of IBC on rotor vibration was measured by examining the oscillatory components of the rotor-balance outputs. IBC had a definite effect on the oscillatory rotor forces and moments. The first figure presents one result showing the influence of 3/rev IBC control on the 4/rev rotor vibrations. The vibration index shown combines the oscillatory 4/rev normal force, in-plane forces, and hub moments into a single metric. Use of a single index was possible because the data showed all five forces and moments were reduced at the same IBC input phase angle. It was shown that a 50–60% reduction in 4/rev

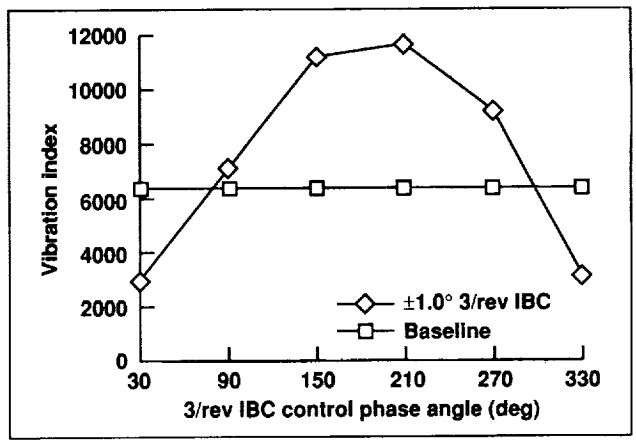


*Fig. 1. Effect of 3/rev individual blade control on 4/rev rotor vibration at 130 knots.*

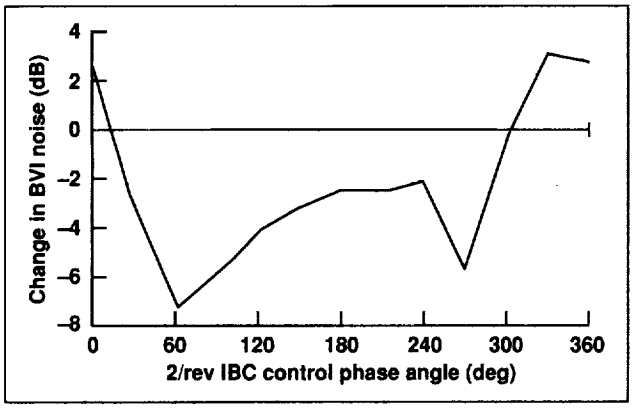


*Fig. 2. Effect of 2/rev individual blade control on blade–vortex interaction noise for descent flight condition at 64 knots.*

oscillatory forces and moments could be obtained using 3/rev control alone.

Acoustic data indicated that 2/rev control was effective in reducing BVI noise. As shown in the second figure, at certain phase angles 2/rev IBC substantially reduced the BVI noise. Use of the Ames Acoustic Survey Apparatus allowed the acquisition of acoustic data over a large range of locations. This data is being reviewed to assess the effects of IBC on noise directivity.

Another focus of the IBC program was to understand how the loads on the control system and rotor blades changed with the application of IBC. Some IBC phase angles decreased the blade loads and others increased them, but the actuator (or pitchlink) loads were always roughly twice the baseline value.

IBC not only changed the rotor power requirements, but also affected the trim state of the rotor. These changes occurred because IBC reduced the adverse effects of blade stall on the rotor. Analysis of the test data is being conducted to verify a 6% improvement in rotor efficiency obtained through IBC.

**Ames-Moffett contact: S. Jacklin**
**(415) 604-4567**
**Headquarters program office: OA**

## Rotor Hub Loads Research

**Sesi Kottapalli**

This analytical study approaches the goal of reducing helicopter rotor hub loads by introducing damping into the blade elastic torsional degree of freedom. Hub load reduction occurs when the blade elastic torsional deflection is modified. In this research, blade torsional damping was introduced as spanwise distributed torsional damping and was applied solely to the blade elastic torsional mode. The fully coupled aeroelastic rotorcraft computer code CAMRAD/JA was used to analytically model the modern, articulated S-76 rotor blade. Substantial reductions in the rotor hub loads were achieved in all three directions for large damping values applied at the frequency of the blade elastic torsional mode. For example, a root torsional damping (an equivalent damping measure) of 528 foot-pound-seconds per radian was applied at 28.5 hertz. The subsequent reductions in hub loads were 15% for the lateral inplane shear, 25% for the longitudinal inplane shear, and 34% for the vertical shear.

**Ames-Moffett contact: S. Kottapalli**
**(415) 604-3092**
**Funded by DDF**

# Hub Load and Noise Reduction by Higher Harmonic Control

Sesi Kottapalli, Stephen Swanson

Open-loop higher harmonic control (HHC) research has been conducted in the 40- by 80-Foot Wind Tunnel of the National Full-Scale Aerodynamics Complex at Ames. This test involved a full-scale, modern, five-bladed, moderate thrust bearingless main rotor. This HHC effort involved obtaining reductions in dynamic hub loads (1/rev and 5/rev) and, separately, reductions in noise due to blade–vortex interaction (BVI). During dynamics testing, the maximum airspeed was 160 knots with the rotor producing a thrust of 14,000 pounds, and with 1/rev and 5/rev control being exercised separately. Full-scale BVI experiments were conducted at 12,000 pounds thrust at 60 and 80 knots with 5/rev control. In the hub load and noise research, testing was conducted with all three modes of control: collective, lateral, and longitudinal. The amplitude and phase in each of these modes were varied to determine their optimum values. It was found that in cruise, at speeds from 120 to 160 knots, the 5/rev side force was reduced substantially by lateral control (first figure). A substantial reduction in the 1/rev normal force was achieved with 1/rev collective control. At the BVI flight condition (descent, 60 and 80 knots), a reduction in BVI related noise up to 5 decibels was consistently achieved by the application of lateral control (second figure).

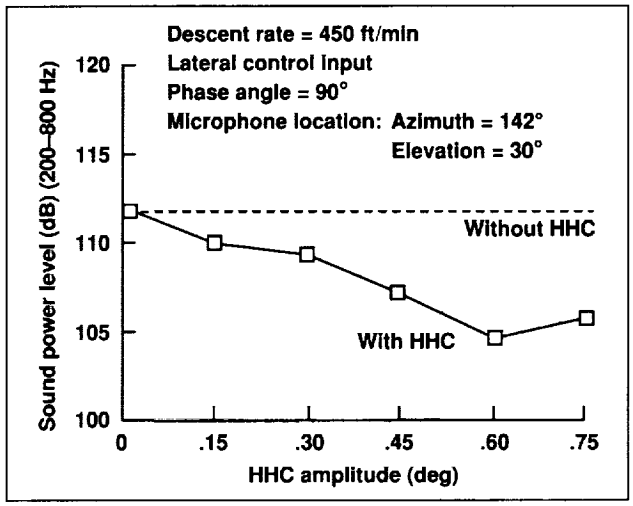


*Fig. 2. Effect of higher harmonic control on blade–vortex interaction noise at 80 knots.*

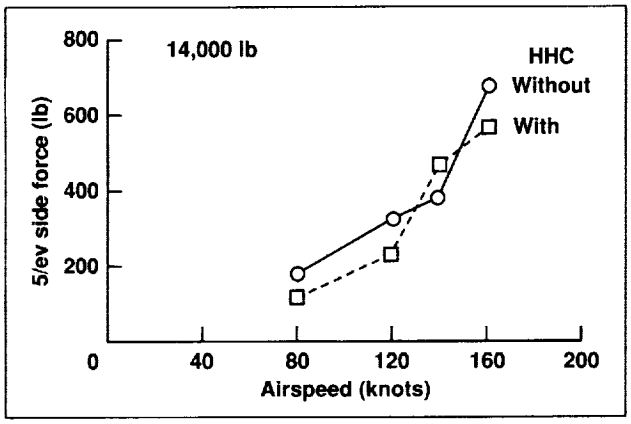


*Fig. 1. Effect of higher harmonic control on side force.*

**Ames-Moffett contact: S. Kottapalli**
**(415) 604-3092**
**Headquarters program office: OA**

# Full-Scale F/A-18 High-Alpha Research

**Wendy R. Lanser, Kevin D. James**

Directional control of fighter aircraft at high angles of attack is difficult to achieve using standard aerodynamic controls. Full-scale tests of the F/A-18 in the Ames 80- by 120-Foot Wind Tunnel demonstrated that forebody flow control by use of either blowing slots or strakes provides ample lateral control at extreme angles of attack. A major goal of the NASA High-Alpha Research Program is to flight test a forebody flow control system that employs strakes as the control effector. The tests of the full-scale F/A-18 in the Ames wind tunnel provided data to augment aerodynamic data taken at small scale to form a thoroughly defined set of flight-control laws for use in the flight tests. Additional research objectives include investigation of the tail buffet phenomenon and detailed measurement of surface pressures

*Fig. 1. Full-scale F/A-18 airframe in Ames 80- by 120-Foot Wind Tunnel.*

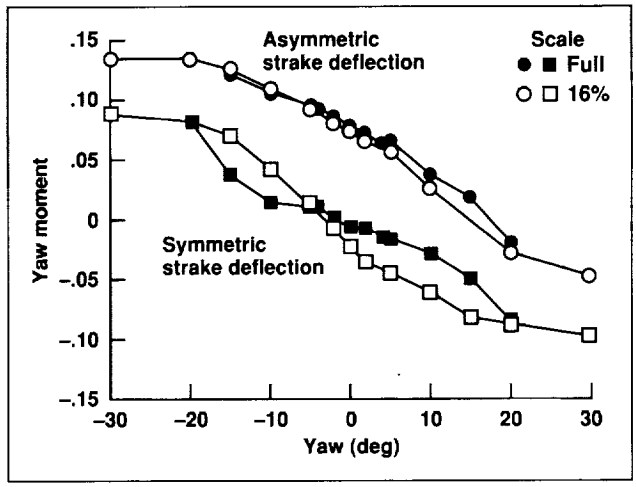


*Fig. 2. Effect of Reynolds number and scale on yaw moment control capability of forebody strakes.*

on the wings and canopy for the development and validation of computational methods. Data was obtained for an angle-of-attack range from 20 to 60 degrees.

The first figure shows the F/A-18 model mounted in the wind tunnel. The forebody strakes, visible on the radome, were remotely actuated during the test. Comparison of the measurements made in the 80- by 120-Foot Wind Tunnel with existing data from 16%-scale-model tests showed some instances of significant difference in lateral control authority. The second figure compares full-scale and 16%-scale measurements of the yaw moment for two separate strake configurations. The differences are primarily due to scale or Reynolds-number effects and show the importance of testing at the largest Reynolds number possible to properly represent the aircraft in a flight-test program.

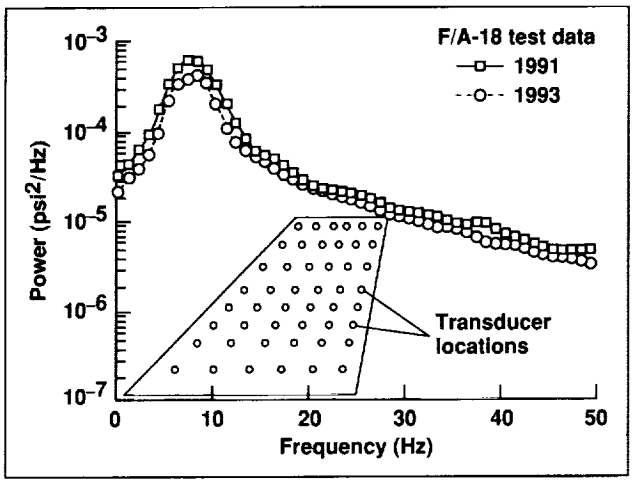


*Fig. 3. Power spectral density of unsteady tail pressure and repeatability validation.*

Unsteady-pressure data was obtained on an 8 × 6 grid of pressure orifices on both sides of both vertical fins (third figure). Also shown is a sample of the power spectrum of the pressure at one point on the port fin. This data, obtained as part of a cooperative effort with the U.S. Air Force Wright Aeronautical Laboratory, is being used to develop an understanding of the flow physics of vortex bursting and the attendant tail buffet phenomena affecting the design and performance of current and future generations of twin-tailed fighter aircraft.

**Ames-Moffett contact: W. Lanser**
**(415) 604-3543**
**Headquarters program office: OA**

## Correlation of the Lynx-XZ170 Flight-Test Results with CAMRAD/JA and R150

**Benton H. Lau, Alexander W. Louie, Costantinos P. Sotiriou, Nicholas Griffiths**

Results from two rotorcraft codes were correlated with flight-test data obtained from the Lynx-XZ170 helicopter. The Lynx XZ170 has a hingeless rotor system featuring four blades with rectangular tip planforms. A NASA technical memorandum was published documenting the steady, level flight conditions at different thrust levels and advance ratios up to and beyond the rotor stall boundary. Rotor performance, control inputs, and blade and control loads were compared with results from the Comprehensive Analytical Model of Rotorcraft Aerodynamics and Dynamics code developed by Johnson Aeronautics (CAMRAD/JA) and the R150 rotor analysis developed by Westland Helicopters Limited and the Defense Research Agency. Effects on blade loads correlation were examined by varying CAMRAD/JA modeling parameters such as lag-damper model, stall model, and wake model. In addition, effects of rotor trim condition on blade structural loads and methods of calculating the loads were investigated. The influence of the fuselage on rotor loads was also examined using the R150 analysis.

The figure compares CAMRAD/JA calculations for the blade bending moments using free-flight trim and wind-tunnel trim options. Near the hub, CAMRAD/JA flatwise moment calculations agree well with the data at low speeds and fairly well at high speeds. At the outboard stations, CAMRAD/JA calculations agree reasonably well with the flight-test data. R150 correlations of the flatwise bending moments are very good near the hub and at the outboard stations, but are only fair at the inboard station. For the edgewise bending moments, both the CAMRAD/JA and R150 correlations with data are

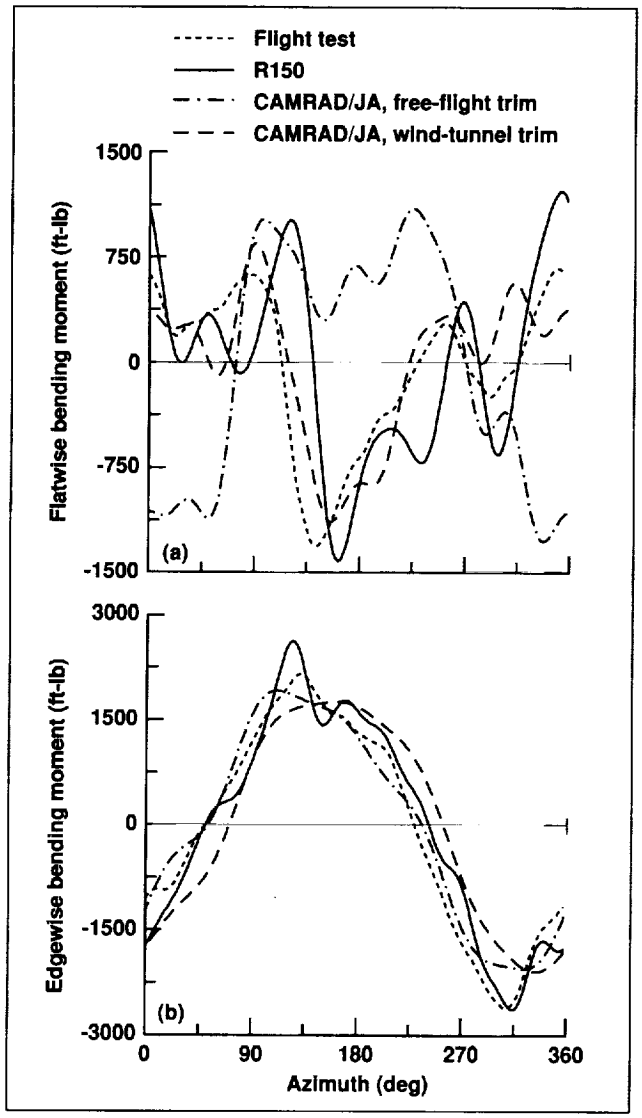


*Fig. 1. Effect of CAMRAD/JA trim option on blade bending moments at an advance ratio of 0.164 and an aircraft weight coefficient of 0.11. (a) Flatwise moment at 3.2% radial station; (b) edgewise moment at 6.8% radial station.*

good near the hub and fair at the outboard stations. Except for a phase difference, the CAMRAD/JA correlation of the lag-damper load is reasonably good using the nonlinear lag-damper model. Although the general trends of the vibratory pitch-link load data are captured by both analytical codes, the details of the waveform are not.

**Ames-Moffett contact: B. Lau**
**(415) 604-6714**
**Headquarters program office: OA**

# Tiltrotor Download Reduction

**Jeff Light**

A test was conducted to measure the rotor performance and download of a model tiltrotor. A 7/38-scale V-22 rotor was tested in conjunction with XV-15 and V-22 wings. The test evaluated two download reduction techniques and assessed some model testing issues. Wing surface pressures were measured along with the rotor performance and wing loads. The first download reduction technique tested used blowing slots on the wing upper surface, and the second used spanwise vortex trapping plates on the upper and lower surfaces.

The upper surface blowing configuration consisted of three spanwise slots in the upper surface of the wing, two near the leading edge and one near the trailing edge. When air was blown through the slots, the pressure on the wing upper surface could be decreased, producing a decrease in wing download. This technique provided modest decreases in the wing download (first figure). The blowing reduced the wing download by 9% at thrust coefficients representative of tiltrotor aircraft (0.016). The benefit of the upper surface blowing technique was greater at lower thrust coefficients.

The vortex trapping plates configuration consisted of spanwise plates perpendicular to the wing on the upper and lower surfaces. The best configuration of plates tested provided a 7% reduction in download at a thrust coefficient of 0.016. A two-dimensional Navier–Stokes analysis was used to model the flow field over the wing to help understand the flow field.

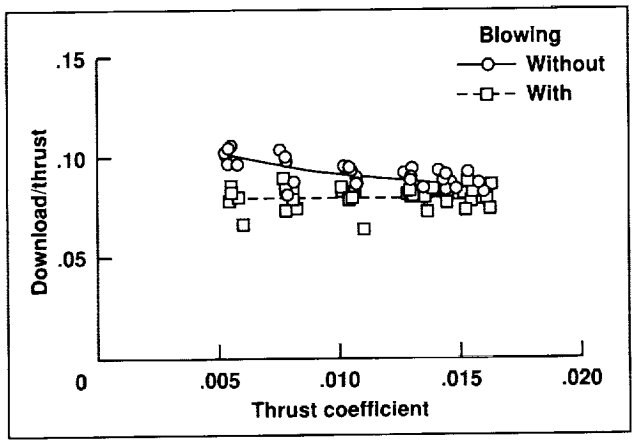


*Fig. 1. Effect of upper surface blowing on wing download.*

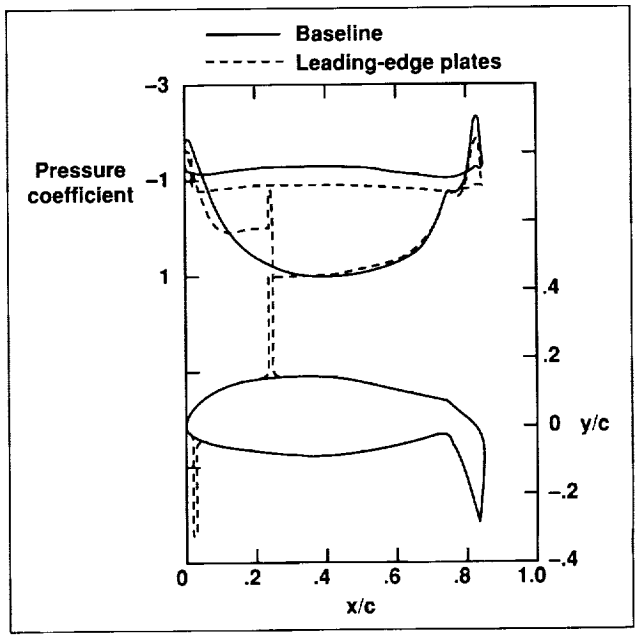


*Fig. 2. Surface pressure and wing geometry for a V-22 wing with vortex trapping plates.*

The wing surface pressures with and without the vortex trapping plates are shown in the second figure. A recirculating vortex is formed by the plate on the upper surface. This vortex decreases the upper surface pressure, and, therefore, the download. The pressure on the wing lower surface was also significantly reduced, providing additional download reduction.

The download on the wing is only part of the rotor–wing interaction phenomenon. The wing also affects the rotor performance. The test examined several parametric changes, including wing sweep, rotor–wing spacing, and wing span, and found changes in both download and rotor performance. A beneficial download reduction was sometimes accompanied with an offsetting decrease in rotor performance. Therefore, overall rotor–wing performance must be considered when examining tiltrotor wing download reduction techniques.

**Ames-Moffett contact: J. Light**
**(415) 604-4881**
**Headquarters program office: OA**

# Parallel Solution of Poisson's Equation

**Wayne O. Miller**

Poisson's equation is an elliptic partial differential equation that is important in describing many physical phenomena. Instances include fluid dynamics, heat transfer, and electromagnetics. Consequently, the solution of Poisson's equation is an important topic of numerical analysis. Further, the growing use of parallel computing requires the development of new solution methods that can be efficiently mapped onto multiple processors. Many traditional scalar algorithms perform poorly when run in parallel because full utilization of all processors is not obtainable. The method presented here was developed to fully utilize all processors of a multiple-instruction, multiple-data parallel computer.

Because Poisson's equation is elliptic, the solution at any point requires information from the entire domain and the boundary conditions. Numerically, this takes the form of a set of coupled equations, with one equation for each discrete point in the domain. As the size or resolution of the domain increases, this set of equations can become prohibitively large and costly to solve.

Domain decomposition is one method for solving large sets of equations, and is part of the approach taken here. The domain is divided into several smaller subdomains, as shown in the figure. Each of these subdomains represents a smaller version of the original problem. The complete solution process is altered from solving one large problem to solving several smaller problems. This is attractive for parallel computing because each of the smaller subdomain problems can be solved on a different processor.

Creating the subdomains involves defining new subdomain boundaries on the interior of the domain. The subdomain problems require boundary values and it is necessary to provide the solution values on these interior boundaries a priori. However, the solution values are not typically known anywhere in the interior a priori, so approximate values must be used. These approximate boundary values couple the subdomain problems and require an iterative solution. Thus, while the global problem has been decomposed into several smaller problems, the smaller problems must be solved several times to converge the solution.

It is possible to determine the exact interior boundary values for certain classes of Poisson's equation. Using the exact boundary values decouples the subdomain problems, thereby requiring only one solution for each subdomain. The exact boundary values are found by mathematically transforming the differential equation into an integral equation. The integral equation contains boundary and domain integrals that can be readily computed. However, the solution of the integral equation is only for a single point in the domain. Finding the solution at any other point in the domain requires another solution of the integral equation. In contrast, a solution of the differential equation gives an answer at all points in the domain.

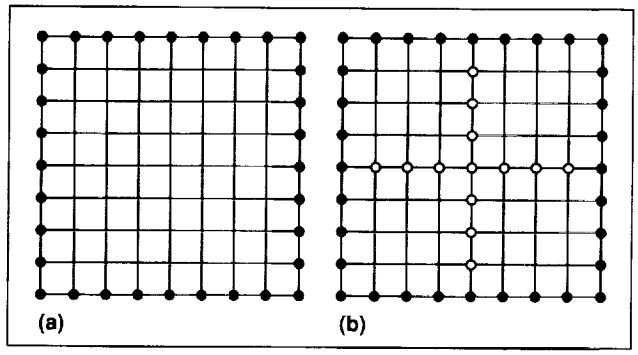


*Fig. 1. Domain decomposition and internal boundary values. (a) Original global domain. Boundary values on filled circles are known; (b) Domain divided into four subdomains. Boundary values needed on open circles.*

The complete method presented here uses domain decomposition to reduce the large global problem into several smaller problems, and uses the pointwise integral solution to find exactly the relatively few interior boundary values. The subdomain problems are thus physically decoupled, and are solved in parallel only one time. The success of the method was found to depend upon the time spent solving the integral equation for the interior boundary values. For certain classes of problems, a nearly perfect parallel speedup was possible, but for others the method was not efficient.

**Ames-Moffett contact: W. Miller/F. Felker**
**(415) 604-6719/6096**
**Headquarters program office: NRC**

# Active Control of Helicopter Blade Stall

**Khanh Q. Nguyen**

Unlike fixed-wing aircraft where stall limits low-speed operations, stall on the rotor limits the high-speed and loading capabilities of the helicopters. At the helicopter operating flight envelope, stall on rotor blades affects handling qualities and creates engine power shortage or excessive vibration causing severe human discomfort and premature fatigue failure of structural components. Stall-induced loads can exceed the design load limits of structural components.

In an effort to expand the helicopter flight envelope, high-frequency blade-pitch actuation is used to alleviate blade stall at high-speed and high-thrust conditions. The analytical study has been carried out using a modified version of the University of Maryland Advanced Rotorcraft Code. One of the modifications includes the automatic stall suppression system, which is configured to minimize the stall areas on the rotor disk. Admissible inputs are the blade-pitch excitations at the harmonics of two to six times the rotor rotational speed, where the input types can be single or multi-harmonic.

The application of the stall suppression system on a highly loaded rotor reveals some unexpected stall-control behaviors. Simulated results indicate that the higher harmonic blade pitches reduce the original stall areas. However, these inputs cause a premature stalling of the originally unstalled areas, resulting in an overall increase in the net stall on the rotor disk (see figure). In particular, the higher harmonic blade pitch used to suppress stall on the retreating side causes premature stall on the fore and aft regions of the rotor disk. Subsequent investigations suggest that an effective input waveform for stall reduction should be active only over the portion of the original stall areas that cover about a quarter of the rotor revolution.

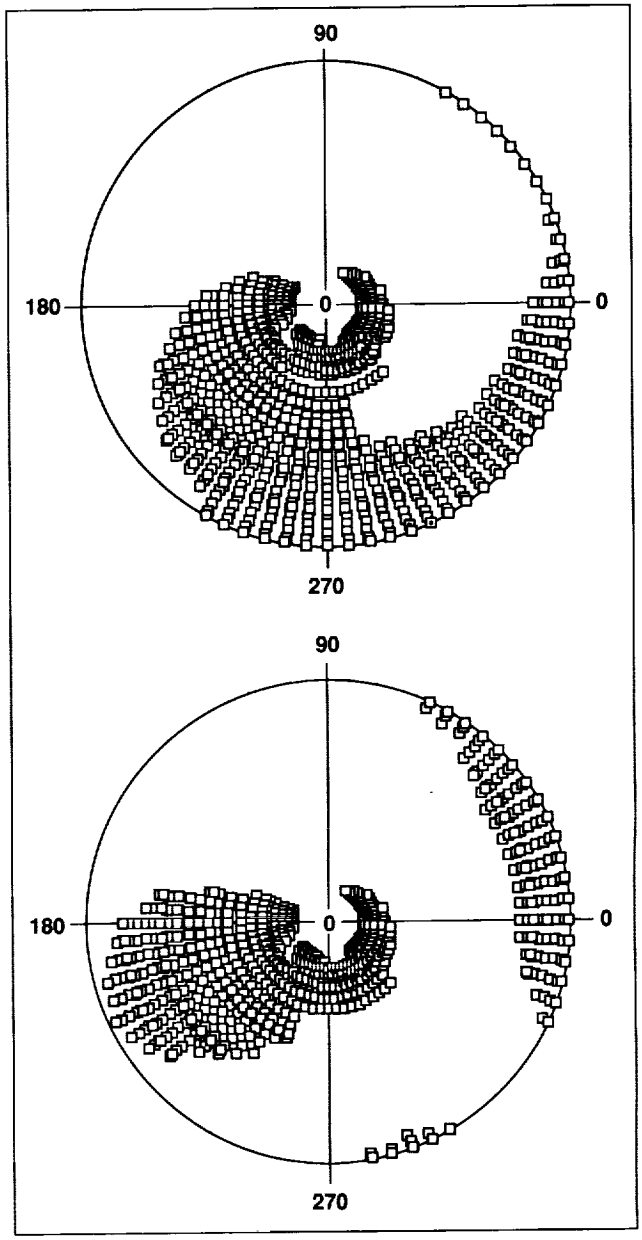


*Fig. 1. Stall areas on a highly loaded rotor (a) without and (b) with two-per-rev blade pitch control.*

**Ames-Moffett contact: K. Nguyen**
**(415) 604-5043**
**Headquarters program office: OA**

# Aeroelastic Stability of Modern Bearingless Rotors

**Khanh Q. Nguyen**

Modern bearingless rotors have evolved from several design processes and are included in current and planned helicopters worldwide. Bearingless rotors are characterized by flexural members that allow the blade flap, lead-lag, and pitch motions without discrete hinges and bearings. The elimination of hinges and bearings significantly reduces the complexity of rotor hub designs making bearingless rotors easier to maintain and to manufacture than conventional articulated or hingeless rotors. The physical simplicity of these designs, however, complicates the analysis of rotor aeroelasticity because of the redundant load path, complex bending-torsion and kinematic couplings, and material nonlinear characteristics.

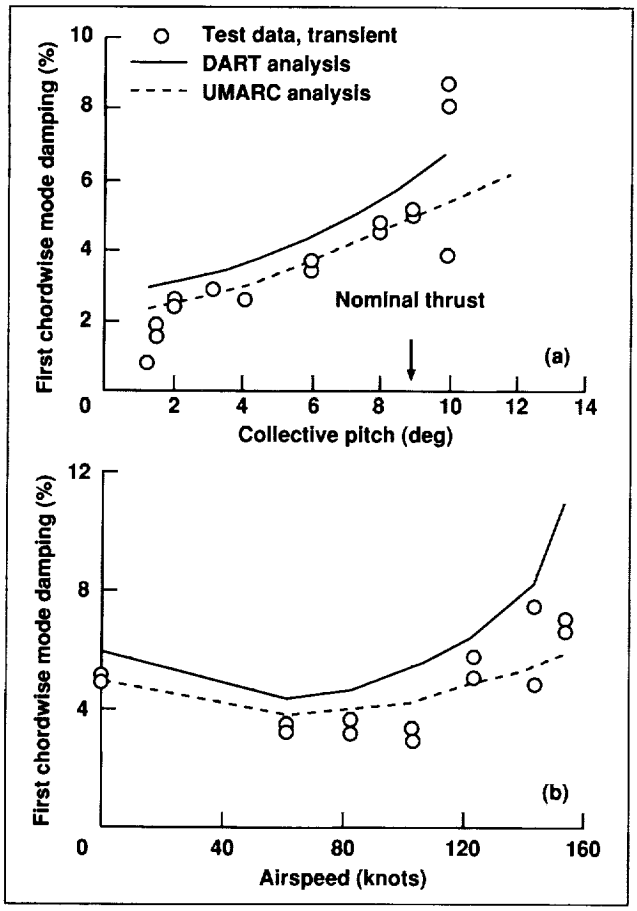


*Fig. 1. Aeroelastic stability of the MDART rotor in (a) hover and (b) forward flight.*

In an effort to provide a new database about bearingless rotors, an aeroelastic stability investigation was conducted on the full-scale McDonnell Douglas Advanced Rotor Technology (MDART) rotor in the Ames 40- by 80-Foot Wind Tunnel. The MDART rotor is a modern, five-bladed, bearingless rotor that incorporates elastomeric dampers to augment the rotor inplane damping. The aeroelastic stability data were acquired over an extensive set of flight conditions, including hover and forward flight.

The aeroelastic stability data were subsequently used in a correlation study comparing test data with the results obtained from two rotorcraft analyses: the University of Maryland Advanced Rotorcraft Code (UMARC) and the McDonnell Douglas Dynamic Analysis Research Tool (DART). Sample results of the correlation study are shown in the figure.

**Ames-Moffett contact: K. Nguyen**
**(415) 604-5043**
**Headquarters program office: OA**

# Rotor Data Correlation

**Randall Peterson**

The use of wind tunnel tests plays a key role, together with analytical prediction and flight test evaluation, in the development of new rotor systems. Such tests are typically performed using a range of rotor system sizes and wind tunnel test facilities. To assure the accuracy of wind tunnel testing methodology, a validation study is in progress using test results from model- and full-scale tests to be compared with flight test data. This study is being conducted under the auspices of the United States/German memorandum of understanding on cooperative research in the field of helicopter aeromechanics. This comparison will determine the ability to accurately predict helicopter flight behavior from wind tunnel experiments and the influence of the test facility on these results. Experimental data from a series of wind tunnel tests, including both model- and full-scale experiments, will be studied to determine the extent to which wind tunnel test results can be used to predict flight behavior.

Results from a recently completed full-scale rotor test in the Ames 40- by 80-Foot Wind Tunnel and a recently completed flight test of a BO-105C helicopter at the Deutsche Forschungsanstalt für Luft- und Raumfahrt (DLR) in Braunschweig, Germany, have been correlated. Rotor hub and blade loads were obtained over a range of advance ratios from 0.1 to 0.34 for a nominal rotor thrust of 5,000 pounds ($C_T/\sigma$ = 0.07). Good correlation of measured blade-root flap-bending moments in the wind tunnel with flight test measurements is shown when the rotor is trimmed to measured flight-test hub pitch and roll moments. Analytical results using the Comprehensive

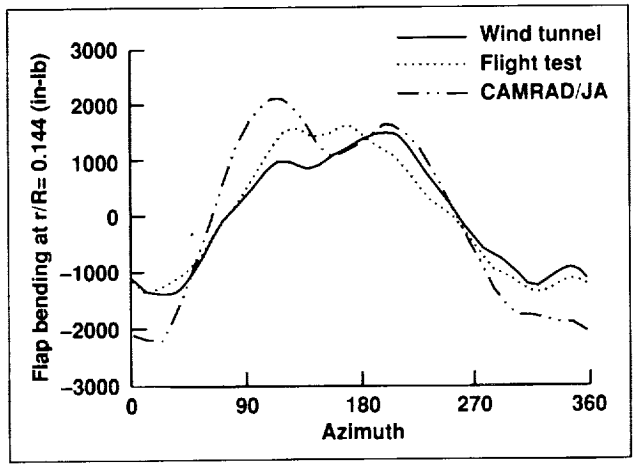


*Fig. 1. Comparison of measured wind-tunnel and flight-test rotor flap bending with analytical results at an advance ratio of 0.197 and 1-G thrust.*

Analytical Model of Rotorcraft Aerodynamics and Dynamics analysis from Johnson Aeronautics shows good correlation for isolated rotor hub moment trim. The figure shows comparisons of wind-tunnel, flight-test, and analytical results of rotor-blade-flap bending at an inboard radial station at a nominal rotor thrust of 5,000 pounds and an advance ratio of 0.197.

**Ames-Moffett contact: R. Peterson**
**(415) 604-5044**
**Headquarters program office: OA**

# High-Lift Aerodynamics Research

James C. Ross

The concept of using a tab at the trailing edge of the main element of a multielement wing was tested at full scale in the Ames 80- by 120-Foot Wind Tunnel. A retired Air Force T-39 aircraft was modified to work as a wind tunnel model (first figure). A lift-enhancing tab is essentially a small split flap (on the order of 1% of the airfoil chord) that is deflected up to 90 degrees. It increases the maximum lift capability of single- and multi-element airfoils at a given angle of attack. The concept can be applied to any element of a multielement airfoil. The test of the T-39 was the first to address possible three-dimensional and scale effects.

The second figure illustrates how a lift-enhancing tab is used on a three-element airfoil. In this case, the tab works by increasing the camber of the main element near the trailing edge. This increase in camber is important because the cove the flap retracts into effectively removes any camber in that part of the airfoil. For the test of the T-39, a variety of tab heights was tested as well as several values of flap gap and overlap.

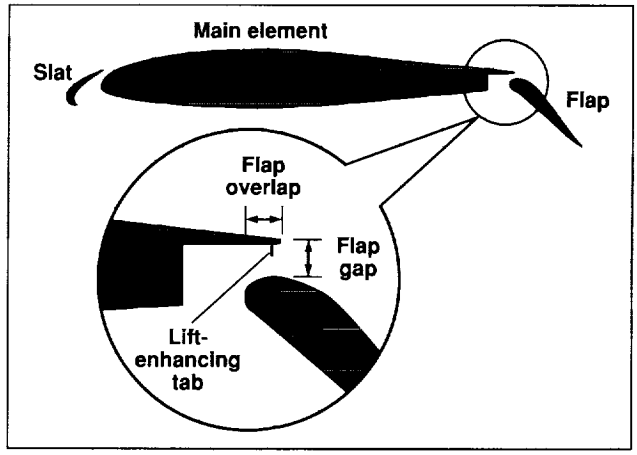


*Fig. 2. Lift-enhancing tab on a three-element T-39 airfoil.*

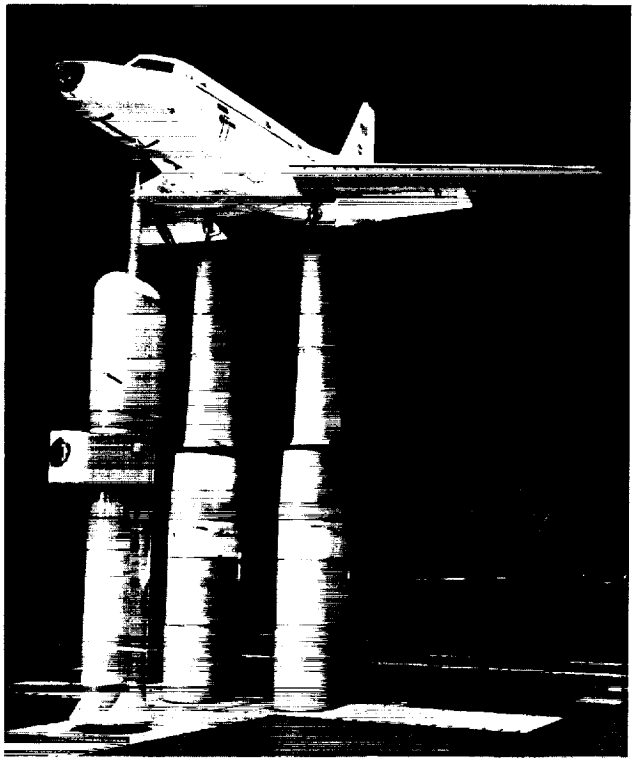

*Fig. 1. Air Force T-39 aircraft mounted in the wind tunnel test section.*

Previous work with two-dimensional, two-element airfoils showed that tabs placed at the trailing edge of the main element could increase the maximum lift by over 10% and reduce the angle of attack required to generate a given lift coefficient by up to 5 degrees. The full-scale tests on the three-element high-lift system of the T-39 showed similar results. One of the most intriguing aspects of the test was that a tab mounted as shown in the second figure made the high-lift performance relatively insensitive to the flap gap and overlap. Additional work is planned to verify this result and to test the concept on modern multielement airfoils.

**Ames-Moffett contact: J. Ross**
**(415) 604-6722**
**Headquarters program office: OA**

# Shuttle Orbiter Drag Parachute Test

James C. Ross, Mario Perez

A drag parachute has been used on the Space Shuttle Orbiter during landings at the Kennedy Space Center since 1992. Some of the deployments have worked very much as anticipated, but at other times the location of the drag parachute was off to one side or the other by up to 10 degrees, rather than centered on the vehicle. The parachute was also much less stable than anticipated. Unsteadiness and off-center location of the parachute lead to increased pilot work load during landings since significant rudder input is required to overcome the lateral forces imposed by the parachute. To investigate the problem and search for solutions, a full-scale test of the Orbiter drag parachute was performed in the Ames 80- by 120-Foot Wind Tunnel.

A photograph of the parachute deployed in the wind tunnel is shown in the figure. The parachute (40 feet in diameter) was tethered to a single strut in the center of the test section in the wind tunnel. A production parachute was tested first to determine its stability characteristics. Two modifications to the parachute were tested in order to find a configuration that would provide sufficient drag with acceptable stability. The first modification was a reduction in the size of the parachute opening. This change increased the stability of the parachute but significantly reduced the drag it produced. The second approach was to increase the porosity of the parachute by removing strips of fabric from the canopy at a variety of locations. This proved to be the best solution because it increased the stability of the parachute without significantly reducing the drag.

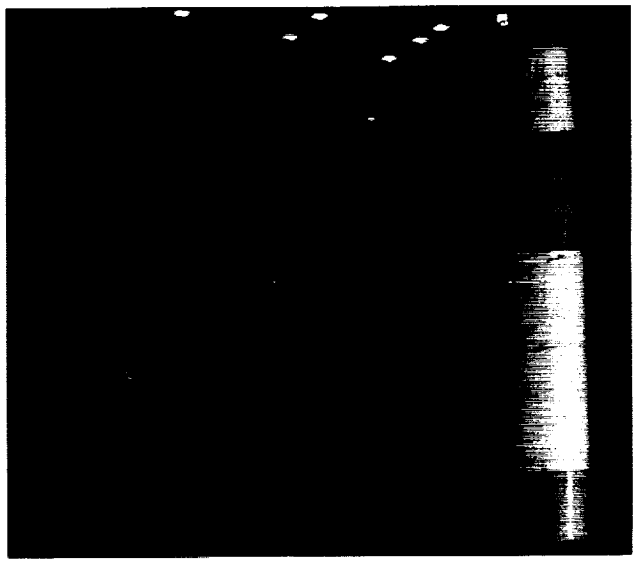

*Fig. 1. Shuttle Orbiter drag parachute in the Ames 80- by 120-Foot Wind Tunnel.*

The time period from initial discussions to completion of the wind tunnel tests was less than four months. The reconfigured parachute was used successfully in the last three Space Shuttle missions of 1993.

**Ames-Moffett contact: J. Ross**
**(415) 604-6722**
**Headquarters program office: OA**

# Evaluation of Wake-Vortex Hazard

**Vernon J. Rossow**

As a part of the Terminal Area Productivity Program at NASA, the wake-vortex research program at Ames Research Center is directed at determining the hazard posed by the wakes of subsonic transport aircraft on any following aircraft in the airport environment during landing and takeoff. A second purpose is to develop guidelines that permit the design of configurations which have wakes that dissipate more rapidly than current designs. The need to alleviate the wake-vortex hazard is necessary because the aircraft fleet of the future will probably include larger jets (on the order of 700 to 1,000 passengers). When these aircraft come into service, the disparity between the large and small commercial transport aircraft will accentuate the possible hazard posed by the wake of one aircraft on following aircraft.

To gain a better understanding of the wake-vortex structure of aircraft currently in the transport fleet and to provide data for the NASA/FAA Terminal Airport Capacity Program, a test in the Ames 80- by 120-Foot Wind Tunnel is being carried out to evaluate the hazard posed by one aircraft on following aircraft. A photograph of the experimental setup is presented in the figure. A model of a transport aircraft is mounted near the upstream portion of the test section to generate a vortex wake. A wing with a planform and shape typical of following aircraft is mounted on a traverse mechanism at the downstream end of the test section. In order to determine results that are indicative of the encounter of an aircraft with a vortex wake, the rolling moment and lift induced by the vortex wake on the downstream model are measured throughout the wake. Since the wind tunnel is large, measurements can be made at distances as large as 30 spans (a scale distance of one mile) behind the wake-generating model. The data provides an evaluation of the hazard posed by various aircraft in the present subsonic transport fleet, and it provides data that can be used to evaluate various theories for the modeling of vortex wakes and for the prediction of wake-induced loads. Future wind tunnel tests are being planned to increase the subsonic transport wake characteristics data bank and to develop design technology for lifting systems that produce less hazardous wakes during landing and takeoff.

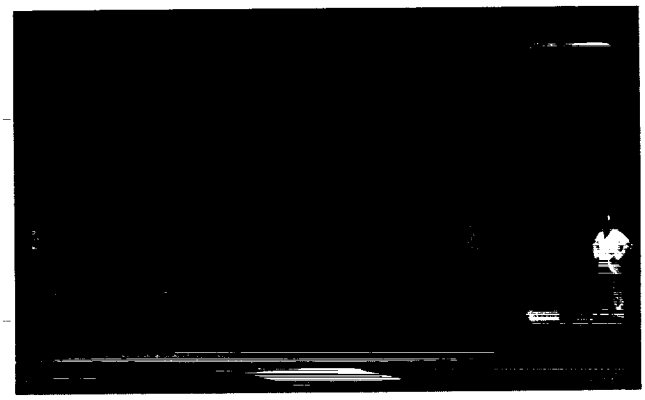

*Fig. 1. Wake-vortex test setup in the Ames 80- by 120-Foot Wind Tunnel.*

**Ames-Moffett contact: V. Rossow**
**(415) 604-4570**
**Headquarters program office: OA**

# Four-Bladed Rotor Research

**Patrick Shinoda**

The Rotorcraft Aeromechanics Branch at Ames Research Center conducted a rotor test in the Ames 80- by 120-Foot Wind Tunnel with a newly acquired Sikorsky S-76 rotor hub/blades system mounted on the recently modified Rotor Test Apparatus in early 1992. This wind tunnel test generated a unique and extensive data base covering a wide range of rotor-shaft angles-of-attack and thrust conditions from 0 to 100 knots. Two research papers have been generated from this test and were presented at conferences in 1993.

In the first paper, "Performance Results from a Test of an S-76 Rotor in the NASA Ames 80- by 120-Foot Wind Tunnel," presented at the AIAA Applied Aerodynamics Conference in August 1993, hover rotor-performance data were compared with calculations based on momentum theory and previously acquired data from other test facilities to evaluate the capabilities of this wind tunnel as a hover facility. Forward-flight rotor-performance data were compared with the calculations from a comprehensive rotorcraft analysis, CAMRAD/JA, to evaluate the analytical modeling in the 0–100 knots speed range. Rotor performance data were also compared with previously acquired S-76 full-scale data from a test in the Ames 40- by 80-Foot Wind Tunnel to evaluate similarities and differences between the two facilities. Hover performance data show significant variations depending on the test configuration. Comparisons with theoretical predictions and other test data suggest that hover testing at an outdoor facility in absence of ground effect is required to make a final determination of the absolute accuracy of the hover data acquired in the 80- by 120-Foot Wind Tunnel. CAMRAD/JA calculations show good correlation with propulsive-force data and a consistent level of overestimation of rotor power throughout the thrust and rotor shaft angle-of-attack envelope for a velocity range of 40–100 knots; below 40 knots CAMRAD/JA power calculations diverge from the data. A comparison of the 80- by 120-Foot Wind Tunnel data with data from a previous 40- by 80-Foot Wind Tunnel test for 60–100 knots velocity range shows good correlation with rotor power and propulsive-force data, except at the higher rotor shaft angles where there are some differences in rotor power. Results from the two S-76 wind tunnel tests suggest that the wind tunnel wall corrections should not be used for rotors operating in a nominal thrust range with rotor diameters up to 55% of the wind tunnel test section width for advance ratio ≥0.150.

The first figure shows the correlation of S-76 rotor-performance data with CAMRAD/JA.

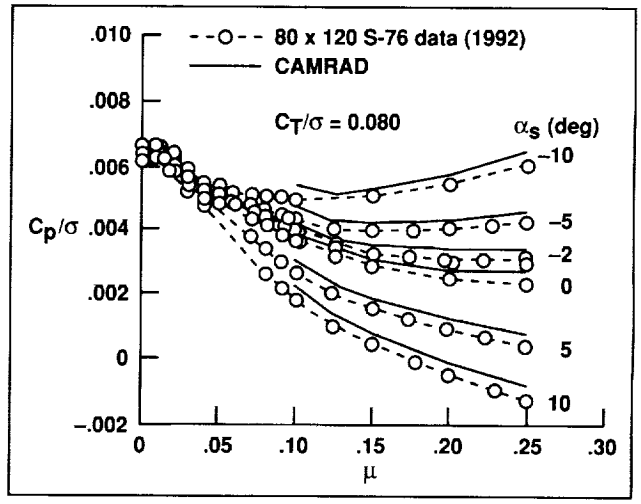


*Fig. 1. The effects of advance ratio and $\alpha_s$ on measured and predicted rotor power; $C_T/\sigma = 0.080$, $M_{TIP} = 0.605$.*

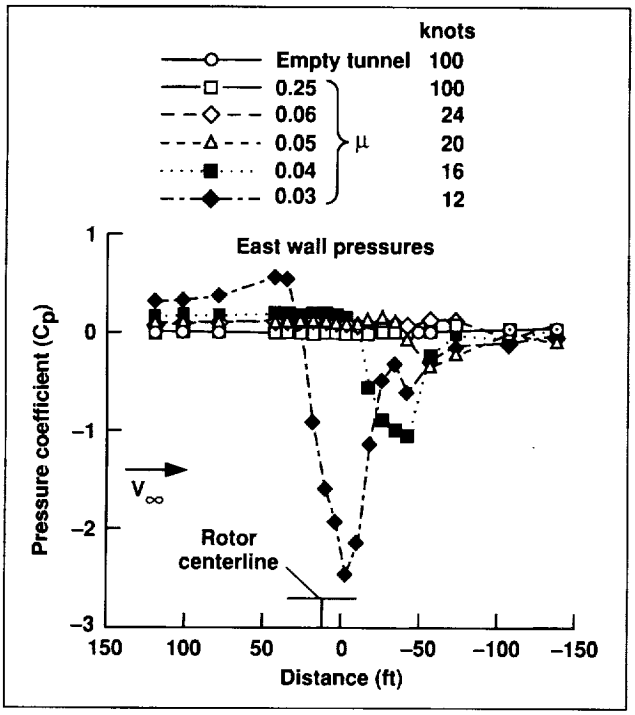


*Fig. 2. Effect of advance ratio (μ) on east tunnel wall pressures; $\alpha_s = -2$ degrees, $C_T/\sigma = 0.100$.*

In the second paper, "Wall Interaction Effects for a Full-Scale Helicopter Rotor in the NASA Ames 80- by 120-Foot Wind Tunnel," presented at the AGARD 73rd Fluid Dynamics Panel Meeting and Symposium in October 1993, three configurations were tested: empty tunnel, test stand body (fuselage) and support system, and fuselage and support system with rotor installed. Empty tunnel-wall pressure data were evaluated as a function of tunnel speed to understand the baseline characteristics. Aerodynamic interaction effects between the fuselage and the walls of the tunnel were investigated by comparing wall, ceiling, and floor pressures for various tunnel velocities and fuselage angles of attack. Aerodynamic interaction effects between the rotor and the walls of the tunnel are also investigated by comparing wall, ceiling, and floor pressures for various rotor shaft angles, rotor thrust conditions, and tunnel velocities. Empty tunnel wall pressure data show good repeatability and are not affected by tunnel speed. In addition, the tunnel wall-pressure profiles are not affected by the presence of the fuselage apart from a pressure shift. Results do indicate that the tunnel wall pressure profiles are affected by the presence of the rotor. Significant changes in the wall, ceiling, and floor pressure profiles occur with changing tunnel speeds for constant rotor-thrust and shaft-angle conditions. Significant changes were also observed when varying rotor thrust or rotor shaft angle of attack. Other results indicate that dynamic rotor loads and blade motion are influenced by the presence of the tunnel walls at very low tunnel velocity and, together with the wall-pressure data, provide a good indication of flow breakdown.

A sample of tunnel wall pressures with the rotor system and test stand present are shown in the second figure. The figure shows that the S-76 rotor system and test stand do have an effect on tunnel wall pressures, but only at very low tunnel speeds.

**Ames-Moffett contact: P. Shinoda**
**(415) 604-6732**
**Headquarters program office: OA**

# Small-Scale, Full-Scale, and In-Flight Measurements of Blade–Vortex Interaction Noise

**David Signor, Mike Watts**

Acoustic measurements of a Messerschmitt-Bolkow-Blohm BO-105 helicopter in flight were acquired using the Ames YO-3A research aircraft. The acquired in-flight acoustic data are being compared for the first time with similar data acquired in a full-scale test of a BO-105 rotor in the Ames 40- by 80-Foot Wind Tunnel and a small-scale BO-105 rotor test in the Deutsch–Niederlandischer Windkanal (DNW).

The acoustic source of interest is blade–vortex interaction (BVI) noise. BVI is typically generated while a helicopter is descending, as during the approach-to-land maneuver. Community acceptance of helicopters continues to be hindered by the impulsive nature of BVI noise generated during approach to landing.

Acoustic data acquired in wind tunnels has been extensively used for code correlation and validation. The primary advantages of testing in a wind tunnel are (1) the ability to accurately control steady operating conditions and (2) reduced cost compared to flight testing. A primary disadvantage is that the walls of the test section may prohibit the flow from behaving as it would if the walls were not there, thus contaminating the acoustic data with reflections. Anechoic wind tunnels that reduce the reflections from the walls have been built (i.e., the DNW). However, even in the open jet configuration the flow is not exactly what would occur in "free air," as evidenced by the need for a "wall correction."

The wall correction involves an arithmetic correction to the rotor shaft angle, so that the corrected shaft angle is more nearly what would be measured in free air. The accuracy of the rotor shaft angle in the wind tunnel is critical because it is included in the calculation of the rotor-tip-path plane angle, which is one of the four primary parameters (advance ratio, thrust coefficient, and tip Mach number are the other three) that must be matched when comparing acoustic data.

Other differences between wind tunnel and flight measurements include the trim state of the rotor, the effect of the fuselage on the rotor wake, and the steadiness of conditions. These differences are

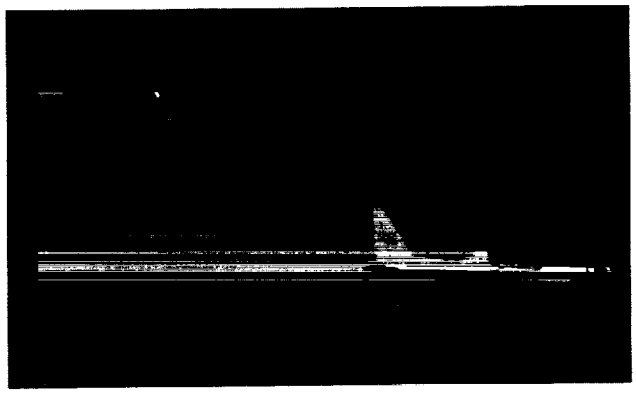

*Fig. 1. BO-105 and YO-3A formation side view.*

significant, and should be considered when comparing flight and wind tunnel data.

Rotors operated in wind tunnels are typically trimmed to minimize the first harmonic of longitudinal and lateral flapping. Rotors operated in flight are trimmed to minimize the moments applied to the hub. This difference can be significant for the BO-105 because the large hinge offset allows large hub moments to occur. Trimming wind tunnel rotors as is done in flight would make the acoustic measurements more meaningful.

Rotor–body interactions may be significant, but they are often ignored. The fuselage that supports the rotor in a wind tunnel is typically designed to be aerodynamic. The wind tunnel fuselage, however, is typically not representative of the actual helicopter fuselage. Rotor–body interactions may affect the wake, causing the blade–vortex miss distances to be different from flight to wind tunnel. Such an effort is expensive, but would generate acoustic fields more representative of actual helicopters.

Flight tests are conducted under the steadiest conditions possible to approximate how rotors are "flown" in the wind tunnel. The pilots are asked not to touch the flight controls during the 30-second data record. This is an unrealistic flight condition and the pilots do make small control inputs during the

30-second data record. Helicopter pilots continually adjust collective and cyclic settings on approach to landing, which changes blade pitch and revolutions per minute. These adjustments introduce large variations in measured noise levels. For comparison, wind tunnel acoustic data acquired while the cyclic and collective controls are varied slightly would be more representative of flight acoustic measurements.

This effort is part of the In-Flight Rotorcraft Acoustics Program established at Ames Research Center. The objectives of the program are to (1) use the capabilities of the YO-3A to measure noise from helicopters and make comparisons with similar wind tunnel measurements, (2) use these comparisons to better understand BVI, and (3) determine how to minimize helicopter BVI.

**Ames-Moffett contact: D. Signor**
**(415) 604-4562**
**Headquarters program office: OA**

## Quiet Microphone for Measurements in Wind Tunnels

**Paul T. Soderman, Christopher S. Allen**

There is a continuing need for aircraft noise reductions to protect airport communities and to comply with current and anticipated airport noise regulations. Consequently, the aeroacoustic study of powered and unpowered aircraft models in wind tunnels has developed into a widespread research tool. As reductions in aircraft noise have progressed, reductions in wind tunnel background noise have been required. Methods to maintain adequate signal-to-noise ratio have proceeded both through facility improvements and improvements in experimental methods. Progress has been made in reducing one important type of background noise—self noise from inflow microphones.

The flow-induced tone eliminator (FITE), shown in the figure, is a new aerodynamic forebody. FITE was designed to minimize flow-induced microphone noise. It was tested in the National Full-Scale Aerodynamics Complex at Ames Research Center, along with the industry standard commercial forebody. Both aerodynamic devices were used to protect identical condenser microphones from wind. The in-flow noise is generated in order of importance by (1) cavity resonances, (2) on-set turbulence, and (3) boundary-layer fluctuations. The flow-induced cavity resonances are tonal and can be very strong. Because the condenser microphones have fairly small cavities near the diaphragm, the resonance tones occur at high frequencies.

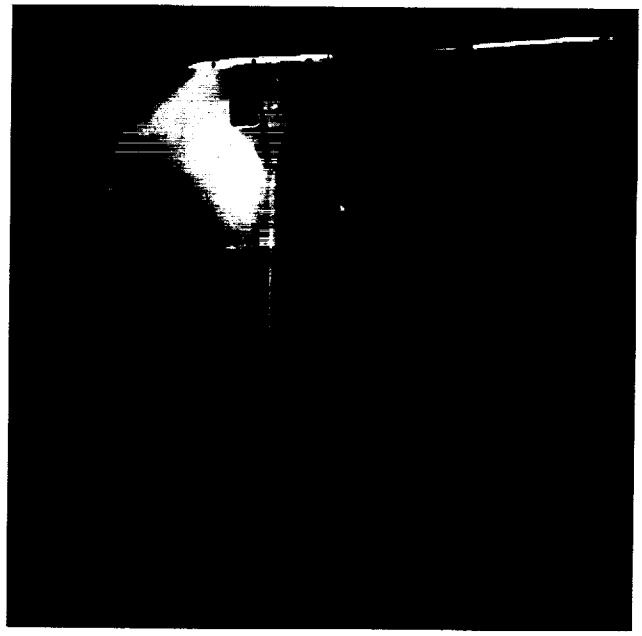

*Fig. 1. FITE forebody and microphone mounted on a wind tunnel strut.*

Results of the analytical and experimental studies showed that the FITE forebody eliminated flow-induced tones produced by the standard forebody installed on the 1/4-inch and 1/2-inch microphones. The tones were up to 40 decibels higher than the broad-band-flow noise. In some cases, the FITE forebody broad-band-flow noise was reduced 2–3 decibels. Directivity pattern and frequency response difference between the two designs were minor.

**Ames-Moffett contact: P. Soderman**
**(415) 604-6675**
**Headquarters program office: OA**

# A Unified Approach for Rotorcraft Aerodynamics

**Paul M. Stremel**

The modeling of rotor flow fields remains a difficult problem. While great strides have been made recently, the ability to efficiently and accurately model the flow field surrounding rotorcraft is lacking. The problem stems from the vortex wake shed from the rotor blades, the convection and diffusion of this vortex wake, and the eventual interaction of the vortex wake with other vehicle components (i.e., rotor blades and fuselage components). An accurate and efficient method to model the rotor wake is required.

Typically, the rotor wake has been modeled by Lagrangian or Eulerian methods. In the Lagrangian method, the rotor wake is represented by vortex filaments that convect and interact through the mutual influence of the vortex wake considered. This method preserves the vortex wake, but is computationally expensive and does not provide an accurate representation of vortex interaction with solid surfaces. In the Eulerian method, the vortex wake is defined on a computational grid and is convected and diffused by the governing equations used to compute the flow. Higher-order computational methods and/or very fine grids are required to minimize the effect of numerical diffusion to preserve the vortex wake. Again, this becomes computationally prohibitive.

Research under development addresses the need for an efficient and accurate rotor-wake model. The new method, vortex confinement, provides a means to compute the development of a vortex wake by Eulerian methods with the elimination of numerical diffusion. Furthermore, no vortex markers are required in the solution, thus allowing the method to be directly coupled with a Navier–Stokes solution.

To demonstrate the method, the flow-field solution of a pitching NACA 0012 airfoil is computed. The computational grid consists of an inner and an outer grid. The inner grid extends 0.05 airfoil chord lengths normal to the airfoil surface and the outer grid extends from the inner grid to 5.0 airfoil chords from the airfoil surface. The flow is computed with and without vortex confinement. When considering the solution without vortex confinement, the solution is calculated by a Navier–Stokes method on the inner and outer grids. When vortex confinement is considered, the Navier–Stokes solution is applied only to the inner grid and the vortex confinement method is used to compute the flow field on the outer grid.

Comparison of the hysteresis loops for the two methods are shown in the first figure. Without vortex confinement, the lift coefficient, represented by "no confine" in the figure, reaches a value of approximately 2.0 and then starts to stall. With vortex confinement, before stall, the lift begins to rise much quicker than that for the "no confine" solution. This increase in lift just prior to stall has been observed experimentally and is the result of the leading-edge

vortex development. On the down stroke, the vortex confine solution demonstrates increased amplitude in the lift oscillations when compared to the "no confine" solution. This is because the vortex confinement method preserves the strength of the shed wake and eliminates numerical diffusion. Similar behavior is shown for the drag and pitching moment.

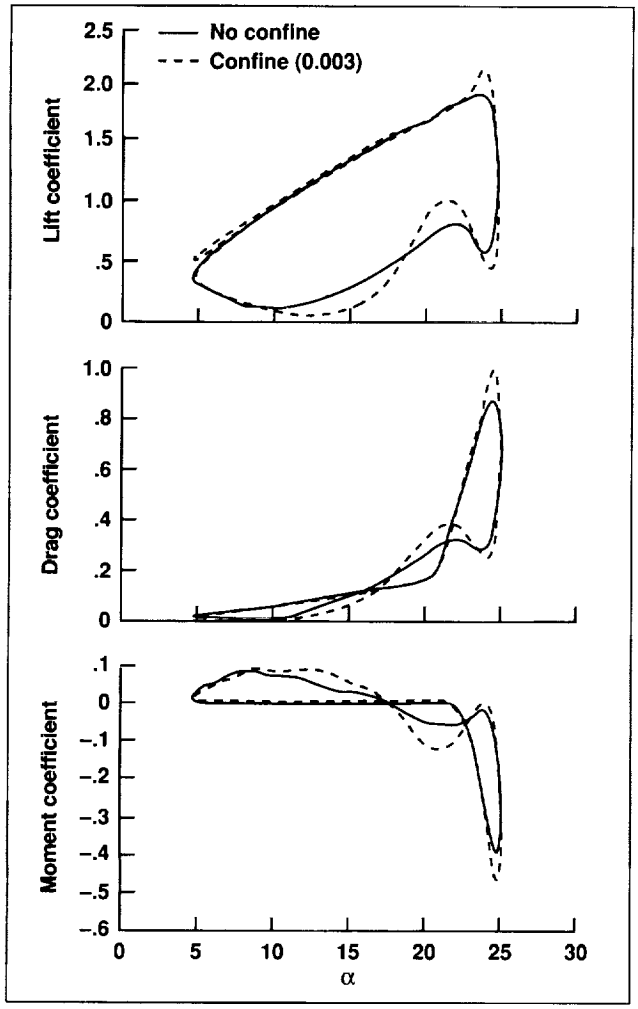


*Fig. 1. Hysteresis loops for a NACA 0012 airfoil, reduced frequency 0.15, Reynolds number 1 million, by Navier–Stokes ("no confine") and Navier–Stokes/vortex confinement ("confine") solution methods.*

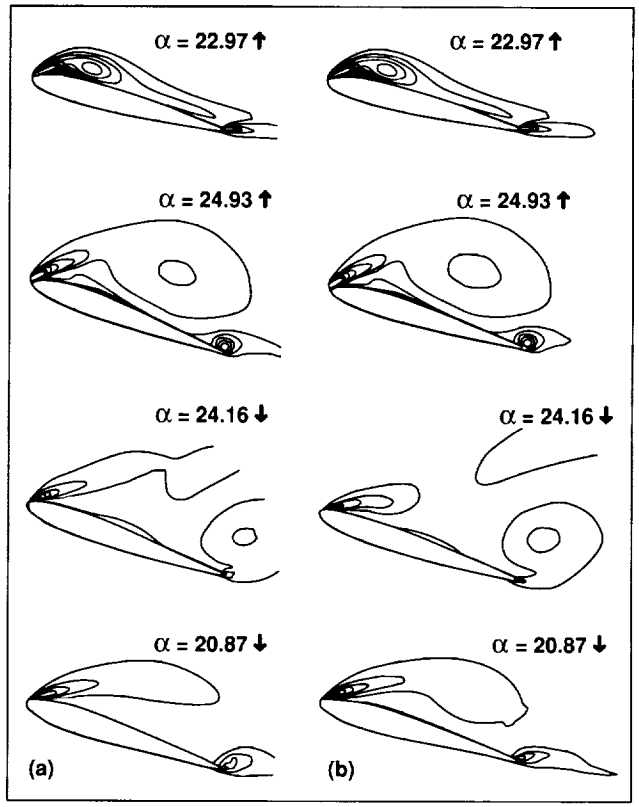


*Fig. 2. Computed equivorticity contours. (a) Navier–Stokes; (b) Navier–Stokes/vortex confinement.*

A comparison of equivorticity contours computed by the two methods is shown in the second figure. The vorticity contours shown are for the NACA 0012 airfoil near stall; therefore, they represent a vortex-dominated flow. The correlations of the vorticity contours are good and demonstrate the ability of the vortex-confinement method to compute vortex-dominated flow fields.

**Ames-Moffett contact: P. Stremel**
**(415) 604-4563**
**Headquarters program office: OA**

# Effect of a Lower-Surface Fence on Airfoil Download

**Paul M. Stremel**

The numerical prediction of download, the drag produced by rotorcraft during hover, is important in the design analysis of rotorcraft. Download limits helicopter performance in hover and is a significant problem in the design of tiltrotor configurations. For tiltrotor configurations in hover, the lifting wing is immersed in the rotor wake normal to the downwash and, therefore, incurs severe download penalties.

To understand the fluid mechanisms of download and to determine a means for its reduction, a method has been applied to the two-dimensional download problem. Plates or fences extending from the airfoil surface parallel to the free-stream flow were included to reduce bluff body drag. Fences extending from the airfoil surface into the wake represent an extension to the splitter plate technique. Splitter plates on cylinders and plates normal to the free-stream flow control the development of the separated vortices in the wake of the body. This effectively streamlines the body, resulting in reduced drag.

The flow about an XV-15 airfoil with a lower-surface fence at -90-degrees incidence was evaluated to determine the influence of a fence on the aerodynamics loading and pressure distribution. Sample results are shown in the figure. A single lower-surface fence is considered at a location of 15% airfoil chord aft of the leading edge and for heights of 15%, 25%, and 30% airfoil chord. The variation from the baseline pressure is shown in the figure, as well as the computed lift, drag, and moment coefficients. The drag is expressed as a ratio of the baseline drag. For a fence of 15% airfoil chord height, the drag is reduced by 11% with respect to the baseline value. The drag is reduced by only 9% when the fence height is increased to 25%, and is reduced by 16% for a fence height of 30% chord. The reduction in the download is directly attributed to the reduction in the suction pressure on the lower surface. However, the development of the leading-edge vortex and the interaction of this vortex with flow about the lower surface fence is quite complex. A study is being conducted to understand the optimum location for minimized download.

**Ames-Moffett contact: P. Stremel**
**(415) 604-4563**
**Headquarters program office: OA**

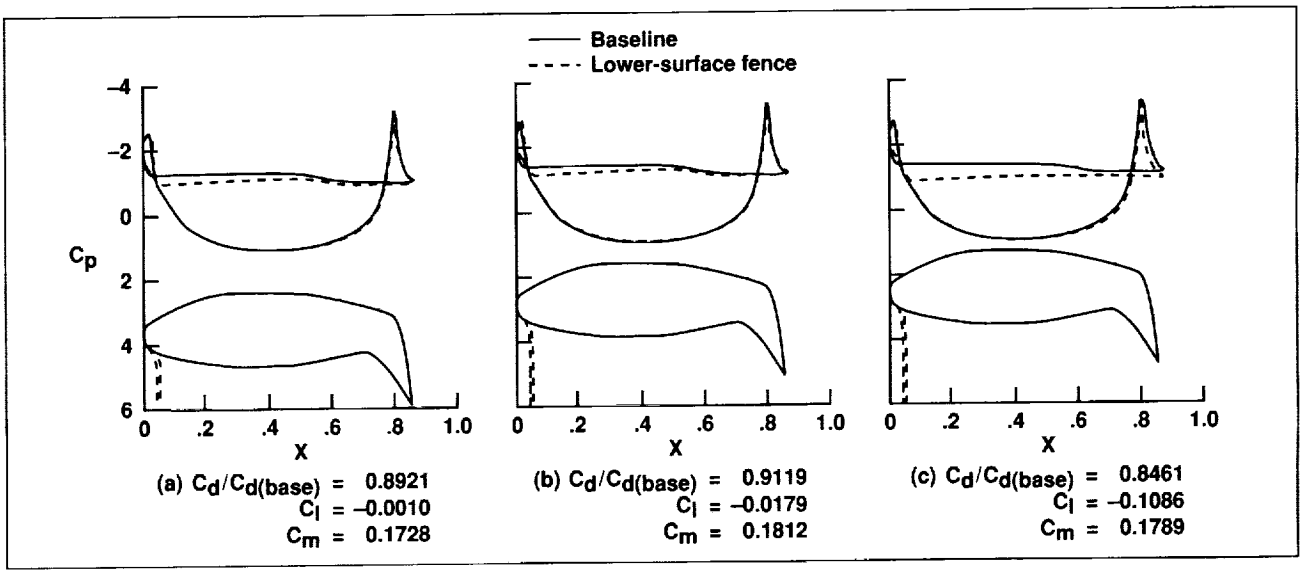


*Fig. 1. Comparison of predicted airfoil average surface pressure coefficients with and without a lower-surface fence, x = 15% chord. (a) h = 15% chord; (b) h = 25% chord; (c) h = 30% chord.*

# Large-Scale Rotor Flow Visualization

**Alexandra Swanson**

Shadowgraphs of blade–vortex interactions were successfully acquired as a preliminary step in supporting rotor aeroacoustics research. Nonuniform inflow free-wake predictions were used to help determine the rotor test conditions and rotor locations of possible blade–vortex interactions. Shadowgraph flow visualization images and acoustic noise measurements were acquired simultaneously. Flow visualization results and predictions show good azimuthal correlation with acoustic noise measurements.

Wake-geometry comparisons were also made between large- and small-scale rotor-flow visualization tests. Wake-geometry predictions and test results show good correlation between large- and small-scale S-76 rotor wake-geometry data in hover. In forward flight, however, these predictions diverge from experimental test data by half a rotor revolution (180 degrees rotor azimuth). This is illustrated in the first figure, for a thrust condition of $C_T/\sigma = 0.08$ at 60 knots, where tip vortex trajectories from the previous blade passages cross 90-degrees azimuth on the advancing side of the rotor disk. More flow visualization studies are required to better validate existing predictive tools.

Simultaneous acquisition of shadowgraph image pairs was demonstrated as a means for acquiring quantitative three-dimensional wake geometry. The second figure shows two simultaneously acquired shadowgraph images (side and top views). The distorted tip vortex is visible in both views. A vortex–vortex interaction is also visible in the side view where tip vortices appear to cross paths. After this interaction, the straight tip vortex becomes diffused and remains diffused. This type of information is needed to develop and validate mathematical wake models that accurately depict the structure of the shed-tip vortex as well as the structural changes the tip vortex encounters as a result of rotor blade and wake interactions.

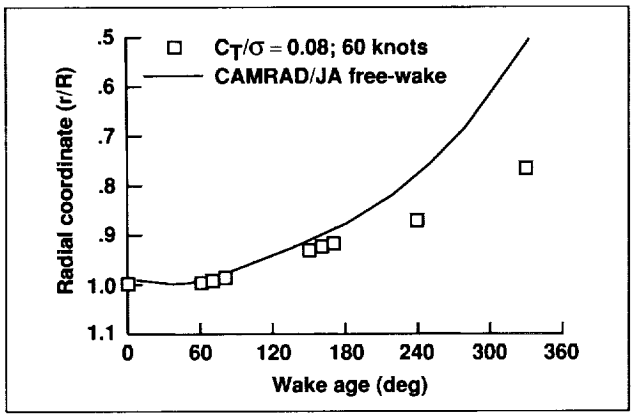


*Fig. 1. Correlation between wake geometry test data and predictions.*

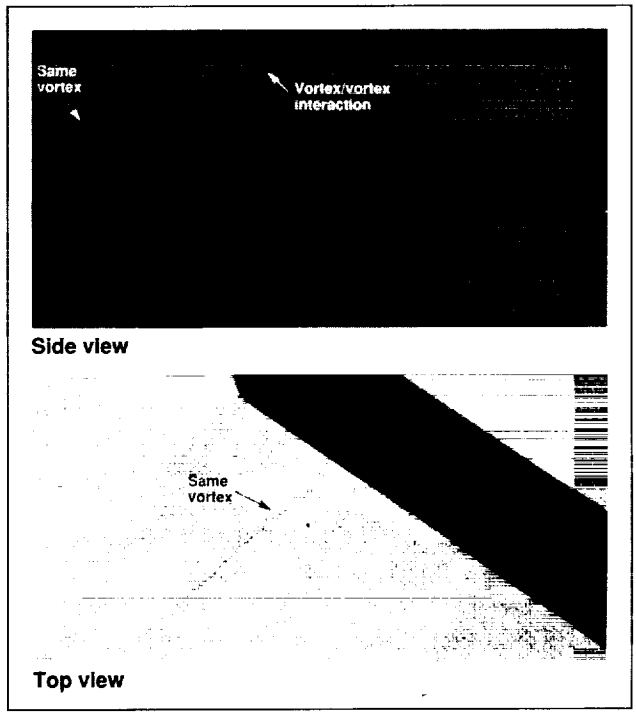


*Fig. 2. Shadowgraphs of tip vortex interactions. (a) Side view; (b) top view.*

**Ames-Moffett contact: A. Swanson**
**(415) 604-6856**
**Headquarters program office: OA**

# Steady/Dynamic Rotor Balance for the Ames Rotor Test Apparatus

**Johannes M. van Aken**

The Ames Rotor Test Apparatus (RTA) was recently modified to include a steady/dynamic rotor balance (S/DRB). The balance gage static load capacities are 22,000 pounds of thrust, 4,400 pounds of shear, and 680,000 inch-pounds of moment. The dynamic load capacities are 5,500 pounds of thrust, 1,100 pounds of shear, and 108,000 inch-pounds of moment. The balance shares a common centerline with the rotor shaft which has an in-line flex-coupling instrumented to measure rotor torque up to a maximum of 430,000 inch-pounds.

Previously the National Full-Scale Aerodynamics Complex (NFAC) wind tunnel scale system was used to measure steady rotor performance. These scale data are contaminated by the airloads on the model-support strut tips and the RTA fairing and require extensive tare runs to correct the scale data. The S/DRB provides a new way to measure rotor loads directly and accurately. The RTA and S/DRB were used to obtain rotor loads for the Sikorsky S-76 rotor, the Sikorsky Bearingless Main Rotor, and the Messerschmitt-Bolkow-Blohm B0-105 rotor in the NFAC 40- by 80-Foot and 80- by 120-Foot Wind Tunnels.

An extensive shake test/dynamic calibration was performed on the RTA S/DRB installation in the 40- by 80-Foot Wind Tunnel. Special shake test hardware allowed dynamic loading at the nominal rotor-hub height without and with shaft rotation. The hardware also allowed steady thrust preload under dynamic-hub shear loading. The shake test hardware-hub mass was varied to represent a nominal rotor system weight with and without the blade mass. Frequency response functions of the S/DRB under various dynamic hub loads were measured and used to determine the S/DRB dynamic calibration matrix at the rotor harmonics up to 60 hertz.

A hub-imbalance test was performed to assess the accuracy of the S/DRB dynamic data reduction. An imbalance mass was located at a radial location and balance data was acquired for rotor revolutions per minute from 2 to 7 hertz. Use of the dynamic calibration matrix showed a marked improvement for the 1-per-rev hub imbalance load prediction compared to the load prediction using the S/DRB static calibration matrix. Work continues on documenting the effects of hub mass, thrust preload, and shaft rotation.

**Ames-Moffett contact: J. van Aken**
**(415) 604-6668**
**Headquarters program office: OA**

# Measurement of Vortex Strength and Core Diameter for a Model Tiltrotor

Alan J. Wadcock, Alexandra Swanson

Vortex strength and core size are equally important in determining the induced velocity field associated with the tip vortices in a rotor wake. It is generally accepted that the most important part of a rotor performance prediction code is the rotor-wake model, especially in the presence of blade–vortex interaction. Unfortunately, there is limited reliable information available on either tip vortex strength or core size and their variation with wake age. If such information were available it could provide valuable guidance for the development of rotor-wake modeling codes.

Additional motivation for the present measurements comes from the increasing use of the shadowgraph technique applied to rotor flow fields. Initially, this technique was used simply to identify the vortex path in space. Recently, attempts were made to infer vortex core size from shadowgraph images. Presently, work is aimed at validating shadowgraph core size estimates by comparing them with direct measurements of core size using hot wire anemometry. The hot wire data were taken in the wake of a model tiltrotor in hover. The first figure shows a typical hot-wire time history corresponding to a high-thrust condition. Simultaneous shadowgraph images are shown in the second figure.

*Fig. 2. Shadowgraph image showing tip vortex and hot-wire probe.*

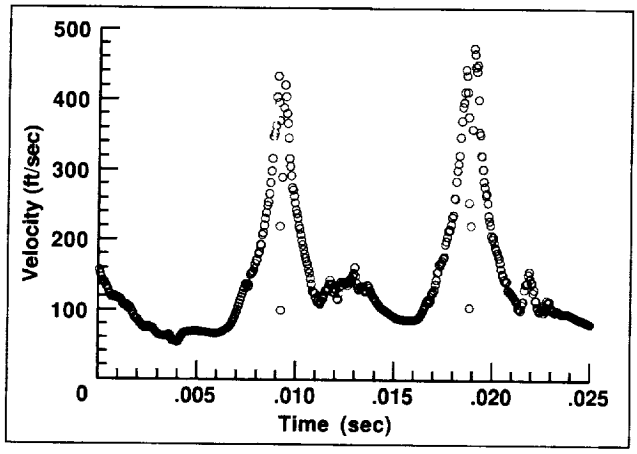


*Fig. 1. Typical hot-wire time history.*

**Ames-Moffett contact: A. Wadcock**
**(415) 604-4573**
**Headquarters program office: OA**

# Rotor/Wing Interactions of Tiltrotor Aircraft

**Larry Young**

Improved prediction of hover rotor/wing interactional aerodynamics to maximize aircraft performance and to minimize noise is critical to the success of tiltrotor aircraft. A first-order analysis has been developed that accurately models the hover rotor-on-rotor and wing-on-rotor interactions of tiltrotor aircraft. The analysis is only valid for hover out of ground effect. An important result of the analysis is that the well-known tiltrotor "fountain effect" comprises two distinct flow phenomena—the importance of a far-wake rotor-on-rotor skew angle effect not previously noted has been accounted for. Also, an initial assessment of the influence of rotor/wing offset distance, wing sweep, and wing span on rotor inflow and performance has been performed. The results of that parametric study demonstrate the considerable influence of wing span on rotor mean inflow and induced power.

**Ames-Moffett contact: L. Young**
**(415) 604-4022**
**Headquarters program office: OA**

# Optical Control of Space Structures

**Maria Bualat, Charles Gary, Meriç Özcan**

In the Optical Control of Space Structures development program, the Ames Photonics Group is applying research in fiber-optic sensors and high-speed optical matrix processing to provide real-time measurement and control which will allow the damping of structural vibrations on space-based platforms.

The use of optics to calculate matrix feedback for the control of truss structures is being studied. Results of this research will be applied to the stabilization of space-based instrumentation platforms such as Space Station Freedom and the Earth Observing System (EOS). For instance, EOS platform vibrations need to be damped at approximately 1,000 hertz so that sensitive scientific instruments can be operated on the platform undisturbed by each other. Optical processing offers greater performance at lower power, mass, and volume than conventional computers for the computation of matrix feedback, increasing the accuracy and resolution of space-based instrumentation.

Optical matrix vector multipliers provide a nearly instantaneous mechanism to compute feedback control signals. Sensor values are fed to the optical processor, and the control algorithm is implemented by the vector-matrix multiplication. The control signals output by the optical processor are converted to electrical signals used to drive the actuators of the plant.

In addition to faster implementation of control algorithms, methods of measuring the vibrational mode amplitudes of a structure are required that are superior to conventional accelerometers. We are investigating distributed fiber-optic sensors for measuring these mode amplitudes directly. The perturbation of light signals in fibers attached to the structure are measured interferometrically, providing enhanced accuracy over conventional sensors; the flexible shape of the fiber sensors allows them to be configured to measure the desired parameters directly.

Currently, a testbed for the prototyping of optical matrix vector processors has been constructed. Work is proceeding in cooperation with NASA Langley Research Center's Control/Structures Interaction (CSI) Laboratory to develop an optical processor for use on platform control testbeds. A ten-bay truss structure identical to that used at the Langley CSI Lab has been installed in order to develop and demonstrate both fiber-optic sensors and the optical-matrix-processor-based control system.

**Ames-Moffett contact: M. Bualat**
**(415) 604-4250**
**Headquarters program office: OA**

# Fiber-Optic Acoustic Sensors for Wind Tunnel Applications

**Young YC Cho, Max B. Reid, Anna H. Pryor**

Acoustic measurements in wind tunnels are subject to certain interference effects that are not found in anechoic chambers. Such effects include wind noise, flow–sensor interaction noise, flow-induced sensor vibration, and deflection of acoustic waves by sensor-induced boundary layers. Furthermore, it is often desirable to investigate specific source regions on the models being studied. Currently existing acoustic sensor techniques are not adequate to cope with these problems.

NASA Ames Research Center has a program to develop new advanced acoustic sensors to eliminate or minimize interference restrictions. The program employs concepts of adaptive arrays with fiber-optic interferometric sensor elements. An adaptive array is a system composed of a number of geometrically configured sensor elements and a real-time signal processor. The signal processing is designed to adjust array sensitivity for enhancing the directivity and the spectral response of acoustic signals. It also provides the real-time manipulation of correlations of signals detected by various sensor elements, which is ultimately used for discrimination of random noise or locally generated pressure fluctuations on individual sensor elements.

The technology of fiber-optic interferometric sensors has matured in underwater acoustics for hydrophone development and is here adapted to aeroacoustics, but with new sensor head designs. This technology utilizes the fact that the light propagating through the optical fiber undergoes phase modulation when the fiber is exposed to external fields. This phase modulation is interferometrically retrieved and processed to determine the external fields. Fiber-optic sensors offer a number of advantages: high sensitivity, wide dynamic range, compact sensor package, light weight, geometric versatility, telemetry capability, and immunity to electrical interference.

NASA's first fiber-optic microphone was developed and fabricated in a breadboard form. A schematic drawing is shown in the figure. This sensor consists of three main components: a laser with an acousto-optic modulator, fiber-optic sensor heads, and an optical detector with signal processors. The components are integrated via optical fibers as

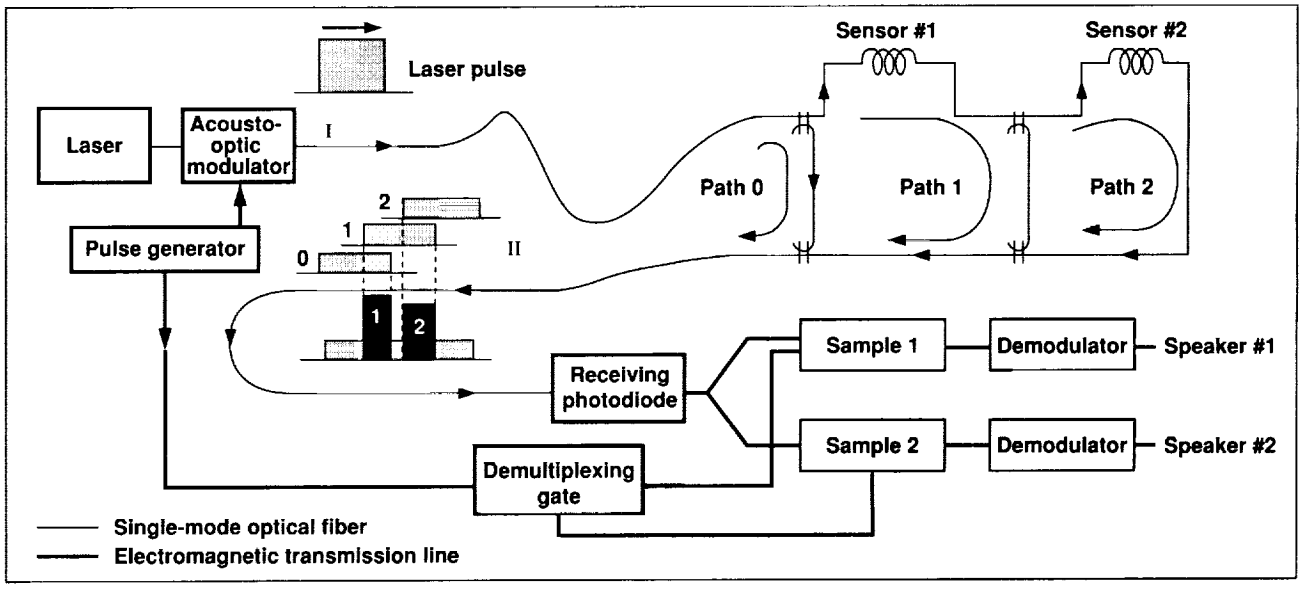


*Fig. 1. Schematic of fiber-optic acoustic sensor.*

transmission lines. The sensor is multiplexed with two sensor heads, each made of single-mode fiber wrapped around a circular cylinder of styrofoam or a torpedo-shaped aluminum body. Extensive laboratory tests are in progress for evaluation of the sensor's acoustic characteristics including acoustic sensitivity, dynamic range, and frequency response. Preliminary test results demonstrated its usefulness for aero-acoustic measurements.

**Ames-Moffett contact: Y. Cho**
**(415) 604-4139**
**Headquarters program office: OA**

## Principal Investigator in a Box

**Silvano Colombano, Michael Compton, Richard Frainier, Nicolas Groleau**

The Principal-Investigator-in-a-Box provides astronaut experimenters in space with an "intelligent assistant" that encapsulates much of the domain- and experiment-related knowledge mastered by the principal investigator (PI) on the ground. Expert-systems technology and flight-qualified personal computers are used to encode the requisite knowledge and make it available to the astronauts. The PI-in-a-Box system performs four major functions: diagnosis and troubleshooting of experiment apparatus, data collection and quality monitoring, detection of important data, and protocol management.

The system software is based on three separate languages: LabVIEW, an icon-based language developed by National Instruments for data acquisition and analysis; CLIPS, a knowledge-based system shell built by NASA; and HyperCard, an interface language developed by Apple Computer. The system functions as a single integrated unit that uses HyperCard-based information displays.

The first experiment to include PI-in-a-Box automation measures human adaptation to weightlessness in the context of the neurovestibular system. This "Rotating Dome" experiment (devised by Laurence Young of MIT) flew with PI-in-a-Box on the SLS-2 Shuttle mission.

In 1993, the PI-in-a-Box team continued efforts started in 1992 to support system use on SLS-2. Support included conducting several astronaut training sessions at Johnson Space Center (JSC); delivery of three system software upgrades; operation of the system on the ground during four preflight and seven postflight scientific data-collection sessions; and ground-based support to the astronauts using the system in space during the two-week SLS-2 mission. Most significantly, PI-in-a-Box was used successfully inflight by four SLS-2 astronauts during their two-week mission. Finally, formal postflight evaluation of the system's performance has begun, and will be completed by 1994.

Follow-on activities include expanding the scope and sophistication of the system to allow increased use (with many experiments) during SLS-4, generalization of the system to new experimental domains, and commercialization of the system's architecture. The SLS-4 effort includes developing new experiments, selecting investigator partners from the list of successful respondents to the SLS-4 "Announcement of Opportunity," and working with hardware- and software-automation groups at JSC and Ames to ensure that the most advanced computing environment is available to the crew of the SLS-4 mission. Generalization to new domains is being pursued by responding to opportunities on U.S. and Russian missions and advanced-technology development for microgravity experiments. The team is currently awaiting results of two proposals for work in these areas. Commercialization or technology transfer is being actively pursued with several companies that have expressed interest as a result of the team's presentation at the July 1993 conference on Innovative Applications of Artificial Intelligence. The team also intends to work closely with the newly formed Commercialization Center at Ames to define and refine the intelligent box concept for industrial use.

**Ames-Moffett contact: S. Colombano**
**(415) 604-4380**
**Headquarters program office: OA**

# Cockpit Studies for Propulsion-Controlled Aircraft

**Joseph L. Conley, Frank W. Burcham**

Research is under way at Ames to develop and test strategies for controlling disabled, multiengine aircraft using only the propulsion system for control. The Propulsion-Controlled Aircraft (PCA) concept, pioneered at the Ames-Dryden Flight Research Facility, consists of a feedback control system commanding symmetric and asymmetric throttle commands that allow a pilot to control the flightpath of an aircraft in the event that the conventional control system is inoperable. The study was motivated by several recent catastrophic accidents involving civil transport aircraft that were caused by total hydraulic failure and the subsequent loss of conventional control (e.g., United Airlines Flight #232 (a DC-10) at Sioux City, Iowa).

A series of experiments investigating PCA cockpit implementation issues are being conducted at the Man–Vehicle Systems Research Facility (MVSRF) in the Human Factors Division at Ames as part of the overall PCA program run by Dryden. The objective of these studies is to determine the best cockpit configuration and implementation strategy for the PCA concept using a generic, twin-jet transport configuration in the six-degree-of-freedom, full-motion Advanced Cab simulator. One study demonstrated that the vertical-speed wheel and heading-select knob from the mode-control panel offered performance superior to that of a sidestick controller in the PCA mode for approach and landing. A second study scheduled for February 1994 will determine which lateral-directional control system command provides better performance in the PCA mode for approach and landing—bank-angle command or heading command. Future plans include more studies in the following areas: autoland systems, engine-out scenarios, and coping with asymmetrically frozen surfaces. In addition, a demonstration of a prototype commercial transport PCA system using the MVSRF's 747-400 level-D-certified simulator is planned for 1995.

Previous studies conducted by the Propulsion and Performance Branch at Dryden have used B-720 and F-15 simulators and various multiengine aircraft to demonstrate sufficient control authority to safely fly and land multiengine aircraft in the PCA control mode. Dryden is also working with McDonnell Douglas on testing PCA systems on MD-11 simulators. Currently, Dryden is conducting a flight test program using an F-15 aircraft to demonstrate the PCA mode for multiengine fighters, and has had excellent results.

This research is intended to develop backup control systems that enable pilots to save lives in the event of a complete failure of an aircraft's conventional flight control system. In addition, PCA concepts may allow airframe manufacturers to eliminate costly and heavy backup systems in the design of future aircraft.

**Ames-Moffett contact: J. Conley**
**(415) 604-5887**
**Headquarters program office: OA**

# Space Shuttle Ground Processing Scheduling

**Ellen Drascher, Michael Hall**

The Space Shuttle Ground Processing Scheduling project is deploying a constraint-based scheduling system at the Kennedy Space Center (KSC). The goal of the project is to assist KSC management in streamlining Shuttle processing. The KSC flow-management team has the responsibility of preparing the Space Shuttle for flight after the orbiter arrives at the KSC Orbiter Processing Facility (OPF). Upon arrival, each orbiter subsystem is inspected, repaired, and tested. The processing within the OPF consists of a set of dynamic and complex activities coordinated by the management team. Execution of a ground processing schedule is plagued by the uncertainty inherent in most complex operations environments. The Ground Processing Scheduling System (GPSS) develops schedules with respect to temporal, resource, and state constraints. The attributes of the "environment" that change over time are represented as state information. This includes the configuration of the orbiter as well as the spatial zones within the OPF. Orbiter configuration includes the positions of the landing gear, payload bay doors, elevons, and rudder speed brake, and the status of the orbiter power and hydraulics systems. The GPSS uses constraint-based iterative repair as its search method. The approach begins with an initial, flawed schedule and then iteratively repairs constraint violations until a conflict-free schedule is produced.

In 1993, the GPSS was successfully deployed to schedule the ground operations of the orbiters Columbia, Endeavour, and Discovery. The Atlantis orbiter is out of service for maintenance and major modifications. During the STS-50 repair cycle of Columbia a number of statistics were kept about the scheduling and processing using the GPSS. These statistics were compared with estimates provided from previous missions, and the conclusion was reached that work was better coordinated with the changing orbiter configuration. The new system drastically reduced weekend overtime. New GPSS features include new decision-making aids, a new explanation facility, and a new schedule hierarchy mechanism. The decision-making aids allow users to "deconflict" their schedules in a more interactive manner. They can now "compress" tasks, reordering them as early as possible without causing conflicts. They can also selectively ignore some constraints and focus on others. The automated deconflict mechanism was also significantly improved in 1993. New heuristics were added that improve computational performance and resulting schedule quality. New deconflict interfaces were also provided.

The plans for the GPSS project are to complete the distributed GPSS system and to continue research on the automated optimization of shuttle ground processing. Multiple orbiter schedules are necessary because of critical resources that are shared among orbiters.

**Ames-Moffett contact: E. Drascher/M. Hall**
**(415) 604-4383/4867**
**Headquarters program office: OA**

# Galileo Image Evaluation Experiment

**Richard F. Haines, Terry L. Grant, Sherry L. Chuang**

The Spacecraft Data Systems Research Branch has been asked to collaborate with the Jet Propulsion Laboratory (JPL) by applying the branch's expertise in image and video quality assessment to an evaluation of compressed images of Jupiter and its major satellites. Although compression was not originally planned for images on the Galileo mission to Jupiter, the loss of the spacecraft's high rate telemetry has made compression a necessity in order to increase the number of images returned. The JPL has developed an Integer Cosine Transform (ICT) compression algorithm for potential application to the image telemetry collected from the Solid State Image (SSI) instrument on board the Galileo spacecraft. The primary questions are What is the acceptable image compression ratio using different quantization tables within the ICT algorithm, and Are important scientific features in an image retained after quantization in the ICT algorithm? The image assessment experiment included a controlled, subjective evaluation of the compressed images by the SSI research team members.

Informal queries to a few team members led to a pretest questionnaire which identified seven image classes that were of interest to them: satellites with and without limbs, satellites with a terminator, Jupiter with and without limb, small bodies, and rings. A program was developed to automate the controlled display of side-by-side images for their comparison at different quantization levels and then to record the selection made. Then, as part of a one-day workshop at Ames Research Center, a total of 15 observers from 11 institutions participated in the image assessment experiment. The Pair Comparisons methodology was employed to evaluate the acceptability of images while varying the quantization tables and quantization levels. The figure shows one side-by-side comparison from the series of image pairs which were presented on workstation monitors to the observers.

The experiment was successful in identifying a degree of acceptance for image compression and in identifying preferred quantization tables for the ICT compression algorithm. It also helped the research team to identify the limits of image compression and the need for a more sophisticated image processing methodology for the Galileo project. A range of compression ratios were found to be acceptable,

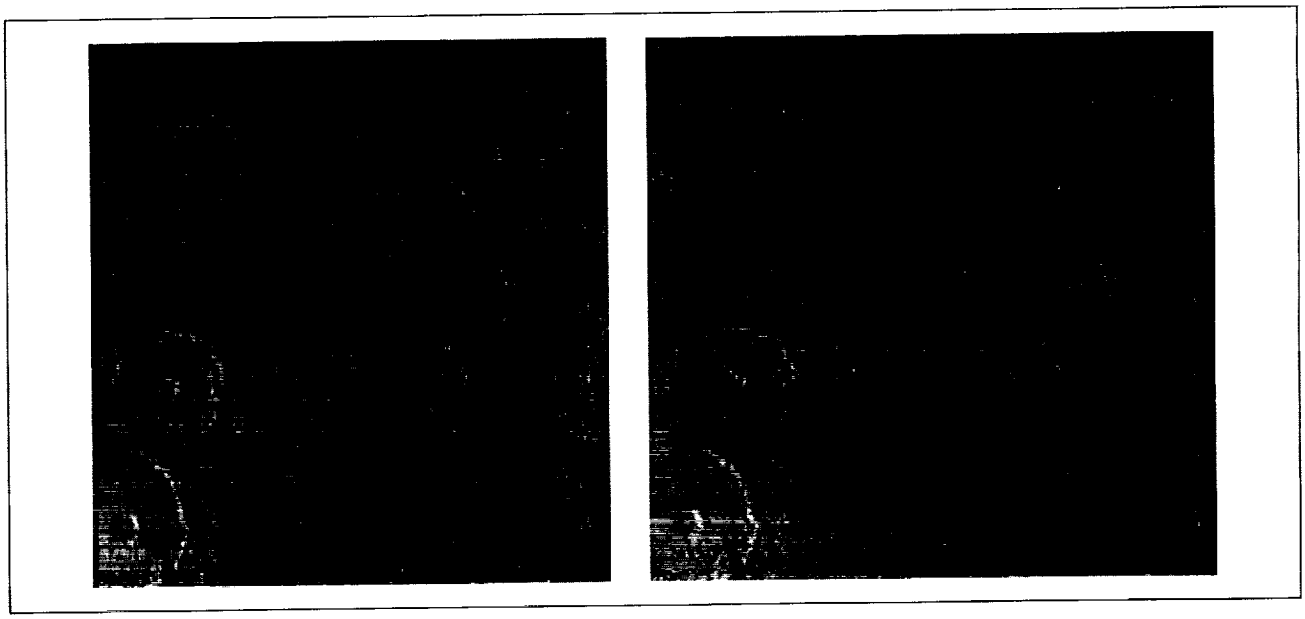

*Fig. 1. Galileo image evaluation. Ganymede image: (a) highly compressed; (b) original version.*

depending on the image class and quantization table used. For example, for Jupiter images, compression ratios of 36:1 to 55:1 were judged visually acceptable. For noisy satellite images, the acceptable compression ratio was only 4:1 to 6:1 under the best conditions. The results are detailed in a final report which has been distributed to JPL and the research team.

**Ames-Moffett contact: T. Grant/R. Haines**
**(415) 604-4200/3373**
**Headquarters program office: OSSA**

## Antarctic Telepresence Remotely Operated Vehicle (TROV)

**Butler Hine, Carol Stoker**

The objective of this project is to determine if telepresence (the projection of the human sensory apparatus into a remote location) and/or virtual environments (highly interactive computer-generated graphics) is a viable approach to scientific operations for planetary exploration.

For many years, scientists have investigated life beneath the permanently ice-covered lakes and dry valleys in Antarctica. This environment is the closest we have on Earth to the conditions that are assumed to have once existed on Mars. Antarctic lakes are explored by divers in dry suits who enter through a hole cut in the ice. There are severe limitations on the length of time and distance a diver can cover in this extreme environment.

Recently, research teams from the Center for Mars Exploration at Ames have begun using remotely operated vehicles (ROVs) to augment these explorations. We are interested in providing advanced teleoperations techniques for the scientists, enabling them to explore the region as if they were diving. Although we are testing the technology on Earth, the ultimate goal is to demonstrate techniques that will be used during the human exploration of Mars.

On 1 December 1992, Ames conducted a live televised news conference with scientists in the Antarctic. The video and data links were put in place during one of the telepresence ROV (TROV) tests, and demonstrated the first long-distance use of telepresence between the U.S. and the Antarctic. Operators at Ames, wearing a helmet-mounted head-tracking display device, remotely controlled a camera platform on an ROV under the ice. The control station is shown in the figure.

*Fig. 1. Teleoperation control station.*

During October and November, 1993, we remotely operated a highly modified version of the TROV vehicle in the McMurdo region from various control consoles at Ames, using advanced telepresence and virtual-environment interfaces. The purpose of the mission was a benthic ecology survey with sample collection. In this experiment, we had full control of all of the vehicle functions from Ames, with trained scientists at the controls.

**Ames-Moffett contact: B. Hine**
**(415) 604-4379**
**Headquarters program office: OSSA/OA**

# Human Exploration Demonstration Project (HEDP)

David J. Korsmeyer, Edward S. Chevers

The Human Exploration Demonstration Project (HEDP) is a multidivision effort that addresses the advanced technology requirements for a planetary surface habitat for humans. The HEDP project began in the fall of 1991 and will conclude in the summer of 1994. The goal was to integrate the specific Ames technologies under development by the Information Sciences Division, the Aerospace Human Factors Division, the Life Science Division, and the Advanced Life Support Division. All of these technologies are necessary to implement an integrated working and living environment.

Four basic goals for the HEDP have been established:

1. Enhance the technology development and evaluation process through synergistic cooperation of multiple Ames divisions.
2. Provide a simulator for evaluation of technology in an integrated system setting.
3. Create a realistic environment for introduction of new technology.
4. Identify promising technology concepts to other Centers for new and existing NASA projects.

The project has developed an integrated demonstration environment which consists of a habitat structure and a life-support-system testbed, a human-powered centrifuge and physiological monitoring system for the crew, a virtual-environment workstation for robotic operations, and centralized data-acquisition and habitat systems health monitoring. There are several robotic systems external to the habitat which are performing activities to provide representative work loads for the crew.

The figure shows the basic components of the HEDP. The HEDP system consists of a working environment contained in a living environment. The living environment consists of the Controlled Environment Research Chamber (CERC) which houses the human-powered centrifuge on its lower floor and the life-support-system testbed. The working environment is made up of the advanced workstations on the upper floor of the CERC which will control and remotely operate systems on the simulated planetary landscape. Use of these devices is not for development

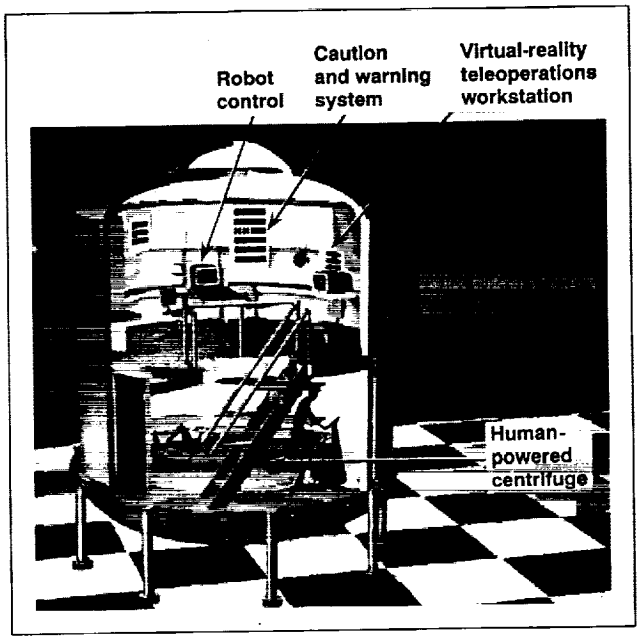


*Fig. 1. Components of the HEDP.*

of robots per se, but to create realistic operational scenarios equivalent to those anticipated on the lunar surface and to develop the robotic controls systems and technologies that will be required. The two environments are coupled through an underlying data network that includes a common set of services and provides a medium for overall system integration. Many of these services utilize artificial intelligence technologies to maximize autonomy and minimize crew work loads.

The HEDP has finished the first two phases of development, and, in phase III, is integrating the component technologies from each division. Phase IV, the system integration and checkout phase, will begin in January 1994. Several demonstrations and an analysis of the completed project are planned to begin in April 1994.

**Ames-Moffett contact: D. Korsmeyer**
**(415) 604-3114**
**Funded by DDF**

# Real-Time Autonomous Machine Vision Control Problems

**Paul W. Ma, John D. Downie, Max B. Reid**

In order to increase the safety and capability of future missions, NASA will need autonomous systems to perform tasks that are either too dangerous or too expensive for humans to perform. Since vision processing is well known as the most computationally intensive aspect of autonomous systems, it can benefit greatly from novel optical processing architectures designed to accelerate these highly computational functions.

The Photonics Group at Ames is using a processing architecture that is based on the optical correlator. The Fourier transform properties of lenses are used along with spatial light modulator devices to correlate input scenes with optical filters especially designed to recognize and track target objects in the scenes. Because the optical computation is highly parallel, it is accomplished much faster than with comparably sized digital electronic systems.

Optical correlator development at Ames has been concentrated recently on the design of appropriate and useful filters. These include binary and ternary synthetic discriminant filters for implementation on the magneto-optic spatial light modulator that are tolerant to prespecified geometric distortions of the target image. Other studies resulted in design algorithms for optimal binary phase and amplitude filters, and ternary filters designed using a simulated annealing technique to minimize the probability of error in a two-class image set. Most recently, we have performed a theoretical analysis of the optimal filter designs for use with images corrupted by signal-dependent noise, such as speckle and film-grain noise.

To apply the correlator technology, an active control system is being built to control a simulated space robotic vehicle (SSRV). The SSRV will be used to address a type of control problem we refer to as station keeping. In a station-keeping control problem, a dynamic vehicle is kept stationary relative to a target regardless of the external forces. Examples for such applications are autonomous space-vehicle docking, autonomous on-orbit construction and maintenance, and undersea-vehicle control.

In a station-keeping function, the user selects the target that the SSRV will track from an input scene obtained from the camera. The information is then passed to an optical correlator, which will track the position of the SSRV relative to the selected target. As the SSRV starts to drift due to external forces, the position information from the optical correlator is used to fire the appropriate thrusters on board the SSRV so the vehicle will remain stationary with respect to the selected target.

Future work in real-time autonomous vision systems involves the implementation of control algorithms on a compact optical correlator. A consortium (OPTICOR) has recently been established with Litton Data Systems, Ford Motor Co., GM Delco, and several government and university laboratories to commercialize optical correlator technology.

**Ames-Moffett contact: P. Ma**
**(415) 604-3586**
**Headquarters program office: OA**

# Propulsion-Controlled Aircraft

**Robert W. Mah**

In the event that most or all of an aircraft's flight control system becomes inoperative, engine thrust may be used to provide sufficient control for safe landing. The Dryden Flight Research Facility is conducting a study of the propulsion control capabilities of airplanes ranging from high-performance fighters (F-15) to commercial jet transports (MD-11), and is investigating conventional methodologies for control of engine throttle. Piloted simulation results show that landings using manual-throttles-only control were extremely difficult, whereas the use of augmented feedback controllers provided major improvements in control capability and enabled safe landings to be made repeatably.

In support of Dryden, Ames-Moffett is investigating the use of nonconventional controllers for propulsion control, and is conducting propulsion control experiments in the Man–Vehicle System Research Facility using the high-fidelity commercial transport simulators (Advanced Cab, Boeing 747-400). The work being performed at Ames-Moffett complements and extends the work being pursued at Dryden. Nonconventional controllers based on advanced neural/fuzzy-logic techniques have the potential for providing improved performance compared to conventional controllers, and for providing effective control in situations in which an airplane may have sustained structural damage.

We are also working with the Aviation Safety Reporting System (in the Ames Aerospace Human Factors Research Division) to investigate incidents of flight control failures in order to better understand the failure modes and the frequency of occurrence. A schematic drawing of the Propulsion-Controlled Aircraft (PCA) flight control concept and a diagram of the PCA features on an F-15 airplane are shown in the figure.

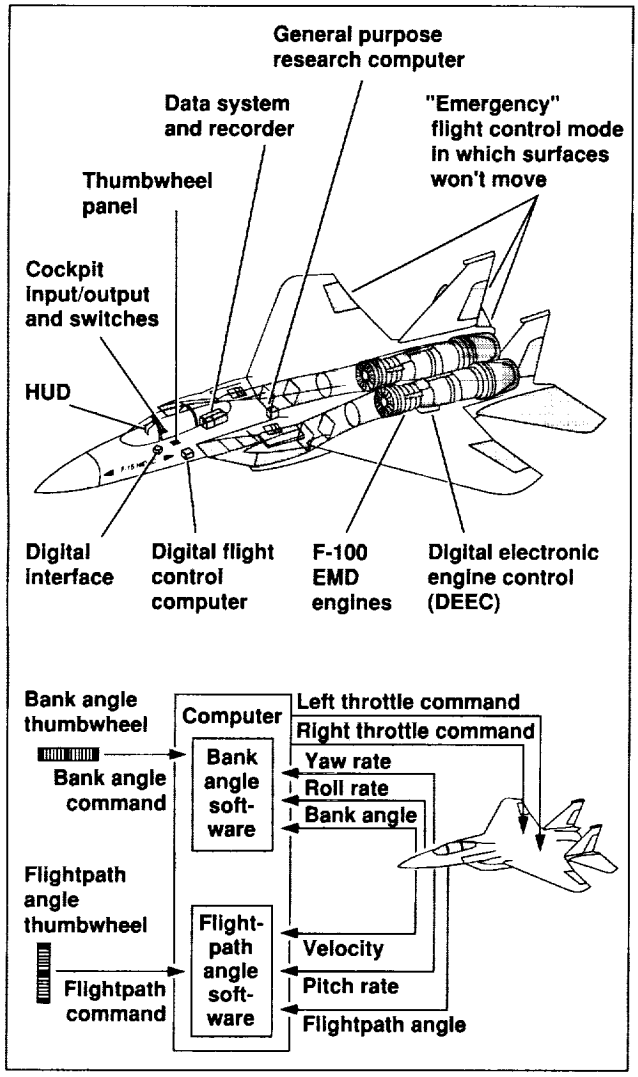


*Fig. 1. Propulsion Controlled Aircraft.*

**Ames-Moffett contact: R. Mah**
**(415) 604-6044**
**Headquarters program office: OA**

# Augmented Monitoring and Diagnosis Application

**Ann Patterson-Hine**

The Data Management System Augmented Monitoring and Diagnosis Application (DMS AMDA) is a software application being developed to enhance baseline monitoring and diagnosis capabilities for the DMS console in the Control Center Complex (CCC) at Johnson Space Center. It will ease the console operator's task by managing and displaying information needed to perform the DMS console functions using a direct-manipulation graphical user interface. The central component of the DMS AMDA is this "status at a glance" (SAAG) capability. This capability allows a console operator to quickly and easily determine whether or not all DMS components are operating nominally. If there are anomalies, the SAAG allows the operator to quickly determine which components are off-nominal, and allows quick access to more information. Nonfunctional components are highlighted in red, allowing quick identification by the operator. The operator can request additional information as an expanded view of the nonfunctional components.

The DMS AMDA project also has the goal of providing a demonstration of advanced automation capabilities for the CCC. Its operation is intended to integrate as seamlessly as possible into the baseline fault detection and management (FDM) functions. Digraph failure models are an integral component in the baseline FDM process for the CCC. In addition to traditional limit sensing and fault annunciation, a diagnostic application that will utilize digraphs as its knowledge base will be provided to all CCC users. The CCC will also provide a tool for developing model-based diagnosis and expert-systems applications and a graphical user interface tool. The DMS AMDA is being designed and developed for this environment. It is the proof-of-concept application for the process of augmenting and utilizing design digraphs for online diagnostics in a software application that integrates traditional fault detection algorithms with automated diagnostic techniques.

For the first prototype of the DMS AMDA, the Crew-Tended Configuration or Stage 6 of the construction of Space Station Freedom (SSF) is the selected domain. At Stage 6, the DMS will consist of four standard data processors, two multipurpose application consoles, and two mass storage units connected by a fiber-optic network. There will also be 18 local busses and more than 40 multiplexer-demultiplexers processing application software.

Digraph models of the DMS, developed during the design phases of the SSF program, will be used to provide candidate failure sets that are consistent with the observed system status. This information will be used by another diagnostic module, implemented using expert-systems and/or model-based diagnosis techniques. This module will narrow down the candidate failures by looking at the system status and behavior compared to a functional description of the system.

**Ames-Moffett contact: A. Patterson-Hine**
**(415) 604-4178**
**Headquarters program office: OA**

# Telepresence and Autonomous Control of Undersea Vehicles

**Daryl Rasmussen, Phil Hontalas, Michael Sims**

Since the earliest days of NASA it has been recognized that the undersea environment offers an accessible and, in many ways, realistic analogue for space environments and missions. The environment is hostile and relatively inaccessible to humans, but is scientifically attractive for a number of reasons. Because of the similarities between operations in space and under the sea, the latter can provide real-world experience in testing and proving technology in preparation for its use in space.

This project includes research in remote human and autonomous operation of undersea vehicles. These vehicles are test platforms for the development and validation of hardware and software technologies for future in-space applications. The focus of the work is in machine vision, virtual reality used for teleoperation, and advanced data analysis. The project is a collaborative effort between the Intelligent Mechanisms (IM) Group, the Photonics Group, the Human Factors Division, the Aerospace Robotics Lab at Stanford University, the Monterey Bay Aquarium Research Institute (MBARI), the Naval Postgraduate School, and the Telepresence Science Working Group (an element of the Ames Research Center's Center for Mars Exploration).

Aside from the work with the Antarctic Telepresence Remotely Operated Vehicle, which is described elsewhere, a major achievement in this project in 1993 was the establishment of a direct T1 connection between Ames and MBARI. This connection allows live video transmission from the MBARI Ventana submersible to the IM lab. The data connection was used to test the application of stereo telepresence techniques developed at Ames on the MBARI vehicle. Live stereo images were sent from the MBARI vehicle and displayed simultaneously at the MBARI facilities in Monterey and at the IM lab at Ames. The demonstration of this technology was so compelling to the MBARI scientists and pilots that they have incorporated this equipment for permanent use on the vehicle.

**Ames-Moffett contact: T. Fong/J. Steele**
**(415) 604-6063/6081**
**Headquarters program office: OA**

# Generator of Parallel-Program Models

**Catherine Schulbach, Jerry Yan, Pankaj Mehra**

A challenging requirement for the rapid availability and effective use of TFLOPS ("trillions of floating point operations per second") computer systems is an understanding of the scalability parameters of both the underlying hardware and the applications software before the fully configured systems are available. The objective is to build better tools to describe the relationship between system parameters and application performance.

Our approach has been to develop methods and tools to model and simulate the hardware architecture and the software application. We have focused on two such tools: (1) the Automated Instrumentation and Monitoring System (AIMS) and (2) the Behavior Description Language and an Experimentation Environment (BDL/AXE). The AIMS is a software tool that automatically instruments parallel FORTRAN and C programs, monitors their execution on a variety of computer architectures, and analyzes their performance by using statistical information and visual displays. BDL is a language used to specify the behavior of application programs; this description is used as input to the system simulator, AXE.

Most of the previous work involved developing application models in BDL, developing hardware systems models in AXE, and simulating the execution of the applications on the hardware model(s). AIMS trace data was used to aid in model development and to produce data to verify the model.

In 1992, we used BDL, AXE, and AIMS to successfully simulate a 7,000-line computational fluid dynamics code (ARC2D) on a model of the iPSC/860 with varying numbers of nodes (powers of 2 up to 1,024). The predicted execution times were within 5% to 10% of measured execution times (for 8–64 nodes) on the iPSC/860; execution time was minimized at 256 nodes, as predicted by the application developer. Early in 1993, we simulated a 5,000-line parallel tridiagonal solver (*xtrid*) and validated it against experimental data. Both models required a great deal of time and effort to develop (e.g., approximately 6 person-months for ARC2D).

This year we focused on automating the process of model development to reduce the amount of effort needed to manually develop models of parallel applications. The Generator of Parallel-Program Models (GPPM) uses AIMS-generated syntactic information about the program, combines it with trace data from AIMS, and uses intelligent regression techniques to discover various numerical attributes of the model (i.e., problem and system sizes). The resulting BDL model is then simulated using the AXE architecture simulator that is the default simulator for BDL models. Currently, AXE can simulate an iPSC/860 with up to 1,024 nodes. We are in the process of building a model for the Thinking Machines Corporation CM-5. At present, our validation only checks the overall completion time of a program.

By building the GPPM, we have demonstrated the feasibility of automated modeling in simulation of message-passing programs. We have identified key issues and developed innovative methods such as grammar-driven interpretation of tracefiles and the use of statistical techniques in driving hierarchical analysis of scalability. Our future efforts will be focused on smarter regression techniques, ways of modeling data-dependent communication patterns, and across-architecture performance prediction.

**Ames-Moffett contact: C. Schulbach**
**(415) 604-3180**
**Headquarters program office: OA**

## Superfluid Helium On-Orbit Transfer (SHOOT) Flight Project

**Jeff Shapiro**

The Superfluid Helium On-Orbit Transfer (SHOOT) experiment was flown aboard the Space Shuttle Endeavour during the STS-57 mission in June 1993. The SHOOT experiment was a demonstration of the technology and operations required to service cryogenically cooled satellites in space. The objectives were to characterize fluid containment, acquisition, mass gauging, and flow metering while liquid helium was transferred between dewars in zero gravity. The experiment was controlled continuously during the mission from the Payload Operations Control Center (POCC) at Goddard.

The Macintosh-based Command and Monitoring System (CMS) software, located in the POCC, communicated directly with the experiment in the space shuttle's payload bay, via standard NASA Communications Network/Tracking and Data Relay Satellite data channels. The CMS software provided a real-time, highly interactive interface by which the scientists controlled the experiment and displayed and analyzed its telemetry. The graphical, point-and-click interface of the CMS, by virtue of intuitive representations of the hardware configuration, greatly facilitated operations. The design of the software was driven by the interface, which was prototyped completely before implementation, and was general enough that it could be used for all phases of the experiment, from engineering tests through flight.

**Ames-Moffett contact: J. Shapiro**
**(415) 604-4713**
**Headquarters program office: OSF**

## Remote Control of the Russian Marsokhod Rover

**Michael Sims, Butler Hine, Terry Fong, Phil Hontalas**

McDonnell Douglas (MDA), with support from The Planetary Society (TPS), hosted representatives from the Russian Marsokhod rover development team in late January and early February of 1993. The team consisted of the Russian Academy of Science's Space Research Institute (IKI), the Babakin Center, and the Mobile Vehicle Engineering Institute (VNIITransMash). Some functional prototypes of the rover were brought to Ames by McDonnell Douglas. The purpose of the Ames visit was to evaluate the potential for applying a virtual-environment control system to control the rover. The figure shows the rover on the Ames simulated planetary surface.

The Ames researchers worked with the Russian software engineers to interface the virtual environment control system with the rover control system. In less than one day, we successfully made the physical link between the systems, reconfigured the rover control software, and began to operate the rover by sending commands via the virtual-reality-based graphical user interface. Subsequently, the Ames Intelligent Mechanisms group (IMG) worked with McDonnell Douglas to test the remote operation of the rover in Moscow via a communications link provided by the French Space Agency (CNES).

*Fig. 1. The Marsokhod rover.*

The success of these tests gave the team sufficient confidence that TPS, the IKI, MDA, and the IMG agreed to attempt remote operations during the next set of rover field tests, which were scheduled for August on the Kamchatka peninsula. The Russians use the terrain around Kozyrevsk and the Tolbachik volcano because it is a good terrestrial analog of the Martian surface. The teams communicated through a telephone channel carried by an Inmarsat communications satellite over the Pacific Ocean. The channel's transmission rate was 2400 bits per second, for an image rate of approximately one frame every five minutes. The crew at the control station at McDonnell Douglas facilities in Huntington Beach, California, commanded the vehicle and collected high-quality mono and stereo images. The testing culminated in a three-hour demonstration on the afternoon of August 31 (California time), during which the team commanded the rover over a 15-meter path and captured a total of 12 images, including five stereo pairs. The stereo pairs were transformed into terrain elevation maps, which were animated by the Virtual Environment Vehicle Interface control software.

This project is an attempt to demonstrate the role of possible U.S. participation in the Russian Mars '96 mission, which is scheduled to launch the Marsokhod rover to the surface of Mars for long-term exploration.

**Ames-Moffett contact: M. Sims**
**(415) 604-4757**
**Headquarters program office: OA/ARPA**

# Real-time Automated Monitoring and Diagnosis System

**Lilly Spirkovska, David Iverson, Stephanie Herrin**

The Research Animal Holding Facility (RAHF) is a Spacelab module designed at Ames that houses and monitors animals for studies of the effects of spaceflight and microgravity. During spaceflight, the RAHF transmits telemetry data to the Payload Operations Control Center (POCC) at Marshall Space Flight Center for ground-based monitoring of the system and the animals. Previously, RAHF telemetry data were displayed in the POCC on text terminals, and anomaly detection and fault diagnosis were performed manually by RAHF payload personnel. Monitoring these displays was a tedious job and finding the cause of detected anomalies involved searching through several volumes of documentation. Also, the telemetry displays did not provide trend information that could be used to detect impending failures.

To aid in failure detection, identification, and recovery, a ground-based automated monitoring and diagnosis system called RAD, for "real-time automated diagnosis," has been developed with support from the Ames Director's Discretionary Fund. RAD presents the telemetry data to payload operations controllers on easily interpreted color graphs that enhance anomaly detection and enable trend identification. It also has user modifiable monitoring rules that are activated whenever a telemetry frame is received. In addition to verifying instantaneous parameter values, RAD monitors parameter trends. The controller is alerted with visual and audible warning signals if any anomalies are detected. The cause of the deviation can be diagnosed and reported to the controller along with the criticality of the failure and possible corrective actions. Both monitoring and diagnosis occur in real time.

The RAD diagnosis system uses knowledge extracted from the Matrix Failure Modes and Effects Analysis (Matrix FMEA) developed by Stephanie Herrin of the Flight Equipment Engineering Branch for reliability analysis of the RAHF. Formal reliability analyses are performed on many engineered systems and contain a wealth of information that can be used to help build automated monitoring and diagnosis systems. This research developed techniques to convert Matrix FMEA information into a diagnostic knowledge base for use with the Fault Tree Diagnosis System developed in the Information Sciences Division.

RAD was used in RAHF readiness tests and was deployed for the SLS-2 Space Shuttle mission in October 1993. During the SLS-2 mission, RAHF payload operators and engineers at Ames, Marshall Space Flight Center, and Kennedy Space Center used RAD extensively to monitor the status of two RAHFs on board Space Shuttle Columbia and the rodents housed in those RAHFs. RAD will also be used for postflight analysis of archived telemetry data.

**Ames-Moffett contact: L. Spirkovska**
**(415) 604-4234**
**Funded by DDF**

# Electronic Chart Displays to Support Geographical Orientation

**Vernol Battiste**

The environments in which civil and military aircraft operate extend from the closely monitored air traffic control system to remote and hazardous areas where little flight guidance is available. Before a flight, pilots plot their course on paper maps and select specific features to use as geographical checkpoints. During ground taxi operations and in flight, they compare visible features in the external scene with those on the maps or in their memory. However, since the loss of geographical orientation remains a significant cause of civil and military incidents and accidents, researchers in the Rotorcraft Human Factors Branch at NASA Ames and at the University of Illinois have conducted research on the information pilots use to maintain geographical orientation and methods of improving the presentation of mission-critical information on advanced displays. To support this research, a highly accurate, low-cost reconfigurable electronic chart display (ECD) system was developed at NASA Ames.

The prototype ECD system uses IBM-PC technology coupled with Global Positioning System (GPS) data. The ECD system was developed with base research and technology funds from NASA and the U.S. Army. The prototype system was ground-tested in late 1991, and flight-tested in NASA's Earth Resources C-130 aircraft in 1992. Results show that GPS data were more accurate than the Inertial Navigation System (INS) currently installed. The flight navigator/photographer rated the ECD system to be as useful as the system currently in use (conventional paper maps and INS), and noted that the ECD afforded greater flexibility; when required to perform other tasks that drew attention away from the map, the navigator could reorient much faster and with less effort using the ECD system. In addition, ground and flight tests have shown that the precision of the system is not limited to the stated accuracy of the GPS receiver, as was expected, but by the pixel size of the scanned map; with a 1:500,000-scale sectional chart, system accuracy is ±165 feet; with a 1:100,000-scale metric topographical chart, accuracy is ±33 feet. The ECD system has been implemented as a ground-based system as well. A scientific ground dispatch station has been developed for the ER-2 SPADE Telescience Missions, which were conducted in 1993. The ECD system provided ground personnel with real-time aircraft position information during all phases of inflight data collection. Coupled with other real-time data from the aircraft's onboard sensors, it allowed scientists to modify flight routing to improve data collection.

In support of the Terminal Area Productivity (TAP) Program, the ECD system was successfully installed and flight-tested onboard Langley Research Center's TSRV aircraft in May 1993. This was accomplished through a collaborative effort between the Ames Rotorcraft Human Factors Branch, the Langley Research Center (LaRC) Cockpit Technology Branch, and the LaRC Advanced Transport Operation System Program Office. The system was installed in an aft equipment rack, and flown during a mission to collect baseline data for the Differential GPS (DGPS) being developed and tested at LaRC for the TAP program. During the mission, flight crew members were invited to observe and comment on the ECD system. Crew comments on display size, update rate, and display resolution were positive. While the aircraft was parked at the DGPS calibration point on runway 28 at Wallops Flight Facility, which was depicted on a 1:6,000-scale map, the mean error using raw GPS data varied less than 19 meters. This variation in map position was well within the published 25-meter GPS accuracy.

The prototype ECD system was developed as a research tool, but has a variety of commercial applications, not limited to flight. This type of system is being extended to most, if not all, vehicle applications in which human operators must relate map position information to a changing out-the-window or synthetic view (e.g., emergency-response dispatch stations and in-vehicle map and information displays for police, firefighters, and others).

We will continue our work in the TAP program to develop advanced taxi map designs integrated with map data bases in support of all phases of flight from push back to arrival at the gate. In addition, we

are working on an agreement with the U.S. Forest Service to develop an ECD system that will be used by the Aerial Commander to structure the air operations in the congested skies over major forest fires. The system will also be used to direct the assault on the fire. In support of this agreement, and also of the need to transfer technology to the private sector, we have entered into a Space Act Agreement and a Technical Exchange agreement with two commercial corporations. The Space Act Agreement (with ASINC, Inc.) will support the development of ECDs for the Forest Service and low-cost ECDs for general-aviation aircraft. The Technical Exchange Agreement (with LOGICON, Inc.) is designed to support the use of voice technology to control advanced map displays.

**Ames-Moffett contact: V. Battiste**
**(415) 604-3666**
**Headquarters program office: OA**

## Ames Spatial Auditory Display

**Durand R. Begault**

Communications in high-stress environments such as spacecraft launch control, air traffic control, 911 operations, and airline cockpits frequently require the monitoring of simultaneous, differentiated communication streams against a background of noise from various sources. In most situations one-earpiece communication systems are used, disabling the operator from using the two-ear (binaural) listening advantage normally present in everyday listening. If communications personnel were able to use both ears, specific advantages would result in intelligibility, with a corresponding benefit in safety.

Studies of speech intelligibility with binaural versus monaural listening have shown that the same level of intelligibility for a given signal against noise can be attained with a lower amplitude of the signal in the binaural case. Binaural hearing is also superior to monaural for separation of a desired stream of auditory information from several, simultaneous auditory streams. This is because separate sound sources normally are emitted from different locations, resulting in each sound source being differentially cross-correlated within the auditory system as a result of differential spectrum and phase information at the two ears. This differential spectrum results from the filtering caused primarily by the outer ears (the pinnae) and head shadowing.

The Ames Spatial Auditory Display (patent pending), developed for Kennedy Space Center, is a prototype device that spatializes launch personnel radio communications. It incorporates four digital signal-processing boards that filter communication streams in the same manner in which the outer ears would filter sounds in everyday hearing. The digital filtering results in the placement of each incoming radio frequency at a different virtual acoustic location. The filter coefficients are stored in a removable programmable memory chip (PROM), allowing the user to select customized virtual auditory positions, or a particular set of pinnae measurements. Preliminary results from intelligibility tests have shown an intelligibility improvement of about 6 to 7 decibels for spatialized radio communications, matching predictions from unaided, normal binaural listening.

The reduction of the likelihood of misinterpreting call signs is an important safety improvement for high-stress human–machine interface contexts. The binaural advantage could also benefit communications personnel because the overall intensity of communications hardware could be reduced without sacrificing intelligibility. Lower listening levels over headphones could possibly reduce the risk of threshold shifts resulting from auditory fatigue, an important factor in operational safety. Another advantage is that users do not need to manually adjust the volume of a desired communication channel as often in order to hear it, allowing for a more "hands-free" operation of communication systems.

**Ames-Moffett contact: E. Wenzel**
**(415) 604-6290**
**Funded by DDF**

# Communicating Quantities to Computers

**Stephen M. Casner, Felix S. Sterling**

A study of airline pilots' use of flight control automation revealed that one reason why crews opt not to use automation in time-critical situations is that it takes too long to configure the automation. Furthermore, it was shown that most of the configuration time is spent entering the quantitative description of the desired flightpath into the flight management computer (see figure).

This research systematically explores a range of techniques for allowing people to communicate quantities to computers. A variety of design dimensions are considered, including (1) how quantities are portrayed, organized, and manipulated in a display, (2) the number of quantities that can be specified at once, and (3) the form in which quantities to be specified are received. In a series of four experiments, subjects performed a variety of data-entry tasks using experimental displays that varied systematically along each of the design dimensions considered. Each experiment measured the time required to enter quantities, the average number of errors made, and the average size of the errors committed when using each experimental display. The results are used to show how, for a given task, a display can be designed to incorporate features that maximize users' performance with respect to time and accuracy.

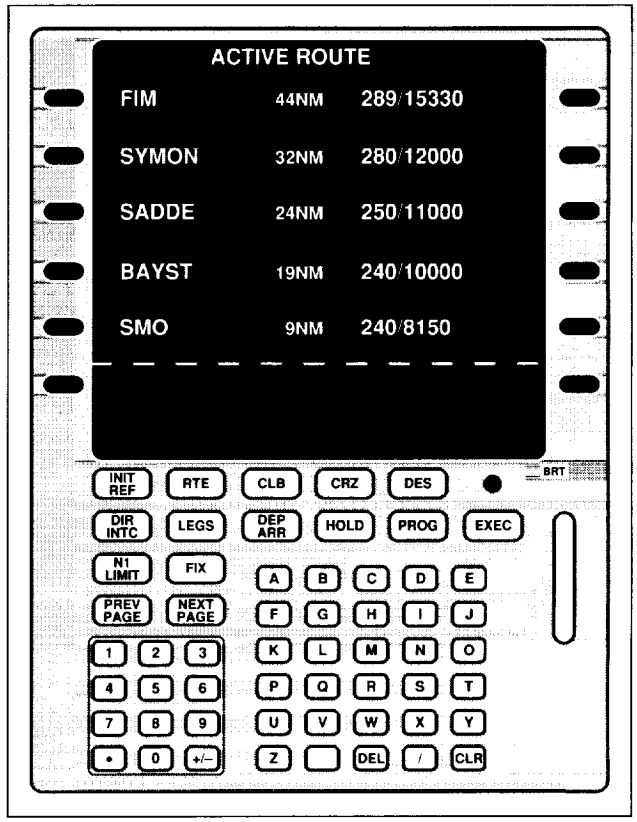


*Fig. 1. Pilot's interface to the flight management computer.*

**Ames-Moffett contact: S. Casner**
**(415) 604-6908**
**Headquarters program office: OA**

## An Electronic Taxiway Map Display for the Flight Deck

**Stephen M. Casner, Dominic Wong**

As commercial transport traffic increases, crews are faced with the challenge of maintaining awareness of other aircraft, both in the air and on the ground. Surface operations are particularly difficult because little support is available for tracking the location of other aircraft. Toward this end, we have developed a prototype of an electronic map display for the flight deck, to be used during airport surface operations. Although our work does not address the problems of global position finding or datalinked communication, the map display provides a framework in which to evaluate the usefulness of providing various types of information to the flight crew, and to evaluate forms in which the information might be presented. The current prototype of the map display presents the following information: (1) a real-time track of the position of all aircraft operating on the airport; (2) data blocks associated with all aircraft, including call sign and type; (3) a graphical plot of the taxi clearance issued to any aircraft; and (4) gate information. In addition, the map display contains a set of "help" functions that allow the crew to (1) obtain the name of any taxiway or runway by pointing to the structure on the map; (2) locate any taxiway or runway by selecting the name of the desired structure.

An early prototype of the map display has been tested in a full-mission study in which all crew interactions with the map display were videotaped. Crews also completed a questionnaire pertaining to their use of and attitude toward having the map display available on the flight deck. A series of part-task empirical studies investigating various design features of the map display are being planned.

**Ames-Moffett contact: S. Casner**
**(415) 604-6908**
**Headquarters program office: OA**

## Advisor Integration Management System (AIMS)

**Kathleen Dammann**

Several research organizations and commercial and military avionics manufacturers are developing "intelligent" aiding systems designed to advise flight crews in specific aspects of their work. These systems are being developed independently and are likely to be based on different formal models. Integrating multiple intelligent advisory systems in the cockpit will raise complex issues in computer science, aeronautics, and human factors. In addition, many of these systems have had little or no interface development. Research is needed to determine what information and what format are best for presenting advisor information to pilots. AIMS work is addressing both advisor integration and interface design.

The AIMS project has a significant computer-science-based component that deals with the requirements and techniques for the integration of multiple expert systems. The advisor integration effort is under way; the first aiding system (Faultfinder, an engine-monitoring and diagnostic advisory system from NASA Langley Research Center) is running at Ames. Other advisor systems are being examined as candidates for integration. Eventually, AIMS will be

incorporated into the Crew-Vehicle Systems Research Facility (CVSRF) Advanced Cockpit Flight Simulator and demonstrated as part of a full-mission simulation study (1995).

A series of part-task studies planned for 1994 will examine the functionality and display of advisor systems, looking at issues such as system explanation, reliability, and machine-generated estimates of advice confidence. The results of these studies will guide the later stages of AIMS development and integration into a full-mission simulation.

**Ames-Moffett contact: K. Dammann**
**(415) 604-0010**
**Headquarters program office: OA**

## Perspective Pathway Attitude Director Indicator (ADI)

**Nancy Dorighi, Stephen Ellis**

The purpose of this work is to investigate whether a perspective pathway format for an attitude director indicator (ADI) provides a significant improvement in pilot spatial awareness over the traditional ADI. Spatial awareness can be seriously affected by the loss of visual or vestibular cues. Since vision can be degraded by weather conditions, and body forces minimized in coordinated turns, the perspective format may better compensate for the loss of these cues, and thus improve overall spatial awareness.

The Tunnel-in-the-Sky is a perspective format that functions much like a flight director, but provides additional information. Its ability to display future path and bank angle may make curved approaches easier to fly because there is more preparation time for control inputs. With less attention required for control, more attention is available for maintaining spatial awareness. The addition of basic ground reference elements to the display may help pilots perceive their location relative to the ground. Furthermore, the information is presented in a body-referenced manner as it would appear out the window, and may therefore be more readily comprehended than with conventional instruments. For example, the traditional two-dimensional ADI provides only a snapshot of the aircraft state, with minimal future trend information. The horizontal or plan-view map format, though appropriate for certain functions, may not be optimal for others because it is not body referenced.

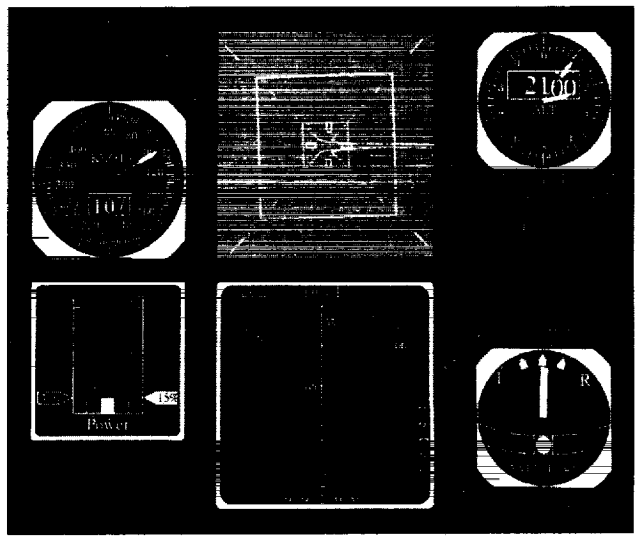

*Fig. 1. Modern glass-cockpit instrument suite.*

We conducted a part-task experiment in which the Tunnel-in-the-Sky was compared to a conventional ADI, within the flight-deck instrument suite of a modern glass cockpit (first figure). The experiment was intended to determine the situation-awareness benefits of a perspective display in a realistic information context. Accordingly, a track-up moving map display was included in the instrument panel. Two modes of control were used, manual and autopilot.

A set of targets was chosen that represented actual terrain features that would be useful ground references during an approach to a major commercial airport. Curved approach scenarios were used to evaluate the effect of the displays during curved and straight flight segments.

Experienced commercial pilots familiar with the airport and area geography were recruited for the experiment. Subjects were seated in front of a graphics color monitor inside a dome and wore a head-mounted tracker with a light pointer for feedback. Spatial awareness was measured by the accuracy and precision of the pilot's judgment of the visual direction to the targets along or near the approach path.

Pilots consistently underestimated the direction to targets in azimuth. The error in their estimate was as high as 20 degrees near the periphery. The level of automation and the type of display did not affect this result. If this phenomenon is present in full-mission simulation, it could be used as the basis for a corrective bias in spatial displays designed to direct pilots' attention to external targets.

Neither the precision nor the underestimation of direction were affected by the trajectory of the approach (curved versus straight). The experimental conditions may not have sufficiently stressed the pilots' sense of spatial awareness to fully test the benefits of the tunnel approach display.

The experimental results did not provide a clear-cut assessment of the benefits of using a perspective tunnel display versus the conventional ADI. In the manual piloting condition, use of the tunnel display reduced directional error as expected. In the automatic control condition, use of the tunnel display unexpectedly increased target directional uncertainty (see second figure). In fact, error was greater for the autopilot condition. This fact suggests that the pilots in autopilot mode may not have been sufficiently engaged in the task to maintain directional awareness to targets. Furthermore, the presence of the track-up map provided a useful source of target orientation information and may have overwhelmed the differences in the two displays. This source of redundancy is likely to be present in future cockpit environments.

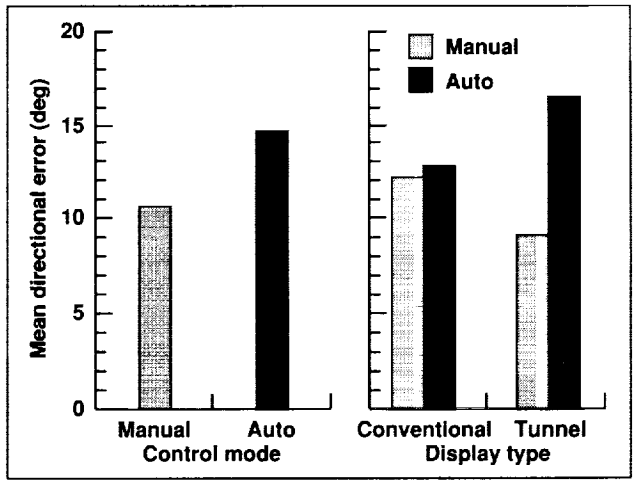


*Fig. 2. Effect of control mode and display type on directional error.*

**Ames-Moffett contact: N. Dorighi**
**(415) 604-3258**
**Headquarters program office: OA**

# Infrared Imagery Video Data Base

**David C. Foyle**

A video-disk-based part-task trainer for flight with infrared imagery is being developed jointly with researchers in Israel under the United States/Israel Memorandum of Understanding on Rotorcraft Aeromechanics and Man–Machine Integration Technology. Previous research has demonstrated that under certain conditions infrared imagery can be problematic for determining navigational and waypoint information. A color television camera, video recorders, and time code generators were installed on the NAH-1S Cobra (NASA 736) helicopter (see figure). The new video capability and the existing infrared system—the pilot night-vision system (PNVS)—were used to collect simultaneous recordings of television and infrared imagery. This imagery forms the image data base for the part-task trainer.

Fifteen flights were successfully completed, resulting in 12 hours of simultaneously recorded, time-stamped infrared imagery and video. Flights were conducted in a variety of environmental conditions, with a bore-sighted television camera and the U.S. Army PNVS sensor. All flights were conducted in areas within a 100-mile radius from Ames Research Center, which included a wide variety of terrain, ground features, and building structures. Flights included daytime flights at 500 feet above ground level, night flights repeating routes flown under daytime conditions, nap-of-the-Earth (NOE) flights in the Western Training Area flown at 50–150 feet above ground level, and approaches to two local area airports at a variety of glide slopes.

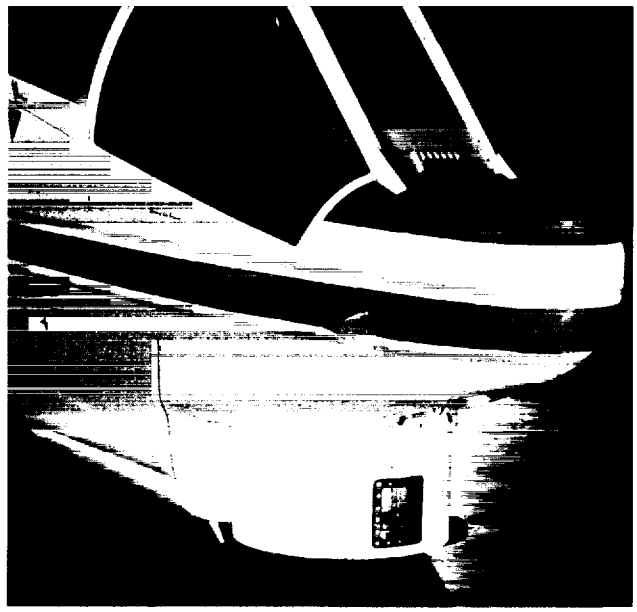

*Fig. 1. NAH-1S Cobra (NASA 736) helicopter outfitted with color television camera in the gun turret.*

The resultant video data base is being incorporated into the infrared imagery part-task trainer, and human-factors experiments assessing the use of infrared imagery are being conducted.

**Ames-Moffett contact: D. Foyle**
**(415) 604-3053**
**Headquarters program office: OA/Army**

# Integrated Mode Management Interface

**Edwin Hutchins, Everett A. Palmer**

Mode management involves understanding the character and consequences of autoflight modes; planning and selecting engagement, disengagement, and transitions between modes; and anticipating automatic mode transitions made by the autoflight system itself. Mode management in the current highly automated airliners is a challenge. The fact that flightcrews are sometimes surprised by autoflight system behaviors has been well documented. When flightcrews wonder what the system is doing, and how to make the plane do certain things, there is a problem. Problems with mode management are also easy to see in Aviation Safety Reporting System reports. Palmer and others have documented several cases in which flightcrew uncertainty about the behavior of glass-cockpit automation led to altitude deviations. The difficulties that pilots have with mode management are understandable, given the nature of the current system. The engineers have created an autoflight system of great utility, but the interface to it is conceptually so difficult that some airline operators do not attempt to train their crews to operate the complicated vertical navigation (VNAV) modes but instead rely on the pilot community to discover and transmit ways of using it in flight.

In order to understand and successfully manage autoflight modes, pilots need to know what modes are available, what conditions must be met before a mode can be selected, what the target value is, who set the target value—the pilot or the flight management system (FMS), how the target is being achieved, and, finally, how to get out of a mode. The interface consists of a vertical mode manager and a lateral mode manager. Autoflight modes are depicted by icons on a graphical display. Mode selection is accomplished by touching the appropriate icon.

The novel features of the mode management interface are (1) the autoflight system's state-display and mode-selection actions are colocated; (2) autoflight modes are depicted by icons on a conceptually meaningful graphical display rather than by strings of characters; (3) icon color and size indicate mode status (engaged, armed, selectable); (4) location of the icons indicates both the source of the target value (FMS or pilot input) and the value of the target (airspeed/Mach number, altitude, heading); (5) display behavior reflects underlying regularities of the autoflight system; and (6) the display of icons is context sensitive so that icons for modes that are not selectable from the present context are not displayed. On the systems currently in use, all mode-select switches are continuously present (as hardware) even though they may not be selectable.

The vertical mode manager hardware consists of a vertical navigation display screen, a speed-select knob, an altitude-select knob, and a vertical-speed-select wheel. The vertical navigation display screen contains an airspeed tape, a vertical profile display, an altitude tape, and four columns for the display of mode icons. Icons on the vertical mode manager show relationships of aircraft pitch and thrust to airspeed/Mach number and vertical flightpath. Target source (FMS or crew input) and target value are indicated by the location of the icon with respect to airspeed/Mach number and altitude tapes.

The lateral mode manager hardware consists of a lateral situation indicator display and a heading-select knob. The lateral situation indicator display is similar in appearance to the current-generation navigation displays except that it contains context-sensitive, touch-selectable mode icons. Icons on the lateral mode manager show aircraft roll guidance for heading and lateral path. Icon display state, color, and size indicate mode availability and mode status (engaged, armed, selectable).

The mode management interface is implemented in C on a graphics workstation. This integrated mode management interface will be implemented in the Ames Advanced Concepts Flight Simulator and evaluated by airline pilots.

Edwin Hutchins is at the University of California, San Diego.

**Ames-Moffett contact: E. Palmer**
**(415) 604-6073**
**Headquarters program office: OA**

# Visual-Motion Cueing in Altitude Regulation

Walter W. Johnson, Jeffery A. Schroeder

Visual flight simulation validity depends on the ability to capture critical information within the visual scene and the motion base. This research examined the role of emergent texture detail and simulator platform motion in altitude regulation tasks. Until recently, presenting multiple levels of detail (LOD) on a simulator has been prohibitively expensive, although it is known that visual scene density affects the salience of certain altitude information, and may directly provide other cues about altitude. When simulators present just a single level of detail, scenes are visually less dense at lower altitudes than at higher altitudes because the simulators cannot "swap in" more highly detailed data bases at lower altitudes, even though objects or features invisible at higher altitudes would be visible at lower altitudes. In fact, even when LOD capability is present, it has not been systematically used to reflect the expected visual density in scenes being depicted. This study examined whether the control of altitude was affected by LOD manipulations that yielded high, medium, and low levels of change in visual density with changes in altitude.

This research also examined the role of platform motion in altitude regulation tasks. It is known that visual information has a strong impact on performance, but the importance of simulator platform motion remains in dispute. The value of platform motion in the regulation of vertical ascent/descent speed was examined in a context where the visual information is known to be deceptive. This case occurs where altitude is varying, and angular or optical flow rate (which is proportional to vehicle path speed divided by altitude) changes with speed and altitude. We therefore examined whether, in a task where pilots had to maintain a constant descent/ascent rate, simulator motion would help the pilots distinguish between changes in flow rate caused by altitude change and changes in flow rate caused by changes in path speed.

Researchers associated with the Rotorcraft Human Factors Research Branch and the Flight Controls and Dynamics Branch addressed this problem in a study designed to examine the value and impact of correct and incorrect LOD implementations. The study, conducted in the NASA Ames Vertical Motion Simulator, examined NASA test pilots' ability to visually (i.e., without instruments) control vehicle altitude in two single-axis tasks: (1) an altitude repositioning task, in which pilots had to double or halve several initial altitudes; and (2) a vertical rate control task, in which pilots had to maintain a fixed climb or sink rate despite a buffeting disturbance.

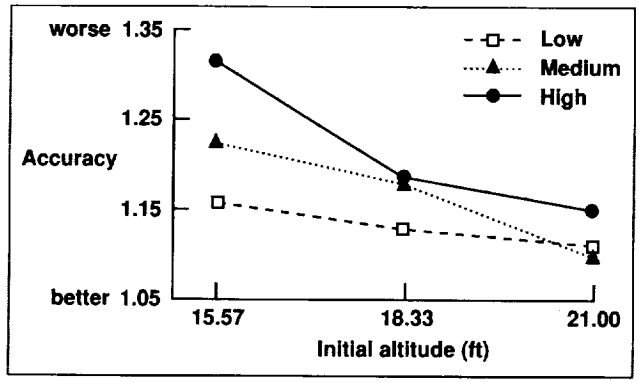


*Fig. 1. Repositioning accuracy as a function of degree of dependence of optical density upon altitude.*

The LOD within the visual scene, composed of hexagons on a flat terrain, was manipulated to generate high, medium, and low linkage between visual density and altitude, while platform motion was either present (and 1:1) or absent. Both the LOD and the motion manipulations had clear effects on altitude repositioning performance: (1) altitude repositioning accuracy was relatively independent of initial altitude when the dependence of optical density on altitude was low (see first figure) and (2) platform motion caused pilots to move less far during each repositioning. These results support the hypothesis that the linkage of optical density to altitude affects performance. They also indicate that an integration of vestibularly sensed platform motion affects the sensed amplitude of movement. For the vertical rate control task, the LOD manipulation had

little effect, but platform motion had a strong effect. The second figure shows that, consistent with expectations, pilots increased speed when climbing (because of the decrease in flow rate with increasing altitude) and decreased speed when descending (because of the increase in flow rate with decreasing altitude). However, the second figure also shows that mean speed was much less affected by movement direction (climb/descend) when platform motion was present, which indicates that the pilots used the motion to sense, and avoid responding to, flow rate changes resulting from the changing altitude. Finally, the second figure shows that platform motion led pilots to generate lower overall vertical rates. This may be due to perceived speed being a summation of information from all cues available, and therefore higher when more cues are present.

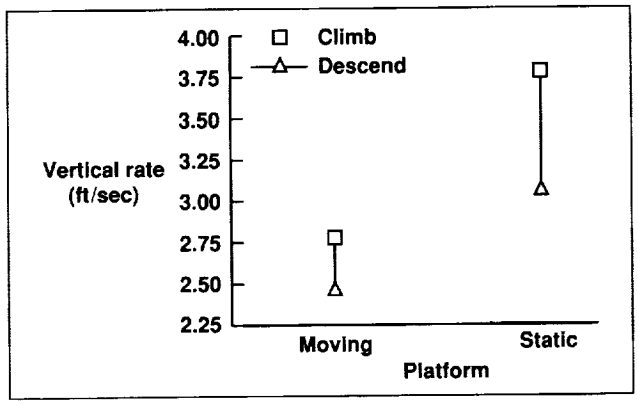


*Fig. 2. Mean vertical rate as a function of platform motion and direction of movement.*

**Ames-Moffett contact: W. Johnson**
**(415) 604-3667**
**Headquarters program office: OA**

## Enhancing Air Traffic Control Displays

**James C. Johnston, Krista Horlitz, Robert Edmiston**

One way to improve human performance is to substitute rapid and reliable perceptual processing of information for slow and unreliable cognitive processing. Our project applies this principle to the performance of air traffic controllers. We are developing and testing new display concepts that enhance the situation awareness of controllers, improving the safety and effectiveness with which they function.

Present air traffic control (ATC) situation-awareness displays provide graphical representation of only a tiny portion of the information needed by controllers (principally, an X–Y map of aircraft positions). Other information—altitude, altitude change, track vector, etc.—is not displayed graphically. This other information is typically available only in an alphanumeric data block, where it must be fixated, identified, and then cognitively interpreted. Very-high-resolution color monitors will be available in future ATC equipment suites, but little is known about how best to take advantage of their capabilities.

Our initial focus has been on designing and testing alternative coding systems for representing aircraft altitude. We have designed a number of different systems that code altitude either continuously or in discrete bands, and that rely on either chromatic or achromatic (black-and-white) properties. We have tested these coding schemes in laboratory part-task experiments in which altitude processing plays a key role. Our preliminary findings are that (1) color coding of altitude is most effective by a considerable margin; (2) some black-and-white schemes are moderately effective; and (3) both discrete-band coding and continuous coding are effective, but continuous coding appears to be acquired more quickly and used more easily. An

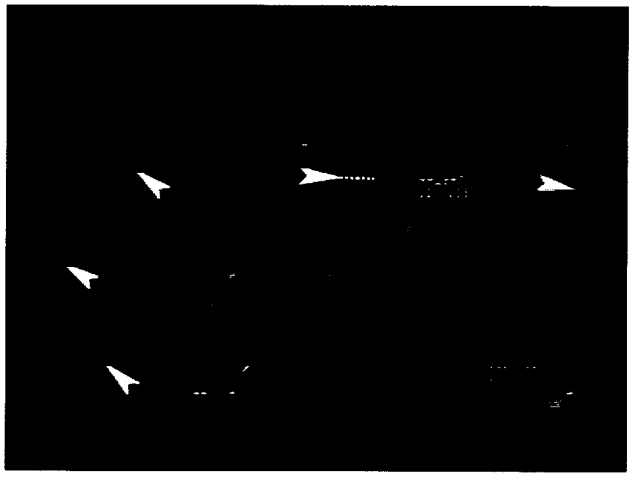

*Fig. 1. Advanced ATC display using integrated aircraft icons to perceptually code altitude (color), track vector (dotted line), altitude change (color of dotted line), and speed (length of dotted line). (See color plate 1 in Appendix)*

additional experiment is being developed to test how well our perceptual coding schemes support the integration of altitude and X–Y position information.

We have also designed an integrated aircraft icon (see figure) that provides perceptual coding of position, altitude, altitude change, track vector, and speed. This integrated icon takes advantage of two important psychological principles: (1) color provides a powerful way to organize the visual field perceptually so that different items can be selected for attention with minimal effort, and (2) multiple items of information can be more rapidly encoded if they are displayed as different properties of one object rather than as separate items.

**Ames-Moffett contact: J. Johnston**
**(415) 604-5686**
**Headquarters program office: OA**

## Perceptually Tuned Visual Simulation

**Mary K. Kaiser**

All flight simulators and synthetic vision systems are limited with respect to computational capacity and data-base size. Computational limitation refers to the limited number of vertices or polygons that can be computed and rendered in any one frame of a simulation. Data-base limitation refers to the limited storage capacity of the hard drives, optical disks, and tapes that hold the many objects that make up the virtual world of the simulator. Research in our laboratory uses models of human visual perception to determine what computational and data-base simplifications can be employed with minimal impact on the veridicality of the visual scene. This research leads to the development of perceptually tuned simplification techniques. Two issues under examination are the impact of removing the rotational component of motion parallax, and how best to emulate the natural emergence of detail as observers approach objects.

When an observer moves past an object, there is a motion-defined rotation of the object relative to the observer. For example, when flying past a building, one initially sees only the near side, but gradually more of another side is revealed. Work in our laboratory suggests that observers may be relatively insensitive to this rotational motion. When asked to judge which of 12 targets in a field has its rotational motion removed, observers were incorrect 25%–50% of the time. As shown in the first figure, the observer's ability to identify the anomalous target decreased with distance. These findings suggest that a common method of computational simplification used in visual simulation (in which billboard representations of objects are shown normal to the observer's line of sight) is perceptually acceptable, especially with more distant objects in the visual field.

The current technique to simulate the emergence of detail is to discretely "page in" more details of data-base objects as the distance to the objects decreases. However, this method is not perfect. If additional details are brought in too late, there is a visible "popping in" of details which attracts attention and distracts the simulator pilot. On the other hand, if these details are paged in well below threshold (to ensure this popping does not occur), the computational savings is negligible.

Another major difficulty with a discrete page-in method is that the data bases are not easily transferable from one flight model to another. For example, the terrain and objects developed for a high-altitude vehicle will not work well in a nap-of-the-Earth simulator because the objects will not page in quickly enough. Furthermore, there will be a blurring of the terrain that was meant for much-higher-level flight (and thus lacks low-altitude detail).

The solution we are pursuing involves short but nonetheless continuous transformations from one object and terrain representation to another. Such transformations will more closely mimic the continuous changes in detail that occur in the real world (see second figure). The research has three phases:

1. Develop techniques likely to simulate the transformation that occurs in objects and textures as observers approach them, and model this transformation on a graphics computer. These techniques are derived from knowledge of the time course of visual perception of objects and textures.

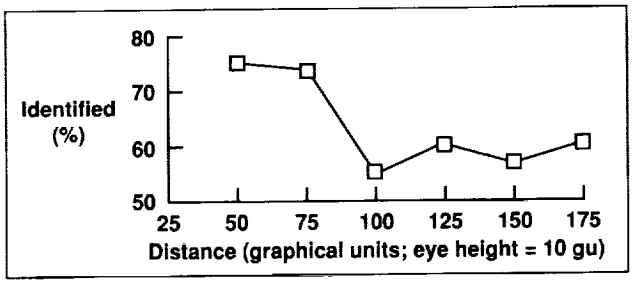


*Fig. 1. Percent of time observers were able to identify an anomalous target in the visual field.*

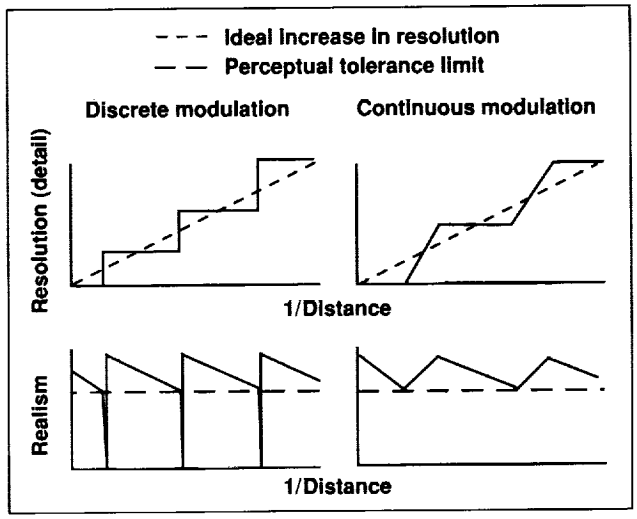


*Fig. 2. Comparison of discrete and continuous level-of-detail modulation with respect to required resolution (which increases computational load) and perceptual realism. The continuous modulation technique allows a sustained level of realism without significantly increasing system load.*

2. Perform a series of psychophysical studies to determine which transformation method best captures the perceptions people have as they approach objects.

3. Optimize the best method and integrate it into a motion simulator and synthetic vision system.

Drawing upon important principles of computer science and perceptual psychology, our research seeks to enhance the perceptual veridicality of visual simulation with minimal increases in computational cost. Such perceptually tuned techniques can be used to best exploit the computational capabilities of simulation hardware.

**Ames-Moffett contact: M. Kaiser**
**(415) 604-4448**
**Headquarters program office: OA**

# Crew Performance in Space-Analogous Environments

**Barbara Kanki, Philip Lieberman**

The high-risk potential for safety and health problems in long-duration space operations requires the timely development and validation of guidelines and intervention strategies for human productivity and well-being. Although our knowledge of the effects of long-term stresses imposed by the space environment on the crew is limited, and we must be cautious in directly generalizing findings from ground-based domains to the space environment, research focusing on teamwork in environments analogous to space can provide a valuable means of identifying potential problem areas and understanding critical issues. Mountaineering teams provide a fruitful analogy to space exploration teams because the mountain environment captures numerous conditions of interest: a harsh, isolated physical location; high-risk, high-stress work conditions; life dependency on fellow team members; and limited access to outside support. We are interested in how teams cope in such environments and what factors contribute to the maintenance of healthy, productive teams.

To ensure human well-being in remote operations it is important to develop an unobstrusive means of monitoring and assessing crew health. For one part of our study of mountaineering teams, we collected speech data via radio transmittals from various waypoints (e.g., base camp and higher camps) in a recent Mt. Everest expedition. Analyses

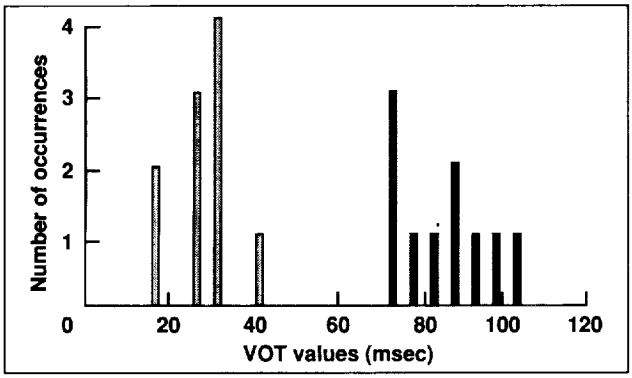


*Fig. 1. VOT range for "g" (gray bars) vs. "k" (black bars) for climber A at base camp.*

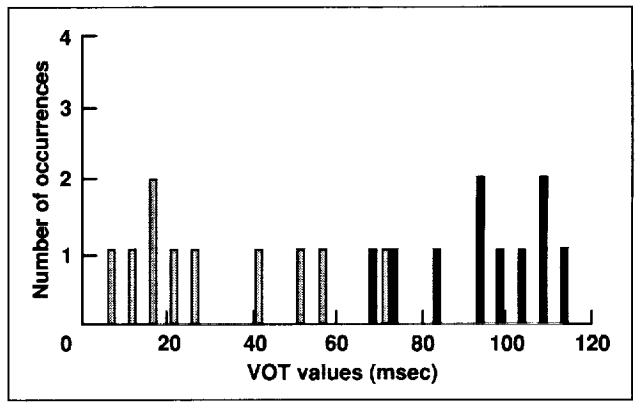


*Fig. 2. VOT range for "g" (gray bars) vs. "k" (black bars) for climber A at camp 2.*

show that acoustic measures derived from speech can be used to detect deficits in fine motor coordination and cognition. Deficits in motor coordination required in speech production as well as deficits in abstract reasoning, working memory, and the ability to comprehend syntax have been reliably tracked in the speech samples collected this year. For example, the figures illustrate differences in "voice-onset time" (VOT) for pronouncing "g" vs. "k." When speakers fail to regulate VOT between critical consonants, communication is greatly impaired. The first figure illustrates good regulation of VOT: each consonant has a distinctive VOT range separated from that of the other consonant by an interval of more than 20 milliseconds. The second figure shows debilitation (presumably a result of anoxia induced by altitude): the VOT ranges are no longer distinct. This technology shows great promise as a clinical tool for studying adaptation to other high-stress environments, and ultimately, for aerospace applications in which real-time, acoustic analysis procedures can provide effective remote monitoring of crew health.

**Ames-Moffett contact: B. Kanki**
**(415) 604-5785**
**Headquarters program office: OSSA**

# The Effects of Flight Deck Automation on Crew Communication

**Barbara Kanki, Elizabeth Veinott, Cheryl Irwin**

Crew communication is a key element in effective coordination of flight operations. It is a means by which the flight task is managed, information is transferred, and a good working atmosphere is established. In addition, it is a primary way in which situation awareness is maintained and standard procedures are carried out. From a research and evaluation standpoint, communications are observable indicators of how well a team is performing and can give us valuable information regarding a crew's response to particular input factors. The input factor in our current investigation is flight deck automation. We are interested in the potential effects of flight deck automation on team performance. We are analyzing patterns in crew communications in order to understand the differences in how crews perform under different automation conditions and how such differences contribute to overall quality of performance. Our ultimate goal is to enhance flightcrew performance by incorporating our findings into training refinements or improved flightdeck design.

In principle, the advances made in new-technology aircraft are expected to yield payoffs for flight operations, but we are concerned about hidden or unanticipated costs that the crew may be required to pay under some conditions. Therefore, Crew Factors researchers are investigating the behaviors and strategies shown by crewmembers as they perform their tasks in highly automated workplaces. Specifically, we have compared crew behavior at two levels of flight deck automation (DC-9 and MD-88), using videotape data obtained from a full-mission simulation study. Although there were no performance differences between crews of the two aircraft, communication behaviors were quite different. Crews used communications differently to accomplish the same performance level, and these differences were related to speaker roles and workload conditions, that is, the phase in which abnormal conditions were introduced into the simulation scenario. For example, as shown in the figure, MD-88 crews asked twice as many questions as DC-9 crews during the abnormal phase. More detailed analyses have also shown that differences in the use of specific types of speech (e.g., commands and questions) are related to aircraft type, indicating that automation may be altering the crewmembers' communication requirements and/or access to information, particularly during the abnormal flight phases.

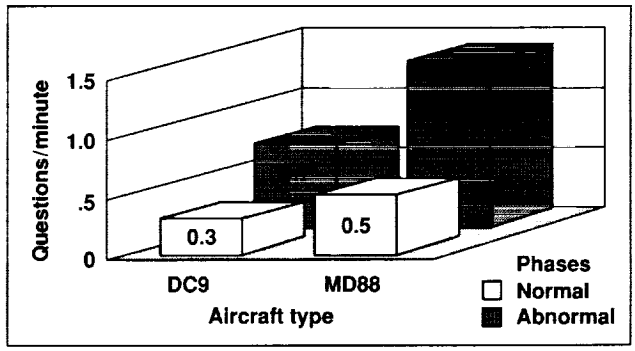


*Fig. 1. Time-adjusted frequencies of crewmember questions, by aircraft type and normal/abnormal phase.*

**Ames-Moffett contact: B. Kanki**
**(415) 604-5785**
**Headquarters program office: OSSA/FAA**

# Information Management and Transfer

**Sandra Lozito, Kevin Corker**

In previous work, the influence of message length and textual format type on communication accuracy and timing were examined in a part-task simulation. This year, an experiment was completed in the Advanced Concept Flight Simulator (ACFS) in a full-mission simulation environment to investigate the performance impact of, and human/system response to, data-linked air traffic control (ATC) and automated flight deck operations. The subjects were twenty pilots (ten crews) from a major U.S. air carrier. The method of data link used was similar to the data-link implementation plans for a next-generation aircraft, and included the capability to review ATC messages and directly enter ATC clearance information into the aircraft systems. Each crew flew experimental scenarios in which data on communication timing, errors and clarifications, and flight procedures were collected. The data on errors and clarifications revealed an interaction between communication modality (voice versus data link) and communication type (air/ground versus intracrew). Results also revealed that voice crews initiated ATC contact significantly more often than data-link crews. Data-link crews performed significantly more extraneous activities during the communication task than voice crews. Descriptive data indicate that the "pilot not flying" accessed the review menu most often, and suggest that pilots had difficulty in accessing the target message within the review-menu structure.

A full-mission simulation, using the Advanced Concept Flight Simulator (ACFS), was designed and has begun. This experiment is intended to explore the integration of data-link technology and air-traffic-control automation. Specifically, the ACFS has been enhanced through the development of the Flight Management System, adding vertical navigation automation, and adding data-link implementation capabilities. To complement these flight deck enhancements, the Man-Vehicle Research Facility (MVSRF) has also integrated Center-TRACON Automation System (CTAS), an ATC advisory tool developed at Ames.

**Ames-Moffett contact: S. Lozito**
**(415) 604-0008**
**Headquarters program office: FAA**

# Perceptual Grouping with Head-Up Displays

**Robert S. McCann, David C. Foyle, James C. Johnston**

Head-up displays (HUD) project instrument information onto a combined glass superimposed on the pilot's forward field of view. It is commonly assumed that HUDs allow the pilot to simultaneously process HUD information and scene information because both sources of information are in the pilot's forward field of view. However, this assumption is challenged by evidence of performance deficits under conditions of divided attention. For example, some investigators have found that detection of runway incursions occur less often with HUDs than with head-down displays, contrary to what would be expected if the HUDs promoted simultaneous processing of HUD and scene information.

In a recent experiment, we tested an explanation for this concurrent-processing deficit. Subjects viewed a simulated approach to a runway on which HUD-like symbology was superimposed (illustrated in the first figure). Each trial began with subjects monitoring either the HUD or the runway for the presence of a three-letter cue (either IFR or VFR). If the cue was IFR, they searched for a target stimulus (stop-sign shape or diamond) among a set of geometric forms on the HUD. If the cue was VFR, they searched for the target among a set of forms on the surface of the runway.

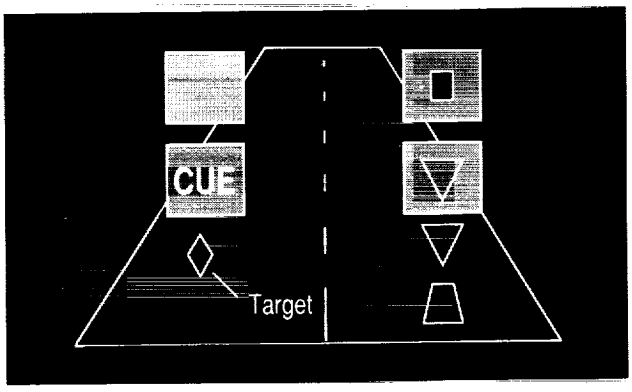


*Fig. 1. Schematic of flight symbology superimposed on an "out-the-window" view corresponding to the runway on final approach.*

The experiment included two kinds of trials: within-domain trials, in which the cue and the target belonged to the same domain (HUD or world), and between-domain trials, in which the cue was part of one domain and the target part of the other. Subjects' responses were faster in within-domain trials than in between-domain trials. An explanation for the between-domain processing penalty assumes that because of the many perceptual cues that distinguish HUDs from the outside scene, the visual system treats the HUD as one perceptual group (the "near domain") and the outside visual scene as another perceptual group (the "far domain"). Attentional limits then prevent subjects from paying attention to both domains at the same time. In between-domain trials, attention must be shifted from the domain containing the cue to the domain containing the target, producing delays in finding the target. In within-domain trials, no switching is necessary, so there are no delays.

The purpose of the present study was to determine which perceptual cue was most responsible for perceptual grouping (and the resulting between-domain processing penalty). Two such cues were particularly salient: color (the HUD was presented in light blue and the world in light yellow) and motion (scene-linked objects appeared to be in motion, consistent with the perceptual changes that accompany normal descent, whereas the HUD symbology was stationary). Accordingly, the present experiment replicated the task described earlier while varying the presence or absence of color cues (either the HUD and the world appeared in different colors, or they appeared in the same color) and the presence or absence of differential motion cues (either the visual scene appeared as it would during final approach, or the scene was "frozen" at a point corresponding to about 4 seconds prior to touchdown). The results of the motion experiment, summarized in the second figure, reveal that the between-domain processing penalty was reduced by 50% when differential

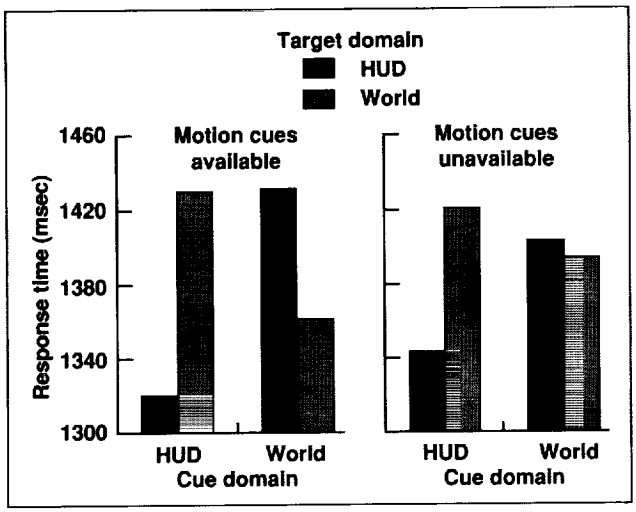


*Fig. 2. Performance results from the motion experiment.*

motion cues were removed from the display. No effects of the presence or absence of the color cues were found.

These results have direct implications for HUD design. They suggest that when a pilot is engaging in phases of flight that require concurrent monitoring of HUD symbology and the outside world, relevant HUD symbology should be made fully conformal with the world. That way, the symbology will be integrated with the natural flow field of the far domain, and should be perceptually grouped with the world rather than with the remaining HUD symbology.

**Ames-Moffett contact: R. McCann**
**(415) 604-0052**
**Headquarters program office: OA**

## A Flight-Management-System Vertical Navigation Tutor

**Christine Mitchell**

Vertical navigation capabilities of the flight management system (FMS) in modern "glass-cockpit" aircraft are often underutilized or misused by pilots. This can be attributed at least in part to an inadequate understanding by pilots of how the FMS interprets and executes a flight plan that a pilot has entered. This project combines a unique vertical profile display with a part-task airline transport simulator. The display provides an otherwise unavailable visual representation of FMS and other vertical navigation (VNAV) modes of the aircraft. A control architecture is embedded into the system to allow the creation of routine flights which the tutor uses as lessons that address key training issues. The tutor controls flight scenarios that help the student pilot explore the content of the FMS vertical profile, FMS execution of that profile through use of the VNAV function, interaction between FMS and other VNAV modes, and the use of FMS VNAV by the pilot for the completion of various in-flight maneuvers. The system is being evaluated on site in the flight training department of a U.S. airline. The evaluation takes approximately six hours per pilot. The initial session is used to assess the subject's knowledge of FMS and VNAV: a formal questionnaire is administered. Four training sessions with the VNAV tutor follow. The tutorial environment consists of the two-monitor 757/767 simulator, augmented with voice- and text-based air traffic control and tutorial messages, and a third monitor which contains the VNAV Profile Display. After the four tutorial sessions, the pilot flies a fifth (evaluation) session that does not incorporate the tutor or the VNAV Profile Display. This fifth session has periodic interruptions at predetermined points in order to allow the experimenter to ask the pilot specific questions to assess VNAV awareness regarding the state of the FMS and other autoflight equipment. These questions are used to determine the subject's understanding of the training material.

Next, a questionnaire is administered that is similar in content to the one used prior to the first session. Comparison of the answers on the two questionnaires serves as a primary source of data in the evaluation. The evaluation of a particular subject concludes with solicitation of the pilot's reactions and opinions about the VNAV tutor.

Christine Mitchell is at the Georgia Institute of Technology.

**Ames-Moffett contact: E. Palmer**
**(415) 604-6073**
**Headquarters program office: OA**

## Crew Activity Tracking System

**Christine Mitchell**

Three requirements for the design of human-centered automated systems were set forth by NASA researcher Charles Billings. First, the human operator must be able to monitor the automated system. Second, the automated system must be able to monitor the human operator. And, finally, each of these two elements must have knowledge of the other's intent. Billings pointed out that cross monitoring can only be effective if the intentions of the human or automated systems are known. Researchers at Georgia Tech are exploring one method of meeting this requirement. They are developing an activity-tracking system that attempts to understand the activities performed by crews of glass cockpit aircraft. The activity tracker focuses specifically on activities that affect the mode awareness of the crew, such as autoflight mode selection and engagement, and associated planning and monitoring activities. The technology will include systems that can provide crews with context-sensitive advice, reminders, and assistance based on dynamic understanding of pilot intent.

The Crew Activity Tracking System (CATS) uses a task-analysis model of crew–automation interactions as its source of knowledge about crew activities. The model of crew activities is structured as a functional decomposition: each phase of flight is decomposed into crew functions which are, in turn, decomposed into subfunctions, autoflight mode selections, tasks, subtasks, and, at the lowest level, observable actions. Each activity in the model has an associated set of conditions for determining the activity's status that is based on the occurrence of a particular event or set of events. By noting the status of activities in the model (e.g., "active," "pending," "done"), a useful description of the crew's current activities is produced. The CATS system analyzes real-time data from a part-task airline transport simulator. CATS accepts aircraft and autoflight system state data, along with data about actions performed by the pilots "flying" the simulator. These data are used to generate predictions and explanations about the activities in real time.

An evaluation will be conducted in which airline pilots fly the part-task simulator. The data obtained will include concurrent verbal protocols from the pilots to be used in assessing the degree of match between the predictions and explanations of CATS and those of the pilots. This phase of the study will be used to validate empirically the adequacy of a computer-based activity-tracking system for correctly inferring operator intent.

Christine Mitchell is at the Georgia Institute of Technology.

**Ames-Moffett contact: E. Palmer**
**(415) 604-6073**
**Headquarters program office: OA**

# Three-Dimensional Primary Flight Display with Terrain Information

**Christine Mitchell, Everett A. Palmer**

An important world-wide aviation safety problem is still the controlled-flight-into-terrain (CFIT) accident. Area-navigation and on-board terrain-elevation data bases offer the potential for improved cockpit displays near terrain.

We have developed a prototype primary-flight-display format designed to reinforce the pilot's model of both lateral and vertical navigation in near-terrain situations. This new display format is referred to as the spatial situation indicator. Specific emphasis has been placed on the terminal phase of flight, with terrain modeling in the vicinity of the destination airport.

The unique design incorporates perspective symbology that depicts the aircraft's predicted position and terrain clearance information for up to 75 seconds ahead of the aircraft. Projection of the flightpath is based on a "fast time" modeling technique described by Grunwald. Traditional flightpaths use the tunnel-in-the-sky approach which presents no reference to the ground elevation. The technique developed for this research uses roll-stabilized vertical lines ("whiskers") positioned at 15-second intervals out to 75 seconds. The figure illustrates the virtual whiskers and flightpath. The whiskers are displayed in equally spaced pairs so that in steady, level flight a perspective path is projected. The whiskers are color coded using green and yellow. The green lower portion (banded in the figure) extends from the aircraft altitude predicted at that interval to the terrain below. Its length therefore is a direct representation of the terrain clearance at that point in the aircraft's path, given no changes in flightpath.

The display also incorporates a dynamically color-coded terrain grid. This color coding is based on predicted aircraft elevation and terrain spot elevations. Dark green is used for safe terrain and dark red for dangerous terrain. The terrain grid is composed of a mesh of triangles, each triangle with sides representing 2 nautical miles. Man-made

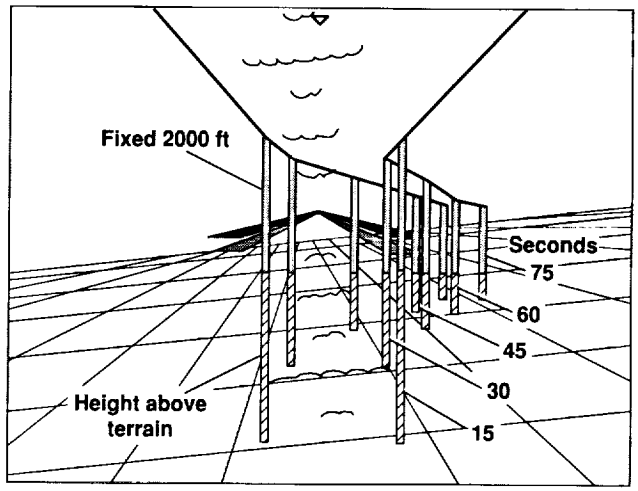


*Fig. 1. Flight display showing projected flightpath.*

obstructions such as radio towers are shown on the terrain grid. Information for building the terrain and obstruction files is obtained from the approach plates for each runway in the scenario.

An experimental evaluation of the display is being conducted by a major U.S. airline. Experiment participants are glass-cockpit flight instructors. Each subject, after training to familiarize himself or herself with the part-task aircraft simulator and interface, will fly three scenarios based on actual controlled flight into or toward terrain as described in a 1991 study by Bateman.

Each participant will use one of three displays: a baseline cockpit display, a primary flight display, or the display with flightpath predictor and ground terrain information. A total of eighteen pilots will participate, six with each display. Attention-diverting tasks are implemented to match as closely as possible the scenarios as they were described by Bateman. Air-traffic-control (ATC) communications are implemented using simple voice communications without supporting electronic intercoms. The experimenter

carries out the ATC communications. The goal of the experiments is to measure how quickly pilots can detect dangerous terrain with the three different display formats. Response time of the pilot for corrective action is recorded, as well as mode control panel inputs.

Christine Mitchell is at the Georgia Institute of Technology.

**Ames-Moffett contact: E. Palmer**
**(415) 604-6073**
**Headquarters program office: OA**

## Team Decision Making in the Cockpit

**Judith Orasanu, Ute Fischer**

Accident and incident reports document the importance of crew judgment and decision making to flight safety. Crews must make decisions when faced with system malfunctions, in-flight emergencies (fires, decompressions, medical problems), bad weather, or airport congestion. Many decisions are aided by checklists, manuals, company procedures, and ground-based support. However, cases often arise for which no guidance exists, or problems cascade. In order to train crews to cope with these situations, or to design cockpit systems to aid decision making, a thorough understanding is needed of the decisions crews actually have to make, sources of difficulty, and factors that ensure good decisions.

The goals of our research are to (1) specify the features of situations that require crew decisions, (2) identify the cognitive demands posed by various types of decisions, (3) define the types of errors likely to be made and the factors that make decisions difficult, and (4) identify effective crew problem-solving and decision-making strategies. Several related approaches are being taken to address these goals:

1. Develop a decision taxonomy to classify types of aeronautical decision tasks
2. Develop a process model of aeronautical decision making
3. Analyze and classify in-flight decisions reported to the Aviation Safety Reporting System (ASRS) using the taxonomy developed
4. Analyze aircrew performance in full-mission simulators to identify strategies associated with effective performance
5. Analyze crew errors detected in National Transportation Safety Board accident reports and simulator performance analyses

Six types of decisions have been identified (see table) based on the following two primary variables that characterize decision problems in the cockpit: (1) ambiguity of cues signaling the problem and (2) response availability. Risk and time pressure serve as constraints on decision processes and amplifiers of problem difficulty. The six types of decisions have been used as a frame for analyzing 94 incidents concerning in-flight decisions reported by flight crews to the ASRS.

Preliminary taxonomy of cockpit decision types

Rule-based decisions (If x, then y)
1. Go/no go (if conditions are normal, continue with planned action OR if condition x exists take alternate planned action)
2. Condition-action (recognize situation x, retrieve preplanned response y)

Adaptive decisions/well structured
3. Choice (multiple response options available; choose one)
4. Scheduling (multiple responses required; prioritize and schedule all)

Adaptive decisions/ill structured
5. Procedural management (unable to diagnose situation; treat as if emergency and take appropriate action)
6. Creative problem solving (diagnose situation; create solution)

The reports have been analyzed according to precipitating events, type of decision, and phase of flight during which the decision was made. Most decisions were precipitated by an aircraft system problem (69%). The focus of the largest percentage of the decisions (43%) was whether and how to change the flight plan (e.g., reject takeoff, divert). Of the six types of decisions, over half (54%) were rule-based (13% Go/No Go, 41% Condition-Action). Choice decisions accounted for 35%, Scheduling 5%, Procedural Management 3%, and Creative Problem Solving 2%. Contrary to typical findings concerning occurrence of accidents, the largest percentage of the decisions were made during the cruise phase of flight (32%). Only 6% were made during takeoff, and 17% during approach and landing. While the ASRS reports should not be seen as a statistically representative sample of all in-flight decisions, they do provide a broad picture of the diverse types of events and decisions that crews have actually encountered in flight.

The decision taxonomy has also been used to specify the cognitive requirements associated with various decisions embedded in scenarios used in studies of full-mission simulators. From these studies we are identifying strategies that are associated with low-error crew performance. The taxonomy is also being used as a frame for characterizing errors, both in the simulator and in accident reports by the National Transportation Safety Board.

Several airlines are using the decision taxonomy in their crew resource management (CRM) courses. It serves to highlight the differences in response requirements and the errors likely to be associated with each type of decision and to sensitize crews to the need for good situation assessment before decisions are made.

**Ames-Moffett contact: J. Orasanu**
**(415) 604-3404**
**Headquarters program office: FAA/OSSA**

## Modeling the Cognitive Activities in Launch Control Operations

**Roger Remington**

Models have been developed previously that describe the cognitive activities necessary for human operators to perform orbiter launch activities. Corresponding research in 1993 has focused on elaborating the cognitive basis of these models. For example, a model of visual search was developed that describes the eye movements, reading patterns, and internal decisions required to find information on a printed page. Coupled with an existing model of page turning, our cognitive model NTD-Soar now simulates a major component of the NASA Test Director's visual information gathering.

The most significant addition to the NTD-Soar model has been the implementation of a natural-language-understanding component. A model of natural language processing, NL-Soar, developed at Carnegie–Mellon University, has been integrated into NTD-Soar. To comprehend an utterance, the NL-Soar component combines syntactic rules that parse utterances using semantic rules that relate the linguistic information to the current context. The result of comprehension is a model of the situation updated to include the meaning of the utterance. The situation model is a nonlinguistic structure that can be used to support reasoning by other components of NTD-Soar. The integration of NL-Soar increases the flexibility of NTD-Soar and should permit it to handle a broad range of anomaly conditions.

Work in progress includes the implementation of a model of human visual selective attention as well as the development of routines for reasoning from the situation model produced by NL-Soar.

**Ames-Moffett contact: R. Remington**
**(415) 604-6243**
**Headquarters program office: OA**

## Fatigue Education and Training Module

**Mark R. Rosekind, Philippa Gander, J. Victor Lebacqz**

The first education and training module on fatigue in flight operations was developed by the Fatigue Countermeasures Program at Ames. The module, entitled "Alertness Management in Flight Operations," has now been presented 21 times to about 1,550 individuals. Presentations have been made for airlines, safety forums, military groups, the National Transportation Safety Board, and industry groups. Interest has been shown by these organizations in using the information for personnel training. Two workshops on implementation of the Fatigue Module have been held at Ames. Three workshop dates for 1994 have been established. We continue in our efforts to educate the aerospace industry about the factors that affect fatigue in flight operations, to provide training on specific fatigue countermeasure strategies, and through their use, to improve flight safety.

A new study is under way in collaboration with the Federal Aviation Administration to examine fatigue in regional airline operations.

**Ames-Moffett contact: M. Rosekind**
**(415) 604-3921**
**Headquarters program office: FAA/OA**

## A.C.T.: Activity Catalog Tool Software

**Leon D. Segal, Anthony D. Andre**

The Activity Catalog Tool (A.C.T.) has been used to analyze cockpit activity in full-mission flight simulations, pilot scheduling strategies during simulated instrument flight, and emergency/police dispatch operations.

A.C.T. is a software tool that we designed for recording and analyzing sequences of activity over time. It runs on the Macintosh® platform. The software is an aid for researchers interested in observing and understanding human behavior in field settings, and can be used to analyze video or audio recordings of behavior. The program is focused on two primary areas: human–machine interactions and interactions between humans. It provides a means by which an observer can record an observed sequence of events, logging such parameters as frequency and duration of each event. The program provides the user with a quantified description of the observed sequence through application of a basic set of statistical routines. It enables merging and appending of several files, and extensive analysis of the resultant data.

**Ames-Moffett contact: L. Segal**
**(415) 604-0011**
**Headquarters program office: OA**

## Design of Propane Supply System Control Panel

**Leon D. Segal, Anthony D. Andre**

Researchers from the Rotorcraft Human Factors Research Branch were asked to assist in designing a control panel for the propane system used in the High Speed Research (HSR) program in the National Full-Scale Aerodynamics Complex. The HSR testing focuses on the analysis of acoustic data produced by a propane-driven jet engine. We were asked to identify human-factors issues that might affect the use of such a system, and to assist in the design of the actual interface, a computer-generated control screen that is new to the HSR wind tunnel facility. Our goal was to design an interface that would be informative, simple, and intuitive. A control panel was designed after extensive interviews with the operators of the system; established human-factors design guidelines were used. The design process included generation and evaluation of multiple display prototypes, and iterative design reviews with the program's test director and systems engineer.

The control panel is now in place in the control room of the Ames 40- by 80-Foot Wind Tunnel.

**Ames-Moffett contact: L. Segal**
**(415) 604-0011**
**Headquarters program office: OA**

## The Importance of Nonverbal Information in the Automated Flight Deck

**Leon D. Segal, Barbara Kanki**

Crew Factors has recently expanded its focus on communication to include nonverbal behaviors that are highly associated with speech. We have analyzed data from a high-fidelity simulation study in which three different types of checklists were used: (1) paper; (2) electronic–manual, on which the user controlled each checklist item; and (3) electronic–automatic, on which the system automatically performed some checklist items.

Analyses showed no differences in the amount of verbal communication used with the different checklist types, but there was significantly more nonverbal activity observed with both electronic checklists. The increases in the ratio of nonverbal activity to verbal communication with the electronic checklists are shown in the first figure, which also highlights the fact that the differences are greatest for the "pilot not flying," i.e., the pilot performing the checklist duty. On the other hand, analyses also showed that monitoring of the pilot not flying by the

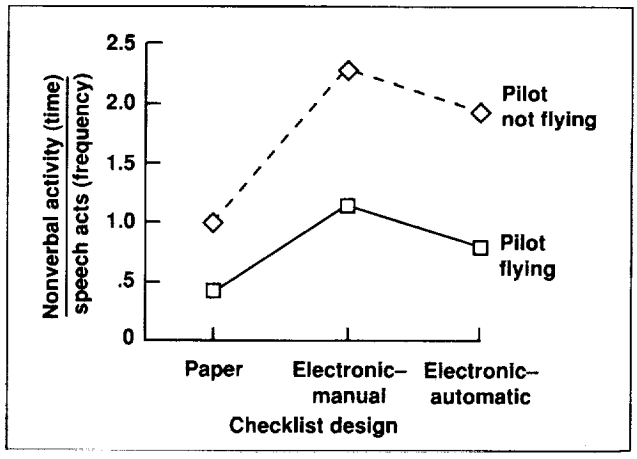


*Fig. 1. Effect of checklist design on nonverbal activity.*

"pilot flying" is greatly increased when the electronic checklists are used (second figure). The results indicate that the nonverbal, visual interaction between the pilots may play an important role in information exchange in the automation-enhanced flight deck. Since effective communication and successful information exchange is crucial to overall team performance, we must anticipate the changes that may result from new technologies in order to facilitate rather than inhibit the communication process. The role of nonverbal communication is expected to have implications for pilot training (e.g., the identification of effective strategies) as well as for future multioperator workstation design.

**Ames-Moffett contact: L. Segal**
**(415) 604-0011**
**Headquarters program office: FAA/OA**

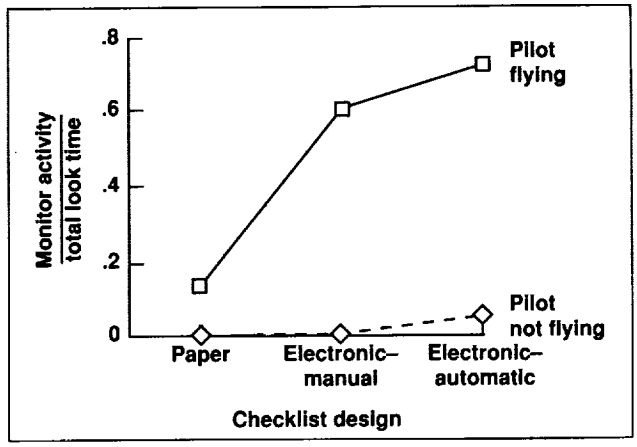


*Fig. 2. Effect of checklist design on monitoring activity.*

## Glass-Cockpit Simulator for Human Factors Research

**Robert J. Shiner**

The glass-cockpit flight simulator, shown in the photograph, was installed this year for operation by the Full-Mission Simulation Branch. The simulator is shown in its baseline (actual aircraft) configuration. In stand-alone operation, it gives the flightcrew the full functionality of a current-technology Boeing 747-400 aircraft flight deck. The simulator, located in the Man–Vehicle Systems Research Facility, is being further configured to support human factors research on issues associated with modern technology in transport aircraft operations.

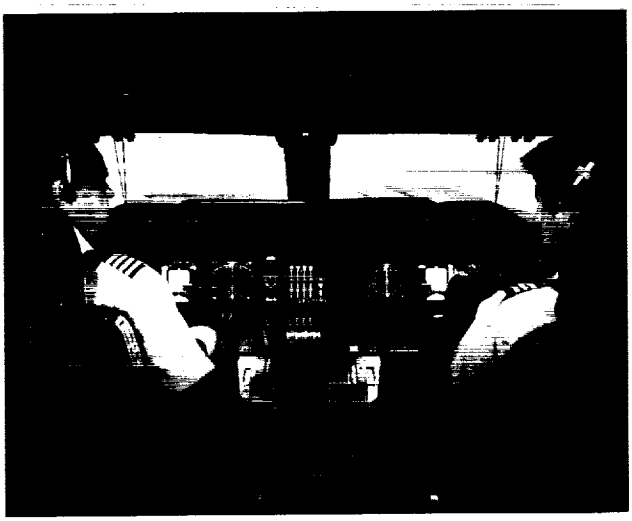

*Fig. 1. Crew station in the glass-cockpit flight simulator.*

The special capabilities of the simulator include normal interactions with air traffic controllers in a fully simulated air traffic environment. Data interchange capabilities permit the aircraft simulator to participate in multiple-aircraft studies with both local simulators and those of other agencies.

After certification by the Federal Aviation Administration, the simulator will support research goals through its enhanced capability to monitor crew and aircraft performance. This capability, coupled with reliable recreation of simulated events through programming and scripting, enables researchers to obtain results from multiple flightcrews and to look for trends in the crews' handling of situations.

The B747-400 simulator has joined the Advanced Concepts Flight Simulator, already in operation. Here, the "conceptual" technology can address possible ways to improve air safety, reduce pilot workload, improve communication among system elements, or lessen crew fatigue.

The new simulator models all aircraft system functions and can simulate a wide variety of weather, visibility, airport, and time-of-day environments. It can also introduce simulated equipment malfunctions for the flightcrew to contend with. Crew performance can be compared in routine, high-workload, and emergency circumstances. The system's high fidelity allows generalization of research findings to the real world of flight operations.

The simulator will also be used in research programs that are part of the National Plan for Aviation Human Factors.

**Ames-Moffett contact: R. Shiner**
**(415) 604-0257**
**Headquarters program office: FAA/OA**

## Man–Machine Integration Design and Analysis System

**Barry R. Smith**

The man–machine Integration Design and Analysis System (MIDAS) is a joint Army–NASA research effort, begun in 1984, to develop computational models for the design of advanced-technology crew stations. The system contains over 400,000 lines of code, and operates on a high-end Silicon Graphics workstation. MIDAS contains a suite of embedded models of human performance (e.g., vision, memory, decision making, and anthropometry) which operate within symbolic and three-dimensional (3-D) computer graphic representations of cockpit equipment and operator tasks. The resulting simulation provides a useful environment for evaluating human–system performance during conceptual design. The past year included several technology-transfer highlights.

**Boeing**. The MIDAS development staff has been collaborating with Boeing Helicopters through a NASA Technical Exchange Agreement (TEA) signed in 1991. The objective of the TEA is to transfer MIDAS code to Boeing, where feasible, to be used in their human engineering design process. In return, Boeing provides real-world user feedback, detailed design and operating requirements information, and applications data to the Ames researchers. MH-47E helicopter data provided by Boeing was used to demonstrate MIDAS capabilities to over 100 visitors in 1993. In addition, extensions and modifications to the MIDAS code are implemented collaboratively. Significantly more software engineering and crew station design expertise has been brought to the project by this collaborative arrangement. Boeing has approximately 60% of the MIDAS code. This includes models for assessing cockpit accommodation (reach, fit), visibility, and legibility, and tools for assessing projected operator workload and for producing animated, 3-D computer graphic controls and displays. Boeing Helicopter is considering the use of MIDAS for their proposed Medium Lift and Vertical Terminal Area Procedures (VERTAPS) programs.

A similar effort has recently begun with the Flight Deck Research group of Boeing Commercial Airplanes. Several components of MIDAS are under study for possible use on their emerging civil transport programs.

**Communications Research Company/Richmond Police Department.** The Communications Research Company (CRC) and NASA Ames Research Center signed a Cooperative Research and Development Agreement (CRDA) in 1993 to adapt and apply MIDAS, as well as other Army–NASA aeronautical human factors tools and expertise, to public safety

technology used by police and fire departments. CRC is a local small business that designs and integrates high-speed wireless communication and navigation systems for emergency response vehicles and 911 dispatch stations. These systems have begun to incorporate cockpit-like technology, such as digital voice data, electronic moving maps, geographic information systems, and satellite-based navigation aids. Because of the similarities between aviation and civil emergency response (complex equipment and high-stress, high-workload tasks) this CRDA will apply human factors methods, empirical findings, and software tools, including MIDAS, to the emergency-response field. The Police Department of Richmond, a local municipality, has also requested the assistance of the Computational Human Engineering Research Office with this endeavor, because they will be a user of future CRC systems. The Richmond Police Department has agreed to make subject matter experts available to Ames researchers, allow observation of actual police/dispatch operations, and serve as a site for field trials of candidate designs developed during this cooperative agreement. MIDAS has been used to replicate 911 dispatch console geometry and to create a prototype of a graphical dispatch decision aid.

**Westinghouse Science and Technology Center.** Westinghouse is engaged in the design of the next-generation nuclear power plant, called the AP600, which is sponsored by the Department of Energy. The conceptual design of the plant is under way, and the Advanced Science and Technology Division has expressed significant interest in cooperating with MIDAS personnel at Ames in applying our tools and models to the power plant console design. The new design is a passive water reactor which is safer and requires fewer personnel as a result of increased automation in monitoring and malfunction diagnosis. MIDAS will be used to create prototypes of operator procedures, advanced checklists, and alternative display designs for a capabilities demonstration planned for late November at Westinghouse. This collaboration will extend the MIDAS application base, link MIDAS to a diagnostic reasoning program that simulates human cognitive function (developed by Westinghouse), and support joint empirical evaluation of the resultant design in full-plant simulation facilities at Westinghouse's Pittsburgh, Pennsylvania site.

**Ames-Moffett contact: B. Smith**
**(415) 604-4264**
**Headquarters program office: Army**

## Visibility of Discrete-Cosine-Transform Quantization Noise

**Andrew B. Watson, Albert J. Ahumada, Jr.**

The Earth Observing System is expected to generate in excess of one terabyte of image data per day. Efficient image-compression techniques will be needed to manage this great flow of imagery. The discrete cosine transform (DCT), the basis of a widely-used compression technique, underlies several emerging international standards for image compression. The artifacts generated by this technique are samples of DCT quantization noise. DCT quantization noise can be produced by uniform random perturbation of each DCT coefficient in each block of an otherwise uniform gray image. A sample of this noise consists of an array of blocks within each of which each DCT basis function has a random amplitude within some range. The ranges of all frequencies except one may be set to zero to produce noise of only a single DCT frequency (see first figure). The visual quality and fidelity of the compressed imagery depends on the visibility of this noise.

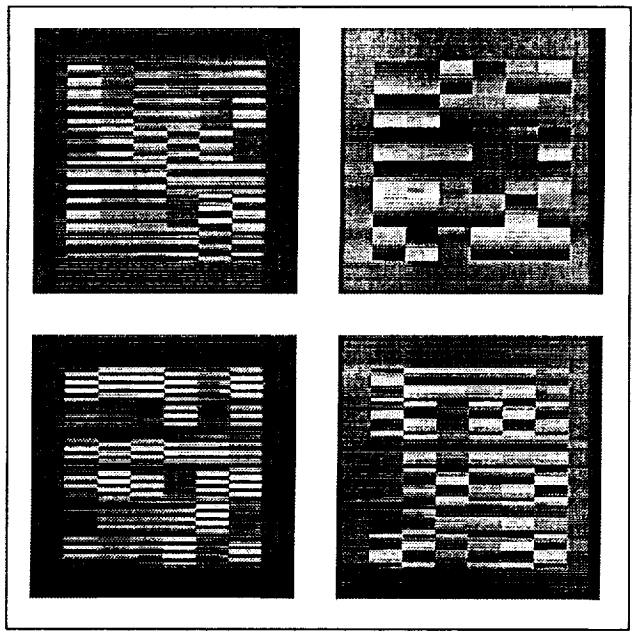

*Fig. 1. Four examples of DCT quantization noise. Each is a 6 × 6 array of basis functions with uniformly distributed amplitudes. The DCT frequencies of the four examples are (0,1), (0,3), (0,5), and (0,7).*

As part of our larger effort (conducted in collaboration with IBM) to apply modern, model-based human-factors principles to DCT-based compression, we have measured the visibility of DCT quantization noise. In particular, we have studied the effects of spatial frequency, display resolution, spatial summation, frequency summation, and contrast masking. The second figure shows the effect of spatial frequency on DCT noise visibility. Other results show that visibility increases as the fourth root of the number of basis functions (image size), and that contrast masking extends over more than an octave of DCT frequency. Display resolution influences visibility in ways that are largely predictable from image size and spatial frequency. We have incorporated the results into our mathematical model of visibility of DCT compression artifacts. These results will allow systematic perceptual optimization of image compression in NASA imaging systems.

**Ames-Moffett contact: A. Watson**
**(415) 604-5419**
**Headquarters program office: OA**

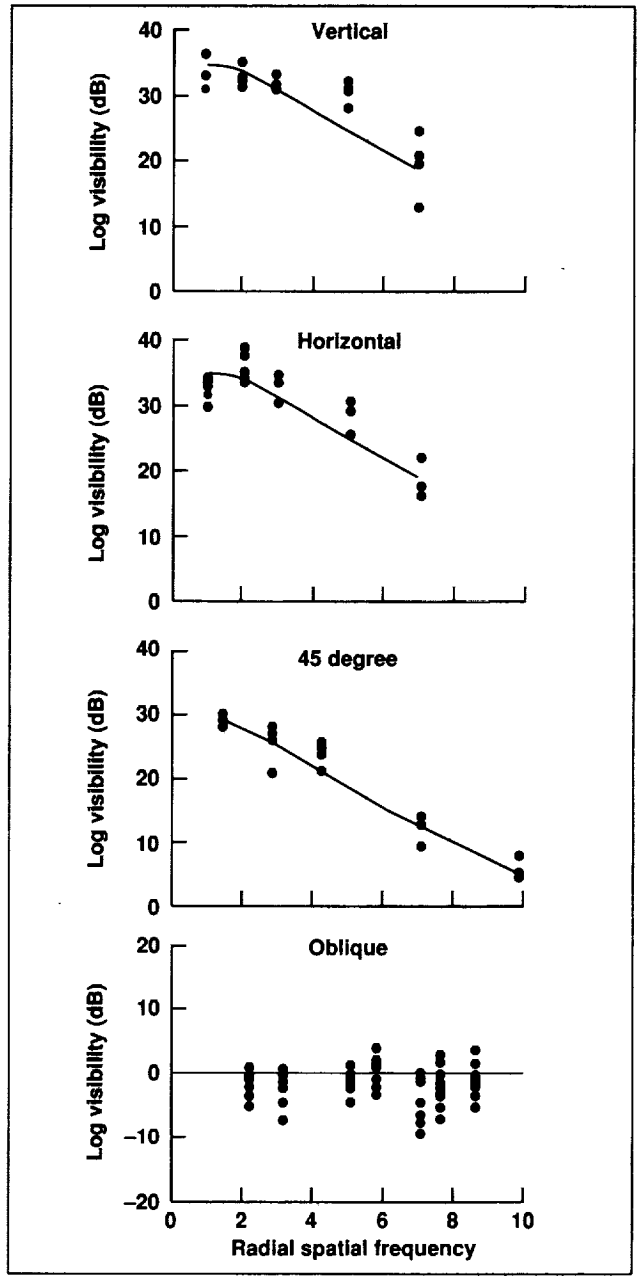


*Fig. 2. Measurements of visibility of DCT basis functions for five observers at a display resolution of 32 pixels/degree, as a function of the spatial frequency of the basis function. Data are plotted separately for vertical, horizontal, 45-degree, and oblique basis functions. The curves in three of the panels show the best-fitting model; in the fourth panel, departures from the model are shown for the oblique frequencies only.*



C-2.

# The Design of Flight-Deck Procedures

**Earl Wiener, Asaf Degani**

Training, standardization, and actual operations in complex human–machine systems depend on an elaborate set of procedures that are specified by management. These procedures indicate the manner in which management intends to have various tasks performed. The intent is to provide guidance and standardization to the operator in order to ensure an orderly, predictable, safe, and efficient means of carrying out these tasks. However, the procedures can become a hodgepodge, with little internal consistency and logic. This is particularly true when an organization operates various pieces of equipment that have been acquired at different times, and for which procedures have been specified by various persons, often under various managements. For example, an airline in the United States may operate fleets of aircraft from 1960s technology (DC9-30) to 1990s technology (B747-400). There may be little consistency between the procedures for the different fleets, or even for various models within fleets. Inconsistent or illogical procedures may lead to nonconformity by flightcrews, and difficulty in transition training for pilots moving from one aircraft to another. In spite of its importance, a basic methodology for procedures has not been examined by the human factors community. This study examines the issue of procedurization from a broad viewpoint. We recommend a process that we call "the four P's": philosophy, policies, procedures, and practices. An organization that commits to this process can create a set of procedures for its fleet that is more internally consistent, that will be better respected by the flightcrews (hence leading to greater conformity), and that will reduce the cost of transition training. The four-P's process is the result of line observations; extensive interviews with airline management, line pilots, and one major manufacturer; and an examination of accident and incident reports involving deviations from standard operating procedures. We have prepared a report that describes the process. Although the report is based on airline operations, we believe that the principles are applicable to other high-risk enterprises, such as nuclear power plants, space flight, law enforcement, military operations, and high-technology medical practice.

Asaf Degani is affiliated with the San Jose State University Foundation and Earl L. Wiener is at the University of Miami.

**Ames-Moffett contact: E. Palmer**
**(415) 604-6073**
**Headquarters program office: OA**

# Integrated Flight/Propulsion Control System Design for ASTOVL Aircraft

William W.Y. Chung

Two integrated flight/propulsion control (IFPC) design methods, applied to the Lockheed Fort Worth Company (LFWC) E-7D short-takeoff-and-vertical-landing (STOVL) fighter with augmented-lift capability (first figure), were evaluated on the Ames Vertical Motion Simulator. One design method is based on explicit model-following with the Linear Quadratic Regulator (LQR) state space design developed by LFWC. The other design method is based on the implicit state-rate feedback and the nonlinear inverse transformation developed by Ames. Two control inceptor configurations (second figure) were also evaluated for approach, precision hover, and vertical-landing flight operations.

Both designs performed well within the operational envelope of the propulsion system. However, both designs experienced deficiencies in control robustness when nonlinear characteristics of the propulsion system were encountered. The problems were all associated with control limit protection or antiwindup protection in the proportional and integral part of the flight control system. After the

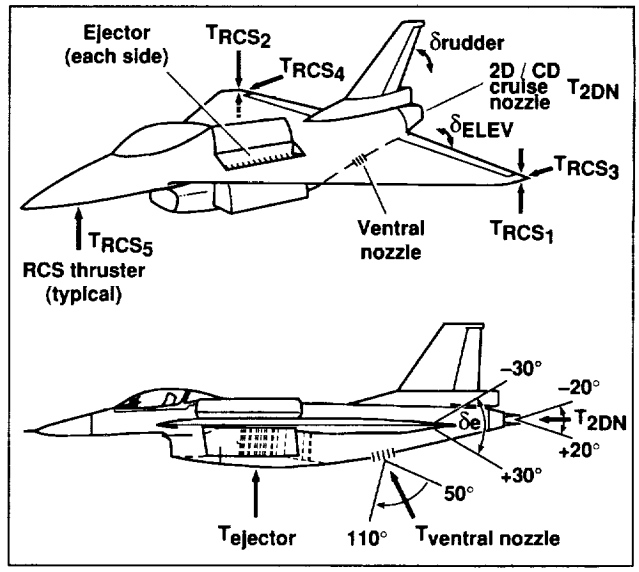


*Fig. 1. Lockheed Fort Worth Company E-7D STOVL aircraft design. (T = thrust; RCS = reaction control system.)*

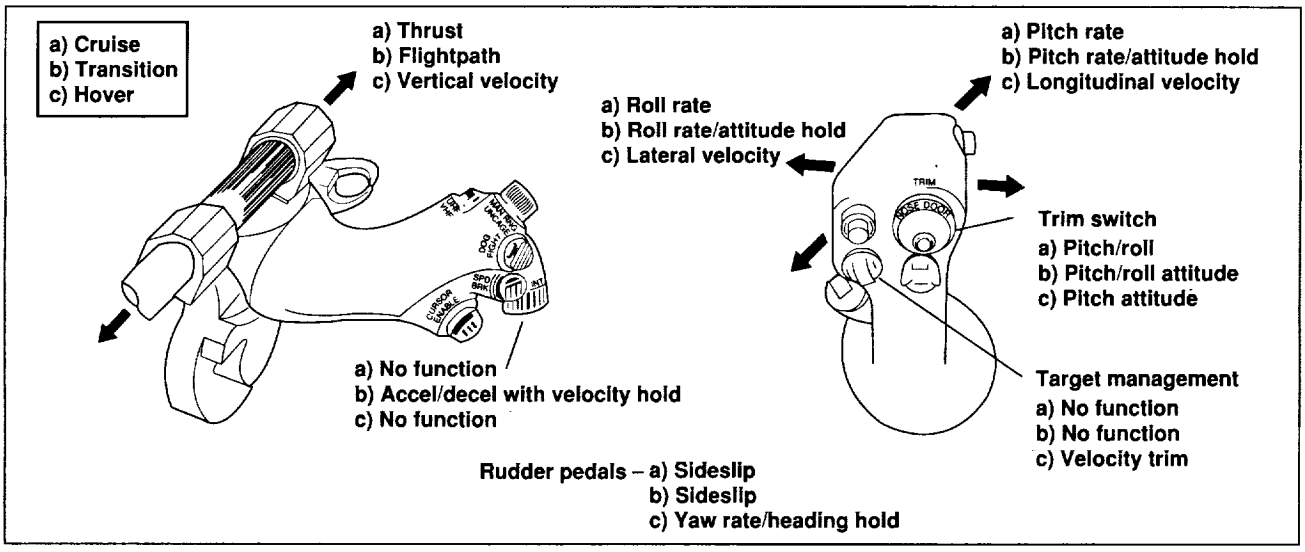


*Fig. 2. Control inceptor/command configurations.*

corrections, the Ames design performed well from transition to hover. Because of time constraints, the LFWC design was evaluated for hover only, and it performed well.

The piloted simulator evaluations highlighted several areas that require improvement in the vehicle design. The evaluation of the control inceptor configurations showed a pilot preference for full-authority engine power control before direct-lift authority was made fully available by the integrated control system. The side-stick force controller was judged unacceptable for precision maneuvers primarily because of its location and orientation in the cockpit. These factors caused undesirable cross coupling which led to increased pilot work load.

The focus of future Ames research efforts on advanced STOVL (ASTOVL) fighter design is to define control power and pitch-coupling control requirements for a lift-fan ASTOVL aircraft configuration, develop a throttle-control configuration for jet-borne flight operation, and generate requirements for control sensitivity of the side-stick force controller.

**Ames-Moffett contact: W. Chung**
**(415) 604-6002**
**Headquarters program office: OA**

## Pilot-Directed Guidance Evaluation

**Richard Coppenbarger**

A fixed-base simulation of an automated rotorcraft obstacle-avoidance system for pilots flying nap-of-the-Earth (NOE) missions was recently carried out on the Ames Vertical Motion Simulator. The evaluation involved a novel concept in rotorcraft control referred to as pilot-directed guidance (PDG). In PDG, pilot inputs are used to control the outer-loop guidance of the vehicle, i.e., to establish a desired direction of travel. An inner-loop obstacle-avoidance system that depends on data from onboard sensors is responsible for supplying whatever additional control inputs are necessary to achieve required obstacle clearance margins. In addition to obstacle avoidance, the PDG system provides for terrain following and airspeed control. The goal of the PDG automation is to reduce the excessive pilot work load often encountered in NOE flight, and thereby increase mission safety and effectiveness.

The simulation incorporated a visual data base constructed from Defence Mapping Agency (DMA) terrain data from the U.S. Army's Hunter-Liggett training facility in California. Numerous trees were randomly added to the data base to provide an obstacle-rich environment. Helmet-mounted display symbology similar to that shown in the first figure was given to the pilots through a Honeywell Integrated Display and Display Sighting System. This system incorporated pilot head tracking in order to

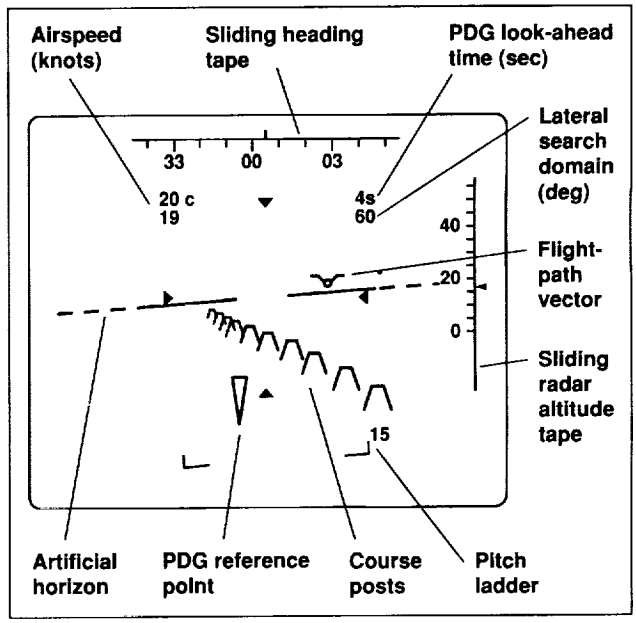


*Fig. 1. Helmet-mounted display symbology for pilot-directed guidance (PDG).*

provide true inertial presentation of symbology. Inertially fixed symbols, similar to croquet wickets, were used to delineate the nominal course that the pilots were asked to fly. An inverted triangular symbol was used as a pilot-controlled reference point

that represented the guidance command being sent to the system via the cyclic and collective controls in the cab. More specifically, forward cyclic was used to command forward airspeed, lateral cyclic was used to command the direction of the reference point, and collective was used to set a commanded ground clearance altitude. Additional controls were given to the pilot to set the look-ahead time of the reference point and to control the angular search envelope for selecting lateral obstacle-avoidance maneuvers. Lateral maneuver options were executed before vertical ones in order to provide the greatest degree of threat protection for military missions.

Three NASA research pilots participated in the evaluation. In order to assess the potential benefits of PDG, pilots were asked to first fly a course under a given set of airspeed and visibility conditions manually, and then fly the same course assisted by PDG. For both manual and PDG flights, pilots were given a target recognition task which served as a surrogate for auxiliary cockpit work load.

Three primary findings of the simulation are summarized in the second figure. First, it can be seen that pilots were able to fly lower, and thus reduce threat exposure, for a greater percentage of the flight time when aided by PDG. This was a result of the ability of the automated system to rapidly detect obstacles and initiate lateral avoidance maneuvers. This benefit of PDG became increasingly evident as visual conditions deteriorated. Second, the PDG system's ability to reduce the number of inadvertent obstacle strikes in a harsh obstacle environment was demonstrated. Significant improvement in collision avoidance was observed with PDG for all airspeed and visibility conditions flown. Finally, pilots reported a lower overall level of cockpit work load when flying with the PDG automation under all conditions tested.

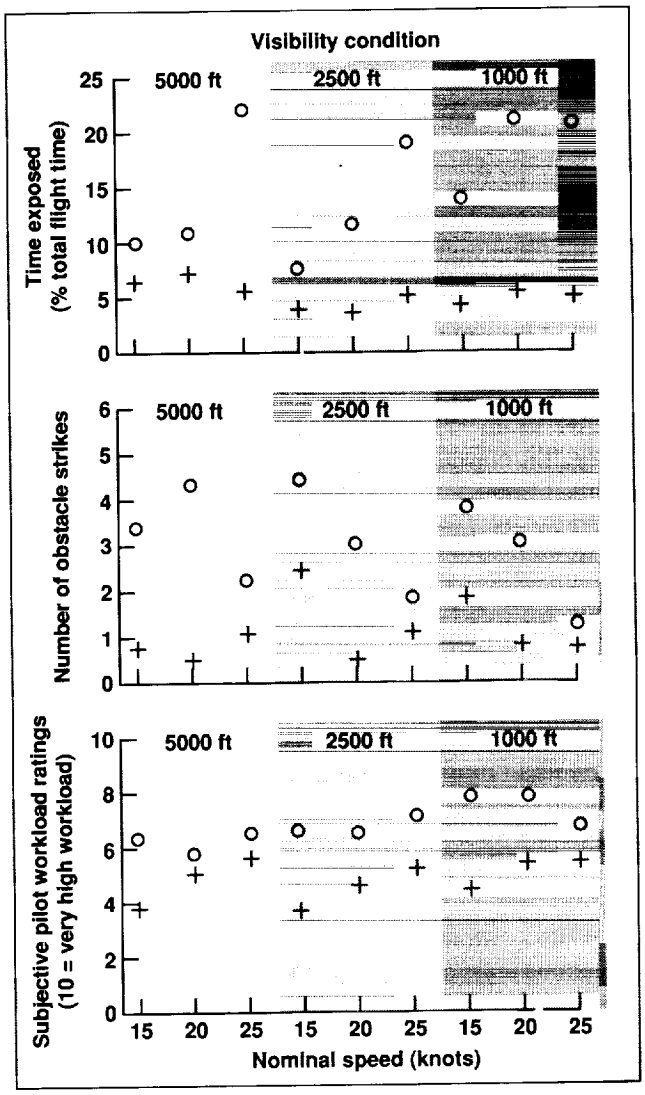


*Fig. 2. Pilot-averaged statistical summaries. + = with pilot-directed guidance (PDG); o = without PDG.*

**Ames-Moffett contact: R. Coppenbarger**
**(415) 604-5433**
**Headquarters program office: OA**

# Air Traffic Simulation Model

George Danek

Pseudo Aircraft Systems (PAS) is a flight dynamics and piloting software system designed to simulate traffic scenarios so that automated air traffic management and control systems can be tested and evaluated in real time and under realistic conditions. PAS was developed in the 1970s at NASA Ames Research Center as an adjunct to research in progress at the time; it is currently used to support the development of the Center-TRACON Automation System. The software has been continually improved over the years to accommodate more complex and sophisticated test requirements. The latest major upgrade to PAS was implemented in fiscal year 1993.

PAS simulates aircraft flight profiles using high-fidelity maneuvering and navigational models, and calculates simulated radar track data representing these flight profiles for each aircraft. The data are used to generate the blips and other information presented on air traffic controllers' radar displays. The air traffic controllers, in turn, use this information to assess the traffic and, using judgment, experience, and any available automated aids, to issue instructions to the pilots of the aircraft to manage traffic flow and spacing.

The major components of PAS are three distinct sets of programs that run on a network of computer workstations. These components are the Simulation Manager, the Pilot Station(s), and the Pilot Manager; the figure shows a pictorial representation of the network. Each component is operated and controlled by its own custom-designed graphical user interface. The Simulation Manager serves as the control center for the overall aircraft simulation and as the computer link between the PAS network and the air traffic control system. The Simulation Manager also contains the kinematic models of the individual aircraft in the simulated traffic scenario. The Pilot Station software runs on a set of workstations that serve as both input devices and information display devices for operators called "pseudopilots." Each pseudopilot controls a number of individual aircraft by issuing commands in response to verbal instructions from air traffic controllers or electronically transmitted datalink commands, in much the same way as an actual pilot controls his aircraft. The commands are predefined strings of alphanumeric characters that are entered using the workstation keyboard. The Pilot Manager relays commands from all the Pilot Stations to the Simulation Manager and, conversely, aircraft state data from the Simulation Manager to the appropriate Pilot Station.

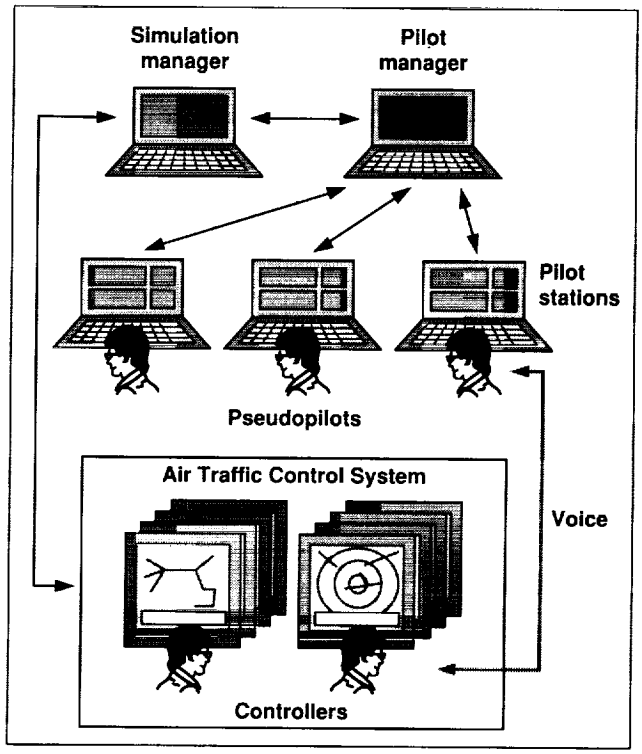


*Fig. 1. PAS network components, connections, and operational interfaces.*

PAS uses a three-degree-of-freedom point-mass model to compute the translational dynamic characteristics of the simulated aircraft. PAS currently contains aerodynamic and powerplant data for six commercial transport aircraft, a representative turboprop aircraft, and a representative single-engine private aircraft. The aerodynamic data include the effects of flaps, spoilers, landing gear, and compressibility. Powerplant data are provided by a special

engine-modeling routine and are derived from actual aircraft engine data.

PAS provides a sophisticated array of piloting and control functions that allow the aircraft to perform a wide variety of maneuvers with minimum pseudo-pilot work load. The piloting logic is implemented as a closed-loop control system with the aircraft model as the controlled element. This implementation results in smooth, realistic maneuvers because changes in state are effected by integrating the equations of motion. The piloting logic can perform both simple maneuvers, such as changes in altitude, and very complex maneuvers, such as holding patterns or automatic navigation of an airway. PAS provides twenty-nine such piloting functions and many of these have several variations.

Because of its primary function as a research support tool, PAS was designed to be flexible and easy to use in order to allow rapid prototyping of changing test conditions. New airspace regions, wind conditions, aircraft types, or traffic scenarios can be implemented by altering data only; the algorithms remain unchanged. The most recent upgrade provided the capability to handle multiple airports and a theoretically unlimited number of aircraft; included more efficient and flexible user interfaces for the operators; and provided simplified setup procedures and improved operational control over the suite of simulated aircraft.

**Ames-Moffett contact: D. Jones/R. Weske**
**(415) 604-5928/3248**
**Headquarters program office: OA**

## Civil Tiltrotor Terminal-Area Operations

**William A. Decker**

Tiltrotor aircraft can supply both military and civilian short-haul air transportation needs. Civil market studies show that tiltrotor aircraft have strong potential as regional air transports, and can relieve the congestion now evident at a number of U.S. airports. A new air and ground infrastructure is needed to realize this potential. The infrastructure must include conveniently located vertiports near population and business centers. Air traffic control procedures and certification standards must be developed for safe, reliable, all-weather operation with minimal community impact.

A series of piloted simulation experiments has been conducted in the Ames Research Center Vertical Motion Simulator to investigate aircraft certification, vertiport design, and terminal operations for civil tiltrotor transports. This joint NASA–Federal Aviation Administration (FAA) effort includes participation by the British Civil Aeronautics Authority, U.S. rotorcraft manufacturers, and potential operators (pilots). Previous simulation experiments were carried out to determine where, during the approach, to conduct the conversion from airplane mode to rotor-borne flight and to study steep approaches in which either basic instruments (showing only approach path tracking error) or more sophisticated cockpit displays with flight director approach guidance were used. As a result of those experiments, the range of approach angles of interest for manual approach path control has been limited to approximately 15 degrees, flown with the assistance of flight director approach guidance. Additional results led to the development of integrated configuration control (flap and nacelle angle settings) and further development of the FAA's Vertiport Design Guide.

A fixed-base simulation was conducted during May and June, 1993, to develop a candidate terminal procedure for steep approaches into a confined urban vertiport, appropriate for flight demonstration by a V-22 Osprey. As a result of previous motion-base simulations on the VMS and this latest fixed-base simulation, the FAA has selected this terminal procedure to serve as the baseline for their

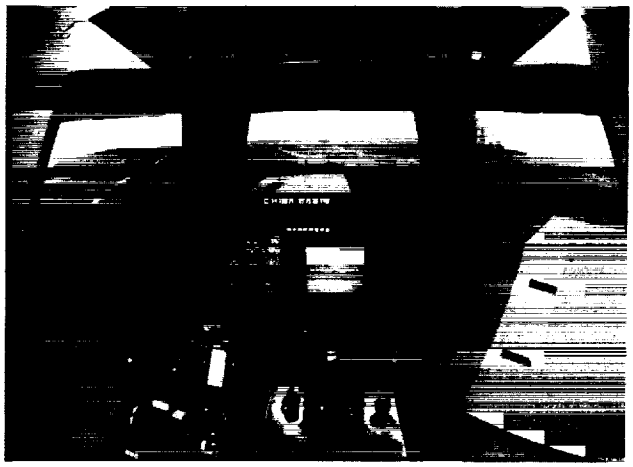

*Fig. 1. VMS cockpit view during approach to a conceptual San Francisco Bay area vertiport.*

vertical-flight-terminal-procedures development program. The procedure focuses on a 9-degree approach path angle, and requires that the aircraft maintain at least a 50-knot airspeed until the final landing decision and commitment in visual conditions is made. Both the airspeed and the approach angle were selected to provide a safety margin for recovery from a single engine failure on approach or a missed approach (forced by poor visibility at the critical decision point). This safety margin is required for airline transport operations that use multiengine rotorcraft which typically cannot hover with one engine failed. The integrated configuration control and automatic flap schedule were further developed to support both conversion to helicopter-mode flight on the approach and movement toward airplane-mode during missed approach and departure operations. Cockpit displays for approach and departure were also further developed.

Operations were conducted for a conceptual urban vertiport atop a parking structure (see figure). Terminal procedures development was further enhanced by placing the vertiport at a possible urban site in the San Francisco Bay area. The natural and man-made obstructions in this terminal area helped to focus procedure development within typical real-world constraints. Significant comments were collected on the vertiport design, marking, and lighting, and have been incorporated in FAA vertiport design projects.

**Ames-Moffett contact: W. Decker**
**(415) 604-5362**
**Headquarters program office: OA**

## Center/TRACON Automation System (CTAS) Deployment

**Heinz Erzberger**

In July 1993, NASA and the Federal Aviation Administration (FAA) hosted a briefing at Ames Research Center for the aviation industry about a NASA-developed automated air traffic control system. The purpose of the briefing was to initiate transfer of the technology to industry for deployment at the 12 busiest terminal-area facilities.

The Center/TRACON Automation System (CTAS) helps air traffic controllers more efficiently manage the flow of aircraft arriving at an airport. The briefing, which was given by members of the CTAS research team at Ames, described the design of CTAS and demonstrated its functions on computer workstations. After the NASA briefing, FAA officials discussed plans for deployment and the potential benefits of the system. The FAA predicts that installing CTAS at just 12 selected airports will save airlines nearly $600 million in operating costs and delays by the year 2000.

The briefing was attended by representatives of 30 organizations, including major aerospace manufacturers, software development firms, airlines, and government agencies.

An important objective of the briefing was to expedite the process of transferring CTAS technology to industry. In response to industry requests, NASA authorized the release of the CTAS software to firms

that intended to compete for the FAA's deployment contract.

CTAS provides three computerized tools that help controllers manage arriving aircraft. These tools bridge the gap between controllers and pilots, improving both the efficiency of air traffic control and the efficiency of each individual flight.

The Traffic Management Advisor (TMA) plans traffic flow and develops efficient landing schedules for aircraft as early as 40 minutes before landing. It assigns aircraft to appropriate runways and selects the legally prescribed minimum spacing between aircraft when creating landing schedules. The TMA also acts as a communications device for exchanging traffic-flow information between en route and terminal-area controller teams.

The Descent Advisor generates advisories to assist en route controllers directing arrival flow into the terminal area.

The Final Approach Spacing Tool provides heading and speed advisories that help terminal-area controllers produce an accurately spaced flow of aircraft on the final approach course.

NASA and the FAA have begun evaluating CTAS at the Denver and Dallas/Fort Worth airports. The automation functions and software validated at these airports will be the basis for the FAA's planned deployment of CTAS at the ten largest U.S. airports.

**Ames-Moffett contact: H. Erzberger**
**(415) 604-5425**
**Headquarters program office: OA**

## Helicopter Linear Model Identification

**Jay W. Fletcher**

NASA and the U.S. Army are currently developing the Rotorcraft Aircrew Systems Concepts Airborne Laboratory, or RASCAL, at Ames Research Center to study advanced flight control and navigation concepts for rotorcraft. The RASCAL will include a programmable, fly-by-wire flight control system, a pilot's helmet-mounted display system, synthetic vision-based navigation aids, and integrated flight/propulsion controls.

A research project associated with the development and use of the RASCAL is the Superaugmented Controls for Agile Maneuvering Performance, or SCAMP, program. Researchers intend to develop new methods of synthesizing the complex flight control systems required for pilots to operate rotorcraft close to the ground (nap-of-the-Earth operation), under low-visibility conditions, with high agility and maneuverability, and while conducting other tasks. The control systems synthesized by these new methods will be proven initially in ground-based simulation and finally in flight on board the RASCAL.

The first flight experiment flown on the RASCAL was conducted in October 1992 to gather data in support of the SCAMP program. With the facility developed only to the point of basic instrumentation, flight data sufficient for the determination of parametric, higher-order models of the aircraft dynamics were collected. Such higher-order models are necessary for the synthesis of modern flight control systems.

An Ames-developed system-identification methodology and software package called Comprehensive Identification from Frequency Responses, or CIFER, was used to identify a relatively high-order, linear model of the RASCAL flight dynamics in hover. This model extends the state of the art in helicopter model identification with regard to complexity and fidelity and builds upon modeling methods previously developed at Ames.

The system identification approach was adopted because significant discrepancies still exist between analytical models of helicopter dynamics derived from first principles and flight test measurements. System identification avoids many of the a priori

assumptions made in analytic modeling which may or may not be valid. The trade-off is a model that is only valid for a limited range of motion and operating conditions, but that "fits" the flight test data by the very nature of its derivation.

In the figure, the response of the identified model to a flight-test-measured longitudinal cyclic control input is compared to the flight-test-measured response of the helicopter and those predicted by two state-of-the-art, analytically derived models (models A and B) of the UH-60. All three models have a similar level of complexity, so the differences illustrated are not due to the detail of the models. It is clear that the identified model does a better job of predicting the overall response of the helicopter to the control input. Significant improvements are seen in the roll attitude, roll rate, and vertical acceleration predictions. These "off-axis" responses are particularly difficult to model analytically, and yet it is critically important to model them well so that the control system can "decouple" the aircraft response. The analytical models have similar deficiencies in this area, indicating that a similar approach to modeling has been taken which is not appropriate.

Other conclusions of this identification study were that including the effects of the main rotor RPM and blade "flapping" in the model is critically important to the RASCAL model fidelity for use in flight control design, and that many of the discrepancies between theory and flight results may be due to an incomplete understanding of the rotor blade dynamics.

The high-order linear hover model identified from the RASCAL flight test data will be used in SCAMP control system synthesis work and ground-based simulations in support of further RASCAL development. It will also serve as a basis for further identification studies which are planned when direct measurement of rotor blade motions become available early next year. The addition of direct rotor measurements will allow the complexity of the rotor dynamics modeling to be increased and important questions about rotor modeling assumptions to be answered.

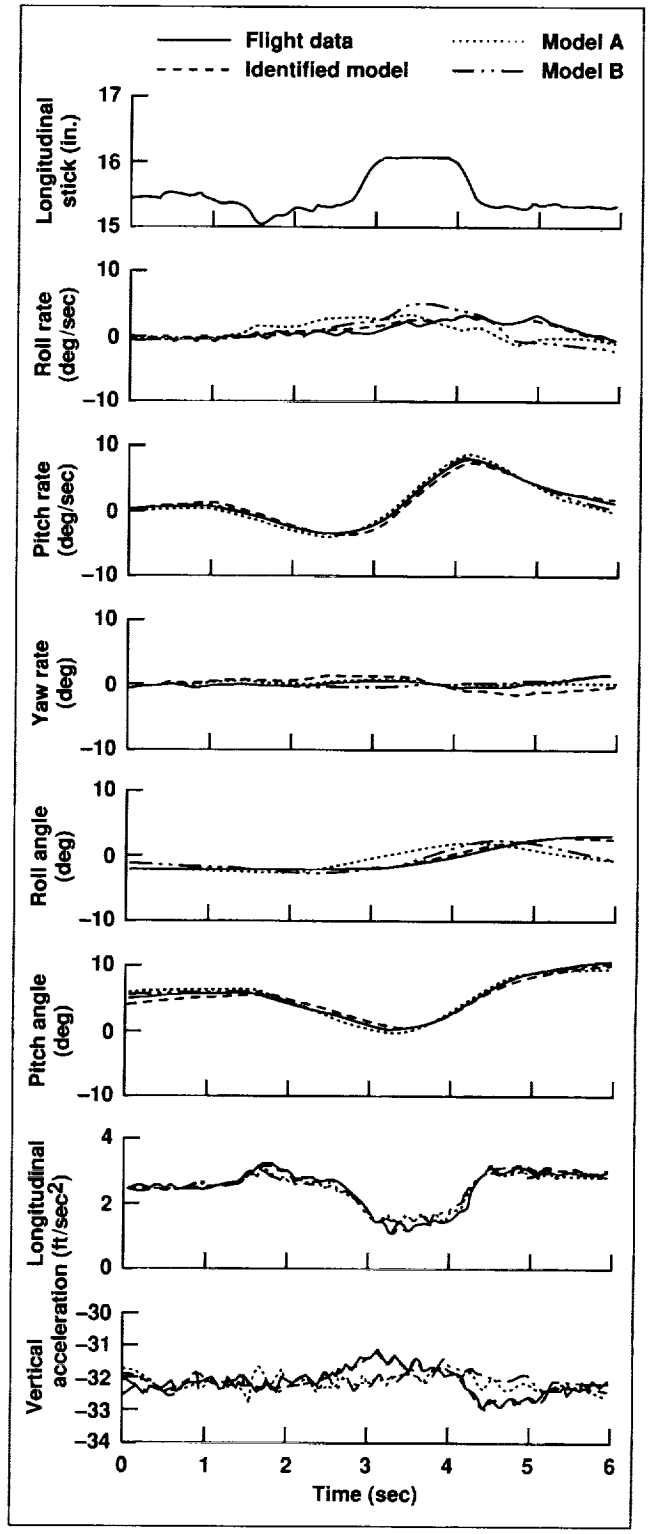


*Fig. 1. Comparison of model time responses with flight data.*

**Ames-Moffett contact: J. Fletcher/M. Tischler**
**(415) 604-6115/5563**
**Headquarters program office: OA**

# Integrated Flight/Propulsion Control V/STOL Flight Research

**John D. Foster, Ernesto Moralez, Dan W. Dorr, Paul F. Borchers, Vernon K. Merrick, Charles S. Hynes**

The Flight Systems and Simulation Research Division at Ames has developed an integrated attitude and thrust vector control system that is currently being flown on the vertical/short-takeoff-and-landing (V/STOL) Systems Research Aircraft (a modified YAV-8B Harrier—see figure). It is a fly-by-wire Digital Flight Control System (DFCS) with mechanical back-up and uses two flight computers to provide fail-safe operations. Additional system elements include a programmable symbol generator for displaying important aircraft state information on the head-up display, a servo control unit for driving the attitude and propulsion servos, and a Global Positioning System (GPS) receiver used for acquiring accurate position information for use in the advanced pursuit guidance algorithms.

Successful engagements of the DFCS in the rate-damping and rate-command modes have been achieved as well as the integration of the GPS into the state estimation algorithms and the identification of structural modes using frequency response identification techniques. The use of the throttle series servo for the mechanization of the vertical-damping control mode allowed the evaluation of a vertical damper in a Harrier aircraft for the first time. This particular mode used the feedback of vertical velocity to the engine throttle to augment the AV-8 Harrier's inherently poor vertical damping characteristics. Further improvements to the AV-8's flying qualities will be demonstrated with an advanced control system that provides direct command of flightpath angle and longitudinal acceleration for the wing-borne regime and a three-axis translational rate command system in the jet-borne regime.

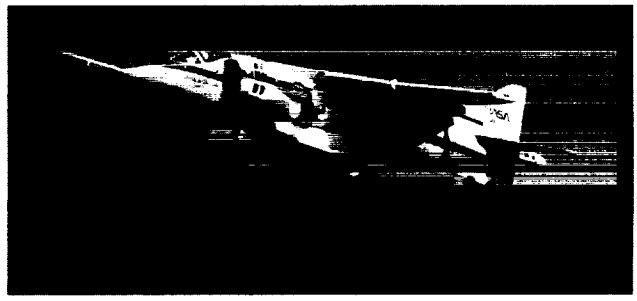

*Fig. 1. V/STOL Systems Research Aircraft (VSRA).*

**Ames-Moffett contact: E. Moralez/D. Dorr**
**(415) 604-6002/6194**
**Headquarters program office: OA**

# Line-of-Sight Determination in Real-Time Simulations

**Frederick G. Kull, Jr., Donald E. Fought**

The Vertical Motion Simulator at Ames Research Center is used to perform aeronautical research on flight vehicles. Many of the simulations require real-time information about intervisibility between moving objects. Examples include own-ship-to-target and missile-to-target intervisibility. Several methods of calculating the line of sight in real time exist. Each method has trade-offs between computation time, storage requirements, and accuracy. This research was undertaken to determine the method best suited to meet the simulation requirements of flexibility, speed, accuracy, storage space, and low turnaround time when a new terrain file is generated.

The first step in testing the algorithms was to select a terrain file. Two distinct terrain file formats were evaluated: the gridpost terrain and the edge terrain. For the gridpost terrain file, a 902-by-772 array was used with a 10-meter post spacing, which resulted in a mapped terrain that covered an area approximately 9 kilometers by 8 kilometers. The edge terrain file consisted of 650 edges and covered an area of 90 square kilometers. The average edge length was 377 meters, with a minimum of 34 meters and a maximum of 2,500 meters. The formats were evaluated with regard to storage requirements and ease of modification.

The gridpost method consists of a two-dimensional data array representing the terrain height at the intersection points on a uniform inertial grid overlying the visual data base. The array indices are X and Y integer coordinates of the axis system defined by the grid, and the terrain height information is stored as inertial Z coordinates in the array. The inertial X and Y coordinates of the lower left post in the grid and the post to post spacing are used to transform inertial positions into the grid axis system. Because of its appearance, such a terrain representation has been called a "bed of nails." There are two simple ways to create such a terrain file. The first method involves dropping vertical lines at the positions of the gridposts onto the visual data base. The second method involves using digital terrain elevation data (DTED) files supplied by the Defense Mapping Agency.

The purpose of any line-of-sight algorithm is to determine if an unobstructed line of sight exists between your eye and a target. Each of the five algorithms tested creates a line-of-sight (LOS) vector connecting the eyepoint and the target. The terrain height is then compared to the altitude of this LOS vector at locations along the length of the vector. If the terrain is higher than the LOS vector at any one of these locations, the line of sight is considered blocked. The LOS algorithms were evaluated on the basis of speed and accuracy.

The four algorithms using the gridpost terrain were (1) the Digital Differential Analyzer (DDA) with rounding, (2) DDA with three-point interpolation, (3) DDA with four-point interpolation, and (4) grid intersection. A visual comparison of a single grid square in the resulting equivalent gridpost terrain models is presented in the figure. The fifth algorithm tested was the intersection of line segments method using the edge terrain. Timing of the various algorithms was accomplished by integrating the LOS software with an existing real-time simulation. The real-time computing system at the VMS facility is

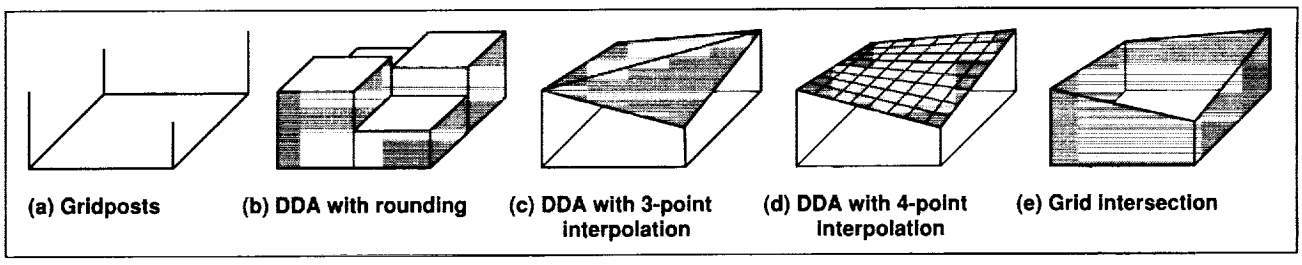


*Fig. 1. Equivalent terrain model comparison.*

equipped to measure the execution time of arbitrary software segments within a real-time frame.

For the gridpost terrain representation, tree and building heights may be added to the terrain height at appropriate gridposts without increasing the required number of posts.

In summary, five methods for determining line of sight in a real-time simulation were tested to select an optimal choice for use at the VMS facility at Ames Research Center. Test results led to the selection of the DDA with rounding method using the gridpost terrain file. The gridpost terrain was desirable because it is easily modified, has acceptable storage requirements for the equipment used, and is compatible with DTED terrain files. The DDA with rounding was the fastest, most efficient algorithm tested. Although it has an accuracy degradation which is due to the rounding process, its speed advantage offsets this small deficiency.

**Ames-Moffett contact: F. Kull, Jr.**
**(415) 604-3861**
**Headquarters program office: OA**

## Satellite Navigation for Precision Approach and Landing

**B. David McNally, Russell A. Paielli, Ralph E. Bach**

Researchers in the Aircraft Guidance and Navigation Branch are working with the Federal Aviation Administration and Stanford University to determine the feasibility of using satellite-based navigation for precision approach and landing guidance. The Global Positioning System (GPS) is a satellite navigation system that provides civil users with 100-meter position accuracy anywhere on the globe. Differential GPS (DGPS), illustrated in the first figure, uses a ground reference GPS receiver at a known position in the local area (at the airport, for example) to compute corrections to satellite measurements. These differential corrections are transmitted by a data link to the aircraft, where they are used to correct the airborne GPS receiver's measurements. DGPS position accuracy of 1–3 meters during approach and landing has been demonstrated in flight by NASA Ames and other organizations. The goal is to develop and flight test improved DGPS methods to achieve both the ±0.3-meter vertical accuracy and the integrity required for precision landing in the worst visibility conditions (Category 3). Ground-based pseudosatellites, which broadcast satellite-like signals, may be necessary to meet the precision landing requirements. Three activities were accomplished during the year.

A DGPS software algorithm which uses the millimeter-accurate GPS carrier phase measurements

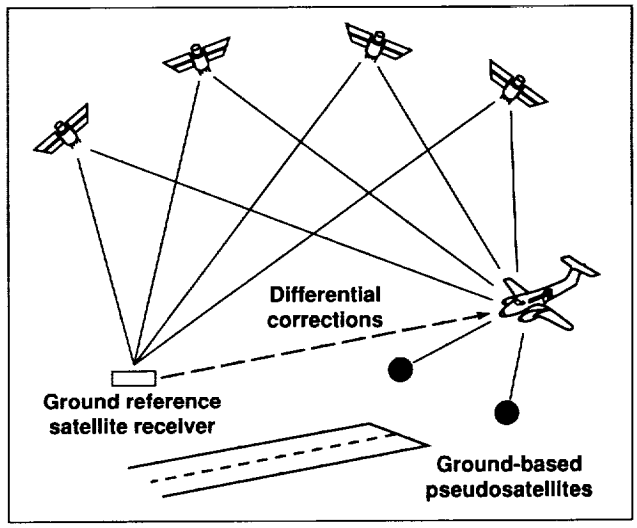


*Fig. 1. Differential Global Positioning System for precision approach and landing.*

for improved accuracy was developed and evaluated with flight data. The algorithm includes a technique called "carrier smoothing" to reduce the uncertainty of the satellite range measurements. An early version of the carrier-smoothing algorithm was validated with data from a 1991 flight test and the results were presented at the January 1993 Institute of Navigation Technical Meeting in San Francisco. A technique

called "integer ambiguity resolution," commonly used in GPS-based land surveying and capable of providing centimeter-accurate results, was also included in the DGPS software. Pseudosatellite data were not used in the algorithm.

To validate the DGPS algorithm, a flight test was conducted with the NASA King Air aircraft at the NASA Crows Landing Facility in February. GPS receivers were used that were capable of tracking all satellites in view and recording all raw satellite range and carrier phase data. Ten straight-in approaches were flown from 15 miles out through touchdown and roll-out while the aircraft was laser tracked to determine its true position. The data were processed with the DGPS algorithm to compute aircraft position (actually, the position of the GPS antenna). The laser tracker solution was then subtracted from the DGPS solution to give the position error. The second figure shows the altitude component of the error plotted against distance to touchdown for the final approach and landing. The ten separate approaches are shown on the graph; the composite average error is ±0.5 meter. These results were obtained using a simplified, more robust version of the algorithm and the accuracy is still very close to that required for precision landing. When integer ambiguity resolution was activated, centimeter-accurate solutions were obtained for five of the ten approaches. The DGPS algorithm and King Air flight test results were presented at the September 1993 Institute of Navigation Meeting in Salt Lake City.

Researchers at Stanford developed a DGPS algorithm which includes pseudosatellite data and installed a prototype system in a Piper Dakota aircraft. NASA Ames supported a flight test of the Dakota system at the Crows Landing Facility in August. Two pseudosatellites were located along the final approach path about 1 kilometer from the runway threshold. Comparison with the laser tracker indicated an altitude accuracy of about ±0.2 meter on final approach. The Dakota test results were

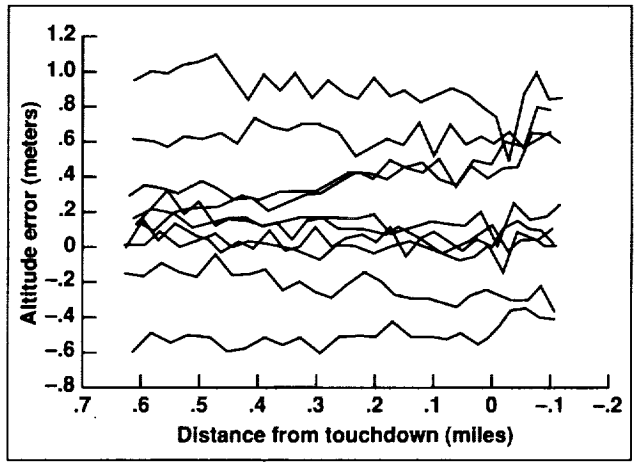


*Fig. 2. DGPS altitude error during final approach and landing for 10 King Air approaches.*

presented by Stanford researchers at the September 1993 Institute of Navigation Meeting.

Aircraft roll, pitch, and heading may be accurately computed by processing GPS satellite data from four antennas mounted on the wings and the fuselage, an application which may prove useful for precision landing. In a joint experiment with Stanford, a satellite-based attitude system was installed on the King Air and a flight test was conducted in January to compare satellite-based roll, pitch, and heading against the same data from an Inertial Navigation Unit, an instrument commonly used for attitude measurement. The test results, presented at the January 1993 Institute of Navigation Meeting, show a ±0.05-degree agreement between the two systems even during dynamic maneuvers to 60 degrees bank angle and 30 degrees pitch attitude.

**Ames-Moffett contact: D. McNally**
**(415) 604-5440**
**Headquarters program office: OA**

# Dynamic Forms

George Meyer, G. Allan Smith

A major new formalism and a collection of algorithms have been developed which will significantly improve the design cycle productivity for automatic control systems. The final development and verification of the mathematical technique of dynamic forms has been completed and published. A dynamic form is defined as a variable together with its time derivatives up to some fixed, but arbitrary, number of derivatives. The variable may be a scalar, a vector, a matrix, a direction cosine matrix, Euler angles, or Euler parameters. A large set of elementary functions and operations has been translated into corresponding functions and operations on dynamic forms. The set is rich enough so that typical system functions occurring in flight control and spacecraft attitude control can be assembled from the members of this set. The resulting collection of algorithms makes the solution of many difficult control problems a routine process.

The methodology applies in all domains that require precise multimode guidance and control of nonlinear, multiaxis processes such as aircraft flight control, spacecraft attitude control, robotics, and process control. Current software design methods for such control systems are prone to errors that are difficult to identify and result in excessive use of manpower, computer, and simulation resources. Using current methodologies, the control-system design problem is particularly difficult and tedious if the process to be controlled evolves on a non-Euclidean state space, as when rotations are present; when a variety of control modes must be provided; and when the process dynamics are multiaxis and nonlinear.

In such cases, the control problem must be formulated and solved in many coordinate systems, and smooth transitions must be provided across these coordinate systems. It is in these transformations that both conceptual and implementation errors are most likely to occur, and it is here that the new methodology is most effective in reducing such errors.

A basic operation in coordinate system transformations is the propagation of a variable together with its time derivatives up to some arbitrary order through a long sequence of complicated functions. There are currently three available differentiation techniques: hand differentiation, symbolic differentiation, and automatic differentiation. Hand differentiation and coding are very tedious and highly unreliable for the typical size of problems being considered. Symbolic differentiation involves the machine translation of, say, FORTRAN code for the system function into the appropriate language, such as MACSYMA, MATHEMATICA, or MAPLE, within which differentiation is defined. Applications of this approach to relatively small systems have been successful. However, for larger systems (4000 lines of FORTRAN) involving deeply nested functions, symbolic methods may be slow and often produce large, unmanageable expressions. The remaining choice for the computation of derivatives is automatic differentiation. Automatic differentiation is based on the fact that Taylor series, which carry derivatives as coefficients, can be propagated through an arbitrary sequence of elementary functions without any truncation error. Thus, automatic differentiation does not suffer from the rapid chain rule fanout of terms which plagues the symbolic differentiation. Furthermore, machine translation into an automatic differentiation language is as practical as it is for symbolic languages. The newly developed theory of dynamic forms represents a particular example of automatic differentiation and is the basis for a formal language for the computer-aided design of automatic control systems.

The dynamic forms have been used at Ames in a simulation study of automatic trajectory control for the AV-8B Harrier V/STOL aircraft. The results show much smoother transitions at trajectory segment junctions and operation over a much greater performance range than previous simulations. The simulation included rapid roll for several revolutions, and a complete loop.

**Ames-Moffett contact: G. Meyer**
**(415) 604-5750**
**Headquarters program office: OA**

# Yaw Motion Cues in Flight Simulation

**Jeffery A. Schroeder, Walter W. Johnson**

In flight simulation, pilots may use visual cues or motion cues or both to perform a particular flying task. For instance, previous research has shown that both visual and motion cues are necessary for many tasks performed in the vertical axis, such as precision landing. However, in the yaw axis, one hypothesis is that the yaw visual cues that a pilot receives from the computer-generated scene are so compelling that the additional motion cue supplied by rotating the cockpit may not be necessary. Thus, although most of today's motion flight simulators can rotate about the yaw axis, the usefulness of this motion has not been demonstrated and may be unnecessary.

With the purpose of determining the usefulness of pure yaw rotational cues, a piloted experiment was completed recently on the NASA Ames Vertical Motion Simulator. The vehicle simulated had the characteristics of an AH-64 Apache helicopter in hover. The pilot was positioned forward of the vehicle center of mass, so yaw accelerations produced lateral accelerations, and yaw rates produced longitudinal accelerations. Five test pilots completed three different tasks with and without moving the cockpit. The first task was a yaw angle change of 15 degrees to be performed as rapidly as possible. The second task was to maintain a zero yaw angle while performing 10-foot vertical translations. Maintaining a zero yaw angle was made a challenge in this task, as the control inputs for the vertical axis also caused a yaw acceleration of the vehicle (typical of a single-main-rotor helicopter). The third task was a hover turn of 180 degrees over a point on a runway. The simulator cockpit visual scene for the latter task is shown in the figure.

For the above tasks, four different cockpit motion configurations were given to the pilot. The first configuration had full motion, that is, the simulation cockpit moved the same amount as the actual aircraft would have moved in each axis (except for the 180-degree hover turn task, in which the simulation cockpit had only part of the full motion because of simulator displacement limits). The second configuration provided full linear accelerations, but it provided no rotational accelerations. The third configuration had full rotational accelerations, but no linear accelerations. The fourth configuration had no motion whatsoever.

*Fig. 1. VMS cockpit visual scene.*

Data collected for each task included pilot–vehicle performance quantities such as vehicle displacement, orientation, rates, accelerations, and stick position. Subjective pilot opinion of the fidelity of the motion compared with actual flight was also gathered. Also, for each configuration, classical signal-detection analysis was used; that is, pilots were asked in each axis if they felt any motion whatsoever. Along with the answer to that question, they were also asked to assign a level of confidence to whether they believed their answer was correct or not.

Preliminary analysis of the data indicates that often pilots perceived yaw rotational cab motion for the configuration in which only linear acceleration was present. Some pilots, however, were more susceptible to the differences in the motion configurations than other pilots. This variability is consistent with previous data on the vestibular differences in humans. Results also indicate that task performance did not change appreciably when yaw rotation was removed, but it did when the linear accelerations were removed.

**Ames-Moffett contact: J. Schroeder**
**(415) 604-4037**
**Headquarters program office: OA**

# Computer Architectures for a Real-Time Passive Ranging Algorithm

**Banavar Sridhar, Ray Suorsa**

The complexity of rotorcraft missions involving operations close to the ground results in high pilot work load. In order to allow a pilot time to perform mission-oriented tasks, sensor-aiding and automation of some of the guidance and control functions would be highly desirable. Automated guidance and control functions for low-altitude flight require detection of obstacles in the flightpath and the range (distance) to the obstacles in order to avoid them. Images from an electro-optical sensor provide a covert way of detecting objects in the flightpath of a low-flying helicopter. Passive ranging consists of processing a sequence of images using techniques based on optical flow computation and recursive estimation. We have implemented and tested a passive ranging algorithm (PRA) off-line using helicopter flight images. The algorithm performs satisfactorily and provides range estimates with an accuracy of 5% to 10%.

Typically, the PRA will receive 512 x 512 8-bit images at frame rates varying from 5 to 30 hertz. The amount of processing time varies from 30 to 200 milliseconds depending on the helicopter speed. The PRA detects distinguishable regions, referred to as features, and tracks them from one image to the next. The number of features can vary from a few hundred to a few thousand depending on the image. The major part of the computation involves the creation and optimization of the correlation function to determine the position of a feature in the next image. The amount of computation varies from a modest requirement of 16 million floating point operations (MFLOPS) to track 100 features at a frame rate of 5 hertz to 2 gigaFLOPs/second (FLOPS) to track 2,000 features at 30 hertz. Currently there is no single off-the-shelf microprocessor that can adequately meet the requirements of a flexible PRA.

Parallel processing technology offers a solution to the computational needs of the passive ranging problem. The challenge lies in the selection of the appropriate multiprocessor technology and the design of an architecture that takes into account the characteristics of the algorithm. Passive ranging involves algorithms from diverse areas such as image processing, numerical analysis, Kalman filtering, and visualization. Thus a hybrid multiprocessor architecture is most appropriate for the algorithm. Clearly, computing power is the dominant criterion in the selection of a processor architecture. Other factors in the choice of the computing architecture are (1) a high-bandwidth interconnection between the various processors, (2) ability to accept video images and other sensor data, (3) weight, volume, and ruggedness of the hardware, and (4) the use of a general-purpose computer as far as possible.

Several architectures were considered as cost effective real-time candidates for the PRA. These were evaluated using the criteria described in the previous section. Here, we describe our experience with four different architectures: (1) A Silicon Graphics Onyx computer with twenty MIPS R4400 processors was used to implement the PRA. The Onyx was able to process 3,549 features per second (FPS) and can meet the modest requirement. (2) The iWarp is a distributed-memory multicomputer developed jointly by Intel Corporation and Carnegie Mellon University. The 16-processor Oak Ridge National Laboratory (ORNL) iWarp was able to process only 524 FPS and was not able to meet the modest requirement. (3) The Honeywell architecture is designed to achieve real-time performance in a single chassis of commercial off-the-shelf hardware. The first figure shows the connections between the various processors. It is estimated that the system can process 200–300 features at a frame rate of 30 hertz. The advantage of the Honeywell architecture is that it is

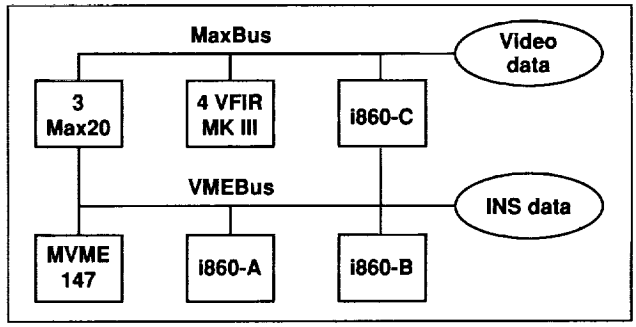


*Fig. 1. Honeywell computer architecture.*

based on flight-tested hardware and provides an early flight-test capability. (4) The ICI computer architecture and interconnection are shown in the second figure. The computation time to process 911 features was 2.56 seconds in a four-processor configuration. Assuming linear speedup, a 36-processor configuration can process 2,700 FPS and meet the modest requirement.

Three architectures, Onyx, Honeywell and ICI, are able to provide real-time passive ranging capability on a modest scale. The rapid advances in processor technology make it possible to achieve real-time passive ranging on a grand scale in the near future, enabling the evaluation of advanced guidance and display concepts for pilot aiding in low-altitude helicopter flight.

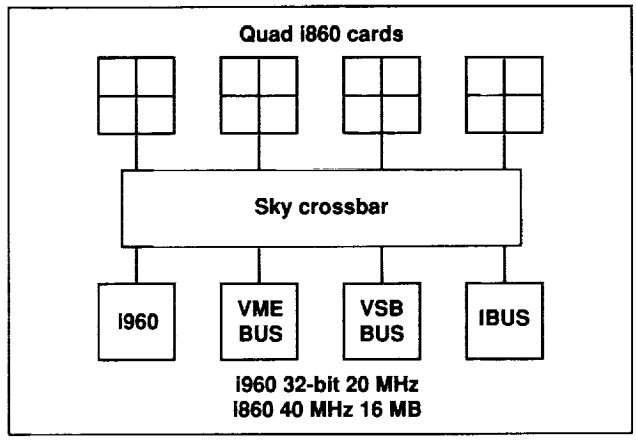


*Fig. 2. ICI computer architecture.*

**Ames-Moffett contact: B. Sridhar**
**(415) 604-5450**
**Headquarters program office: OA**

## Computer Aiding for Low-Altitude Helicopter Flight

**Harry N. Swenson, Richard E. Zelenka**

Helicopters operating in combat conditions fly close to terrain, vegetation, and man-made structures for masking. This is an extremely demanding and difficult piloting task, especially in rugged terrain, at night, or during adverse weather conditions. In these flight environments, pilots expend most of their energy in safely controlling the helicopter from one masked position to the next. Therefore, a significant portion of mission time is spent hovering and navigating. Automation to help with these duties would allow the pilot more time for mission functions (i.e., reconnaissance, targeting, support, evacuation, etc.). The NASA Ames Research Center and the U.S. Army Command/Control and Systems Integration Directorate have developed and flight evaluated an automation aid to support these near-terrain helicopter operations. This aid includes a near-terrain trajectory-generation algorithm and visually coupled helmet-mounted display symbology, developed at NASA during the past few years.

The joint NASA/Army flight evaluation of this near-terrain flight automation aid has been successfully completed on the Army's NUH-60 STAR (Systems Testbed for Avionics Research) helicopter. Four NASA and Army research pilots have completed the engineering flight evaluations, which included 12 variations in flight conditions, terrain masking performance, and display parameters. The flight mission over which the evaluations were conducted is shown in the first figure superimposed on a contour map of the terrain. The mission includes 12 navigation waypoints (marked by Xs and connected by a dashed line). It starts in the northeast corner, then travels southwesterly to a teardrop course reversal and back to the start. Also displayed in the first figure is an example ground track flown by the pilot following the display symbology. The helicopter ground track does indeed follow the mission waypoints as well as the terrain contours, thus

providing a more masked trajectory. The second figure shows the helicopter altitude and terrain profile during the mission. The clearance altitude for the example was set at 150 feet above the terrain. As shown in the figure, the automation aid helps the pilot fly the helicopter at 150 feet set clearance altitude for a majority of the example run. The flight evaluations are the first successful attempt to bring digital terrain information into piloted control of a helicopter. The flight evaluations have been significantly extended during the year by the Army. The Army has conducted a subsequent flight evaluation, modifying a pair of night-vision goggles to accept the NASA-developed display symbology. An operational flight evaluation was also conducted during the year. Research pilots from the helicopter industry (Sikorsky Helicopters, Boeing Helicopters, and McDonnell Douglas Helicopters) as well as Army and Navy active-duty pilots flew the NUH-60 STAR helicopter

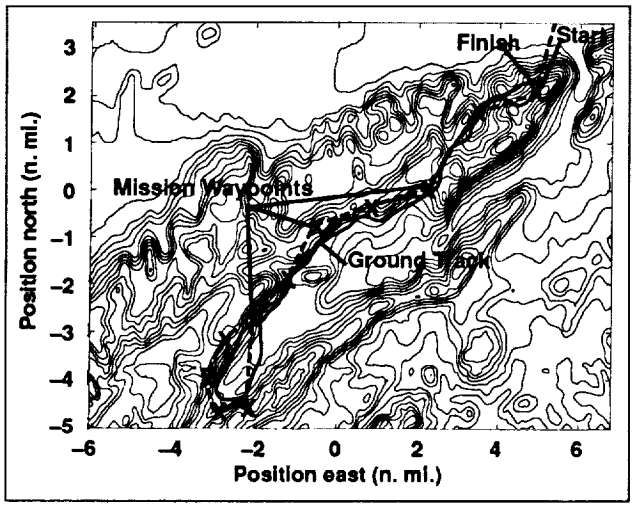


*Fig. 1. Flight evaluation mission and ground track.*

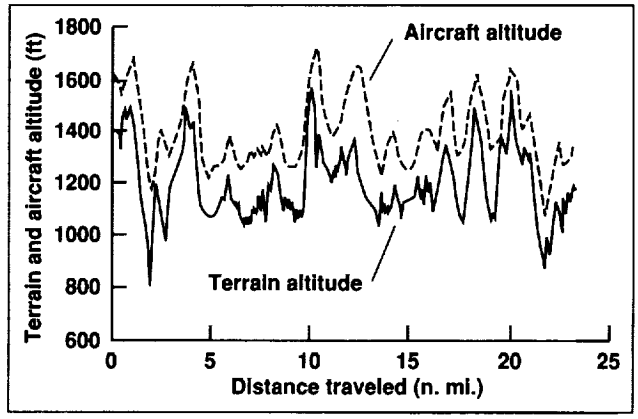


*Fig. 2. Helicopter altitude and terrain profile.*

using the near-terrain automation. The pilots indicated that this automation would be highly desirable for helicopter operations in combat conditions, especially at night or during poor weather.

These flight evaluations completed the first phase of the joint NASA/Army Computer Aiding for Low-Altitude Helicopter Flight Project. The second phase of the flight evaluations includes the addition of a wide-field-of-view, forward-looking laser range sensor to support operations at or below 25 feet above the terrain. A successful piloted simulation was conducted at Ames to develop the necessary enhancement to the near-terrain automation aid. Integration of these enhancements are currently being conducted by the Army to allow flight evaluations during 1994.

**Ames-Moffett contact: H. Swenson**
**(415) 604-5469**
**Headquarters program office: OA**

# Advanced Rotorcraft Flight Control Design

Marc D. Takahashi

Future civilian and military rotorcraft will require capabilities for operations in degraded visual environments and adverse weather conditions. In addition, military rotorcraft will need high levels of agility and maneuverability. A high-gain flight control system is one means of enhancing these capabilities by improving the disturbance rejection, stability, and tracking performance. Disturbance rejection is the resistance of the rotorcraft to outside disturbances, such as wind gusts: to reduce pilot work load in turbulent conditions, it is desirable to have a high level of disturbance rejection. Stability is the system's ability to return to equilibrium after being disrupted: without feedback in the flight control laws, helicopters are inherently unstable and require constant attention by the pilot to stay upright. Many current helicopters, even with conventional flight control laws engaged, are unstable. The tracking performance determines how closely the pilot can follow a prescribed path or a moving target. All of these qualities or capabilities—disturbance rejection, stability, and tracking—affect the pilot work load and performance in tasks such as air-to-air combat, nap-of-the-Earth flight, instrument approaches, carrier operations, oil-rig operations, and emergency services.

Design of high-gain flight control laws for rotorcraft is problematic because the high-order effects of the rotor dynamics become significant. The coupling between the rotor and the fuselage must be considered in the design process along with the coupling between the pitch and roll axes. Overcoming these effects is increasingly difficult using current flight control design methods, thus improved methodologies are needed.

*Fig. 1. RASCAL UH-60 research aircraft.*

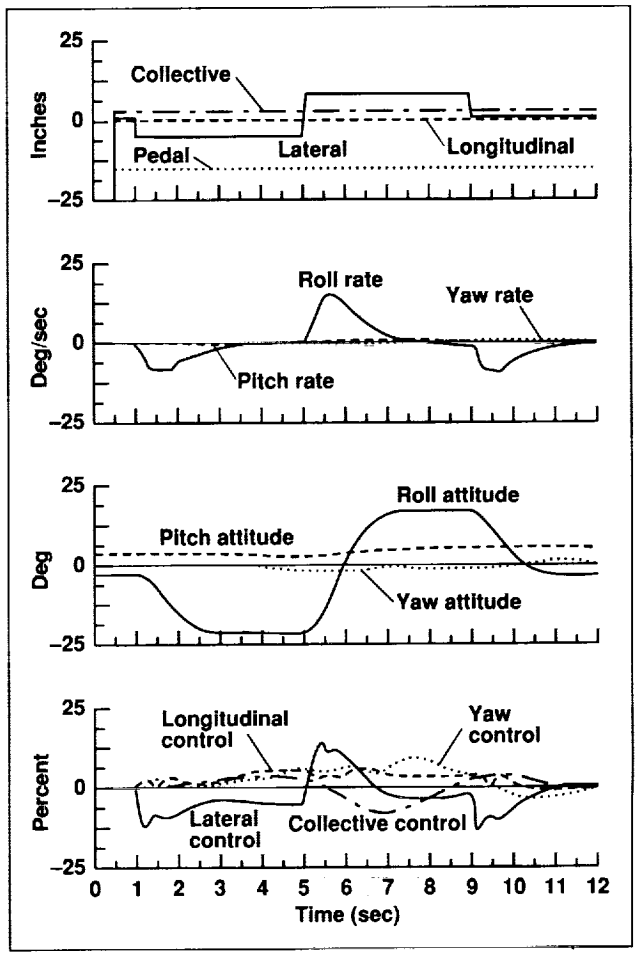


*Fig. 2. Response of the nonlinear analysis model with the H-infinity control law.*

An approach to apply an H-infinity multivariable method to the design of rotorcraft pitch and roll axis flight control laws was recently developed. A direct relationship between the H-infinity design parameters and the crossover frequency, stability margins, and feedback gain magnitudes was established. The crossover frequency directly controls the disturbance rejection and the crispness of the aircraft response to the pilot's control inputs. The stability margins

determine the sensitivity of the system to variations such as changes in gross weight and altitude, whereas the gain magnitudes determine the sensitivity of the system to sensor noise.

The design approach was applied in analysis using linear and nonlinear helicopter models configured as the Rotorcraft-Aircrew Systems Concepts Airborne Laboratory (RASCAL) UH-60 Black Hawk (first figure), which is the research vehicle that will be used to demonstrate feasible control law methodologies. The linear model includes the flap and lag rotor degrees of freedom and inflow states. The nonlinear models also include these dynamics as well as the nonlinear lead–lag damper, component level engine model, sensor delays, and nonlinear actuator dynamics. Two sets of control laws were developed, one that uses conventional rigid-body sensors only and one that uses both conventional sensors and rotor flapping angle sensing. The laws were designed to meet the quantitative requirements in the current military rotorcraft handling-qualities standard. The second figure shows the nonlinear response of the helicopter configuration using the H-infinity control law to a doublet lateral stick input. The design response type is attitude command, which yields a steady-state attitude response to a step control input.

The control law that uses rotor state sensing was shown to pass half as much sensor noise as the design without rotor sensing, indicating a potential to achieve twice the control-system gain using such measurements. Furthermore, the design with rotor state sensing was able to tolerate more uncertainty in the modeling of the dynamic characteristics of the vehicle. During moderate maneuvers, the design without rotor state sensing showed more undesirable oscillations in the roll response than the design with rotor sensing.

**Ames-Moffett contact: M. Takahashi**
**(415) 604-5271**
**Headquarters program office: OA**

## Field Site Evaluation of the Traffic Management Advisor

**Leonard Tobias**

An integrated assessment of Traffic Management Advisor (TMA) was conducted at the Denver Air Route Traffic Control Center (ARTCC) and the Denver TRACON in January 1993. TMA is a sequence and schedule tool for planning of arrival traffic, and is one of the main tools of the Center/TRACON Automation System (CTAS).

The assessment addressed the effectiveness of TMA for supporting various traffic management activities. Both human factors issues and system performance were included. TMA has been installed in the Traffic Management Units at both the ARTCC and the TRACON in order to develop and assess the tool interactively with the field site staffs. In the configuration assessed, TMA was operated in a one-way mode, i.e., TMA received arrival planning data from the Host Computer System at the Denver ARTCC, but no TMA-generated data was passed back to the Host for transmission to the radar control positions. Furthermore, TMA did not receive any data from the TRACON's computer system.

Prior to the installation of TMA at the TRACON, the only means of obtaining information on arrival traffic currently in Center airspace was by voice communication with the Center, or from knowledge obtained from historical experience. Since TMA provides a graphical picture of traffic in the Center airspace destined for the TRACON, it provided advance warning of a change in traffic conditions which was helpful in a variety of ways. It assisted the traffic management staff in deciding when to open or consolidate positions. It assisted in decisions related to traffic load distribution, i.e., rerouting of aircraft to equalize workload at the TRACON. It helped the staff decide on the optimum time to make needed changes in operating parameters, such as airport acceptance rate.

At the Center, the existing metering system was used operationally while TMA was used in a background mode by an additional traffic management specialist. TMA was evaluated for use in supporting decisions on when to meter and when to release aircraft for feeder airport departures. A comparison of decision times generated by the TMA traffic management specialist with those generated by the existing planning system demonstrated that TMA could support these types of planning functions.

The success of this nonoperational assessment of TMA at Denver has contributed to the decision to install the one-way TMA at the Dallas-Fort Worth TRACON and, in addition, the one-way TMA is being considered for installation in fiscal year 1994 in the Chicago, Southern California, and Seattle TRACONs. Furthermore, the decision has been made to conduct a TMA limited operational assessment at Denver in fiscal year 1994 in which TMA actually replaces the existing metering system during busy arrival traffic periods. A two-way link will therefore be needed so that TMA-generated planning data can be displayed at radar control positions at the Denver ARTCC. The two-way link has been developed and is being tested, and the plan for a TMA operational assessment has been approved.

**Ames-Moffett contact: L. Tobias**
**(415) 604-5430**
**Headquarters program office: OA**

## A High-Fidelity Video Delivery System for Real-Time Flight Simulation Research

**Daniel A. Wilkins, Carl C. Roach**

Image-generating systems have evolved rapidly in the past few years to the point where they are capable of providing very-high-fidelity video presentations. In the flight simulation environment at Ames Research Center the aircraft simulator is located hundreds of feet from the image generators. To ensure high scene fidelity at the simulator, the transmission architecture of the video must be considered.

A fiber-optic system was installed and tested in the distribution of high-fidelity output of the image generators that drive the cockpit and flight displays. The optical system proved to be transparent in the distribution system. Video signals at the remote display devices were virtually identical to those at the image generator. The fiber-optic system proved to be very reliable even though it traveled through a 200-foot, constantly moving catenary. This system also affords minimum electrical noise interference and produces high-definition scene content.

Image generators use high line rates and have very rapid video transitions that produce very-high-fidelity displays. This fidelity is not required for researcher observation and recording. For those purposes the video is electronically converted and reduced to a standard video format similar to that used in a commercial broadcast studio. In this format the video can be recorded and observed on broadcast-type video equipment. This format also allows the use of existing or "off the shelf" (OTS) processing and distribution equipment.

The head-up display (HUD) was changed from a point-to-point graphic display system to a raster system. This change allowed the use of the standard video-transmission-system equipment and eliminated the special amplifiers and hardware required for direct-current distribution.

**Ames-Moffett contact: D. Wilkins**
**(415) 604-0628**
**Headquarters program office: OA**

# 11-Foot Transonic Wind Tunnel Wall Interference Study

**M. Jahed Djomehri, Pieter Buning, Larry L. Erickson**

The objectives of this study are to simulate 3-D transonic flows about a semispan model mounted in the NASA Ames 11- by 11-Foot Transonic Wind Tunnel, to understand the wall interference effect of the tunnel slotted walls in the test section, and to validate the flow solver data with the experiments. In the long term, our objective is to provide a predictive-capability tool for experimental data acquisition procedures.

The computational approach is based on the Chimera grid procedures which allow simple hyperbolic grid generation about the individual components of the model and the interior of the tunnel's box-like test section. Additional box grids at the test section entrance and exit have also been provided to maintain uniform flows at the upstream and downstream stations of the test section; no attempt has been made to model the tunnel geometries in these regions, i.e., the nozzle-shaped geometry of the tunnel walls upstream and other complex geometries downstream of the test section. The Navier–Stokes flow solver Overflow, developed at Ames, has been used to simulate viscous flows about the model with the Baldwin–Lomax turbulence model. A porous-type boundary condition method has been incorporated in the code to account for the flow behavior near the tunnel slotted walls.

Solutions were computed for a Boeing semispan wing-body floor model, mounted on the 11-foot test section floor, for various tunnel operational Reynolds numbers, flow-stream Mach numbers, and incident angles. Pressure coefficient measurements taken at several spanwise stations corresponding to experimental pressure tap locations were used to compare the CFD results with wind tunnel test results for the model. Comparison for cruise conditions and for low angles of attack appear to be in good agreement. Some discrepancies at the trailing edge and at the wing tip are evident in the data and are attributed to the geometry of the grid in these regions. A few of the CFD results obtained have also been compared with "free air" computations about the same model, i.e., flows about the model without the tunnel walls, resembling a free flight environment. Comparison of CFD results between the free air and confined tunnel air-flow computations indicates that the tunnel wall boundary conditions have been effectively implemented. Although the two sets of CFD results are in relatively close agreement, the latter more accurately predicts the experimental results.

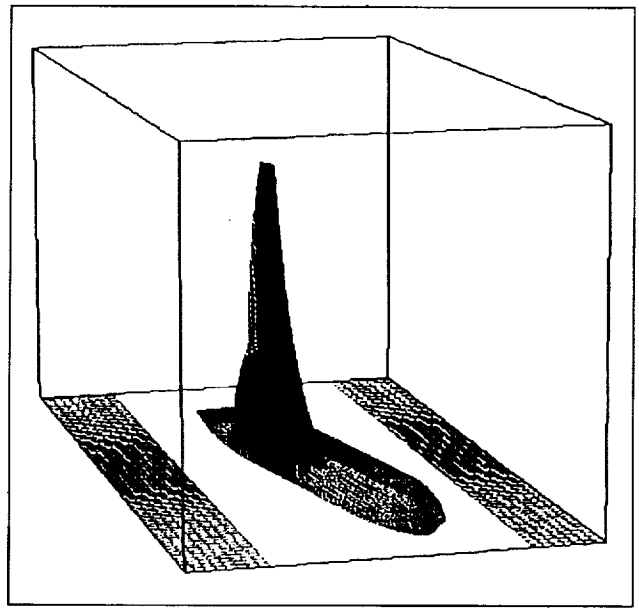

*Fig.1. Chimera grid for semispan Boeing model mounted in the test section of the Ames 11- by 11-Foot Transonic Wind Tunnel at incidence $\alpha > 0°$.*

The Chimera grid approach delivers capabilities for flow simulations about further complex geometries and allows simulation of internal-viscous-flow-type calculations for the wind tunnel flows. It provides data on the wall interferences of the tunnel as well as a means for code validation by direct comparison of the CFD with experimental data.

Additional calculations are planned to assess the versatility of the overall approach with further improvements to the grid and/or boundary conditions about the trailing edge and about the wing tip, and to apply alternative turbulence models.

**Ames-Moffett contact: M. Djomehri**
**(415) 604-6216**
**Headquarters program office: OA**

# A Practical Stress–Strain Law for Designing with Rubber-Like Materials

Larry L. Erickson

The objective of this study was to obtain a practical stress–strain law for rubber-like materials, so that the problem of designing with such materials is simplified.

The stress–strain law resembles the familiar Hooke's law equations used for metal-like materials, and employs two material properties, Young's modulus (E) and Poisson's ratio (ν). But instead of employing conventional engineering stresses ($f_i$, force per original area), true stresses ($t_i$, force per current deformed area) are used. E relates uniaxial $t_i$ to strain ($e_i$), and is assumed constant. However, ν is not taken to be 0.5, the value normally assumed for rubber-like materials. Instead, ν is solved for by imposing the complete, as opposed to linearized, condition of incompressibility. The first figure shows how ν varies as a function of the principal extension ratios $\lambda_i = 1 + e_i$ for biaxial tension loading. At 100% strains, ν drops to about 0.3, 40% below the small-deformation value of 0.5. It is only at zero strain that ν takes on the value 0.5.

How well the predicted biaxial stresses follow the experimental nonlinear behavior of rubber is illustrated in the second figure. Here, the variation in $f_1$ with extension ratio $\lambda_2$ is shown for fixed values of $\lambda_1$ that vary from 1.05 to 2.5. The variable Poisson's ratio theory predicts that along each $\lambda_1$ equal

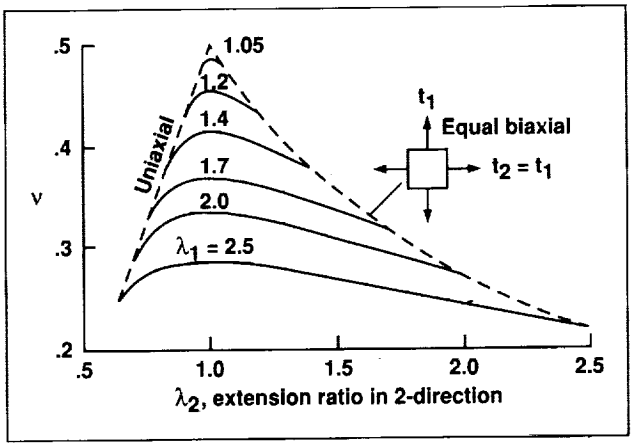


*Fig. 1. Variation in Poisson's ratio with principal extension ratios for biaxial tension.*

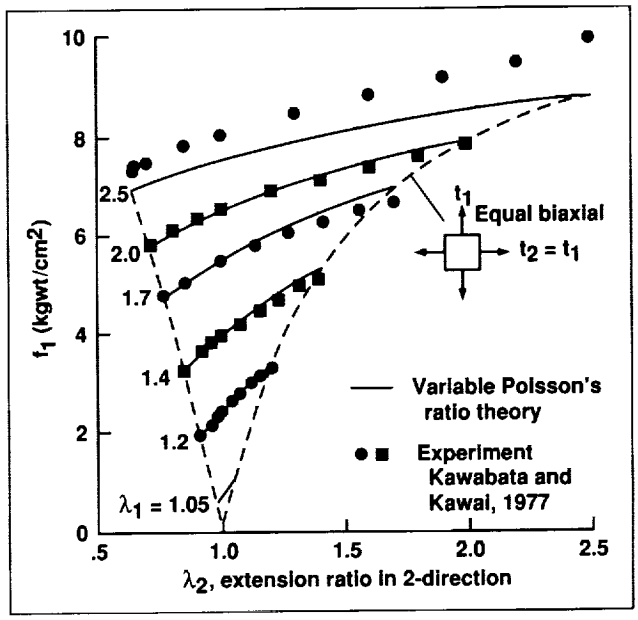


*Fig. 2. Comparison of predicted and experimental stresses for biaxial tension.*

constant curve, the slopes decrease with increasing strain. This behavior agrees with the experimental results, which are shown by the solid symbols. The variable Poisson's ratio theory agrees quite well with the experimental results out to a $\lambda_1$ of about 2.0 (doubling of length).

Designing with elastomeric materials is a difficult problem. Conventional approaches employ curve fits to experimental data, from which estimates for various partial derivatives of the work of deformation (W) are obtained. This is a difficult, time-consuming process, and the correct form of these derivatives is still a matter of debate.

The current formulation takes a much simpler approach. Rather than seeking a form for W, it directly relates stress and strain with equations that resemble the well known Hooke's law familiar to most practicing engineers. The theory needs only one experimental constant, E. No curve fitting of experimental data is needed. The theory appears to be useful for strains up to about 100%, which covers the

range for which most rubber-like materials are used for engineering purposes (tires, seals, etc.).

The theory has also been used to compute $W(I_1, I_2)$ and the partial derivatives of W with respect to the two strain invariants $I_1$ and $I_2$. This analytic derivation of the derivatives should lead to a better understanding of the complicated material behavior of rubber-like materials, and should help resolve some of the current controversies regarding experimental results.

The approach may also have applications to the behavior of other essentially incompressible materials—for example, biological materials, and the plastic deformation of metals.

**Ames-Moffett contact: L. Erickson**
**(415) 604-6217**
**Headquarters program office: OA**

## Computational Studies of a High-Performance Diffuser

**Michael J. Fletcher, Gary B. Cosentino, Mark J. Won**

The use of computational techniques for analyzing and designing aerodynamic components has become standard practice because of the long lead times, excessive costs, and limited parametrics and diagnostic information associated with wind tunnel tests. The present work examines the results of a computational study conducted on a representative high-performance inlet diffuser duct.

The diffuser used in this study is shown in the first figure. The throat station is elliptical in cross

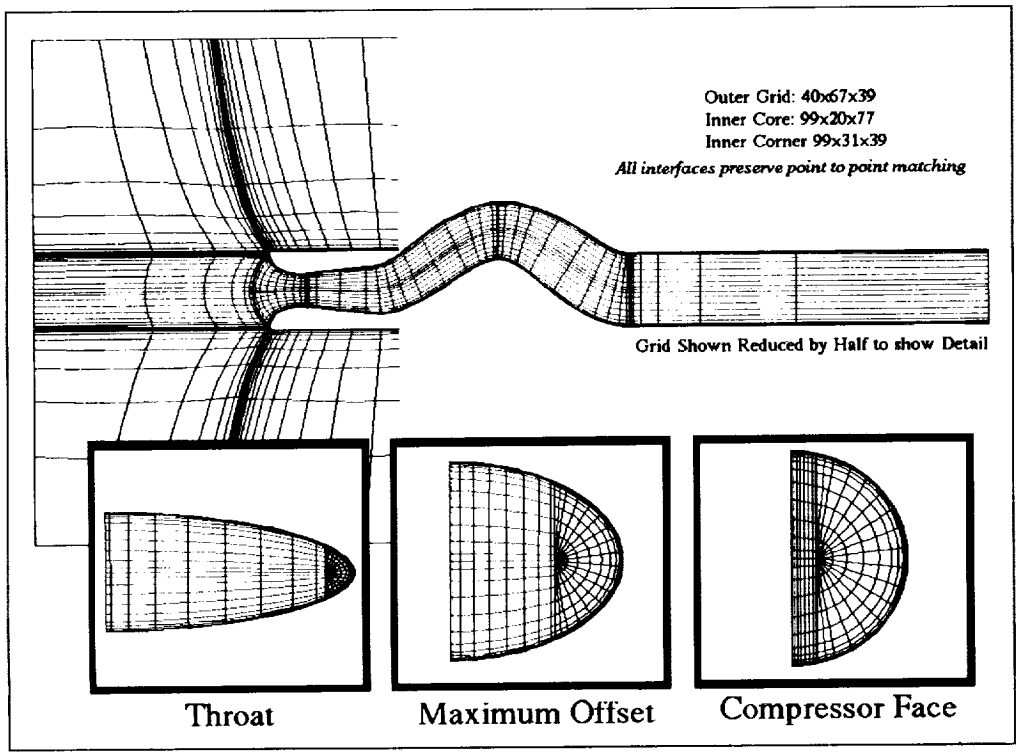


*Fig. 1. Side view of the diffuser showing the grid topology.*

section and has an aspect ratio of 3.85. The elliptical cross section gradually changes to become fully circular at the simulated compressor face location. The length of the duct is 4.0 times the compressor face diameter and the area of the compressor face is eighteen percent larger than the area of the throat station. The design flow value for the diffuser was chosen to yield a throat Mach number of 0.75. The one additional feature of this diffuser that makes it particularly representative of a high-performance inlet is the high degree of curvature throughout the duct. Although this diffuser is not designed for any specific aircraft application, its features are representative of high-performance aircraft inlets.

The computational results were obtained using the RANS3D flow solver. Recent development of RANS3D has led to the ability to analyze both external flow fields, such as those about a wing or body, and internal flow fields, such as diffusers. This work provided some of the initial validation of RANS3D's ability to predict internal flow characteristics as well as a means to develop and examine the boundary conditions necessary for defining an internal flow problem.

One of the most important aspects of computational fluid dynamics studies is the grid topology used to solve the problem of interest. No flow solver can overcome the problems associated with a poor grid, therefore care was taken when creating the grid for this diffuser problem. With diffusers that are circular in cross section, a simple O-type grid can be used to define the internal flow-field volume. But if the geometry is noncircular, as in this study, then an O-type grid can result in poor resolution in some regions and severe grid-cell distortion in others. In an effort to circumvent these problems, a novel grid topology was developed in which the interior of the diffuser was defined by an H-type grid capped by an O-type grid to define the corner regions. This topology, which is shown in the first figure, allowed for better resolution of the diffuser in the regions of interest and also improved the problems of grid-cell distortions.

Another important benefit of the two-grid topology was the elimination of the singularity at the collapsed edge of the O grid. Ordinarily, a special averaging technique must be imposed at this point to enforce the boundary condition of the flow field. Although many averaging techniques have been investigated, none have proved satisfactory for

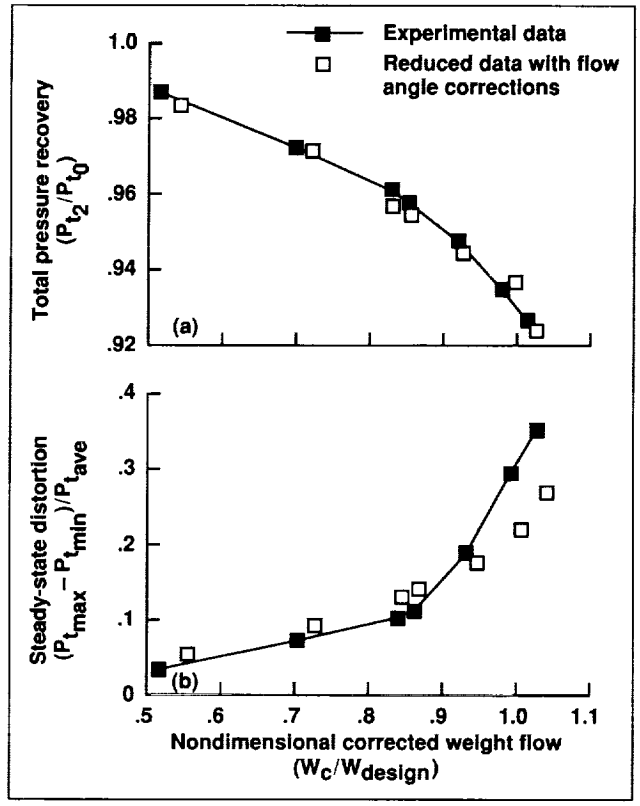


*Fig. 2. Total pressure ($P_t$) recovery (a) and steady state distortion (b) at the engine face.*

internal flows. By carefully aligning the O-type and H-type grids, the information at the singularity of the O-type grid can be obtained from the interior of the H-type grid, thus eliminating the problems associated with the requirement for averaging to obtain a boundary condition.

Results were obtained for a number of different flow conditions and these were compared to the experimental results from a static inlet model tested in the Propulsion Simulation Calibration Laboratory at Ames Research Center. The second figure shows comparisons of the predicted and measured total pressure recovery and steady-state distortion at the compressor face. The total pressures show good agreement at all flow rates, but for steady state distortion, the agreement falls off above about 95% of the design flow value. In addition to these results, it was also found that the grid dependency in the computational solutions, although reduced, was not eliminated (as was hoped) by using the O-type and H-type grids.

In conclusion, the RANS3D flow solver was shown to provide reasonable results for a complicated internal flow-field geometry. New boundary conditions suitable for internal flows were developed and tested in the RANS3D code. In addition to the work on the code, a new approach to internal grid topologies was examined in an effort to eliminate some of the problems associated with single O-type grids used in internal flows.

**Ames-Moffett contact: M. Fletcher**
**(415) 604-5923**
**Headquarters program office: OA**

## Integration of Numerical and Experimental Wind Tunnels (I_of_Newt)

**Dennis J. Koga**

A new program called Integration of Numerical and Experimental Wind Tunnels (I_of_Newt) has been undertaken to provide remote-access wind tunnel capabilities and real-time integrated comparisons between experimental and computational data in the Ames Unitary Plan Wind Tunnels. The primary objective is to provide more useful and comprehensive information for Ames wind tunnel customers.

The I_of_Newt program will include experimental techniques such as pressure-sensitive paint (PSP) for nonintrusive detection of surface pressures, temperature-sensitive paint and infrared thermography for temperature measurement and boundary-layer transition detection, body-deformation mapping, and laser vapor screen and global velocimetry techniques for off-body flow-field measurement.

The unique feature of the I_of_Newt implementation is that data from these experimental measurement methods are centrally maintained, along with traditional wind tunnel run parameter data and precomputed computational-fluid-dynamics (CFD) results, to provide a complete and comprehensive analysis of the data. The figure shows an example of a comparison graphic that is available to investigators in the wind tunnel control room. The PSP result was obtained using a NASA-Ames-developed, automated, real-time PSP data acquisition system in the 11- by 11-Foot Transonic Wind Tunnel. The CFD results were precomputed for the same model geometry and flow conditions, including the presence of the slotted transonic wind tunnel walls. This comparative information was also delivered to a remote customer site via data networks.

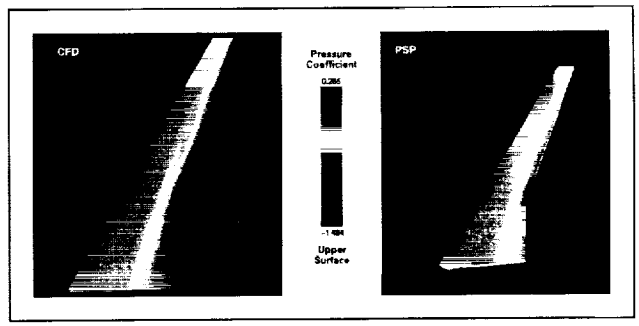


*Fig. 1. I_of_Newt real-time display of CFD and pressure-sensitive paint data. (See color plate 2 in Appendix)*

Future work on I_of_Newt will incorporate additional experimental techniques into the data-base structure, provide a link with the NAS Cray supercomputers to run near-real-time CFD cases in support of wind tunnel model modifications, and ultimately establish a more complete two-way communication link to remote customers. A remote-access wind tunnel will enhance the efficiency and quality of aerodynamic testing.

**Ames-Moffett contact: D. Koga**
**(415) 604-6285**
**Headquarters program office: OA**

# Cartesian CFD Analysis of a High-Lift Delta-Wing Configuration

**John E. Melton, Francis Y. Enomoto**

Although the variety of complicated geometries that have been analyzed using computational fluid dynamics (CFD) continues to expand, the process of grid generation remains both tedious and difficult. Until this obstacle is overcome, two of the major promises of CFD will remain unfulfilled: rapid aerodynamic analysis of novel configurations, and a dramatic reduction in the wind tunnel testing of configurations with flap and control-surface deflections. Despite the many advances in interactive grid generation techniques, the time to completely grid and analyze complicated geometries is still measured in weeks, and sometimes in months. For engineers involved in the design of new aircraft, rapid turnaround requirements often necessitate time frames of one to two days as the absolute maximum for the analysis of complete configurations. Until flow fields about arbitrarily shaped geometries can be numerically simulated in a timely and robust fashion, the analysis of new configurations and the effects of control-surface deflections will continue to constitute a large majority of aircraft wind tunnel investigations.

Unfortunately, the techniques currently used for interactive structured grid generation and unstructured tetrahedral grid generation still require large amounts of human interaction. In most cases, substantial specialized training is necessary before the grid generation and flow solver codes can be used effectively, and even those who are highly skilled in the process would not describe it as productive, enjoyable, or efficient. The current research in Cartesian grid generation and flow solution algorithms is intended to demonstrate that these Cartesian approaches have the potential for becoming the first highly automated techniques for the inviscid Euler analysis of arbitrary geometries.

Methods that use Cartesian grids for the aerodynamic analysis of complicated geometries are not as numerous as the more conventional multiblock structured or tetrahedral unstructured methods, but they are currently gaining popularity for a variety of reasons. Cartesian grids are natural candidates for multigrid algorithms, and Cartesian cells can be easily subdivided in order to provide the increased grid resolution necessary for capturing surface geometry details. Cell subdivision can also be performed for each flight condition, thus providing efficient off-body grid resolution for the study of important flow-field structures such as shocks and vortices.

Cartesian approaches employ a fundamentally different strategy for discretizing and simulating the flow fields about complex geometries. Instead of using complicated body-fitted grid topologies with "simple" boundary-condition routines, "simple" Cartesian grids are combined with sophisticated boundary-condition routines. An important consequence of the absence of a conventional body-fitted grid is the shift in the grid-generation philosophy away from increased interactivity and toward complete automation.

The first figure shows an initial application of the Cartesian Euler technique to a representative cranked-delta-wing configuration. Two configurations, one with flaps undeflected and the other with

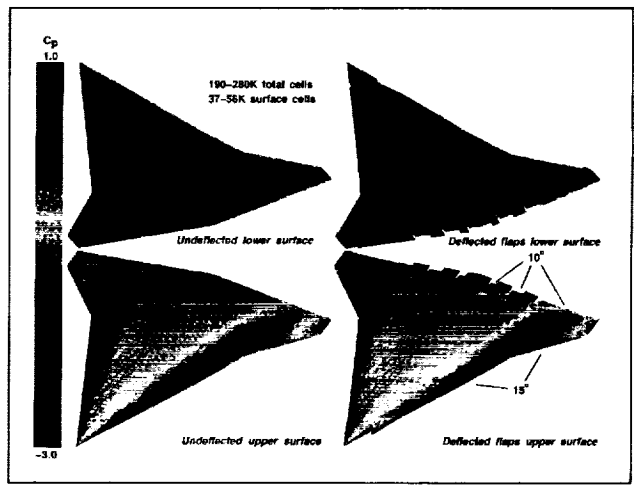


*Fig. 1. Grid and surface pressure coefficient distributions for two cranked-delta-wing configurations. (See color plate 3 in Appendix)*

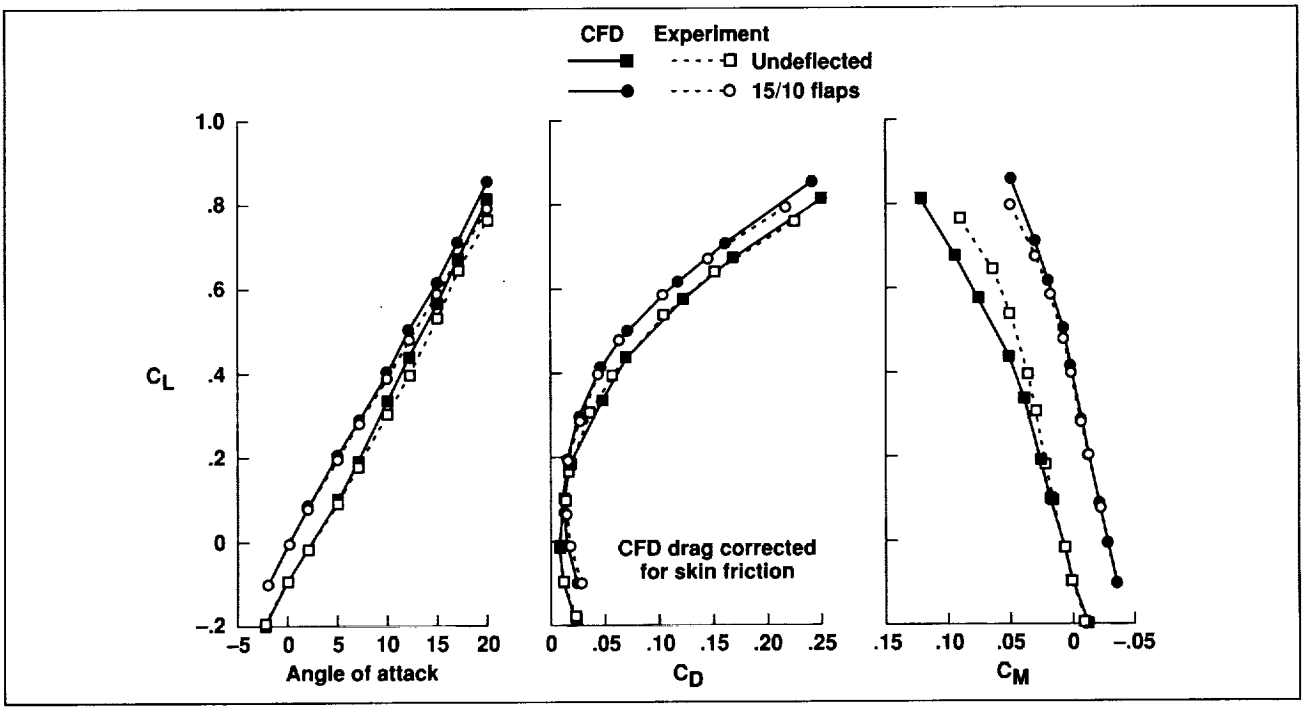


*Fig. 2. Comparison of Cartesian Euler CFD predictions with experimental data.*

leading- and trailing-edge flaps in a takeoff configuration, were analyzed at a flight Mach number of 0.2. For the takeoff configuration, a large portion of the leading edge was deflected down 15 degrees, and the three separate trailing edge flaps were deflected down 10 degrees. The upper and lower surfaces of the wing are colored by the value of the local pressure coefficient. The automatic refinement of the grid around the edges of the wings and flaps is clearly evident. The computational predictions for the two configurations are compared with experimental data over a wide range of angles of attack in the second figure. (Unlike the experimental data, the CFD solutions did not include the effects of the fuselage.)

The CFD geometry descriptions for the wings consisted of networks of abutting panels, and the entire list of grid-generation instructions were contained in three files with a total of 20 command lines. The grid generation for each configuration required approximately 3 single CPU hours of Cray C-90 time, and each flow solution required approximately 30 minutes and 38 megawords of memory for each Mach number/angle of attack combination.

**Ames-Moffett contact: J. Melton**
**(415) 604-1461**
**Headquarters program office: OA**

# Application of NURBS Curves to Airfoil and Wing Design

David A. Saunders, Robert A. Kennelly, Jr.

Nonuniform rational B-spline (NURBS) curves and surfaces have been widely adopted by the computer-aided design and manufacturing (CAD/ CAM) industry because they provide a means of representing all of the standard geometric shapes in a precise, unified mathematical form. Furthermore, the CAD system has become a vital component of the aerodynamic design process, both in preparing tool paths for numerically controlled machining of wind tunnel models and in preparing surface grids for analysis of designs via computational fluid dynamics (CFD).

Since CFD analysis and design-by-optimization are now indispensable for effective aerodynamic design, it is desirable that the CFD flow solvers use the same geometric representation as the CAD systems—the NURBS representation.

Starting with software utilities in the DT_NURBS package available to NASA from the David Taylor Research Center, additional software suited to airfoil and wing design has been developed at Ames and applied successfully.

First, in order to keep the necessary number of design variables (control point coordinates) modest, an improved method for approximating a given curve (such as an airfoil or its camber line) was developed in place of the standard linear method, which requires considerably more control points for adequate precision (see example in the figure).

Other utilities were required, such as those for determining airfoil thickness and area, and for discretizing such curves appropriately, before CFD design with the new representation could begin. Two transonic full-potential flow solvers, FLO6QNM and R22OPT, were interfaced with the NURBS utilities, and the design-by-optimization capability of these solvers was applied to the oblique all-wing (OAW) supersonic transport project.

The basic cabin section was designed initially as an 18-control-point (nonrational) 4th-degree B-spline curve, although considerably more control points were required subsequently as the design was refined.

Careful tailoring of the downstream tip cap section with a 12-control-point/4th-degree B-spline curve representation of the camber line minimized the likelihood of flow separation in this most troublesome region (as verified by Navier–Stokes calculations with the Ames flow solver OVERFLOW).

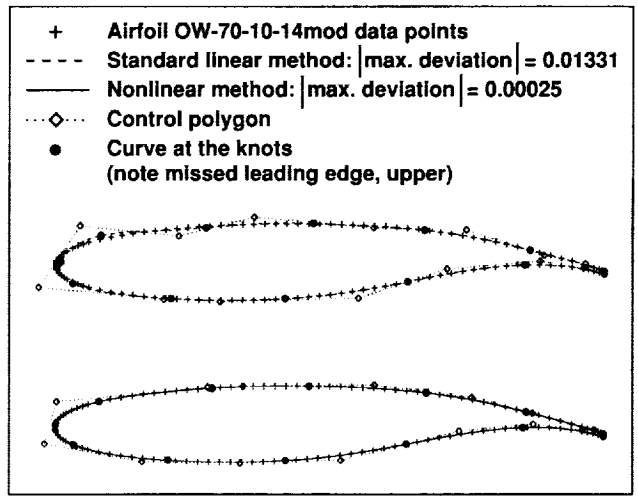


*Fig. 1. Standard and improved NURBS curve fits. The weakness of the standard linear least squares method of approximating a typical airfoil as a B-spline curve is illustrated (lower half of the figure, particularly near the leading edge, where the standard fit is quite inadequate). The improved method optimizes the knots (where the piecewise polynomials meet) as well as the control point coordinates, by solving a nonlinear least squares problem. The result is a more viable starting point for CFD design-by-optimization of the airfoil in NURBS form—the form now preferred for compatibility with modern CAD systems.*

The final OAW wing was supplied to the CAD system compactly as 101 B-spline section curves which were readily derived from the four actual defining sections. Arranging for the latter to use *identical knots* allowed the lofting (a mixture of nonlinear and linear tapering of chord and thickness) to be done by straightforward scaling of the control points of the four main stations. A NURBS surface with full fidelity was easily constructed from these sections on the CAD system. Wind tunnel testing of two OAW designs as 7-foot models is scheduled for spring 1994.

**Ames-Moffett contact: D. Saunders**
**(415) 604-1480**
**Headquarters program office: OA**

# Computation of Aero-Optical Effects for Airborne Observatories

**Christopher A. Atwood**

A technique that determines the optical distortion caused by computed density fields has been developed. The method allows the results of unsteady computational fluid dynamics (CFD) simulations to be used in the analysis of the optical performance of airborne sensors. This type of distortion can manifest itself in the twinkling of stars on clear nights, for example.

The approach uses a time sequence from a flow solution computed via the Reynolds-averaged Navier–Stokes equations. The shear-layer flow above the telescope or other sensor is used to directly compute the optical degradation caused by large-scale density fluctuations.

The method passes a series of light rays through a tessellated structured grid, each tetrahedron of which possesses a local mean index of refraction. The index of refraction is a function of the local density of the gas and the wavelength of the light. After tracing a grid of rays through a series of instantaneous density fields, the time and spatial variation of optical-path distortion is obtained. Using this phase-distortion information, instantaneous and time-averaged far-field diffraction patterns can be computed. Only the phase distortion resulting from fluid scales resolved by the CFD solution can contribute to the optical analysis.

The aero-optical codes were applied to two- and three-dimensional U.S. Army Airborne Optical Adjunct (AOA) and Stratospheric Observatory for Infrared Astronomy (SOFIA) configurations. The figure shows a proposed SOFIA concept, which is

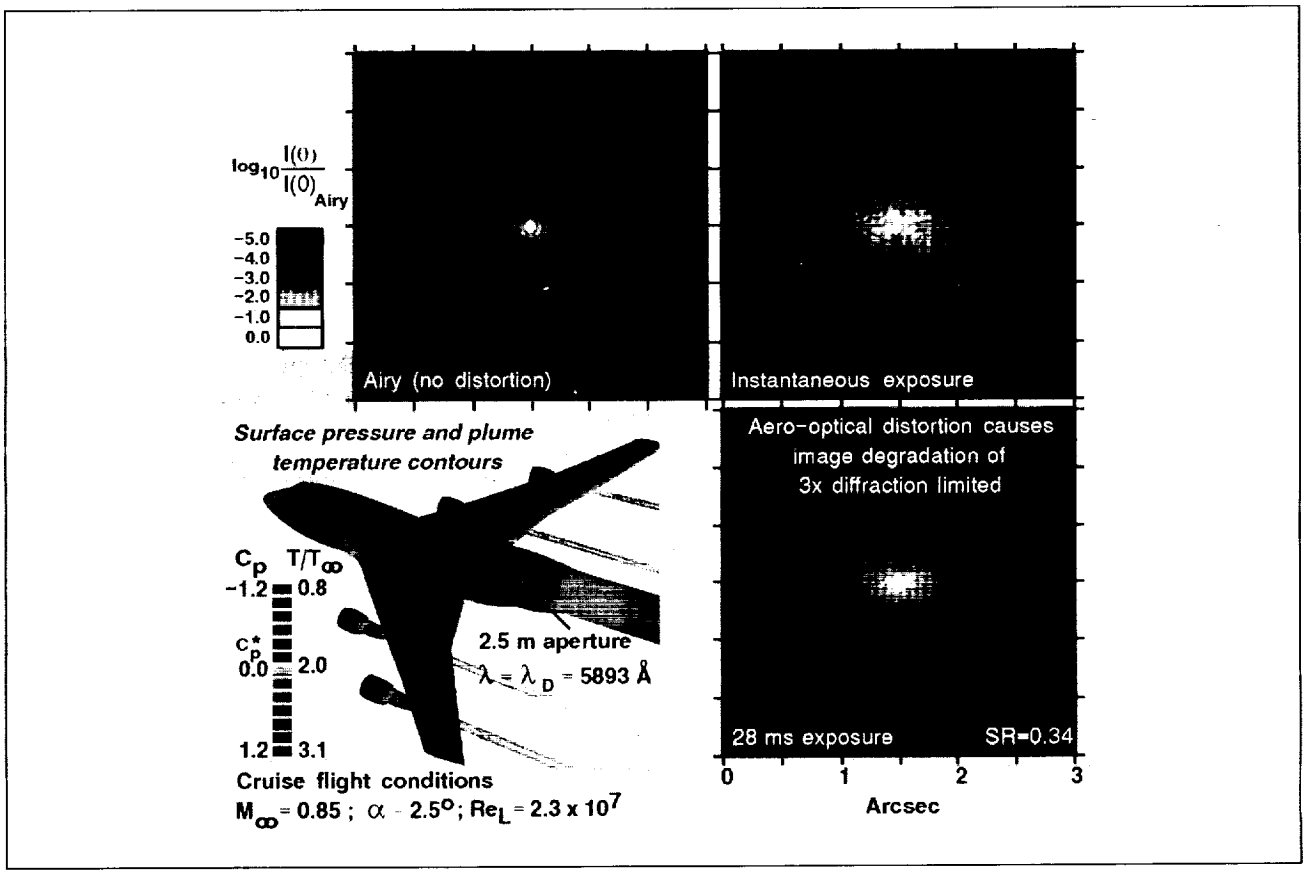


*Fig.1. Computed optical distortion for the proposed Stratospheric Observatory for Infrared Astronomy (SOFIA).*

plotted with surface-pressure and engine-plume-temperature contours. The figure also shows the simulated image produced by the observatory for an instantaneous- and a long (0.028-second) exposure response to a point source of light (analogous to a distant star). Comparison of the distortion-free, or Airy, diffraction image with the instantaneous- and long-exposure images reveals a degradation in resolution caused by the large-scale aero-optical effects.

The aero-optical codes allow integrated computational analysis of the coupled fluid and optical fields about realistic geometries. This capability provides an estimate of the aero-optics portion of the total optical distortion, and hence reduces potential expenditures for other system components.

**Ames-Moffett contact: C. Atwood/T. Holst**
**(415) 604-3974/6021**
**Headquarters program office: OSSA**

## Geometry Data-Exchange Standard

**Matthew W. Blake, Patricia A. Kerr, Scott A. Thorp, Jin J. Chou**

Geometry data exchange between design and analysis systems has been a major stumbling block to engineers attempting to use computational fluid dynamics in the design of new products. The most popular current method for exchanging this geometric data is to use the Initial Graphics Exchange Specification (IGES). IGES provides a super-set of geometric representation options for translating data between systems. This set of representation options presents a problem, because nearly every computer-aided design (CAD) vendor and every analysis software package has a different representation. Thus there may be a situation in which System A may represent a circle in one way, but System B only reads a circle represented a different way. Both are legal IGES representations, but the two systems cannot exchange data.

NASA has developed a subset of IGES that is capable of representing any simple or complex geometry based on nonuniform rational B-splines (NURBS). The document defining this subset is entitled, "NASA Geometry Data Exchange Specification for Computational Fluid Dynamics," often referred to as NASA-IGES. If two systems can both read and write data in this form, they will be able to exchange geometry data rapidly and accurately. Engineers should then be able to rapidly pass geometry data between design and analysis systems.

The NASA-IGES protocol is being utilized and supported by personnel at five NASA centers. It provides a consistent method for the exchange of geometry data between different engineering systems. We are currently developing software to process any IGES file into the NASA-IGES form and are planning to expand the specification to geometry topology information for use in automating the analysis process.

**Ames-Moffett contact: M. Blake**
**(415) 604-4978**
**Headquarters program office: OA**

# Navier–Stokes Prediction of Maneuver Aerodynamics

**Neal Chaderjian, Lewis B. Schiff**

Improved maneuverability of modern tactical fighter aircraft can be achieved by flying at high angles of attack. This performance gain is a result of the nonlinear lift obtained from vortices that form on the leeward side of the aircraft. If the angle of attack is sufficiently large, vortex asymmetries can form and result in a sustained roll oscillation known as wing rock. This phenomenon can be dangerous and can restrict the aircraft's useful flight envelope.

The Navier–Stokes Simulation (NSS) code numerically integrates the time-dependent, three-dimensional Reynolds-averaged Navier–Stokes equations. The goal is to provide an experimentally validated computational fluid dynamics (CFD) tool for computing wing rock and other aircraft motions. Present investigations focus on a 65-degree-sweep delta wing with subsonic turbulent flow conditions. The NSS code has the capability to treat complete aircraft geometries.

Previous results showed that the NSS code could predict the aerodynamics of a delta wing for static roll and forced dynamic roll motions. Static and time-dependent forces, moments, and wing surface pressures were in excellent agreement with experimental data. These computations were carried out at 15 degrees angle of attack and for roll angles up to 42 degrees. At this angle of attack, there was no vortex breakdown (vortex breakdown may accompany wing rock).

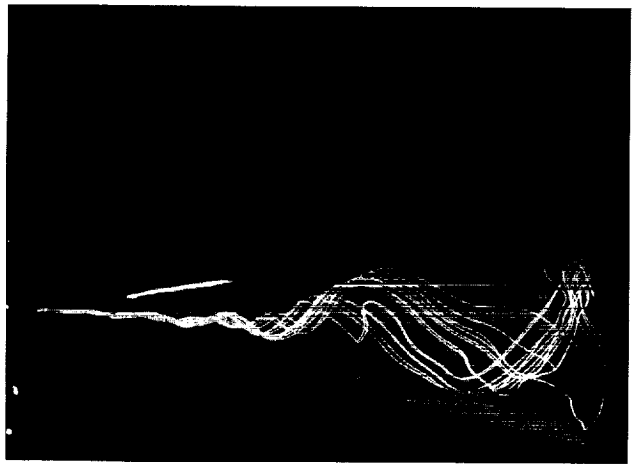

*Fig. 1. Visualization of vortex breakdown at −5 degrees of roll. (See color plate 4 in Appendix)*

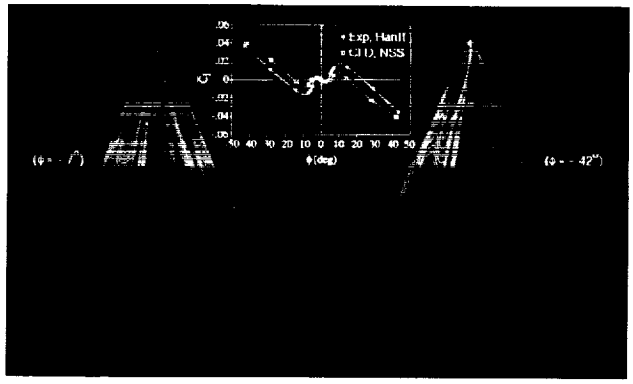


*Fig. 2. Comparison of computational and experimental $C_l$ and visualization of leeward-side surface pressures. (See color plate 5 in Appendix)*

A follow-on study was carried out this year at 30 degrees angle of attack, where vortex breakdown does occur. The objective of this research was to determine if the NSS code could capture a static rolling-moment nonlinearity that was observed in an experiment. Static roll angles up to 42 degrees were investigated. The resulting flow fields were highly nonsteady as a result of vortex breakdown. The first figure shows a perspective view of the delta wing and the leeward-side vortices. The left wing vortex (pilot's view) is yellow, and the right wing vortex is green. At −5 degrees of roll, the left wing is rotated to a lower position than the right wing. Vortex breakdown is apparent in the scatter of particle traces used to visualize the vortex cores. The left wing breakdown position is closer to the wing apex, whereas the right wing breakdown position is closer to the wing trailing edge.

The second figure shows the mean static rolling-moment coefficient ($C_l$) versus roll angle. A negative slope corresponds to a region of static roll stability, and a positive slope corresponds to a region of static roll instability. There are five trim points (zero $C_l$), three of which are statically stable in roll (negative

slope). The computational results are in good agreement with the experimental results. Also shown in the figure are planform views of the leeward-side surface pressures for –7 and –42 degrees of roll. Blue contours indicate low pressures; red contours indicate high pressures. Vortices cause local low-pressure regions on the wing. At –7 degrees of roll, the left wing vortex breaks down closer to the wing apex, whereas the right wing vortex breaks down closer to the wing trailing edge. This is apparent in the blue and yellow contours of the right vortex extending farther downstream than the contours of the left-side vortex. The difference results in a negative (statically unstable) rolling moment. At –42 degrees of roll, the left wing vortex breaks down near the wing apex, and the right wing vortex does not break down at all. The right wing vortex (red contours) is very weak, however. The result is a positive (statically stable) rolling moment. These computational results help explain the presence of the rolling-moment nonlinearity.

Future plans include the numerical simulation of forced roll motions and a damped free-to-roll motion with vortex breakdown, and then wing rock.

**Ames-Moffett contact: N. Chaderjian**
**(415) 604-4472**
**Headquarters program office: OA**

## Supersonic/Transonic Wing-Body Design Optimization

**I-Chung Chang, Francisco Torres**

A newly developed wing-design code, based on the three-dimensional Euler equations and a constrained numerical optimization technique, has been used to enhance the performance of high-speed airplane wing-body configurations. The new design tool consists of three major modules: (1) a flow solver, (2) a numerical optimizer, and (3) a geometry modifier. These modules interface with each other as a single design tool that is efficient, robust, and fast.

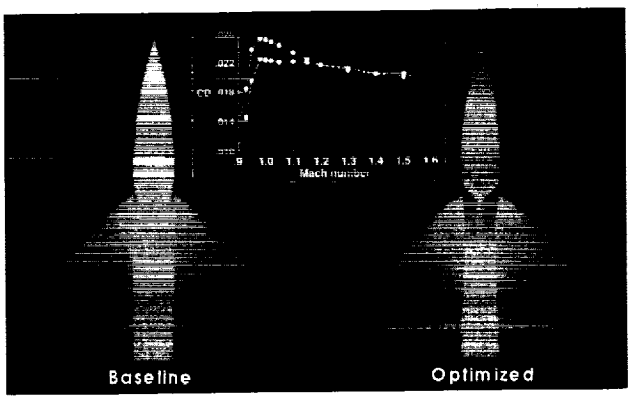


*Fig. 1. Comparison of baseline and optimized wing-body configuration. (See color plate 6 in Appendix)*

The new code has the capability of not only modifying the wing but also of automatically modifying the fuselage. It has been used to improve the lift-to-drag (L/D) ratio of wings in the presence of fuselages for cruise conditions at both transonic and supersonic speeds. Pressure coefficients predicted by the design code for a well known wing-body model at different flight speeds up to Mach 1.2 were in excellent agreement with experimental data.

A test case was performed on a simple wing-body geometry consisting of an ogive cylinder fuselage with a clipped delta wing. The figure shows this configuration with the Mach contours for the baseline and optimized results. The results confirm Whitcomb's supersonic area rule numerically. In this case, the fuselage was modified during the design process while the wing remained unchanged. In order to achieve minimum drag, the total longitudinal distribution of cross-sectional area, wing and body, would have to be equivalent to that of a minimum-drag body of revolution. Since the wing was fixed, the design process modified the body shape, resulting in a "coke bottling" of the fuselage. This can be visually observed at the wing–body interface in the

figure. Thus, the area rule effect was obtained numerically using the new computational-fluid-dynamics (CFD) design tool. The graph in the figure shows the drag rise reduction between the baseline and optimized configurations over a range of Mach numbers from 0.9 to 1.6. It can be seen that there was indeed an improvement in the new wing-body design, which demonstrates the usefulness of the code. Because of the modular aspects and versatility of the new design tool, it is feasible to extend its capability to handle more complex configurations and eventually an entire aircraft.

**Ames-Moffett contact: I. Chang**
**(415) 604-6396**
**Headquarters program office: OA**

## Sonic Boom Propagation and Prediction

**Samson Cheung**

The sonic boom produced by current commercial supersonic transport is too environmentally disruptive for routine overland flight. By properly distributing the airplane lift, the pressure pulse associated with the sonic boom can be alleviated. In the design cycle of low-boom aircraft, sonic boom prediction must be accurate and efficient. The objective of this research is to develop an efficient and accurate computational method for prediction of sonic-boom wave propagation.

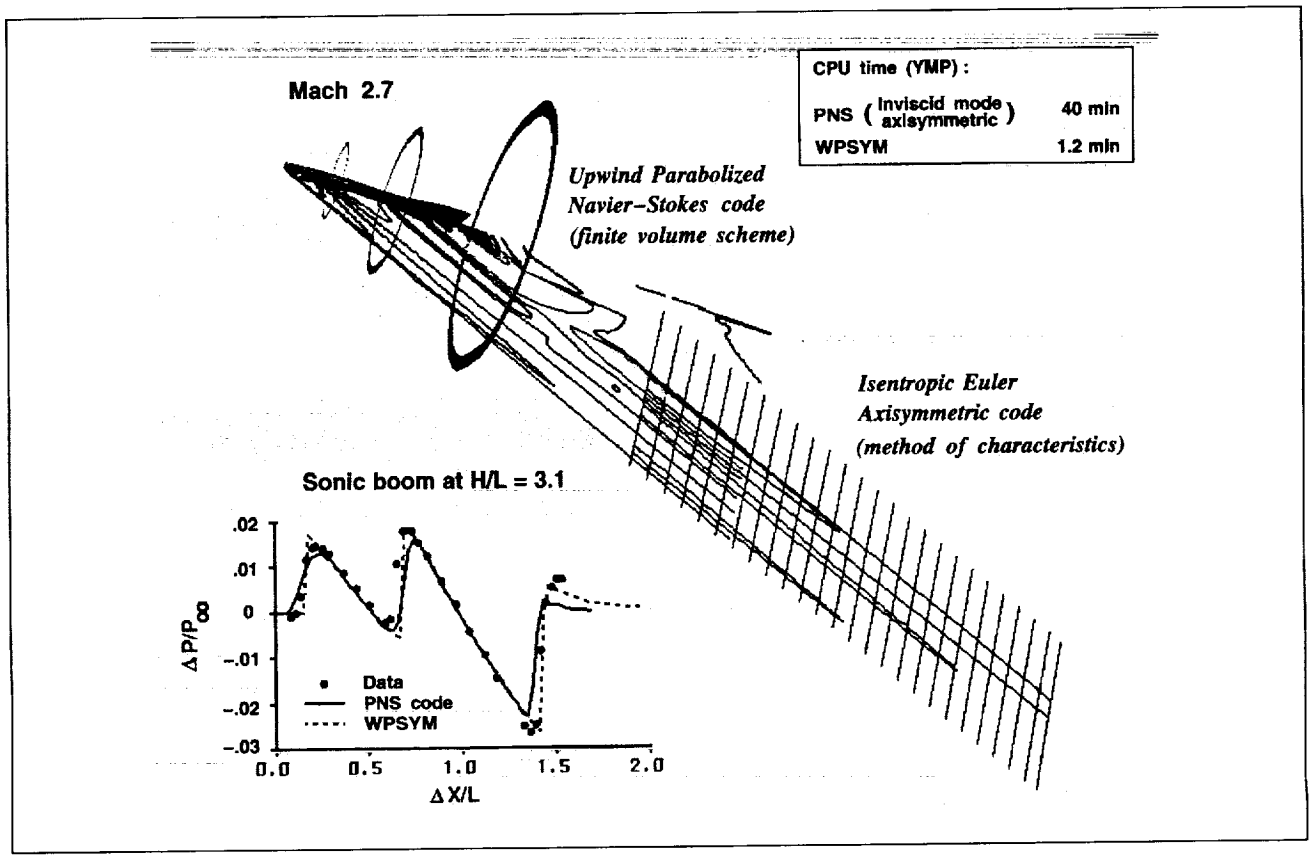


*Fig. 1. Wave-propagation prediction capability.*

Recently, computational fluid dynamics (CFD) was applied to calculate the near-field solution in the low-boom airplane design process for high-speed civil transport (HSCT). However, only low-order extrapolation methods were used in sonic boom propagation prediction because current CFD methods are too expensive for far-field calculations. The present wave-propagation code uses a higher-order method in a computationally efficient manner, allowing timely and accurate solutions to low-boom HSCT problems.

The equations solved by the present wave-propagation code are the steady-state Euler equations. The flow is assumed to be axisymmetric with constant total enthalpy and constant entropy. The system of the equations is converted to the form of Burger's equations and the equations are solved by the method of characteristics.

The figure shows that the near-field solution is supplied by a three-dimensional (3-D) CFD code for a generic wing-body configuration. The CFD code solves the 3-D parabolized Navier–Stokes (PNS) equations. The PNS solution at about one body length downstream of the vehicle is then interfaced with two sonic-boom prediction codes, namely, the current axisymmetric wave-propagation code (WPSYM) and an axisymmetric PNS code. The plot in the figure shows the sonic boom at 3.1 body lengths (H/L = 3.1) under the vehicle. The results show that the current wave-propagation code defines the sonic boom shocks sharply and accurately with a computational speed 40 times faster than the axisymmetric PNS code.

This efficient sonic-boom-prediction code has allowed CFD low-boom airplane design to be performed in current supercomputer facilities.

**Ames-Moffett contact: Dr. Samson Cheung**
**(415) 604-4462**
**Headquarters program office: OA**

## Atomic Oxygen Fluorescence Excitation Using a Raman-Shifted Excimer Laser

**Douglas G. Fletcher**

Atomic oxygen is an important species in high-enthalpy and reacting airflows (such as scramjet combustor flows) because its concentration determines many of the primary reaction rates. Consequently, considerable effort has been directed toward the development of methods for exciting oxygen atom fluorescence, which can provide an indication of relative concentration without perturbing the flow. A new approach for inducing oxygen atom fluorescence with less complex laser instrumentation has recently been demonstrated. In this approach, a pressurized gas cell containing pure deuterium is used to Raman-shift a tunable argon-fluoride (ArF) excimer laser. Raman-shifting involves directing a focused laser pulse into a cell containing a pure, Raman-active gas. Stimulated Raman scattering in the focal volume within the cell gives rise to a number of output laser pulses which are separated from the input laser wavelength by integral multiples of the characteristic Raman frequency shift of the cell gas. Output pulses at longer wavelengths than the input pulse wavelength are termed Stokes orders, and the number and intensity of the Stokes orders produced by the Raman shifter depend on the input laser energy level and cell pressure. When an ArF excimer laser operating at 193.11 nanometers in the ultraviolet is used to pump a deuterium-filled gas cell, second and third Stokes orders are generated at 218.4 and 233.6 nanometers, respectively. The photon energies of these orders sum to match the excitation energy (88,631 wave numbers) of a strong, two-photon oxygen atom transition.

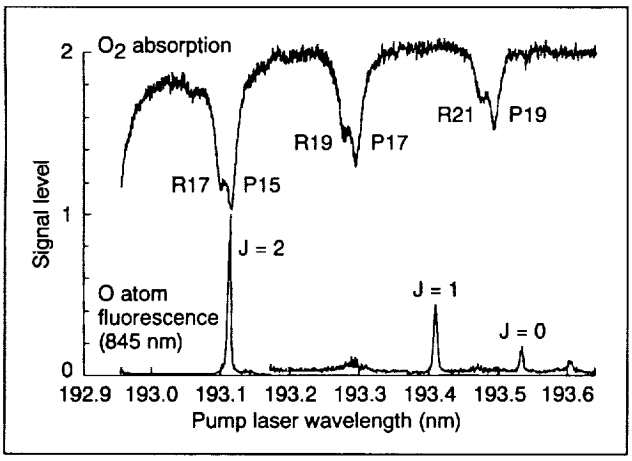


*Fig. 1. Atomic oxygen (O) fluorescence signal measured in room air after photolysis of molecular oxygen ($O_2$) as the ArF excimer laser is scanned through the central portion of its tuning range.*

To demonstrate this Raman-shifted, ArF excimer laser excitation approach, an oxygen atom population was created in room air from molecular oxygen absorption and predissociation at 193 nanometers. After a short time delay, the second and third Stokes-order pulses from the deuterium-filled Raman shifter are combined to excite the photolytically created oxygen atoms to a fluorescing state. The 845-nanometer fluorescence from the excited oxygen atoms is then recorded by a photomultiplier tube. The 193-nanometer pulse energy is recorded at the same time by a phototube to monitor the oxygen atom population at the measurement location and to provide a wavelength calibration as the excimer laser is scanned through its tuning range. Results from the demonstration experiment are shown in the figure, where the photomultiplier and phototube signals are plotted as a function of ArF excimer laser wavelength. The upper curve is the 193-nanometer pulse energy, and the minima result from increased absorption in the room air at wavelengths that correspond to rotational transitions of molecular oxygen. These transitions are identified in the figure by their rotational quantum numbers. The lower trace is the 845-nanometer oxygen atom fluorescence, which has three distinct peaks corresponding to two-photon transitions from the three energy levels of the ground state. As shown in the figure, all three oxygen atom transitions lie within the tuning range of the Raman-shifted, ArF excimer laser.

Previous laser-based approaches for exciting this two-photon atomic oxygen transition required the use of a YAG-pumped dye laser system which was usually operated near 226 nanometers. The results of the demonstration experiments show that the Raman-shifted, ArF excimer laser excitation approach now offers a capability that is comparable to commercially available YAG-pumped dye lasers but uses considerably less complex instrumentation.

**Ames-Moffett contact: D. Fletcher**
**(415) 604-6457**
**Headquarters program office: OA**

# Forebody Tangential Slot Blowing

Ken Gee, Yehia M. Rizk, Lewis B. Schiff

An aircraft flying at a high angle of attack may encounter control problems. The flow about the aircraft becomes unsteady and asymmetric, leading to a loss of directional control of the aircraft. Overcoming this problem will increase the safety and maneuverability of high-performance aircraft. This may be accomplished by developing methods that provide the pilot with sufficient side force and yawing moment to control an aircraft flying at a high angle of attack. One such method of providing the necessary side force and yawing moment is forebody tangential slot blowing.

Forebody tangential slot blowing consists of air being ejected tangential to the surface from a thin slot located close to the nose of an aircraft. This jet of air alters the flow field about the nose and fuselage of the aircraft such that a side force and yawing moment is created. A slot located to the pilot's right will create a side force and yawing moment directed to the right.

The forebody-tangential-slot-blowing method is being analyzed by computational fluid dynamics (CFD) for use on the NASA High-Alpha Research Vehicle (HARV). Solutions are obtained using the HARV geometry at typical flight conditions. The first figure illustrates the solutions that show the effect of blowing on the flow-field characteristics. Blowing causes the vortex on the blowing side to burst sooner than the vortex on the nonblowing side. The flow aft of the burst point is unsteady and impinges upon the vertical tails.

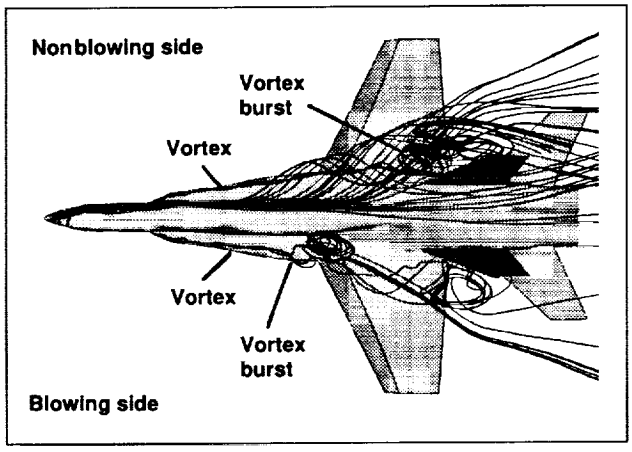


*Fig. 1. Effect of forebody tangential slot blowing on flow field about the HARV.*

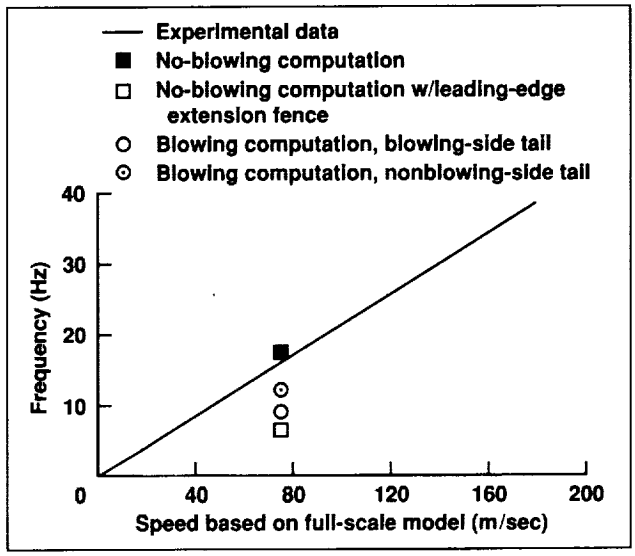


*Fig. 2. Effect of forebody tangential slot blowing on dominant frequency of aerodynamic loads about vertical tails.*

The unsteady flow about the vertical tails can lead to tail buffet or harmonic oscillations of the vertical tails. Tail buffet is harmful because it can lead to structural failure. Since forebody tangential slot blowing causes a change in the flow field, it also alters the frequency of the aerodynamic loads over the vertical tails, shown in the second figure. The computed solutions indicate that blowing changes the dominant frequency of the airloads over the vertical tails. Such changes must be understood if

forebody tangential slot blowing is to be a viable method of generating side force and yawing moment.

An understanding of the effects that forebody tangential slot blowing has on the flow field about high-performance aircraft will lead to a more efficient blowing system, and thus to greater maneuverability and safety. CFD is being used to analyze such effects. By combining CFD with experimental research, a thorough understanding of forebody tangential slot blowing may be developed.

**Ames-Moffett contact: K. Gee**
**(415) 604-4491**
**Headquarters program office: OA**

## Aeroelastic Computations for Aircraft Wings on Parallel Computers

**Guru P. Guruswamy, Chansup Byun**

Aeroelastic computations for aircraft pose several challenges to engineers, particularly computations for flows associated with shock waves and vortices. Because of their multidisciplinary nature, the aeroelastic computations are an order of magnitude more expensive than single-discipline computations. The maximum computational speed on the current serial computers has nearly been reached. The objective of this research is to perform aeroelastic computations on realistic configurations using the much faster parallel computers.

In this work, the three-dimensional Navier–Stokes equations of motion coupled with the finite-element structural equations of motion are solved using a time-accurate numerical integration scheme with configuration-adaptive dynamic grids. A domain-decomposition method suitable for parallel computers is used. In this method, the computational domain is divided into fluids and structural domains. The information between domains is communicated using the virtual zone concept. The fluids domain is solved in parallel with the structural domain in separate cubes (group of processors). Within each domain (cube), computations are also performed in parallel.

Based on the above approach, a new version of the Euler/Navier–Stokes Aeroelastic (ENSAERO) computer code that solves the Euler/Navier–Stokes equations simultaneously with the finite-element structural equations of motion for wings has been developed on the Intel iPSC/860 computer. The fluids part of ENSAERO, including the moving grid, is

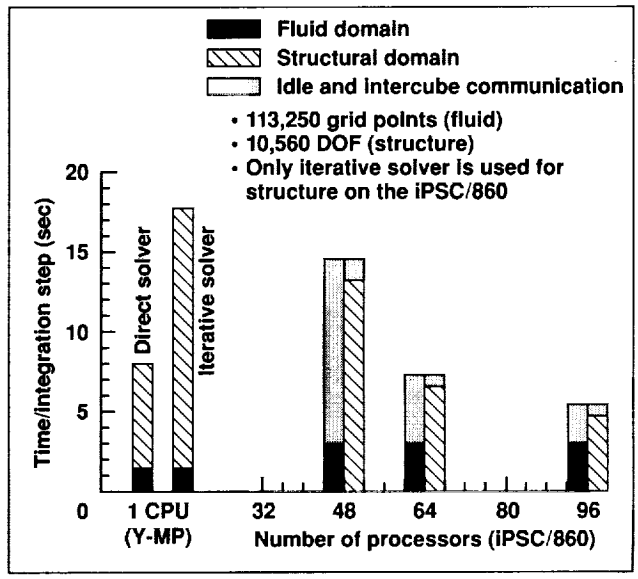


*Fig. 1. Performance of wing version of ENSAERO on Intel iPSC/860 computer.*

computed in a cube of 32 processors using the Euler equations, and the finite-element structures part of ENSAERO is computed in a cube using up to 64 processors. Increase in the computational speed is in two parts. First, computations for each discipline are done in parallel within the cube. Next, fluid and structural computations are done in parallel. The first figure shows the scalability of structural computations

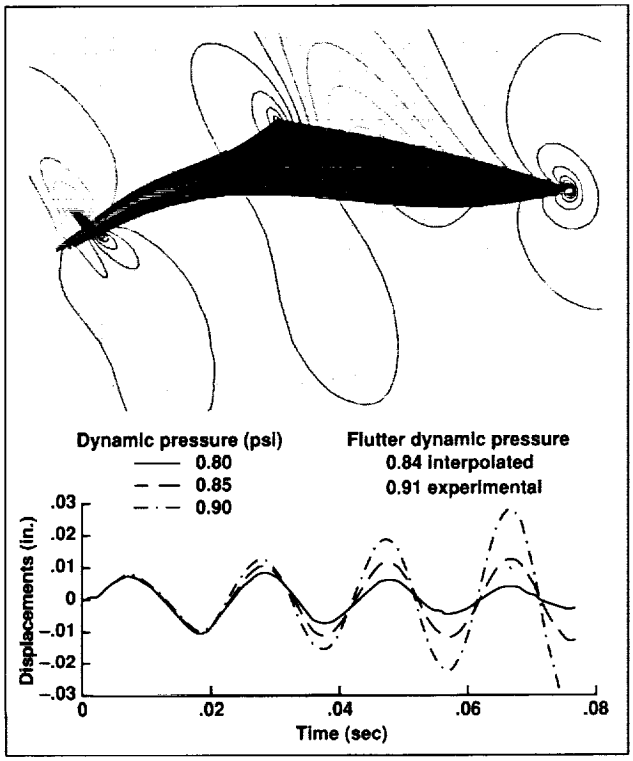


using 16, 32, and 64 processors. The second figure demonstrates computation of flutter speed for a typical wing.

The successful implementation of ENSAERO (wing version) with finite-element structures on the Intel computer is a major stepping-stone in the development of general-purpose computer codes to solve fluid/structure interaction problems on parallel computers.

**Ames-Moffett contact: G. Guruswamy**
**(415) 604-6329**
**Headquarters program office: OA**

*Fig. 2. Computation of flutter speed using parallel version of ENSAERO (Mach number = 0.854, angle of attack = 0.0 degrees).*

## Aeroelastic Computations for Wing-Body Configurations

**Guru P. Guruswamy, Chansup Byun, Shigeru Obayashi**

The main objective of this research is to develop general-purpose software to solve fluid structural interaction problems for aerospace vehicles, using the Euler/Navier–Stokes flow equations, coupled with finite-element structural equations on the state-of-the-art supercomputers. This report describes the work that has been completed for wing-body configurations.

The three-dimensional Euler/Navier–Stokes equations of motion, coupled with the finite-element structural equations of motion, are solved using a time-accurate numerical integration scheme with configuration-adaptive dynamic grids. This moving-grid capability can model oscillating control surfaces by using a shearing-grid concept. A computationally efficient domain-decomposition method suitable for both serial and parallel computers is used for aeroelastic computations. The computational domain is divided into fluids and structural domains, and the equations in these domains are solved using finite-difference and finite-element methods, respectively. The information between domains is communicated using a virtual-surface concept.

A new version of the Euler/Navier–Stokes Aeroelastic (ENSAERO) computer code that solves the Euler/Navier–Stokes equations simultaneously with the plate/shell finite-element structural equations of motion has been developed for wing-body configurations on a Cray C-90 computer. The code is demonstrated for a typical wing-body configuration. The body and wing are modeled using shell and plate

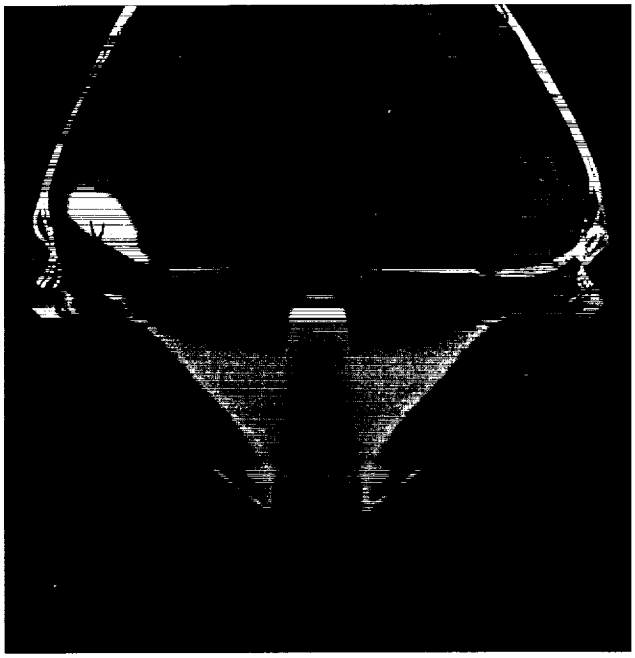

finite elements, respectively. Computations are done for transonic/vortical flows. These computations are the first of their kind to use computational fluid dynamics methods. The first figure demonstrates unsteady flow computations over a typical high-speed civil transport (Boeing Arrow wing-body) configuration with oscillating control surfaces. The second figure demonstrates the aeroelastic computations over a typical transport wing-body configuration.

Completion of this work lays an important foundation for the development of general-purpose, multidisciplinary codes that deal with fluid/structural/control interaction problems.

**Ames-Moffett contact: G. Guruswamy**
**(415) 604-6329**
**Headquarters program office: OA**

*Fig. 1. Unsteady flows over a wing-body configuration with oscillating control surfaces. (See color plate 7 in Appendix)*

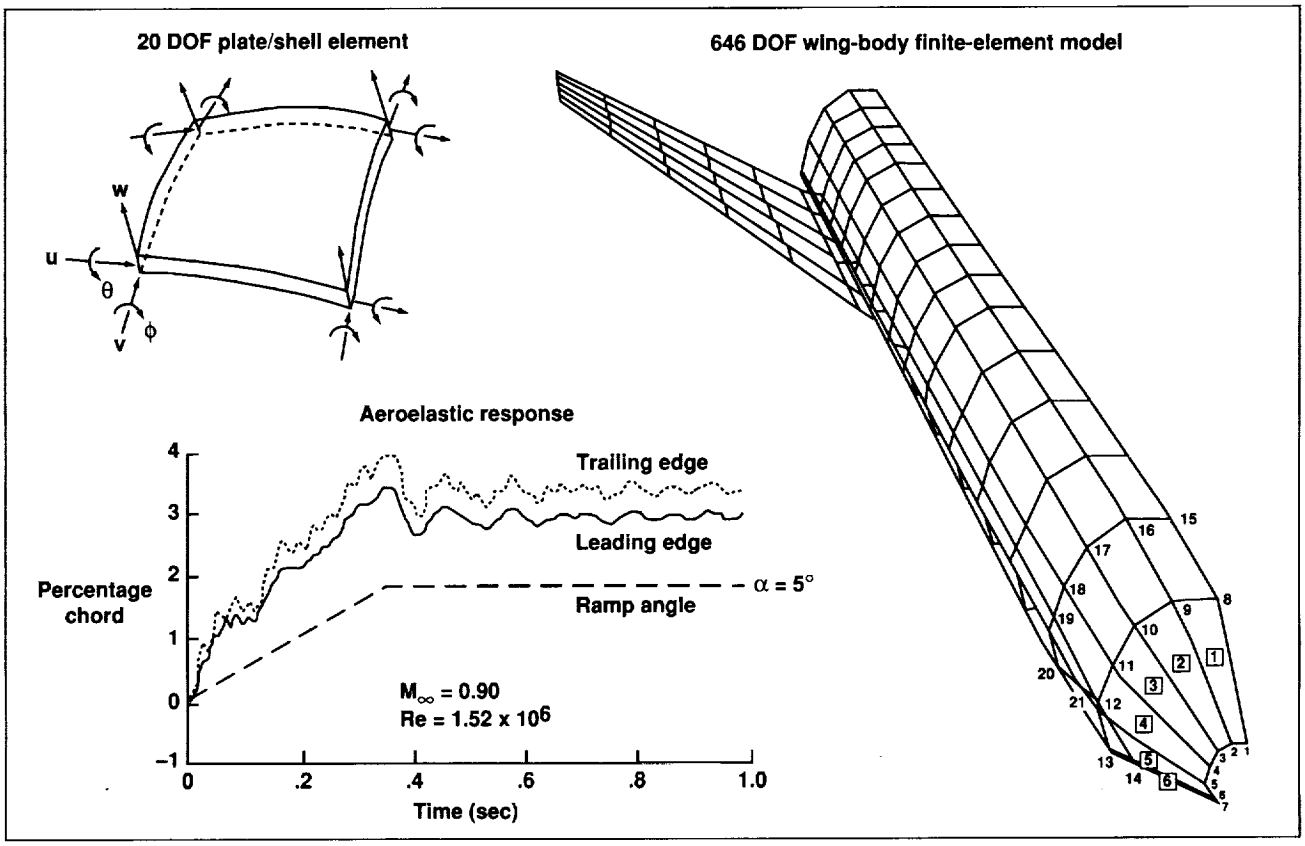


*Fig. 2. Aeroelastic response of a typical wing-body configuration.*

# The LU-SGS Scheme for a Viscous Compressible Flow Code

**Goetz H. Klopfer, Seokkwan Yoon**

It is well known that the finite-volume form of the diagonal Beam–Warming scheme has a time-step restriction. For constant time steps, the largest Courant–Friedrichs–Levy (CFL) numbers are less than ten. The CFL number is a nondimensional time step. With judicious time-step scaling, the maximum CFL number can be as high as 75. For numerical simulation of a realistic aerodynamic configuration, several dozen zones may be required, and much user input is required to determine the optimum time step and time-step scaling. Furthermore, for simulating unsteady viscous flows a constant time step is required, and the allowable CFL number of 10 is much too low for such a simulation to be practical. The objective of the present work is to use an alternative algorithm to the diagonal Beam–Warming scheme in the three-dimensional compressible Navier–Stokes code, CNSFV, so that the severe time-step restriction is avoided. For steady flows, larger time steps will allow faster convergence to steady state. For unsteady flow, the time-step restriction will be based solely on accuracy considerations, rather than algorithmic limitations. The LU-SGS (lower–upper symmetric Gauss–Seidel) algorithm

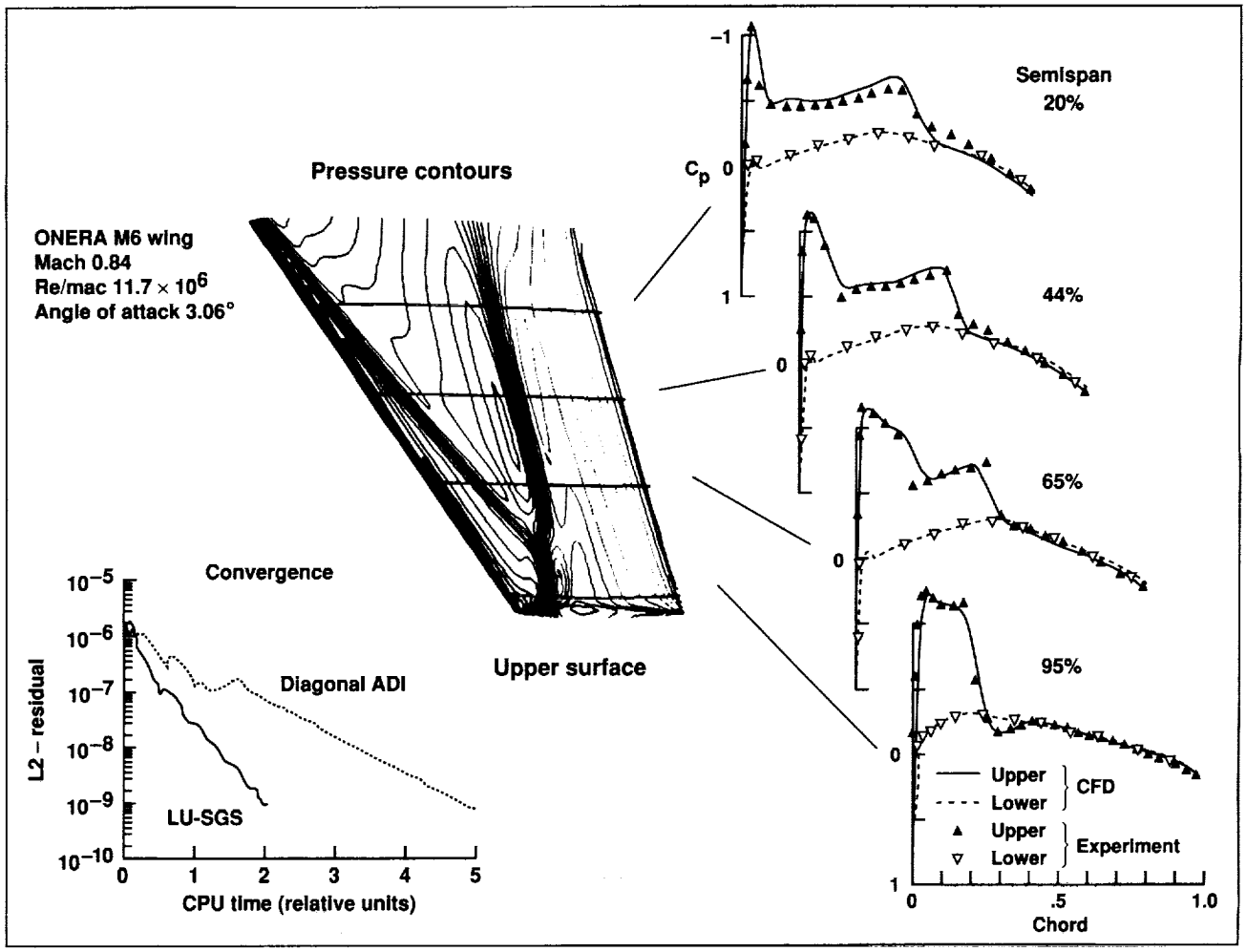


*Fig. 1. Comparison of the LU-SGS and diagonal Beam–Warming schemes and CNSFV code validation.*

has unconditional linear stability. Hence, this scheme is implemented in the CNSFV code and is validated by simulating a transonic turbulent flow around the ONERA M6 transport wing.

Computations have been performed for the ONERA M6 wing at Mach 0.8339, an angle of attack of 3.06 degrees, and a Reynolds number of 11.72 million for turbulent flows with both the diagonal alternating-direction-implicit (ADI) and the LU-SGS schemes in the CNSFV code. The turbulence model is the Baldwin–Lomax model. The grid consists of four zones with a total mesh size of $193 \times 49 \times 35$ points. The normal grid spacing at the wing surface is sufficiently fine to resolve the viscous sublayer. The steady-state results obtained with both schemes are indistinguishable and are compared to experimental results, as shown in the figure.

However, the computational cost for the LU-SGS has been reduced by a factor of two. The actual CFL numbers that were run with the LU-SGS scheme were 200,000, and no time-step scaling was necessary.

A multizonal compressible Navier–Stokes code has been improved by replacing the diagonal ADI algorithm with the LU-SGS scheme. With the new scheme, the code is much more robust, requires no user intervention to determine the optimum time step or time-step scaling, converges faster, and requires only half the computer time to obtain the same convergence level.

**Ames-Moffett contact: E. Tu**
**(415) 604-4486**
**Headquarters program office: OA**

## Boundary-Layer Transition at High Lift

**George Mateer, Daryl Monson**

Boundary-layer transition is the point at which a laminar boundary layer becomes turbulent. Identifying this location on airfoils at large angles of attack is important because the location plays a major role in determining the flow at the airfoil's trailing edge. This flow, in turn, defines the performance of flap systems.

Recently, a new technique for identifying transition was developed at Ames. This new and innovative testing technique, called the fringe-imaging skin-friction (FISF) method, was developed to measure global skin friction and the location of boundary-layer transition on wind tunnel test bodies. It has the advantages of being simple and easy to use, and a location map for the entire model can be obtained in a single wind-tunnel run. The method was used to map transition on a modern, supercritical airfoil in the NASA Ames High-Reynolds-Number Channel II facility. This data will be used in conjunction with surface pressure and flow-field measurements to form a validation data base for the development of numerical simulations of wing flows.

The figure shows transition on the airfoil as it undergoes angle-of-attack ($\alpha$) and Reynolds-number

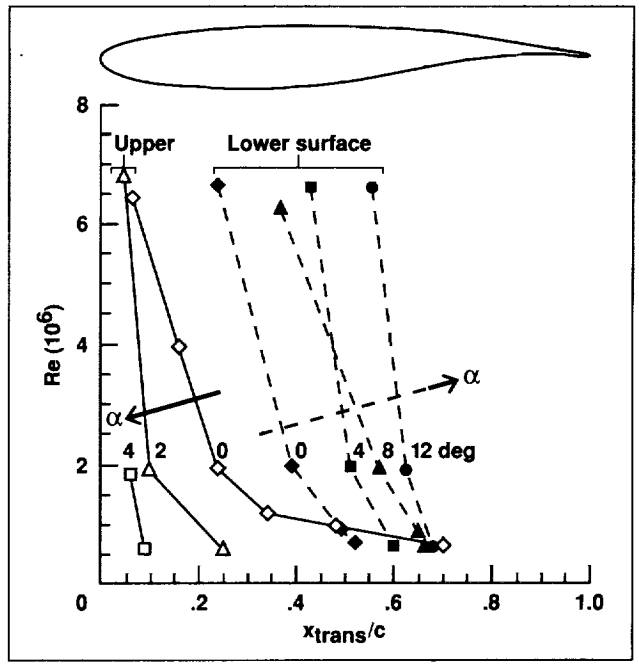


*Fig. 1. Boundary-layer transition location measurements.*

(based on chord) variations at a constant free-stream Mach number of 0.2. These results are noteworthy because they illustrate two opposite trends of transition with angle of attack. As $\alpha$ increases, transition moves forward on the upper surface and rearward on the lower surface. This feature is a significant test for any simulation that attempts to model the transition process. Once a computer code has been developed, it can be used to design optimal high-lift systems.

**Ames-Moffett contact: G. Mateer**
**(415) 604-6255**
**Headquarters program office: OA**

## GDCF: Interactive Domain Connectivity Software

**Karen M. McCann, Robert L. Meakin**

Overset grid systems are a popular means of analyzing geometrically complex fluid-dynamics problems by computational methods. The advantages of the approach are manifold: geometric complexities are reduced to multiple geometrically simple subproblems; simplified relative motion between component parts is easily addressed; and efficient and accurate flow solvers are readily available. However, in order to take advantage of the benefits of the approach, there must be a means of establishing connectivity among the members of the system of overset grids.

Algorithms have been developed to perform this domain-connectivity function automatically. Currently available software for performing this function is either easy to set up but computationally inefficient, or computationally efficient but very difficult to set up. A new software package called GDCF (Graphical Domain Connectivity Functions) has been developed to minimize the human resources required to use the most computationally efficient domain-connectivity algorithm currently available: Domain Connectivity Function in Three Dimensions (DCF3D).

DCF3D uses analytical shapes to create Chimera-style holes, and a combination of inverse-map and gradient-search methods to efficiently establish domain connectivity among systems of overset grids. DCF3D users must supply the grids, Euler parameters (for moving-body problems), and information describing the analytical shapes. The GDCF code is a graphical tool that greatly simplifies the preparation of this input data for DCF3D. GDCF is written in C (C computer language) and runs on SGI IRIS workstations; it has extensive on-line help to aid first-time users. We estimate that using GDCF to prepare input instead of hand crafting the input data gives an order-of-magnitude reduction in user time.

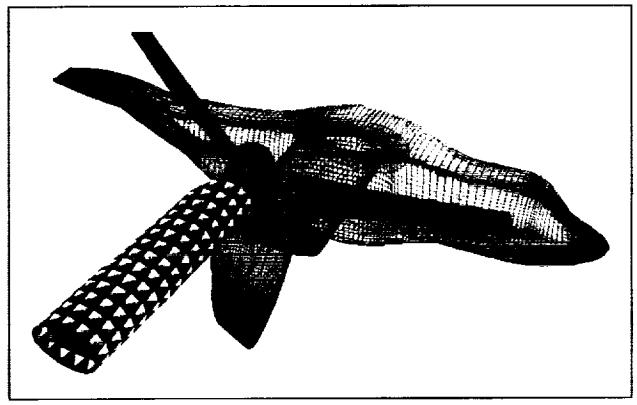

*Fig. 1. GDCF frustum shape surrounds one propeller blade of the V-22 tiltrotor.*

The figure shows a three-dimensional display from GDCF: a frustum hole-cutter shape is being placed over one of the propeller blades of the V-22 tiltrotor aircraft. The shape is drawn with a new technique called "corner-shaded polygons" that was developed to improve three-dimensional visibility.

The combined use of GDCF and DCF3D to satisfy domain connectivity requirements for systems of overset grids minimizes the human and computational resources required.

**Ames-Moffett contact: K. McCann**
**(415) 604-3973**
**Headquarters program office: OA**

# Unsteady Simulation of Flow about the V-22 Tiltrotor Aircraft

**Robert L. Meakin**

The objective of this research has been to apply dynamic overset grid methods to the V-22 tiltrotor aircraft in order to demonstrate the state of the art for unsteady simulation about complete tiltrotor aircraft, define associated computational costs, and identify algorithm components that need improvement in order to ensure accuracy and robustness for general applications.

Overset grid techniques developed for simulating the Space Shuttle solid-rocket-booster separation sequence and aircraft store separation have been used as the basis for tiltrotor simulations, which directly include rotor and/or nacelle motion. The V-22 tiltrotor aircraft was selected as the test geometry for the project because of the future possibility of obtaining experimental data for comparison with computational results.

An unsteady thin-layer Navier–Stokes simulation of flow about the V-22 tiltrotor aircraft in a 75-knot free stream in helicopter mode was carried out. The computation directly simulated the rotor-blade motion using approximately 1,500 time steps per blade revolution. The figure shows pressure coefficient histograms for a point on the wing upper surface and two points along the fuselage. Results of the simulation were used to generate animations of the unsteady pressure field on the aircraft surface, as well as unsteady smoke simulations with smoke releases from one of the blade tips and hubs. Results of the simulation and algorithmic enhancements resulting from this project were presented at the AIAA 11th CFD conference held in Orlando, Florida, in July 1993.

The present unsteady V-22 simulation was made possible by dynamic overset grid methods developed for store-separation-like problems. However, rotorcraft applications have several unique complications. For example, although the motion of rotor blades is relatively simple, the extent of their path greatly increases the degree of connectivity that may exist between grid components. Accordingly, a significant improvement in efficiency of the "DCF3D" domain connectivity algorithm was needed in order to carry out the present V-22 simulation. Rotor blades deform in flight as a function of aerodynamic and forced

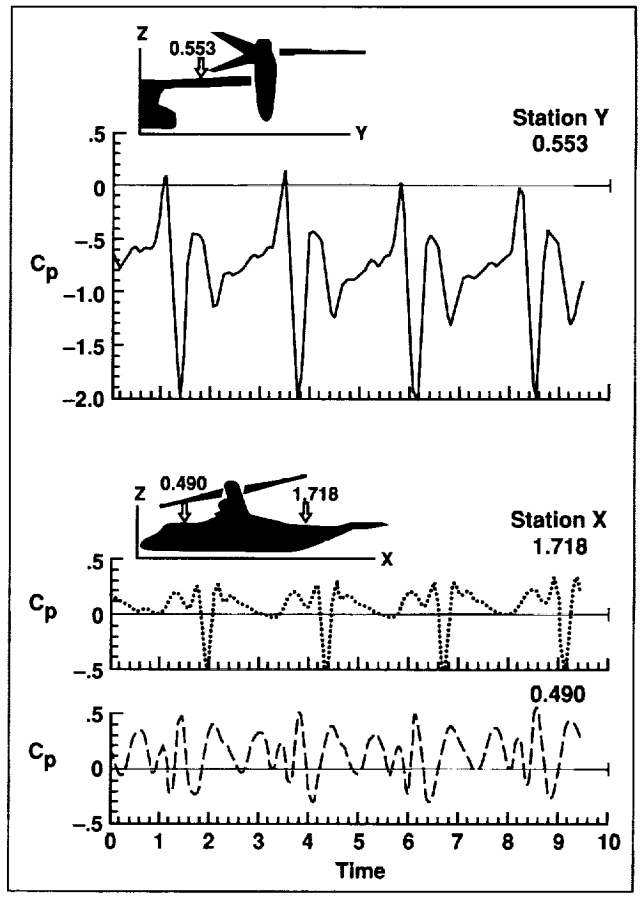


*Fig. 1. Pressure coefficient histograms for a point on the wing upper surface and two points along the fuselage.*

loadings and blade materials. Rotor blades were assumed rigid in the present simulation; however, deformation will be included in future applications. The present simulation demonstrates that computational methods can be a valuable tool in the analysis of present and future tiltrotor designs. The simulation has also illuminated algorithmic components that need further improvement and generalization.

**Ames-Moffett contact: R. Meakin**
**(415) 604-3969**
**Headquarters program office: OA**

# Hypersonic Waverider Research Vehicle Analysis

**Gregory A. Molvik**

In support of the Hypersonic Research Program, computational fluid dynamics (CFD) was utilized in the conceptual design process for a hypersonic research vehicle (HRV). Engineering methods are traditionally used in the conceptual design process but can produce erroneous results in regions where simplifying assumptions break down. Furthermore, these simplified methods lack the capability to predict any unforeseen physics associated with a particular design. CFD can significantly improve the accuracy and detail of the results, but not without a penalty. Significant computer resources are required for a complete CFD analysis of an HRV with an integrated propulsion system.

The current HRV design (Mach number = 8.0) consists of a waverider forebody with an integrated hydrocarbon scramjet engine. Waverider configurations have received a high degree of interest for their potentially high lift-to-drag ratios and their flow quality at the inlet plane. These characteristics are desirable for HRV missions; however, the performance of the propulsion-integrated configuration may be much lower than that of the pure waverider shape. The propulsion system for the HRV is a hydrocarbon scramjet with augmented preburning. Hydrocarbon fuels offer sufficient specific impulse performance, heat sink capability, and the potential for reduced vehicle size compared with hydrogen-powered designs. In addition, the handling and infrastructure requirements for the hydrocarbon fuels have a distinct advantage compared to cryogenic hydrogen. Because of the slow reaction rates of a hydrocarbon/air mixture in a supersonic stream, a mechanism is required to provide sufficient fuel/air temperatures for burning within the combustor. The concept used here is an augmented preburner in which a small amount of fuel is burned with on-board liquid oxygen and injected into the airflow upstream of the main fuel-injector locations, thus ensuring that main fuel combustion is present and uninterrupted.

A nose-to-tail CFD analysis was conducted on the present design to determine the aerodynamic performance of the integrated waverider design and to assess the feasibility of the current engine concept. The codes used for this analysis are the TUFF and STUFF hypersonic codes developed at Ames Research Center. These codes offer many of the features required for accurate hypersonic flow-field computations including upwind fluxes and fully coupled chemistry. The TUFF code is a time-marching code. It is generally used to obtain solutions in the subsonic or separated regions of the hypersonic flow field. The STUFF code employs a space-marching algorithm that can obtain a solution in relatively little computer time. For the results presented below, the STUFF code was used to obtain nozzle and external solutions. The TUFF code was used to obtain the solution within the combustor.

The first figure shows the current HRV design along with CFD-predicted pressure contours on several crossflow planes. The bow shock remains attached to the waverider leading edge for the entire length of the vehicle. This feature is desirable

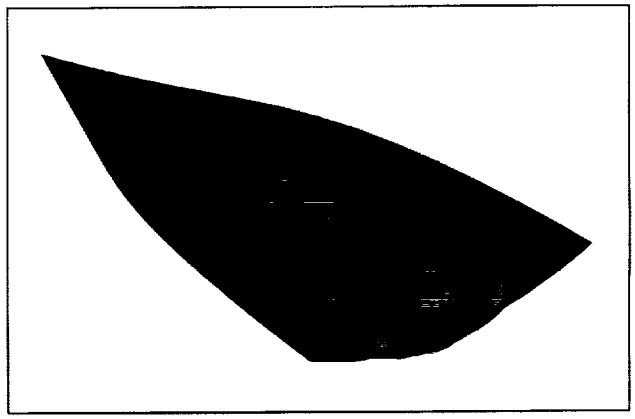

*Fig. 1. Current HRV design, with pressure contours shown. (See color plate 8 in Appendix)*

because any spillage of the high-pressure gases onto the upper surface would reduce vehicle performance. The influence of the propulsion system on the pure waverider flow field is also shown in this figure by numerous pressure waves. These CFD results also show that the flow-field quality at the inlet face is very good: the flow is uniform, and little spillage is observed.

The current scramjet engine design is shown in the second figure, along with water contours at seven axial locations. This figure clearly shows the mechanism that is employed in the current design. The hot preburner gases emerge from the preburner injector ports and mix with the oncoming air stream, but there is still a core of very hot gas just before the main fuel injection station. This hot core, falling just above the main fuel injection, serves as a "pilot light" for main fuel injectors, causing combustion of the main fuel to instantaneously occur. The main fuel injectors produce a significant amount of penetration without traversing the entire height of the scramjet. This figure indicates that the concept of preburning does indeed accomplish the task of maintaining combustion at the main fuel injection station and that an injector can be designed to provide significant flow-path penetration without unstarting the engine.

The use of CFD in the conceptual design process proved to be invaluable. It answered critical questions concerning the basic concepts involved in the design of an HRV. The nose-to-tail analysis of the waverider HRV has clearly shown the benefits of the current design and has revealed areas for improvement. The analysis of the liquid-oxygen-augmented preburning hydrocarbon scramjet indicates that the concept is viable and does indeed produce uninterrupted combustion of the main fuel within the scramjet engine.

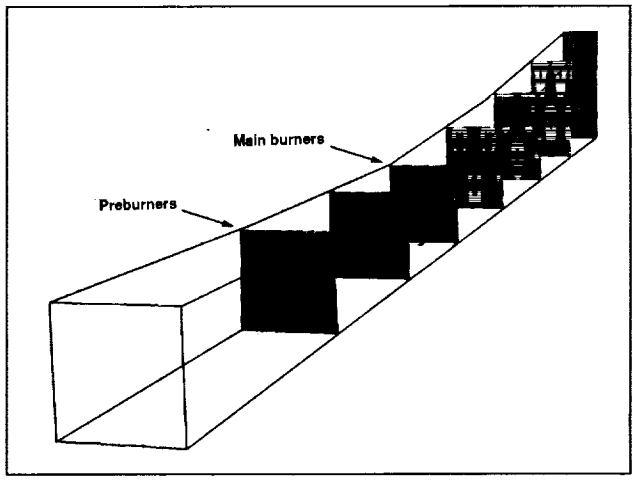


*Fig. 2. Current hydrocarbon scramjet concept, with water contours shown. (See color plate 9 in Appendix)*

**Ames-Moffett contact: G. Molvik**
**(415) 604-4483**
**Headquarters program office: OA**

# Global Skin Friction Measurement by Oil-Fringe Interferometry

**Daryl Monson, George Mateer**

The importance of data on skin friction in aerodynamic testing has stimulated a continuing effort to develop reliable instrumentation for its measurement. Recently, a new and innovative testing technique, the fringe-imaging skin-friction (FISF) method, has been developed at Ames Research Center to measure global skin friction and the location of boundary-layer transition on wind-tunnel test bodies. The concept involves the application of a line of oil to a test surface (e.g., a wing) before a run, as illustrated at the upper left in the accompanying figure. During the run, surface shear causes the oil to flow downstream in the shape of a wedge. After a run, the oil is illuminated to produce interference fringe patterns as shown in the upper right image in the figure. Lubrication theory and optical interferometry can be used to relate the local skin-friction coefficient, $c_f$, to the local fringe spacing in the image, fs, as shown at the lower left of the figure. A typical measured normalized $c_f$ distribution on the wing is shown at the lower right. The sudden rise in $c_f$ near the wing leading edge is indicative of boundary-layer transition and corresponds in location to the sudden increase in fringe spacing observed in the upper image. Absolute values of $c_f$ can be obtained with the FISF method by solving for the constants in the equations at the lower left. These values show excellent agreement with computer predictions of $c_f$ on the described wing.

The FISF method has few limitations, and several future applications of the method are planned. These include hypersonic, separated, and transonic shock-wave/boundary-layer interaction flows. The FISF method should be a valuable addition to the techniques available for measuring skin friction in wind tunnel testing.

**Ames-Moffett contact: D. Monson**
**(415) 604-6255**
**Headquarters program office: OA**

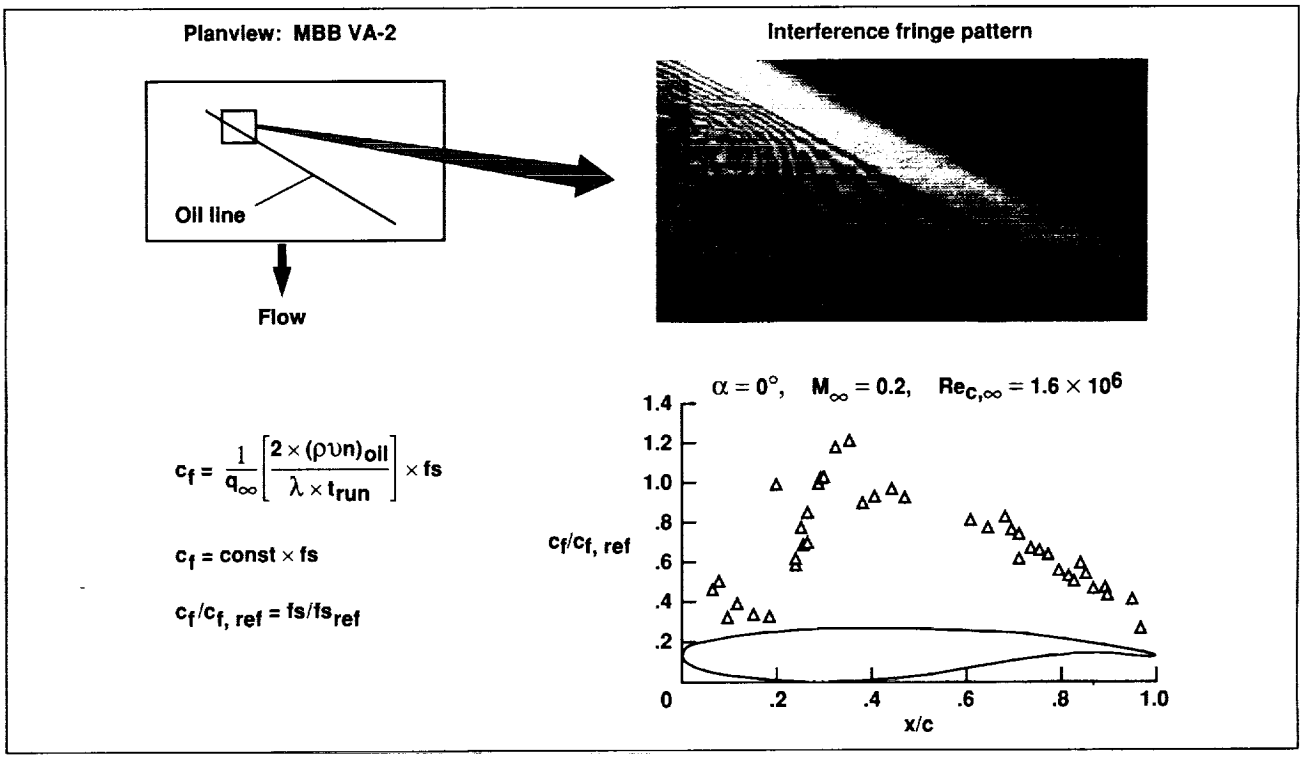


*Fig. 1. Fringe-imaging skin-friction (FISF) technique.*

# Computational Investigation of High-Alpha Aerodynamics

**Scott M. Murman, Yehia M. Rizk, Lewis B. Schiff**

The improvement of flight quality in the high-angle-of-attack regime requires a full understanding of the dynamics of the aircraft. Computational simulations can provide this understanding by supplying details of the entire flow field, which cannot be obtained by other methods. These simulations present a challenge to computational fluid dynamics (CFD) methods because of the complex geometry of a full aircraft and the unsteady, vortex-dominated flow fields that occur at high angles of attack.

Computations of the flow about NASA's High Alpha Research Vehicle (HARV) were performed and evaluated against available flight-test data. The figure shows the results of three separate computations performed to assess the effects of engine power on the external flow field of the HARV. Here, the external flow and the internal flow through the engine inlet diffuser were computed concurrently. The figure shows the trajectory of particles released from the tip of the wing leading-edge extension (LEX) on the HARV. The trajectories on the upper surface of the LEX correspond to the trajectory of the LEX vortex core. When the trajectory of the core rapidly expands, the vortex is said to have "broken down," and the ensuing motion is highly chaotic. This chaotic motion downstream of the vortex breakdown causes unsteady loading on the aircraft wings and tail, which can affect performance and safety.

The image at the top of the figure is the result of a computation that simulates the HARV without flow through the engine inlet; the second image corresponds to an idle engine setting, and the image at the bottom shows a simulation of a maximum-power engine setting. As the mass flow rate through the engine is increased by increasing the engine power, the position of the LEX vortex breakdown is seen to move downstream. This behavior has also been noted in flight testing, and the CFD solutions can be used to better understand the physics of this type of external and internal flow coupling.

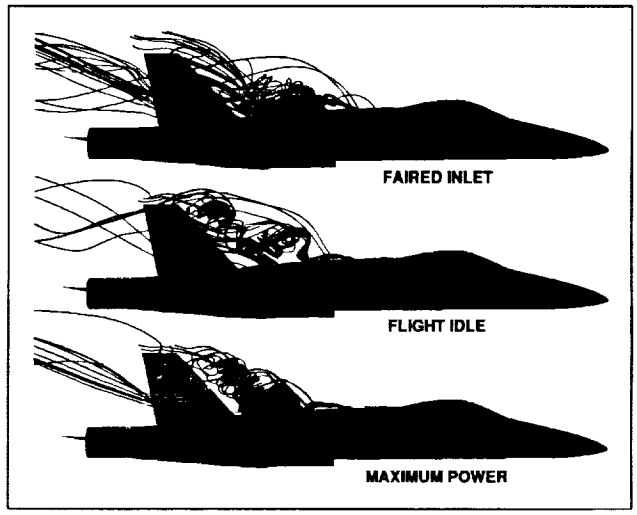


*Fig. 1. Effects of engine power on HARV leading-edge-extension vortex breakdown.*

**Ames-Moffett contact: S. Murman**
**(415) 604-4470**
**Headquarters program office: OA**

# Numerical Simulation of a Self-Similar Turbulent Plane Wake

**Michael M. Rogers, Robert D. Moser**

Turbulent wakes evolve "self-similarly" once they reach a developed state. That is, mean profiles of flow statistics at different points in the layer evolution will collapse when scaled by the appropriate length and velocity scales. For the plane (two-dimensional in the mean) wake examined here, the appropriate scales are the local maximum velocity deficit and the wake half-width.

In many cases of practical interest, a wake is formed when turbulent boundary layers from either side of a streamlined body meet at the rear end of the body (e.g., an airfoil). We have attempted to mimic this situation computationally by generating a direct numerical simulation (resolving all scales of turbulent motion) of a turbulent plane wake begun from co-flowing turbulent boundary layers. The initial boundary-layer turbulence was obtained from previous direct numerical simulations generated by Philippe Spalart.

Previous numerical simulations of three-dimensional turbulent wakes have not been able to achieve self similarity because of either insufficiently high Reynolds numbers or an insufficient sample of eddies in the computational domain. We have overcome both these limitations by considering a Reynolds number (based on velocity deficit and half-width) of 2,000 in a large streamwise domain. The computation required up to $512 \times 195 \times 128$ modes to accurately resolve this flow and used over 200 hours of Cray C90 CPU time.

After going through a transitional period in which the layer evolves from turbulence with boundary-layer characteristics to turbulence that is typical of wakes, a self-similar period is indeed obtained. During this period, integrated statistics scale as they should for a self-similar layer, and scaled mean velocity, Reynolds shear stress, and root-mean-square vorticity profiles collapse. The scaled mean velocity profiles and Reynolds shear stress profiles at five stations are shown in the first figure.

The structure of the vorticity field in the self-similar wake is very complex, containing many small-scale eddies of both signs of all three vorticity components. A contour plot of the spanwise vorticity at a point in the self-similar period is shown in

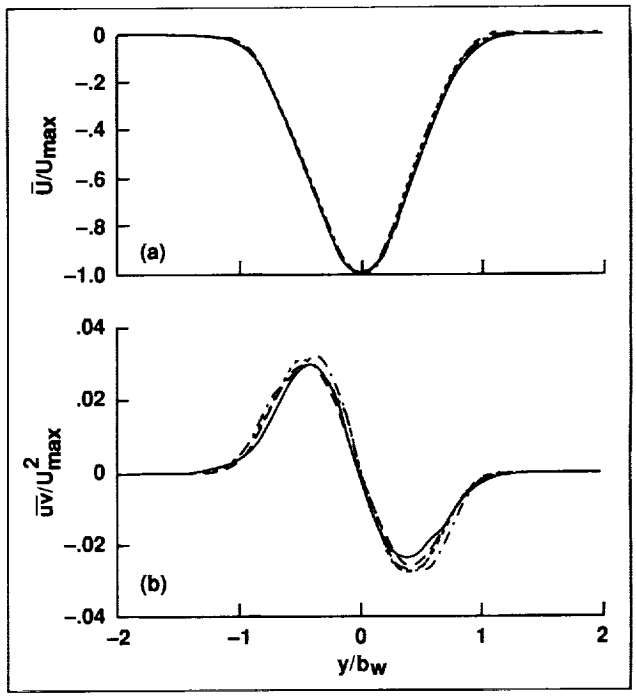


*Fig. 1. Scaled cross-stream average profiles of (a) mean velocity and (b) Reynolds shear stress at five stations in the self-similar region ($b_w$ = wake thickness).*

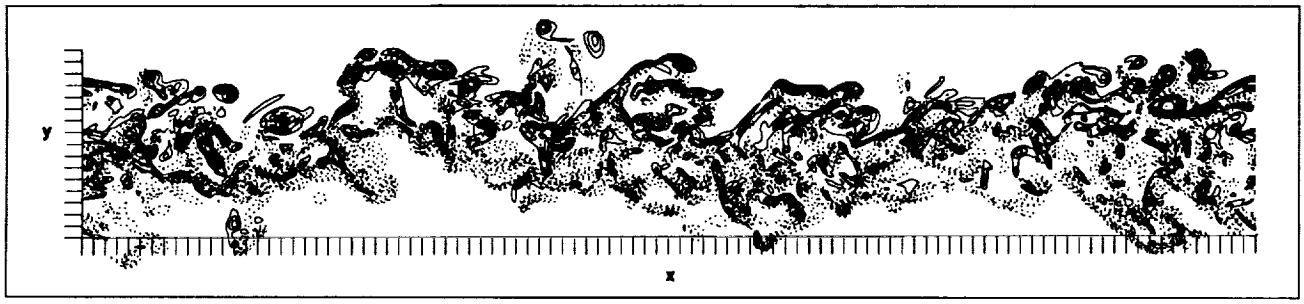


*Fig. 2. Spanwise vorticity contours (solid = negative, dotted = positive) at a point in the self-similar region.*

the second figure. The flow appears much more complicated, with less large-scale "coherent structure," than many researchers have thought.

In addition to simulating the hydrodynamic flow field, the concentration of a passive (leaving the velocity field unaffected) chemical species was tracked in order to directly address mixing in the flow. The resulting concentration fields are used for flow visualization, for testing turbulent flux models, and for modeling simple chemical reactions.

**Ames-Moffett contact: M. Rogers**
**(415) 604-4732**
**Headquarters program office: OA**

## Computations of Flow Over a High-Lift Wing

**Stuart E. Rogers**

The incompressible Navier–Stokes equations are solved using the INS3D-UP code for high-lift wing configurations. The code uses an artificial compressibility approach. The convective terms are upwind differenced, resulting in third-order accuracy in space. The equations are solved using an implicit Gauss–Seidel line-relaxation method which provides a very robust code. Complex configurations are handled using the Chimera overlaid-grid approach in which multiple bodies are individually discretized; the resulting grids then overlap in a random fashion. Information is passed between the grids by interpolation of the change in the dependent variables in the interior of one grid and use of that grid as a boundary value on another grid. The effects of turbulence are modeled using the one-equation Baldwin–Barth formulation.

The code has been used to solve the flow over the wing of a T-39 Sabreliner with a flap deployed at 40 degrees, as shown in the figure. A total of

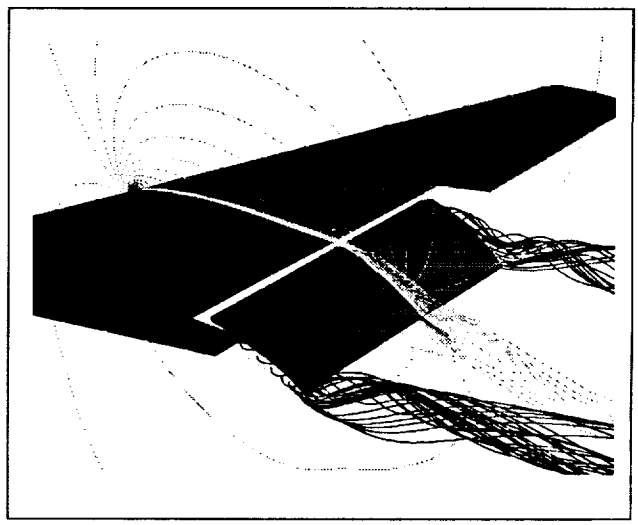

*Fig. 1. Velocity magnitude contours and particle traces on T-39 wing.*

585,000 grid points were used in six overset grids. Separate grids were used to resolve the surfaces of the wing, the wingtip, the flap cove, the flap, and each squared-off end of the flap. The procedure represents an initial solution for this configuration for which a number of grid-topology and grid-generation issues have been studied and addressed. This geometry was chosen because a full-scale T-39 aircraft will be tested in the Ames 80- by 120-Foot Wind Tunnel. The initial computations will give some insight into the complex flow over this wing, and will help in the instrumentation of the experimental configuration. The flow was computed on the NAS Cray 2 computer. The computations used 10 CPU hours and converged in 150 iterations.

This computation is the first Navier–Stokes solution of the flow over a multielement wing and represents a new computational capability. The INS2D/INS3D codes have become significant tools in the study of high-lift systems as a result of their ability to handle complex geometries and their use as a test platform for the development of advanced turbulence models.

Additional enhancements to the grid topology are under way which should help to resolve the geometry. Additional zones will then be added to include the leading-edge slat to the computations. These results will be validated upon completion of the first experimental work with this geometry. Work will then begin on a combined CFD/experimental study of high-lift configurations using the T-39 wing and a more modern high-lift system.

**Ames-Moffett contact: S. Rogers**
**(415) 604-4481**
**Headquarters program office: OA**

## Skin-Friction Transducer and Aircraft Ice-Detection System

**H. Lee Seegmiller**

A new transducer is being developed to measure aerodynamic skin friction. This rugged, flush-mounted device measures the thickness of a thin film of oil on a model or aircraft surface. The rate of thinning of this oil wedge is related to the skin friction at the surface. Previously the thinning rate was determined by optical interferometric methods using a laser beam; these methods require optical access, are sensitive to vibration, and are tedious in application. The new transducers project an electrostatic field from flush electrodes into the space above the model surface. The presence of oil at the surface alters the capacitance of the transducer and is detected by a capacitance bridge. Preliminary calibrations indicate that sensitivities to the required micrometer ($10^{-6}$ meter) changes in oil thickness can be achieved.

During tests to evaluate the effect of temperature change on the transducer, a sensitivity to water was noted as the transducer was cooled below the dew point. This effect can be mitigated with a surface coating, but a useful application of the effect is proposed. For this application, a modified transducer was designed to exploit the sensitivity to water as an aircraft ice detector. A United States patent disclosure has been submitted to the Ames Patent Counsel which describes an aircraft ice-detection system that employs two devices. One device detects the formation of ice during flight or ground operations and provides a measurement of the accumulated ice thickness. The second device is useful for aircraft that are treated with deicing fluid during ground operations. Contamination of the deicing fluid by snowfall or freezing rain can permit ice to reform and cause an accident during attempted takeoff. The second device provides a timely warning to the flight crew of the need for reapplication of deicing fluid.

**Ames-Moffett contact: H. Seegmiller**
**(415) 604-6211**
**Headquarters program office: OA**

# Network-Based Parallel Flow Simulation

**Merritt H. Smith**

The availability of supercomputer resources is often a limiting factor on the use of state-of-the art computational methods in the aircraft design process. At the same time, engineering workstations have a significant but under-used computational capability. The purpose of this research is to examine ways to use the power of multiple workstations, working in parallel, to solve the Navier–Stokes equations for complex aircraft configurations.

Previous work has shown the effectiveness of the Chimera overset grid technique in the solution of the three-dimensional Navier–Stokes equations over complete aircraft. The multiple grids used in Chimera have a natural parallelism wherein each grid is essentially autonomous, with communication required only at grid boundaries. If each grid can be updated by a separate process, and these processes spread among multiple workstations, it should be possible to harness a large fraction of the workstations' combined power.

The widely used overset grid flow solver OVERFLOW has been modified to run in a heterogeneous parallel environment. The flow field is solved for on the individual grids by separate but interdependent processes spread over a network-connected system of workstation processors. Inter-process communication employs the Parallel Virtual Machine (PVM) software library developed by Oak Ridge National Laboratory. Sustained performance exceeding 50 million floating-point operations per second (MFLOPS) has been achieved with the combination of nine commonly used workstation processors. This is one-third of the speed of a Cray Y-MP processor running the original serial code (OVERFLOW). The accompanying graph indicates that proportionately greater performance will be achieved for larger problems with more grids.

The use of workstations for large-scale flow computations will result in savings of both time and money. Most aerospace companies and research institutions have a large number of engineering workstations whose processors spend the vast majority of the time idle. These processors are usually connected by computer networks such as Ethernet. So, with no additional hardware expenditures, an organization may significantly increase its effective computer resources by using network-based parallel computing techniques. Monetary savings will be seen in a reduced demand for costly supercomputer time. Local control of the workstations will allow faster and more predictable job turnaround than if a centralized computing facility was used. Additionally, this work provides a means of exploiting the dramatic increases in workstation speed and memory coming in the near future.

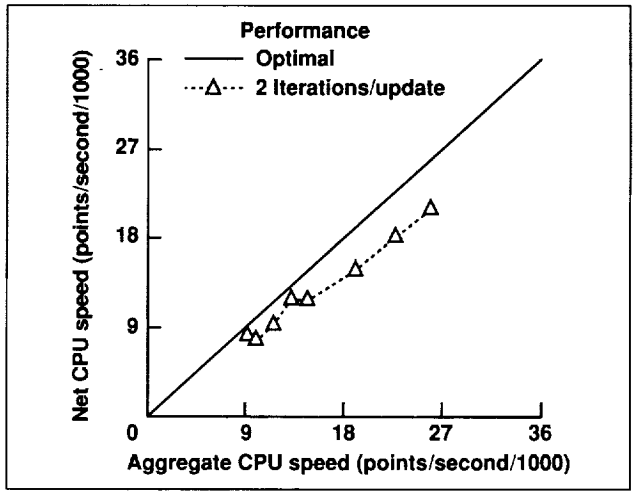


*Fig. 1. Parallel performance of the OVERFLOW–PVM flow solver on a cluster of network-connected workstations computing the flow over a wing defined by nine grids.*

The current grid-by-grid parallel decomposition may use no more processors than grids in the problem. Future work will focus on modifications of the flow solution algorithm to allow the use of multiple processors on each grid. The methodology employed in this work appears to be extremely receptive to multidisciplinary simulation. The current work will therefore be expanded to include modules from other areas such as structures and propulsion.

**Ames-Moffett contact: M. Smith**
**(415) 604-4493**
**Headquarters program office: OA**

# Dynamic Mesh Adaption for Three-Dimensional Unstructured Grids

**Roger C. Strawn, Rupak Biswas**

This research is aimed at solving problems in rotary-wing aerodynamics in which rotor-wake systems and acoustic waves are extremely complex. The key to modeling these flow features with computational fluid dynamics is to minimize any numerical dissipation that can artificially diffuse the rotor wakes and acoustic signals. This is accomplished by using dynamic solution-adaptive grids and flow solvers that are appropriate for the resulting unstructured meshes. The solution-adaptive approach adds and removes points locally, providing higher resolution for moving flow features such as rotor-wake vortices and acoustic waves.

An efficient new procedure has been developed for the simultaneous coarsening and refinement of three-dimensional, unstructured tetrahedral meshes. An innovative data structure allows the mesh connectivity to be rapidly reconstructed after mesh points are added and/or deleted. These local grid modifications enhance the resolution of rotor wakes and acoustic signals and drastically reduce any numerical dissipation in the solutions.

The figure shows the solution-adaptive mesh and nondimensional pressure contours for a rotor in hover. The direction of rotation is counterclockwise, and the Mach number at the tip of the blade is 0.95. A strong shock is present on the blade surface which propagates to the far field as a very loud acoustic signal. The dynamic mesh-adaption scheme has automatically increased the mesh resolution along the surface shock and acoustic wave. As a result, the acoustic signal is very accurately reproduced.

The key to success for dynamic mesh adaption is the ability to efficiently add and delete points from the grid. For an unsteady flow, this coarsening/refinement step must be completed every few time steps, so its efficiency must be comparable to that of the flow solver. It must also have a reasonable memory requirement. The new mesh-adaption scheme has all of these attributes. In addition, it can be applied to a variety of important NASA problems in areas other than rotorcraft aerodynamics.

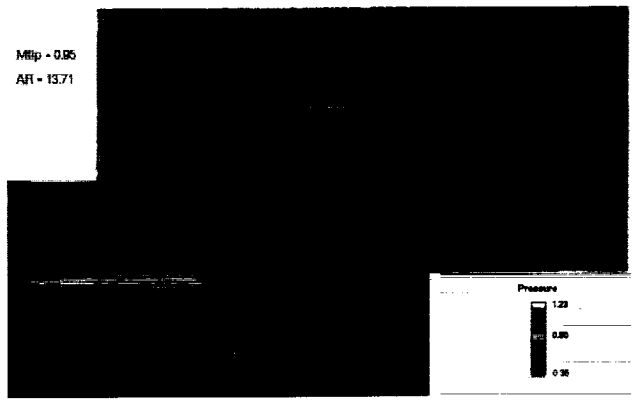


*Fig. 1. Solution-adaptive mesh and pressure contours for modeling high-speed impulsive noise from a three-dimensional helicopter rotor blade. (See color plate 10 in Appendix)*

**Ames-Moffett contact: R. Strawn**
**(415) 604-4510**
**Headquarters program office: OA**

# Unsteady Canard–Wing-Body Aerodynamics

Eugene L. Tu

The objective of the current work is to improve the understanding of complex unsteady aerodynamics of canard configurations and to study the effects of canards on the stability of aircraft. By accurately simulating the flow field about a canard–wing-body geometry undergoing pitch-up and oscillatory motions, dynamic stability characteristics of the configuration can be determined. Results from this study validate the capability of computational fluid dynamics (CFD) to predict and improve the aerodynamic performance of canard-configured aircraft.

Using a CFD flow solver, the Navier–Stokes equations are solved for the flow about a canard–wing-body configuration that is performing a rapid pitch-up maneuver and undergoing pitch oscillations. A patched multizoned grid scheme is used which allows for a mismatched interface

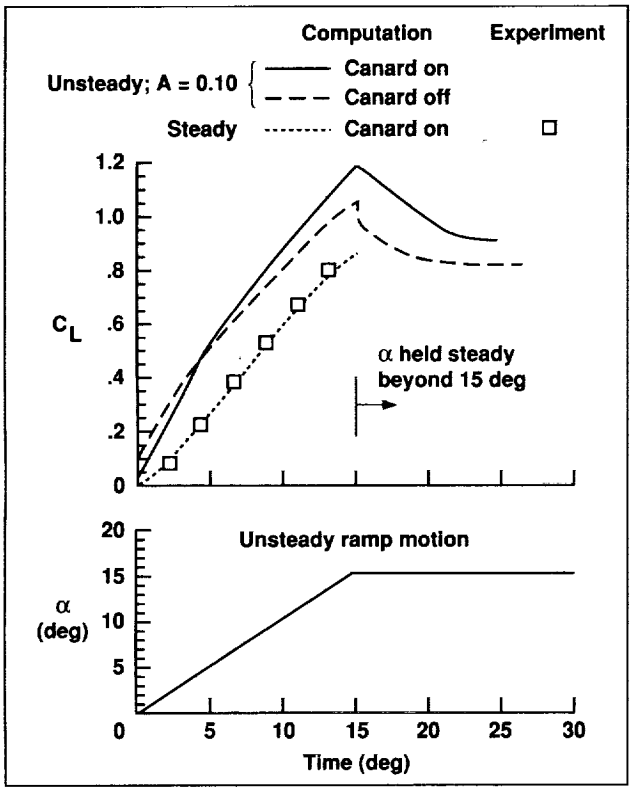


*Fig. 1. Effect of the canard on unsteady lift during the pitch-up ramp motion (nondimensional pitch rate (A) = 0.10).*

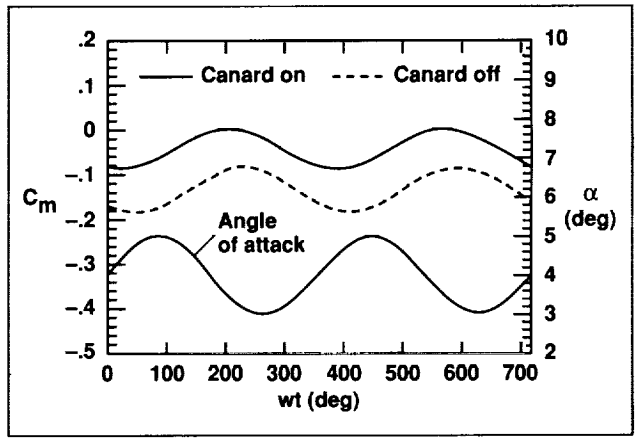


*Fig. 2. Time histories of pitching moment for the oscillating canard–wing-body configuration.*

between the close-coupled canard and wing regions. The canard can be easily repositioned relative to the wing by using this grid scheme. The Baldwin–Lomax algebraic eddy-viscosity model is used to model the effects of turbulence.

Computations are made at high subsonic to transonic Mach numbers of 0.70 to 0.90, angles of attack of –2 to 16 degrees, and Reynolds numbers (based on mean aerodynamic chord) of 1.52 to 3.05 million. The first figure illustrates the effect of the unsteady pitch-up motion on the computed lift curves for the configuration with and without the canard. The horizontal axis represents nondimensional time (in degrees). For reference, the motion of the configuration is illustrated in the lower portion of this figure. The steady-state computational and experimental lift curves are also illustrated in the first figure. As time increases, the unsteady case shows a significant increase in lift over the steady-state case at the same angles of attack. Furthermore, the first figure shows that more unsteady lift is generated when the canard is present.

The second figure illustrates the effect of the canard on the configuration that is oscillating with a mean angle of attack of 4 degrees. For this case, the amplitude of the oscillation is 1 degree and the reduced frequency, k, is 0.236. A significant phase

difference is noted between the canard-on and canard-off cases and with respect to the time history of the angle of attack. By performing a Fourier analysis on time histories of lift and moment, the longitudinal dynamic stability characteristics of the configuration can be predicted. The third figure illustrates the comparison between the computed and experimental oscillatory stability parameters for the configuration with and without the canard. These results demonstrate that CFD can be used to perform dynamic stability analysis on future advanced canard-configured aircraft.

**Ames-Moffett contact: E. Tu**
**(415) 604-4486**
**Headquarters program office: OA**

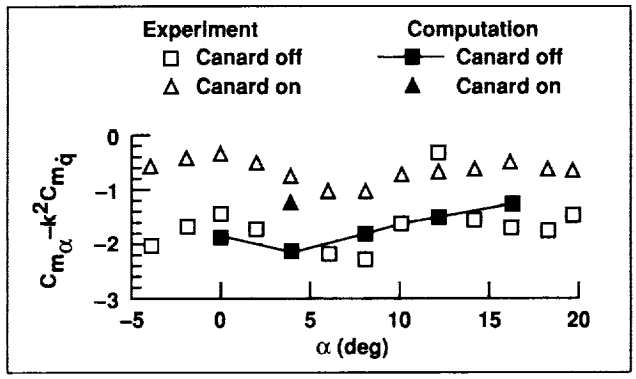


*Fig. 3. Effect of the canard on the pitch oscillatory longitudinal-stability parameter.*

## Turbulence Modeling Used in Design of a High-Lift Experiment

**John Viegas**

An efficient numerical algorithm was used in the design of an experiment to develop improved turbulence models for use in high-lift airfoil flow studies. These models are needed to improve the design of high-lift single- and multielement wing systems slated for the next generation of transport aircraft.

Usually, computational fluid dynamics codes play a major role in understanding the flow after an experiment has been completed. In this study, the computer's resources were used in the early stages to test the feasibility of the design prior to the expensive process of cutting metal. A wide variety of wind-tunnel test sections were studied in conjunction with many configurations of airfoil and airfoil–flap combinations. The objective was to create an experiment that would simulate the flow features of a high-lift wing-flap combination (slot flow, confluent boundary-layer flow, wake/jet boundary-layer interaction, and/or trailing-edge separation).

The algorithm was used to solve the incompressible Navier–Stokes equations for four different models of turbulence: two one-equation (turbulent viscosity) models, and two two-equation (turbulence energy and dissipation rate) models. These models are representative of the types of turbulence models that would be expected to be applicable to high-lift wing flows. A convenient grid package was developed that enabled wind tunnel models, or the tunnel itself, to be modified to yield the desired flow features, such as a curved wake in an adverse pressure gradient. The computations showed that the flows affected the turbulence models distinctly, thus this type of experiment could be used to discriminate between models.

The figure shows the streamlines and reversed-flow regions for an example configuration computed by two turbulence models. In this case, a pressure gradient is imposed on the flow as the tunnel expands through a 14.5-degree half angle from 4 inches to 14 inches in height. Wall jets energize the boundary layer at the expansion corners and help keep the flow attached throughout the expansion. An 18-inch plate 1/4 inch thick is centered in the tunnel

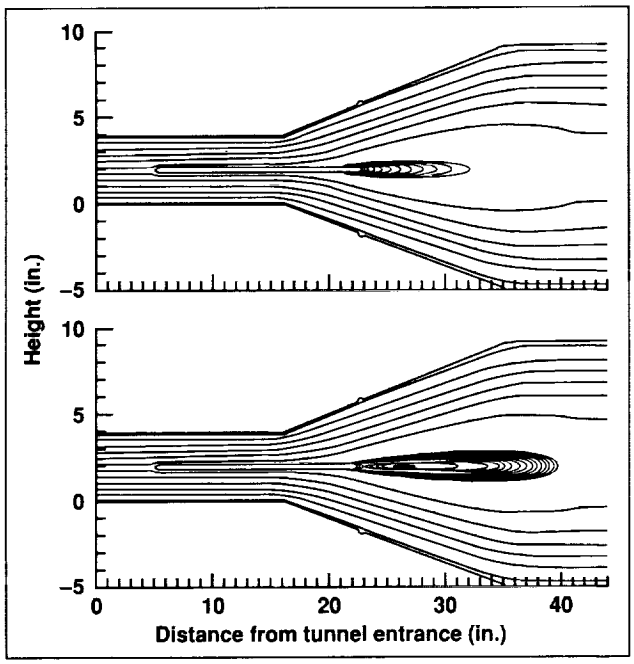


*Fig. 1. Comparison of streamline pattern and region of reversed flow for two turbulence models applied to the wake in an adverse pressure gradient.*

beginning at 5 inches from the left boundary. The flow is from left to right. In the wake of the plate, the flow is reversed. This reversed-flow region is indicated on the figures by superimposed contours of negative velocity that are attached to the back of the plate. On the figures, the differences in the streamline locations, their shape, and the size of the reversed-flow regions show how the turbulence models react to the pressurized expansion differently. Many computations of this type with other tunnel configurations were used in the design of an experiment that should be a useful tool to test a turbulence model's ability to accurately simulate the wake region in a high-lift environment.

**Ames-Moffett contact: G. Mateer/D. Driver**
**(415) 604-6255/5396**
**Headquarters program office: OA**

## Experimental and Numerical Study of a Turbulent Boundary Layer with Pressure Gradients

**Jonathan H. Watmuff, Philippe R. Spalart**

The flow in the vicinity of the surface (i.e., the boundary layers) of an airplane is most likely to be turbulent. The shear stress at the surface forms a large component of the overall drag. Currently, the prediction of the shear stress for design purposes depends on turbulence models. These models have a number of adjustable constants which are tuned against experimental data. Unfortunately, extrapolation to other geometries and Reynolds numbers has proved to be unreliable. Our knowledge of turbulent flows is far from complete despite their practical importance.

Direct numerical simulation (DNS) is an alternative to experiments that provides full details about all flow quantities. Although DNS requires extremely large amounts of memory and supercomputer time, this obstacle will diminish with the ever-increasing power and reduced cost of computational resources. Nevertheless, DNS is in its infancy and validation is required as the technique is extended to more complex flows. Prior to this investigation, DNS was capable of handling only the relatively trivial case of a low-Reynolds-number two-dimensional flow over a flat surface with zero pressure gradient. In this project, DNS was extended by Spalart to handle the case of an adverse pressure gradient (APG). A closely matched experimental investigation (EXP) was performed by Watmuff, and the results of the two approaches were compared.

The boundary layer first develops in a favorable pressure gradient (FPG) to help the turbulence recover from the trip (EXP) or inflow (DNS) without unduly increasing the Reynolds number. Relatively good agreement is observed at the end of the FPG,

as shown in the first figure. In the APG region of most interest, downstream, there are some differences between the two data sets. In the second figure, the wall shear-stress coefficient $C_f$ is shown versus the streamwise distance, x (the APG is applied at x = 0.6). The DNS value is definitely too low at x = 0.4 meter as a consequence of the recovery from the inflow conditions in the FPG region. From x = 0.6 to 0.8 meter, the agreement is quite good. This generally is observed with other quantities as well. The difference of 12% at x = 1 meter is interesting and worthy of comment. In the experiment, a Preston tube was used to measure the shear stress, an indirect method that assumes the "law of the wall," i.e., that the velocity profile close to the surface is universal. Direct measurements of the shear stress from the velocity gradient are subject to considerable uncertainty because of the small differences in wall

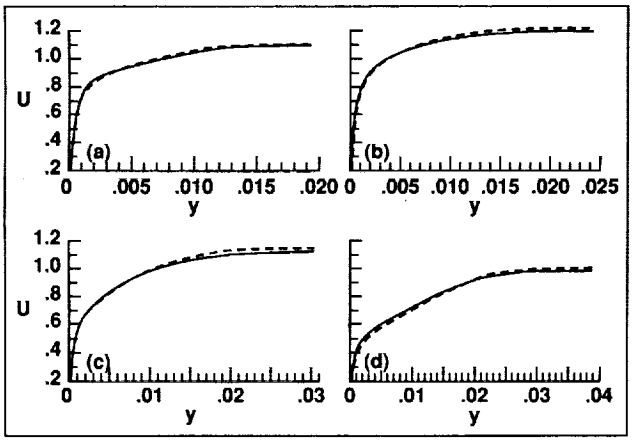


*Fig. 1. Velocity profiles. (a) x = 0.4, (b) x = 0.6, (c) x = 0.8, (d) x = 1.0 m (dashed line = EXP, solid line = DNS).*

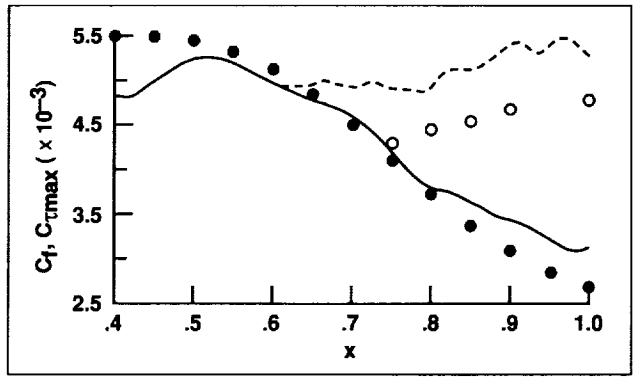


*Fig. 2. Shear-stress coefficients. Dots = experiment, lines = DNS.*

distance. In the simulation, the shear stress was calculated directly from the velocity gradient, and it is as reliable as the other quantities. The DNS results suggest a moderate failure of the law of the wall with APG. This finding is controversial, since the law of the wall is one of the most widely accepted properties of turbulent boundary layers.

The turbulence models mentioned earlier fail to predict this flow adequately. The direct comparison in this joint study provides confidence in the overall results and an immediate estimate of the uncertainties, such as the shear stress differences noted above. The results are ready for use in the scrutiny of turbulence models. The DNS technique has been advanced for use with more complex flows.

**Ames-Moffett contact: S. Davis**
**(415) 604-4197**
**Headquarters program office: OA**

# Physics of a Wingtip Vortex

**Greg G. Zilliac, Jim S. Chow, Jennifer Dacles-Mariani, Peter Bradshaw**

The performance of virtually every fluid-dynamic machine, from the household fan to the space shuttle, is, to some degree, affected by the flow over wings. In the past, typically, the approach to wing design has included costly parametric studies of wing contours and wingtip shapes in wind tunnels. With the emergence of computational fluid dynamics as a design tool, the amount of wind tunnel testing required to design an efficient wing has been reduced; yet questions remain concerning the accuracy of the computer-generated flow fields.

The flow in the vicinity of a wingtip is a fairly difficult test case for a Navier–Stokes code. Under typical flight conditions, highly skewed turbulent boundary layers detach from the surface of a wingtip and roll up into a tightly wound vortex. The mean velocity in the vortex core has been found to be almost twice the free-stream velocity, and the turbulence levels in the core are much higher than previously thought.

The purpose of this study is to compare a measured and computed wingtip flow field and to identify the shortcomings of the computational techniques. An extensive data base of measured and computed results for the flow over a rectangular wing with rounded tip has been analyzed. The Reynolds number based on chord was 4.6 million, and the angle of attack was 10 degrees. The figure shows a comparison of the measured and the computed mean velocity fields. These results illustrate that the Navier–Stokes predictions are a close approximation of the flow field everywhere with the exception of the vortex core. In the vortex core, the peak axial velocity is underestimated by nearly twenty percent. The probable cause of this underestimation is a deficiency in the capability of the turbulence model used in the computations.

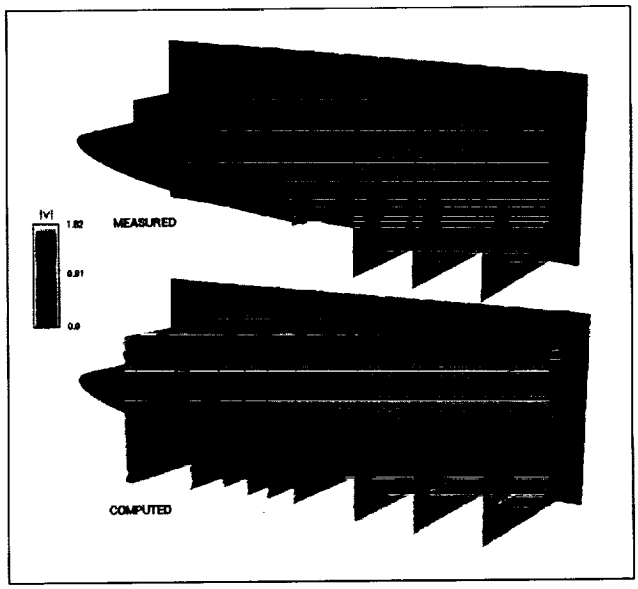


*Fig. 1. Comparison of measured and computed mean velocity. (See color plate 11 in Appendix)*

**Ames-Moffett contact: G. Zilliac**
**(415) 604-3904**
**Headquarters program office: OA**

# Combustion Enhancement by Pulsed Detonation Waves

**Jean-Luc Cambier, Henry Adelman, Gene Menees**

This study was focused on obtaining an understanding of the interaction between pulsed blast waves and a fuel–air mixing layer in a supersonic combustor (scramjet), such as the one proposed for the National Aerospace Plane (NASP). A fundamental challenge in this type of combustor is to be able to mix and burn the fuel (hydrogen) with air rapidly enough while both fluids are moving at high speed. Recent research in hypersonics has shown that the rate of mixing is diminished at high speeds, as a result of compressible effects: the mixing layer radiates some of the convective energy as acoustic waves and shock waves, instead of generating vortical flow for mixing. However, this effect can be applied in reverse, i.e., the mixing layer can also absorb acoustic energy, or energy from shock waves, and transform it into vortical flow. The design of a supersonic combustor could therefore benefit from this principle, if an attempt were made to maximize the interactions between shock waves in the combustor and the mixing layers. This design idea is used in a proposed engine concept called the Pulsed Detonation Wave Augmentor (PDWA). In this concept, shock waves (or blast waves) are generated at the ends of small tubes embedded within the combustor walls, and propagate into the supersonic combustor stream where fuel and air are being mixed. The tubes are periodically filled with a combustible mixture, which is then ignited. A detonation wave is rapidly formed and propagates down the tube at high speed: as it reaches the tube exit, it decays into a strong blast wave, which propagates into the supersonic stream in the combustor. The tubes are rapidly filled again with a fresh mixture, and the process is repeated at a high cycling rate. Multiple tubes, operated in sequence, can be used to maximize the effective firing rate of the "detonation tubes."

The concept has several design options. Its effectiveness may depend on many factors, such as the location of the tubes with respect to the mixing layers, and the overpressure behind the blast wave. The mixing layers can be "free," i.e., within the core

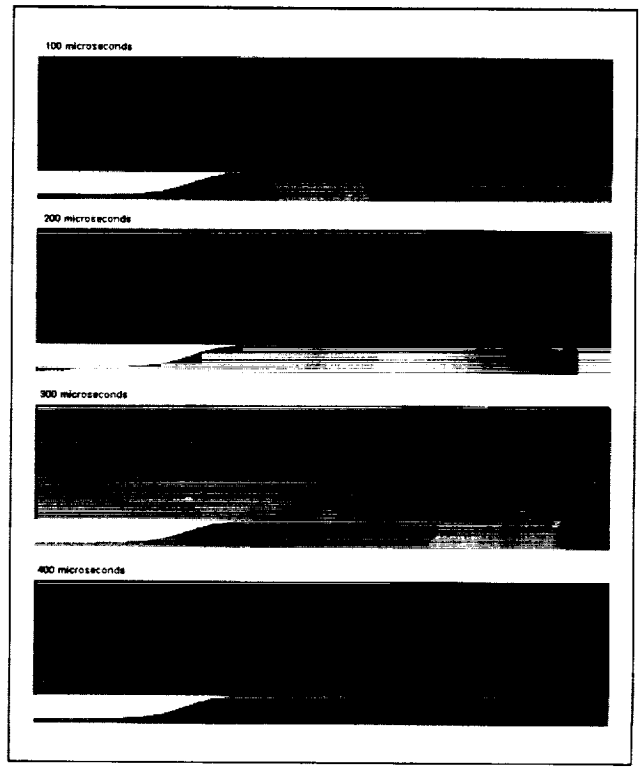


*Fig. 1. Time sequence for the transverse coupling case. Blast waves propagate into the supersonic combustor through two holes in the side of the detonation tube. The fuel layer can be seen in the center of the combustor. (See color plate 12 in Appendix)*

of the supersonic stream, or "bounded," i.e., near a combustor wall. In one design option, the blast waves are generated from small holes in the sides of the detonation tubes; this is called "transverse coupling," because the blast waves propagate mainly in a direction transverse to the main combustor flow. A second option uses a shorter tube and directs the blast wave in the same direction as the combustor flow, the axis of thrust; this option is called "axial coupling." The blast waves can have several beneficial features. First, they can enhance the mixing by

generating the necessary vortices, on several length scales. Second, the passage of a strong shock can rapidly heat the fuel–air mixture and trigger immediate combustion, thus enhancing the rate of combustion. Third, the detonation wave is an efficient propulsion mechanism, and will enhance thrust as well.

To investigate the effectiveness of this concept, numerical simulations of the fluid dynamics were performed, using standard methods of computational fluid dynamics (CFD). The simulations included the computation of chemical processes in time-accurate fashion, in order to determine the effect on ignition delay (combustion enhancement). The computations were done in two dimensions only, and turbulent effects were omitted. This provided a worst-case scenario, since three-dimensional and turbulent effects would further increase the mixing rate in the combustor. The two options of transverse and axial couplings were studied, for a single cycle of the detonation tube. The first case—transverse coupling—showed mixed results: as the blast waves interact with the fuel layer, they produce strong vortices, and effectively stimulate the mixing and combustion, as expected (see first figure). However, the high pressure generated at the holes in the sides of the detonation tube also generates strong oblique shocks within the combustor flow. These oblique shocks are a problem because they raise the entropy production within the combustor flow and lower the propulsive efficiency. As one attempts to diminish the strength of these oblique shocks by lowering the pressure in the detonation tube, the interaction with the fuel layer is also decreased. This configuration is therefore not considered optimal.

In the axial coupling configuration, the blast wave diffracts at the tube exit and propagates downstream. Thus the high-pressure region is swept along with the combustor flow. Axial coupling should therefore minimize the losses in efficiency, and this was indeed verified. The efficiency of this configuration at promoting mixing and combustion is also observed to be very good. The mixing layer is compressed and heated by the passage of the blast wave, which triggers an immediate combustion of the fuel in that region. The fuel layer is then pushed by the blast wave and starts to roll up. This process

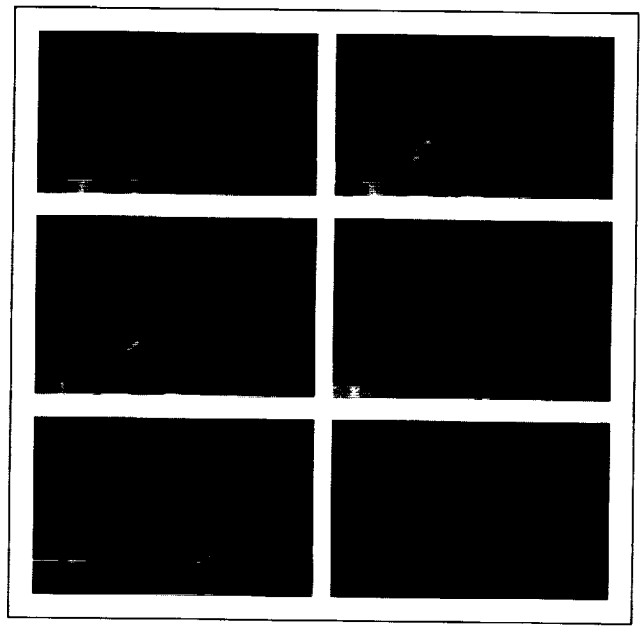

*Fig. 2. Time sequence of temperature contours, PDWA operation. Rapid combustion is seen in frame 2 (75 microseconds). The fuel layer (green contours) is seen to roll up and break up. Strong mixing vortices are generated. (See color plate 13 in Appendix)*

creates regions of strong vorticity as well as a stretching of the mixing interface, both of which enhance mixing. Further heating and ignition takes place at various locations during the interaction between this single pulse and the mixing layer. These features can be seen in the second figure, which shows a time sequence of the temperature contours. A detailed examination of the flow also reveals that, as the shock moves through the fuel layer, interface instabilities (called Richtmeyer–Meshkov instabilities) are seen to develop. These are known to promote mixing, and occur for unsteady shock waves only. Another feature that was observed in both configurations studied was the existence of a transmitted shock within the fuel layer, which could propagate faster than all other flow structures because of the very high speed of sound in the pure fuel ($H_2$). This feature may be of interest in other applications, notably external combustion.

The preliminary computational results show that the principal goals of the study—enhancement of mixing, combustion, and thrust—can be simultaneously achieved, with the required minimal efficiency losses, if the design configuration is carefully chosen. The thrust enhancement comes from the detonation wave itself, which is an efficient propulsive mechanism (near-constant-volume combustion). The detonation can be directly initiated in the appropriate mixture with minimal electrical power. It is clear that the concept has enormous potential, and it should be verified experimentally, as well as theoretically, through a progressive series of tests and more detailed numerical simulations. Variations of the PDWA concept can also be considered and applied, for example in stimulated external combustion or nozzle combustion. If successful, the PDWA concept may lead to significant improvements in the performance of hypersonic air-breathing engines.

**Ames-Moffett contact: J. Cambier/H. Adelman**
**(415) 604-4283/3468**
**Headquarters program office: OA**

## A Three-Dimensional Self-Adaptive Grid Code

**Carol Davies, Ethiraj Venkatapathy**

Computational fluid dynamics has become an important tool in analyzing and predicting a wide variety of complex flows. Even with supercomputers available, the demand for modeling and accurately predicting the flow around complete three-dimensional (3-D) aircraft and spacecraft requires efficient solution strategies. One such strategy is to use solution-adaptive grid refinement methods. A 3-D, self-adaptive grid code (SAGE) has been developed for single or multiple finite-volume or finite-difference grids. SAGE is a robust, user friendly, efficient, and well documented code. It has been widely distributed within NASA and throughout the aerospace industry and universities.

In SAGE, the 3-D adaption takes place as a sequence of one- and two-dimensional adaptions. The error-minimization method of redistributing grid points is based on the self-adaptive grid scheme proposed by Nakahashi and Deiwert. The procedure is analogous to using tension springs to minimize the error and torsion springs to maintain smoothness and orthogonality between the grid lines. The solution on the adapted grid will be more accurate than the original solution as a result of the grid point redistribution. SAGE can be used either on a single grid or on multiple grids. It is available as a stand-alone code or within FAST, an interactive, user-friendly, flow analysis graphical software developed at Ames

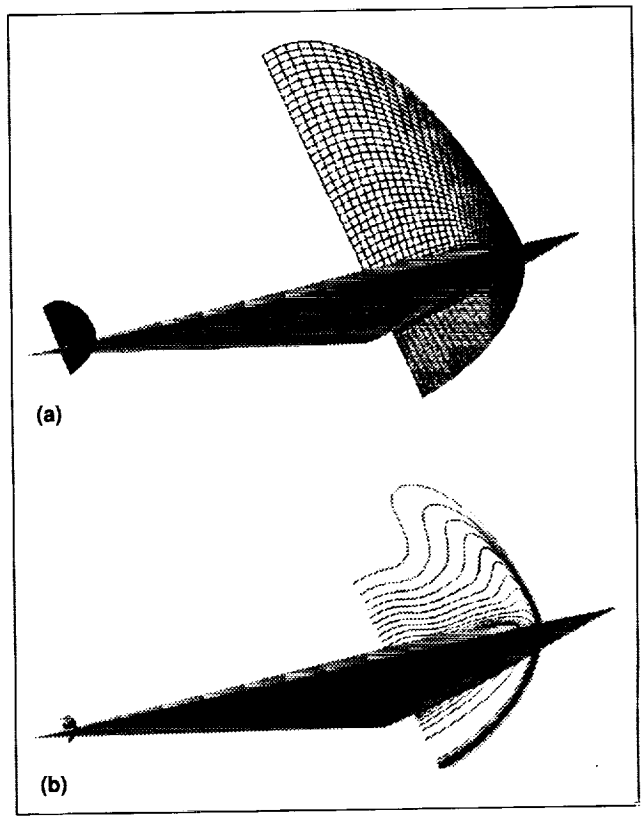


*Fig. 1. Example of grid adaption for the NASP model (with fig. 2). (a) Original, nonadapted grid; (b) Mach contours from the original grid solution.*

Research Center. SAGE is highly portable and can be used in a wide range of computing platforms such as supercomputers, workstations, and personal computers. The multigrid option was developed as part of the Government Work Package related to the National Aerospace Plane (NASP) program and has been made available to NASP contractors.

The figures show an example of grid adaption performed for the National Aerospace Plane model. Two grid planes from the nonadapted zonal grids are shown in part (a) of the first figure and the initial solution is shown as Mach contours in part (b). The outer shock in part (b) is clearly seen as the high-gradient region represented by the clustered contour lines. The grid points on each of the grids were redistributed according to flow gradients and the adapted grid is shown in the second figure.

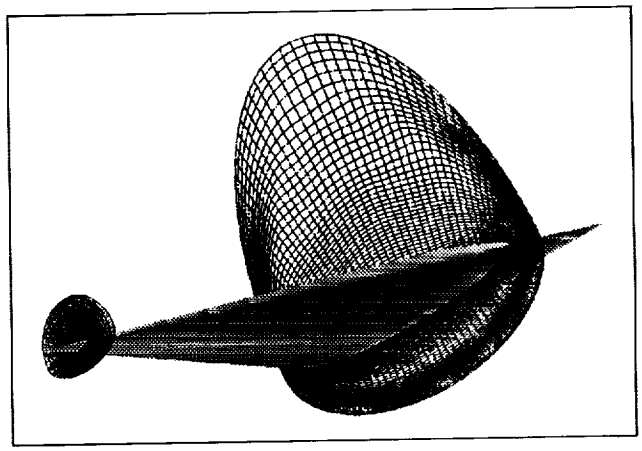

*Fig. 2. Final adapted grid based on the original grid and the solution.*

**Ames-Moffett contact: G. Deiwert**
**(415) 604-6198**
**Headquarters program office: OA**

## Thermal Protection System Technology Transfer

**Daniel B. Leiser**

A noteworthy example of useful technology transfer from NASA to industry, paving the way for future commercial applications, is the transfer of heat-shield-tile processing techniques from Ames Research Center to Rockwell International at Kennedy Space Center. Rockwell requested specifications for several different tile materials. Some processing specifications developed in the mid-1970s had to be modified to account for the cleaner fibers now used in making these materials. Specifications for a 22-pound-per-cubic-foot, all-silica tile (AIM-22) and a fibrous refractory composite insulation produced at 12 pounds per cubic foot (FRCI-12) were sent to Rockwell, along with processing equipment and drawings for the casting towers needed to press the individual tiles. Rockwell personnel successfully produced both variations of tiles at the Kennedy Space Center facility. These materials are currently being used, in place of flight tiles, as machining and processing fixtures for fabricating flight tile materials, resulting in a $10.4 million savings to the Shuttle program. In addition, the use of a flight-certified version of these tiles has been approved for future Orbiter installation with an estimated savings of about $22 million.

**Ames-Moffett contact: D. Rasky**
**(415) 604-1098**
**Headquarters program office: OACT**

# Accuracy of Continuum Methods in Slightly Rarefied Flows

**Forrest E. Lumpkin III, Iain D. Boyd, Ethiraj Venkatapathy**

Aerospace vehicles experience conditions ranging from the near vacuum of space to the more dense lower atmosphere. Theories appropriate at these two extremes are, respectively, free molecular flow and continuum fluid dynamics. Whereas these theories are each valid at one of the two extreme conditions, the limits of their accuracy between these extremes is not well known. It is thus not always clear when and where a set of continuum equations such as the Navier–Stokes equations begins to fail. At a certain altitude, for example, Navier–Stokes predictions are invalid in the low-density wake behind a blunt reentry vehicle even though they are valid elsewhere in the flow. Knowledge of the critical altitude when this invalidity occurs is important to the designer of such a vehicle.

Evaluation of the Navier–Stokes equations can be achieved by comparing their solutions with the results of simulations that are based on a more general theory. The direct-simulation Monte Carlo (DSMC) method is accurate for conditions ranging from free molecular to continuum and has been used to analyze flows that approach the limit at which continuum theory applies. Unfortunately, the method requires a rapid increase in computational effort with increased density and therefore becomes impractical at some density. Advances in computer performance have recently allowed meaningful comparisons of DSMC and Navier–Stokes simulations of a complicated flow to be performed.

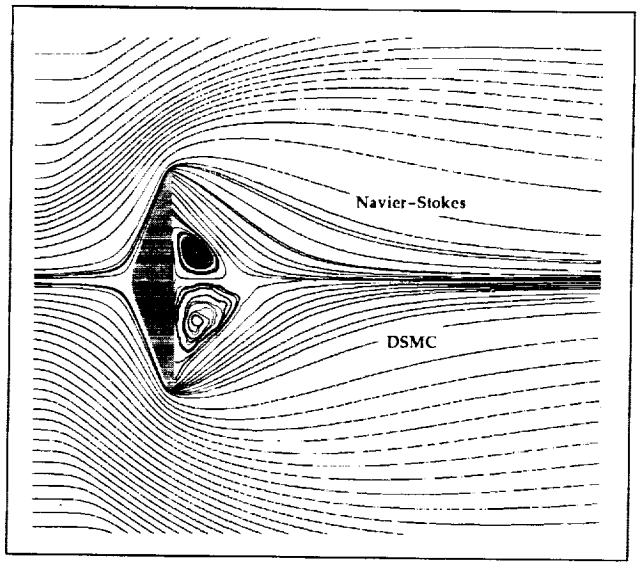


*Fig. 1. Comparison of Navier–Stokes and DSMC particle traces at 92 kilometers; Knudsen number = 0.0162.*

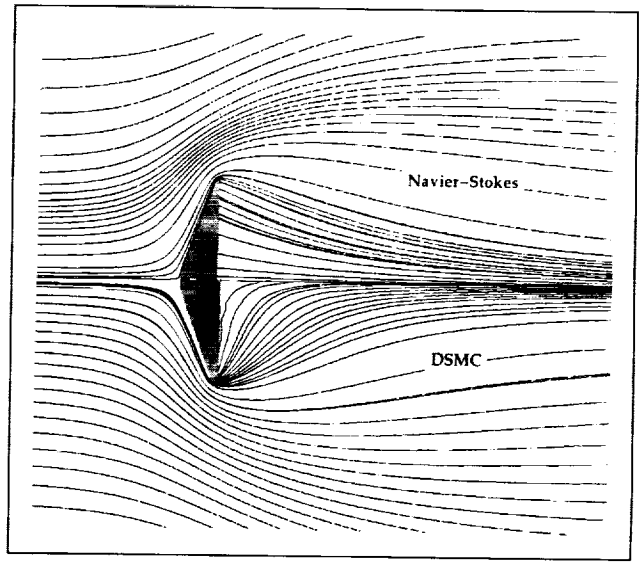


*Fig. 2. Comparison of Navier–Stokes and DSMC particle traces at 105 kilometers; Knudsen number = 0.146.*

Such comparisons between DSMC and Navier–Stokes simulations are illustrated in the accompanying figures, in which computed particle traces are compared for flow over a 70-degree

blunted wedge with a slightly rounded shoulder at two different free-stream densities. The first figure presents results for Mach 29 flow at a density that is equivalent to a 92-kilometer altitude. This density corresponds to a free-stream Knudsen number of 0.016 for a body diameter of 1.7 meters. At these conditions, results from the two methodologies essentially agree. For example, both exhibit a separation point approximately half way between the vehicle shoulder and the vehicle center line. Other predicted features of the flow at these conditions are in good agreement as well. However, at lower densities, disagreements between the two methodologies occur. The second figure presents results for a density nine times smaller than employed for the results in the first figure, which is equivalent to an increase in Knudsen number and altitude to 0.146 and 105 kilometers, respectively. The particle traces in the second figure show a large difference in flow angle in the wake region. A base pressure several orders of magnitude smaller than the DSMC results was predicted by the Navier–Stokes equations as well.

The above results show that current continuum methods based on the Navier–Stokes equations fail to accurately predict conditions in the wake of a blunt body when the free-stream Knudsen number exceeds a value of approximately 0.02. Thus, if such a design is sensitive to wake features at Knudsen numbers exceeding this value, the Navier–Stokes equations should not be used for the analysis. For lower altitudes, where the Knudsen number is below 0.02, the designer can confidently employ the Navier–Stokes equations.

**Ames-Moffett contact: F. Lumpkin**
**(415) 604-3475**
**Headquarters program office: OACT**

## Computational Analysis of Conestoga Launch Vehicle Flow Field

**Grant Palmer, Ethiraj Venkatapathy, Pieter Buning**

The Conestoga launch vehicle is a small, commercially developed rocket designed to lift payloads of up to 2 tons into low-Earth or geosynchronous transfer orbits. The configuration consists of six booster rockets surrounding a central core motor. Four of the booster rockets have vectoring nozzles, which means that the nozzle can be turned to trim the vehicle.

Before the Conestoga launch vehicle was flown, several important design questions had to be answered. In order for the vectoring nozzles to turn, their motors must overcome the force due to external pressure on the nozzles. Aerodynamic forces on the pieces connecting the boosters to the core motor and total vehicle drag must be assessed. It was necessary to determine whether hot exhaust gas from the nozzle recirculated back into the vehicle and whether there was significant outflow between the boosters and core motor.

Answers to these questions were obtained by a computational fluid dynamics (CFD) analysis, using the OVERFLOW code, of the flow around the vehicle at flight conditions. OVERFLOW, developed at NASA Ames, is a multiple-grid fluid dynamics solver that includes advanced turbulence models and a state-of-the-art memory-allocation system. Thirty-two grids with a total of 2.8 million grid points were used to characterize the Conestoga configuration.

The figure shows normalized surface pressure contours over the vehicle at a point in its ascent when the free-stream Mach number is 0.8. The pressure values have been normalized by the free-stream pressure. The highest pressures occur in the stagnation regions of the boosters and core motor and in the region of the forward connecting pieces. There are areas of moderately high pressure on the nozzle shrouds, but on the vectoring nozzles themselves the surface pressure is at or below free-stream pressure. Analysis of the velocity field in the base region indicated only small amounts of the hot nozzle exhaust gases recirculating back to the nozzle and shroud region.

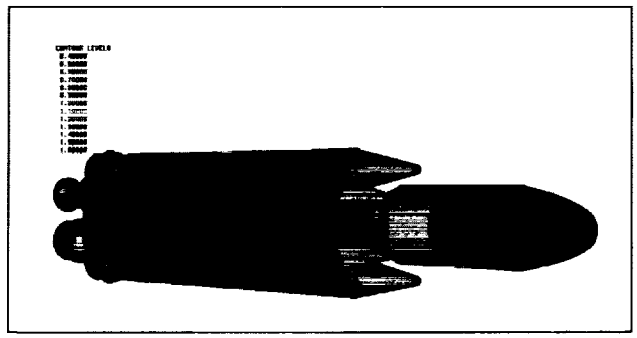

*Fig. 1. Normalized surface pressure over the Conestoga launch vehicle. (See color plate 14 in Appendix)*

**Ames-Moffett contact: G. Palmer**
**(415) 604-4226**
**Headquarters program office: OACT**

## Multitemperature Nozzle Flow Code NOZNT

**Chul Park, Dikran S. Babikian**

The computer code NOZNT enables one to predict the flow along the centerline of the expanding nozzle of a high-enthalpy wind tunnel such as an arc-jet wind tunnel, a gun tunnel, or a shock tunnel. The code is one-dimensional, and accounts for the thermochemical nonequilibrium processes that occur in the nozzle. Several chemical nonequilibrium codes have been written in the last three decades. These conventional nonequilibrium flow codes assume that only one temperature characterizes the flow. None of them so far has been validated by experiment. The existing experimental data on chemical composition at the end of expansion disagree with the values calculated by the existing codes: the codes overestimate the concentration of atomic oxygen and underestimate the concentration of atomic nitrogen, among other differences. Some additional experimental data on the vibrational temperatures of the molecules have been obtained recently at Ames Research Center. The conventional codes cannot reproduce the behavior of vibrational temperatures at all.

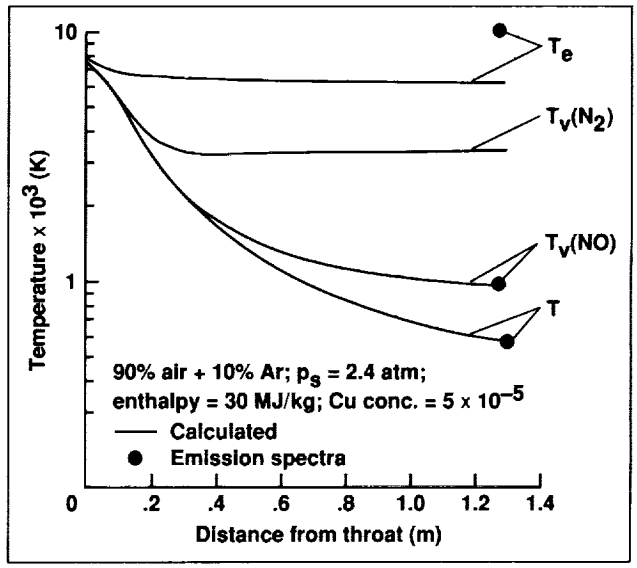


*Fig. 1. Comparison between calculated and measured temperatures along the nozzle. (Experimental data from an arc-jet wind tunnel at Ames Research Center.)*

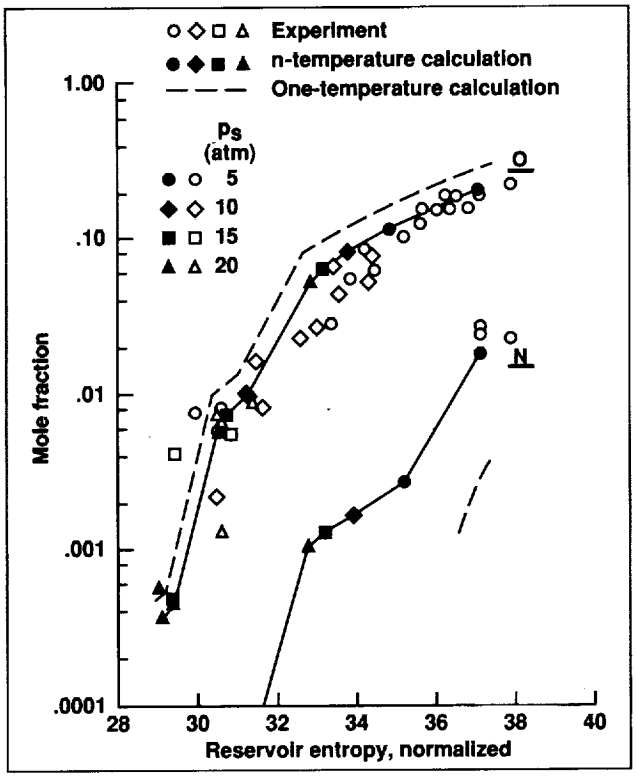


*Fig. 2. Comparison between the measured species concentrations at the nozzle exit and the concentrations calculated using the NOZNT code and one-temperature models. (Experimental data from an arc-jet wind tunnel at Arnold Engineering Development Center.)*

Unlike the existing codes, the NOZNT code correctly reproduces the experimental data. This agreement between theory and experiment is brought about by introducing separate vibrational temperatures for each molecule and electron temperature, leading to a multitemperature model. The code tracks each temperature using the most up-to-date information on interactions among the temperatures, and accounts for the effects these different temperatures have on chemical reaction rates.

In the first figure, the experimental data on the rotational, vibrational, and electronic temperatures obtained in an arc-jet wind tunnel at Ames are compared with the calculations made with the NOZNT code. The code reproduces the measured values fairly well. In the second figure, the experimental data on the concentrations of atomic oxygen and nitrogen obtained in an arc-jet wind tunnel at Arnold Engineering Development Center are compared with the calculations made by the NOZNT code. The figure also shows the values calculated by the conventional one-temperature model. Here, the NOZNT code yields values that are closer to the measured values than the one-temperature model does.

**Ames-Moffett contact: C. Park**
**(415) 604-5394**
**Headquarters program office: OACT**

# Relaxation Phenomena in Expanding Nitrogen Flows

**Surendra P. Sharma**

The relaxation in expanding hypersonic flows is a complex phenomenon. It is customary to measure the rate of relaxation in expansion flows by comparing it with that in compressed flows, such as the flow behind a normal shock wave. Available experimental data indicate that relaxation in expanding flows occurs 5–70 times faster than in flows occurring behind a normal shock. Such a large scatter in the data has been of concern for several decades.

Experimental and analytical investigations of expanding flows in nitrogen were conducted at the NASA Ames Electric Arc-driven Shock Tube (EAST) Facility. The flow expansion is simulated by installing a two-dimensional (2-D) nozzle insert in the driven section of the shock tube. A 2.6-kilometer-per-second shock is generated in 150-torr nitrogen, which reflects off the nozzle insert wall and creates a stagnant reservoir of nitrogen gas at 5600 kelvin and 100 atmospheres.

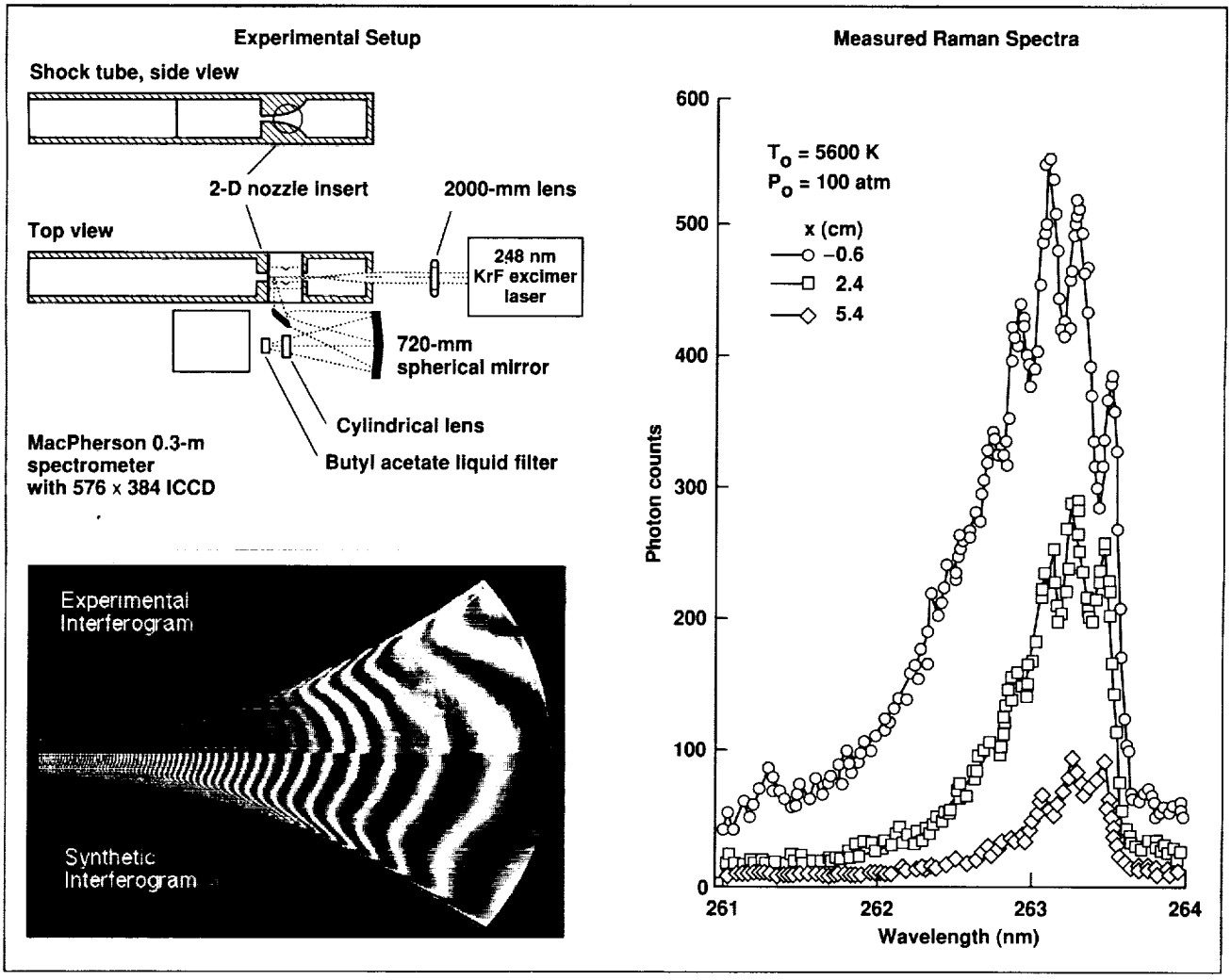


*Fig. 1. Raman-scattering experimental setup, interferograms, and typical Raman spectra.*

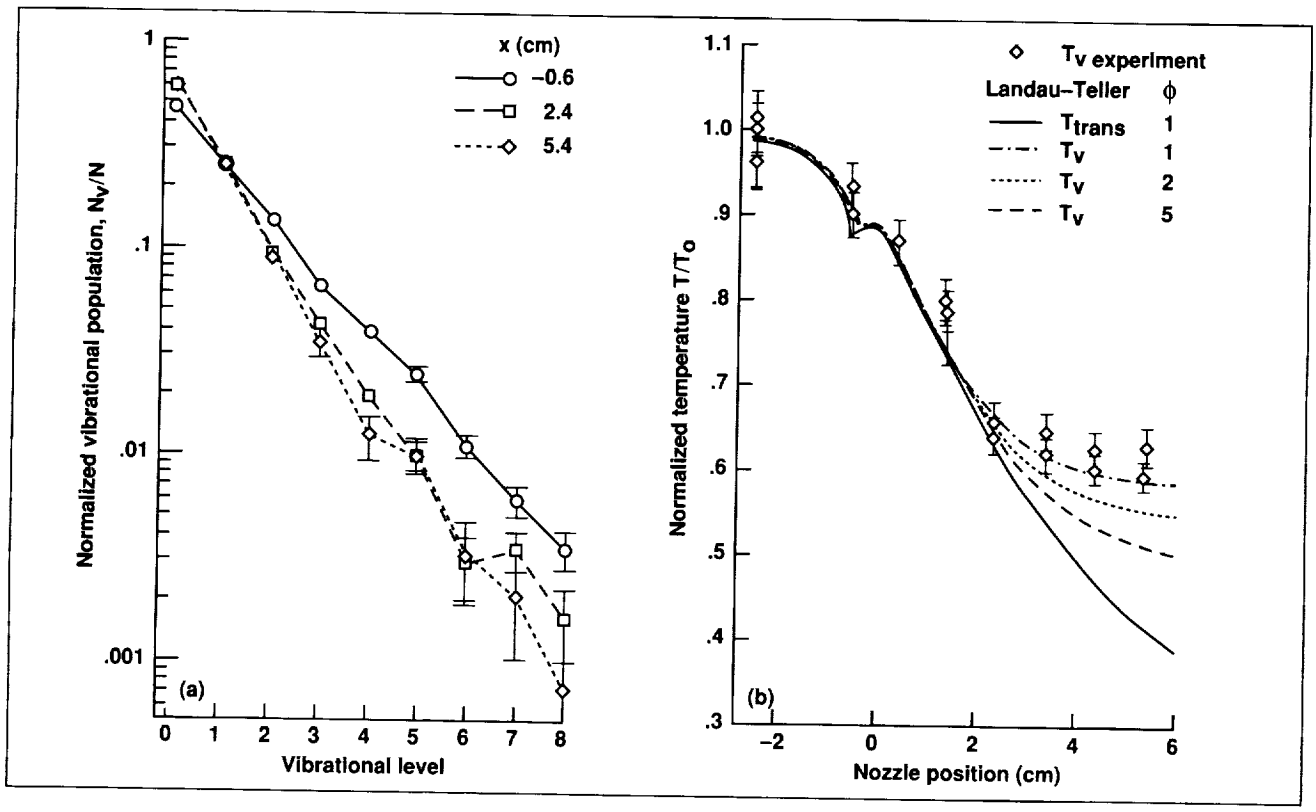


*Fig. 2. (a) Measured normalized vibrational populations; (b) normalized temperatures along the nozzle axis.*

The shock-heated gas expands through the nozzle, generating a steady-state nozzle flow (Mach = 4 at the nozzle exit) for about 0.001 second. The vibrational population distribution at various nozzle stations is measured with spontaneous Raman-scattering spectroscopy. Raman scattering is an inelastic scattering process in which light incident on a molecule is shifted in frequency as the molecule undergoes a transition to a new internal energy state. The intensity of Raman scattering is related in a simple way to the number density at each vibrational level and is a measure of the vibrational population distribution at the point where the Raman-scattered light is collected. The Raman spectrum is excited with a krypton-fluoride excimer laser operating at 2480 angstroms. The laser pulse probes the test gas, as shown in the first figure. The collection scheme images the focal volume of the beam onto the slit of a spectrometer. The spectrometer is equipped with a grating and an intensified charged coupled device (ICCD) camera which provide spectral resolution of 1 angstrom. The background emission is rejected by gating the intensifier to operate only during the laser pulse and by using a butyl-acetate filter to absorb the Rayleigh-scattered light. Spontaneous Raman spectra taken from three of the seven stations along the nozzle axis are shown in the figure. The columns of pixels on the 2-D ICCD array are binned to form "superpixels," each of which is designated by a symbol in the spectrum.

The nozzle flow field is computed by two different computational schemes. A 2-D Navier–Stokes calculation is performed to predict boundary layer effects and effects caused by vertical and streamwise velocity components in the rapidly expanding nozzle. The 2-D code utilizes the standard Landau–Teller relaxation equation to predict energy

transfer from the vibrational to the translational mode. Comparison of a synthesized interferogram using the 2-D results with an experimental interferogram is also shown in the first figure. The second type of code solves the vibrational master equations to determine vibrational energy transfer along with the quasi-1-D fluid dynamics equations. The 2-D flow solution is used to determine an effective quasi-1-D nozzle contour, which is used in the quasi-1-D calculations.

The results for the vibrational temperature measurements for all seven stations in the nozzle are shown in the second figure. At least two measurements were made at each station. The data have been normalized by the stagnation temperatures inferred from shock speed measurements as discussed above. Included in this plot are curves from the quasi-1-D computations using the Schwartz, Slawsky, and Herzfeld (SSH) and Landau–Teller models. Only a single curve is included for translational temperature since all calculations yield virtually identical results for this property. The experimental data do not fall along a single line, yet the overwhelming evidence shows a relaxation rate that is reasonably well described by, and certainly not much faster than, the simple Landau–Teller relaxation. Based on these results, an upper limit of 1.5 can be placed on $\phi$; that is, the relaxation rate in an expanding flow of nitrogen is at most 1.5 times faster than that in flows behind a normal shock.

This measured value of $\phi$ is considerably lower than previous estimates, which lie in the range 5–70. It is well known that the presence of even a small amount of impurity can significantly increase the relaxation rate, hence the purity of the test gas is very important. Most of the scatter seen in previous measurements has been blamed on test gas impurities. In the present measurements extreme care was taken to minimize the impurities in the system. This is the first time that spontaneous Raman scattering was used to provide direct measurement of the vibrational population in a spectroscopically clean facility. It is encouraging to see that the theoretical predictions based on SSH theory also agree with the experiments.

**Ames-Moffett contact: S. Sharma**
**(415) 604-3432**
**Headquarters program office: OACT**

# Thermal Protection Material Property Database

**Thomas Squire**

The Thermal Protection Material Property Database, or TPS*X*, is a personal-computer-based program that serves as a data base for advanced thermal protection material properties. The TPS*X* data base program provides an easy user interface for retrieving material property information in a variety of forms, both graphical and textual. The data base itself consists of a set of text files that can be easily modified and expanded to include new materials. The primary purpose of TPS*X* is to maintain a high-quality source of often-used thermal protection material properties in a convenient, easily accessible form, for distribution to aerospace communities in government and industry. TPS*X* runs on an IBM personal computer, or compatible machine, under the Microsoft Windows operating system. This system provides an easy and familiar "point and click" user interface. By simple menu choices, a user can display material property information in a tabular form, a graphical form, or as a report. For example, a user can display a graph of a material's thermal conductivity as a function of temperature at several pressures. A built-in unit converter makes it effortless to present data in a variety of unit systems, such as the International System of Units (SI) or the English system. In addition, there is an option to view digitized photographs of the materials.

TPS*X* also provides a means of converting the data into a form that can be used in existing computational analysis tools, such as finite-element thermal- and stress-response programs. TPS*X* formats the data appropriately, in the correct units, and outputs it to the screen or to a file on the computer's hard disk. This file can then be included in the input to the analysis program. TPS*X* consists of the computer program itself and associated data files. These data files contain the actual property data such as density, thermal conductivity, specific heat, and tensile strength. Additional data, such as a periodic table of elements and a chemical species data base, are also included in TPS*X*. The program accesses these files, then presents the information in the form requested by the user. TPS*X* comes with an existing property data base of thermal protection materials developed at the NASA Ames Research Center.

Although TPS*X* was developed for use in the design of thermal protection systems, it is general enough to be used as a repository for any material property data. Users can create their own data base by using a simple text editor. The format of the data files is "command driven." This means each new line contains a command that tells the TPS*X* program exactly what information to expect. This makes it possible to include as much or as little data as the user requires. The data base accepts property values that depend on as many as two independent values. Thus it is possible to include thermal conductivity as a function of both temperature and pressure, or material strength as a function of temperature and orientation.

Future enhancements to TPS*X* include (1) a simple one-dimensional thermal analysis module to estimate material temperatures under a given heating condition; (2) a module to predict the heating conditions for reentry trajectories used in the design of thermal protection systems; and (3) the ability of the program to be ported to other computer platforms, such as the Macintosh computer. Currently TPS*X* has been distributed in an "alpha" test version to Johnson Space Center and several industry customers. The general distribution of the complete program is expected in fiscal year 1994.

**Ames-Moffett contact: D. Rasky**
**(415) 604-1098**
**Headquarters program office: OACT**

# Accidental Earth Entry of Radioisotope Thermoelectric Generators

**Michael E. Tauber, Paul F. Wercinski, Lily Yang, Frank Milos**

The upcoming Cassini spacecraft mission to Saturn will require the use of radioisotope thermoelectric generators/general-purpose heat sources (RTG/GPHS). After launch in October 1997, the spacecraft will be accelerated on its journey to Saturn by close fly-bys (gravity assists) of Venus, Earth, and Jupiter. The Earth gravity-assist trajectory will carry the spacecraft within 200 kilometers of the Earth at a speed of 19.4 kilometers per second. Should the spacecraft experience a guidance or control malfunction before or during the Earth fly-by, there is a small probability that an accidental entry into the atmosphere could occur which would cause the RTGs to be released. Each of the three RTGs contains 18 GPHS "bricks." Each brick, in turn, holds two heat-shield-encased cylinders, and each cylinder contains iridium capsules that hold 100 grams of radioactive plutonium oxide fuel (see first figure). This study was done to determine if the bricks will provide sufficient heat shielding to prevent release of the radioactive fuel during entry at 19.4 kilometers per second from an altitude of 95 kilometers and at entry flightpath angles from about –8 degrees to –90 degrees. The work was done in response to a request from NASA Headquarters to support the Cassini project office at the Jet Propulsion Laboratory.

The heating of bodies entering the Earth's atmosphere at nearly 20 kilometers per second has not been calculated previously with any degree of confidence. Although the bricks that hold the fuel-containing cylinders are approximately 10 centimeters square, the heating along most trajectories is dominated by thermal radiation from the high-temperature, incandescent gas in front of the body, rather than conduction through the boundary layer. The interaction of intense radiative heating with the vaporizing, finely woven carbon–carbon heat shield material is an extremely complex phenomenon and was approximated in the analysis by considering only sublimation—the phase change from solid to vapor. Other forms of energy transport into and from the carbon heat shield were neglected. The validity of considering only sublimation was based on experimental data from high-power laser-beam irradiation of the carbon heat-shielding material. Nonetheless, the computation of the heating rates and the resultant heat-shield vaporization was a challenging task.

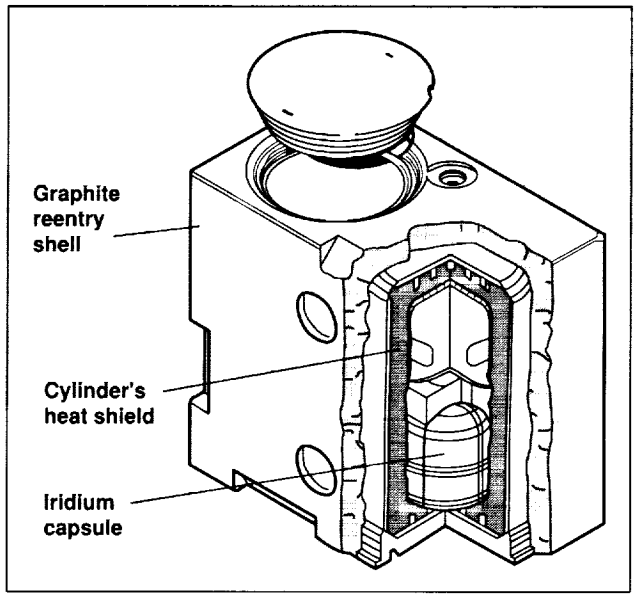


*Fig. 1. Cutaway view of general-purpose heat source (GPHS) brick.*

At the hypervelocity speeds encountered here, the bricks tend to be aerodynamically stable with their bluntest faces forward, and the cylinders are stable when their axes are perpendicular to the air stream. After the brick's face burns through, the cylinders fall out of the cavity in the brick and continue the descent. During their release from the brick, the cylinders are expected to acquire some angular momentum, which causes them to rotate.

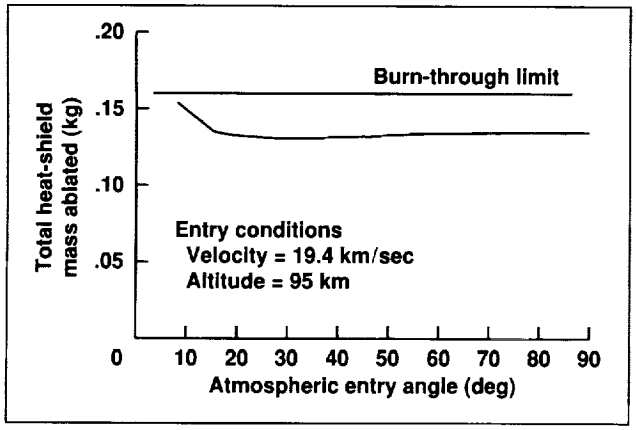


*Fig. 2. Heat-shield mass loss as a function of atmospheric entry angle.*

The heating along more than 50 trajectories was calculated for a variety of scenarios. It was found that the bricks burn through, generally, but that the heat shield of a rotating cylinder does not burn through (see second figure), and therefore no radioactive fuel is released. In the unlikely case that the cylinder does not rotate, a portion of the heat shield that is facing the air stream could burn through, however, and some plutonium oxide fuel could be released into the atmosphere.

**Ames-Moffett contact: M. Tauber/P. Wercinski**
**(415) 604-6086/3157**
**Headquarters program office: OACT/OSSA**

## High-Speed Propulsive Nozzle Flow Simulations

**Ethiraj Venkatapathy**

The nozzle part of the high-speed propulsion system is complex. An efficient, quiet nozzle design is needed for the success of the high-speed civil transport (HSCT) system. In the nozzle, the hot engine-exhaust flow is allowed to mix with the cooler fan flow through multiple mixers, and the mixed flow is expanded through the afterbody of the nozzle downstream of the mixer. Propulsive thrust is extracted from the one-sided nozzle ramp. The mixing between the hot and cold flow can cause high noise levels. An understanding of the dynamics of the flow in the nozzle is essential for improving the nozzle's noise and thrust performance. Computational simulation of the high-speed nozzle flow can provide the necessary insight for the optimum nozzle design.

In collaboration with General Electric Aircraft Engines Company (GE/AE), computational analysis of a high-speed civil transport nozzle has been carried

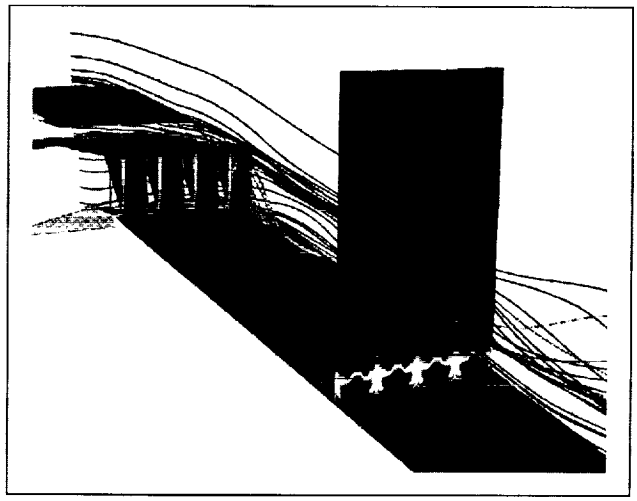

*Fig. 1. Surface pressure, total temperature, and particle traces. (See color plate 15 in Appendix)*

out using a three-dimensional flow solver. The flow solver known as FL3D, which was developed at NASA Ames, has been successfully applied to a number of high-speed nozzle flow problems. The FL3D solver is a stable, versatile, validated, and easy-to-use code. The solver can be used in the analysis of complex configurations either with a single grid or with multiple grids. GE/AE has adapted FL3D as a design tool and is using it to solve a wide variety of commercial aircraft engine flows in addition to the HSCT nozzle flow.

From the computed solution for the GE/AE HSCT nozzle configuration, a composite picture of the fluid dynamics is depicted in the figure. The one-sided nozzle wall, the primary hot core region upstream of the chute-mixers, the secondary fan flow region, and the external flow region are all shown in the figure. The surface pressure contours are plotted all along the walls, and particle paths from the hot and cold flow regions are computed and shown as red, blue, and yellow lines in one of the modules. The red lines represent the particles from the hot core, and the blue and yellow lines represent particles from the cooler outer flows. In addition, the total temperature contours on a plane downstream of the mixer is also shown. Large separation within the chute region was observed both experimentally and from the computed solutions. The computed solutions were able to provide helpful insight into the complex flow dynamics.

**Ames-Moffett contact: G. Deiwert**
**(415) 604-6198**
**Headquarters program office: OACT**

# Decision Analysis for Development of Life-Support-Systems Technology

Mark G. Ballin

With resources becoming increasingly limited, it is important to be able to make sensible and defensible technology investment decisions. Applied research and technology development (R&TD) is often characterized by uncertainty, risk, and significant delays before tangible returns are obtained. Therefore, making decisions about which technologies to advance and what resources to devote to them is a challenging but essential task. For life-support systems for piloted spaceflight, new technology concepts typically are characterized by nonexistent data and rough approximations of performance, uncertain future flight program needs, and a complex, time-intensive process to develop the technology to a flight-ready status.

A methodology known as decision analysis was developed to address investment decisions that are characterized by high complexity, cost, and uncertainty. Decision analysis is an outgrowth of game theory, operations research, and management science. It imposes logic and structure on complex problems, thereby capturing the process by which a decision is made. It also provides a practical method for accounting for the limits of knowledge that may be available at the time a decision is needed. The viability of decision analysis is well established in fields that are strongly dependent on risk mitigation, such as oil exploration geology.

An initial study to assess the viability of using decision analysis to make R&TD recommendations for life-support technology was successfully completed in 1993 at Ames Research Center. Several advanced carbon dioxide removal concepts were assessed for application to a human lunar return

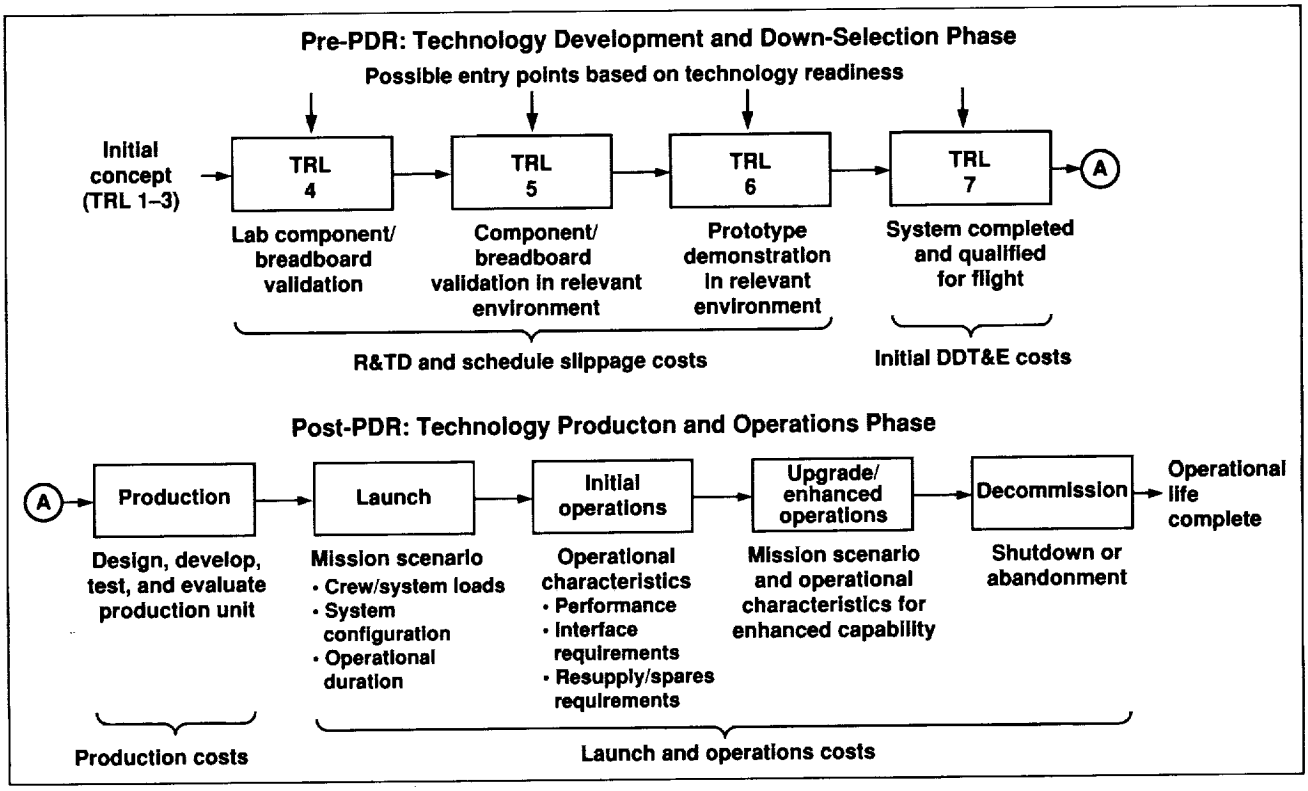


*Fig. 1. Simplified model of technology development, emplacement, and operational life cycle. (PDR = preliminary design review.)*

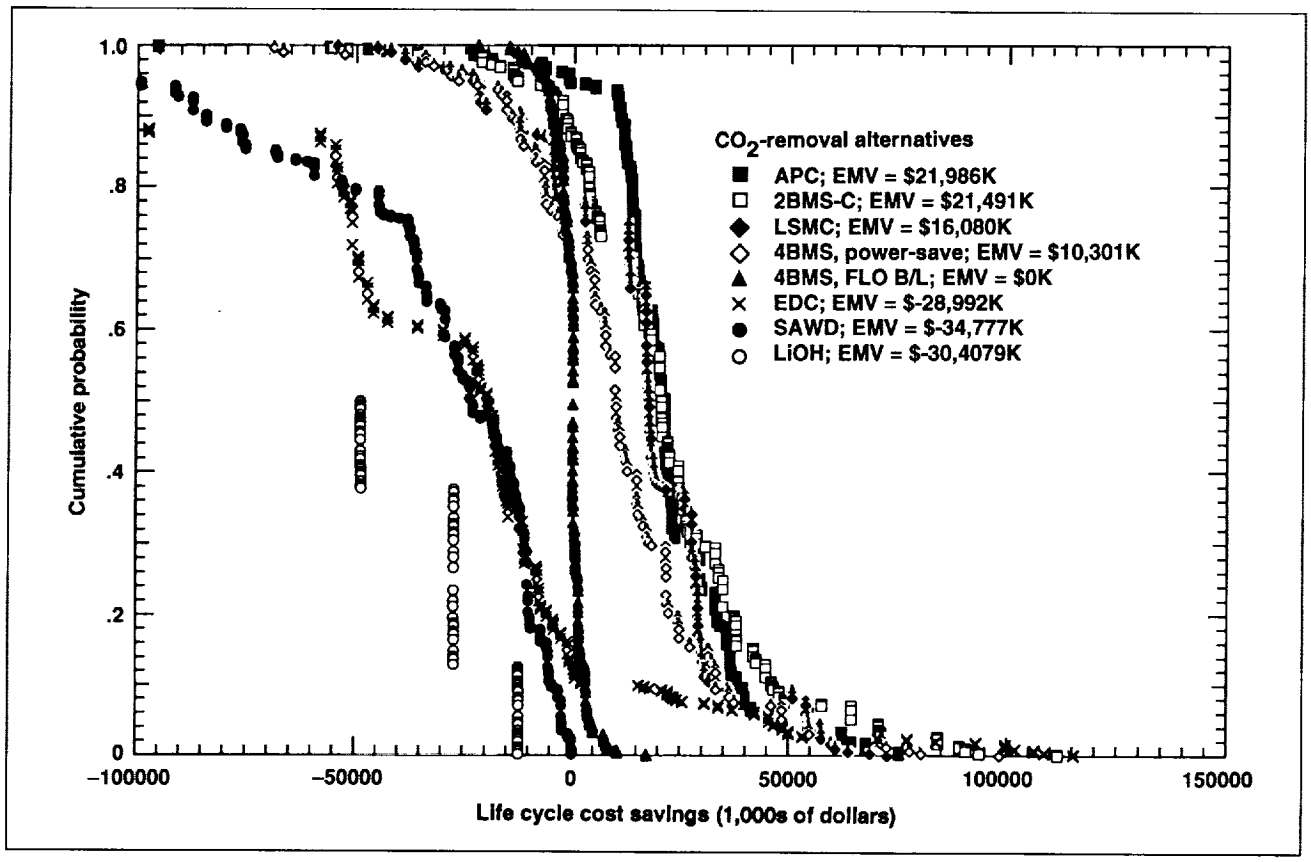


*Fig. 2. Cumulative distributions of life-cycle cost savings of various concepts for one life-support-system technology ($CO_2$ removal). (EMV = expected monetary value.)*

mission scenario known as the First Lunar Outpost. An approach was developed that accounts for the uncertainties in each technology candidate's cost and performance parameters as well as programmatic uncertainties such as mission architecture. Life cycle cost savings relative to a baseline, adjusted for the cost of money, was used to evaluate each of the technology concepts.

Because the focus of the study was to make recommendations in support of flight programs, a model containing the technology development steps and the operational life cycle was required. A simplified model of an idealized NASA hardware development program was developed for the study (see first figure). The model makes use of the commonly used "technology readiness level" (TRL) measure. One form of quantitative result obtained from the study was the cumulative probability distribution of projected life-cycle cost savings, shown in the second figure. From this type of distribution, a decision maker can understand the levels of risk associated with levels of benefit for a particular technology.

The decision analysis methodology was found to provide a consistent decision-making strategy for development of new life-support technology. It provides insight that is not possible from more traditional analysis approaches. It establishes a consistent decision-making framework, it accounts for the risk preferences of the decision maker, and it enables a systems analyst to estimate the value of reducing uncertainties through further study or testing. Most important, decision analysis enables the R&TD management role to be shifted from that of balancing competing demands for resources to that of

defining program goals and the assumptions needed to assess a project's merit. The decision maker can assess the ability of a proposed technology development project to deliver the performance promised and evaluate its chances of being successfully completed with the proposed resources. Impartial decisions can then be made concerning which efforts to support.

**Ames-Moffett contact: M. Ballin/P. Cheng**
**(415) 604-5771/6975**
**Headquarters program office: OA**

## Effect of Particle Size on Supercritical Water Oxidation

**John W. Fisher**

Advanced life-support systems for space, especially systems that include growing plants for food, require the recovery of resources—primarily carbon dioxide and water—from various hydrocarbon wastes. Supercritical water oxidation (SCWO) of wastes is one of several possible techniques for oxidizing waste organics to recover the carbon dioxide and water. "Supercritical" means that the system is operated at temperatures and pressures above a critical point so that separate liquid and vapor phases cease to exist. For water the critical temperature is 374°C and the critical pressure is 3,210 pounds per square inch. Supercritical water oxidation has the advantages of fast kinetics, complete oxidation, and minimization of undesirable side products. However, the SCWO process requires further development before it can be implemented in space life-support systems. One SCWO development need is in the area of destruction of insoluble solids, such as inedible biomass or human waste. Insoluble solids must be introduced into an SCWO reactor as particles, and the size of the particles can affect the rate of reaction.

Particle size can affect the rate of reaction in various ways. Large particles with density higher than the supercritical water may settle out in a reactor. Settling and clumping of solids can slow the reaction rate considerably. Even without settling, particle size affects reaction rate because of diffusion or heat transfer effects. Larger particles take longer to heat up to reaction temperature. Also, larger particles have a smaller proportionate surface area exposed to the

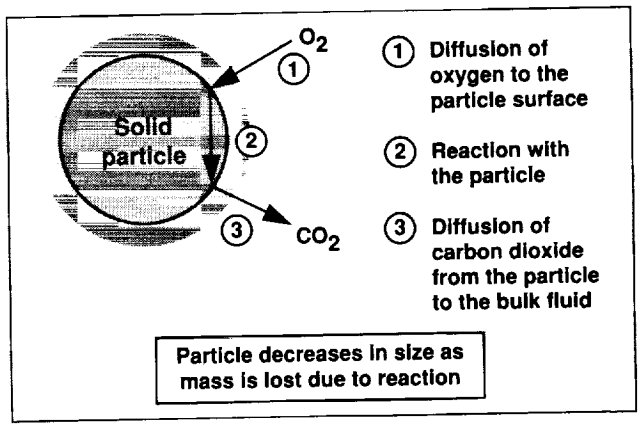


*Fig. 1. Reaction and diffusion with solid particles.*

oxidizing gas surrounding the particles. The first figure illustrates the diffusion process that takes place at the surface of a particle. It is generally true that smaller particles will react faster, but there are significant difficulties involved in grinding material to very small sizes. More equipment, more system complexity, and more energy are required to grind to small sizes. The approach being taken is to determine SCWO reaction conditions that will require minimal feed preparation. Experiments were conducted in a stirred autoclave reactor, constructed of corrosion-resistant Hastelloy 276C. The reactor feed-injection and sample-removal systems are capable of operating while the reactor is at supercritical conditions. The ability to inject and sample at supercritical conditions

is valuable because data evaluation problems that are associated with long reactor heat-up times can be avoided. A continuous reactor system with the ability to pump solid slurries at supercritical conditions is being fabricated. The continuous system will be more like an actual flight system and will permit development of slurry handling and process control.

The second figure is a graph of some of the data obtained to date. It clearly shows that the reaction rate was faster for smaller particles. Reactions were run at pressures of about 4,000 pounds per square inch and temperatures of about 720°F. The experimentation is continuing. It is possible that at higher temperatures the particle-size effect will be negligible. Besides particle size, other significant process parameters will eventually be studied, including temperature, agitation, and waste composition.

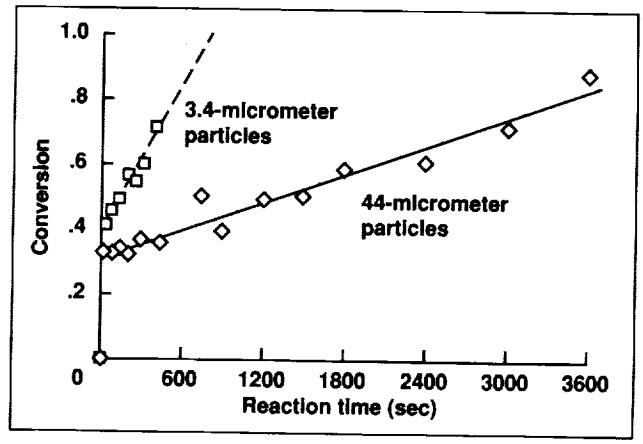


*Fig. 2. Particle conversion obtained at 720°F for 3.4-micrometer and 44.2-micrometer particles. Lines represent zero-order fit of the data.*

**Ames-Moffett contact: J. Fisher/R. Lamparter**
**(415) 604-4440/1159**
**Headquarters program office: OSSA**

## Thermal Regeneration of Spent Lithium Hydroxide

**Venkatesh Srinivasan, Bernadette Luna**

Exploration of planetary surfaces will require portable life-support systems to provide a continuous supply of breathable air. These systems will need to be able to support many missions without resupply of air from Earth. A lightweight, regenerable carbon dioxide absorber will be required.

Lithium hydroxide is the carbon dioxide absorbent of choice. Its high carbon dioxide absorption capacity per unit mass makes it the lightest absorbent for use as a scrubbing agent, but it has been thought to be nonregenerable, which makes it undesirable for use in portable life support systems. Silver oxide, an alternative scrubbing agent under consideration, is regenerable, but a silver oxide life support system would weigh at least five times more than a comparable lithium hydroxide system. Since a light-weight system is essential to astronauts on a planetary surface, the feasibility of regenerating lithium hydroxide from lithium carbonate (the spent material) was investigated.

Lithium hydroxide is currently manufactured from lithium carbonate and calcium oxide by a series of steps (precipitation, separation, screening, etc.), almost all of which require gravity. Processing that requires gravity would not be practical in a zero-G environment, but could, in principle, be accomplished on a planetary surface. However, there is a possibility that a thermal regeneration process could be used which is potentially simpler and may not require a gravitational field. This thermal regeneration process was investigated and the initial results have shown that it may, in fact, be possible to regenerate lithium hydroxide by thermally decomposing lithium carbonate under carefully controlled conditions.

Judging from other studies of the thermodynamics and kinetics of thermal decomposition

of carbonates, we believe that careful heating of spent lithium hydroxide absorbent will lead to its decomposition, resulting in the release of absorbed carbon dioxide, and leaving a product that may be reused. The absorbent currently used by NASA has been carefully engineered to be nondusting and to have good carbon dioxide absorption properties—specifically, high porosity and surface area. It is essential that any regeneration process preserve these special properties as much as possible. A sample of the spent absorbent was heated in a vacuum to 680°C. Subsequent analysis of the product showed that 70% of the original material had decomposed. Studies of the surface using a scanning electron microscope showed some changes but no major degradation. The micrograph in the first figure shows

*Fig. 1. Scanning electron micrograph (800X) of a sample of spent lithium hydroxide regenerated to >99% lithium carbonate.*

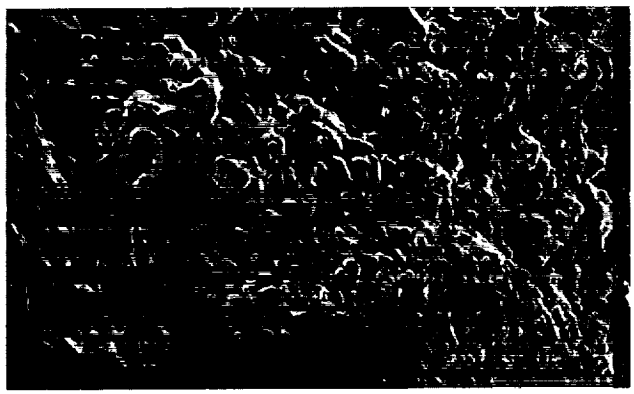

*Fig. 2. Scanning electron micrograph of a sample of spent lithium hydroxide after heating. There is some "smoothing" of edges, but grain size is retained.*

the sample before heating, and the second figure shows the sample after heating was completed. These results are very promising for the development of a new process that is simple (no moving parts) and yet enables the reuse of lithium hydroxide as a carbon dioxide absorbent.

**Ames-Moffett contact: V. Srinivasan/P. Cheng**
**(415) 604-1417/6975**
**Headquarters program office: OAST**

# Semiclosed Plant Growth Chamber Model

**Ann Blackwell, Scott Maa, Mark Kliss, Charles Blackwell**

Several NASA projects for the Space Station will support research on the influence of gravity on the development and maintenance of living systems. These projects will include small, semiclosed plant growth chambers in which the environmental conditions are controlled to an accuracy that permits scientific experimentation in various simulated-gravity conditions from $10^{-6}$ to 2 times the gravity at the Earth's surface. A model and simulation of a plant growth chamber system can be used to predict, before actual construction of the system, whether the environmental conditions in the design will provide the accuracy required by the scientific community. The research effort reported herein is a collaborative effort of the Systems Engineering and Analysis Office of the Centrifuge Facility Project and the Flight Experiments Development Group of the Advanced Life Support Division.

NASA's Computer Aided System Engineering and Analysis (CASE/A) program, originally developed as a simulator for the Space Station's life support system, was chosen as a potentially useful application program for computer simulation of the dynamic response of a plant growth chamber system. The purpose of the research was to identify and implement modifications to CASE/A to extend its function to simulation of the fluid and thermal dynamics of the environment of plants in small, controlled-environment systems.

The laboratory version of Ames Research Center's Salad Machine, a unique application of controlled ecological life support system (CELSS) technology, was selected as a model-validation system. The laboratory version of the Salad Machine consists of a hydroponic plant growth chamber, a fluorescent lighting system, an air-to-water heat exchanger, a water chiller, an air mover, interconnecting air ducting and fluid plumbing, and nutrient and carbon dioxide ($CO_2$) supply systems. A mathematical model of the biophysical processes important in determining the thermal and fluid dynamics of the Salad Machine was developed. This model was implemented in CASE/A by using existing CASE/A subroutines where possible, and modifying others or developing new routines as necessary. To account for temperature, relative humidity, and gaseous variations in the plant chamber, it was necessary to create and incorporate a thermal submodel into CASE/A's routines. A condensing heat exchanger subroutine developed at Ames replaced the CASE/A subroutine. Modifications were made to the "pump," "valve," "passive," and "controller" subroutines.

Two scenario studies have been completed, in which the response of the modified CASE/A simulation was compared to the measurements made on the actual Salad Machine system: (1) an unlighted-switched-to-lighted, low-humidity environment without plants in the system and (2) a changing-$CO_2$-level environment with plants in the system. The first figure shows the comparison between the

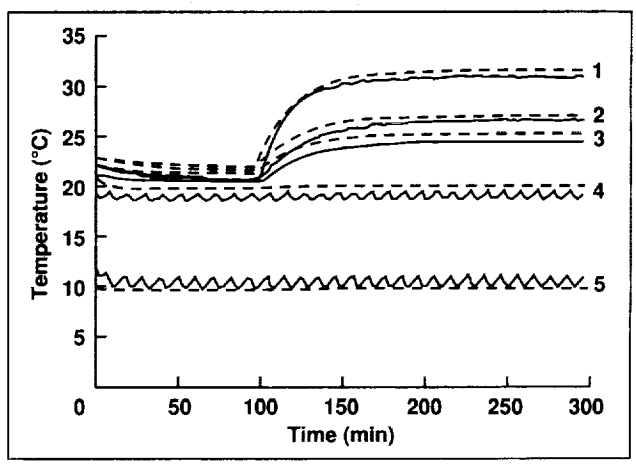


*Fig. 1. Measured (solid lines) and simulated (dashed lines) temperature responses of the Ames Salad Machine for an air-mover speed of 1200 rpm. The air mover was turned on at 0 minutes. The lights were turned on at about 100 minutes. Temperatures measured were (1) chamber ceiling, (2) chamber wall, (3) air entering the heat exchanger, (4) air leaving the air mover, (5) air leaving the heat exchanger.*

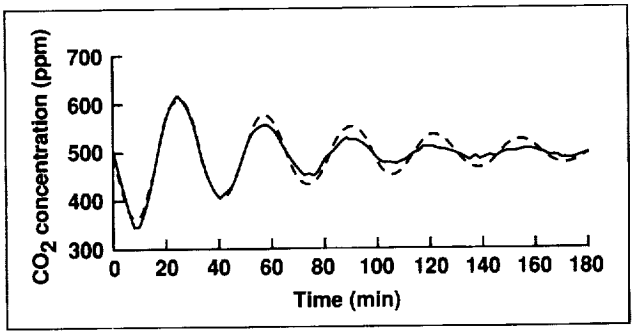


*Fig. 2. Measured (solid line) and simulated (dashed line) responses of the Salad Machine containing plants. The $CO_2$ concentration was raised to 1300 parts per million (ppm) and the chamber concentration command set point was set to 500 ppm. The initial draw-down from 1300 ppm is not shown.*

simulated and measured temperatures at five locations throughout the system for scenario 1. The second figure shows the comparison between simulated and measured $CO_2$ concentration in the plant growth chamber for scenario 2. For the two scenarios studied, the level of success that was achieved by the simulation in replicating the measured performance of the system was very high for temperature and $CO_2$, high for pressure, and moderate for relative humidity.

Many of the processes that were expected to have significant impact on the system behavior at the level important to the study were already resident in CASE/A. Several processes critical to achieving the extent of system replication desired had to be added to the existing program or significantly modified. The study showed that the potential for developing CASE/A into a tool adequate for forecasting the dynamic behavior of small, semiclosed plant growth chamber systems is very high. Some important aspects of the simulation remain to be addressed, including the evaluation of the model performance under high-humidity conditions and the development and evaluation of a completely interactive plant growth chamber–plant physiological model.

**Ames-Moffett contact: A. Blackwell**
**(415) 604-6540**
**Headquarters program office: OLMSA**

# Jet Exhaust Study for SOFIA

**Ann S. Dinger, Edward W. Dunham, Edwin F. Erickson, Stephen P. Klotz, David G. Koch, Robert N. Yee**

A study was performed at Ames to evaluate the potential effects of engine exhaust plumes from a Boeing 747 aircraft on the infrared sensitivity of the SOFIA telescope. The telescope was installed in a cavity aft of the wings. Even though the telescope in actual use will not look through the jet exhaust plume, the concern was that the thermal infrared (IR) from the exhaust gas from the JT9D-7 engines could scatter into the telescope beam and cause an undesirable increase in the IR background.

The nature of the signal was described, actual plume measurements were made, and stray light calculations were performed to quantify the IR background at an image plane that is reimaged from the telescope. To better understand the plume, exhaust gas abundance and thermodynamic properties were obtained from the engine manufacturer, Pratt and Whitney. The IR emissivity of the plume was calculated from that data. Development of the plume downstream of the engine was predicted, including evolution of the streamlines and mixing and cooling of the gases. Because of the considerable amount of modeling involved, measurements from the Shuttle Carrier Aircraft were used to verify the predicted emission levels. The measured temperature profiles, absolute power, and fluctuations were close to those anticipated and were used in the final stray-light modeling. The emission from the engine tail cone was included in the analysis.

The stray-light modeling was performed using the program APART/PADE. The model included the telescope, tertiary mirror, Nasmyth tube, reimaging optics and cold stop, aircraft cavity, cavity door, shear-layer control surfaces, aircraft wing, and outboard engine tail cone (not shadowed by the wing). Mirror surfaces were modeled for scatter from expected surface particulate contamination. Martin Infrablack coating was assumed for the stray-light control surfaces. Besides the plume and the engine tail cones, atmospheric emissions from the tropopause and from the Earth's surface at 12 micrometers were included unwanted sources. Background calculations were made in bands centered on six wavelengths from 4.5 to 100 micrometers.

The results of the investigation indicate that without taking any remedial action to reconfigure the telescope for improved rejection of the exhaust plume background, the only situations where the exhaust plume would be a problem are at low elevation angles (25 degrees) for high-spectral-resolution observations near water or near carbon dioxide spectral lines for wavelengths less than 10 micrometers.

**Ames-Moffett contact: E. Erickson/A. Dinger**
**(415) 604-5508/4924**
**Headquarters program office: OSSA**

# High-Temperature Semiconductor Bolometers

**John Goebel**

Missions to the outer planets enter a thermal environment similar to that encountered in cryogenic laboratory experiments. Many of the experiments considered for these missions use infrared detectors to measure the thermal emission from the planets and their moons. With currently available bolometric thermal detectors, infrared spectra and images of only limited quality can be produced. As the probe moves out of the relatively warm environment of the Earth's solar orbit into the colder reaches of the outer planets, the sensitivity achievable by pyroelectric and thermoelectric detectors drops significantly. Ironically, the theoretical sensitivity of an ideal thermal infrared detector increases with decreasing temperature. It would be beneficial to take advantage of this free increase in sensitivity and thereby improve the quality and quantity of scientific information that can be returned by future probes.

We have developed a detector concept that takes advantage of the cold environment near the outer planets. It is capable of achieving near theoretical sensitivity when used as an infrared bolometric detector. The detector utilizes a semiconducting crystal appropriately doped to be at maximum sensitivity over the ambient temperature range in any of several outer-planet environments. No refrigeration is required in the spacecraft, although thermal isolation from the spacecraft, especially if the latter is heated, would be necessary. This concept is intended to overcome the shortcomings of pyroelectric and thermopile detectors in missions to the outer planets.

Selection of an appropriate semiconductor material for a particular outer planet is based on the ambient temperature of the planet, e.g., 35 kelvin for Pluto. Then a semiconductor crystal and appropriate dopant are chosen as a thermistor to maximize sensitivity in the ambient environment. For example, silicon (Si) crystals doped with phosphorous have suitable resistivity and temperature coefficient of resistance at and below 50 kelvin for use in a Pluto environment. Then the selected thermistor element is incorporated in a composite bolometer construction. Infrared radiation is coupled to the thermistor by a blackened substrate to which the thermistor is attached. The composite bolometer is electrically and thermally coupled to the radiation-cooled ambient-temperature spacecraft structure by fine-diameter wires. Support structures used in other composite bolometer designs can be used for mechanical rigidity. This design is also compatible with photolithographic replication techniques for use in one- and two-dimensional detector array structures.
A prototype thermistor has been tested in the laboratory at liquid-nitrogen temperature (77 kelvin). This temperature is approximately that of the planet Neptune. With an indium-doped Si (Si:In) crystal, a resistivity of 100 kilo-ohms was achieved in a dark environment. Si:In has an activation energy of 150 millielectron volts and a temperature coefficient of resistance in excess of 2 per kelvin.

**Ames-Moffett contact: J. Goebel**
**(415) 604-3188**
**Headquarters program office: OA**

# Variable Temperature Performance of an Si(Li) Detector Stack

G. Scott Hubbard, Robert E. McMurray, Jr., Robert G. Keller, Paul F. Wercinski

We have previously reported data from laboratory experiments and Monte Carlo analysis for a Silicon(Lithium) (Si(Li)) gamma-ray detector stack. This configuration is intended to provide moderate resolution (full width at half-maximum (FWHM), 5–10 kiloelectronvolts (keV) at 1000 keV)) over a broad temperature range (<90 kelvin to 230 kelvin). This temperature range is consistent with the requirements of spaceborne applications that use ambient (passive) cooling for orbiting platforms (100 kelvin) or for Mars surface operations (130–230 kelvin). Such an approach provides an attractive alternative to the poorer resolution of scintillators (~60 keV at 1300 keV) and the cryogenic cooling requirements of Germanium (≤100 kelvin).

Leakage-current measurements indicated that acceptable device performance (FWHM < 10 keV at 662 keV) could be expected up to ~230 kelvin, where leakage current was ~10 nano-amps. However, it is well known that leakage current is only one contributor to detector performance; it has been asserted that performance often degrades as a function of temperature faster than indicated by direct-current measurements. In addition, the literature provides little experimental data on the performance of Si(Li) detectors at temperatures above that of liquid nitrogen. The present work addresses this absence of data, providing variable temperature resolution measurements from 85 to 245 kelvin.

We evaluated six 5-millimeter-thick detectors and two 1-centimeter-thick detectors, all with a 2-square-centimeter active area. These devices were fabricated using standard lithium drifting techniques employed at the Lawrence Berkeley Laboratory (LBL) silicon detector laboratory, with no special attention to elevated-temperature operation. Selection and optimization of the preamplifier (provided by LBL) was driven by the need to compensate for competing noise sources across the broad temperature range of interest. Our choice for the present experiments was an alternating-current-coupled preamplifier with input circuit selected for lower capacitance, and leakage current varying from a few pico-amps to >50 nano-amps.

To establish suitability of Si(Li) devices over the range of interest, and to provide a basis for comparison with our previous leakage-current measurements, five Si(Li) devices were selected, on the basis of room-temperature noise performance, from a larger group of detectors. Results of Cesium-137 gamma ray resolution measurements vs. temperature for all these detectors are shown in the first figure. Electronic and environmental noise performance was not optimized;

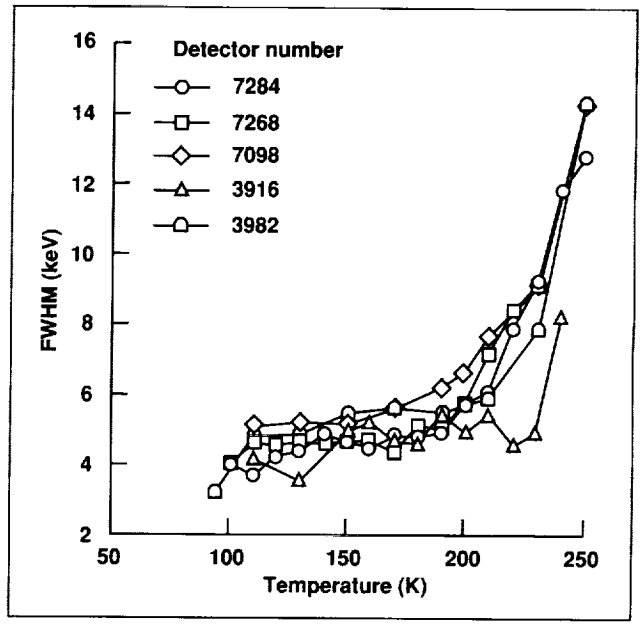


*Fig. 1. Temperature dependence of full-width-at-half-maximum (FWHM) peak width of five 5-millimeter Si(Li) detectors.*

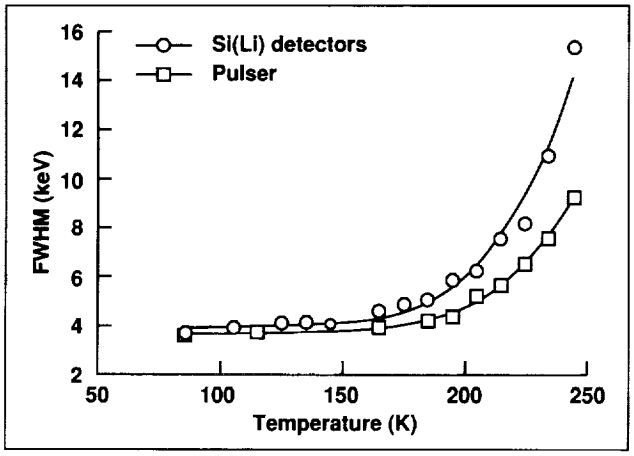


*Fig. 2. Temperature dependence of FWHM peak width of a 2-centimeter-high detector stack and of the electronic pulser noise contribution.*

rather, the results were used for qualitative screening only. As can be seen, the resolution variation among devices is relatively small (±20%) up to temperatures of approximately 200 kelvin. In addition, such detectors individually met the key resolution criteria of <10 keV up to 230 kelvin. From these results, we concluded that even without special fabrication or selection procedures, devices on hand at LBL should yield stacks that respond consistently to variable-temperature operation.

A 2-centimeter-high-detector-stack resolution of 3.92 keV up to 150 kelvin, as shown in the second figure, was obtained through standard multichannel analyzer output analysis. Electronic noise as determined by a precision pulser is 3.68 keV for the same temperature range. The quadrature subtraction of these noises yields a silicon contribution of 1.4 keV. At higher temperatures this relationship does not hold. These results suggest that "normal" Si(Li) device performance may be obtained up to ~150 kelvin, but that an excess noise mechanism begins to dominate at higher temperatures.

In summary, the Si(Li) stack measured exhibits the required resolution over the temperature range of interest. We have observed an FWHM for 662 keV of ≤5 keV for temperatures ≤ 200 kelvin and ≤10 keV for temperatures ≤ 230 kelvin. Judging from the results so far, further improvements are possible in detector noise performance. In order to demonstrate spectrometer performance, we plan to read out individual device signals from the stack elements and apply previously developed detection algorithms to the measurement of multiline spectra.

**Ames-Moffett contact: G. Hubbard**
**(415) 604-5697**
**Headquarters program office: OA**

# Heat Switches for Applications at Temperatures Below 10 Kelvin

Ali Kashani, Ben Helvensteijn

Several NASA astrophysics missions, such as the Large Deployable Reflector (LDR), require refrigeration systems that would cool some of their components to a temperature of 2 kelvin. A magnetic refrigerator is one system that could provide cooling to 2 kelvin. Magnetic refrigeration is based on magnetic cycling of a paramagnetic refrigerant. During parts of the refrigeration cycle, thermal contact must be made between the refrigerant and the 2-kelvin heat source or the 10-kelvin heat sink. A liquid-gap heat switch and a gas-gap heat switch, respectively, are developed to accomplish these tasks.

Both heat switches are configured as two matching surfaces which are separated by a narrow gap. A switch is on when its gap is filled with helium and off when the gap is emptied. This filling and emptying is accomplished by an activated-carbon pump (ACP). The carbon adsorbs helium when cooled and desorbs it when heated. The 2-kelvin heat switch is a liquid-gap heat switch, used to reduce the required heat transfer surface area, taking advantage of the high thermal conductivity of the liquid. The 10-kelvin heat switch is a gas-gap heat switch and thus requires a much larger heat transfer area.

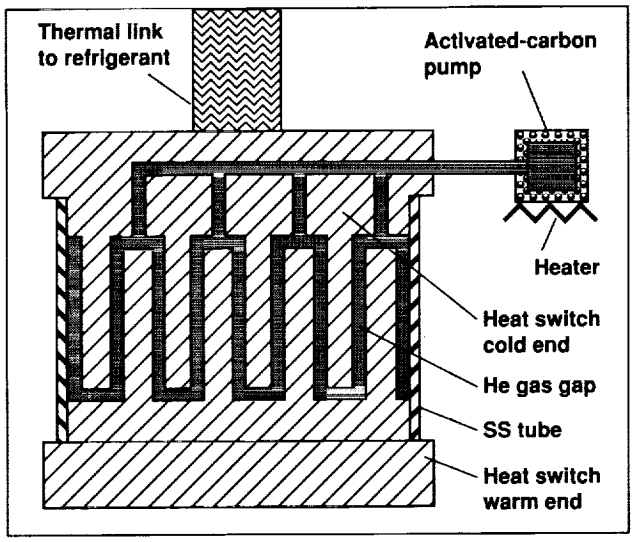


*Fig. 1. Schematic of the 10-kelvin gas-gap heat switch.*

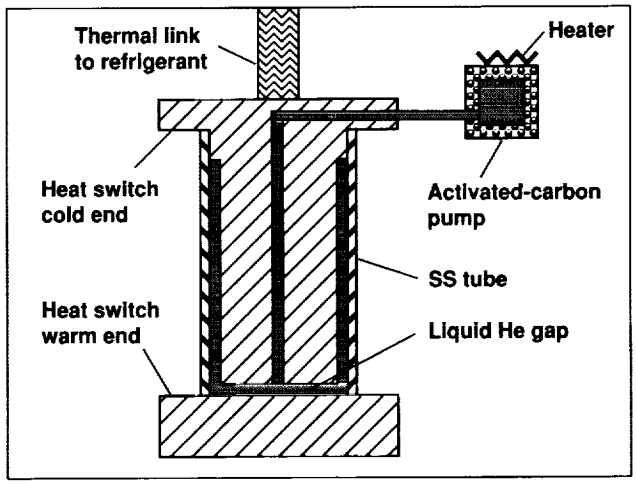


*Fig. 2. Schematic of the 2-kelvin liquid-gap heat switch.*

The 10-kelvin heat switch consists of two finned copper cylinders, shown schematically in the first figure. The fin patterns on the two cylinders are mirror images of one another. When the cylinders are put together, the fins are separated by a gap of 0.010 centimeter. A thin-wall stainless steel tube holds the two cylinders together and seals the gap volume. The fins are 2.5 centimeters long and the diameter of the heat switch is also 2.5 centimeters.

When the heat switch is off and a temperature difference of 8 kelvin is maintained between its warm and cold ends, 10 milliwatts is conducted. In the on state, the switch conducts 0.25 watt with a 0.2-kelvin temperature drop developing across it. The turn-on time of the heat switch is on the order of 30 seconds; its turn-off time is less than one minute.

The 2-kelvin liquid-gap heat switch consists of two high-purity copper cylinders that are positioned end to end separated by a 0.010-centimeter-wide gap, as shown in the second figure. The two cylinders are held together by a thin-wall stainless steel tube

which is 2.5 centimeters in length. The diameter of the switch is about 1.3 centimeters.

In the off state, when the temperature difference across the heat switch is 8 kelvin, 1 milliwatt is conducted from the warm end to the cold end. In the on state the switch conducts 50 milliwatts with the temperature drop developed across it being 0.08 kelvin. The heat switch turns on in less than a minute; however, its turn-off time is on the order of three minutes.

**Ames-Moffett contact: A. Kashani**
**(415) 604-6534**
**Headquarters program office: OA**

## Focal-Plane Arrays for Space Infrared Astronomy

**Mark E. McKelvey, Robert E. McMurray, Jr., Craig R. McCreight**

The development of focal-plane detector array technology that will allow reliable background-limited operation in the radiation environment found in Earth orbit is a key requirement for successful infrared (IR) astronomy from space-based platforms such as the Space Infrared Telescope Facility. A team at Ames Research Center is evaluating the performance of a number of detector and readout-device technologies to determine their suitability in space IR astronomy applications.

Impurity band conduction (IBC) focal plane detector arrays produced by several manufacturers are under study for applications in the 5–30-micrometer wavelength range. IBC detectors rely on a thin, highly doped IR-active layer to provide high quantum efficiency from a small detector volume, minimizing the ionization cross section for cosmic-ray events. A high-purity blocking layer keeps the high doping levels in the IR-active layer from resulting in excessive dark current. IBC arrays also exhibit wider spectral response than alternative photoconductor (PC) architectures, without many of the anomalies associated with PC devices. IBC architectures are well suited to modern epitaxial fabrication methods. The technology has progressed to the point where large-format hybrid focal-plane arrays (FPAs) sensitive to IR wavelengths as long as 28 micrometers can be reliably produced.

Recently, two 256- by 256-element arsenic-doped silicon (Si:As) IBC detector arrays developed by Hughes Aircraft Company have been evaluated. The bulk of the data were obtained by grantees visiting Ames Research Center from the University of Rochester.

The detector arrays are based on CRC-644 multiplexers implementing a source-follower-per-detector scheme with nondestructive read capability for use in a variety of sampling modes.

Performance parameters were measured at various bias voltages, temperatures, and wavelengths at background photon fluxes on the order of $10^5$ photons per pixel per second with excellent results (equal or superior to manufacturer's claims). Dark currents as low as 18 electrons per second were measured, with a strong onset of thermally activated current at temperatures above 8 kelvin. Effective responsive quantum efficiencies ($G\eta$) as high as 3.8 were observed at 11.5 micrometers at effective biases of near 4 volts. Measured detective quantum efficiency ($\eta/\beta$) was near 20%. The rough bias independence of $\eta/\beta$ indicates that background-limited performance is obtained for effective bias values greater than 0.7 volt. A transfer-function-limited well capacity of $3 \times 10^5$ electrons was observed.

The measured dependence of $\eta/\beta$ on bias voltage is consistent with an IR-active layer that is completely depleted even at relatively low biases. The measured bias dependence of input capacitance (typically

54 femtofarads) is consistent with this hypothesis. Responsivity was found to vary only weakly with temperature between 5 and 8 kelvin.

Also under way is a project aimed at the development of readout circuitry optimized for operation at cryogenic temperatures. Present metal oxide semiconductor (MOS) transistors suffer degraded noise performance at temperatures below roughly 20 kelvin. A systematic study of the effects of detailed changes in the transistor structure is required to improve the technology. To this end, a contract has been placed with Hughes Aircraft for the manufacture of 1- by 32-element readout circuits and smaller test structures, optimized for use at 1.5 kelvin. A number of process splits are planned, with each containing a unique variant of the baseline design for each device. Evaluations of the performance of devices from each split will yield important information to be used in future cryogenic electronics designs. This project involves significant collaborative testing at the University of Arizona.

Further experimentation and optimization of both full hybrid FPAs and elemental electronic devices will continue in the next year, with emphasis on maturing IBC technology and improved readouts to enhance overall IR focal plane performance in NASA space- and ground-based astronomy applications.

**Ames-Moffett contact: M. McKelvey**
**(415) 604-3196**
**Headquarters program office: OA**

# Spectral Reflectance and Leaf Chemistry

**Jennifer Dungan, Pamela Matson, Vern Vanderbilt, Lee Johnson, Tina Billow**

Under a NASA Headquarters research program to find scientific evidence for or against the need for a high-spectral-resolution Earth Observing System (EOS) instrument, members of the Ecosystems Science and Technology Branch designed an experiment to test the possibility that the biochemical makeup of tree leaves can be remotely sensed by high-spectral-resolution spectroradiometers. Other studies have suggested that it may be possible to monitor canopy biochemical contents using remote sensing, but few experiments have been accomplished under controlled conditions. If such monitoring were possible, the status of forests in many parts of the world could be determined, adding to the scientific community's understanding of forest ecosystem processes.

The "forest" used in this experiment was grown in the laboratory of Pamela Matson. Two-and-a-half-year-old Douglas fir seedlings were fed according to three different fertilization regimes for two months to create a variable biochemistry of the fir needles. Typically, tree foliage will respond to varying fertilization treatments with different chlorophyll, nitrogen, and amino acid concentrations. Starch and sugar concentrations may also vary depending on the growth stage of the plants. These chemicals absorb light at specific wavelengths, which is why many laboratory tests include spectrophotometric methods. The physical structure of plant canopies (the shape and arrangement of branches and foliage) and the soil also have a large influence. Initial results from this experiment show that the reflectance in one part of the spectrum may change by over 100% as a result of reorientation of the canopy.

The seedlings were arranged in basins to create a miniature forest canopy and then were transferred to a turntable marked off in 10-degree increments. Two spectroradiometers, one belonging to Ames and the other loaned by the Jet Propulsion Laboratory, were used to collect spectra simultaneously. A solar radiometer was used nearby to monitor atmospheric transmission. The canopy measurements were made in November of 1992, when cloudless weather allowed collection of spectra at every turntable orientation for each of the three fertilization-treatment groups. Experiments over the course of six days began at about 10:30 a.m., continued through solar noon (when the sun is highest in the sky), and concluded at 2:00 p.m.

With outdoor measurements completed, the trees were returned to the laboratory to be stripped of their needles for chemical analysis and for laboratory spectroradiometric measurements. The group collected approximately one thousand spectra to analyze from the outdoor component of the experiment. Work in 1993 focused on calibration and processing of these spectra, as well as collection of ancillary data on a second tree species (big-leaf maple) at the leaf and canopy level. As expected, clear differences caused by the chlorophyll differences between groups that had high and low fertilization treatments were observed in both species in the visible portion of the spectrum. Further analysis will determine if differences in other portions of the spectrum can be attributed to variations in foliar chemistry.

**Ames-Moffett contact: J. Dungan**
**(415) 604-3618**
**Headquarters program office: OSSA**

# Stratospheric Photochemistry, Aerosols, and Dynamics Expedition (SPADE)

**Stephen Hipskind**

The SPADE mission, conducted from and managed by the Ames Research Center, was the first dedicated field campaign to obtain atmospheric measurements in support of the High Speed Research Program/Atmospheric Effects of Stratospheric Aircraft (HSRP/AESA). The HSRP is charged with assessing the environmental impact of a projected fleet of high-speed civil transports (HSCTs), with emphasis on the potential chemical perturbations that would affect the production or loss of stratospheric ozone. The measurements for SPADE were made from the NASA ER-2 aircraft with a suite of fast-responding instruments taking chemical, dynamical, and aerosol particle data.

Sixteen state-of-the-art instruments were developed and flown on the ER-2 by an international team of scientists and engineers from Ames, other NASA centers and government agencies, universities, and the Canadian Atmospheric Environment Service (AES). The instrument teams included collaborators from the U.K., Germany, Iceland, Italy, Australia, the People's Republic of China, and France in addition to the team from Canada. The Ames effort was a collaboration between the Earth System Science Division, which manages the project, and the Science and Applications Aircraft Division, which operates the aircraft and provides the engineering support for the instrument integration.

The experiment was conducted in three phases. The first phase, conducted in November 1992, was the integration and flight testing of the instruments. Many of the instruments had flown previously in the polar ozone-depletion studies, but there were several new instruments and many significant changes to existing ones. New instruments provided the capability for measuring hydroxyl radicals, carbon dioxide, and the visible and ultraviolet portion of the solar spectrum. This was one of the most ambitious payload integration efforts yet undertaken on the ER-2.

The second phase of the SPADE mission was conducted from 30 April 1993 through 18 May 1993. This was the primary scientific phase in which one 2-hour check flight and eight 8-hour data-gathering flights were carried out. There were four latitudinal survey flights and four pseudo-diurnal flights across sunrise and sunset. This phase of the SPADE mission accomplished all of its stated objectives and extended the state of scientific knowledge of the stratosphere in several key areas. First-ever measurements of the nitrogen-oxide-emission index of the ER-2 engine were made from several wake crossings. The new instruments provided first-ever measurements of key chemical species which will provide needed constraints on current photochemical assessment models. SPADE particle measurements will provide important insights into the evolution of stratospheric aerosols released by the Pinatubo eruption. Overall, the results from SPADE will lead to a better understanding of important photochemical and transport processes in the stratosphere and how they may be affected by future stratospheric aviation.

**Ames-Moffett contact: S. Hipskind**
**(415) 604-5076**
**Headquarters program office: OA**

# Spectroscopic Analysis of Biochemical Concentrations in Plants

**Lee Johnson**

The goal of this research was to determine whether the reflectance of Douglas-fir foliage is influenced by total nitrogen (TN) concentration in the leaves, and to assess the possibility of using this information to predict TN values in other plants. The study was undertaken to provide fundamental information regarding the feasibility of deriving biochemical information from plant canopies over large areas by means of remote sensing instrumentation.

The design of the study (species selection, timing of fertilization) was intended to induce differences in foliar TN and chlorophyll concentration while minimizing changes in other chemicals and in leaf structure. Two-year old Douglas fir seedlings (n = 100) were transplanted in spring 1992 and grown under a medium-level nitrogen (N) treatment (15 milligrams per liter) for five months in a greenhouse. Plants were watered twice a day. After termination of summer growth and two months prior to analysis, the seedlings were randomly divided into three groups which received low, medium, or high levels of N (5, 15, or 55.5 milligrams per liter) three times per week to produce a wide range of foliar TN concentrations.

In November 1992, needles were removed from each tree, and reflectance measurements of all the needles on each tree were made with a laboratory spectrophotometer. The instrument performed bidirectional reflectance measurements with channel centers ranging from the 400- to the 2498-nanometer region, at a spectral resolution of 10 nanometers, a sampling interval of 2 nanometers, and signal-to-noise ratio >10,000:1.

Stepwise regression equations were developed to relate the reflectance values to TN concentration in a subset of foliage samples. The derived equations relied primarily on the longer (>2000 nanometers) wavelength region for TN estimation. In particular, the spectral region near 2160 nanometers was particularly diagnostic of TN concentration, probably because of the nearby presence of a major N–H (nitrogen–hydrogen organic bond) absorption feature. The regression equations were subsequently used to predict with high accuracy the TN concentration of validation samples (samples that were not included in the formulation of the regression equation).

The results of the study indicate that fresh foliage reflectance is influenced by foliar TN concentration. These spectral indicators, measured by a laboratory spectrophotometer, may be used to make reliable predictions of TN concentration in other leaf samples of the same species. These data may ultimately be linked with plant-canopy and atmospheric radiative transfer models to address requirements for remote sensing instrumentation.

**Ames-Moffett contact: L. Johnson**
**(415) 604-3331**
**Headquarters program office: YSE**

# Using Satellite Imagery to Understand Carbon Dioxide Exchange Between the Terrestrial Biosphere and the Atmosphere

**Christopher Potter**

One of the clearest signals of human impact on a global scale is the rapidly rising concentration of greenhouse gases such as carbon dioxide ($CO_2$) in the atmosphere as a result of combustion of fossil fuels and deforestation. Whereas human-driven changes in the composition of the atmosphere are well documented, interactions and feedback between the biosphere (plants, animals, and microbes) and the changing atmospheric composition are not adequately understood.

As Earth System scientists seek to predict future responses of the planet to global warming, it is critical that they begin with accurate estimates of current patterns of carbon flux and storage. Ecologists are refining our understanding of the seasonal changes in the way climate and soils control exchange of $CO_2$ between the land surface and the air. In preindustrial times, fluxes between the atmosphere, land, and ocean pools were in a relatively steady state. However, when climate and land use change at a rapid pace, the existing patterns of carbon flux and storage may be dramatically altered.

By the use of recently assembled satellite images of the surface of the globe, a team of investigators from NASA Ames Research Center, the Carnegie Institute of Washington, D.C., and Stanford University have completed a study of the role of terrestrial plants and soils in the cycling of carbon to and from the atmosphere. Historical climate and land-surface data sets are used as additional inputs to drive the model at 1-degree latitude/longitude resolution. This research has produced a dynamic picture (called the Carnegie-Ames-Stanford Approach (CASA) biosphere model) of the contemporary balance between photosynthetic fixation and microbial respiration of $CO_2$.

The CASA biosphere model estimates photosynthetic fixation of $CO_2$ in terrestrial net primary production (NPP) at 48 petagrams ($10^{15}$ grams) carbon per year. This flux is ten times the annual fossil fuel emission of $CO_2$. Our modeling efforts show that 60% of terrestrial NPP occurs at tropical latitudes.

The use of satellite sensor data to estimate NPP captures many of the effects of land cover change (urbanization, deforestation, and cultivation) on the dynamics of the carbon cycle. Human-induced changes in the rate of cycling of carbon in agricultural soils are included in the model design through increased microbial decomposition rates. We are also investigating the global impacts of agricultural fertilizers on greenhouse gas fluxes.

In the CASA model, carbon from plant residues stored in the soil and at the surface of forest and grassland soils (in what is called litter) is divided into separate pools, depending on the residence times of the plant residues in the ecosystem. Residence times of litter–soil carbon pools (expressed as the steady-state pool size divided by the sum of annual losses) are generally shortest for ecosystems of the tropics. Both nonwoody (leaves and roots) and woody litter are represented in the model, along with soil microbial carbon pools. Soil organic carbon is divided into a SLOW pool (with residence time of one to several decades), and an OLD pool (with residence time of one to several centuries).

The CASA model shows that SLOW soil carbon makes up the single largest pool in most ecosystems. Steady-state pools of SLOW soil carbon (in the top 30 centimeters) contain 300 petagrams of carbon, whereas standing litter represents global storage of around 170 petagrams. The distribution of stored carbon in litter and soil carbon pools varies greatly with latitude. There are large carbon pools in northern boreal/temperate forests and also in tropical ecosystems. With the exception of the OLD carbon component, these large pools have a residence time of less than 70 years. The carbon stored in these pools may be released to the atmosphere at much faster rates if the climate warms significantly. Deforestation and biomass burning can also greatly accelerate losses of soil carbon from soil pools.

Global models like the CASA Biosphere formulation of net ecosystem production can reveal patterns in the functions and interactions of the

biosphere–atmosphere system at scales not observed before the advent of satellite technology. Future work will include an attempt to evaluate the effects of deforestation and land use change on global trace gas fluxes. Expected contributions of this work include (1) an understanding of process controls on trace gas fluxes between terrestrial ecosystems and the atmosphere and (2) an explanation of the role of forests and their loss in global biogeochemical cycles and climate change feedbacks. Principal collaborators include Pamela Matson (University of California, Berkeley), Christopher Field (Carnegie Institute), and Peter Vitousek (Stanford University).

**Ames-Moffett contact: C. Potter**
**(415) 604-6164**
**Headquarters program office: OSSA**

## Grapevine Remote-Sensing Analysis of Phylloxera Early Stress

**Joan Salute, Roy Armstrong, Cindy Bell**

The Grapevine Remote-Sensing Analysis of Phylloxera Early Stress (GRAPES) project is a collaborative effort to develop methods for using remotely sensed data and geographic information system (GIS) technology for the early detection of phylloxera infestation and other conditions that affect vineyard yield. Phylloxera are aphid-like insects that damage grapevines by feeding on the roots, ultimately killing the vines. A phylloxera infestation is crippling California's $14 billion/year wine industry. Approximately 65% of the 34,000 vineyard acres in the Napa Valley, California, are planted on rootstocks susceptible to phylloxera. The only known remedy for the infestation is to replant the vineyards on rootstock believed to be resistant to the newest strain of phylloxera, biotype B. The cost of replanting vineyards is about $25,000 per acre. Many vineyards cannot absorb this cost along with the financial loss associated with reduced wine grape crops. The GRAPES project is designed to research the epidemic with the use of NASA-developed technology.

Team members from the Earth System Science Division at Ames, the Robert Mondavi Winery (RMW), the University of California Cooperative Extension, the University of California, Davis, and California State University, Chico, will research and develop the use of field-, aircraft-, and satellite-based remote sensing data to detect phylloxera both before and after visual symptoms are apparent and to assess the magnitude of its effects. A GIS will be developed to analyze and characterize the spatial and temporal spread dynamics of the infestation.

The wine growing industry has not been a commercial user of remote sensing data, and it is hoped that the market segment will open up as a result of this project. The team of investigators will pursue four related remote sensing/GIS tasks for study sites in the Napa Valley: (1) determine the relationship of spectral response to vine health as affected by phylloxera, (2) study factors affecting the spatial patterns of phylloxera infestations to assess the risk of future infestations, (3) characterize land use and land use changes that affect the wine market, and (4) identify the location of introduction of phylloxera biotype B to the Napa Valley.

An extensive field experiment was conducted during the 1993 growing season for task 1. Within one field, plots of 40 vines were identified in each of four categories: #1) phylloxera infestation with visual symptoms (three plots), #2) phylloxera infestation with no visual symptoms (three plots), #3) no phylloxera (three plots), and #4) artificial stress applied to

the roots (damaging the roots), no phylloxera (two plots). On seven dates between May and October, 1993, the following measurements were made for one leaf on each vine in each plot: chlorophyll estimate, leaf area, spectral reflectance, and nitrogen, phosphorous, and potassium content.

Consistently throughout the growing season, category #1 vines had significantly different spectral reflectance curves than categories #2, #3, and #4. This was surprising in the May data, because at that time, even though phylloxera infestation had been apparent in 1992, all of the newly formed leaves looked healthy. This was encouraging, and work on the task continued throughout the summer. Analysis to date has not been able to distinguish category #2 from category #3, but analysis of the 1993 data continues.

Because differences between categories #1 and #2 were apparent at the leaf level, measurements were then taken at the canopy level. In late July, a Compact Airborne Spectrographic Imager (CASI) was flown over the test sites to acquire detailed spectral data. The data were of 1.5-meter spatial resolution, which allows identification of individual vines. Global position system (GPS) measurements of the plots were taken to geographically correct the CASI data. Initial analysis of the CASI data revealed category #1 phylloxera infestations quite easily. Our collaborators at RMW were surprised at the amount of infestation obvious in the CASI imagery and at the increased information available in CASI data as opposed to aerial photography.

For task 2, the GIS is under development. Hydrology, soils, and transportation network layers have been created. Past phylloxera infestations are being incorporated from historical photography. Cultural factors for fields are being incorporated from RMW data bases.

For task 3, land use analysis is under way for Thematic Mapper (TM) satellite scenes from July 1987 and June 1990. Additional data have been ordered. Task 4 will begin in 1994. Overall, results are very encouraging. Data collected throughout the 1993 growing season are being analyzed.

**Ames-Moffett contact: J. Salute**
**(415) 604-5596**
**Headquarters program office: OACT**

## Validation of Regional Simulations of Radiative Transfer

**Douglas L. Westphal, Eric J. Jensen, Stefan A. Kinne**

Our goal is to develop and validate parameterizations of cloud microphysics and radiative transfer suitable for use in general circulation models (GCMs). Our approach is to use a regional weather prediction model as a testbed for these parameterizations and to compare the simulated cloud and radiative fields with observations made during field programs such as NASA's First International Satellite Cloud Climatology Program Regional Experiment (FIRE). We use the Pennsylvania State University's mesoscale model, adapted for use at Ames Research Center. We have added an explicit, size-resolving cloud model and a 44-band radiative transfer model which allows us to make accurate radiative calculations during a simulation and also allows us to directly model many of the radiation observations with a minimum number of assumptions. For example, we can model lidar backscatter, 6.7-micrometer radiance, 0.55-micrometer albedo, or 10-micrometer downwelling irradiance at the surface.

An extensive set of radiative measurements were made at Coffeyville, Kansas, during FIRE by surface and airborne instruments. These measurements are adequate for testing the model's prediction for Coffeyville but do not contain the information necessary for a regional validation of the predicted cloud and radiative fields. Satellite observations do provide the necessary regional coverage. By doing the forward problem with our model, we simulate the

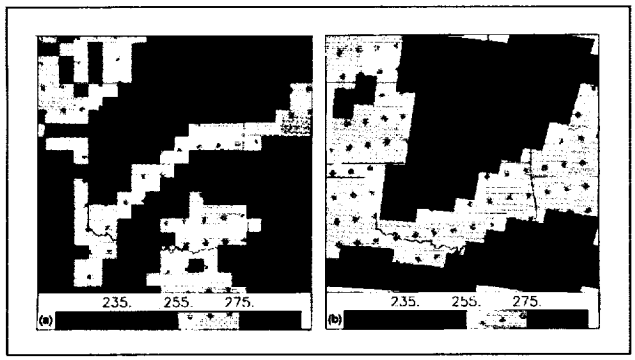


*Fig. 1. 11-micrometer blackbody temperatures ($T_b$) at 1600 Greenwich mean time on 26 November 1991 for the FIRE study region. Kansas and Oklahoma are in the center of the figure. (a) Derived from GOES satellite data by Minnis (Langley Research Center); (b) diagnosed from the model at 16 hours into the simulation.*

satellite radiances and make direct comparisons between the pixel and grid point radiances as often as every half-hour. We are conducting comparisons to determine systematic differences for cloudy and clear conditions and to determine the sensitivity of the modeled radiation fields to model constants and to the modeled cloud microphysics. As an example we compare the 11-micrometer blackbody temperatures ($T_b$) observed from satellite at 1600 Greenwich mean time on 26 November 1991 (part (a) of the figure) with those diagnosed from the model at 16 hours into the simulation (part (b)). A mid-level disturbance forced the cloud field that appears as an area of low $T_b$ (light shading) with a SW–NE orientation. NASA and other aircraft sampled this cloud field as it passed over Coffeyville. The low values of $T_b$ over Texas and Oklahoma were due to clouds at middle and low levels that came from the SSW. The simulated field of $T_b$ (part (b)) for the subdomain of the model corresponding to satellite analysis is in general agreement with the satellite analyses except that it lacks the clouds over Texas and eastern Oklahoma and the surface temperatures are cooler than those observed over Arkansas and west Texas.

**Ames-Moffett contact: D. Westphal**
**(415) 604-3522**
**Headquarters program office: OMTPE**

## Basic and Applied Research in Ion Trap Mass Spectrometry

**Carla M. Wong, Peter T. Palmer**

There has been an ever-increasing interest in recent years to develop smaller, faster, and more sensitive instrumentation for a host of environmental monitoring applications. Inevitably, the instrumentation developed for these applications represents a trade-off between analytical capabilities (i.e., sensitivity, selectivity, and speed) and real-world constraints (size, weight, power). This is particularly evident in the area of atmospheric analysis. Whereas a variety of sensors and other specialized instruments have been developed to monitor permanent gases of environmental significance (e.g., ozone, methane, carbon dioxide), few, if any, instruments are capable of performing on-line, real-time analysis of a variety of volatile organic compounds in the atmosphere.

Ion-trap mass spectrometry is one of the more recent developments in mass spectrometry (MS) instrumentation. The ion trap is the most sensitive of all mass analyzers and is capable of detecting species at the attomole ($10^{-18}$ moles) level. It can provide tandem MS (MS/MS) data to enable direct analysis of selected compounds. Finally, it is inherently smaller, simpler, and more efficient than other types of tandem mass spectrometers. Recent efforts have focused on enhancing the applicability of the ion trap

MS/MS experiment for on-line, real-time monitoring, and on further developing expert system software to provide specialized knowledge for autonomous analysis. Collectively, these advances have resulted in the development of an instrument with exceptional sensitivity and versatility, smaller size, functional simplicity, and a high degree of automation.

This technology has been successfully employed to characterize and quantitate emissions of volatile organic compounds (VOCs) from a variety of life support testbeds. It also opens up new opportunities for environmental monitoring, including simultaneous monitoring of various permanent gases that play a role in global warming, and on-line, real-time monitoring of VOCs that represent by-products of anthropogenic and biogenic processes. Future efforts will focus on (1) developing a field-deployable instrument; (2) porting the expert system software to a PC platform; and (3) further reducing space, weight, and power requirements. These technological advances will enable laboratory, field, and aircraft deployment for direct monitoring applications that were previously unfeasible. This approach has potential usefulness in NASA applications in atmospheric and ecosystem monitoring as well as in a host of applications in the environmental, toxicological, pharmaceutical, and clinical markets.

**Ames-Moffett contact: C. Wong**
**(415) 604-4294**
**Headquarters program office: OACT**

# Progress in High-Resolution Microwave Survey (HRMS) Search Capabilities

**David Harper, Peter Backus, Edward Olsen**

The NASA High Resolution Microwave Survey (HRMS), formerly called the Search for Extraterrestrial Intelligence (SETI), began its operational phase on October 12, 1992. On October 1, 1993, Congress voted to terminate the project. During this one-year period the HRMS conducted the most comprehensive search yet made for indications of intelligent life elsewhere in our galaxy. Microwave observations using radio telescopes were conducted using the Targeted Search engineering design model, which has about a sixth of the final configuration's capability, and the Sky Survey prototype, which has about a sixteenth the capability of the final design. In this short time and with equipment that had only a fraction of the planned capability, these observations examined many times the search space covered by all previous searches combined. These observations provided field experience that helped improve operational concepts, refine the control software, and evaluate interference-handling techniques to be used in the final versions of the equipment. The Targeted Search prototype can process 10 megahertz at a time, at 1-, 7-, and 28-hertz resolutions, in both left and right circular polarizations. The Sky Survey prototype can examine 40 megahertz at a time at 19-hertz resolution for one polarization.

The project had planned to conduct over 100,000 separate observations and cover the entire sky six times. Control software was developed to automate the observing sessions. This automation included scheduling, controlling two radio observatories, coordinating as many as 10 computer systems, conducting signal verification procedures, and "intelligently" collecting data.

The Targeted Search used 200 hours of observing time at the 1000-foot Arecibo Observatory in Puerto Rico to observe 25 solar-type stars that are within 100 light years of Earth. About 300 megahertz in the 1300- to 2400-megahertz band were examined for narrow-band signals of technological origin. Each observation of a star followed an on-target, off-target, on-target procedure, each step lasting either 92 or 299 seconds. A total of 15 signals passed the initial criterion of being present only when the antenna was pointing at the target star, and these were then subjected to further tests. All proved to be of terrestrial origin.

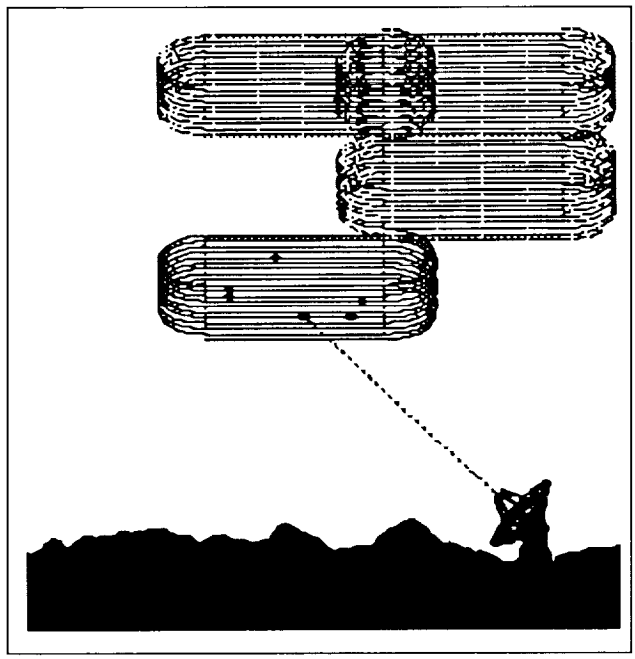

*Fig. 1. Sky Survey scan pattern.*

Until the project's termination, the Sky Survey was continuously observing with the 34-meter Venus Development Station at NASA's Deep Space Communications Complex in Goldstone, California. The system covers the sky by rapidly driving the antenna through precise 90-minute-duration "race track" patterns that are 1.4- by 30-degree rectangles. The first figure shows the racetrack pattern used in the Sky Survey. This pattern is repeated to cover the entire sky. Sixty-three sky frames were completed. Candidate signals are verified by switching the system to a targeted mode to obtain higher sensitivity. Three signals required further investigation but were determined to be caused by statistically expected temperature fluctuations in the receiver. The data collected will be provided to the National Space

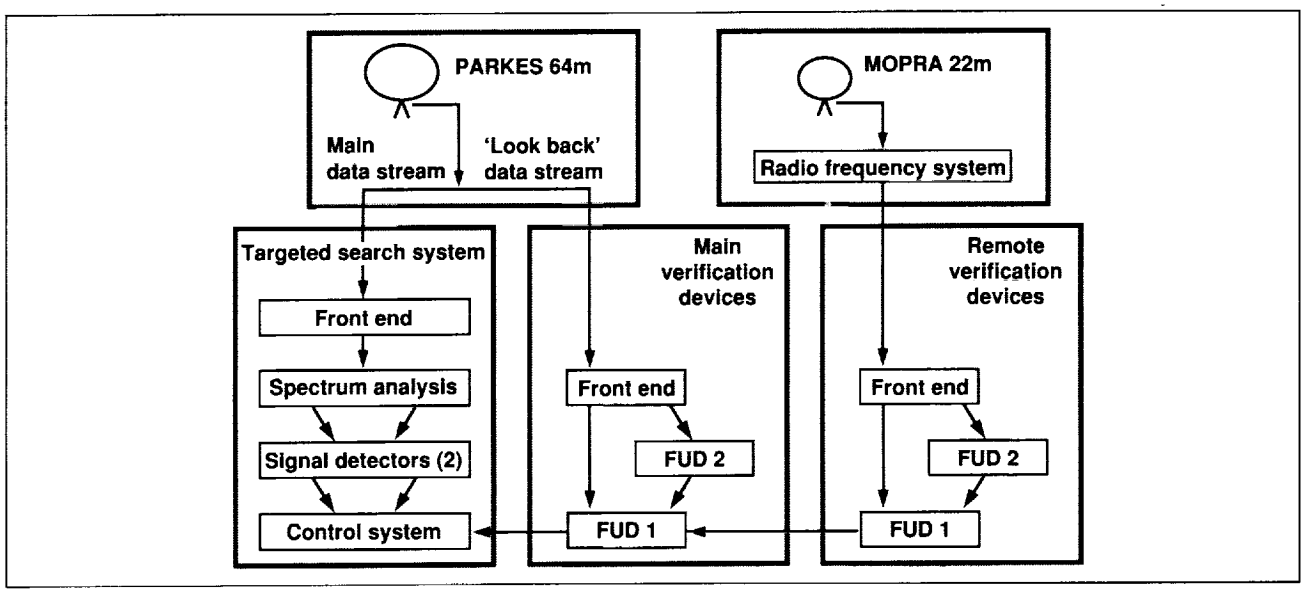


*Fig. 2. Targeted Search configuration using two observatories. FUD = followup device.*

Science Data Center later this year and will be available to anyone after another year.

The Sky Survey also completed a series of observations of the hydrogen and hydroxyl emission lines, designed to enhance radio astronomy spin-offs and to improve interference excision. Results of these observations will be published this year. The Sky Survey's unique capabilities were used to search for the lost Mars Observer spacecraft. Small areas of the sky, centered upon Mars and along the projected hyperbolic fly-by trajectory, were observed using a modified candidate reobservation strategy. This strategy would have detected the spacecraft's low-gain antenna even if the spacecraft was tumbling. A similar set of observations was used to search for the Landsat Satellite.

The project team has developed comprehensive systems for the reception, analysis, and processing of observatory data. The control software automatically conducts the observations, including creating and executing session schedules and coordinating two separate radio observatories and at least 10 distinct computer systems. The second figure shows the final Targeted Search configuration that was planned for the 1994 Australian deployment. The main Targeted Search system and primary Follow-Up Device are at Tidbinbilla, and the remote Follow-Up Device is at Parkes. All activity at the two sites is directed by the Targeted Search Control System.

Other achievements included enhancements of a commercial electronic design software that the manufacturer added to the package. The project developed the world's broadest-band low-noise receiver. This receiver would improve the observing efficiency by increasing the range of frequency bands available at any one time and would be a useful tool for radio astronomy in general. The project's signal analysis research has spurred interest from the medical field for use in diagnostic medical imaging technology. The project team has developed connections with parallel-processor and signal-processing experts in preparation for future HRMS development. In association with the National Science Foundation, it has also developed educational materials for grades 3–9.

**Ames-Moffett contact: D. Harper**
**(415) 604-3060**
**Headquarters program office: OSSA**



C-3

# Biological Verification of a Noninvasive Technique to Quantify Material Properties in the Tibia

Sara Arnaud, Teresa Hutchinson

The Mechanical Response Tissue Analyzer (MRTA) is an instrument that uses (1) a magnetic shaker to generate a brief, low-frequency vibratory stimulus to the skin surface over the center of a well-supported long bone (the ulna or the tibia) and (2) a small curved aluminum probe that detects the resonant response of the bone at the same site. In a few seconds, the response is analyzed with an algorithm that calculates the bending stiffness of the bone (EI). The instrument is the result of the combined efforts of Don Young (Ames Research Center) and Charles Steele (Stanford University), who originated the system to quantify material properties in long bones; Robert Marcus (Stanford University), who demonstrated the potential of the instrument for understanding changes in bone biomechanics with aging; and Gait Scan, Inc., a small company that designed the instrument for use in the clinical setting.

The measurement of EI in the human ulna has been fairly well documented by investigators at Stanford University. Stiffness in the tibia, a weight-bearing bone of interest to NASA, has been more difficult to determine because of the more irregular structure and more complex resonant response in this bone. Essential to the development of the clinical test for EI in the tibia is verification of the results generated by the MRTA instrument by comparing them to results from standard biomechanical testing. B. Martin at the University of California, Davis, collaborated with us to do the objective measurements in excised tibias of rhesus monkeys whose bones had been tested earlier, in vivo. The figure shows the correlation of EI measured with the MRTA in the intact animal and by standard testing in the excised bone. These results provide the essential biological validation of the tibial measurements made with the newly designed instrument. The results of earlier tibial measurements and these recent results indicate that the newly designed MRTA can provide an accurate, direct but noninvasive measure of EI in the clinical setting for research studies that include evaluation of the material properties of long bones.

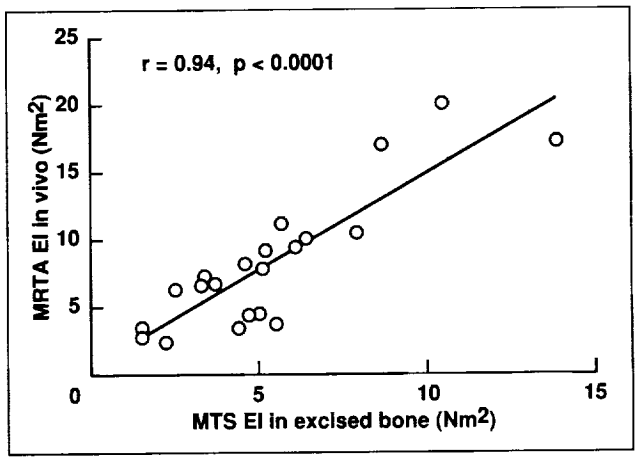


*Fig. 1. The relationship between the bending stiffness (EI) measured in vivo with the MRTA instrument and the EI obtained by objective mechanical testing of the same bones after the bones were excised.*

**Ames-Moffett contact: S. Arnaud**
**(415) 604-6561**
**Headquarters program office: OSSA**

# Urinary Calcium Loss and Dietary Sodium

**Sara B. Arnaud, Meena Navidi, Jennifer Harper**

It is well known that the excretion of calcium in the urine is related to the amount of sodium in the diet. The possibility that dietary salt has a major influence on urinary calcium loss during spaceflight was suggested by the high-sodium diets (about 240 milliequivalents per day (mEq/d)) of astronauts during the Skylab mission, and by our observations of healthy ambulatory men and volunteers exposed to 6-degree head-down tilt (HDT) bed rest. We compared the relationship of calcium and sodium excretion in 24-hour urine specimens from 10 healthy male volunteers whose dietary analyses showed high-normal daily intakes of sodium (200 mEq/d) and from 10 whose sodium intakes were relatively low (110 mEq/d). Measurements of the excretion of calcium and sodium in the urine, each expressed in terms of creatinine excretion, an index of lean body mass, were correlated in the high-salt group ($r = 0.66$, $p < 0.05$) but not in the low-salt group ($r = 0.09$, not significant). Both groups consumed about 900 milligrams of dietary calcium per day.

When these same relationships were examined in HDT bed-rest subjects on diets controlled to provide low (120 mEq/d) or high (200 mEq/d) levels of sodium, we found unexpected evidence for an effect of dietary sodium on calcium loss. Increases in urinary calcium were correlated with urinary sodium only in bed-rest subjects fed the higher-sodium diets ($r = 0.71$, $p < 0.001$). There was no increase in urinary calcium at the end of the fourth week of bed rest in subjects consuming the lower-sodium diets, and urinary calcium was not related to urinary sodium. These findings confirmed known effects of high levels of dietary sodium on calcium excretion of normal active men, and also revealed an unexpected effect of dietary sodium on the calcium loss that occurs during bed rest.

To determine the factors that alter the sensitivity of the kidney to sodium-induced calcium excretion during HDT bed rest, we proposed studies of the effect of dietary sodium on calcium excretion in a flight-simulation model in the rat. This basic research required the construction of a metabolic cage for a rat spaceflight model and experiments to define the response of the kidney in this species to dietary sodium. The first figure is a photograph of the metabolic cage constructed by G. Mulenberg and colleagues at Ames. It is designed to collect urine specimens from the rat, uncontaminated by feces or food, during periods when the animal is exposed

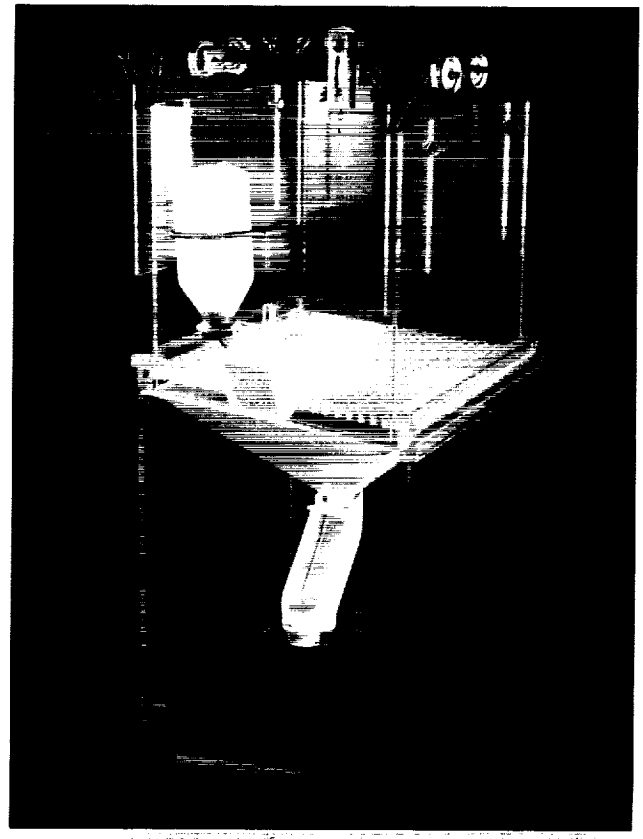

*Fig. 1. The metabolic cage designed to collect urine specimens uncontaminated by feces or food. The animal is housed in the upper section of the cage, where the suspension apparatus (designed by E. Holton) is shown. The food supply is outside the cage, easily accessed through a short tunnel. Excretions pass through the grid floor to the device in the center of the square funnel, which allows urine to pass directly into the first test tube through slits on the side of a ramp; fecal pellets travel along the ramp and enter only the second tube.*

to a spaceflight model designed by Ames researcher E. Holton. This model unloads the hind limbs by tail suspension and causes a cephalad fluid shift.

The results of experiments that compare the measurements of urinary calcium during normal weight bearing and during 20 days' exposure to the flight-simulation model at two levels of dietary sodium (normal and high) are shown in the second figure. Mature male rats fed diets containing 8% salt and normal amounts of calcium show increases in urinary calcium during unloading of the hind limbs ($p < 0.05$), whereas those fed diets with normal amounts of salt do not. Further experiments in this rat spaceflight model will allow us to define the critical elements in the renal regulation of calcium excretion and metabolism that are sensitive to high-salt diets. Whereas it is not possible to extrapolate from rat to human directly, an animal model that shows a response similar to that of a human in a given situation can provide guidelines for the human experiments that will be required to make firm dietary recommendations.

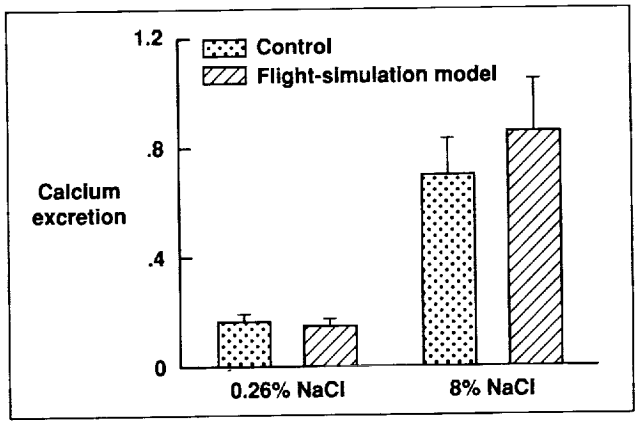


*Fig. 2. Comparison of urinary calcium excretion in control (dotted bars) and flight-simulation-model (lined bars) rats fed normal (0.26% salt) and high-salt (8% salt) diets. There is increased excretion of calcium in the urine of all rats fed high-salt diets compared to those fed normal diets ($p < 0.001$) and greater calcium loss in the flight-simulation-model rats fed high-salt diets than in control rats ($p < 0.05$).*

**Ames-Moffett contact: S. Arnaud**
**(415) 604-6561**
**Headquarters program office: OSSA**

## Exercise in Lower-Body Negative Pressure

**Richard Ballard, Donald Watenpaugh, Suzanne Fortney, Gita Murthy, Alan R. Hargens**

Acclimation to microgravity leads to deconditioning to normal Earth gravity (1 G). Specific problems include muscle atrophy (particularly of "antigravity" muscles such as the soleus), bone demineralization, reduced neuromuscular coordination, postflight orthostatic intolerance, and reduced upright exercise capacity. Exercise protocols and equipment for astronauts in space are still under development; recent calculations suggest that all exercise regimens in space so far have lacked sufficient loading to maintain preflight musculoskeletal mass. Force levels generated by bungee-cord-assisted, treadmill exercise are limited by harness discomfort.

Lower-body negative pressure (LBNP) has been used as a test of orthostatic tolerance on Earth and as a countermeasure during spaceflight to prevent postflight orthostatic intolerance. In essence, an LBNP device consists of a partial vacuum chamber surrounding the lower body and sealed at the waist. Normally, the LBNP chamber incorporates a saddle to allow the legs to remain relaxed, thereby maximizing blood flow and other fluid movement to the lower body. Either syncope from reduced arterial pressure to the head or seating discomfort from prolonged pressure against the saddle usually limits LBNP levels to 30–50 millimeters of mercury (mmHg).

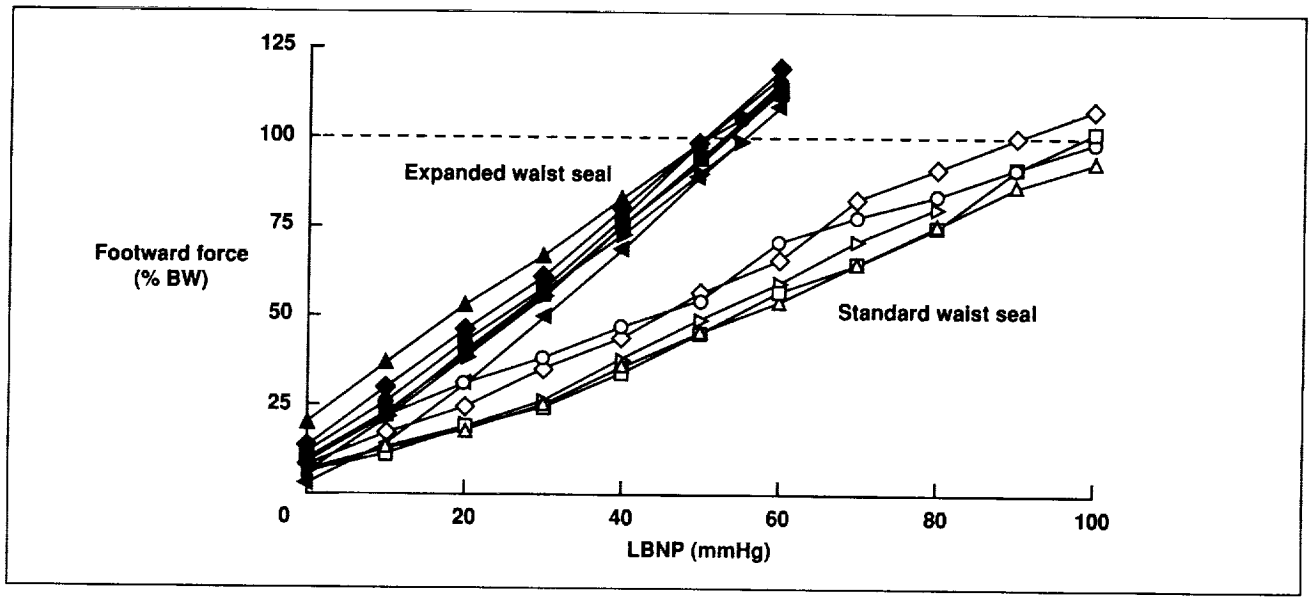


*Fig. 1. An expanded waist seal (filled symbols) effectively increases a subject's waist cross-sectional area such that one body weight is achieved with approximately 53 mmHg LBNP, whereas a standard waist seal (open symbols) requires 100 mmHg LBNP.*

Previously, we documented that footward force in an LBNP chamber without a saddle is a product of the body cross-sectional area at the waist seal and the LBNP level. If the negative pressure acts only through the cross-sectional area of the subject's waist, a negative pressure level of approximately 100 mmHg is necessary to generate one body weight (BW) of footward force. Supine exercise during 100-mmHg LBNP produces ground-reaction forces equivalent to 1 G, but greater cardiovascular stress than that during upright exercise in 1 G.

We hypothesized that the amount of negative pressure required to generate one BW could be decreased by expanding the area through which the pressure produces force, thus creating a more Earth-like ratio of cardiovascular to musculoskeletal stress. A flexible neoprene waist seal was attached at its outer edge to the LBNP chamber, such that part of the force created by suction acting on the seal was distributed on the chamber and part was applied to the subject. Shoulder straps attached to the waist seal permitted transmission of some force to the upper body, allowing spinal as well as lower-body loading. The area spanned by the flexible seal between the subject and LBNP chamber could be varied by increasing or decreasing the dimensions of the elliptical opening through which the subject placed their body into the chamber. In nine supine subjects, we found that if the waist seal area equaled twice the subject's waist cross-sectional area, the slope of the footward force/negative pressure relationship increased from the previously established 0.99% BW/mmHg LBNP to 1.75% BW/mmHg, such that the negative pressure necessary to produce one BW decreased from approximately 100 mmHg to 53 ± 2 mmHg (mean ± standard deviation; see first figure).

In a subsequent study of eight healthy male volunteers, heart-rate response to supine graded LBNP treadmill exercise with an expanded waist seal and 55 ± 3-mmHg suction was compared to the heart rate during upright running in 1 G. The second figure shows the supine LBNP exercise chamber developed at Ames Research Center. The average heart rate during upright treadmill exercise (161 ± 4 beats per minute) was similar to that for exercise during supine LBNP (162 ± 4 beats per minute). Thus, increasing

the waist seal area to twice the subject's waist cross-sectional area during supine exercise provided cardiovascular response equivalent to that of upright exercise in 1 G.

Reducing the negative pressure required to generate one BW of force lowers the risk of syncope, hernia, and petechiae associated with higher levels of LBNP stress. Exercise within LBNP addresses the interdependence of cardiovascular and musculoskeletal systems and may provide a practical alternative to centrifugation during long-duration spaceflight.

**Ames-Moffett contact: R. Ballard/A. Hargens**
**(415) 604-5747/5746**
**Headquarters program office: OSSA**


*Fig. 2. The LBNP exercise device.*

## An Optical Technique for Measuring Muscle Oxygenation

**Gregory A. Breit, Alan R. Hargens, Jeffrey H. Gross, Britton Chance**

In chronic compartment syndrome (CCS), the pressure inside an exercising muscle increases to an abnormally high level, resulting in reduced local blood flow and consequent cramping and pain. Astronauts may experience CCS in flight or after return to Earth. This condition is currently diagnosed by clinical signs along with intramuscular pressure readings using a catheter inserted into the painful muscle. We have investigated dual-wave near-infrared (NIR) spectroscopy, a technique to determine skeletal-muscle oxygenation noninvasively, as a means for detection and diagnosis of CCS.

The NIR spectroscopy technique is summarized in the first figure. Infrared (IR) light from a source placed on the skin surface is scattered randomly within the muscle tissue and sensed by two detectors that respond to light wavelengths of 760 and 850 nanometers. The amount of IR light that is absorbed as it passes through the tissue depends on local blood oxygenation. The difference between light intensities at the two wavelengths, which is a reliable index of tissue oxygenation, is detected by a differential amplifier. Because the pain associated with CCS is caused by inadequate muscle-tissue

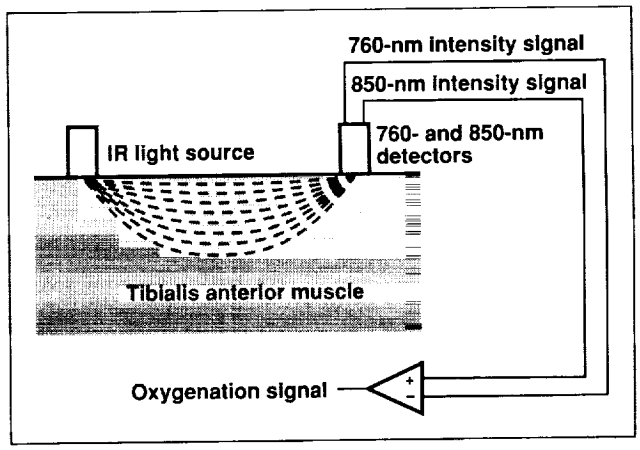


*Fig. 1. Principle of operation of the NIR spectroscopy technique.*

oxygenation, we hypothesized that NIR spectroscopy could detect this condition in an exercising muscle.

We conducted a study using seven healthy male and three healthy female subjects, aged 23–49. On two separate days, subjects were asked to perform ankle flexion/extension exercise for 14 minutes.

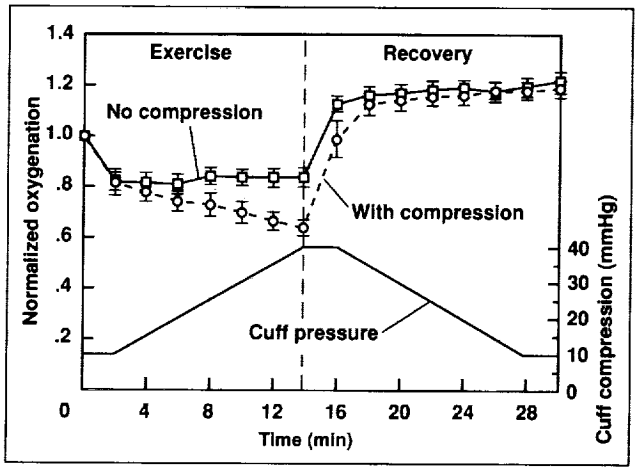


*Fig. 2. Muscle oxygenation patterns measured in the tibialis anterior muscle by the NIR spectroscopy technique during and after exercise. Simulation of CCS by external cuff compression has a significant effect on these patterns.*

On both days, the NIR spectroscopy device was placed over the tibialis anterior muscle of the shin to monitor oxygenation patterns during and after exercise. On one day, CCS was simulated by placing a compression cuff over the lower leg and inflating it gradually from a pressure of 10 mmHg to 40 mmHg over the duration of the exercise. After termination of exercise, the cuff was gradually deflated at the same rate back to 10 mmHg.

The results are summarized in the second figure. Without CCS induction (no external compression), the muscle exhibited a normal oxygenation pattern, reaching a decreased steady-state level during exercise and recovering rapidly after exercise ceased. In contrast, during simulated CCS, muscle oxygenation decreased significantly more with exercise. Furthermore, post-exercise recovery of muscle oxygenation was significantly slower with simulated CCS than that under normal conditions.

There is no noninvasive technique currently in use for the diagnosis of CCS. The results of this study suggest that NIR spectroscopy may be an effective diagnostic tool for identification of this syndrome. Future studies using actual CCS patients will be necessary to further evaluate the technique's efficacy.

**Ames-Moffett contact: G. Breit/K. Hutchinson**
**(415) 604-0519/5747**
**Headquarters program office: OSSA**

## Cutaneous Microvascular Flow in the Foot in Various Gravitational Environments

**David Chang, Gregory A. Breit, Jorma Styf, Alan R. Hargens**

External compression of the human skin increases tissue pressure and decreases cutaneous blood flow. With sufficient compression, blood flow is totally occluded. Long-term reduction of cutaneous blood flow leads to pressure sores in bed-ridden patients and ulceration and tissue necrosis in diabetics. On Earth, human feet are regularly exposed to variable levels of external compression in the form of weight bearing during normal daily activities, and therefore the soles of the feet must contend with low states of blood flow. However, Earth's 1-gravitational-unit (1-G) environment increases local blood pressure in the foot as a result of hydrostatic effects, and may counteract microvascular occlusion caused by orthostatic weight bearing. Therefore, in this study we hypothesized that cutaneous blood flow in the sole of the human foot has lower tolerance to weight bearing in weaker gravitational fields.

Human subjects (six males, six females; aged 18–49, body weight 42–86 kilograms, height 152–183 centimeters) underwent whole-body tilting at four angles: 90 degrees (upright) (1 G), 22 degrees (0.38 G), 10 degrees (0.17 G), and 0 degrees (supine) (0 G). These positions simulated the gravitational environments of Earth, Mars, the Moon, and microgravity, respectively (first figure). Cutaneous capillary blood flow was monitored on the plantar surface of the heel by laser Doppler flowmetry (second figure) while weight-bearing load was

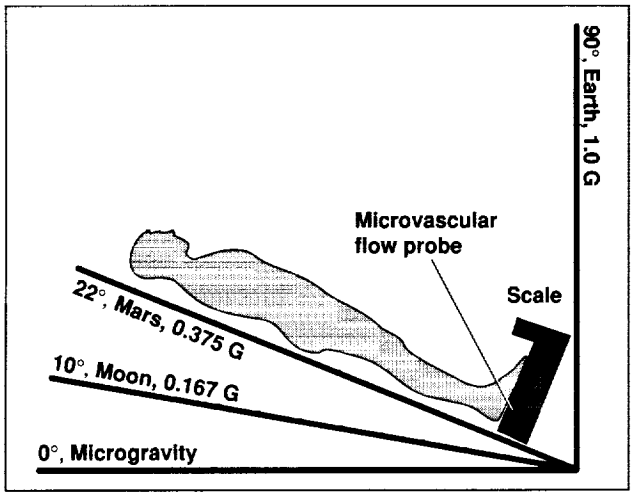


*Fig. 1. Tilt protocol to simulate different gravitational environments. At foot level, the gravitational environments of Earth, Mars, the Moon, and microgravity are produced with head-up tilt angles of 90, 22, 10, and 0 degrees, respectively.*

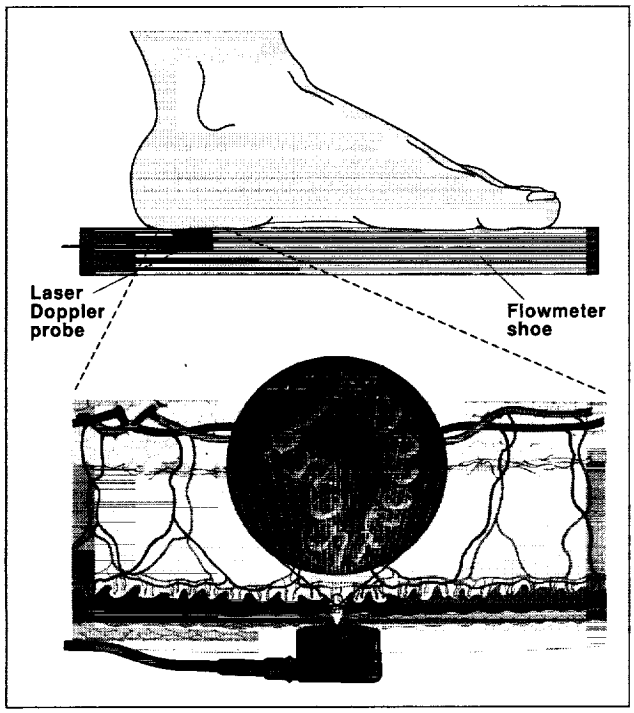


*Fig. 2. Human foot instrumented with laser Doppler flowmeter. The laser Doppler probe measures capillary blood flow in an approximately 1-cubic-millimeter volume of tissue by emitting a low-intensity laser light penetrating 3–4 millimeters into the skin.*

measured beneath the same foot with a calibrated scale. Mean arterial pressure in the foot was calculated by adding the hydrostatic pressure to the continuously recorded heart-level blood pressure for each subject. At each tilt angle, subjects increased weight bearing on one foot in graded load increments of one kilogram beginning with zero. The weight-bearing load at which null flow first occurred was determined to be the critical closing load (CCL). Subsequently, the load was reduced in reverse steps until blood flow returned; this point was determined to be the critical opening load (COL). The CCL and the COL were normalized to each subject's body weight.

The CCL and the COL decreased linearly with reduction of G level (third figure). Furthermore, the threshold for microvascular occlusion correlated directly with the magnitude of local arterial pressure at the level of the foot ($r = 0.71$). Also, CCL and COL were significantly different ($p < 0.0005$).

Microvascular blood flow in the sole of the human foot is less tolerant to external compression as gravity and local blood pressure are reduced. As the simulated gravitational field is reduced, both CCL and COL decrease. Our data suggest that in space, the foot sole is less tolerant to weight bearing and more prone to compression-related injuries as a result

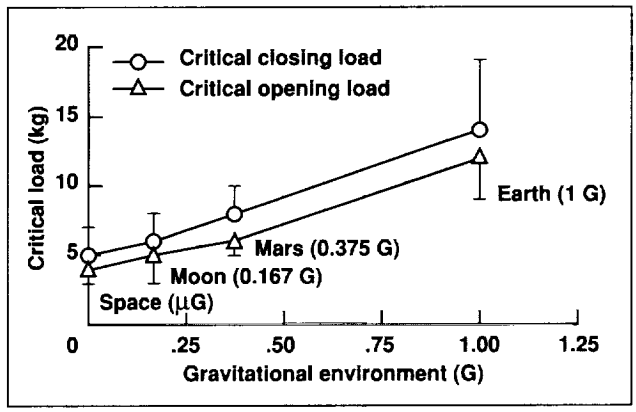


*Fig. 3. Critical closing and opening loads for different simulated gravitational environments. G levels less than that of Earth produce lower local blood pressures in the foot during orthostasis. Consequently, compression thresholds for microvascular occlusion in the sole of the foot at G levels below 1 are lower.*

of loss of gravitational blood pressures. The results of this study should be considered in the designing of extravehicular activity (EVA) suits and exercise hardware for astronauts. The observed relationship between local perfusion pressure and occlusion thresholds also has important implications for the treatment and prevention of skin ulcers in patients on Earth.

**Ames-Moffett contact: D. Chang/A. Hargens**
**(415) 604-5747/5746**
**Headquarters program office: OSSA**

## Noninvasive Determination of Structural Properties of Bone

**Tammy Cleek, Robert Whalen**

The cross-sectional asymmetry and curvature found in long bones such as the tibia or femur are related to musculoskeletal forces present during the development and maintenance of bone. Without normal loading, as in long-term paralysis or with certain congenital defects, long bones develop like straight, and then circular, tubes. Various methods have been used to determine bone structural properties that reflect the growth and loading history of an individual. Computed tomography (CT) has been used to obtain the desired three-dimensional information from bones noninvasively. However, this method is both costly and not readily accessible to most researchers.

Bone densitometry methods such as dual-energy X-ray absorptiometry (DXA) are commonly used to analyze regional and whole-body changes in bone mineral content. Bone densitometry has also been used to obtain information on cross-sectional properties of bone in a single scan plane. Using three DXA scans, we have extended the method to obtain the principal moments of inertia (Imin, Imax) and orientations of the principal axes of each scan cross section. Cross-sectional properties are combined along the bone length to create whole-bone models. The torsional strength and stiffness of a long bone is characterized by these measures along with bone material properties.

We applied this three-scan method to aluminum phantoms and cadaver long bones. Our preliminary efforts focused on investigating the feasibility of our algorithms with phantoms of known material properties and geometries. Initial results showed that our methods are successful in computing principal

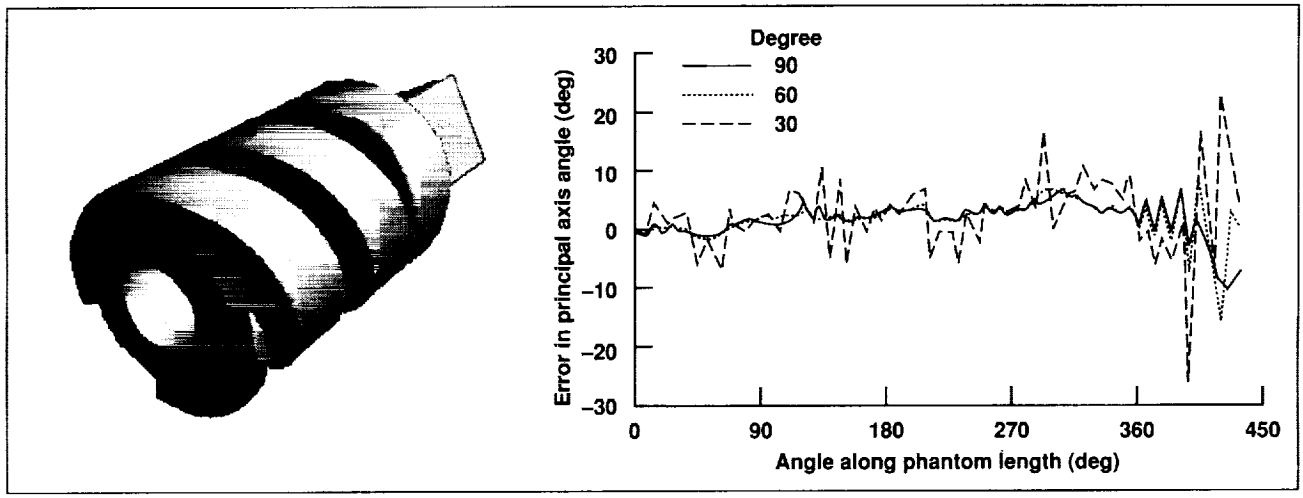


*Fig. 1. Error of computed principal angle of tapered helix along phantom length with scan-included angles of 30, 60, and 90 degrees.*

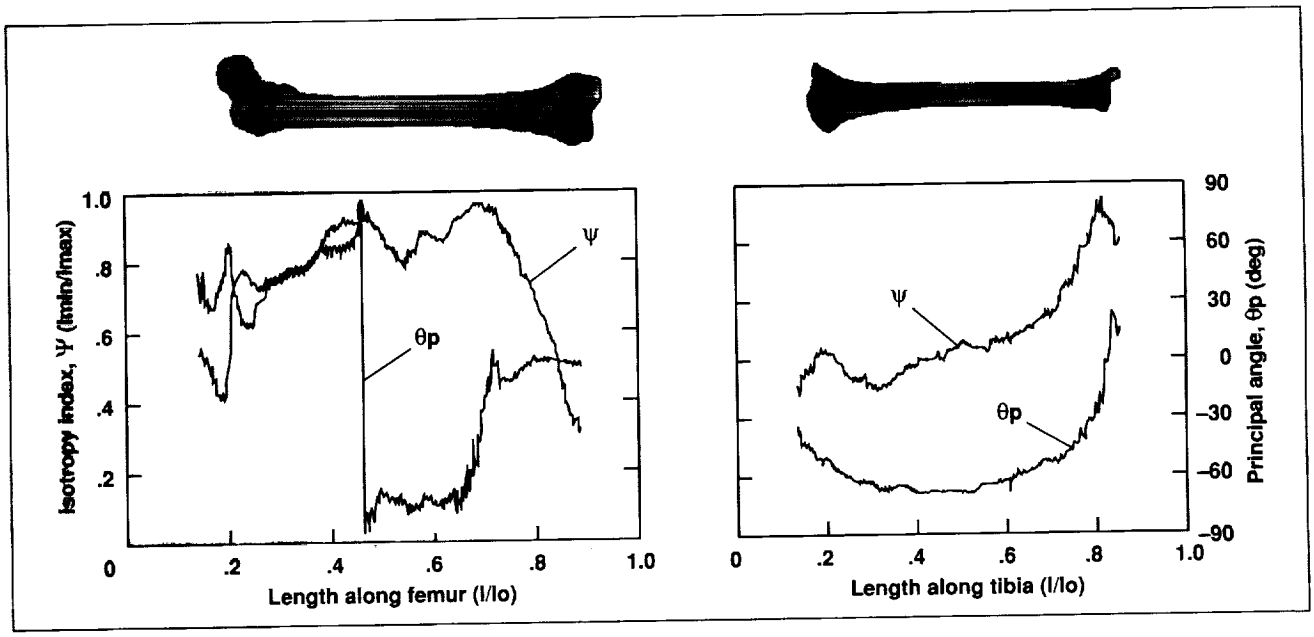


*Fig. 2. Computed isotropy index (ψ) and principal angles (Θp) for female right femur and tibia. Coordinate frame (viewed from distal ends): 0 degrees: medial; 90 degrees: anterior; –90 degrees: posterior.*

moments of inertia and principal angles from the analyses of three scans taken at 0, 45, and 90 degrees. The next phase of development involved the verification of the accuracy and sensitivity of the method with respect to different DXA scan resolutions, the included angle of the scans, and the isotropy index (Imin/Imax). These factors are important in determining the usefulness of the technique for future in vivo studies.

Aluminum phantoms and a cadaver femur and tibia were scanned along their entire lengths at several orientations by means of the whole-body and normal- and high-resolution spine-scan modes with a Hologic DXA machine. Computed section properties were compared using three different scan conditions. Scan directions included an initial position and ±15, ±30, and ±45 degrees from that position to yield scan-included angles of 30, 60, and 90 degrees.

The high-resolution spine-scan mode was not more accurate than the normal spine-scan mode in computing section properties, despite its having twice the point resolution. The whole-body scan, despite its coarse resolution, also showed some promise in computing section properties; further investigation is needed to explore the limitations of this mode.

Calculated principal moments of inertia were within 3% and principal angles were within 2 degrees of the expected value of all phantoms, using included angles of 60 and 90 degrees. Increased errors were observed in the tapered helical tube phantom when the included angle was reduced to 30 degrees as the helix approached a circular cross section, as depicted in the first figure.

The isotropy indexes of phantoms with elliptical and eccentric circular cross sections were similar to values that may be found in bone and were calculated accurately regardless of included angle and phantom orientation. The isotropy index of the helix scanned in spine mode steadily increased from ~0.5 to 1.0 for all included angles. Increased error was observed as the included angle was reduced. The errors were greatest as the helix approached a circular cross section with no unique principal-axis orientation.

A cadaver female right femur and tibia were scanned and the cross-section properties were computed (see second figure). The femur was highly isotropic (0.80–0.98) in the midshaft, suggesting a regular cross section in this region. The orientation of the cross section of the femur underwent a continuous twist along the bone length and is indicated by the principal angle profile. The tibia was highly isotropic only toward the ankle (distal end).

The calculated principal moments of inertia and principal angles were in excellent agreement with

expected values for phantoms scanned with included angles of 60 and 90 degrees. The algorithm was also insensitive to changing cross-sectional shape and isotropy values. These results are promising for future in vivo studies of bones such as the tibia, which have changing cross-sectional shapes and isotropy values and must be scanned without interference from the fibula, necessitating scanning with smaller included angles. We believe this method will provide a means to follow the changes in bone mineral distribution that occur with changes in daily activity patterns, spaceflight, age, osteoporosis, fracture healing, and spinal cord injury.

**Ames-Moffett contact: T. Cleek**
**(415) 604-0518**
**Headquarters program office: OSSA**

## Oculomotor and Perceptual Responses to Pitched Optical Backgrounds

**Malcolm M. Cohen**

In several previous studies, we demonstrated that the apparent elevation of a visual target is altered when the magnitude of the gravitational–inertial force acting on an observer is changed. Furthermore, we showed that the effect of the gravitational–inertial force can be reduced when the target is presented against a well-structured optical background. We also showed that an optical background whose surfaces are not aligned with gravity can similarly alter the apparent location of a target that is viewed against it.

We hypothesized that a pitched optical background elicits an optostatic response—an unconscious and involuntary change in the direction of gaze—and that this response causes the eyes to rotate with the pitch of the background toward a line that is normal to its rear surface. When the background is pitched upward (or downward), the direction of gaze also rotates upward (or downward), but to a lesser extent than the background itself. If the observer is unaware of this involuntary change in the direction of the gaze, the observer will misperceive the location of a target viewed against the background. This optostatic response, which we recently measured in our laboratory with an infrared video system, is described below.

We systematically altered the orientation of an optical background for each of 16 subjects by having them look into a pitchbox that was erect or pitched at angles as large as ±20 degrees from the vertical. The interior edges of the pitchbox were dimly illuminated by electroluminescent strips. Our subjects adjusted the position of their eyes, and of a target on the rear wall of the box, so that they felt their eyes were pointing horizontally and so that the target appeared to be at eye level. With the rear wall of the pitchbox oriented at –20, –10, 0, +10, and +20 degrees from the vertical, we recorded the actual position of the target, and we used an ISCAN infrared video system to register the position of our subjects' eyes.

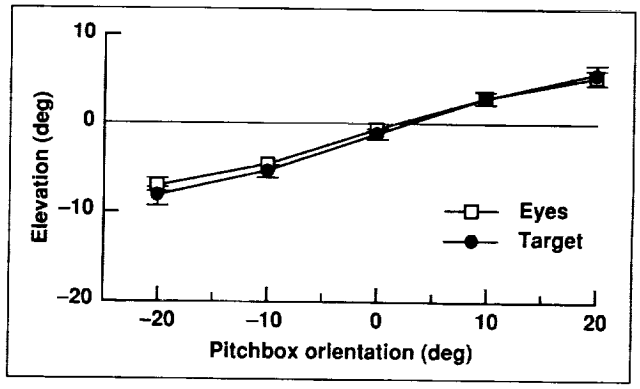


*Fig. 1. Effects of pitchbox orientation on settings of the eyes and settings of a visual target to apparent eye-level horizontal.*

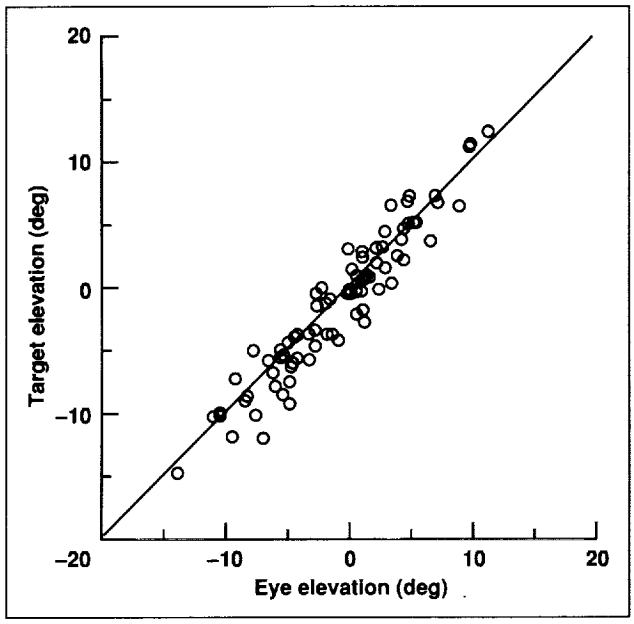


*Fig. 2. Eye elevation versus target elevation when both the eyes and the target are perceived to be at eye-level horizontal. These data represent settings from each of the 16 subjects tested at each of the 5 pitchbox orientations used in this study.*

Our results demonstrated that changes in the orientation of the pitchbox caused the target to appear displaced from its objective position with a slope of 0.34 degrees per degree of pitch of the box, and that the eyes deviated in the same manner, as shown in the first figure. Furthermore, on a subject-by-subject basis, the magnitude of the errors in setting the eyes to the horizontal was highly correlated with the magnitude of the errors in setting the target to eye level, as shown in the second figure. Thus, we argue that the ability of our subjects to localize a visual target with respect to apparent elevation depends on their ability to know the position of their eyes, and that undetected changes in the position of the eyes brought about by the optostatic response shown here are directly responsible for the errors in the perceived location of the target.

**Ames-Moffett contact: M. Cohen**
**(415) 604-6441**
**Headquarters program office: OSSA**

## Hindlimb Suspension Affects Posture and Gait

**Nancy Daunton**

The hindlimb suspension model simulates some of the effects of microgravity exposure on rats by unloading the hindlimbs, which produces changes in the structure, physiology, and biochemistry of the hindlimb neuromuscular system. The effects of suspension on hindlimb function, and in particular on posture and gait, have received little attention, even though it is important to evaluate the functional as well as the structural changes that are elicited by chronic microgravity exposure.

As part of our ongoing studies of the effect of chronic altered-gravity conditions on neuromuscular function in rats, we investigated the impact of hindlimb suspension on the posture and gait of adult rats. In addition, to ensure that we discriminated between effects of unloading (as would occur in microgravity) and those that might be caused by tail restriction (a consequence of the suspension procedure), a control group in which the tail was suspended but not the hindlimbs (which remained loaded) was used in addition to the normal (nonsuspended) control group.

Posture and gait were assessed after 14 days of suspension. In the unloaded animals, as in astronauts returning from long periods in microgravity, significant changes in gait and posture were seen. For example, animals walked more slowly and with a broader base than normal, in an apparent attempt to enhance stability during walking. Some of these effects were observed in the loaded, tail-suspended animals as well as the unloaded ones, which suggests

that the restriction of normal tail use during hindlimb suspension affects neural circuits involved in the control of posture and locomotion.

Some of the effects of suspension on gait disappeared over the 35 days of post-suspension testing. However, some postural changes (e.g., elevation of the pelvis during walking) were still significant on the 35th day (see figure). These results suggest that exposure in simulated microgravity for only 14 days can induce widespread changes in posture and gait, and that some of these changes may be very long lasting or even permanent. Further studies will be done to determine the most efficient behavioral and/or pharmacological methods for restoring normal posture and gait in animals chronically exposed to altered gravity conditions.

**Ames-Moffett contact: N. Daunton**
**(415) 604-4818**
**Headquarters program office: OSSA**

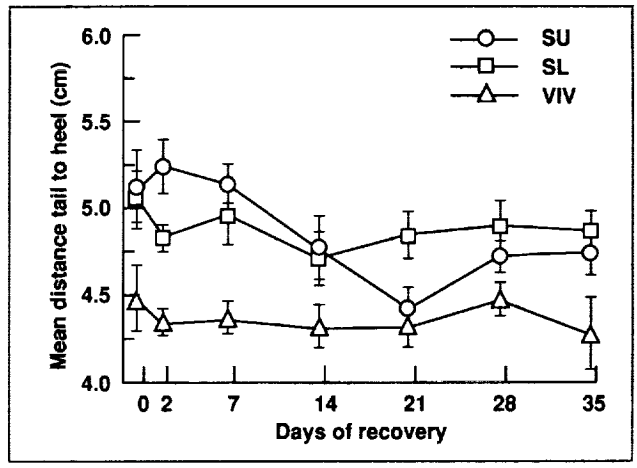


*Fig. 1. Long-lasting change in posture during walking in rats after 14 days of suspension. SU = animals suspended with hindlimbs unloaded; SL = animals suspended with hindlimbs loaded; V = vivarium animals housed in suspension cage but not suspended.*

## Growth Hormones, Exercise, and Muscle Atrophy

**Richard E. Grindeland, J. K. Linderman**

Previous studies have shown that secretion of growth hormone (GH) is markedly reduced in actual or simulated spaceflight in rats and humans. We have now shown that monkeys also sustain dramatic reductions in growth hormone as a result of spaceflight: at 3 and 11 days after flight, GH is almost undetectable in their blood. Moreover, the levels of a second growth-promoting hormone, insulin-like growth factor-I, parallel those of GH. Earlier data revealed decreased brain levels of factors that regulate GH secretion, but we now have unequivocal evidence that microgravity during spaceflight also reduces GH secretion by direct inhibition of growth-hormone-producing cells (Type II somatotrophs) in tissue culture. Reduced secretion of GH is physiologically important because of its many effects on metabolism and growth, including growth of skeletal muscles. Loss of muscle mass in space is primarily due to decreased synthesis of protein. Because of the well known effects of GH on protein synthesis, we hypothesized that the presence of GH would prevent or ameliorate loss of muscle mass in space. We treated groups of rats with either GH or saline solution. GH alone was found to be ineffective in preventing muscle atrophy in rats without a pituitary gland, but when combined with exercise, GH prevented muscle atrophy in simulated microgravity. In studies of rats with their pituitary glands intact, daily high-intensity exercise alone prevented atrophy of fast-twitch, but not slow-twitch, muscles, as determined by the weights of the muscles. More important, in the gastrocnemius, a predominantly fast-twitch muscle, the combination of exercise and GH maintained the protein fraction of muscle that is responsible for contraction (myofibrillar protein) at the same level as that in ambulatory control animals (part (a) of the first figure). As shown in part (b) of the first figure, the combination of exercise and GH increased the synthesis of myofibrillar protein, which suggests that stimulation of synthesis by exercise and GH was at least partially responsible for maintaining protein content. The results in the first figure suggest that GH and exercise may be useful in preventing the

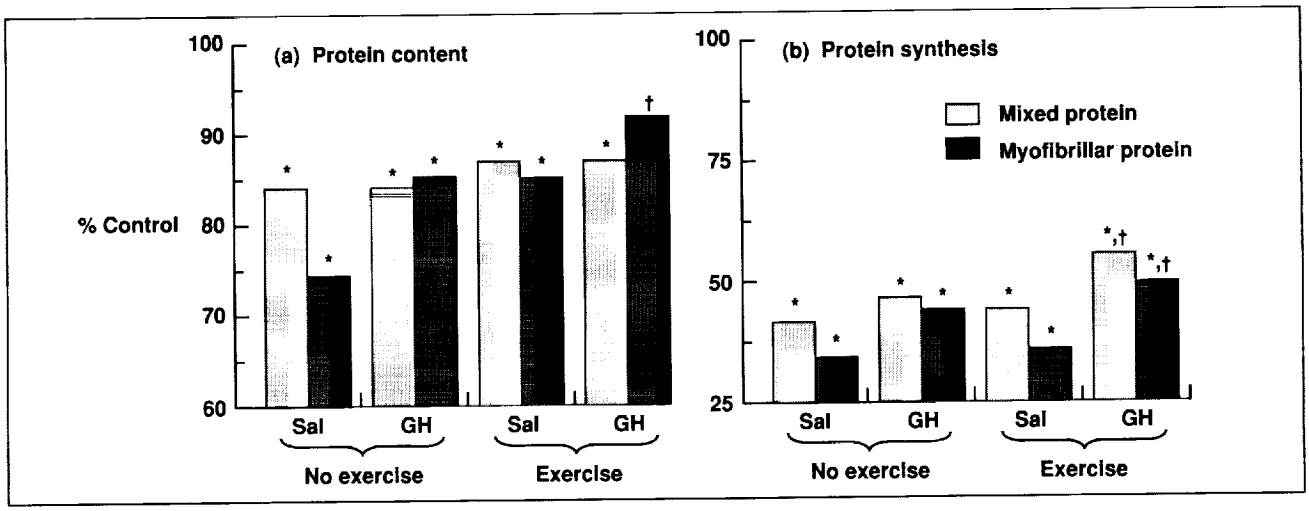


*Fig. 1. The effect of daily high-intensity exercise and growth hormone (GH) on protein content and synthesis in the gastrocnemius muscle of hindlimb-suspended rats, expressed as a percentage of ambulatory control. Sal = saline; * = significantly less than control; † = significantly greater than hindlimb-suspended, nonexercised animals.*

muscle atrophy and dystrophy that is associated with spaceflight.

The effect of a bout of exercise, with and without GH, on stimulating synthesis of contractile protein in atrophic muscle would indicate the optimal frequency with which muscles should be loaded to prevent atrophy during weightlessness, and whether GH enhances the effect of exercise. The second figure indicates that protein synthesis was decreased more in the soleus, a slow-twitch muscle, than in the gastrocnemius—a result that is consistent with the fact that slow-twitch muscles atrophy more in space than do fast-twitch muscles. In part (a) of the second figure, it can be seen that the stimulation of protein synthesis by a bout of high-intensity exercise was greater in the soleus than in the gastrocnemius. However, as shown in part (b), exercise did not restore synthesis in the soleus to the same extent as in the gastrocnemius. It remains to be determined whether other components of muscle loading, such as duration, may be more effective in restoring protein synthesis in slow-twitch muscles. Furthermore, GH does not appear to enhance the effect of a single bout of exercise in stimulating contractile protein synthesis. More work is needed to fully understand the interactive effect of GH and exercise in maintaining contractile protein content during microgravity.

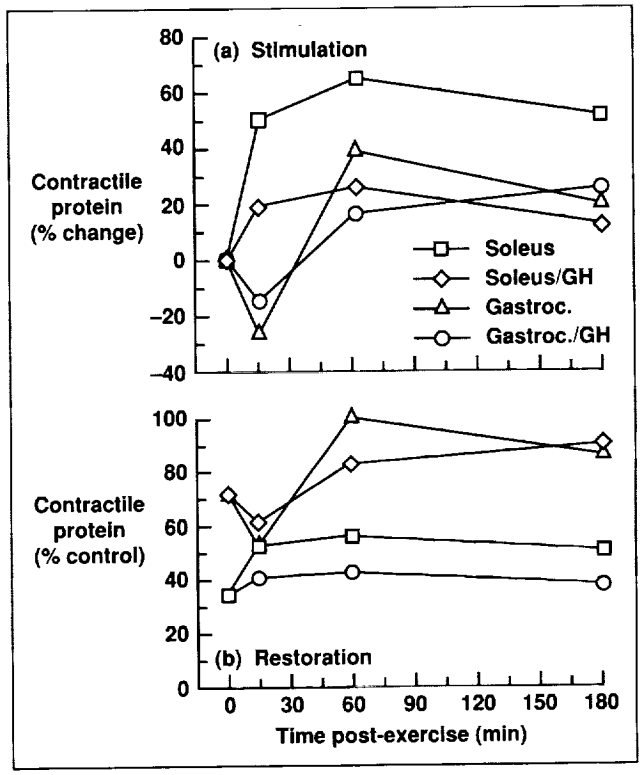


*Fig. 2. The effect of a single bout of high-intensity exercise and growth hormone (GH) on restoration of protein synthesis, expressed as a percentage of control, and stimulation of protein synthesis, expressed as percent change in synthesis compared to hindlimb-suspended, nonexercised animals.*

**Ames-Moffett contact: R. Grindeland**
**(415) 604-5756**
**Headquarters program office: OSSA**

# External Force and Cell Behavior

**Rosalind A. Grymes**

We are using two methods to evaluate cellular behavior under conditions of varying physical force. First, we have developed a prototype clinostat. This instrument supports the cultivation of cells under conditions of vectorially averaged gravity. There is a constant (small) force perpendicular to the direction of rotation, and the vector of the 1-G gravitational force is constantly shifting. The gravity-vector-shifted cells show a marked alteration in intercellular contacts, in colony morphology, and in growth kinetics in alkaline media. We have completed construction and prototype testing of the clinostat and its companion instrument, the vertical rotational control.

Our second method of evaluating force variation uses the Flexercell Strain Unit™. This instrument transmits a mechanical stretch over a 24-millimeter flexible membrane. Monolayers of cells are grown on the flexible-membrane support and are subjected to predetermined regimens of flexing at precisely controlled amplitude and frequency. Cellular response is measured by DNA synthesis and by direct cell counts. Various dermal and corneal fibroblast cell strains with a range of proliferative capacities have been examined. The dermal fibroblasts also provide reference points along a timeline that starts with fetal growth and ends with senescence. These are (1) young cells, (2) aged cells, and (3) Werner's syndrome (WS) cells. WS is a genetic advanced-aging disorder. Many of its clinical symptoms involve the skin and connective tissue. In culture, dermal cells from WS patients fail to respond to growth factors such as platelet-derived growth factor (PDGF), indicating a fundamental defect of signal transfer. Similarities between the generalized response failures of senescent cells and of those exposed to microgravity are the basis for our choice of this age-range model.

In determining the response of normal cells to various regimens of applied mechanical stretch, we noted two significant and related behaviors. First, the behavior of stretched and control cultures became more and more similar in sequential experiments, regardless of the applied-stretch protocol. In the first figure, the cumulative results of multiple stretch regimens are combined. The two curves, control and stretch, cannot be distinguished within one standard deviation. This adaptation is not related to the applied stretch; it is a result of the dynamic interaction between the cells and the flexible membrane mediated by the ability of the membrane to resist intracellular tension generated by cytoskeletal structures.

Normal aged cells were compared with those derived from the prematurely aging WS cells. We observed a large response to the applied growth factor under the stretched conditions only, whereas normal aged cells responded to the applied PDGF under either the stretched or the static condition. Subsequently, we observed a gradual shift in the ability of these cells to mount a mitogenic response to the soluble growth factor PDGF as they continued

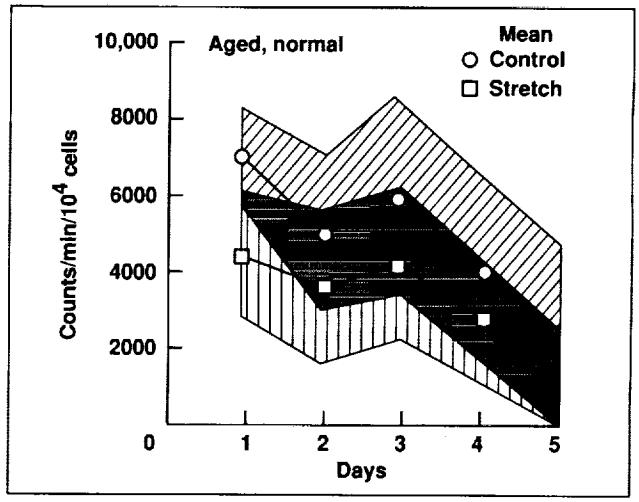


*Fig. 1. Cumulative results from multiple studies of different stretch regimens using normal, chronologically aged dermal fibroblasts. The control and stretch cultures do not differ significantly from each other, as their curves lie within one standard deviation value, as indicated by the shaded regions.*

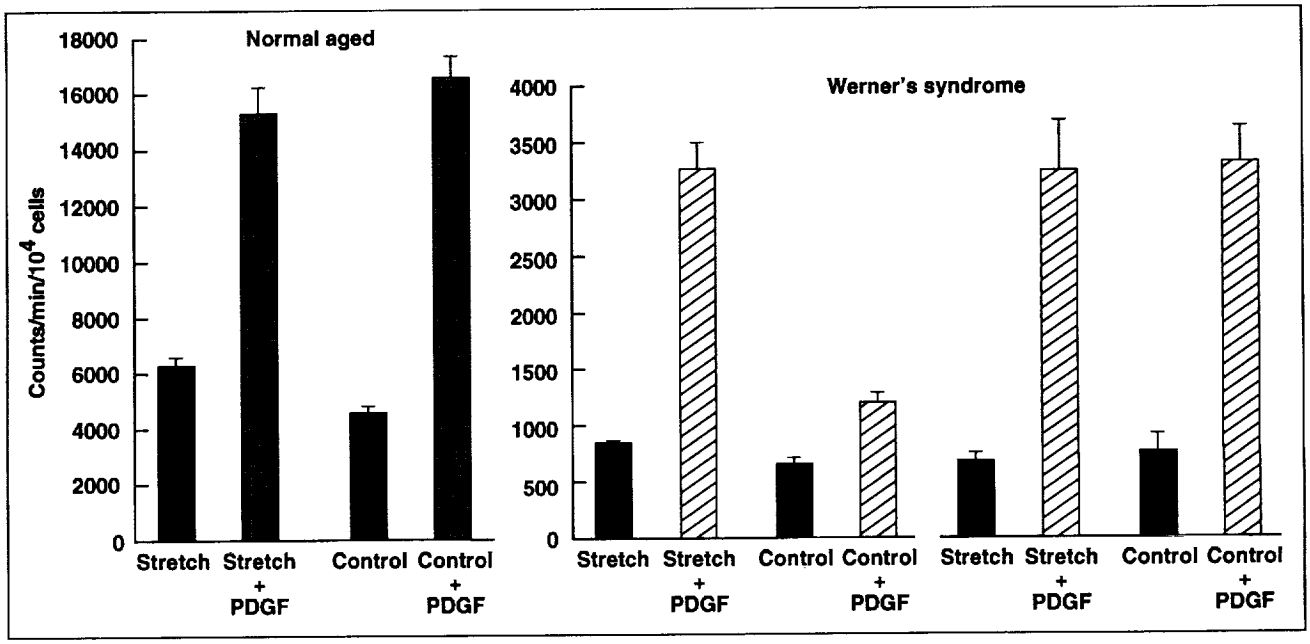


*Fig. 2. DNA synthesis by normal aged and WS dermal fibroblasts. The right-hand graph gives results from two separate, temporally sequential experiments on the WS cells. Each bar represents the mean of six independent determinations, plus or minus one standard deviation.*

to adapt to the malleable substrate. The results of these studies are shown in the second figure. The dynamic interaction between the cells and their substrate is a powerful stimulus which results in an adaptive behavior that rewires the cells' internal signaling pathways and permits the normal PDGF response to occur.

We also noted that the skin cells aligned their cell bodies parallel to the direction of applied stretch. In the circular wells in which the cells are grown, this resulted in a radial array of cells like the spokes of a wheel. All cell strains examined required a specific minimum of cell-to-cell contact to initiate this orientation behavior. The application of cytoskeleton-destabilizing drugs, which affect orientation behavior in a dose-dependent fashion, can be observed by immunofluorescence microscopy. The central role of the cytoskeleton in the perception of stretch and the cell's response to stretch has been established, and we have determined that force perception and response behavior depend on the presence of an interconnected cell population of critical size.

**Ames-Moffett contact: R. Grymes**
**(415) 604-3239**
**Headquarters program office: OSSA**

# Gravity Tolerance in Snakes

**Harvey B. Lillywhite, Richard E. Ballard, Alan R. Hargens**

Gravity affects all organisms, particularly terrestrial animals that are large or vertically oriented. Humans and giraffes, for example, have cardiovascular systems that are specially adapted to circulate the body fluids against the force of gravity and to maintain adequate blood flow to the brain. Snakes, however, are unique in the extent and range of their cardiovascular adaptations to variable gravity.

Today, the 16 families and approximately 2,700 species of snakes in the world occupy nearly every available habitat except the polar regions, high mountain tops, and deep oceans. Some snakes are aquatic, many are terrestrial, and others are strictly arboreal. Arboreal species are characterized by morphological and physiological adaptations that maintain cardiovascular homeostasis during changes in posture (e.g., during tree climbing). Aquatic species, however, exhibit severe hemodynamic and cardiopulmonary problems when they are removed from their natural environment and oriented vertically in air. Semiaquatic species and nonclimbing terrestrial species are intermediate in cardiovascular responses to gravity. Thus, snakes demonstrate a diverse range of adaptation to gravitational influence on the cardiovascular system. Regulatory responses of tree-climbing snakes to vertical posture resemble those of humans to standing upright, and the gravitational problems experienced by nonclimbing snake species resemble the cardiovascular deconditioning observed in humans after bed rest and spaceflight.

To evaluate the nature and extent of vascular adaptations to gravity, blood flow to the head in snakes from various habitats was continuously monitored while the snakes underwent centrifugation. Centrifugation allowed forces in excess of 1 G to be applied along the longitudinal axis of the snakes. The cardiovascular responses in aquatic, terrestrial, and arboreal species could then be compared. After approval of the protocol by the NASA Ames Animal Care and Use Committee, snakes were placed in long tubes and mounted on a 4-foot-radius centrifuge, head toward the center. Headward blood flow was measured using a surgically implanted Doppler flow cuff around the carotid artery, and centrifugal force ($G_z$) at the tail was measured by an accelerometer. $G_z$ was increased stepwise, in 0.25-G increments, every 10 minutes until the carotid flow fell to zero. Tolerance was defined as the $G_z$ level at which carotid flow could not be maintained.

The figure illustrates the $G_z$ tolerance of various snakes, from aquatic to semiarboreal. In general, the

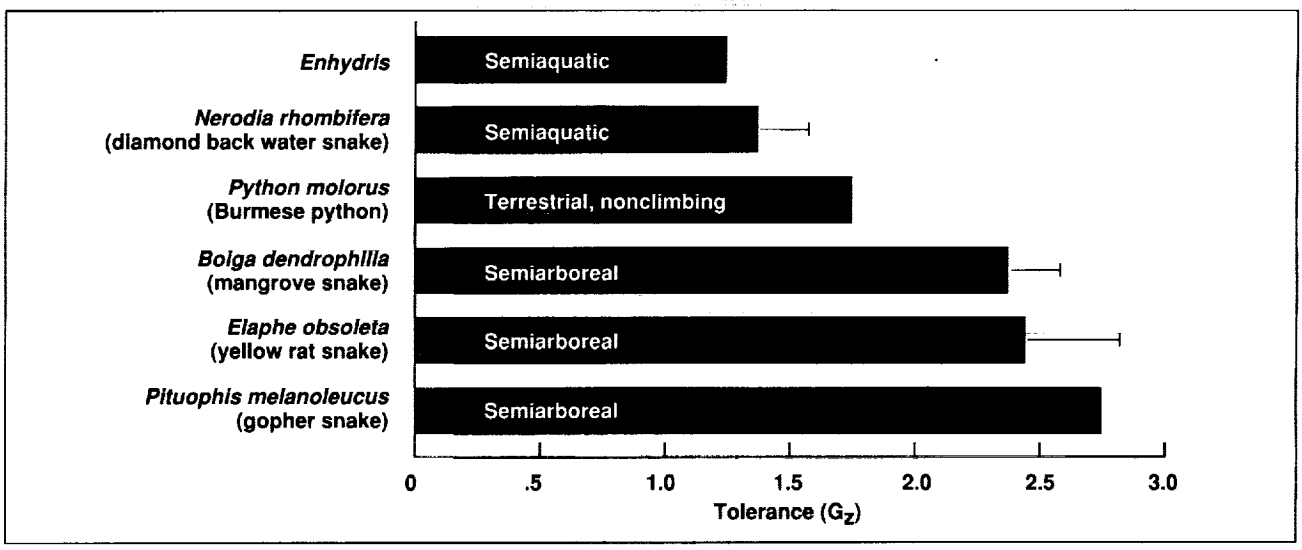


*Fig. 1. $G_z$ tolerance in snakes from various habitats.*

semiarboreal snakes had the greatest capacity to maintain cardiovascular function in the face of gravitational disturbance. These species have firm muscle tone and tight skin, similar to an antigravity suit, whereas aquatic, semiaquatic, and nonclimbing terrestrial species have more flaccid bodies with looser skin. In addition, nonclimbing snakes have poorly developed physiological mechanisms for dealing with gravity. We are currently investigating physiological and morphological changes that accompany 3 months of daily acclimation to hypergravity in the semiarboreal snake *Elaphe obsoleta*. Because of their elongate body shape and extensive range of adaptations to gravity, snakes are ideal models for studying cardiovascular adjustments to microgravity and return to normal gravity after spaceflight.

**Ames-Moffett contact: R. Ballard/A. Hargens**
**(415) 604-5747/5746**
**Headquarters program office: OLMSA**

## Intramuscular Pressures Produced by Elastic and Inelastic Leggings

**Gita Murthy, Richard E. Ballard, Gregory A. Breit, Donald E. Watenpaugh, Alan R. Hargens**

The musculovenous pump of the human leg is critical in counteracting the effects of gravity. Muscle contraction increases intramuscular pressure, compresses the veins, and improves venous return to the heart (see first figure). The valves within the veins prevent retrograde blood flow. Intramuscular pressure (IMP) probably decreases with prolonged spaceflight or bed rest, as a result of tissue dehydration and loss of muscle mass and/or muscle tone. In order to increase IMP and improve peripheral circulation, compression devices are used clinically. The efficacy of these devices—for example, the elastic stocking or the inelastic legging—has been well documented. Clinically, these stockings or leggings are used for the treatment of venous insufficiency and leg swelling and to prevent venous stasis and orthostatic intolerance (the inability to stand upright).

The purpose of our study was to compare the effects of elastic and inelastic compression on leg IMP, an objective index of calf-muscle pump function. IMP in the soleus and tibialis anterior muscles was measured with transducer-tipped catheters (first figure) in 11 healthy volunteers. Each volunteer was tested under three conditions: (1) control (no legging); (2) elastic legging; and (3) inelastic legging. Pressure data were recorded for each study condition while the volunteer was recumbent (lying down), sitting, and running. To allow objective comparisons, the inelastic legging was adjusted in the upright posture to approximate the specified compression of the elastic legging.

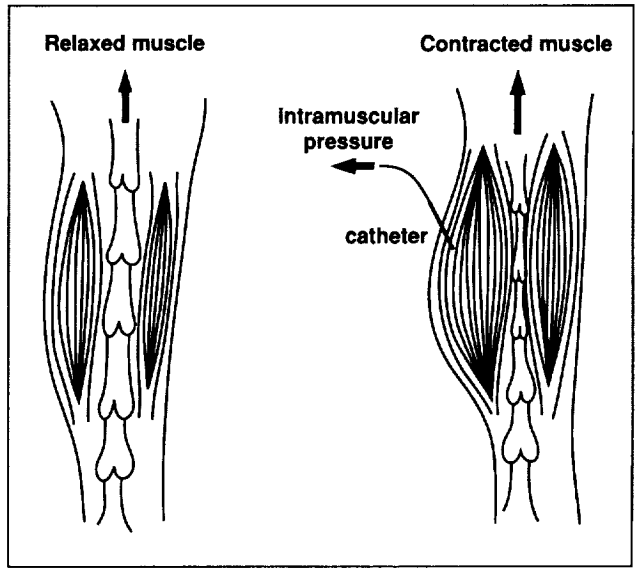


*Fig. 1. The muscle pump during relaxation and contraction. During muscle contraction, the intramuscular pressure increases and empties the veins, driving blood back toward the heart against gravity.*

During recumbency, the elastic legging produced a significantly higher IMP of 25 ± 1 millimeters of mercury (mmHg) in soleus muscle and 28 ± 1 mmHg

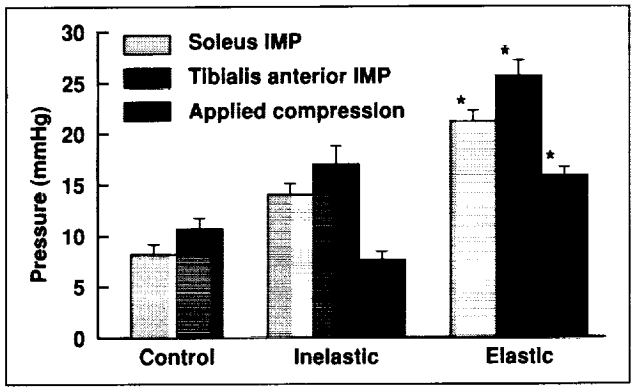


*Fig. 2. Intramuscular pressures in the soleus and the tibialis anterior produced by elastic stockings and inelastic leggings. * indicates significantly higher ($p < 0.05$) pressures than with inelastic leggings.*

in tibialis anterior muscle; the inelastic legging produced IMPs of 14 ± 1 mmHg and 16 ± 1 mmHg (see second figure). Mean IMPs produced by both elastic and inelastic leggings were significantly higher than control values (8 ± 1 mmHg in soleus and 11 ± 1 mmHg in tibialis anterior muscles) during recumbency. During sitting and running, peak IMPs generated by elastic and inelastic leggings were similar.

Leg compression of 20 mmHg during recumbency, in the absence of the high local blood pressure associated with upright posture, is known to impair venular outflow and decrease local muscle perfusion. Therefore, elastic leg compression applied over a long period of time in the recumbent posture may impede microcirculation and put tissue viability at risk. On the other hand, inelastic leggings do not compress leg tissues at levels above 20 mmHg during recumbency. Our study suggests that inelastic leggings counteract orthostatic intolerance in patients with venous insufficiency without the detrimental compression of leg tissues in supine posture that is associated with elastic leggings. Inelastic leggings may also help prevent orthostatic intolerance in astronauts after spaceflight.

**Ames-Moffett contact: G. Murthy/A. Hargens**
**(415) 604-5747/5746**
**Headquarters program office: OSSA**

## Automated Reconstruction of Neural Tissue

**Muriel D. Ross, Kevin Montgomery, Rei Cheng**

Neuroscientists have long wanted to visualize neural tissue in three dimensions. With the advent of computer technologies, a goal has been to automate the visualization process using serial sections photographed in a transmission electron microscope (TEM). Only at the TEM level can accurate measurements of cellular parts be obtained and details of cell-to-cell communication observed, so that neural functioning can be better understood. Such accuracy is particularly important in understanding the functional significance of any changes in neural structures that may occur in the space environment.

Earlier computer-based reconstruction methods relied on conventional photography. Either photographs (called micrographs) were scanned into a computer to digitize them, or contours of objects were traced from micrographs using a digitizing pad. The methods were labor intensive and less accurate than an automated method that begins with direct digitization from the TEM. Here, we report the first successful automatic acquisition of images from the TEM and computer-based recombining (mosaicking) of individual micrographs to reproduce the entire

section electronically. We developed algorithms for automated alignment of contours, but their extraction from the digitized sections still requires operator interaction. It is anticipated that complete automation will be achieved within the year.

Our present method consists of six parts: image acquisition, mosaicking, object-contour extraction, registration, visualization, and modeling. Sections cut from embedded tissue previously prepared for TEM study are mounted on slotted grids coated with a thin film of a material called Formvar. This supports the section for viewing in its entirety in the TEM. Each section is aligned in the microscope so that orientations of all sections are similar. This provides a rough alignment of objects in the sections at the outset, making later registration of contours easier.

Image acquisition is by a 1,024- by 1,024-element charge-coupled device (CCD) camera mounted on a Zeiss 902 TEM and connected to a Silicon Graphics (SGI) Indigo graphics workstation. The workstation is used to control the TEM stage. Software automatically translates the section in predetermined measured steps, with each step encompassing a micrograph that is then recorded in digitized form. The digitized micrographs are stored and then transferred over the Ames Ethernet network to an SGI Indigo in the Biocomputation Center. There, the individual micrographs are reassembled as sections (mosaicked) with our software and a CM 5 (connection machine). The process is repeated for every section in the series. This often entails recording 100 to 200 or more sections and storing as much as 10 gigabytes of data.

Objects of interest are identified from the digitized sections, and their contours are traced with the aid of a mouse. Each contour that belongs to a specific object (for example, a nerve ending or cell) is recorded with a number that identifies the object. If 24 different objects are traced, 24 identifying numbers are used in the data base. After contour retrieval, the objects must be registered (brought into alignment) with as much precision as possible. An algorithm for estimating alignment is used and the registered, successive contours are displayed on the monitor. The investigator can interactively modify the rotation and translation of objects, or scale them as necessary.

The registered contours are connected to one another by triangles, forming a mesh or grid-like structure, in a process called tesselation. The objects can be visualized in grid form, as shaded solids, or in transparent mode, using software (Ross 2.3) developed in the Biocomputation Center. The reconstructed objects can be rotated and viewed from any angle, or sliced into to reveal internal structure. The grid form is used in models to simulate neural functioning more accurately than is possible using architectures that are based on expected, rather than actual, design.

Our current, semiautomated method of reconstruction is a step toward full computer automation. It permits reconstructions to be completed in about one-third of the time previously required. The method also eliminates expensive, conventional photography and the resulting chemical waste. We use the method, called Recon 1.2, to reconstruct gravity-sensor neural tissue exposed to microgravity. The software is being made available to others interested in advancing the software or in using it in their own research.

**Ames-Moffett contact: M. Ross**
**(415) 604-4804**
**Headquarters program office: OSSA**

# Human Neck Compliance Exceeds Leg Compliance

**Donald E. Watenpaugh, Gregory A. Breit, Richard E. Ballard, Stanley Zietz, Alan R. Hargens**

Leg vasculature should exhibit limited compliance, or distensibility, in order to prevent excessive pooling of blood during orthostasis, yet little physiologic need exists for low vascular compliance in the upper body. We therefore hypothesized that vascular compliance of the leg is less than that of the neck.

To measure compliance at the two sites, we monitored volume changes in 1-centimeter calf and neck segments with gallium/indium-in-silastic strain-gauge plethysmography in nine subjects (six males, three females; ages 20–47) at the following tilt-table angles: 90 (head-up tilt), 54, 30, 12, 0 (horizontal supine), –6 (head-down tilt), –12, –6, 0, 12, 30, 54, and 90 degrees. Each position was held for 30 seconds, and data were averaged over the last 5 seconds of each interval. Compliance was calculated as the slope of the segment-volume/local-venous-pressure relationship, using interpolated jugular and leg venous pressure data collected under similar conditions in an earlier study by Katkov and Chestukhin (Russian Ministry of Health).

We found that mean calf compliance was $4.6 \pm 1.0 \times 10^{-2}$ milliliters per millimeter of mercury (ml/mmHg) (mean ± standard error), whereas neck compliance was six times greater at $28.2 \pm 4.1 \times 10^{-2}$ ml/mmHg (see figure). Responses of segment volumes to tilt were nearly instantaneous, which suggests that blood-volume translocation accounted for the changes. The relatively low leg compliance is attributed to stiffer vascular and connective tissues, better-developed neural control of capacitance, and calf-muscle contraction during head-up tilt. We conclude that the leg is better adapted than the neck to resist vascular distention with increased local vascular pressures. This research provides fundamental knowledge of how blood vessels have adapted to gravity.

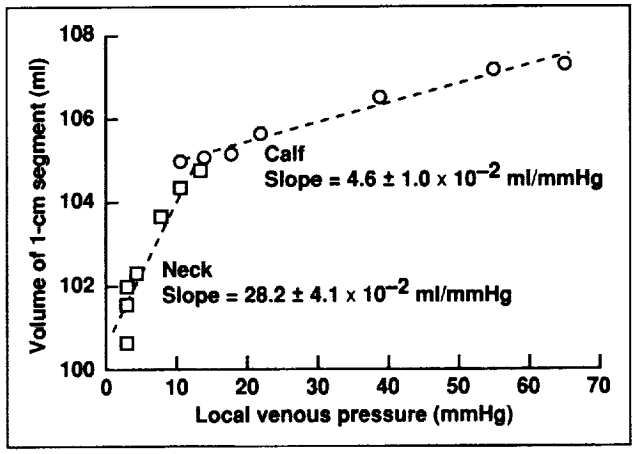


*Fig. 1. Mean neck compliance (slope of the segment volume/local pressure relationship) compared with calf compliance.*

**Ames-Moffett contact: D. Watenpaugh/A. Hargens**
**(415) 604-5747/5746**
**Headquarters program office: OSSA**

# The Measurement and Manipulation of Telepresence

**Robert Welch**

We have been investigating the perceptual experience of human observers when they are placed in a "virtual environment." In general, a virtual environment is one in which the sensory world is created by a computer and then fed to a head-mounted display or television monitor viewed by the observer. Virtual environments are also interactive: the observer's hand and body movements are signaled to the computer, causing the sensory world to change appropriately. It is of particular interest that observers frequently report that they feel they are actually in the situation that is being presented to their senses, rather than watching it from some distance, as in a movie theater. We refer to this experience as "telepresence." The aim of our research program was to measure this phenomenon quantitatively and, at the same time, to determine how it is influenced by several selected variables.

The virtual environment we used entailed a simulated automobile-driving task. Each subject sat in a mock-up of a car and looked at a monitor that depicted a computer-generated road and surrounding landscape as viewed through the windshield of the car. The subject's performance task was to "drive" the car as quickly and safely as possible over one circuit of the driving course, which was depicted as a winding road. Although performance measures (time to complete one circuit and number of times the car left the road) were obtained, they were not the focus of the present investigation. The subjects were told that the sensory and/or motor conditions of the driving task would differ from trial to trial and that after every two trials they would be asked to compare the two situations they had just experienced and indicate which situation produced in them a greater feeling of telepresence. We then carefully explained what we meant by this term. Every possible pairing and both orders of the various virtual environments were used.

In one of three experiments, we examined the potential effects of the "pictorial realism" of the scene. In one situation, the scene was presented as a flat, colorless terrain. In the second scene, color was added. In the third scene, hills and color were added, but the color was inappropriate. Finally, in the fourth and presumably most realistic situation, the scene contained hills and appropriate colors. The results of this experiment indicated that, in general, as realism increased, experienced telepresence also increased.

In the second experiment, we reexamined the effect of pictorial realism and, in addition, looked at the role of the presence or absence of a delay between the subject's actions and the resulting sensory feedback. Besides confirming the previous results on realism, we found, as expected, that feedback delay weakened telepresence.

In the third experiment, we examined the roles of realism and subject interactivity. In one condition, the subjects' steering and accelerator movements led to immediate sensory effects. In the other condition, subjects were told that they would not be using the steering wheel or accelerator pedal, but would merely view the visual scene in the passive manner of a passenger in the car. The results further confirmed the effects of realism and appeared to show that telepresence is stronger if subjects have some control over their sensory experience. In this research program, we have demonstrated for the first time the feasibility of quantitatively assessing the psychological experience of telepresence. And we have begun to determine some of the variables that influence the strength of this experience. These results, and those of our future planned experiments, will help us understand the nature of telepresence and, simultaneously, the nature of the sense of presence that we all experience in the real world.

Besides its relevance to these theoretical questions, this investigation should lead to the development of better virtual environments. The ultimate goal of many developers of virtual environments (often referred to as virtual reality) is to create situations that are so realistic that observers find it difficult or impossible to distinguish them from the real thing. This is the aim of those who create virtual environments for entertainment purposes. Another reason for wanting a virtual environment to produce a strong sense of telepresence is the possibility that this experience can improve task performance. Whether this notion is actually true is an empirical question, which we hope to examine at a later date.

**Ames-Moffett contact: R. Welch**
**(415) 604-5749**
**Headquarters program office: OSSA**

## Long-Term Skeletal Loading During Daily Activity

**Robert T. Whalen, Gregory A. Breit, Jason M. Quintana**

Recent theoretical and experimental studies of bone remodeling suggest that a bone's mineral density and strength are affected by the magnitude, rate, and frequency of the mechanical loads applied to it. Throughout a typical day, the human leg experiences a wide range of external loads ranging from zero to one body weight (BW), plus intermittent peaks of 1.2–1.3 BW during walking and 2.0–3.0 BW during running. The precise amount of time a typical person's legs are subjected to these various forces is unknown. Such knowledge may be crucial to understanding the relationship between daily loading histories and bone formation.

We have developed a portable system for long-term monitoring and recording of foot ground reaction forces (GRF). The system consists of an insole capacitive force sensor, placed in one shoe that connects to a compact data logger worn on a belt around the waist. The data logger (5 × 2.5 × 1.5 inches) contains a microprocessor, a capacitance signal conditioner, an analog-to-digital converter, a liquid-crystal text display, a removable 2-megabyte memory card (for data storage), and a serial data port (for communication to an external computer). The system is powered by two standard 9-volt batteries attached to the belt. Every 0.01 second, the GRF from the insole sensor is recorded, analyzed, and stored by the data logger. Using a sophisticated filtering algorithm to record only significant maxima and minima of the GRF, up to two weeks of loading data can be stored on a single memory card. The data logger also calculates loading rates (in BW/second), maintains a running total of duration at force levels partitioned into 0.1-BW intervals (a time–force histogram), and keeps a count of the number of steps taken at each force level.

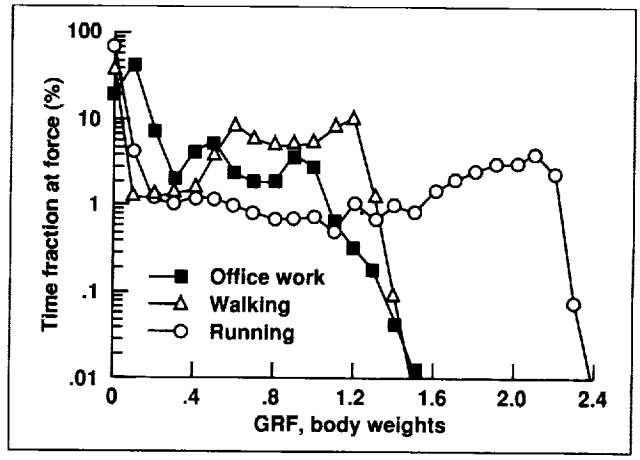


*Fig. 1. Representative time–force histograms for running, walking, and sedentary office work. Each point represents the percentage of time the instrumented leg spends at each force level. Note logarithmic scaling of vertical axis.*

We have used the system to compare three types of activities: running, walking, and sedentary office work (based on a total of 25 hours measured over several days). The first figure illustrates the differences between the time–force histories associated with these three activities. During office work, the leg is loaded in excess of one BW only 1.3% of the time, in contrast to walking (20.2%) and running (22.8%). The leg experiences loading greater than 1.5 BW less than 0.02% of the time during both office work and walking, compared to 18.6% during running. The relatively large fractions of time spent at 0 BW during walking and running (39.4% and 64.4%, respectively) correspond to the swing phase of the gait cycle—the time during which the leg swings from back to front between steps.

The second figure demonstrates the differences between the three activities with respect to the frequency and average peak rate of loading. We found that the typical office worker takes, on average, approximately 5 steps per minute, in contrast to 80 steps per minute during running. Mean peak load rates also show significant differences, ranging from approximately 6 BW/second during office work to 79 BW/second during running.

We believe that long-term monitoring of GRF to obtain habitual individual loading histories may provide new insights into the role of mechanical stresses on the formation of bone. For example, a decline in daily activity level with age has been suggested as a factor that contributes to a loss of bone density. Also, some research suggests that osteoarthritis results from the cumulative effect of high impact forces and load rates. Current theoretical and experimental models depend on load magnitude, load rate, and number of cycles to predict bone-formation patterns. Our system is the only currently available method for accurate, long-term measurement of these variables in humans. This method may also be used to evaluate exercise activities in space and to establish equivalent loading histories compared to Earth activity levels.

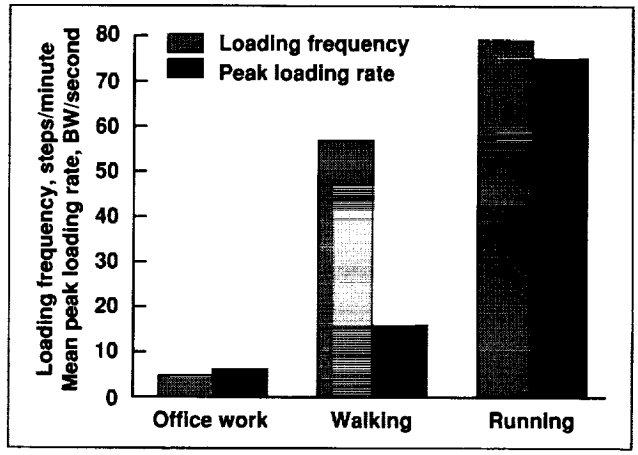


*Fig. 2. Average loading frequency and peak loading rate for running, walking, and sedentary office work.*

**Ames-Moffett contact: R. Whalen**
**(415) 604-3280**
**Headquarters program office: OSSA**

# Cosmos 2229

**James Connolly**

On the 29th of December, 1992, NASA Ames Research Center took part in the last of a series of eight joint U.S./Russian Biosatellite missions that have spanned a period of just over 20 years. Cosmos 2229, which flew from December 29, 1992, to January 10, 1993, carried 11 U.S. experiments. This brings to 104 the total number of U.S. experiments flown on these Russian unmanned biosatellites. Many life sciences disciplines have been represented, and important findings have emerged. Valuable pieces of flight and ground hardware, developed to support these joint missions, have had important applications for shuttle missions and will have applications for space stations in the future.

The Cosmos series of missions has contributed a large percentage of the accumulated information on the effects of microgravity on living systems. Various species, including microbes, plants, invertebrates, fishes, rats, and primates, have been used over the years to examine the effects of space microgravity on living systems. Each species has contributed an important piece to the puzzle of how biological systems adapt to the absence of gravity and how these processes relate to behavior in the gravitational environment of Earth.

The Cosmos 2229 mission focused on studies of the effects of microgravity on neurobiological, musculoskeletal, immunological, and regulatory mechanisms in the rhesus monkey. Data analyses are under way and published results from these investigations will soon be available. Much of the focus of this mission involved furthering research and pursuing insights gained from previous ground and flight studies. Key scientific objectives in neurosciences included investigating the processing of sensory inputs by the central nervous system, to aid in understanding the adverse vestibular effects experienced by crewmembers in space and by older people on Earth. Bone mineralization studies explored noninvasive methods to determine the source and degree of the increased bone fragility that was noted on earlier missions. The primary focus of the immunology studies was on assembling more information on the overall functioning of the immune system in response to the stress of spaceflight. Regulatory physiology studies in microgravity were designed to examine temperature regulation and circadian timekeeping, two critically important control mechanisms in vertebrates.

The Cosmos 2229 mission, like its predecessors, provided NASA with a testbed for new pieces of flight-support equipment. Ground and flight hardware were developed to support vestibular-ocular reflex, neuromuscular, bone bending strength, and temperature regulation experiments. Several elements of the flight hardware designed for this mission are being incorporated into the design of hardware for the next U.S. life sciences spacelab mission.

As part of the Biocosmos series of collaborative biosatellite missions, Cosmos 2229 represented the culmination of long-standing teamwork between scientists and engineers from Russia and the United States. The future holds many possibilities to extend this mutually beneficial working relationship, with opportunities for U.S. participation in a new series of Russian biosatellite missions. There will be expanding opportunities for joint experimentation on the Russian Mir space station, beginning with a kind of "exchange program" that will involve a U.S. astronaut aboard Mir and a Russian cosmonaut aboard the U.S. Shuttle. The joint use of resources by the two countries should substantially reduce costs and eliminate redundant scientific experimentation. At the same time, the future gains anticipated from continued biological research in space will be accelerated.

**Ames-Moffett contact: P. Davies**
**(415) 604-3608**
**Headquarters program office: OSSA**

# Secondary Payloads Flown on Space Shuttle Missions

**Joellen Jarvi**

In fiscal year 1993, NASA Ames Research Center managed four secondary-payload missions involving animal studies. Each flight carried one or more animal enclosure modules (AEMs) which housed groups of five to eight adult rats. There were two payloads within the Physiological Anatomical Rodent Experiment (PARE) series, PARE.02 and PARE.03, and two within the Physiological Systems Experiment (PSE) series, PSE.02 and PSE.03.

The AEM is an automated piece of hardware that houses adult rats within a self-contained habitat inside a standard middeck locker enclosure. In this function it is easily loaded and integrated and can thus fly more frequently than more complex habitats such as the Research Animal Holding Facility. Because of its automated mode, compact size, and inflight inaccessibility, it is best suited for simply designed experiments that primarily involve examining specific parameters before and after exposure to microgravity.

The 1993 PARE series payloads were focused on studies of the musculoskeletal system. In addition to the studies of the principal investigators, the payloads supported a biospecimen sharing program that made flight tissues available to a number of other researchers. PARE.02, which involved a 6-day flight launched on 13 January 1993, examined the routine contractile properties of antigravity skeletal muscle associated with peak twitch and tetanic force production and assessed the endurance properties of the muscle during repetitive contractions in an isometric mode. Preliminary analyses indicate that rodent antigravity muscles are functionally altered after only 6 days in microgravity.

PARE.03, launched 8 April 1993, was designed to examine several aspects of bone mineralization after a nine-day exposure to microgravity. The experiment yielded some surprising results. Postflight examination of tissues from flight animals showed a decrease in the production of certain chemical messages necessary for bone formation that was followed within 24 hours by a dramatic rise in these chemicals that leveled off within 72 hours of landing. This response could be a means of compensating for the slowed bone growth during flight. The significance of this finding is that it may give scientists a means of identifying the genes involved in initiating cortical bone formation, which could eventually lead to development of a drug to stimulate the production of new bone. Such a drug could have profound benefits both for astronauts on long-duration missions and for people on Earth who suffer from bone-weakening disorders.

The PSE series payloads were developed by Pennsylvania State University, one of NASA's Centers for the Commercial Development of Space (CCDS). PSE.02 was a 10-day mission launched 23 October 1993. PSE.03 was launched on 21 June 1993 and recovered 10 days later. Two AEMs were used on each flight to provide a replicate environment to improve statistical validity. As both PSE flights involved tests of proprietary pharmaceutical compounds, details of the experiment results have not yet been made public.

**Ames-Moffett contact: P. Davies**
**(415) 604-3608**
**Headquarters program office: OSSA**

# Results from Spacelab-J

**Kenneth Souza**

The STS-47 mission, launched on the Orbiter Endeavour in September 1992, carried as part of its payload the NASA/Japan-cosponsored Spacelab-J, which included life sciences microgravity experiments. Ames Research Center participated in this mission with the inclusion of two important life science payloads: the Autogenic Feedback Training Experiment (AFTE) and the Frog Embryology Experiment (FEE). Hardware for both investigations was designed, developed, and fabricated at Ames. A description of the experiment protocols and associated hardware appears in the Ames 1992 Research and Technology report. The present report emphasizes the scientific results from these two studies.

A high priority for NASA has been to find an effective treatment for space motion sickness. The AFTE uses a behavioral medicine approach that involves training in physiological self-regulation as an alternative to pharmacological treatment. The rationale for using AFT to treat motion sickness is based on the observation that there are profound autonomic nervous system changes associated with this disorder which are, although highly idiosyncratic, repeatable over time. Knowledge of the physiological and behavioral indicators of human adaptation to the microgravity environment are used in a behavioral-medicine training technique to facilitate adaptation. AFT has successfully increased tolerance to motion sickness during ground-based tests in over 200 individuals under a variety of test conditions.

For the SL-J mission, crewmembers underwent preflight training beginning 1 year prior to flight to provide a sound physiological database and to document the amount of physiological control obtained by the subjects as they became more proficient at using AFT. During the mission, the physiological responses of the control and AFT subjects were monitored and recorded for the first 3 mission days using the Autogenic Feedback System-2 (AFS-2). The AFS-2 is a portable battery-powered belt that records and displays several physiological parameters. AFT has now been tested on six crewmembers; a thorough testing requires 16 individuals in space, 8 treatment and 8 control subjects. Future studies are planned to obtain the necessary data for evaluating this treatment.

The FEE was designed to investigate the effects of microgravity on fertilization and development in the African clawed frog, *Xenopus laevis*. The amphibian egg is known to be particularly sensitive to gravity; on Earth, fertilized eggs rotate within the fertilization envelope so that the animal-vegetal axis is aligned with the gravity vector. Eggs experimentally inclined with respect to gravity form their dorsal structures on the side of the egg that is uppermost in the gravitational field. To examine whether gravity is required for normal development, four female frogs were artificially induced to ovulate in microgravity. Eggs were fertilized with a previously prepared sperm suspension and placed in plastic chambers, half of which were incubated in microgravity and the remainder incubated on a 1-gravity centrifuge. The centrifuge capability within the Frog Embryology Unit allowed an isolation of the microgravity effects of space from other spaceflight-related influences that may affect the experimental outcome. Ovulation was induced inflight and proceeded on schedule. Fertilization efficiency exceeded 70 percent in the centrifuge and microgravity flight groups. Gross morphology of embryos and larvae examined at a variety of developmental stages was generally similar in the flight microgravity and flight control groups, with some distinct differences: (1) a significant thickening of the blastocoel roof was present in the microgravity group; (2) blastopores of the microgravity group were displaced toward the vegetal hemisphere; (3) lung volume in the microgravity group was significantly smaller than that in the centrifuge control group; (4) swimming behavior of tadpoles fertilized preflight and launched at the neurula stage developed upwardly bent tails and swam in backward somersaults both during flight and immediately postflight; (5) tadpoles fertilized and hatched in space did not exhibit looping behavior similar to that of the larvae fertilized preflight; and (6) tadpoles in the microgravity group tested within 5 hours postflight for their ability to follow a rotating pattern of vertical stripes exhibited a stronger response than did the centrifuge control group.

**Ames-Moffett contact: P. Davies**
**(415) 604-3608**
**Headquarters program office: OSSA**

# Outer Heliosphere and Termination Shock

**Aaron Barnes**

The expansion of the solar wind into the local interstellar medium creates a cavity called the heliosphere. It is generally believed that the expansion of the wind changes abruptly from supersonic to subsonic flow at some heliocentric distance within the range of 50–200 astronomical units (AU), via a shock wave, usually called the heliospheric termination shock. Pioneer 10, at present the most distant spacecraft from the Sun, is located at more than 58 AU heliocentric distance near the solar equatorial plane. It is possible that the spacecraft will encounter the termination shock within the next several years. The Ames plasma analyzer aboard Pioneer 10 would be the primary instrument involved in making such a discovery.

In 1992 we developed a self-consistent gas-dynamic model of the response of the termination shock to upstream variations in the solar wind in order to estimate the speed of the shock as it moves back and forth. In 1993 this model was generalized in several different directions: (a) response to disturbance by an interplanetary gas-dynamic shock wave, (b) incorporation of a magnetic field within the model, and (c) incorporation of an energy sink that is a result of acceleration of energetic particles at the shock. In models (a) and (b) we find that, for typically observed variations in solar wind density, the shock speed would be approximately 50–200 kilometers per second, and a typical inward or outward excursion would be on the order of 1–10 AU; these conclusions are essentially identical to those of the previous gas-dynamic model, which therefore appears to be fairly robust. However, model (c) indicates that if energetic-particle acceleration is an important dynamical process at the shock, the motion of the disturbed shock would be substantially slower than in the gasdynamic case.

In 1991 there were frequent mass ejections from the solar corona, which propagated into the outer heliosphere. The entire heliosphere exhibited frequent high speeds not observed during other phases of the solar cycle. The subsequent period (through September 1993) was quieter and the heliosphere appeared to be approaching conditions more typical of solar minimum.

Plasma data from Pioneers 10 and 11 (Ames) and Voyager 2 (Massachusetts Institute of Technology (MIT)) have been reprocessed. The new ARC data set is basically the same as the earlier version, but it is statistically more complete; however, the MIT data set was significantly altered by the reprocessing. Consequently, we repeated an earlier comparison of the two data sets and found one major result to be different from that of earlier analyses. An apparent celestial-longitude asymmetry in temperature which, if real, could possibly have been a signature of interaction with the interstellar medium, disappears in the latest analysis. We now conclude that the outer heliospheric plasma data show no indication of interaction with interstellar material.

**Ames-Moffett contact: A. Barnes**
**(415) 604-5506**
**Headquarters program office: OSS**

# Carbon Soot in the Upper Troposphere and Lower Stratosphere

**David F. Blake**

In recent years it has become increasingly apparent that aerosol-size particles (those particles smaller than about 1 micrometer, or about one hundredth the diameter of a human hair) in the stratosphere can affect the climate and the environment on a global scale. The effects include (1) reduction of the amount of ozone in the Antarctic stratosphere. Ozone is thought to be catalyzed by reactions that occur on the surfaces of polar stratospheric cloud particles; and (2) the recent slight cooling of the Earth's atmosphere, thought to be caused by the injection of large amounts of sulfuric acid aerosol from the eruption of Mt. Pinatubo in the Philippines. Because of the importance of these changes, much effort has been put into detecting and monitoring trends in the types and amounts of natural and anthropogenic aerosols present in the upper troposphere and lower stratosphere.

We are collecting and analyzing carbon-soot aerosol particles from the upper troposphere and lower stratosphere to determine the amounts present there and the extent to which natural and anthropogenic sources appear to contribute to the soot load. Soot is collected on thin wires that are exposed to the atmosphere on the wings of DC-8 and ER-2 aircraft. These wires are then examined by scanning electron microscope, and the soot particles (which are about 0.1 micrometer in diameter) are counted and characterized. From the numbers of soot particles on the wires and the volume of air swept past the wires during their exposure in the upper atmosphere, absolute concentrations of soot per cubic meter of air can be calculated. We have made these calculations for samples collected from 45 degrees south latitude to 90 degrees north latitude. The results are plotted in part (a) of the figure.

The measured latitudinal distribution of soot at 10–11 kilometers altitude was found to correlate with commercial air-traffic fuel consumption (part (b) of the figure). Fuel burning by jet aircraft produces carbon-soot aerosol particles with a morphology similar to those collected on the wires.

The measured abundance, total mass, and total surface area of carbon-soot aerosol are

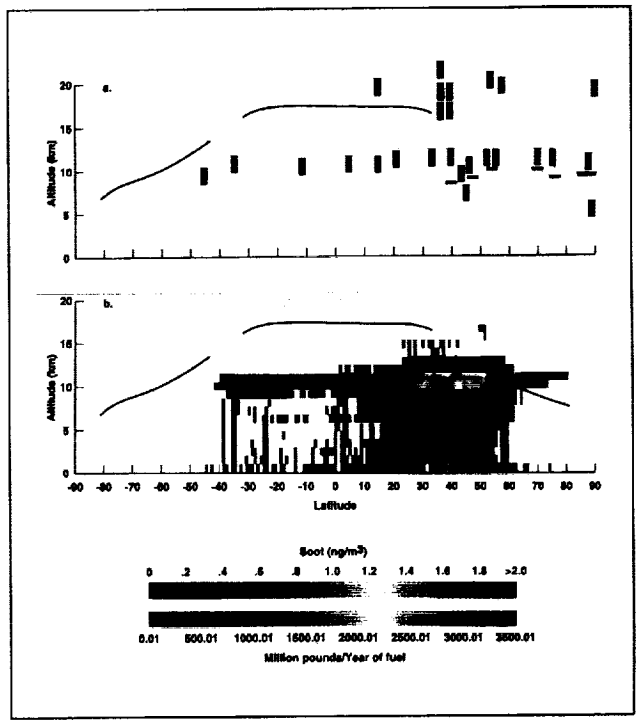


*Fig. 1. Comparison of observed upper-troposphere soot concentration and calculated aircraft fuel burning. (a) Observed soot concentrations in the upper troposphere and lower stratosphere. Tropopause height from 90 degrees south to about 35 degrees north, drawn as an idealized curve, as obtained from a reference publication. Tropopause heights from about 38 degrees north to 90 degrees north, drawn as discrete line segments on the plot, were measured during the flight on which the soot data at the same latitude were taken. (b) Fuel consumption by commercial aircraft during 1992. Idealized tropopause height drawn from a reference publication as in (a) above. Northern and southern hemisphere tropopause height is shown for wintertime. (See color plate 16 in Appendix)*

10–1,000 times less than those measured for naturally occurring sulfuric acid aerosol. It appears from this comparison that, relative to sulfuric acid aerosol, soot does not play a direct role in the chemistry of

the lower stratosphere or upper troposphere. It remains to determine the extent to which carbon-soot aerosol particles act as nuclei for sulfuric-acid aerosol formation. However, calculations of mass balance suggest that aircraft soot injected at altitude does not constitute a significant source of condensation nuclei.

Measured soot concentrations in the upper troposphere at tropical latitudes are uniformly low, suggesting that biomass burning does not contribute significantly to the carbon-soot load at this altitude. Low soot values in the lower stratosphere of these same regions indicate that very little soot penetrates the tropopause from these sources, but more data are needed before a quantitative assessment can be made with assurance.

**Ames-Moffett contact: D. Blake**
**(415) 604-4816**
**Headquarters program office: OSS**

## A Space Mission to Find Other Earth-Size Planets

**William Borucki, David Koch, Edward W. Dunham, Harold Reitsema**

A new method is being developed to detect planets orbiting other stars. The photometric method is the first practical method by which we should be able to determine how many other Earth-size planets exist in habitability zones of other stars. The method entails searching for Earth-size planets beyond our solar system by using a special telescope that can stare continuously at several thousand stars simultaneously while watching for eclipses. New telescope designs and detector technology make possible the observation of the large number of stars at the high precision required to find Earth-size planets. The mission is included in NASA's new Discovery class of better, faster, and cheaper missions.

The idea behind the detection method is straightforward. When a planet in orbit around a star passes in front of that star as viewed by an observer, the light from the star is dimmed by a small amount, as in an eclipse. The decrease in light will be much smaller than in a solar eclipse because the apparent size of the planet's disk relative to the star is very small when viewed from a great distance. Measuring this small change in the star's brightness requires the use of high-precision light detectors called charge-coupled devices (CCDs). These detectors operate on the same principle as those used in video cameras and camcorders. The brightness changes caused by planetary eclipses are so small that they are masked by the fluctuations in the atmosphere that cause stars to twinkle. Therefore, the telescope must be placed in orbit, above the atmosphere, to overcome the brightness fluctuations. By watching the stars for several years, it will be possible to determine which changes are due to the periodic eclipses associated with a planet orbiting a star (as in the case of the Earth orbiting the Sun once a year) and which are due to the natural, but less regular, variations in the star's brightness, such as those caused by star spots. Once two eclipses of a star have been seen, then the period, amplitude, and duration of future eclipses can be predicted and the discovery verified.

If current theories on the formation of planetary systems are correct, then roughly 50 planets beyond our solar system should be detected if 5,000 sun-like stars are monitored. (Because of the low probability of getting the appropriate geometric alignment, only 1% of planetary systems like our own will display transits.) If few or no planets are detected, then planetary systems like our own must be rare—the Earth might be unique in the Cosmos, and the theories of stellar and planetary formation must be revised.

**Ames-Moffett contact: W. Borucki**
**(415) 604-6492**
**Headquarters program office: OSS**

# Telepresence for Planetary Exploration

**Geoffrey Briggs**

Although the global characterization of Mars has not yet been achieved, plans are already under way to continue the surface exploration begun by Viking, including the deployment of mobile robots. Although robotic surface mobility has thus far been achieved only with difficulty for the Moon (the 1972 Lunakhods), United States and Russian missions are being developed that will provide limited mobility on the Martian surface, from which round-trip light-travel times reach 40 minutes. Such mobile laboratories, designed for sites where water may once have covered the Martian surface, will be important in the geologic and exobiological exploration of Mars. Eventually, human explorers will join the search for evidence of past primitive life on Mars, but they, too, will require mobile surface robots to extend their exploration across a planet which has a surface area comparable to the continents of Earth. Research at Ames is being carried out jointly by exobiologists, planetary geologists, and information-systems scientists to develop an effective human–robot control interface for Mars scientists—an interface that takes advantage of new telepresence and virtual-environment advances.

The Ames Telepresence Remotely Operated Vehicle (TROV)—a small, submersible robot that in December 1992 was successfully operated in Antarctica under telepresence control from Ames—has been substantially improved and has been returned to Antarctica for more testing under a joint NASA/National Science Foundation research agreement. Changes include the addition of a second camera (to provide stereo images), a manipulator arm, and a precision navigation system; and the use of fiber-optic cables to improve signal transmission to the surface. Operations are planned for the McMurdo Sound rather than the ice-covered lakes of the Dry Valleys. In the Sound the TROV will dive to depths inaccessible to human divers, in a truly exploratory mode. Telepresence control will be exercised from both the dive hole and from Ames (via satellite link). From Ames it will also be possible to control the vehicle in a virtual-environment mode in which the operations are first rehearsed in a computer memory (in which an increasingly detailed computer model of the local environment will be built, derived from the stereo images). Such operations will closely resemble the system required to operate a rover on the surface of a distant planet, where light-transmission delays introduce substantial complications.

It is somewhat serendipitous that it has been possible during the last year to demonstrate the use of the telepresence/virtual-environment interface for the control of a real planetary rover prototype, the Russian 1996 Marsokhod, over a satellite link. The Planetary Society and the McDonnell Douglas Corporation sponsored a tour of the Russian vehicle to several NASA centers in spring 1993. During an unplanned stop at Ames for several days, an effective interface between the Ames virtual-environment laboratory and the Marsokhod was created. The vehicle could then be driven around the Ames lunar-surface simulator under both direct (telepresence) and delayed (virtual environment) control. In October, the simulation was taken a major step forward when the Marsokhod was operated on a volcanic plain in Kamchatka, Russia, from California using the telepresence/virtual-environment interface (at the McDonnell Douglas Corporation). During the several-hour satellite hookup, the Marsokhod was directed to move and to acquire images that were then used to create a virtual environment of the test site.

The progress made in 1993 has set the stage for future demonstrations on Mars when the Jet Propulsion Laboratory's Rocky rover will be launched as a part of Mars Environmental Survey (MESUR) Pathfinder in 1996 and the Russian Marsokhod will be deployed as part of a comprehensive orbiter-lander-balloon program. Testing of the system will continue using Carnegie-Mellon University's Dante rover on the active volcano Mt. Spurr in Alaska in spring 1994.

**Ames-Moffett contact: G. Briggs**
**(415) 604-0218**
**Headquarters program office: OSS**

# Rims on Chondrules: Markers of Early Solar System Events

**Ted E. Bunch, Julie M. Paque**

Meteorites and their components provide insight into processes and physical/chemical conditions of the early solar nebula and other environments associated with the accretion of small bodies. Some of this information lies hidden in the somewhat mysterious fine-grained (less than 0.002-millimeter), dark, opaque rims of unequilibrated ordinary chondrites (UOCs) and carbonaceous chondrites. These rims have been considered by some researchers to be markers of major changes in elemental and isotopic compositions in the solar nebula. The researchers suggest that the rims are the result of dusty material melted by localized heat sources, then accreted as melt onto "cold" chondrules. In contrast, the formation of these rims has been considered by others to be not the result of nebular events, but rather to be the products of flash-heating events (e.g., transient atmospheric ablation) during planetary accretion. Production and/or modification of rims during atmospheric entry onto a parent body is a scenario that can be verified by examining ablation crusts produced on meteorites during their entry into Earth's atmosphere. Comparison of ablation-crust features with opaque rims on UOC chondrules will indicate whether this is a viable method for the production of chondrule rims.

Terrestrial ablation crusts on UOCs and carbonaceous chondrites have been examined both texturally and chemically. Ablation crusts have the following distinct characteristics. (1) The bulk composition of the crust is a reflection of the bulk chemistry of the host object, including similar sodium, potassium, and phosphorus levels but with the exception of much lower sulfur. (2) Boundaries between unmelted bulk meteorite and crust silicates are physically sharp over distances of microns, similar to the boundaries between rims and their chondrules. However, compositional transition zones extend inward from the boundaries for tens of micrometers. (3) Melted meteorite matrix in the crust is compositionally similar to unmelted matrix and is texturally and chemically similar to rims. (4) Mineral texture and chemistry at chondrule/rim and meteorite/ablation-crust interfaces indicate that significant thermal processing has occurred. Overall, the comparison of ablation crusts with rims strongly suggests that opaque rims are formed by the melting of dusty accretion mantles.

Calculations of rim melting that results from entry into a transient atmosphere of a parent body of low-scale height indicate that encounter velocities in the range of 2–4 kilometers per second are sufficient to melt the outer parts of chondrules. If the thermal conductivity of porous accretionary rims is as low as that of powdered chondrite, then gas-dynamic deceleration could have produced totally or partially melted rims on chondrules without melting the chondrule itself. The results of this work demonstrate that the formation of melt rims on chondrules is more consistent with short heating times (seconds to tens of seconds) associated with planetary environments than with any constrained event in the solar nebula.

**Ames-Moffett contact: T. Bunch**
**(415) 604-5909**
**Headquarters program office: OSS**

# Cometary Coma Chemical Composition (C4) Mission

**Glenn C. Carle, Ben Clark, Bonnie O'Hara**

Cometary exploration is very important to space science. Because comets are presumed to be remnants of the early solar nebula, they are expected to provide fundamental knowledge about the origin and development of the Solar System. They are also vital to an understanding of the source of volatile substances, and even life itself, in the inner Solar System.

The Cometary Coma Chemical Composition (C4) mission, a comet rendezvous mission, is now being studied as a candidate for the new Discovery program. This mission is a highly focused and usefully limited subset of the Cometary Rendezvous Asteroid Flyby (CRAF) mission. The C4 mission will concentrate on measurements that will produce an understanding of the composition and physical makeup of a cometary nucleus. The core scientific goals of the C4 mission are (1) to determine the chemical, elemental, and isotopic composition of a cometary nucleus; and (2) to characterize the chemical and isotopic nature of its atmosphere. A related goal is to obtain temporal information about the development of the cometary coma as a function of time and orbital position.

Four short-period comets—Tempel 1, Tempel 2, Churyumov–Gerasimenko, and Wirtanen—which all appear to have acceptable dust production rates were identified as candidate targets. Mission opportunities have been identified beginning as early as 1998. Tempel 1, with a launch in 1999, however, is the baseline comet for studies and planning of the C4 mission.

The C4 mission incorporates two scientific instruments and two engineering instruments in the payload to obtain the desired measurements. The scientific instruments are (1) an advanced version of the Cometary Ice and Dust Experiment (CIDEX)—a mini-CIDEX with a sample collection system, an X-ray fluorescence spectrometer, and a pyrolysis-gas chromatograph; and (2) a simplified version of the Neutral Gas and Ion Mass Spectrometer (NGIMS). These instruments have substantial history; they are based on those developed for the CRAF mission. The engineering instruments are a simplified Comet Dust Environmental Monitor (SCODEM) and a navigational camera, NAVCAM. Whereas neither of these instruments will be permitted to establish research requirements, it is anticipated that significant scientific returns will be obtained.

**Ames-Moffett contact: G. Carle/B. O'Hara**
**(415) 604-5765/5770**
**Headquarters program office: OSS**

# Catalytic Decomposition of Methane by the Photolysis of Acetylene

Samuel M. Clegg, Thomas W. Scattergood

The photochemistry of the outer planets and satellites is dominated by hydrocarbon reactions, because of the presence of a relatively large amount of methane ($CH_4$). Acetylene ($C_2H_2$), a product of the photolysis of methane, is also photolyzed to produce other gases, including methane, ethane ($C_2H_6$), ethylene ($C_2H_4$), and propane ($C_3H_8$). Previous experimental results determined that the photolysis of acetylene will catalytically decompose methane and produce methyl radicals ($CH_3$). The reaction of two methyl radicals would result in the production of ethane. This could explain the production of ethane in Titan's atmosphere, where there is an atmospheric average of about 6% methane.

In a typical acetylene photochemical experiment, the amount of methane produced increases with increasing acetylene pressure. When acetylene is photolyzed in the presence of methane, methane is catalytically decomposed, which results in a decrease in the amount of methane remaining in the sample, as shown in the first figure. The amount of methane that is catalytically decomposed depends on the amount of methane present in the original sample;

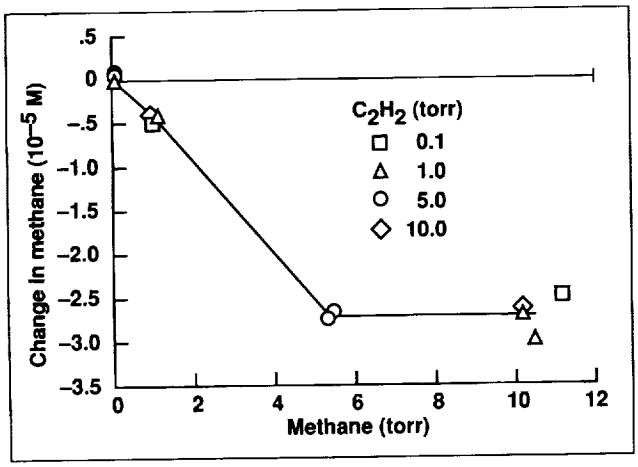


*Fig. 1. The catalytic decomposition of methane by the photolysis of acetylene ($C_2H_2$).*

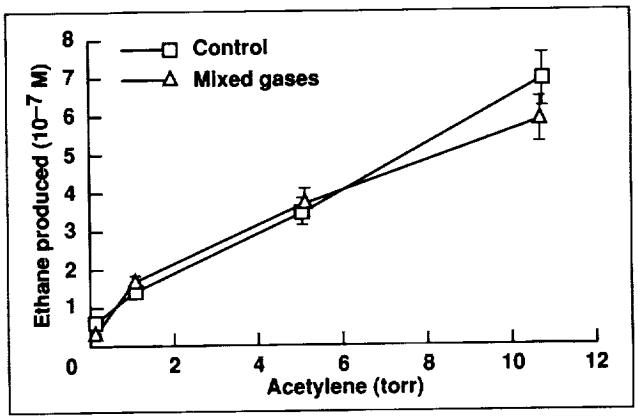


*Fig. 2. The production of ethane by the photolysis of acetylene with and without methane present in the original sample.*

that is, as the methane pressure in the original sample increases, the amount of methane catalytically decomposed increases. Theoretically, this would lead to an increase in the amount of ethane produced in the experiments. The second figure shows, however, that the catalytic decomposition of methane did not produce an increased amount of ethane compared to the amount produced by the photolysis of acetylene alone.

Therefore, the catalytic decomposition of methane by the photolysis of acetylene does not explain the production of ethane in Titan's atmosphere. However, experimental results reported within the last year indicate that the photolysis of methane does produce methyl radicals that will react to produce ethane, a reaction believed not to have been previously observed.

**Ames-Moffett contact: S. Clegg**
**(415) 604-3219**
**Headquarters program office: OSS**

# Particle–Gas Dynamics in the Protoplanetary Nebula

**Jeff Cuzzi**

Flattened disks of dust and gas have been shown to form as a natural byproduct of stellar formation. The global thermal and dynamical properties of these disks have been established. The physical and chemical properties of primitive meteorites provide clues to these processes.

Our paper on particle–gas dynamics in a settled midplane layer of centimeter- to meter-sized particles is in press. Our self-consistent numerical models of particle settling and diffusion in self-generated turbulence clearly show that gravitational instability in a settled particle layer is much more difficult to achieve than was previously thought, if not impossible. We completed an extension of the model to include a particle size distribution. The importance of this is that more easily dispersed, smaller particles might sap the turbulent energies and smooth the overall velocity gradient responsible for maintaining turbulence to the point where the largest particles might be able to achieve gravitational instability. New and interesting behavior is seen in the coupled solutions, but the gravitational instability still appears to be beyond reach even for meter-size particles. A second paper is in preparation.

In a second thrust, we have implemented on the Numerical Aerodynamic Simulation (NAS) supercomputer (the Cray Y-MP) a fully three-dimensional direct numerical simulation model of solid particles in turbulence. The model was developed by K. Squires and J. Eaton, then of Stanford University. We have extended this model to larger grids, converted it to the Y-MP, and added a variety of visualization and classification schemes to explore the clumping of appropriately sized particles in turbulence. We have found that clumps develop that are on the order of the Kolmogorov length scale in their smallest dimension. The particles so affected seem to be of sizes that agree well with size-sorted "chondrules" in primitive meteorites. Even as clumps get stretched out in shear regions between turbulent eddies, particles remain concentrated to a degree much higher than average. Our belief is that this process might be responsible for the first accumulation of planetesimals, with sizes of tens to hundreds of meters. We next plan to incorporate the effects of particle damping in turbulence on clump stability and longevity.

**Ames-Moffett contact: J. Cuzzi**
**(415) 604-6343**
**Headquarters program office: OSS**

# Planetary-Ring Dynamics and Morphology

**Jeff Cuzzi**

Planetary ring systems are quite similar to each other in their combinations of diffuse rings of material interspersed with belts or ensembles of mountain-sized "moonlets." We hope to understand these similarities in terms of the conditions of formation and the operation of similar processes in different environments. From an understanding of the structure and dynamics of planetary rings, we hope to gain insight into the process by which planets form from their own protoplanetary particle disks. The work involves a group which includes J. Scargle and C. Levit (Ames Research Center), R. Hogan (Synernet, Inc.), A. Dobrovolskis and L. Dones (University of California, Santa Cruz), M. Showalter (Stanford University), and K. Young (National Research Council Fellow).

We completed a detailed study of color variations in the main rings of Saturn using the complete set of highest quality Voyager-2 color image data. Images were scanned and profiles combined into ratios. Different regions of the rings display significant variations in their spectral shape between 3,500-, 4,000-, and 5,500-angstrom filters, clearly indicating particle composition differences. Not only are the C ring and Cassini Division compositionally distinct from their surroundings with transitions on 1,000-kilometer-length scales, but within the B ring several distinct subregions are found which exhibit color variations on a radial scale of a few hundred kilometers. The subregions differ in the spectral shape of these variations. These results indicate a degree of compositional heterogeneity that is intriguing from the standpoint of ring origin. The short radial length scales in the B ring, in light of rapid dispersal processes, argue for geologically recent events. These results will help guide observations by the Cassini spacecraft.

In a second effort, we performed detailed numerical integration of the orbits of tens of thousands of test particles under the nonlinear, simultaneous gravitational perturbations of several nearby "ringmoons" in the outskirts of the Saturn ring system. The results displayed for the first time that material evolves in a chaotic fashion over a much larger region than was previously believed. That is, orbits of any small objects in the region can be perturbed into a state in which orbit crossings and ongoing collisions are common. These results cast doubt on the prevailing concept that the "kinky" F ring of Saturn can be a steady-state feature, and supports the idea that it is merely one of a succession of transient features that might appear in the region. These models can be easily extended to the ringmoon systems of Jupiter, Uranus, and Neptune, in which similar ensembles of closely spaced moonlets are found.

**Ames-Moffett contact: J. Cuzzi**
**(415) 604-6343**
**Headquarters program office: OSS**

# The Ames Submillimeter Array Photometer

**Jacqueline A. Davidson, Thomas Roellig, Maureen Savage**

Since 1990, we have been developing a ground-based, background-limited, submillimeter/millimeter array photometer for astronomical observations. Within the past year, the photometer construction has advanced to the point where it can be tested in the laboratory. The photometer is optimized for operation at 730- and 870-micrometer wavelengths, but it also operates at 1.1 millimeters. It uses an array of 5 × 5 monolithic bolometer detectors, each illuminated through diffraction-limited light concentrators. The photometer will have its first engineering run on the telescope in 1994, but is expected to achieve a system noise equivalent flux density of about 0.1 jansky/$\sqrt{\text{hertz}}$ and spatial resolution of 25 arc-seconds at 800 micrometers on a 10-meter telescope such as the Caltech Submillimeter Observatory (CSO) in Hawaii. This sensitivity will enable measurements of 10-millijansky sources (such as radio-quiet quasars) to a signal-to-noise level of 5 in half an hour of integration. The photometer will be able to achieve this sensitivity because the array of bolometers will allow for the subtraction of correlated sky noise (a common problem in the submillimeter range) and the bolometer detectors will be cooled to temperatures below 0.1 kelvin. To achieve these low temperatures we have constructed, in collaboration with colleagues at the University of

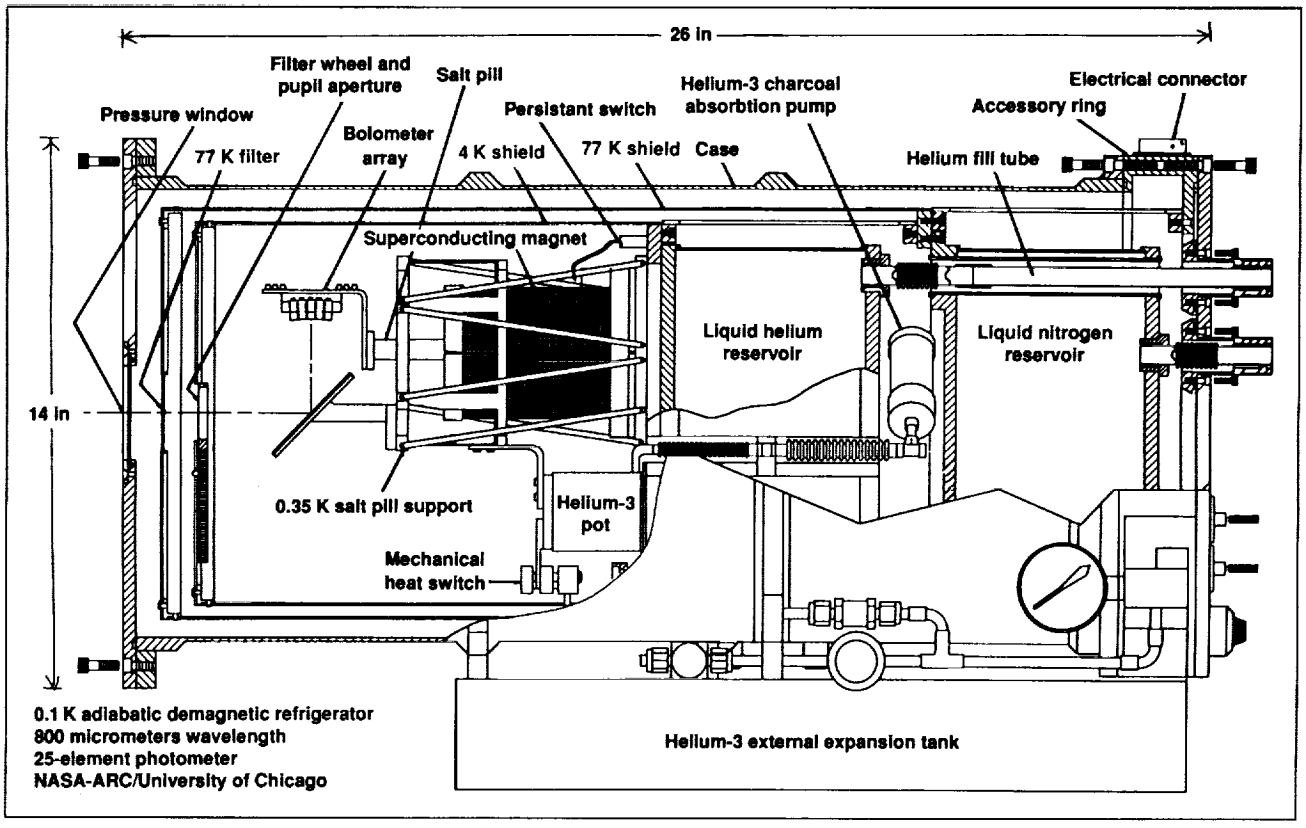


*Fig. 1. Cutaway view of the Ames submillimeter array photometer, showing the adiabatic demagnetization refrigerator.*

Chicago, an adiabatic demagnetization refrigerator (ADR) to cool the 25 bolometers and their optics. This refrigerator is housed in the photometer, as shown in the figure. The ADR consists of a paramagnetic salt pill that lies in the core of a superconducting magnet. Our design suspends the salt pill by means of a helium-3-cooled support structure. This design allows for operation of the photometer on the telescope without pumping on the helium-4 reservoir. Once the ADR is optimized, it is expected to maintain a temperature of $0.10 \pm 0.01$ kelvin for over 15 hours.

The Ames ADR photometer is scheduled for first use on the CSO in late August 1994. The initial observations will be made of distant quasars and of cold, dark clouds in the outer parts of our galaxy.

**Ames-Moffett contact: J. Davidson**
**(415) 604-5531**
**Headquarters program office: OSS**

## Thermal Springs: Fossil Sites on Earth and on Mars?

**David J. Des Marais, Jack D. Farmer**

Fossilized bacteria are plentiful in the mineral deposits surrounding volcanic hot springs such as those in Yellowstone National Park. Some dry stream channels in volcanic regions on Mars appear to emerge from springs. By delivering water and dissolved nutrients to the sunlit surface of Mars, springs could have been ideal sites for supporting life on an otherwise dry and hostile planet. On Earth, the temperature and chemical gradients associated with thermal springs support a diverse population of organisms (see first figure). The precipitating minerals can entrap bacteria and preserve them. Thus, the search for fossils on both Earth and Mars should target ancient spring sites. Our research team included Malcolm Walter (Macquarie University, Sydney, Australia) and Nancy Hinman (University of Montana).

As a first step, we located and examined ancient spring deposits for fossils. The bacterial colonies create distinctive surface textures in the opal deposits that vary as temperatures decline away from the spring. We investigated whether these textures are preserved as the silica, deposited initially as opal, is converted to quartz. In North America, we found the distinctive bacterial textures in deposits ranging in age from a few thousand to several million years. These were located in Yellowstone National Park and Steamboat Springs, Nevada. In the Drummond Basin, Queensland, Australia, we confirmed that 300-million-year-old quartz spring deposits had retained many of the surface textures we had observed in Yellowstone National Park. These

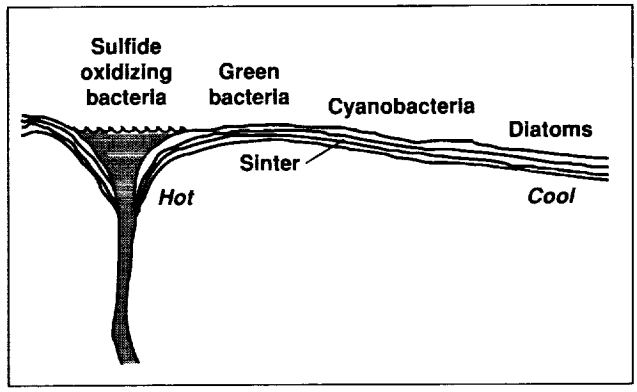


*Fig. 1. Schematic cross section of a thermal spring, showing the stream, deposits, and microorganisms often found there.*

*Fig. 2. Dao Valles, near Hadriaca Patera, Mars. This feature (lower middle of photo) has been interpreted to be a large spring on the flanks of an ancient volcano (upper middle of photo).*

quartz deposits are highly resistant to weathering; therefore they are good prospective areas for finding preserved fossils.

Thermal springs create features that can be detected by remote sensing. These features include rock alteration by the heated waters and the spring deposits themselves. Alterations in rock can be identified by detecting variations in the rock's magnetic properties and in the spectral characteristics of reflected sunlight. The siliceous or carbonate spring deposits can be detected in the infrared region of the light spectrum. On Earth, these approaches have been used successfully to search for hydrothermal ore deposits. Future orbital missions will examine both visible and infrared radiation from Mars. A search for ancient spring sites such as the one shown in the second figure will be an important first step in the search for an ancient Martian biosphere.

**Ames-Moffett contact: D. Des Marais**
**(415) 604-3220**
**Headquarters program office: OSS**

## Airborne Astronomy

**Edward W. Dunham, Edwin F. Erickson, Jacqueline A. Davidson**

For the past quarter century, an airborne astronomy program has been conducted from Ames Research Center that provides observation opportunities for astronomers from both domestic and foreign institutions. The program's major facility is the Kuiper Airborne Observatory (KAO), a 0.9-meter telescope in a Lockheed C-141 aircraft. The broad spectral regime accessible from the telescope's operating altitude of 41,000 feet, and its ability to deploy to locations around the world, allows investigation of a wide variety of astrophysical processes.

This year, astronomers have used the KAO to make observations of (1) organic molecules in the interstellar medium, (2) star-forming regions, (3) our galactic center, (4) starburst galaxies, (5) calibration objects for the European Infrared Space Observatory (ISO), (6) Saturn's satellite Titan, and (7) an occultation of a star by Neptune's satellite Triton during 49 flights from Moffett Field, New Zealand, Hawaii, and Punta Arenas, Chile. The total number of flights was low because of unexpected delays in the installation of a new shear-layer control system and an upgraded computer system. Once the KAO began flights in March, the success rate was high, with only four aborted flights.

The KAO is under continuous technical development to improve its reliability and scientific performance. Activities this year included completion of a major upgrade to the on-board computer systems and replacement of the shear-layer control "fence" with a fairing aft of the telescope cavity. A continuing program will result in significant improvements in near-infrared image quality. Work in progress includes tuning of the telescope's pointing control system, modification of the cavity's environmental control system, and investigation of the parameters of systems that could be used for image-motion compensation.

New questions arise that require observations of fainter objects and observations with better angular resolution. These needs will be filled by the Stratospheric Observatory for Infrared Astronomy (SOFIA), the proposed next step in the airborne astronomy program. SOFIA will carry a 2.5-meter telescope in a Boeing 747 aircraft, and will achieve about ten times better sensitivity and three times better angular resolution than the KAO. The following questions will be addressed by airborne astronomers using SOFIA: What is the structure, composition, and chemistry of planetary atmospheres? How do protoplanetary disks form and evolve? How are bipolar outflows and disk formation involved in star-birth processes? Is there a black hole at our galactic center? How do stars form in different types of galaxies? What fuels starbursts and active galactic nuclei? The National Research Council's report on priorities in astronomy and astrophysics in the 1990s (the Bahcall report) places SOFIA as the highest-priority new NASA initiative in the moderate-cost category.

Since much of the radiation in the universe is found at infrared wavelengths that are not observable from ground-based telescopes, SOFIA's ready and frequent access to these wavelengths will provide a capability critical to the understanding of many important astronomical phenomena. The United States has established world leadership in infrared science through detector technology, the KAO, the Infrared Astronomy Satellite (IRAS), and the Cosmic Background Explorer (COBE). If developed as planned, SOFIA will continue this tradition. Its development will start in 1995, and operations will begin just after the turn of the century.

Historically, SOFIA has been planned as a collaborative venture, with the United States providing the aircraft and associated systems and Germany providing the telescope. After several years of uncertainty as a result of events in Germany, German participation now appears more likely. This year, researchers at Ames and in U.S. industry carried out studies of critical-path technology items, and a plan for largely in-house development at Ames was formulated. The projected cost of the project has been reduced by plans to use existing hangar facilities for integration and testing and by use of in-house manpower.

**Ames-Moffett contact: E. Dunham**
**(415) 604-5523**
**Headquarters program office: OSS**

# Exploring the Solar System Through Stellar Occultations

**Edward W. Dunham**

Recent observations have revealed the first of what is likely to be a large population of small, icy bodies in the most distant reaches of the Solar System. These objects are similar in size to the asteroids, but are much more distant from the Sun, and are most likely made of ices rather than silicate rocks. A similar, but very large and nearby, object is Chiron, which has an orbit lying between those of Saturn and Uranus. Even the most basic properties of Chiron, its size and surface brightness, are unknown but could be determined by means of a stellar occultation. In addition, if Chiron is icy, it may have a tenuous "atmosphere," or coma, like a comet. The dust in the coma would also be detectable in an occultation of a bright star.

Realization of the promise of the stellar-occultation method is dependent on the availability of suitable instrumentation and of timely, reliable prediction of occultations. The investment in instrumentation over the last two years bore fruit this year. The large-format charge-coupled device (CCD) camera system used with the Crossley telescope at Lick Observatory successfully provided prediction astrometry for an occultation by Triton and another by the Pluto/Charon system. A portable CCD occultation photometer system was completed; it successfully recorded the Triton occultation aboard the Kuiper Airborne Observatory (KAO). This observation was made in collaboration with J. L. Elliot and C. Olkin from Lowell Observatory. A near-infrared array camera system was successfully modified for occultation work at Lick Observatory by K. Gilmore and D. Rank, but was not used aboard the KAO because we were able to predict, before departing on a deployment to Australia, that the occultation track of Pluto would pass north of the Earth, while the track of its satellite, Charon, would graze Antarctica. Although it was disappointing to discover that the occultation would not be observable, it was pleasing to see the precision of the prediction, a few hundred kilometers error at a distance of 4.5 billion kilometers!

Next year, improvements to the astrometric procedures will be a major focus. Improvements will be made in three areas: (1) increased accuracy of the prediction early in the prediction process in order to ease the burden of logistical planning for the occultation observation; (2) an increase in the ultimate accuracy of the prediction, allowing application of the stellar-occultation method to smaller and/or more distant objects; and (3) reduction of the effort required to produce a reliable prediction. In addition, a major effort will be made to observe an occultation by the enigmatic object Chiron to determine its size and surface brightness.

**Ames-Moffett contact: E. Dunham**
**(415) 604-5523**
**Headquarters program office: OSS**

# Site Selection for Mars Exobiology

Jack D. Farmer, David J. Des Marais

Results of the Viking life-detection experiments suggest that living organisms do not now exist in surface environments on Mars. However, liquid water, regarded as a basic requirement for terrestrial life, was apparently abundant on Mars earlier in its history, evidenced by the presence of extensive channel networks, large lake basins, and possibly even a global ocean. Given the wetter and warmer conditions that existed on Mars earlier in its history, microbial life may have evolved and flourished there for a time and then become extinct in surface environments as the planet lost its atmosphere and began to cool. To evaluate the possibility that there was life in the past on Mars will require the systematic exploration of the planet for a fossil record. Given the vast number of potential sites on Mars, how can we best optimize this search for a fossil record? More important, what can we do now to lay a foundation for future exploration efforts?

In collaboration with colleagues at Arizona State University and the U.S. Geological Survey, we have been developing methods for the selection and prioritization of exobiological sites on Mars using Viking data. Initially, potential sites were screened for geomorphic criteria believed to be indicative of past hydrological activity. Geological terranes of prime interest included fluvial-lacustrine (stream-fed lakes), spring (both subaerial thermal and subaqueous), and high-latitude (above 40°) periglacial environments, where stable ground ice may exist. Sites possessing features indicative of hydrological systems of longer duration (e.g., channel networks with higher-order tributaries) and basinal areas lying at low elevation (see figure) were assigned a higher priority because of the enhanced opportunity for accumulation of a sedimentary record in these areas and because of the persistence of liquid water near or at the surface, as a result of higher atmospheric density.

The study began with a review of the 83 sites listed in the Mars Landing Site Catalog (MLSC) (a NASA Reference Publication), and was subsequently expanded beyond the MLSC to include a broad-based regional reconnaissance of Mars (still under way). Our preliminary study resulted in the identification of 25 sites of exobiological interest. Detailed descriptions and exploration strategies for each site will appear in the second edition of the MLSC along with a review of our methodology.

*Fig. 1. Parana Valles, the Margaritifer Sinus region of Mars. Note the well developed dendritic valley systems that terminate along the northeast margin of the basin, the proposed target area for high-resolution imaging and infrared spectroscopy.*

It is essential that high-priority exobiology sites be represented in site recommendations for high-resolution remote imaging during future orbital missions. Remote imaging of these sites will ensure the availability of detailed geological and compositional information needed to refine site priorities for future Mars surface missions. Over the past year, recommendations for high-resolution imaging were

presented to imaging teams for both Mars Observer and Mars '94/'96. Site recommendations were also used to refine landing targets for the Mars Environmental Survey (MESUR) Pathfinder mission. We are continuing to develop our methods for site selection and to expand and refine exobiological priorities for future high-resolution imaging. This information will provide a basis for detailed landing-site studies for exobiology, as well as for the development of site-specific exploration strategies for future surface missions.

**Ames-Moffett contact: J. Farmer**
**(415) 604-5748**
**Headquarters program office: OSS**

## Integrated X-Ray Laboratory Breadboard Module for Mars Geologic Exploration

**Mark L. Fonda**

An integrated X-ray fluorescence/X-ray diffraction (XRF/XRD) breadboard module was developed and successfully tested to demonstrate the feasibility of combining these two powerful techniques.

The XRF/XRD module, developed by the ARACOR Corporation under the NASA Small Business Innovative Research Program, is illustrated in the first figure. The module combines XRF/XRD techniques while using a thinned, backside-illuminated, charge-coupled device (CCD) detector configuration. The module uses an iron-target, 9-watt X-ray tube with a 10-millicurie, cadmium-109 isotopic X-ray source. The operation of the X-ray tube is filtered with a manganese potassium-edge filter, creating a monochromatic beam covering a diffraction d-spacing range of 1.5–13 angstroms while also allowing for detection of elements from oxygen to chromium.

In order to meet Mars mission-compatibility constraints, a nonscanning powder camera configuration was chosen; a specific X-ray tube was selected to reduce power consumption to below 15 watts; and a specific geometry below 20 centimeters was chosen to limit examination time for a sample to less than

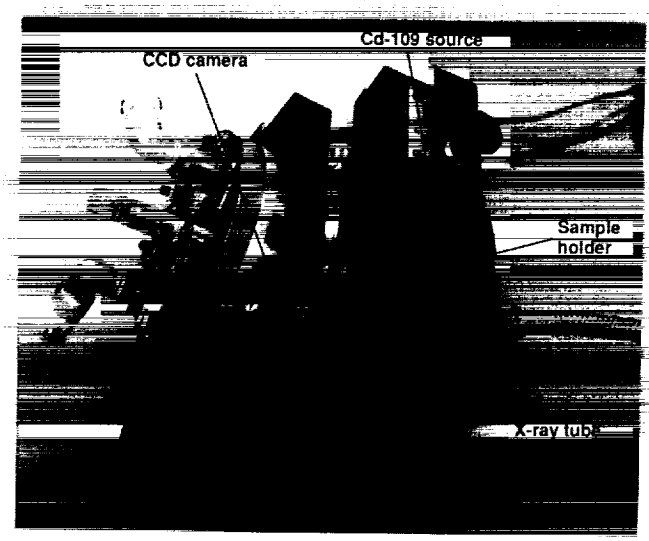


*Fig. 1. XRF/XRD breadboard module.*

4.5 hours. Once assembled, a filtered, collimated X-ray beam was diffracted over a wide range of angles, producing a diffraction signature of several different sample mixtures on a stationary, commercial CCD detector.

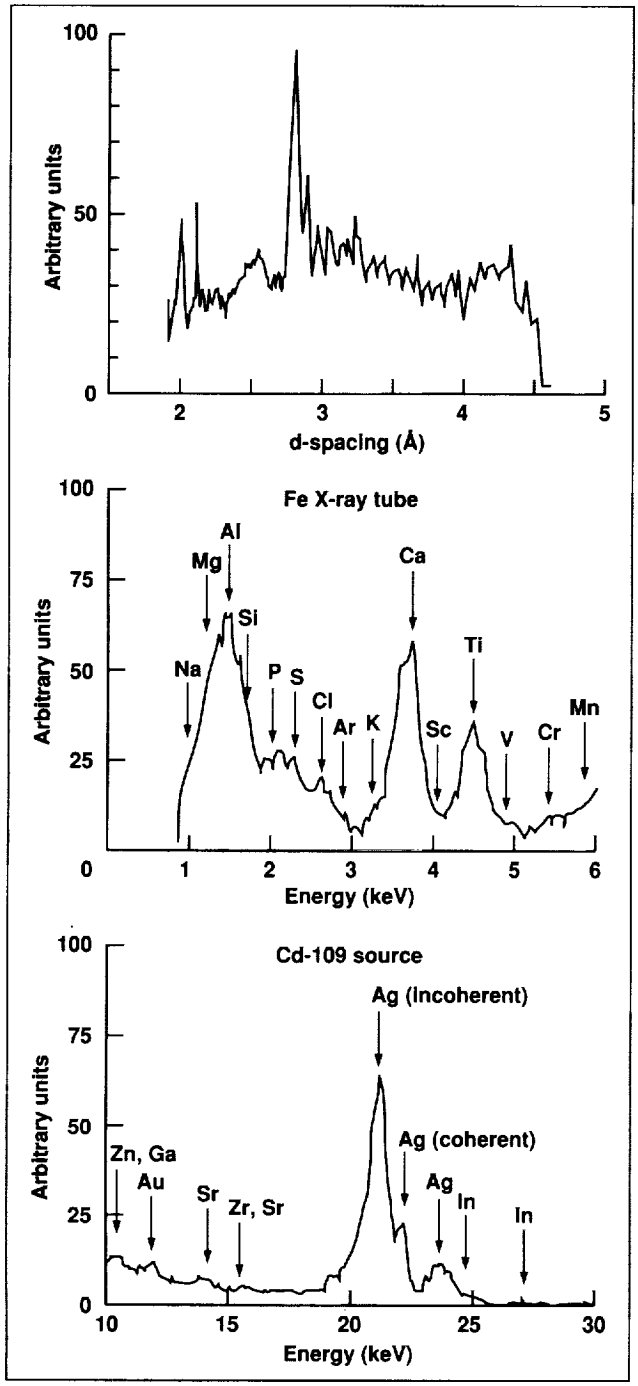


*Fig. 2. Representative XRF/XRD breadboard test results. Top graph: XRF/XRD diffraction signature for halite; middle and bottom graphs: XRF/XRD fluorescence analysis of 80% palagonite/20% mineral mixture.*

The data recorded by the CCD was used to form the diffraction pattern. The image was divided into concentric arcs about 0.05 degree wide, and the total number of events contained within each arc was determined. The geometry of the CCD and the sample analyzed establishes the relationship between a particular arc location on the CCD and the corresponding d-spacing. This was used to produce plots of the number of events as a function of d-spacing. Fine-grained sample mixtures, approximately 10 milligrams per sample, were placed in the sample holder and analyzed.

A series of XRD/XRF experiments was run to determine the spectral and d-spacing resolution performance parameters of the module as well as the impact of the small diffractometer radius on the identification of the samples tested. Our test approach included a series of pure crystalline samples, such as halite, to determine d-spacing resolution and to characterize the signal-to-background noise ratio; we followed these pure sample tests with more complicated mixtures of crystalline and amorphous samples to demonstrate the module's ability to identify major constituents in the mixture. The experiments were performed in a simulated Martian environment consisting of an atmosphere of 8 torr of $CO_2$ at a temperature of –50°C. Examples of measured results involving a sample mixture of 80% palagonite and 20% crystalline materials are illustrated in the second figure.

**Ames-Moffett contact: M. Fonda**
**(415) 604-5744**
**Headquarters program office: OSS**

# Gravity-Independent Solid-Particle Generator

**Mark L. Fonda, C. Fred Rogers**

A gravity-independent solid-particle generator breadboard was developed by TRW Inc., under NASA contract, to support the Gas-Grain Simulation Facility (GGSF) experiment and hardware studies. The GGSF is a multidisciplinary research facility being developed at Ames Research Center. An examination of the scientific and technical requirements for the GGSF revealed a need for dry-particle generation with a particle size range of submicrometers to tens of micrometers, and particle concentrations of less than one to more than $10^8$ per cubic centimeter.

The test setup for the development effort is shown in the first figure. It consists of a sample holder, a dilution section, an aerodynamic deagglomerator, and a test chamber, together with control circuitry, optical diagnostics, and a particle-collection system. The sample holder accommodates up to 200 milligrams of dry powder, which is mixed with dilution air in the dilution section. The deagglomerator consists of closely matched, mating cones spaced to provide a conical, annular gap in which strong aerodynamic shear is accomplished with small volumes of carrier gas. The deagglomerated particles are delivered to the test chamber which, in the current version, is a transparent cylinder equipped with optical and filter-sampling ports. The sample holder and dilution section are unique, gravity-independent components developed in the course of this research. To quantify performance, several

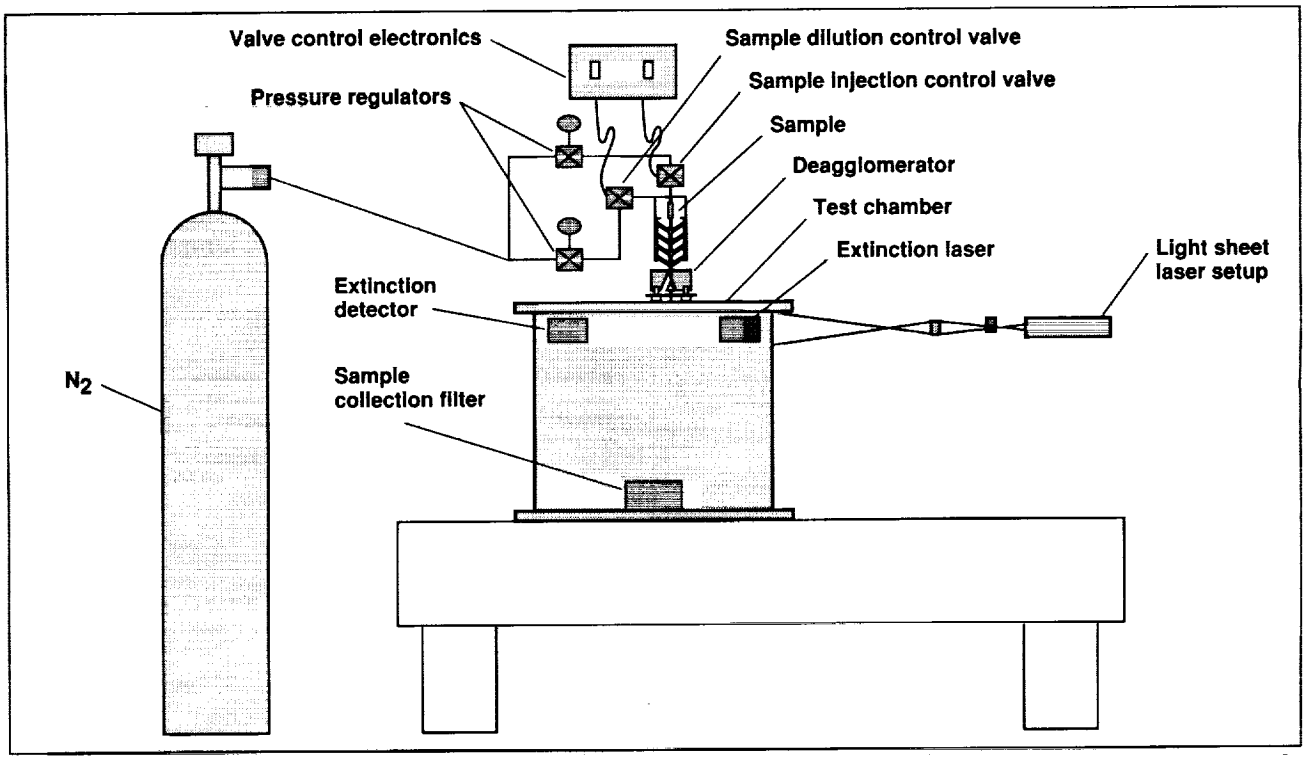


*Fig. 1. Breadboard test configuration.*

diagnostic techniques were used. The primary method involved collection of the dispensed particles on a filter and subsequent optical or scanning-electron-microscopic determination of the percentage of monoparticles. A laser beam passing in front of the particle-generator output was monitored for extinction as another diagnostic, since dilution of the particles was found to be related to the percentage of monoparticles.

A third diagnostic was employed for a limited time in order to qualitatively monitor the cloud motion in the test cell after dispensing. This was a sheet of laser light optically viewed.

To verify the adequacy of the developed particle-generator concept, a series of performance tests were carried out using representative particle samples of 2.1- and 10.2-micrometer glass spheres, and 5–10-micrometer geological dust. Tests with these samples were performed as a function of carrier-gas pressure and aerodynamic slit width. Deagglomeration data were obtained at 30, 60, and 120 pounds per square inch (gauge) pressure, for slit widths of 39, 79, and 118 micrometers and concentrations of approximately $1 \times 10^{-4}$ grams/centimeter$^3$ to approximately $15 \times 10^{-4}$ grams/centimeter$^3$, with at least three concentrations for each pressure and slit width. The second figure illustrates the test results for deagglomeration efficiency as a function of pressure.

These tests indicated that predictable and repeatable results can be obtained from the particle-generator concept, although particle concentrations were not high enough to meet the entire range of GGSF requirements. The most significant findings

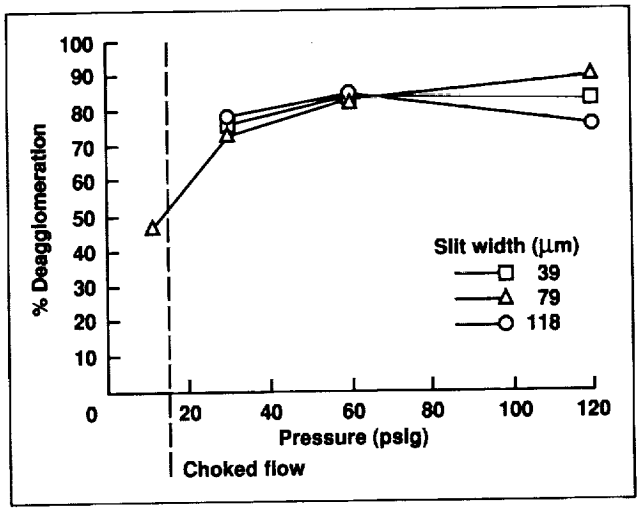


*Fig. 2. Test results for deagglomeration efficiency as a function of carrier-gas pressure.*

were that the solid-particle generator can achieve better than 90% deagglomeration, and that the repeatability was approximately 10%.

Future plans for the solid-particle generator include further sample-holder and dilution-section studies aimed at increasing the particle throughput, and tests of the deagglomeration efficiencies for particles in the 0.1–1.0-micrometer size range.

**Ames-Moffett contact: M. Fonda/C. Rogers**
**(415) 604-5744/0527**
**Headquarters program office: OSS**

# In Situ Particle-Measurement Concept for Aerosols

**Mark L. Fonda, C. Fred Rogers**

A broad-range diagnostic tool was required for performing nonintrusive, in situ measurements of particle size (0.01–1,000 micrometers) and concentration (up to $1 \times 10^8$ particles per cubic centimeter) in support of the Gas-Grain Simulation Facility (GGSF) experiment and hardware advanced-technology development studies. The GGSF is a multidisciplinary research facility being developed at Ames Research Center. The feasibility of measuring particles smaller than 1 micrometer and at varying concentrations up to $1 \times 10^8$ per cubic centimeter using ensemble diffraction techniques was demonstrated by Insitec Measurement Systems, Inc., under a NASA Phase-I Small Business Innovative Research contract.

The feasibility study entailed redesigning the optical system of a current in situ optical light-scattering device to perform large-angle light-scattering measurements with high sensitivity. The system needed the capability to measure the smaller particle sizes (0.01–1 micrometer) at dilute particle concentrations. The existing signal processor and software were modified to perform real-time measurements in an evolving planetary aerosol simulation experiment. A large-angle optical system was breadboarded and integrated with an existing NASA-provided optical reaction vessel in which polymerization reactions of acetylene that produced submicrometer-sized particles were performed. The first figure is a schematic diagram of the test

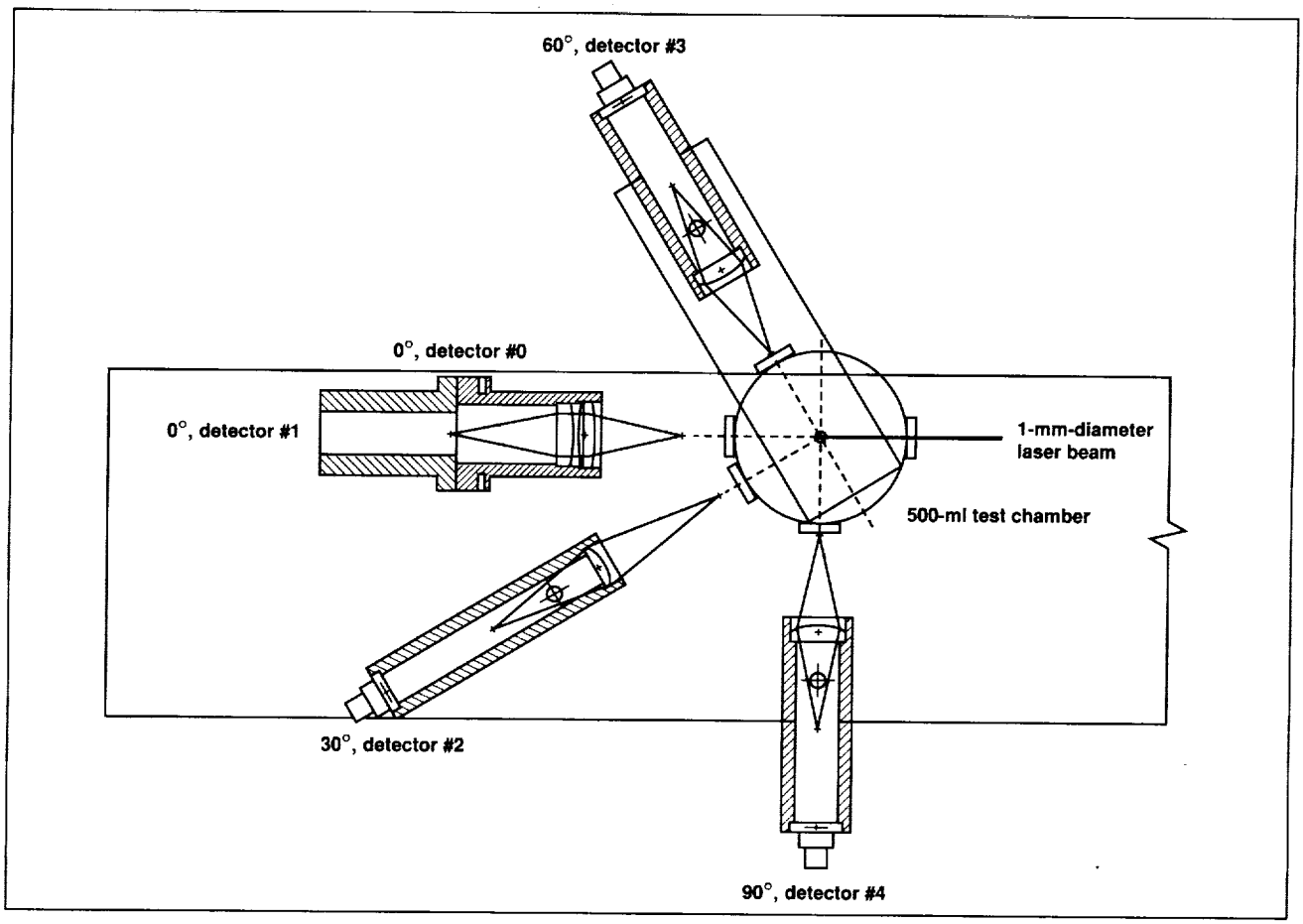


*Fig. 1. Schematic diagram of the small-particle ensemble scattering instrument.*

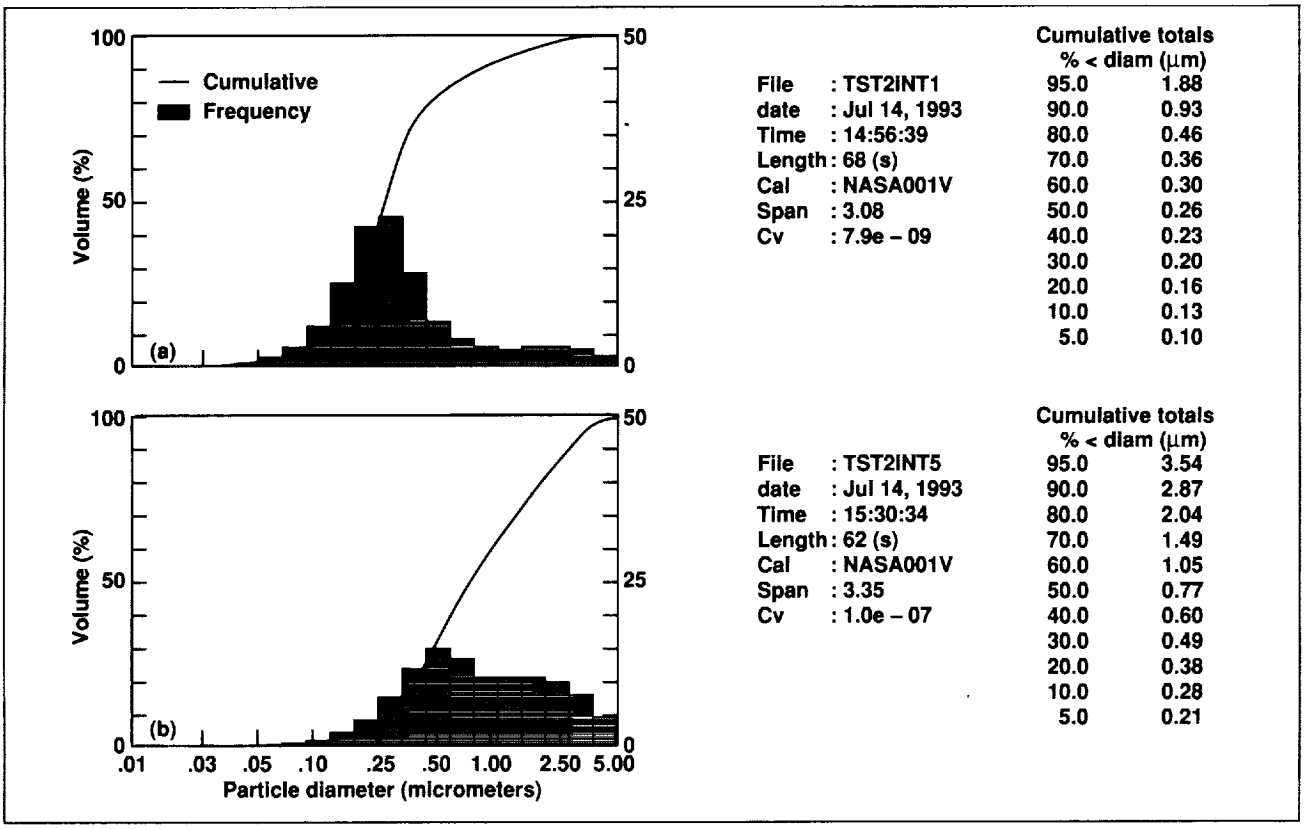


*Fig. 2. Initial (a) and final (b) particle size distributions.*

configuration. The experiments were performed under vacuum from 1 to 0.1 torr, and time-dependent measurements of the particle size distribution were obtained.

The experiments demonstrated the feasibility of this technique to measure in real time a broad range of particle sizes at varying concentrations. The instrument concept measured a time-dependent growth of particle size and total particle concentration as a function of reaction pressure. Measurement results indicate a non-Gaussian distribution of particle shape that changes over time as the aerosol population is formed. The second figure shows representative measurement results.

Future plans for the in situ particle size and concentration measurement system include (1) increasing the number of angular light-scattering detectors to refine sensitivity and resolution capability and (2) combining polarization ratio scattering methods to measure particle sizes of less than 0.1 micrometer.

**Ames-Moffett contact: M. Fonda/C. Rogers**
**(415) 604-5744/0527**
**Headquarters program office: OSS**

# Rovibrational Intensities of the Isotopes of Carbon Monoxide for the Ground Electronic State

**David Goorvitch, Charles Chackerian, Jr.**

Electric dipole transition matrix elements for rovibrational transitions in the ground state of the seven carbon monoxide (CO) isotopes are calculated for all the transitions in the fundamental, first, and second overtone bands with the vibrational quantum number (v) less than or equal to 20 and the angular momentum quantum number (J) less than or equal to 150. Because of its large dissociation energy and the relatively high abundance of its constituent atoms, carbon monoxide in its several isotopic forms is observed in a variety of astrophysical sources. Since many of these sources are quite hot, the molecular emissions can be observed from highly excited vibrational levels that may or may not be in local thermodynamic equilibrium. The main isotopic forms $^{12}C^{16}O$ and $^{13}C^{16}O$ have been observed in a variety of astrophysical sources such as stellar photospheres, comets, interstellar shock waves, and the interstellar medium. The minor isotopic forms are also observable in several of these astrophysical sources. The presence of these minor isotopic forms of CO provides evidence of the nuclear processes that occur in the interiors of stars. We have used the electric dipole moment function calculated previously by Chackerian and his colleagues and the numerical wavefunctions calculated by the method of Goorvitch and Galant to calculate the rovibrational transition moments for all these transitions. These calculated transition moments, combined with highly accurate term values and transition frequencies reported in the literature, allow the calculation of the Einstein A values, the oscillator strengths, and the temperature-dependent strengths. The matrix elements of the transition moments are given as a polynomial expansion in terms of the angular-momentum quantum numbers. The maximum degree for each of the polynomial fits is derived using orthogonal polynomials which are tested for statistical significance.

**Ames-Moffett contact: D. Goorvitch**
**(415) 604-5502**
**Headquarters program office: OSS**

# Evolution of the Martian Atmosphere

**Robert M. Haberle, Dan Tyler, Christopher P. McKay, Wanda L. Davis**

The terrestrial planets—Venus, Earth, and Mars—reside in the same neighborhood of the Solar System, all have solid surfaces, and all are enveloped by gaseous atmospheres. However, the mass and composition of their atmospheres vary widely: Venus has a massive 90-bar carbon-dioxide atmosphere, Earth has a moderate 1-bar nitrogen/oxygen atmosphere, and Mars has a tenuous 6-millibar carbon-dioxide atmosphere. Since each of these planets is thought to have originated with an atmosphere of similar mass and composition, mainly carbon dioxide and water vapor, planetary scientists have long sought to understand how these atmospheres have evolved to their present condition.

For Mars the problem is particularly intriguing, because there is evidence that very early in its history, 3.5–4.5 billion years ago, its atmosphere was much more massive than it is today. Fluvial features characterize much of the planet's ancient, heavily cratered terrain; these features have been interpreted as having developed in an early climate that was warmer and wetter than the Martian climate today. These warm and wet conditions are thought to be the result of the greenhouse effect of a dense carbon dioxide atmosphere. If Mars did start out with a more massive carbon-dioxide atmosphere, where has it gone?

We have constructed a model to simulate the evolution of the Martian atmosphere from some initial size 3.8 billion years ago to its present state. Our goal is to determine plausible values for the size of the initial atmosphere and in what reservoirs it now resides. The model accounts for the change in solar luminosity with time, the greenhouse effect, chemical weathering of carbon dioxide in carbonate rocks, storage of carbon dioxide in the regolith and polar caps, and escape of the atmosphere to space. We have found that the best agreement with current conditions occurs for starting pressures of less than 1 bar. However, this is not enough carbon dioxide to produce a strong enough greenhouse effect to explain the fluvial features. This fact suggests that the fluvial features must have been formed in a much colder environment than was previously thought possible. We have also found that the atmosphere may have catastrophically collapsed into the polar caps during its evolution to present conditions. This collapse occurs when heat transport into the polar regions is not sufficient to prevent polar caps from forming. Once formed, the polar caps determine the surface-pressure–vapor-pressure relationship. The possibility of atmospheric collapse in the long-term evolution of the Martian atmosphere has not previously been recognized.

The experience gained with our model has illuminated the key processes involved in the evolution of the Martian atmosphere. Further work on these processes, particularly atmospheric heat transport and chemical weathering, will be carried out to better understand when and where they become important. For now, it appears that Mars has been cold through most of its history and that, if it did begin with a massive carbon-dioxide atmosphere, most of that atmosphere must be stored as carbonate in near-surface materials. The search for carbonates by future missions will therefore provide important clues about the planet's early history.

**Ames-Moffett contact: R. Haberle**
**(415) 604-5491**
**Headquarters program office: OSS**

# Is ATP Synthesized by a Vacuolar-Like ATPase in Extremely Halophilic Bacteria?

**Lawrence I. Hochstein, Darian Lawson**

According to current dogma, the superfamily of proton-translocating ATPases evolved from an enzyme that resembled both the vacuolar ATPases found in the Eucarya and the vacuolar-like ATPases found in the Archaea. In this phylogeny, the evolutionary line from the progenitor led to the vacuolar-like ATPases found in the Archaea, the Eucaryal vacuolar enzyme (which is incapable of synthesizing ATP), and the ATP synthases. A necessary corollary of this hypothesis is that the vacuolar-like ATPases in the Archaea must synthesize ATP. Thus it is important to determine whether the Archaeal ATPases do indeed synthesize ATP.

Previous studies by this laboratory established that ATP synthesis in the Archeon *Halobacterium saccharovorum* takes place under conditions that are inconsistent with the operation of the organism's vacuolar-like ATPase and that ATP synthesis is catalyzed by the ubiquitous ATP synthase. To ascertain whether this characteristic was unique to *H. saccharovorum*, we examined the synthesis of ATP in other extreme halophiles: *H. salinarium*, *Haloferax mediterranei*, *H. volcanii*, and *Haloarcula hispanicum*. The experimental design was derived from the differential sensitivity of the vacuolar ATPases and ATP synthase. The former are inhibited by the thiol reagent N-ethylmaleimide and nitrate; the latter are not. On the other hand, the latter are inhibited by azide whereas the former are not. ATP synthesis in these organisms was inhibited by azide but not N-ethylmaleimide and nitrate, thus extending the original observation in *H. saccharovorum* that ATP synthesis is inconsistent with the operation of the vacuolar-like enzyme.

The specificity of azide is the critical element in identifying the ATPase responsible for ATP synthesis. Azide can act as a protonophore (i.e., by collapsing the gradient of protons). If it does so, then the inhibition of ATP synthesis by azide would be an indirect effect rather than a direct effect on the enzyme responsible for ATP synthesis. In order to establish that azide was not acting as a protonophore, the effect of azide on substrate-level phosphorylation was examined. If azide acts as a protonophore, it should inhibit the net synthesis of ATP during substrate-level phosphorylation. The arginine-dependent synthesis of ATP is an example of substrate-level phosphorylation and did not affect the net synthesis of ATP. The presence of azide was not affected by the inhibitor, which is consistent with the notion that azide acts at the level of the ATP synthase.

These results indicate that ATP synthesis in the extremely halophilic Archaea is not catalyzed by a vacuolar-like ATPase and that the suggested phylogeny of the proton-translocating ATPases does not account for the origin and evolution of the ATP synthase.

**Ames-Moffett contact: L. Hochstein**
**(415) 604-5938**
**Headquarters program office: OAST**

## The Center for Star Formation Studies

**David Hollenbach, Pat Cassen**

The Star Formation Summer Workshop in 1993 was held at Wellesley College and included, in addition to Center scientists, about 100 astrophysicists from around the world. The topics discussed included the structure of molecular clouds, the formation of clusters of stars and binary stars, theoretical models of protostellar winds, and the evolution of disks of gas and dust around protostars.

The main focus of work in 1993 was the structure of the interstellar clouds that gravitationally collapse to form stars or clusters of stars, the collapse of these clouds to form protostars and their dusty, orbiting disks, and the evolution of these disks which feed mass to the protostar and form planets. M. Wolfire, D. Hollenbach, and A. Tielens modeled the clumpiness of interstellar molecular clouds and showed how the observed spectra from the carbon monoxide molecule indicated a large number of substellar-mass clumps. C. McKee at the University of California, Berkeley, showed how magnetic fields and the turbulent velocities of these clumps support a molecular cloud against gravitational collapse. Eventually, however (according to F. Shu and D. Galli at the University of California, Berkeley), the slow diffusion of the neutral gas through the ions and magnetic field and the dissipation of turbulence lead to the collapse of the dense regions in each molecular cloud. The collapse leads to the formation of a protostar and an orbiting disk of gas and dust. The shock formed when the collapsing cloud impacts this system has been modeled by D. Hollenbach and D. Neufeld (Johns Hopkins University). It was found that those interstellar dust particles that hit the disk beyond a radius of about the Earth–Sun orbit will survive the shock. Therefore, coagulated interstellar dust particles may be found in comets and meteorites that originated in the outer Solar System. P. Cassen, L. Tomley (San Jose State University), and T. Steiman-Cameron showed that the dusty, orbiting disks become gravitationally unstable and rapidly evolve to dump disk material onto the star, the time scale depending on the rate of cooling in the disk.

**Ames-Moffett contact: D. Hollenbach**
**(415) 604-4164**
**Headquarters program office: OSS**

## Photoevaporation of Disks Around Young Stars

**David Hollenbach**

Stars form by the collapse of rotating interstellar clouds of gas and dust. The angular momentum in the rotating clouds ensures that much of the collapsing material does not fall directly onto the protostar, but falls on a disk of gas and dust that orbits the star. Viscosity in these disks causes the material to spiral onto the star, and the star grows in mass. The time required for the formation of a star is about 100,000 years. Around low-mass stars like the Sun, the orbiting disks last perhaps ten million years and eventually form planets.

High-mass stars are very luminous in ultraviolet photons. With colleagues F. Shu and D. Johnstone of the University of California, Berkeley, we have shown that the ultraviolet photons heat the surfaces of the orbiting disks to 10,000 kelvin, and that the disks around high-mass stars rapidly evaporate back to the interstellar medium in about 100,000 years. Therefore, planets do not have as much time to form as low-mass stars do. In addition, the model explains the existence of dense, hot, ionized plasma that has

been observed at radio and infrared wavelengths around high-mass stars. The origin of this high-pressure plasma has long been a mystery.

Low-mass stars like the Sun also produce a modest amount of ultraviolet radiation as they form, especially during the phase of accretion of material from the disk onto the star. The photoevaporation models show that the orbiting gaseous disk around the early Sun could be dispersed in about ten million years, with most of the photoevaporative loss from the region beyond Saturn. The models therefore provide an explanation for the lack of hydrogen gas on Uranus and Neptune compared to Jupiter and Saturn: the gas was evaporated before the rocky cores of Uranus and Neptune grew large enough to gravitationally attract the (mostly hydrogen) disk gas.

Data from NASA's Infrared Telescope Facility, as well as from future NASA infrared missions such as the Stratospheric Observatory for Infrared Astronomy (SOFIA) and the Space Infrared Telescope Facility (SIRTF), will test predictions of these models. In future work we will study the hydrodynamics of these outflows.

**Ames-Moffett contact: D. Hollenbach**
**(415) 604-4164**
**Headquarters program office: OSS**

## Planetary Protection Implementation on Future Mars Lander Missions

**Robert Howell, Donald L. DeVincenzi**

A workshop was held on the subject of planetary protection implementation for Mars Lander missions. It was sponsored and organized by the Exobiology Implementation Team of the United States/Russian Joint Working Group on Space Biomedical and Life Support Systems. The objective of the workshop was to discuss issues for the Russian Mars '94 mission that is under development, and for future Mars Lander missions including the planned Mars '96 and U.S. Mars Environmental Survey (MESUR) Pathfinder and Network missions.

Invited presentations covered the following topics: exobiology science objectives for Mars exploration, current international policy on planetary protection, planetary protection requirements developed for earlier missions, mission plans and designs for future U.S. and Russian Mars landers, biological contamination of spacecraft components, and techniques for spacecraft bio-load reduction. The recent recommendations of the U.S. Space Studies Board (SSB) on this subject were also summarized.

Much of the discussion focused on the recommendations of the SSB. The SSB proposed relaxing the planetary protection requirements for those Mars Lander missions that do not contain life-detection experiments, but maintaining Viking-like requirements for those missions that do contain life-detection experiments. The SSB recommendations were found to be acceptable as a guide for future missions, although many questions about interpretation were raised, which are summarized in the workshop report. Significant among the concerns was the need for (1) more quantitative guidelines to prevent misinterpretation by project offices and (2) better access to and use of the Viking database of bioassays to specify microbial burden targets. Among the questions raised were How will the SSB recommendations be integrated with existing COSPAR policy and How will they apply to and affect Mars '94, Mars '96, MESUR Pathfinder, and MESUR Network missions?

An additional topic that was considered briefly was the identification of issues related to planetary protection considerations for Mars sample-return missions. These issues will form the basis of a follow-on joint U.S./Russian workshop.

**Ames-Moffett contact: R. Howell**
**(415) 604-4223**
**Headquarters program office: OSS**

# Interpretation of Paleoenvironments Using Compound-Specific Isotope Analysis

**Linda Jahnke**

Compound-specific isotope analysis by means of gas chromatography–combustion–isotope ratio mass spectrometry (GC–C–IRMS) is a new tool being applied in the field of organic geochemistry. The recycling of carbon in ancient ecosystems was a complex process. Then, as today, microbially mediated aerobic and anaerobic processes resulted in the formation and eventual deposition of specific organic compounds we refer to as biomarkers. These compounds are molecular fossils that can be used to identify specific groups of ancient bacteria. The use of GC–C–IRMS now affords an opportunity to further refine the field of biomarker analysis and contribute to a broader understanding of the organisms and processes that made up paleoenvironments.

Two stable carbon isotopes occur naturally, carbon-12 ($^{12}C$) and carbon-13 ($^{13}C$). Biochemical processes often result in the synthesis of molecules depleted in $^{13}C$ relative to $^{12}C$. Such carbon isotopic fractionations are described by the term $\partial^{13}C$. Photoautotrophy is a biological process whereby the energy of sunlight is used to convert carbon dioxide ($CO_2$) to cellular material. This process, mediated by the enzyme ribulose-bisphosphate carboxylase (RuBPC), is responsible for most of the organic carbon present on Earth today and results in a $\partial^{13}C$ of –27‰ (the more negative the number, the more depleted in $^{13}C$). Several bacterial processes can be involved in the recycling of photosynthetically produced organic carbon back to either $CO_2$ or methane (methanogenesis). The methane produced is depleted still further in $^{13}C$ (–40‰ to –80‰). In contrast to the abundance of information on carbon isotope fractionations associated with photoautotrophy and methanogenesis, little information exists regarding the fractionations taking place during bacterial growth on methane and any further fractionations that might occur during synthesis of the lipid biomarkers. Specific groups of lipid biomarkers are normally synthesized by more than one metabolic group of bacteria, so isotopic signatures for individual molecules could provide a powerful tool for understanding the component processes that made up ancient ecosystems.

Working with an organic geochemist, Roger Summons (Australian Geological Survey Organization), we have been able to show that a distinct isotopic fractionation occurs when bacteria grow on methane. The carbon fractionation depends primarily on the initial methane-oxidizing step, which is carried out by an enzyme, methane monooxygenase (MMO). Two types of MMO, a membrane-bound and a soluble form, can be expressed depending on the environmental conditions under which the cells are grown. Whereas both MMO enzymes result in considerable carbon isotopic fractionation, the fractionation with the membrane-bound enzyme is the greatest, –30‰ versus only –16‰ (relative to the initial methane) for the soluble. Additional strong $^{13}C$ depletion takes place during synthesis of the lipid biomarker pool, so the hopanes and sterols that are characteristically synthesized by these methanotrophic bacteria can be as negative as –40‰. This provides an unambiguous means for determining whether similar molecules extracted from ancient organic sediments were synthesized by methanotrophic bacteria or by another metabolic cell type.

**Ames-Moffett contact: L. Jahnke**
**(415) 604-3221**
**Headquarters program office: OSS**

# FOSTER: Flight Opportunities for Science Teacher Enrichment

**David G. Koch, Garth Hull, Carl Gillespie**

NASA has continued to place major emphasis on pre-college educational outreach programs. The goal of the Flight Opportunities for Science Teacher Enrichment (FOSTER) project at Ames Research Center is to provide an enriching experience on board the Kuiper Airborne Observatory (KAO), a C-141 aircraft equipped with a 36-inch telescope. In 1993, the first group of ten teachers from the San Francisco Bay Area flew on the KAO. Before their flights, they attended a series of workshops in which they received background information on contemporary astrophysics, suggestions for classroom activities and other curriculum-supplementing materials, and an orientation for their upcoming flight. The project has included participation by astrophysicists at Ames, the Education Programs office, and the Science and Applications Aircraft Division. A significant portion of the work is being performed by the project teacher, Edna DeVore, and others at the SETI Institute under a NASA grant.

A second group of teachers (ten more from the Bay Area and two from Hawaii) attended a one-week workshop at Ames in June and were scheduled for flights in the fall. Plans are under way for the third group, which will include teachers from an additional ten schools affiliated with the principal investigators and guest investigators from around the country.

The FOSTER project has been well received by the pre-college science teaching community. The teachers have found this to be an enriching experience in which they have been able to witness the excitement, hardships, challenges, discoveries, teamwork, social relevance, and educational value of scientific research. They have been able to take what they have learned into their classrooms and use it to teach their students the relevance of science. The project will continue to expand yearly until it becomes a national program flying 50 teachers per year. With the advent of the Stratospheric Observatory for Infrared Astronomy (SOFIA), a Boeing 747 aircraft with a 100-inch telescope, it will be possible to fly 100 or more teachers per year.

**Ames-Moffett contact: D. Koch**
**(415) 604-6548**
**Headquarters program office: OSS**

## The Submillimeter Wave Astronomy Mission

**David G. Koch, David Hollenbach**

A small Explorer mission is being planned to determine the abundance of species that have been predicted to be gas coolants in molecular clouds. The Submillimeter Wave Astronomy Satellite (SWAS) is a small Explorer mission for measuring chemical species important in star-formation processes. The mission will address such issues as (1) stability of clouds against collapse, (2) variations in star-formation efficiencies in different regions, and (3) the processes whereby energy is removed, permitting stars and planets to form. The SWAS mission, headed by Gary Melnick of the Smithsonian Astrophysical Observatory, is being developed for launch in June 1995. The instrument is under construction at Ball Aerospace, with delivery planned to Goddard Space Flight Center for spacecraft integration in mid-1994. An acousto-optical spectrometer with 1,400 channels and 1-megahertz spectral resolution is being provided by collaborators at the University of Cologne in Germany. Investigations into efficient planning algorithms were conducted this year at Ames. The operating constraints on the SWAS spacecraft are unique. Therefore, customized approaches had to be developed for efficient support of mission planning to maximize the scientific return.

**Ames-Moffett contact: D. Koch**
**(415) 604-6548**
**Headquarters program office: OSS**

## Enhanced Ion Mobility Spectrometry (IMS) Sample Ionization

**Daniel R. Kojiro**

For exobiology experiments on board spacecraft or space probes, a wide range of chemical species must often be detected and identified. The limited amount of power and space available for flight instruments severely limits the number of instruments that can be flown on a given mission. It is important, then, that these experiments use instrumentation with universal response, so that all species of interest can be analyzed.

Ion mobility spectrometry (IMS) has developed into a powerful analytical technique for the analysis of gases. Normal laboratory and commercial operation of IMS uses a reaction region with a radioactive source irradiating the host gas to produce a water-cluster reactant ion for sample ionization. This ionization mechanism is rather selective and restricts the range of chemical species that can be detected and identified by IMS.

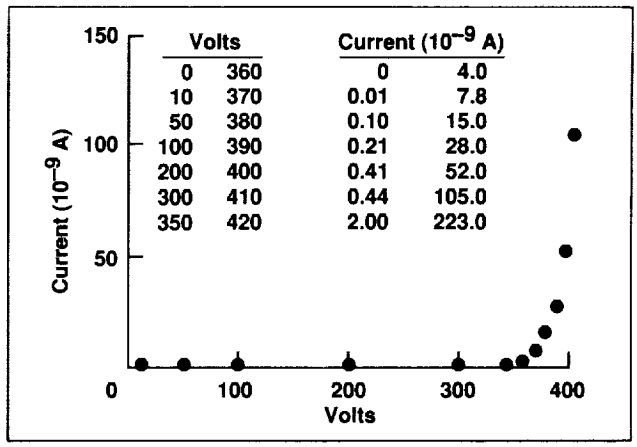


*Fig. 1. Change in current as voltage is increased between the repeller plate and ring 1.*

One possible method of universal IMS sample ionization would use metastable helium. In the presence of a strong electric field, helium can be "excited" to a higher-energy, metastable state through collisions with beta particles emitted by a radioactive source. These excited, metastable helium atoms can ionize molecules with ionization potential below 19.8 electron volts.

Combining this ionization technique with IMS may result in a gas-chromatography (GC) detector with universal response that provides sample identification independent from GC retention time identification. The figure shows the current produced in an all-helium IMS system with the electric field between the repeller plate and ring 1 in the reaction region increased to levels at which a metastable ionization detector (MID) operates. These IMS background-current levels increased in a manner similar to those in the MID. To further study the effect of metastable ionization on IMS response to simple alkanes, a dry-helium IMS system was modified to enhance IMS ionization through the use of metastable helium, again by increasing the voltage between two rings in the reaction region. The modified dry-helium IMS could be operated with or without the enhanced ionization. A coupled mass spectrometer was used to identify the ions.

The table shows the results of hydrocarbon responses from injections of the dilute hydrocarbon mixture made with the enhanced ionization on and off and equivalent drift fields. Although the same ions were produced in both cases, background-reaction ion intensities increased by a factor of four and sample molecule ion intensity increased by a factor of 1.5 to 2.

Further experiments are being developed to study the processes occurring in this enhanced ionization reaction region. Whether the increased ionization is the result of metastable ionization, glow discharge, other highly reactive species produced by metastable helium, or a combination of processes has yet to be determined. It is clear that an increase in sample ionization can be achieved using this enhanced ionization reaction region with possible increases in sensitivity. If metastable helium does play a major role here, then the IMS may also provide valuable information on the processes that occur within the metastable ionization detector.

Net peak ion intensities with and without enhancement

| Chromatographic peak | Ion (amu) | Peak ion intensity: No enhancement (gain 4) (mV) | Peak ion intensity: Enhancement calculated at gain 4 (mV) |
|---|---|---|---|
| Ethane | 28 | 2,000 | 4,200 |
| | 29 | 550 | 1,100 |
| Ethylene | 28 | 900 | 2,200 |
| | 29 | 135 | 500 |
| Propane | 28 | 500 | 1,500 |
| | 29 | 525 | 1,400 |
| | 43 | 675 | 750 |
| Isobutane | 43 | 760 | 1,100 |
| | 57 | 90 | 80 |
| Butane | 28 | 150 | – |
| | 29 | 50 | 100 |
| | 43 | 830 | 1,100 |
| | 57 | 230 | 220 |

**Ames-Moffett contact: D. Kojiro**
**(415) 604-5364**
**Headquarters program office: OSS**

# High-Speed Gas Chromatography with Thermal Modulation on a Fused-Silica Capillary Column

Diem Q. Le, José R. Valentin, John B. Phillips

Conventional gas chromatography (GC) has long been used in the detection and measurement of gases in complex mixtures. In GC, a mobile phase (inert gas) carries the components of a gaseous mixture through a column that contains a stationary phase. The interaction between the sample components and the stationary phase results in differences in the elution times of each component of the mixture.

This analytical technique has proved to be valuable on previous planetary missions. On such missions, the time available for GC application is limited, and a decrease in the analysis time is crucial to gaining additional information. High-speed gas chromatography (HSGC) was developed to increase the speed of GC analysis. Temperature programming has proved to be more effective on HSGC's short fused-silica column because the column is heated directly by an electrical current instead of an oven. Other advantages of HSGC are the increase of detection limits and improvements in the separation power of the technique. The high performance of this simplified instrumental setup increases the potential of HSGC to be used in small flight projects or probes in future planetary missions.

In this study, a thermal desorption modulator was used to introduce the sample into the column. The modulator, shown in the first figure, contains an adsorbent (stationary phase) within a short length of fused-silica tubing coated with a thin film of electrically conductive paint. The role of the modulator is

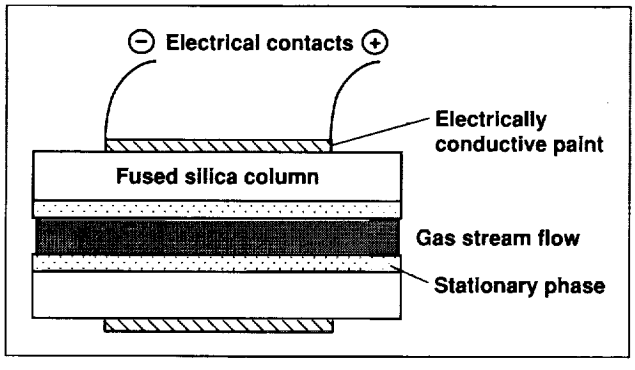


*Fig. 1. Thermal desorption modulator.*

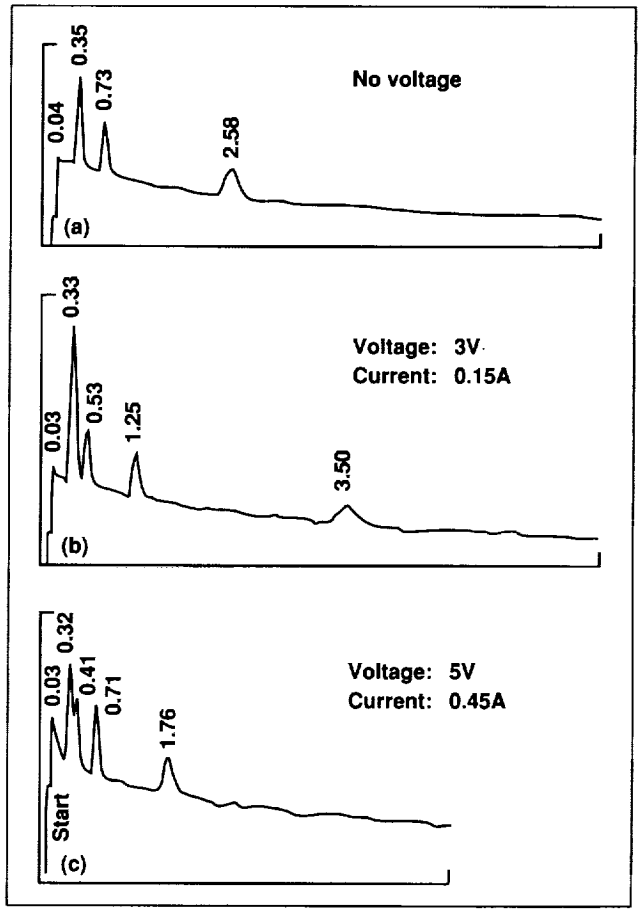


*Fig. 2. Chromatograms obtained from a coated fused-silica capillary column packed with alumina. (a) The chromatogram of a nonheated column; (b) and (c) results obtained after applying 3 volts (0.15 amp) and 5 volts (0.45 amp).*

to strip sample substances out of the mobile phase and accumulate them for some period of time in the adsorbent. On command from a signal generator (computer or other electronic device), an electrical current passes through the paint, rapidly heating the modulator and the adsorbent within it. The components are then released from the adsorbent and they form concentration pulses in the gas stream entering the column, where the separation occurs.

Part (a) of the second figure shows the chromatogram of a single injected sample mixture of light gases (methane, ethane, propane, butane) when the modulator, i.e., the column, is not electrically heated. Only three sample peaks, in the order methane, ethane, and propane, are detected for the duration of the 10-minute run. Part (b) displays the elution of butane after 3 volts (0.15 amp) are applied to the column. The increase in voltage and, in turn, temperature of the column not only allowed for the desorption of butane, but also increased the elution speed of ethane and propane by 28% and 52%, respectively. As the voltage increased to 5 volts (0.45 amp) (part (c)), the methane and ethane peaks overlapped with a decrease of 43% and 73% in retention times, respectively. Thus, HSGC shows its ability to perform fast and sensitive detection of volatile substances in a sample mixture.

Increasing the speed of gas chromatography improves its sensitivity, its resolving power, and its ability to follow changes in a sample. Faster chromatographic peaks are sharper, and detection sensitivity is therefore enhanced. Faster chromatography produces more information per unit of time, allowing measurements to be made more frequently. All of these advantages indicate that HSGC will enhance the information return from any future planetary missions.

**Ames-Moffett contact: J. Valentin/D. Le**
**(415) 604-5766/3212**
**Headquarters program office: OSS**

## The Search for Life on Mars

**Rocco L. Mancinelli, Melisa R. White**

Other than Earth, Mars is the only planet in our solar system that may have had conditions early in its history favorable for the origin and early evolution of life. During the Viking Mission, analyses of the Martian surface were made to determine its chemical composition and to search for a possible biota. Results of three life-detection experiments suggested that the probability of extant life on Mars is very low. These experiments did reveal, however, that the surface is oxidizing. A gas chromatography/mass spectrometry (GC/MS) experiment found no organic matter on the surface of Mars.

Mars is currently a cold (210 kelvin), dry (0.03–0.1% water, by volume) planet with a thin (8 millibars) carbon-dioxide atmosphere. Photographs reveal carved features (e.g., the Valles Marineris) which suggest that liquid water may once have flowed across the Martian surface. If liquid water flowed on the surface of Mars early in its history, then the atmosphere would have been much denser than it is today and the temperature warmer than it is today. Because Mars is in the inner solar system and is composed of the same material as Earth, the products of outgassing during its formation should have been similar to those of Earth, that is, primarily carbon dioxide and nitrogen. Although similar, Mars and Earth were not identical.

Among the critical differences between Earth and early Mars was the partial pressure of dinitrogen. Mars is postulated to have had 18 millibars of dinitrogen compared to greater than one bar on Earth. We have shown that this difference is not critical for biological nitrogen fixation. Data from the Viking X-ray fluorescence experiment and analyses of Shergotty–Nakhla–Chassigny (SNC) meteorites indicate that all of the elements necessary for the origin of life are present on Mars. Because life is known to exist at all temperatures where liquid water exists (110°C to –20°C) and at low pressures

such as are found on Mars, the Martian temperature and pressure regimes would not, in and of themselves, preclude the origin of life. The radiation regime of early Mars was not unlike that of early Earth, so it would not have hindered the development of life but would have influenced where life might have arisen and how it might have evolved. The physical features (for example, temperature, pressure, and radiation regimes) of Mars are only important in that they control the state of water. Because liquid water is essential for life, water must exist as a liquid for life to arise and evolve.

We know that Mars today does not possess liquid water at its surface. This means that any liquid water that did exist at the surface dissipated when the planet turned cold. As the planet became cold and dry, any life that may have evolved would have sought refuge in protected niches. Terrestrial analogs of such life in protected niches include microbial mats growing beneath the ice-covered lakes in the Antarctic Dry Valleys, cryptoendoliths growing beneath the surface of sandstone rocks in the Antarctic Dry Valleys, and endoevaporites, that is, those organisms inhabiting dry gypsum–halite crusts. We study the ecology of these terrestrial analogs to determine what traces such life on Mars might have left (that is, biomarkers).

Biomarkers of a past Martian biota would include key morphological (fossils), chemical (specific organic or inorganic compounds), or isotopic signatures of living systems that could be used to determine if the life process occurred on Mars. Given that, in the near term, missions to Mars will be unmanned and relatively simple, it will be impractical to search for these biomarkers. What can we do to gain insight into the possibility of a past Martian biota? The first thing that must be done is to better characterize the past Martian environment. Specifically, we must determine whether liquid water existed in sufficient quantity and for a sufficient length of time to allow life to arise. To do this remotely during unmanned missions requires the ability to analyze the composition and mineralogy of the Martian surface material. Several techniques have been proposed for accomplishing this task (for example, X-ray diffraction; differential thermal analysis/GC (DTA/GC) or DTA/MS; differential scanning calorimetry/GC (DSC/GC) or DSC/MS). Because DTA/GC shows great promise, we are actively defining experiments for unmanned missions to Mars using DTA/GC to determine the mineralogy of the Martian surface.

The results of our research on the interaction between the environment and living systems (ecology) and the physical environment's impact on evolutionary processes will be important in understanding the origins of life on Earth and on Mars.

**Ames-Moffett contact: R. Mancinelli**
**(415) 604-6165**
**Headquarters program office: OSS**

# Particle Dispersion Experiment: Preliminary Results

**John R. Marshall**

The Particle Dispersion Experiment (PDE) (see first figure) was designed to test technologies for future Space Shuttle and Space Station experiments that will be concerned with the dispersion of aerosols and related particulate clouds. The PDE successfully tested a gas-pulse method of dispersing granular materials inside eight modular experiment chambers. The technique demonstrated the ability of an air pulse to redisperse particles when they are already free-floating in a chamber. The PDE was also designed to enable a limited parametric study of the aggregation of the dispersed particles caused by electrical interparticle forces. Such forces are prevalent on natural materials when dust is injected into planetary atmospheres by volcanic eruptions, meteorite impact, and dust storms. Electrostatic aggregation is inevitable in natural dust clouds and is a major factor controlling the longevity of the dust palls. The PDE showed that aggregation experiments can be conducted in small chambers, that aggregating natural materials form amorphous and filamentous structures, and that aggregation can lead to the formation of "giant" (larger than 1 centimeter) particle clusters with commensurably large electrical fields around them (see second figure). The observed growth of the electrical fields has important implications for our understanding of the aggregation process and, of course, the behavior of natural dust clouds.

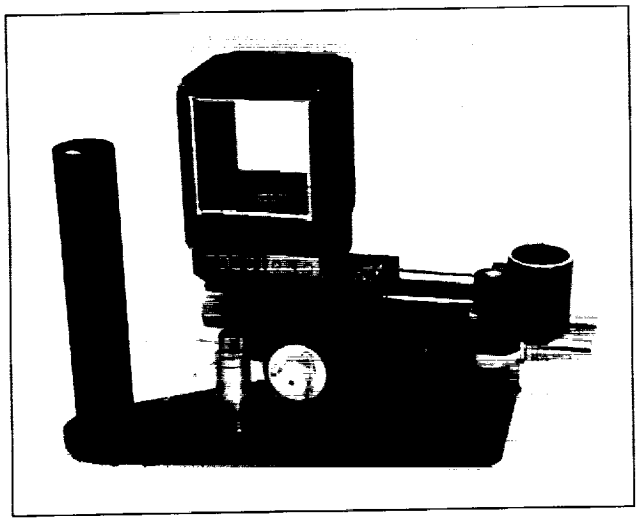

*Fig. 1. Flight hardware for the Particle Dispersion Experiment.*

*Fig. 2. Giant aggregate formed from 400-micrometer particles in microgravity. The field of view is 5 centimeters in diameter.*

**Ames-Moffett contact: J. Marshall**
**(415) 604-4983**
**Headquarters program office: OSS**

# The Past Climate on Titan

**Christopher P. McKay, James B. Pollack, Regis Courtin**

Titan is the largest moon of the planet Saturn and is the only moon in the solar system with a substantial atmosphere. Its atmosphere is mostly nitrogen and has a pressure one and a half times larger than sea-level atmospheric pressure on Earth. In these respects Titan's atmosphere is the most similar to Earth's. Methane is found in Titan's atmosphere and results in the formation of an organic smog layer via chemistry similar to that in current theories of the origin of life on Earth. Titan's atmosphere has a greenhouse effect that is much stronger than the Earth's. However, the organic smog layer produces an antigreenhouse effect that cuts the greenhouse warming in half. The surface of Titan remains unknown, hidden by the thick smog layer, but it may be an ocean of liquid methane and ethane.

In order to understand the evolution of Titan's atmosphere, we have developed a coupled atmosphere-and-ocean model of Titan's surface. The atmospheric model is a one-dimensional, spectrally resolved, radiative–convective model. The ocean thermodynamics are based on solution theory. The ocean, composed entirely of methane ($CH_4$) 3.5 billion years ago, becomes progressively enriched in ethane over time. The partial pressures of nitrogen ($N_2$) and $CH_4$ in the atmosphere are dependent on the ocean's temperature and composition. We find that the resulting system is stable against a runaway greenhouse effect. Accounting for the decreased solar luminosity in this case, we find that Titan's surface temperature would have been about 20 kelvin colder 4 billion years ago. If there was no ocean, but only small $CH_4$ lakes, the temperature change would have been 12 kelvin. In both cases we find that the surface of Titan may have been covered by ice about 3 billion years ago. In the case of small methane lakes, condensation of $N_2$ provides the ice, whereas in the ocean case, the ocean freezes (see figure).

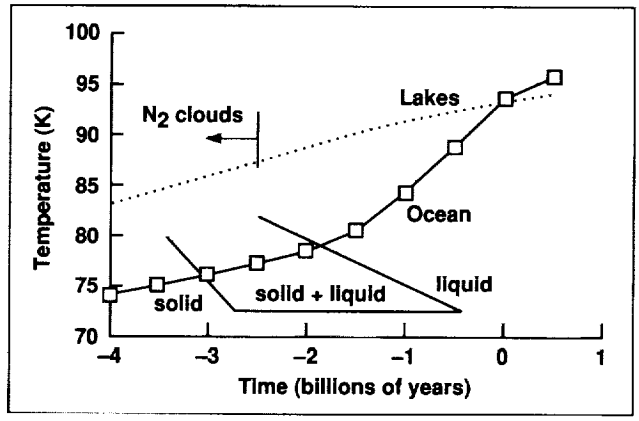


*Fig. 1. Time history of pressure and temperature for the coupled atmosphere-and-ocean model. The phase diagram for the freezing of the ocean is shown where it intersects the temperature history. Also shown, by the dotted line, is the temperature history of the surface without an ocean: in this case there are only lakes.*

The dominant factor influencing the evolution of Titan's surface temperature is the change in the solar constant—amplified, if an ocean is present, by the temperature dependence of the solubility of $N_2$. Accretional heating can dramatically alter the surface temperature; a surface thermal flux of 500 erg/square centimeter/second, representative of small levels of accretional heating, results in a 20-kelvin change in surface temperature.

Regis Courtin is at the Observatory of Paris-Meudon.

**Ames-Moffett contact: C. McKay**
**(415) 604-6864**
**Headquarters program office: OSS**

# The Detection of Molecular Hydrogen in Interstellar Ices

Scott A. Sandford, Lou J. Allamandola

As part of an ongoing study of the properties of interstellar and solar system ices, we have been investigating the chemistry that occurs when analogs of these ices are exposed to ultraviolet (UV) radiation. These studies have demonstrated that photochemistry plays an important role in the composition of interstellar and cometary materials. Irradiation destroys many of the molecules in the original ice and produces a host of new molecules and radicals. When the temperature of these ices is raised, these species become mobile, react, and produce new, complex materials. When the temperature exceeds 150 kelvin, the ice sublimes and an organic residue is left.

The organic residue is important because its spectrum is similar to that of the organic material in the diffuse interstellar medium. Thus, the diffuse medium appears to contain an abundant organic component created by the UV photolysis of ices in dense molecular clouds. This suggests that the carbon-rich materials that eventually become incorporated into newly forming planetary systems already exhibit a large degree of molecular complexity.

One of the key questions associated with this process has to do with the hydrogen balance during photolysis. The production of the residue requires that a great deal of hydrogen be removed from the original carbon-carrying ice species. Hydrogen removal is apparent when one notes that the major carbon carrier in the original ices is methanol (H/C = 4) while the resulting residue is similar to an aliphatic hydrocarbon having H/C ≈ 2.3.

We carried out experiments that demonstrated that most of the hydrogen is lost when hydrogen atoms removed from the molecules in the ice recombine in situ to form molecular hydrogen ($H_2$). This $H_2$ can be detected within the ice through a weak infrared absorption feature it produces near 4,137 $cm^{-1}$ (2.417 micrometers). Studies have indicated that typical interstellar ices might be expected to contain large amounts of molecular $H_2$ (up to 30% relative to $H_2O$) and that, despite its great volatility in pure form, some $H_2$ would remain in $H_2O$-rich interstellar ices up to temperatures of about 70 kelvin.

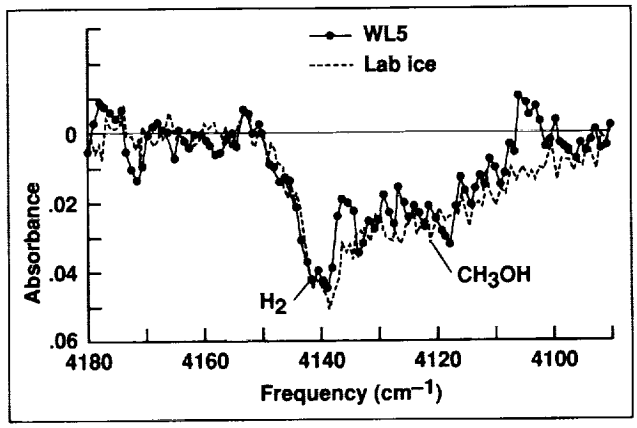


*Fig. 1. A comparison of the spectrum of WL5 with that of an $H_2O$:$CH_3OH$:$H_2$ = 10:5:1 laboratory ice analog at 15 kelvin. $H_2$ frozen into interstellar ices produces the narrow absorption at 4,141 $cm^{-1}$ (2.415 micrometers). The broader feature centered near 4,125 $cm^{-1}$ is due to methanol ($CH_3OH$) in the ice.*

Inspired by the prediction that interstellar ices might contain $H_2$, we began an observing program with Thomas Geballe of the Joint Astronomy Centre (Hilo, Hawaii) to search for the $H_2$ ice feature using the CGS4 spectrometer at the United Kingdom Infrared Telescope (UKIRT) on Mauna Kea, Hawaii. On 20 April 1993 we detected the $H_2$ feature along the line of sight toward WL5, an object deeply embedded in the rho Ophiuchus dark cloud (see figure). The strength, position, and profile of the absorption band are consistent with an in situ formation by photolysis and indicate that the $H_2$ is present in great abundance (after $H_2O$, it is the second most abundant component known in the ices toward WL5!). We are continuing to search for this absorption feature in the spectra of other dense clouds and are actively considering the many implications the presence of large amounts of $H_2$ in interstellar and cometary ices will have for their chemical and physical properties.

**Ames-Moffett contact: S. Sandford**
**(415) 604-6849**
**Headquarters program office: OSS**

# Diode Laser Spectroscopy of Stable Isotopes of Carbon and Oxygen in Soils

**Todd B. Sauke, Joseph F. Becker**

Variations in the ratios of stable isotopes of carbon and oxygen in Martian rock and soil samples can be caused by several factors, such as the fractionation that occurs as a result of past or present volcanism, the incorporation of carbon dioxide from the atmosphere onto the Mars surface, or the existence of other reservoirs of carbon or oxygen, i.e., water or possibly organic carbon that has been formed by biological or nonbiological processes. Measurement of the isotopic variations can provide much important information about and insight into the planet's physical and chemical evolution, including possible past inhabitants. We are developing a stable isotope laser spectrometer (SILS) that uses high-resolution tunable diode lasers to measure ratios of stable isotopes of carbon and oxygen in carbon dioxide obtained from soil and rock samples. Because modern high-temperature diode laser systems are reliable, lightweight, rugged, and operate at temperatures in excess of 200 kelvin, they are well suited for flight hardware applications. Laser spectroscopy offers several important advantages over conventional mass spectrometry for measurements on a planet's surface. For example, the complex and detailed sample preparation and purification necessary for reliable mass-spectrometer measurements are unnecessary when a laser spectrometer is used, because contaminant gases typically do not interfere with the measurement. The goal is to develop an instrument for laser-spectroscopic isotope analysis of planetary soils and ice on possible near-term Mars missions such as the Mars Polar Pathfinder, Mars Environmental Survey (MESUR), or Mars Rover with Sample Return mission.

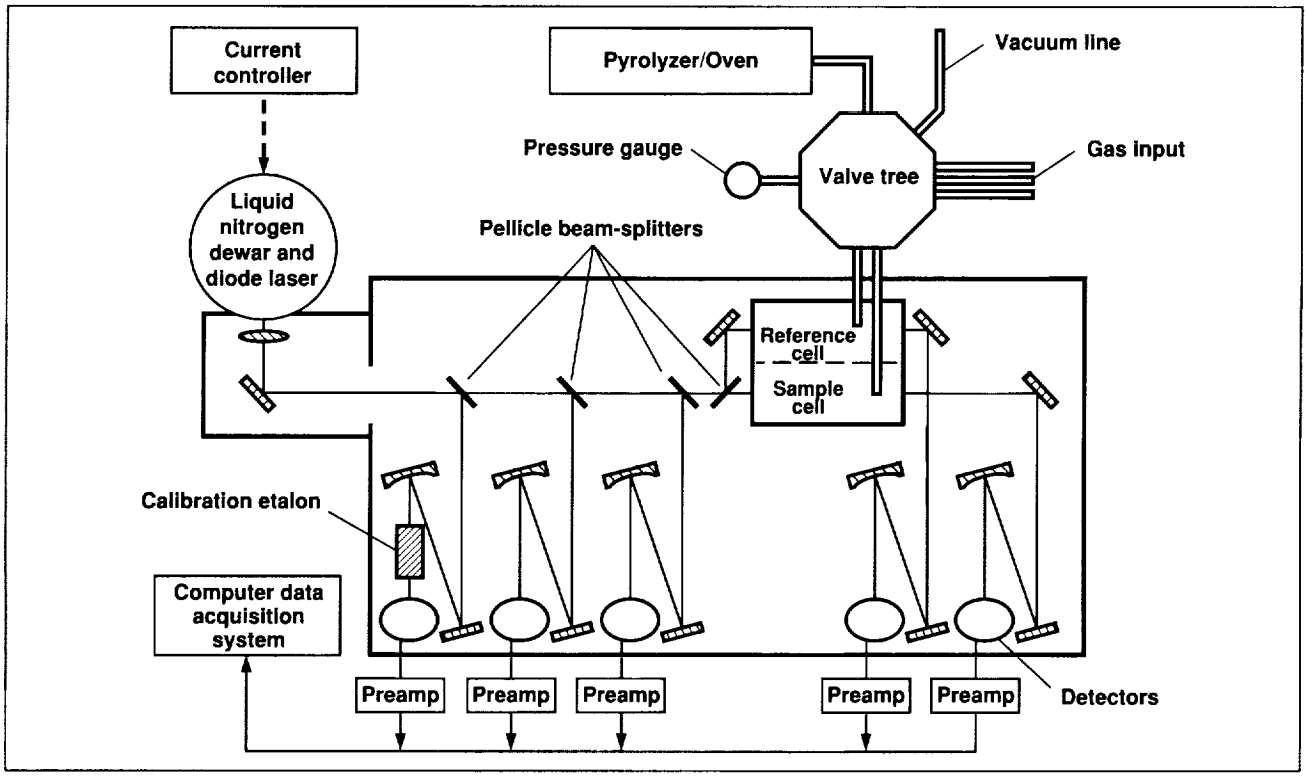


*Fig. 1. Schematic diagram of the stable isotope laser spectrometer (SILS-II) and pyrolyzer for soil carbon combustion.*

Major accomplishments for the year include the design and construction of a second-generation SILS (SILS-II) and the integration of this new instrument with a pyrolysis oven for processing soil analogs. These developments provide further progress toward our goal of measuring the ratios of carbon and oxygen stable isotopes in soil and ice samples on planetary surfaces. The figure is a schematic diagram of the SILS-II instrument and pyrolyzer.

The SILS-II instrument has increased the number of available instrument beams to five; two were available in SILS-I. This increase permits the simultaneous acquisition of calibration spectra and eliminates inaccuracies caused by system drift during data acquisition; system drift with time was evident in the analysis of data acquired using SILS-I. In addition, the new instrument has integrated, thermally coupled sample-reference cells that will reduce any temperature difference between sample and reference gases. This feature will eliminate any inaccuracies resulting from the temperature dependence or from absorption strength of spectral lines having different rotational quantum numbers.

The integration of a pyrolysis oven with the laser spectrometer provides the capability to analyze isotopic abundances in solid samples such as ice and soils. In planetary-exploration applications such as the Mars Polar Pathfinder mission, ice samples acquired from various depths of the north polar ice cap could, upon heating, yield carbon dioxide ($CO_2$) gas samples that would then be analyzed to determine values of $^{13}C/^{12}C$ and $^{18}O/^{16}O$. For a landing site south of the ice cap, carbon in acquired soil samples could be combusted in an oven to form the $CO_2$ for a laser-spectrometric determination of $^{13}C/^{12}C$. The integration of a pyrolysis oven into SILS-II provides capabilities applicable to NASA planetary exploration missions designed to provide information of importance to geologists and planetary scientists.

**Ames-Moffett contact: J. Becker/T. Sauke**
**(415) 604-3213**
**Headquarters program office: OSS**

## Wavelet Methods for Astronomical Time Series

**Jeffrey D. Scargle**

Much of the astronomical data obtained from NASA Great Observatories and other space-based telescopes are in the form of measurements over time of the brightness of an object. The brightness of many astronomical objects is highly variable, as a result of explosive or chaotic processes such as the accretion of matter onto a condensed star or black hole. "Wavelets" provide new analysis techniques for dealing with such data.

Wavelets are quasi-oscillatory basis functions that are localized in time (in contrast to the purely oscillatory basis functions in Fourier analysis). A new generation of analysis techniques has been developed to deal with both time-series data, such as those discussed above, and image data. These methods allow efficient smoothing, reconstruction, modeling, characterization, and compression of scientific data.

In collaboration with David Donoho of Stanford University, I have developed wavelet-based algorithms and collected them in a unified software package that forms a toolbox for time-series analysis. We include extensions of the basic wavelet transform techniques, including the ability to handle unevenly spaced data (of particular importance in astronomy), wavelet packet analysis, and time-frequency distribution methods (for the study of how the harmonic content of a signal can evolve in time). These routines will be provided to the community as a coherent package of routines in several data-analysis languages including MatLab, Octave, and IDL, as well as low-level programming languages such as FORTRAN and C, as part of a project funded by the NASA Astrophysics Data Analysis program.

One of the most useful signal diagnostics to arise from wavelets is the "scalegram," the wavelet analog of the power spectrum in Fourier analysis. Scalegram analysis of a long, high-time-resolution observation of

the low-mass X-ray binary (LMXB) Sco X-1, from the European X-ray satellite EXOSAT, led to the conclusion that the X-ray luminosity varies stochastically on time scales from milliseconds to hours. The nature of this variability—as quantified with both power spectra and scalegrams—agrees well with the "dripping handrail" accretion model, a simple dynamical system that exhibits transient chaos. This work has been carried out in collaboration with Donoho, James Crutchfield (University of California, Berkeley, and the Santa Fe Institute), James Imamura (University of Oregon), Thomas Steiman-Cameron (University of California, Santa Cruz) and Karl Young (National Research Council Fellow at Ames). In this model, both quasi-periodic and low-frequency noise, long known to arise in this star system, are produced by radiation from blobs with a wide size distribution as a result of accretion and subsequent diffusion of hot gas, the density of which is limited by an unspecified instability. Thus two observable characteristics (quasi-periodic oscillations and very-low-frequency noise) are seen as different aspects of the same chaotic physical process rather than two distinct physical processes as previously thought by the astronomical community.

Subsequently we have found that the dripping-handrail model appears to explain the observed temporal characteristics of a wide variety of astronomical sources, including such diverse objects as X-ray pulsars (rotating neutron stars that emit copious X-radiation) and active nuclei of galaxies. The common denominator seems to be accretion, thought to play a role in formation of the objects. Our simple, deterministic model thus may be a paradigm for a whole suite of astronomical sources that exhibit apparently stochastic (random or chaotic) luminosity changes.

**Ames-Moffett contact: J. Scargle**
**(415) 604-6330**
**Headquarters program office: OSS**

## Noise-Reduction Techniques Used to Process Multiplex Gas-Chromatographic Signals

**Maxine R. Shao, José R. Valentin**

Gas chromatography (GC) is an established technique used for the analysis of planetary atmospheres. Multiplex gas chromatography (MGC) is a refinement of GC in that it increases the signal-to-noise ratio (S/N) of the chromatographic signal, thereby allowing the determination of low-concentration chemical components.

The output from an MGC experiment is in a convolved form. Part (a) of the first figure shows a typical output, which, until deconvolved, is not interpretable. Part (b) shows the deconvolved chemical signal (chromatogram). In this study, both deconvolution and a filtering technique were applied to increase the S/N of MGC outputs.

The MGC signal output was computer simulated. Experimental parameters, such as the number of modulated impulses and the modulation input sequence, were varied. Two different deconvolution algorithms were applied to determine which yielded the most accurate results. Keeping all the experimental parameters fixed except the input modulation sequence, ten simulations were performed. These trials allowed a mean value of the peak heights of particular components and a standard deviation of the mean to be calculated. Given that this was a simulation, the exact input response function was known, thereby allowing a direct comparison with the values found after the deconvolution and filtering techniques were applied.

The filtering technique used to further increase the S/N is a method wherein chemical signals (peaks) of relatively large heights are mathematically subtracted from the MGC output. This output, after being deconvolved, demonstrates how the removal of the effect of these peaks positively affects the S/N of the resulting chromatogram. Part (a) of the second figure shows the chromatogram after the largest peak, at a

retention time of 101 seconds, has been removed. Part (b) shows the same chromatogram after the remaining peak, at 151 seconds, has been removed. Part (b) not only demonstrates the increase in S/N from the initial chromatogram (part (b) of the first figure), but also shows the recovery of a small peak, at 85 seconds, that was previously lost in the noise.

The deconvolution technique selected for these graphs was cross-correlation. Although it yielded an error of less than 13% for the accurate recovery of the two large peaks, in this case it failed to recover the small peak at all. After the filtering technique was

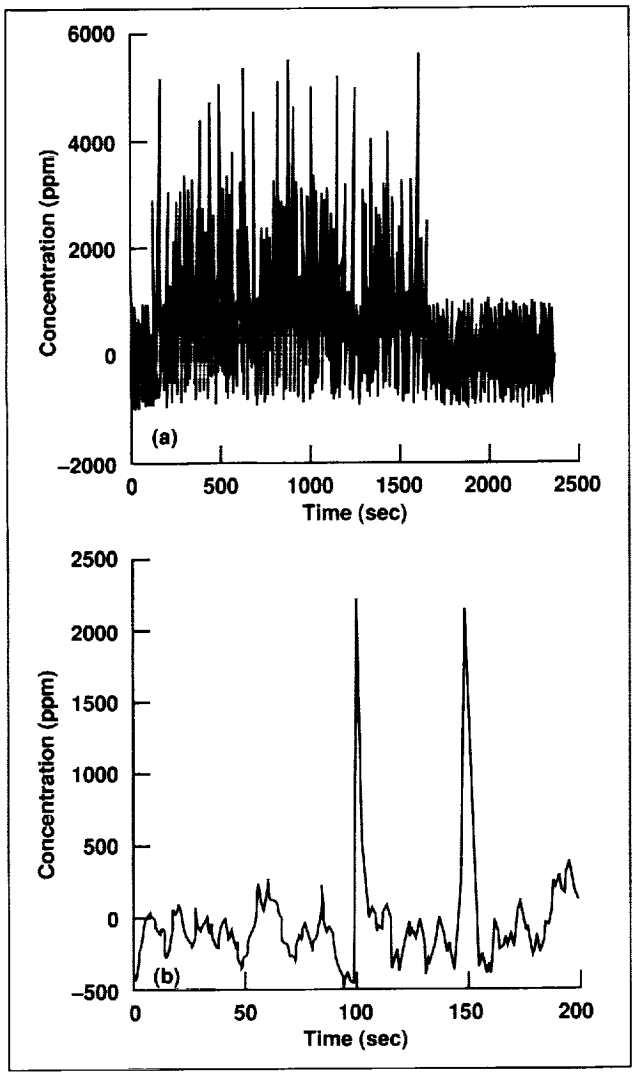


*Fig. 1. (a) Simulated MGC output in which the noise added about the baseline has an amplitude of 1,000 parts per million; (b) the deconvolved chromatogram.*

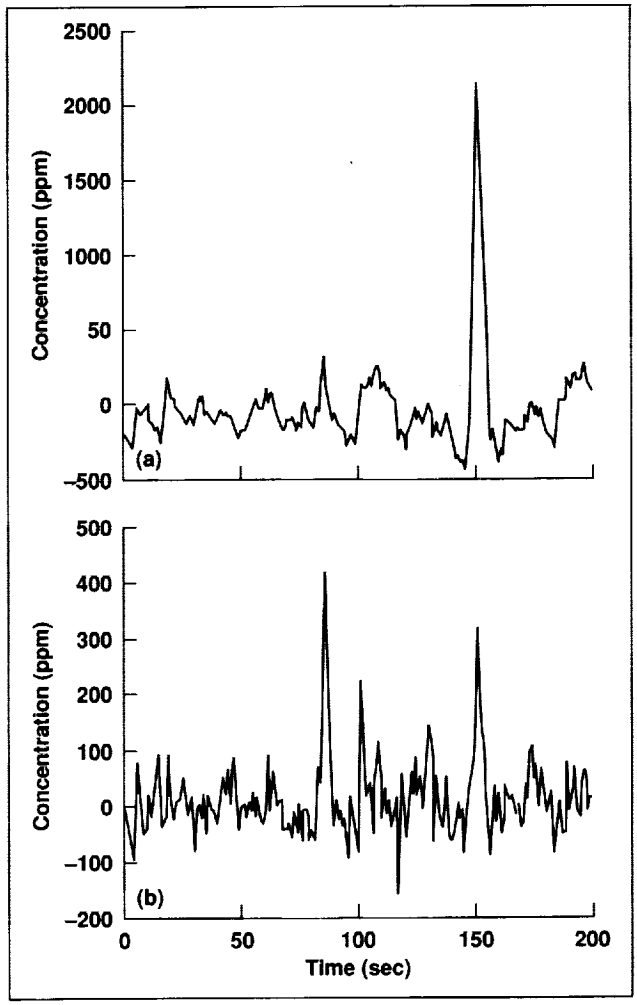


*Fig. 2. (a) Deconvolved chromatogram after the large peak at retention time of 101 seconds has been removed; (b) the same chromatogram after the remaining large peak at 151 seconds has been removed.*

applied, the small peak at 85 seconds was recovered with the small error of 5%, whereas in general this peak was recovered with a 25% error.

The noise amplitude before deconvolution was set in this simulation to be equal to 1,000 parts per million. Part (b) of the second figure shows the dramatic reduction in noise to less than 150 parts per million.

**Ames-Moffett contact: J. Valentin/M. Shao**
**(415) 604-5766/3212**
**Headquarters program office: OSS**

# Bonded Stainless-Steel Porous Layer Open Tubular (PLOT) Columns

Thomas C. Shen, Michael M. Fong

Fused silica tubing has been used in capillary columns for many years because it is inert and can be modified. Because the material is brittle, it is difficult to install and breaks easily on impact. Although coating columns with a polyimide can increase their strength, polyimide shrinks and becomes brittle at temperatures above 360°C. Shrinkage of the polyimide coating leads to spontaneous column breakage under normal stress. For this reason, polyimide-coated fused silica columns are not suitable for space missions. In addition, most bonded fused silica capillary columns are found to bleed, when a sensitive detector is used. In order to overcome these problems, an inert, coated stainless-steel capillary column was studied, and a bonded in situ polymerization Porous Layer Open Tubular (PLOT) stainless-steel column was developed. A PLOT column, with the adsorbent deposited on the wall of the column as a thin layer, results in open tubes with very high permeability so that very long columns, with high separation power, can be used. PLOT columns are particularly well suited for the analysis of light hydrocarbons, light gases, and light polar volatiles at or above ambient temperatures. A colloidal silica is fused onto the stainless-steel column at 1,000°C. Colloidal-silica-fused columns have better adhesion, durability, and crack resistance than unfused PLOT columns. These fused silica-coated columns have the following advantages: (1) they are easy to install because of the strong metal support, (2) they have higher resistance to shock damage, and (3) they do not bleed at temperatures below 150°C.

The figure shows the chromatogram of the separation of four inert gases and five hydrocarbons using the developed in situ polymerization bonded PLOT column. This column is made from the in situ polymerization of divinylbenzene and trivinylcyclohexane in a polymer-coated stainless-steel tubing. A number of data analysis techniques

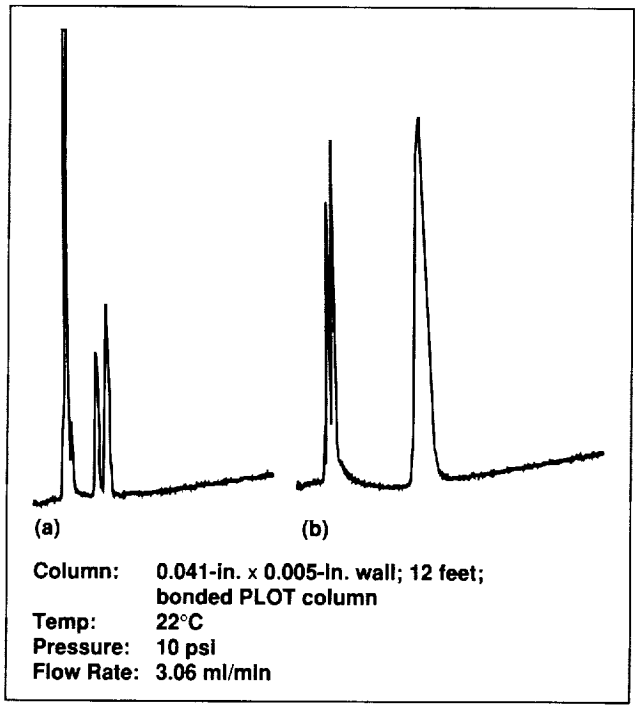


*Fig. 1. Gas chromatography separation of in situ polymerization bonded PLOT column.*

are being employed to optimize these gas-chromatographic results. Different sizes and concentrations of colloidal silica will be tested in order to obtain optimized adhesion, coating, and binding of the polymers, which will result in a better separation of compounds.

**Ames-Moffett contact: T. Shen/M. Fong**
**(415) 604-5769/1156**
**Headquarters program office: OSS**

# Numerical Experiments on Galaxy Structure and Evolution

**Bruce F. Smith**

Numerical experiments on galaxy models are providing new insights into the structure and dynamics of galaxies. Recent work on the internal dynamics of galaxies is yielding important clues to the nature of activity observed near the centers of galaxies, including the Milky Way. This work was done in collaboration with Richard H. Miller at the University of Chicago. The experiments were performed on the supercomputers at the Numerical Aerodynamic Simulation (NAS) Facility at Ames.

The figure shows views from various directions of the warping of a disk galaxy (yellow particles) after it has been captured by a larger, nearby galaxy (blue particles). The numerical experiments on the dynamics of the disk have led to the identification of various oscillatory modes and central activity in the galaxy models which are also indicated by observations of galaxies. Significant velocity differences are observed between the nucleus and the rest of a galaxy. Many observations also indicate a significant shift of the nucleus of a galaxy from the center as defined by the outer brightness profiles. The numerical experiments indicate systematic motions of a galaxy's nucleus that are surprising. These center motions are seen as the galaxy's dynamical evolution is followed in the computational experiments; the complex oscillations observed in the experiments indicate that the central regions of galaxies almost certainly are not in a static, steady state. These results bear directly on issues of nuclear activity seen in many galaxies, including our own. The results were recently published, and were included in the first video publication in the Astrophysical Journal.

The center motions raised the question of whether global motions that affect an entire galaxy are also present. Such global oscillations have also been found experimentally. The global oscillations of the galaxy models can be described in terms of characteristic motions of the entire galaxy. The most important modes can be described as (1) a breathing mode in which all parts of the galaxy move in and out in unison, and (2) a mode in which the galaxy sloshes: as material from the center moves out, the material in the outer portions moves inward, and then the pattern reverses as the oscillation progresses.

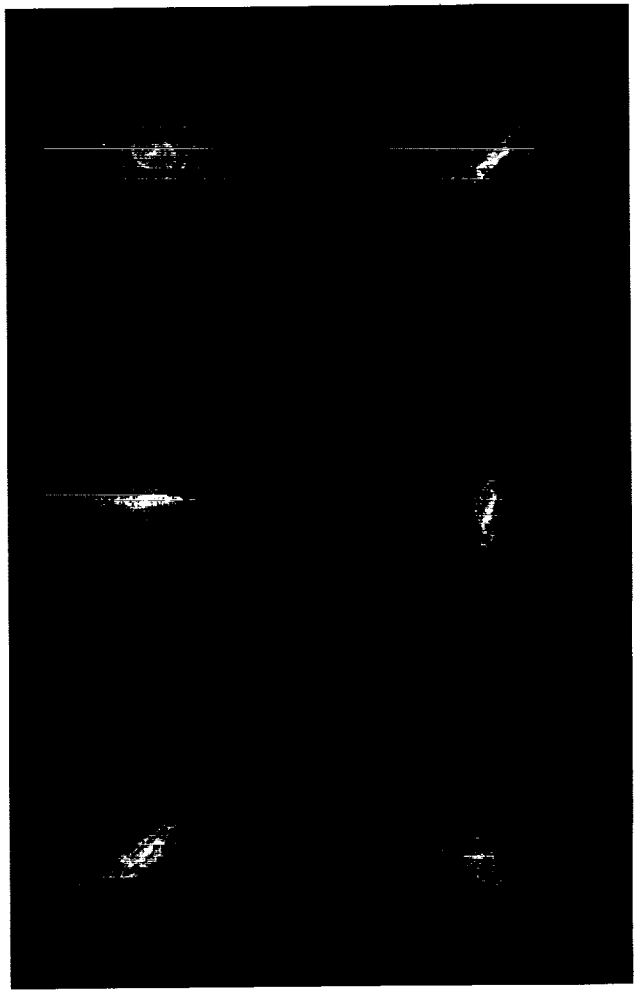

*Fig. 1. The warping of a disk galaxy (yellow particles) after it has been captured by a larger, nearby galaxy (blue particles). (See color plate 17 in Appendix)*

These global oscillations may have profound effects on our understanding of the shapes, dynamics, and evolution of galaxies.

The observational data on the morphology and kinematics of galaxies give us fascinating glimpses of these objects. The use of complementary computational experiments has become essential in our attempts to understand these beautiful, challenging objects.

**Ames-Moffett contact: B. Smith**
**(415) 604-5515**
**Headquarters program office: OSS**

## The Twisted Disk in the Galaxy NGC 4753

**Thomas Y. Steiman-Cameron**

Although a galaxy's shape is one of its most fundamental attributes, the shapes of galaxies are poorly known and understood. This is because most of the material in galaxies is unseen "dark matter." Therefore, the most obvious aspect of a galaxy, its visual appearance, tells us very little about the galaxy's true shape. New approaches are necessary to evaluate the distribution of matter, both luminous and "dark," in galaxies.

Particularly promising aids for evaluating the distribution of matter are the disks that are often found at unusual orientations in galaxies. Although many galaxies have disks, most disks lie in a plane along a principal axis of the luminous galaxy. What is required to investigate dark matter are disks that are warped and twisted and inclined with respect to a principal plane. These disks permit us to study the gravitational pull of the dark matter on the disk, and thus allow us to evaluate the overall distribution of material in the galaxy.

Recent work performed at Ames, in collaboration with Richard Durisen of Indiana University and John Kormendy of the Institute for Astronomy in Hawaii, used theoretical models of how a disk evolves in a nonspherical galaxy coupled with observations to determine the shape of a specific galaxy. The galaxy in question, NGC 4753, provides an ideal opportunity for such an investigation. NGC 4753 possesses prominent and chaotic-appearing dust lanes (see the top photographs in the figures). The dust is presumed to lie in a highly twisted disk that is thought to be the product of material captured from another galaxy. The nonsphericity of the galaxy causes the disk to change its orientation with time, a process referred to as precession. Precession is faster at smaller distances from the center of the galaxy than at larger distances; this difference is what causes the disk to become twisted.

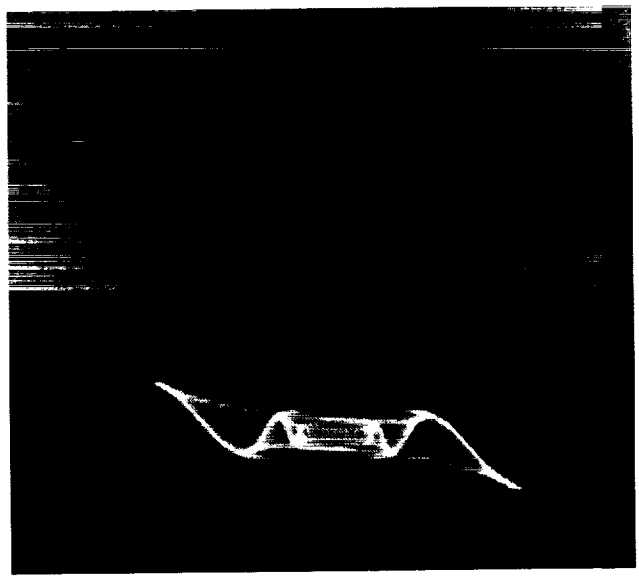

*Fig. 1. (Top) The galaxy NGC 4753, showing the complex structure of its dust lanes; (bottom) the appearance of a highly twisted disk model that was fitted to the dust lanes.*

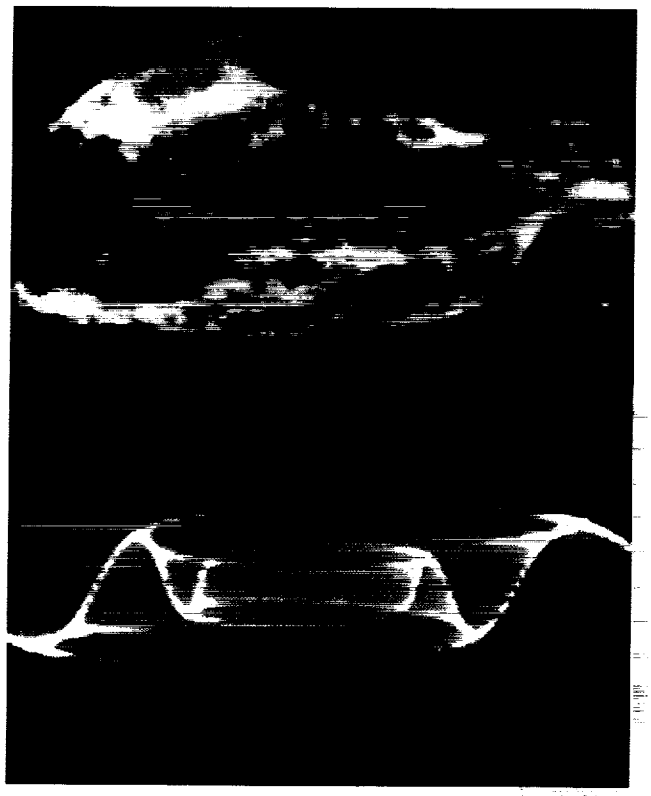

*Fig. 2. (Top) The inner regions of NGC 4753. The image has been processed in a manner designed to accentuate the dust lanes; (bottom) the twisted-disk model.*

Theoretical models allow one to predict the degree of twisting as a function of the shape of the underlying galaxy. Thus, by determining the true shape of the twisted disk we have been able to assess the distribution of matter in NGC 4753. The bottom panels in the figures display the appearance of a twisted-disk model that was fitted to the observed dust lanes. The model indicates that the unseen matter is nearly spherical but flattened slightly, somewhat like a hamburger bun. The distribution of dark matter is less flat than the galaxy's luminous matter. Also, most of the galaxy's mass must be dark matter to account for the severe twisting.

This study has provided the most accurate determination to date of the three-dimensional shape of a galaxy. Since shape is the product of a galaxy's formation and subsequent evolution, knowledge of shapes provides important insight into the underlying physical principles guiding the global structure of these island universes.

**Ames-Moffett contact: T. Steiman-Cameron**
**(415) 604-3120**
**Headquarters program office: OSS**

## Low-Gravity Aerosol Experiment Modeling

**David M. Stratton**

Aerosols (multiphase suspensions of liquid or solid particles in a gas) are important in a wide range of scientific disciplines, from astrophysics and cosmology to atmospheric science and climatology. Laboratory experiments on aerosols are limited in duration and particle size (or particle size distribution) because of gravitational settling. Levitation techniques may keep particles aloft longer, but such techniques have drawbacks such as suspending only specific sizes or restricting particle motion.

Aerosol experimentation in Earth orbit has been proposed both by NASA (the Gas-Grain Simulation Facility) and by the European Space Agency (the Columbus proto-planetesimal dust aggregation experiment). The very low gravitational accelerations in an Earth-orbital experiment would greatly decrease particle settling, allowing much longer experiments on aerosols with arbitrarily wide particle size distributions.

A potential problem for low-gravity aerosol experimentation is the limited size of the experiment chamber. Ground-based laboratory experiments are typically done in large chambers to minimize the

effects of the chamber walls on the experiment. In Earth orbit, volume is an expensive commodity that must be minimized. With increased potential for wall effects linked to the decrease in gravitational settling, several questions arise concerning the feasibility of these low-gravity aerosol experiments: (1) How do wall effects in a low-gravity aerosol experiment compare to those in a similar ground-based experiment? (2) Can the design of the experiment facility or the choice of experiment parameters reduce these wall effects? (3) Can wall effects be characterized so that they might be effectively removed from the data, allowing conclusions drawn from a contained experiment to be applied to a spatially unbounded aerosol?

A computer model of a low-gravity aerosol experiment has been developed to begin to examine these questions. The model contains algorithms for particle aggregation, Brownian diffusion, and particle loss resulting from particles touching and sticking to the chamber walls. It tracks the size distribution and spatial distribution of the aerosol particles as they evolve through time. If the output from this model is compared with that from models of ground-based experiments and from models of spatially unbounded

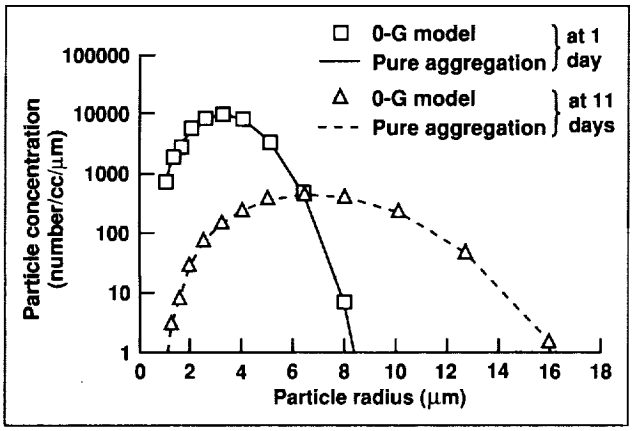


*Fig. 1. Particle size distributions for initial particle size of 1.0 micrometer by the low-gravity model prediction and by pure aggregation.*

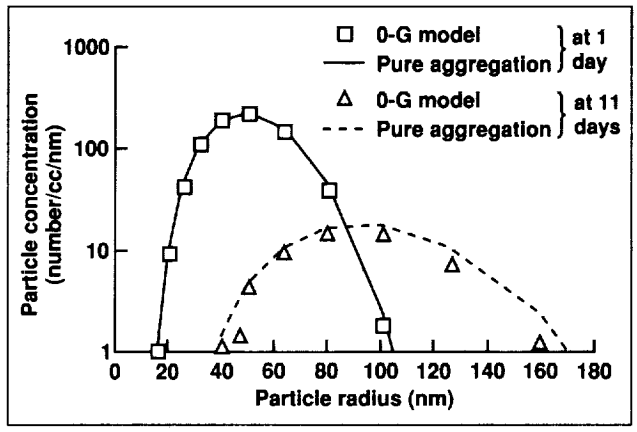


*Fig. 2. Particle size distributions for initial particle size of 10.0 nanometers by the low-gravity model prediction and pure aggregation.*

aggregation, the potential benefits of various low-gravity aerosol experiment configurations can be assessed.

At this point, the computer models indicate that ground-based experiments exhibit more particle loss than low-gravity experiments in similar volumes. This finding is based on tests with initial particle radii of 1.0 micrometer and 10 nanometers with initial concentrations of one million per cubic centimeter, and in an experiment volume 28 by 28 by 44 centimeters. As shown in the figures, the low-gravity model's particle size distribution remains remarkably similar to that in the spatially unbounded case even after a simulated experiment duration of 11 days. Both runs of the ground-based experiment model show no particles left after the first day. Further work in this area could investigate (1) the effects of particle size and concentration on the wall effects and on particle loss rates and (2) the importance of the experiment chamber's shape and size.

**Ames-Moffett contact: D. Stratton/J. Huntington**
**(415) 604-4204/3675**
**Headquarters program office: OSS**

# The Upcoming Collision of Comet Shoemaker–Levy 9 with Jupiter: Predictions

**Kevin Zahnle**

The pieces of Comet Shoemaker–Levy 9 are expected to strike Jupiter during the week of 21 July 1994. The comet presently consists of a score of fragments in orbit about Jupiter. The parent body was tidally disrupted on 8 July 1992, the date of its previous close approach. It is not known where the comet was before then. Whatever its origin, its terminus appears clear enough: the fragments will enter the Jovian atmosphere on or about 21 July 1994 at an escape velocity of approximately 60 kilometers per second and at entry angles near 45°. The impacts will occur on the far side of the planet as viewed from Earth; they will occur near the limb as viewed by Galileo, however, and near the center of the disk as viewed by Voyager 2.

We predict the catastrophic disruption and consequent explosion of comet fragments hitting Jupiter. If the largest pieces are as dark as Comet Halley, the upper limit of the fragment size is 5 kilometers across. If the fragments are this large, the collisions will release energy of about $10^{30}$ ergs, comparable to the energy released by the Cretaceous–Tertiary impact that destroyed the dinosaurs. But it seems more likely that the pieces are smaller, around 1 or 2 kilometers in diameter, so that the largest collisions would release a hundred times less energy. Our description of disruption and deceleration is directly based on our models of similar phenomena that occurred on Venus and Earth (described in the 1991 and 1992 Ames R&T reports). In these models we integrate equations describing aerodynamic drag and ablation of a spreading, fragmenting impactor. The Jovian impact will test these models. In our model, 1-kilometer-diameter comets penetrate to the 10-bar level, tens of kilometers below the water clouds.

In contrast to smaller, more familiar explosions, the energy released by kilometer-scale comets when they strike Jupiter is large enough that the explosion breaks through the atmosphere, the fireball expanding hundreds of kilometers above the Jovian cloud tops. We numerically model the explosion produced by 1-kilometer-diameter impactors in two dimensions using the astrophysical hydrodynamics code ZEUS–3D (work with Mordecai-Mark Mac Low, University of Chicago). Our simulations begin either with hot cylinders with dimensions suggested by the disruption and deceleration model or with an initial wake constructed from a moving line charge. The models with wakes evolve about twice as fast as the initially confined models.

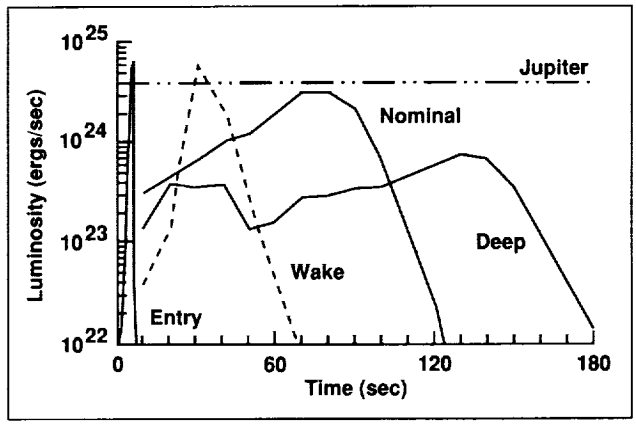


*Fig. 1. Predicted luminosity of the entering bolide and the subsequent fireball produced by a 1-kilometer-diameter comet striking Jupiter. The "deep" explosion is placed 1 scale height (50 kilometers) below the "nominal" explosion. The "wake" model assumes an entry shock produced by a moving line charge. Total sunlight reflected by Jupiter is shown for comparison.*

The numerical simulations are both qualitatively and quantitatively illuminating. The figure shows predicted light curves produced by the fireball. For atmospheric entry, light curves were computed assuming thermal radiation by clean Jovian air with a surface area consistent with the (changing) cross-sectional area of the impactor. On entry the largest bolides become very bright, possibly as bright as Jupiter for observers placed to see them, although for kilometer-sized impactors the luminosity peak is obscured by clouds. The time for entry is about 10 seconds. For the fireball, light curves were computed from the numerical simulations assuming

a grey atmosphere. Metals from the vaporized comet provide electrons that dramatically increase the opacity of Jovian air at low temperature; the resulting effective radiating temperature of the fireball is about 3,000 kelvin. The fireball rises through and above the atmosphere, brightening at first with increasing surface area, but later fading to invisibility as the temperature drops and the opacity plummets. The time for this process is about 100 seconds.

**Ames-Moffett contact: K. Zahnle**
**(415) 604-0840**
**Headquarters program office: OSS**

# Coadsorption of $CO_2$ and $H_2O$ on Mars

**Aaron P. Zent, Richard Quinn**

Physical adsorption is the process whereby molecules in a fluid phase concentrate at an interface. It occurs at every interface between a fluid and a solid. The Martian atmosphere is a fluid, and it is in contact with an enormous amount of surface area, the regolith. It has been understood for some years that more water and carbon dioxide ($CO_2$) may be adsorbed in the regolith than are present in the observable atmosphere. The regolith is probably the major reservoir of exchangeable volatiles on the planet.

Models of the regoliths' role in the Martian climate are based on the adsorptive behavior of water and $CO_2$, which are measured in laboratory experiments that involve only one gas or the other. If the relationships in the regolith materials do not mimic those seen in the laboratory, then estimates of the total volatile inventory in the Martian climate will be wrong. There is evidence that the presence of water will affect the adsorptive behavior of $CO_2$. To explore the importance of coadsorption, we have undertaken the first measurements of the simultaneous adsorption of water and $CO_2$ under conditions appropriate to the Martian regolith.

Our results suggest that the surface coverage of water is very low as a result of the low partial pressure of water buffered at the polar caps. Where fractional coverage approaches 0.5 monolayer, however, the amount of adsorbed $CO_2$ begins to decrease relative to its value at a relative humidity (RH) of 0 (see figure). This suggests that where RH is greater than about 60%, published adsorption isotherms may overestimate the inventory of adsorbed $CO_2$. This is a critical region because the previously established adsorption isotherms showed that almost all $CO_2$ was adsorbed poleward of 60° latitude, in exactly the places where the highest surface coverage by water would be anticipated. Numerical modeling of the climatic effects of coadsorption continues.

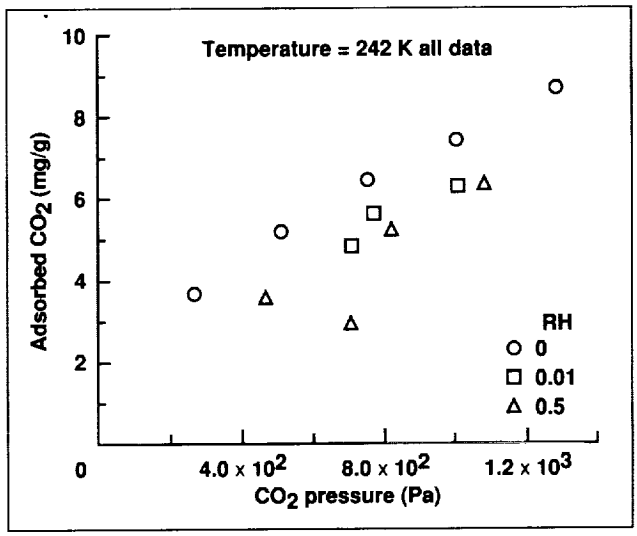


*Fig. 1. The adsorption of $CO_2$ at relative humidity of 0, 0.01, and 0.5. When the relative humidity becomes high and the fractional coverage of $H_2O$ approaches 0.5 monolayer, $CO_2$ is displaced from adsorption sites.*

**Ames-Moffett contact: A. Zent**
**(415) 604-5517**
**Headquarters program office: OSS**

# The Electrochemistry of the Martian Soil

**Aaron P. Zent, Christopher P. McKay**

Possible interpretations of the results of the Viking Biology Experiments suggest that more than 1 part per million of a thermally labile oxidant, perhaps hydrogen peroxide ($H_2O_2$), and about 10 parts per million of a thermally stable oxidant are present in the Martian soil. We have reexamined these results and their implications for future missions, including their possible effects on human health and engineering. We conclude that further characterization of the reactivity of the Martian regolith materials is warranted. If our present understanding is correct, however, the oxidant does not pose a hazard to humans.

There are difficulties with explaining the reactivity of the Martian soil by oxidants. Most bulk phase compounds that are capable of oxidizing $H_2O$ to $O_2$ as in the Gas Exchange Experiment (GEx) are thermally labile or unstable against reduction by atmospheric $CO_2$. Models invoking trapped $O_2$ or peroxynitrates ($NOO_2^-$) require an unlikely geologic history for the Viking Lander 2 site. Most suggested oxidants, including $H_2O_2$, are expected to decompose rapidly under Martian ultraviolet radiation. Nonetheless, we conclude that the best model for the Martian soil contains oxidants produced by heterogeneous chemical reactions with a photochemically produced atmospheric oxidant. The GEx results may be due to catalytic decomposition of an unstable oxidizing material by $H_2O$.

We show that interfacial reaction sites covering less than 1% of the available soil surfaces could explain the Viking Biology results. Because of (1) the low concentration of reactive agents, (2) the fact that the reactive agents are probably composed of elements that are common in the soil, and (3) the observed instability of these agents, it is unlikely that a sample return mission would be effective in identifying them. Methods for in situ characterization of the oxidant must be developed that are consistent with the dry state of the soil. Traditional terrestrial methods of characterizing the standard oxidation–reduction potential (Eh) of the soil are unsuitable. Alternative methods must be developed; one approach under development involves exposing a wide variety of materials to the Martian regolith and monitoring their reaction.

**Ames-Moffett contact: A. Zent**
**(415) 604-5517**
**Headquarters program office: OSS**

# The Constant-Current Loop: A New Paradigm for Resistance Signal Conditioning

Karl F. Anderson

A novel interface circuit, originally developed for high-temperature structural testing, makes strain gages and resistance temperature detectors (RTDs) significantly easier to use in a variety of applications. Its key advantage is that, unlike a Wheatstone bridge, the new circuit is unaffected by parasitic resistances stemming from lead wires and electrical connectors. Fewer connecting wires may be required in multi-sensor installations; other advantages include linear output, high sensitivity (twice that of a Wheatstone bridge), and a bandwidth that extends to dc. This innovation is the subject of various patent applications.

In the first figure, a sensor and a reference resistor are shown wired in series. A current regulator completes the circuit, forcing a known, constant current through the loop. The system output $V_{out}$ is simply the difference between the voltage across a gage $V_g$ and that across the reference resistor $V_{ref}$. By solving a few circuit equations, the voltage difference can be related to a sensor's output signal $\Delta R$:

$$V_{out} = V_g - V_{ref} = I[(R + \Delta R) - R_{ref}]$$

where

$$R_{ref} = R$$

$$V_{out} = I(\Delta R)$$

The effect of lead-wire resistances $R_{w3}$ and $R_{w4}$ can be ignored, provided the measuring circuit has a sufficiently high input impedance. As a rule of thumb, if the impedance of the measuring device is at least one million times that of the lead wires, negligible voltage will drop across the leads.

Ordinarily, the initial resistance R of a gage will be slightly different than that of the reference resistor $R_{ref}$, causing a correspondingly small offset in the output. But once calibrated, this offset can be subtracted in data reduction (a procedure common to Wheatstone-bridge measurements).

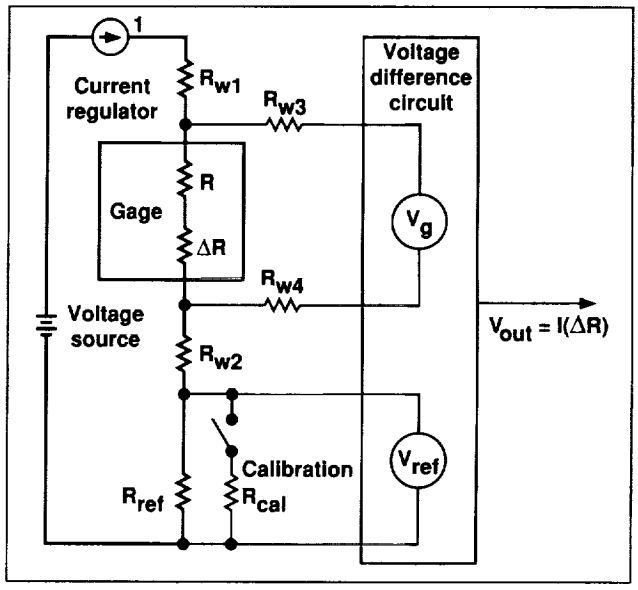


*Fig. 1. The fundamental current loop circuit.*

The second figure illustrates a practical means to accomplish the voltage-difference function. A stable instrumentation amplifier component reproduces the gage voltage $V_g$ at a point in the circuit where it can subtract directly from the reference voltage $V_{ref}$. The gain K is typically selected somewhere between one and ten.

Multiple gages may be included in the same current loop. Their outputs are sensed by subtracting the same reference voltage $V_{ref}$ from each individual gage voltage $V_g$ with separate voltage-difference circuits.

Multiple gages in the same current loop can be wired in additive and subtractive groups. The circuit can then accomplish analog computations with greater linearity than those computed by the Wheatstone bridge.

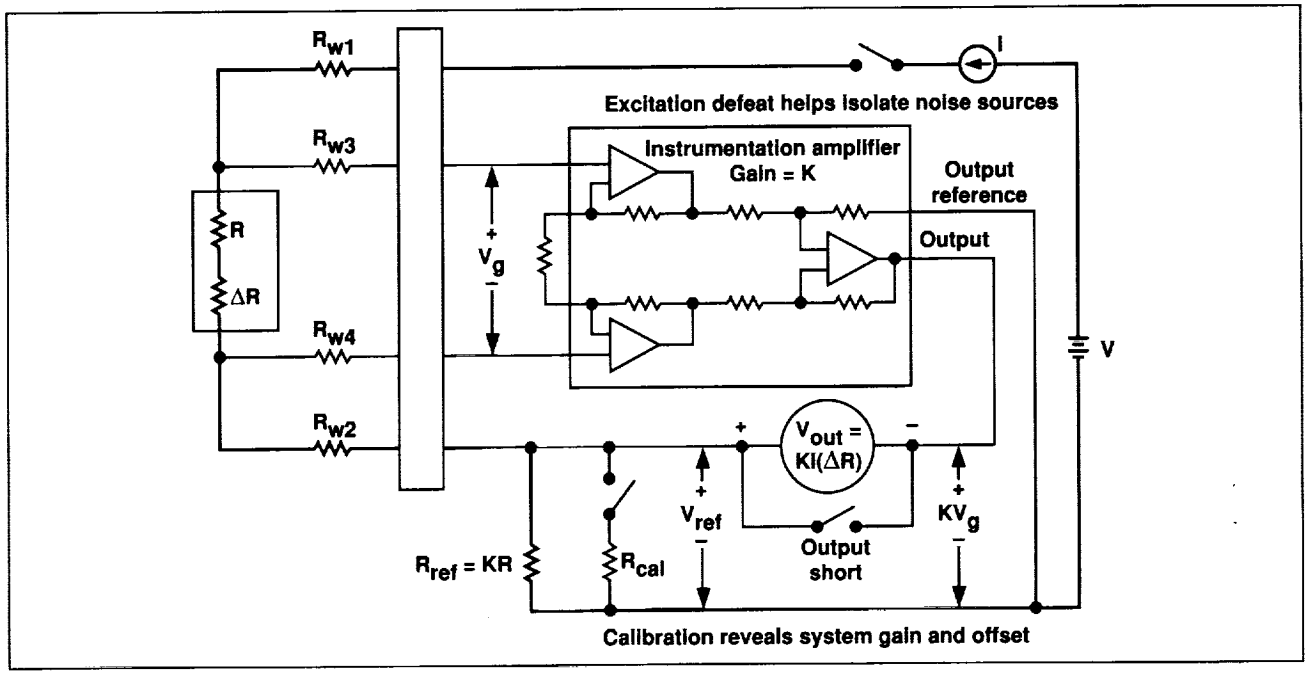


*Fig. 2. A practical current loop system.*

Of course, the circuit is not without disadvantages. In order to make lead-wire resistances irrelevant, the circuit requires four lead wires to hook up a single gage. However, a three-wire current-loop configuration is practical if one accepts a drawback of the Wheatstone bridge: Lead-wire resistance must track with changes in temperature, pressure, and so forth. In multigage applications, for example a strain gage rosette, the constant-current loop has the advantage of using fewer wires per gage than a Wheatstone bridge.

**Ames-Dryden contact: K. Anderson**
**(805) 258-3549**
**Headquarters program office: OA**

# Flight-Test Results for the Landing Systems Research Aircraft

**John F. Carter**

The goal of the Landing Systems Research Aircraft (LSRA) is to gather research data regarding orbiter landing-gear failure modes and effects and orbiter tire/surface response characteristics. In order to achieve this goal, a Convair 990 medium-range jet transport was modified with a test fixture mounted between the two main landing gears (see figure). This test fixture can be vertically extended onto a runway while being rotated through a steering angle. The initial flight-test phase of this vehicle has been completed at the Kennedy Space Center (KSC) and the results are being used in planning orbiter missions.

There were four goals for the flight test at the Kennedy Space Center: (1) to validate the LSRA as a tire test facility on the KSC orbiter runway, (2) to validate Langley Research Center (LaRC) orbiter tire-wear models, (3) to validate (LaRC) tire-force models, and (4) to demonstrate tire performance on simulated orbiter profiles to verify current landing crosswind limits for the orbiter.

During a typical landing test sequence, the LSRA makes a final approach with the flaps up. At touchdown, spoilers are deployed as the vehicle derotates. When the speed of the LSRA matches the test-profile condition, the test fixture is activated and the test gear is automatically extended and rotated through test profiles of vertical load and slip angle. Upon completion of the test, the test gear is retracted.

Validation of the LSRA on the KSC runway was performed by simulating a time history of an actual shuttle landing. The tire wear of the LSRA test tire was then matched against photographs of the orbiter main-gear tires from that landing. Rockwell International provided time histories of load, slip, and speed

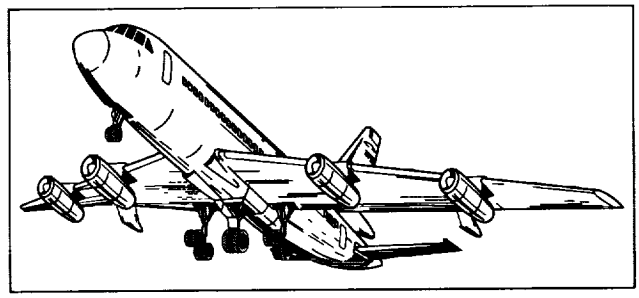

*Fig. 1. The Landing Systems Research Aircraft.*

derived from orbiter flight STS-51D. These commanded time histories were programmed into the LSRA, and a test run was executed. The resulting LSRA test tire matched the orbiter tire photographs very well, thus validating the LSRA as a tire test facility for this application.

Once confidence was gained in the LSRA through validation, the remaining work was completed with the following results: (1) side forces on the KSC runway were somewhat lower than predicted by the LaRC model, (2) drag forces are lower than predicted by the LaRC model, (3) tire wear is much higher than predicted by the LaRC model, and (4) crosswind limits for orbiter landings on the KSC runway may have to be modified because tire wear is greater than predicted.

**Ames-Dryden contact: J. Carter**
**(805) 258-2025**
**Headquarters program office: OA**

# Predicted Performance Improvements in a Thrust-Enhanced SR-71

Timothy R. Connors

NASA is evaluating the use of the SR-71 Blackbird as a mother ship for the hypersonic air-launch option (HALO) vehicle. The SR-71 would carry the unmanned vehicle to an altitude of 70,000 feet at a flight speed of Mach 3.0, where it would separate, fly automatically to very high Mach, and then be retrieved later for reuse. The SR-71 is capable of shouldering the weight and size of this type of vehicle in a back-mounted configuration but would have a shortage of excess thrust in the transonic speed range because of the large drag increase.

Pratt & Whitney (West Palm Beach, Florida) studied the feasibility of increasing the thrust of the SR-71's engines. They concluded that the engine control could be easily modified to increase thrust by means of a hotter-running core section. Also, nitrous oxide could be safely injected into the afterburner section to provide additional thrust with only minor engine hardware changes.

An aircraft performance-prediction computer program is used at Dryden to determine various performance indices for different aircraft. It was altered to include the SR-71-specific data and was used to predict the changes in Blackbird performance with the addition of the HALO vehicle and thrust enhancement.

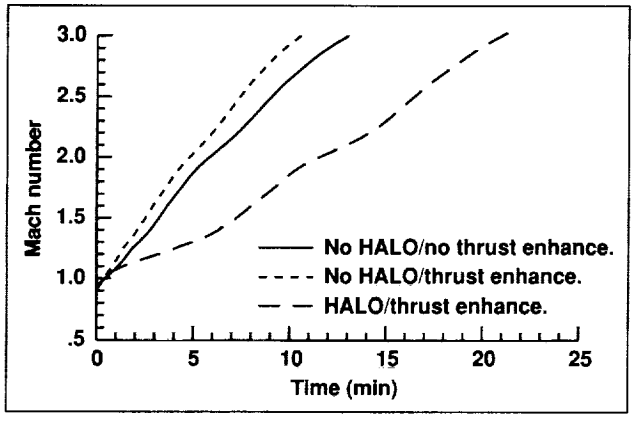


*Fig. 1. Comparisons of SR-71 acceleration times.*

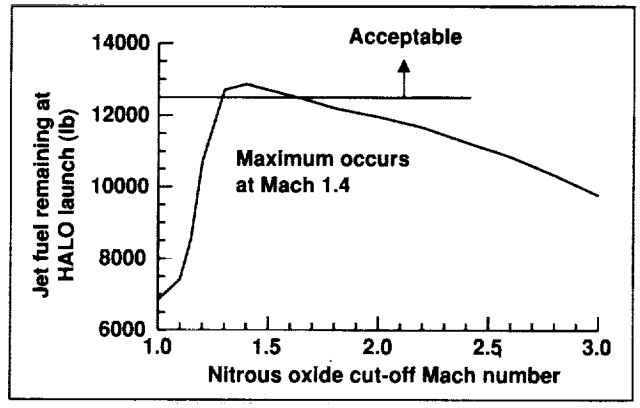


*Fig. 2. Jet fuel remaining as a function of nitrous-oxide cut-off at Mach 1.4.*

Simulated climb profiles were flown to the HALO launch condition at a constant equivalent airspeed of 500 knots. When nitrous oxide was used, it was injected at a flow rate per engine of 8 pounds per second. The first figure displays the Mach-versus-time traces with and without thrust enhancement. Without the engine upgrade, the SR-71 could not accelerate through the transonic flight regime with HALO. The simulation predicted a 20% improvement in the acceleration time of the SR-71 with no HALO using the engine upgrade. When HALO is added, the effect is substantial. It takes the vehicle combination more than 21 minutes to reach the launch speed.

The first figure shows that the vehicle can theoretically reach the target launch condition with HALO, but it was also necessary to see if the required amounts of jet fuel and nitrous oxide exceeded the SR-71's capacity. The Blackbird requires a minimum of 12,500 pounds of jet fuel to return to base from the launch point. Longer nitrous-oxide burn times result in large improvements in excess thrust and corresponding reductions in acceleration time, but the process is very fuel-inefficient. Once past the transonic drag pinch, the benefits of nitrous injection

wane rapidly. As the second figure shows, maximum jet fuel remaining at the HALO launch condition occurs when the nitrous injection is terminated at Mach 1.4. This maximum value barely exceeds the required amount.

The HALO vehicle has recently undergone a major design iteration and is now substantially smaller. The SR-71 performance model will be modified to reflect the change in the aerodynamic data. The large reduction in weight and drag will provide a much greater margin between the amount of jet fuel remaining after HALO launch and the amount required to safely return to base.

The thrust enhancement would allow the rigorous performance requirements of a HALO-type mission to be met. In addition, it would allow the SR-71 to carry heavier, higher-drag captive-carry experiments to the high-speed end of the envelope, and to collect research data for a much longer period than would be possible otherwise.

**Ames-Dryden contact: T. Conners**
**(805) 258-3324**
**Headquarters program office: OA**

## A Flight-Test Fixture for Aerodynamic Research

**John H. DelFrate, David M. Richwine**

A wide variety of basic aerodynamic research experiments have been conducted during the past 30 years on a specially designed, fin-shaped flight-test fixture (FTF). This fixture has provided well-defined, steady, uniform flow over a large Mach- and Reynolds-number envelope when installed on an F-104 aircraft. The FTF is easily modified to accommodate experiments and the means to transmit resulting data to the ground station. Upon completion of experiments, the FTF can be quickly removed to allow the aircraft to carry on its normal support duties while the FTF is free to be modified for the next experiment.

In recent years a successor fin with additional capability, called the FTF-2, was designed and built, and is undergoing initial flight testing on an F-15B (see first figure). The FTF-2 design required a multidisciplinary effort to meet the objective of obtaining good flow quality for aerodynamics and fluid-mechanics research experiments while maintaining a functionally flexible configuration. The design effort focused on a larger fixture that took into consideration the prior experience with the F-104/FTF combination as well as F-15B operational considerations.

The design effort resulted in a rectangular-shaped fin with a replaceable 12° elliptical leading edge, as shown in the first figure. The FTF-2 was fabricated primarily from carbon fiber and epoxy and designed for flight speeds up to Mach 2. The FTF-2 is 107 inches long, 32 inches high, and 8 inches wide. It consists of an upper and a lower section with the upper section designed to carry instrumentation. The lower section is removable and designed to carry the experiments.

The F-15B/FTF-2 combination recently completed initial flight testing up to speeds of Mach 1.3. Surface flow visualization and handling-quality tests were conducted in this flight phase. Flow visualization showed that the flow is predominantly streamwise with some flow unsteadiness at higher speeds. Some downwash effects were observed near the top of the nose piece at supersonic speeds. Because of its modular construction, the FTF-2 can be modified to improve flow quality if necessary. Handling qualities with the FTF-2 installed on the F-15B are similar to those present when the F-15B is

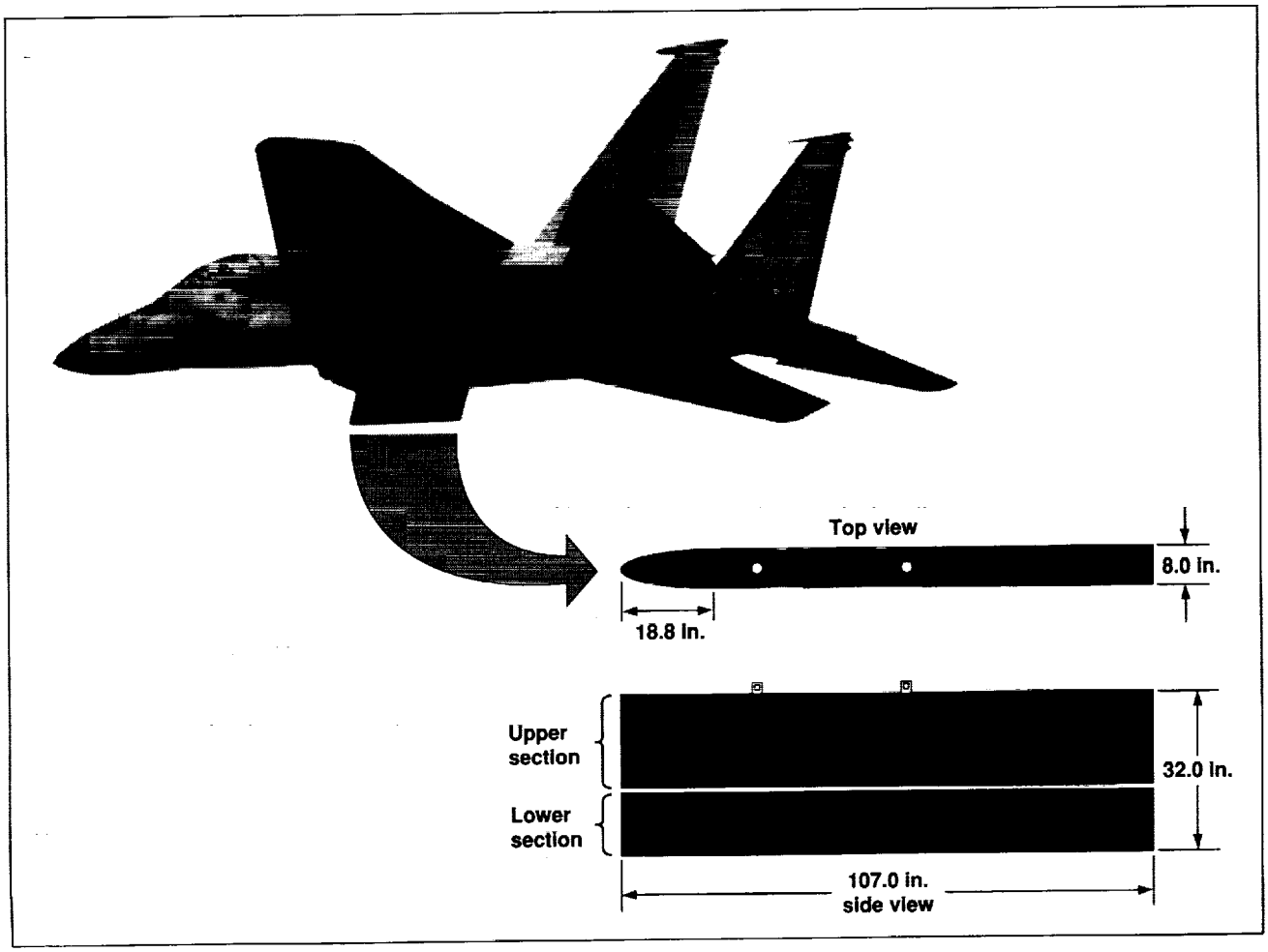


*Fig. 1. Placement and dimensions of the FTF-2.*

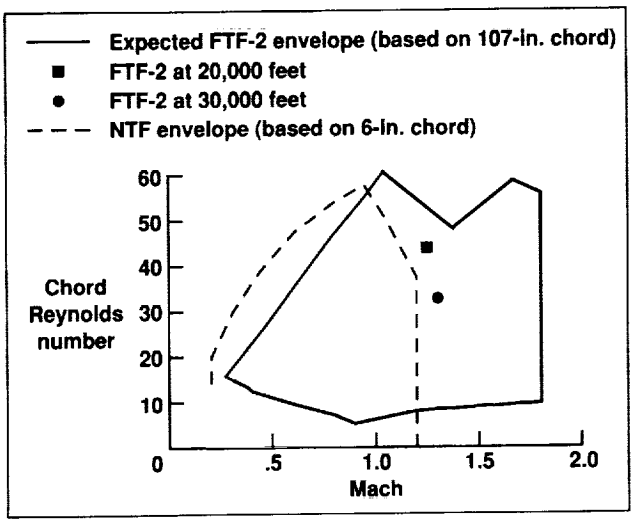


*Fig. 2. Mach- versus Reynolds-number comparisons.*

configured with the centerline fuel tank. The second figure shows a comparison of the maximum Reynolds-number values achieved at 20,000 and 30,000 feet in this first flight phase along with the anticipated full flight envelope. The test envelope of the National Transonic Facility is included to provide an example from a ground test facility.

**Ames-Dryden contact: J. DelFrate**
**(805) 258-3704**
**Headquarters program office: OA**

# Sonic Boom Near-Field Flight-Test Measurements

L. J. Ehernberger, Edward A. Haering, Stephen A. Whitmore

The near-field sonic boom overpressure signatures of the SR-71 airplane were measured using the noseboom of a close-flying F-16XL aircraft at the Ames-Dryden Flight Research Facility. Vertical separation distances between the aircraft ranged from less than 100 feet to more than 500 feet for the tests performed at 50,000 feet altitude and Mach 1.8. Such data are needed to establish the validity of computational fluid dynamics (CFD) solutions for sonic boom strength near the generating aircraft where strong nonlinear effects are present, as well as the subsequent propagation to ground level. Development of the near-field shock-wave characteristics occurs a few body lengths below the airplane and is generally beyond the space available for measurement in wind-tunnel tests. Both CFD and wind-tunnel tests are needed for the design of "low boom" supersonic aircraft configurations that would be environmentally compatible with flight routes over sensitive areas. Low-boom aircraft would be economically viable for many more transoceanic and transcontinental city pairs than would conventional-planform supersonic aircraft, which would be restricted to subsonic flight over most land routes.

Previous in-flight measurements of near-field sonic boom overpressure were obtained for the B-58 and B-70 aircraft during the 1960s. These were limited, however, to vertical separations of at least 1,500 feet and lateral separations of more than 160 feet when flying at the generator airplane altitude. For the 1993 flight tests, the pilot positioned the F-16XL below and to the rear of the SR-71. As the F-16XL moved forward, the SR-71 near-field overpressure was measured at the pitot and static pressure orifices on a conventional flight-test noseboom. Variations in the total pressure data depict the local shock wave structure of the SR-71, as represented by the curves for two probe distances in the first figure. Separate FPS-16 tracking radar were used to obtain the relative positions of the aircraft. Prior to the SR-71 mission, the flight-test technique was demonstrated by probing below an F-18 airplane. Trajectory reconstruction techniques using onboard acceleration and altitude data are also being used to enhance the detailed features of the basic radar trajectory positions and velocities. To confirm the pitot pressure measurements of the sonic boom signature, the static-pressure amplitude and phase data are being reinterpreted in the frequency domain and deconvoluted to extract the true static-pressure time history.

As is evident in the first figure, flight-test results also show the behavior of the overpressure features, or sonic boom signature, in terms of distance from

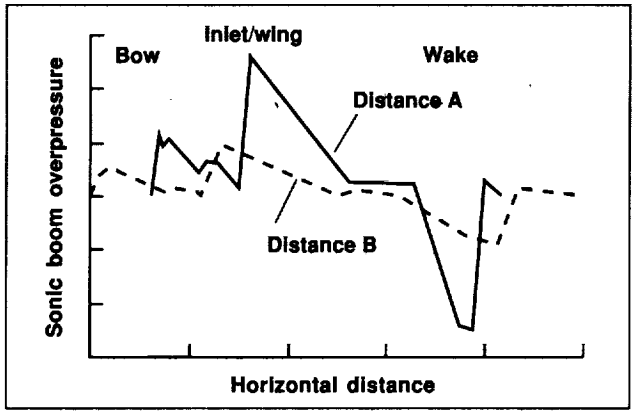


*Fig. 1. Sonic boom overpressure signatures for two distances from the SR-71.*

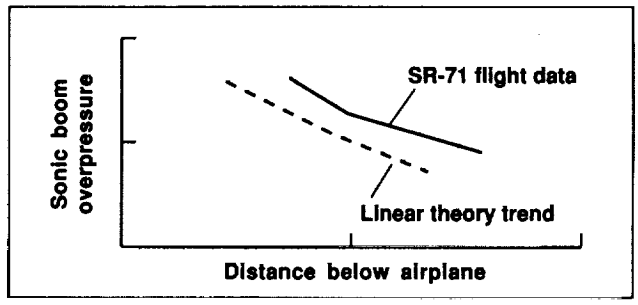


*Fig. 2. Overpressure vs. distance from the SR-71, from flight data and theory.*

the SR-71 as the shock wave forms in the near field. As distance from the generating aircraft increases, overpressures decrease and the signature length increases. The flight-data trend for the decrease in overpressure with distance is compared with the linear-theory trend in figure 2. Validation of CFD codes with these data is critical to their use in the design and development of low-boom supersonic passenger aircraft.

**Ames-Dryden contact: L. Ehernberger**
**(805) 258-3699**
**Headquarters program office: OA**

## Vibration Parameter Estimation with Error Bounds

**Lawrence C. Freudinger**

Ground-based and in-flight vibration tests (experimental modal analysis) are required for new or modified aircraft to ensure that the aircraft are safe to fly. These tests measure the effects of aerodynamic forces and control-system forces on the airframe's vibration characteristics. In particular, the goal is to monitor the vibrations in flight and to identify unstable flight regions before entering them. Failure

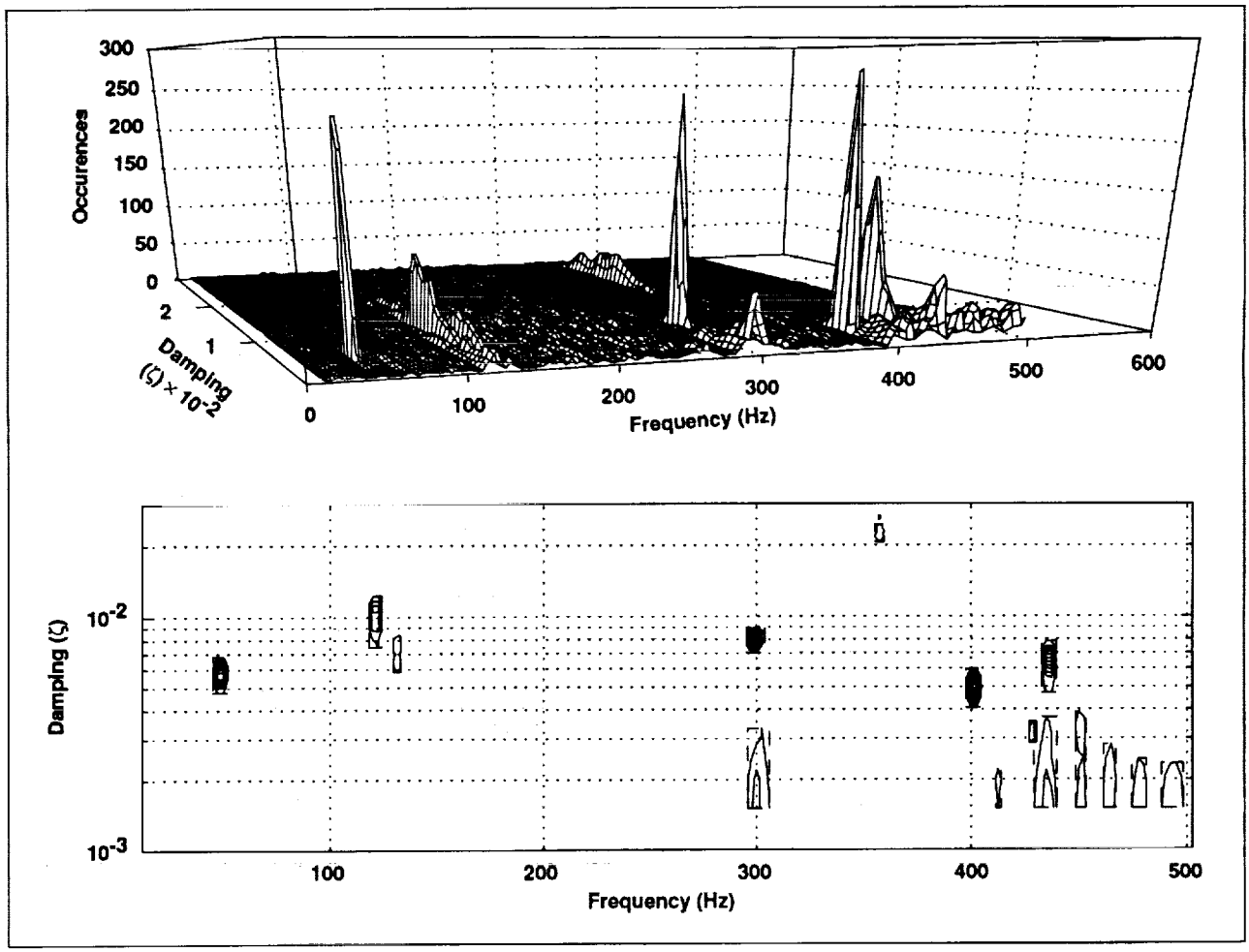


*Fig. 1. Two-dimensional histogram of all pole estimates: perspective view (top) and contour view (bottom).*

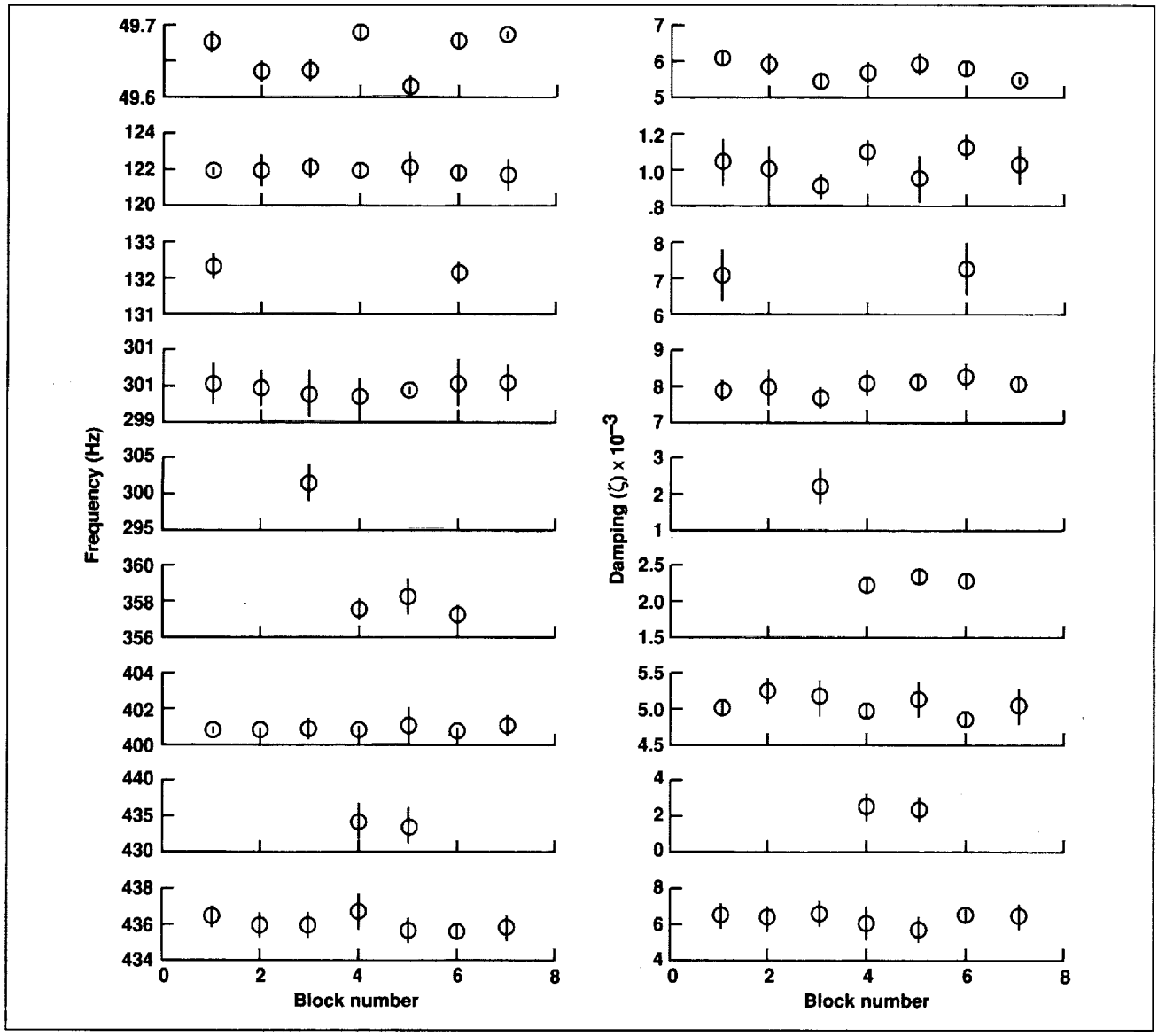


*Fig. 2. Results from experimental data analysis: frequency estimates (left) and damping estimates (right) versus run number.*

to identify these unstable regions can result in loss of the aircraft.

Improved techniques for observing the vibration characteristics of aircraft are being developed at the Ames-Dryden Flight Research Facility. Specifically, Dryden researchers have begun to investigate null space methods for estimating pole values (frequency and damping) in autoregressive systems.

In spite of significant efforts by many researchers to extract the "best" estimates possible, it turns out that most algorithms in widespread use today do not provide an adequate indication of the uncertainty of these estimates. Null space methods can generate redundant sets of estimates of a system, an ability that can be exploited to generate empirical error bounds on the estimates. This is possible by overspecifying the number of modes active in the measured data. A large degree of overspecification yields many estimates, some of which are not useful (these are often called computational poles). To sift through all these

estimates and decide which ones are useful, nontraditional methods for viewing the results and establishing error bounds are required.

One approach to establishing the error bounds uses two-dimensional histograms to heuristically separate meaningful estimates from those that are unreliable. For example, the first figure shows two views of a histogram indicating the distribution of frequency and damping estimates derived from separately analyzing seven sensor time histories from the same structure. The upper drawing is a three-dimensional perspective view of the number of pole estimates generated versus both frequency and damping. The lower drawing is a contour map of the same information viewed from above. The contours were chosen to isolate the dominant peaks. The lowest-level contour (in this case 10% of the maximum value in the histogram) identifies regions containing the pole value for a particular mode. The estimate and its error bound are subsequently defined as the average and standard deviation of all the pole values within a particular region.

The second figure displays the results derived from the first figure. The left column shows the resulting frequencies with error bounds plotted against the data set number. The right column shows the corresponding damping estimates, also with error bounds. These results represent only estimates that have a confidence factor above 50%; consequently, the nine poles indicated in the first figure correspond to the nine tallest peaks in the second figure.

This approach to vibration parameter estimation for linear systems displays attributes that make it a viable approach for experimental modal analysis. Research efforts to further understand the characteristics of null space methods are under way, as are efforts to improve and automate the calculation of error bounds.

**Ames-Dryden contact: L. Freudinger**
**(805) 258-3542**
**Headquarters program office: OA**

## Pressure-Sensing Performance of Upright Cylinders in a Hypersonic Boundary Layer

**Steven A. Johnson**

Measuring boundary-layer stagnation pressures in a high-Mach-number/high-stagnation-temperature environment is a fundamental problem for future hypersonic flight vehicles. For the hypersonic flight regime, the practice of using conventional rakes that employ protruding pitot tubes is not an option because of the likelihood of heating-related failure of the pitot tubes.

A rake without the protruding pitot tubes is an attractive alternative to a conventional rake design. By eliminating the protruding pitot tubes, the survivability of the rake would be ensured, but the pressure-sensing accuracy is unknown. As a result, the Ames-Dryden Flight Research Facility and Langley Research Center conducted the first such experimental investigation of the pressure-sensing performance of upright cylinders in a Mach-10 boundary layer. In this study, upright cylinders of 0.25-inch, 0.5-inch, and 1-inch diameter and a

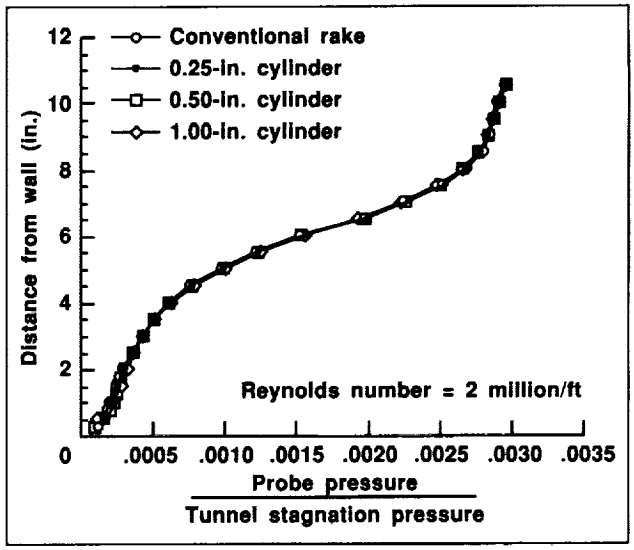


*Fig. 1. Comparison of conventional rake pressures and the cylinder leading-edge pressures.*

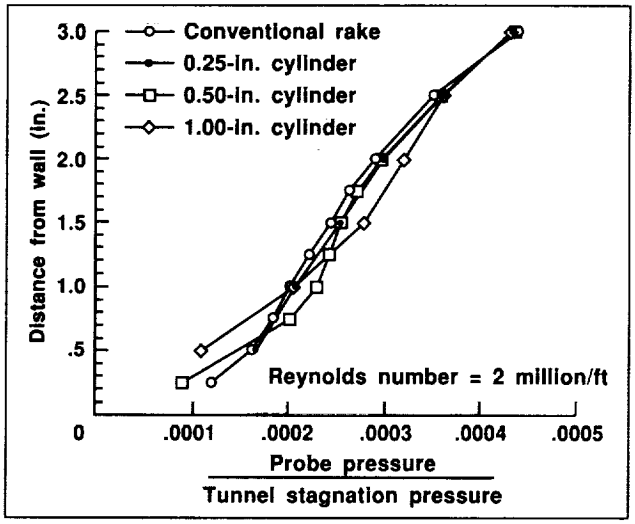


*Fig. 2. Pressure comparison for the first three inches from the wall.*

conventional rake were placed in the test-section sidewall boundary layer of Langley's 31-Inch Mach-10 Wind Tunnel. Boundary-layer pressure profiles measured on the leading edges of the three cylinders were compared to conventional rake measurements over a freestream Reynolds-number range of 0.5–2.0 million per foot.

The results of the test are summarized in the two figures. As shown in the first figure, the cylindrical rakes show no distortion of the "overall" boundary-layer stagnation pressure profile. On the other hand, a closer look near the wall (second figure) does show a diameter influence on pressure measurement. As the cylinder diameter increases, the pressure profiles deviate more from the conventional rake values. This is due to the influence of the separation bubble that is positioned at the wall/cylinder junction and scales with cylinder diameter. These results are significant in that boundary-layer pressure measurements can indeed be acquired in a hypersonic flow with a simple design that does not require protruding pitot tubing.

**Ames-Dryden contact: S. Johnson**
**(805) 258-3096**
**Headquarters program office: OA**

## Signal Management for Analysis in Real Time

**Richard Larson**

The flight-test monitoring requirements at the Ames-Dryden Flight Research Facility have increased in complexity with each new flight-test program. Consequently, the Western Aeronautical Test Range (WATR) has recently upgraded the mission control center (MCC) to provide additional flexibility and improvement to the real-time display capabilities. The MCC now contains high-speed UNIX workstations that support a variety of application programs.

A new type of real-time monitor that utilizes this added capability has been installed and used extensively for the X-31A flight-test program. The monitor is called the Signal Management for Analysis in Real Time (SMART) display. The SMART display works by processing a series of rules (written in C) of the system and parsed (developed in house) to trigger a message(s) to a message stack on the monitor. The message stack contains time-tagged information formatted in both textual strings (which can be in color) and as data in engineering units (see figure). The example in the figure shows that the POST STALL request was made, but did not engage because of reasons contained by the submessages (identified by an asterisk) below. When an event occurs as defined by a rule, the message(s) are added to the top of the stack and previous messages are pushed down. For cleared events, the messages are removed and the stack automatically compresses. No information is lost or missed by the SMART display, because all messages can be latched on the monitor (user option) or written to a log file for later printout. Since the

SMART display converts raw information into an analyzed, interpreted result, the engineer monitoring this display does not need to have expert knowledge of the system. Even though a large number of signals are processed, the message stack is small because only off-nominal events need to be displayed at a given time.

The knowledge base file constructed for the X-31A program contains the elements shown in the table.

In conclusion, the SMART display has proved to be very usable in providing real-time analysis of problems during X-31A flights. It has even detected problems that would have been completely missed by conventional monitors. This capability has enhanced safety of flight for the X-31A and has significantly shortened trouble-shooting time during flight anomalies by minimizing the need or amount of post-flight data processing for analysis.

**Ames-Dryden contact: R. Larson**
**(805) 258-3740**
**Headquarters program office: OA**

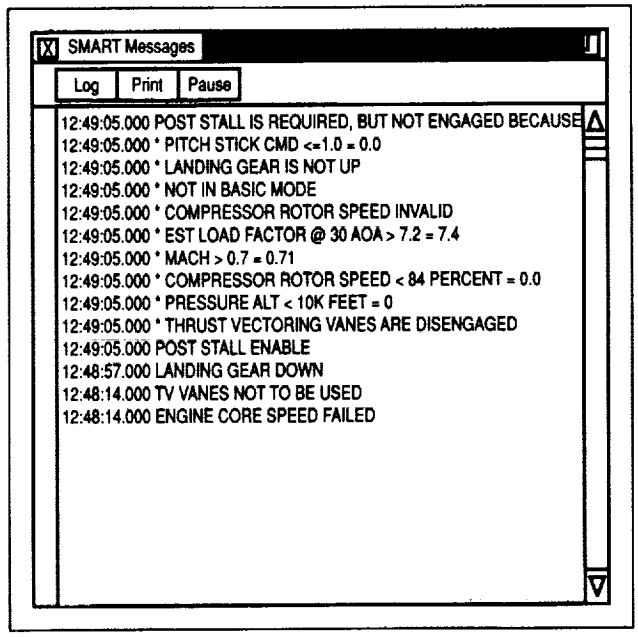


*Fig. 1. SMART message stack.*

Elements of the knowledge base file for the X-31A program

1. Telemetry validity checks and SMART update rate
2. Pre-takeoff testing
   a. Automatic signal validity testing during ground preflight (120 parameters)
   b. Correct Flight Control System (FCS) configuration
   c. Automatic reporting of any preflight built-in-test failures
   d. Check for correct takeoff trim
3. In-flight testing
   a. Check for any flight limits exceeded
   b. Give FCS configuration status
   c. Convert FCS fail codes (434) into a textual string with piloted action advisory
   d. Compute max/min of selected signals during flight-test maneuvers; printout at completion of test point
   e. Compute max/min of selected signals during entire flight; printout at touchdown
   f. Compute gun/missile shoot-conditions criteria with hit/miss analysis during close-in combat flight test
4. Post-flight testing
   a. Peak FCS frame throughput with time tag during flight
   b. Peak hinge moment loads during flight

# Propulsion-Controlled Aircraft Flight Results

**Trindel Maine**

Because of several accidents in which all or major parts of the flight control system were lost, the Ames-Dryden Flight Research Facility has established a research program to investigate the capability of a Propulsion-Controlled Aircraft (PCA), using engine thrust for flight control. The NASA F-15 airplane has been modified and has served as the first airplane to intentionally demonstrate this PCA capability, with landings made with no movement of the conventional flight control system.

Initial flight studies in the NASA F-15 with the pilot manually controlling the throttles and all flight controls locked showed that it was possible to maintain gross control. For instance, a climb could be initiated by adding an equal amount of power to both engines. Bank control could be achieved by adding power to one engine and reducing power to the opposite engine. Using these techniques, altitude could be maintained within a few hundred feet and direction to within a few degrees. These same flights showed that it was very difficult to land on a runway. This was due to the small control forces and moments of engine thrust, difficulty in controlling the airplane phugoid and dutch roll motions, and difficulty in compensating for the slow engine response. Studies in flight simulators at Dryden and

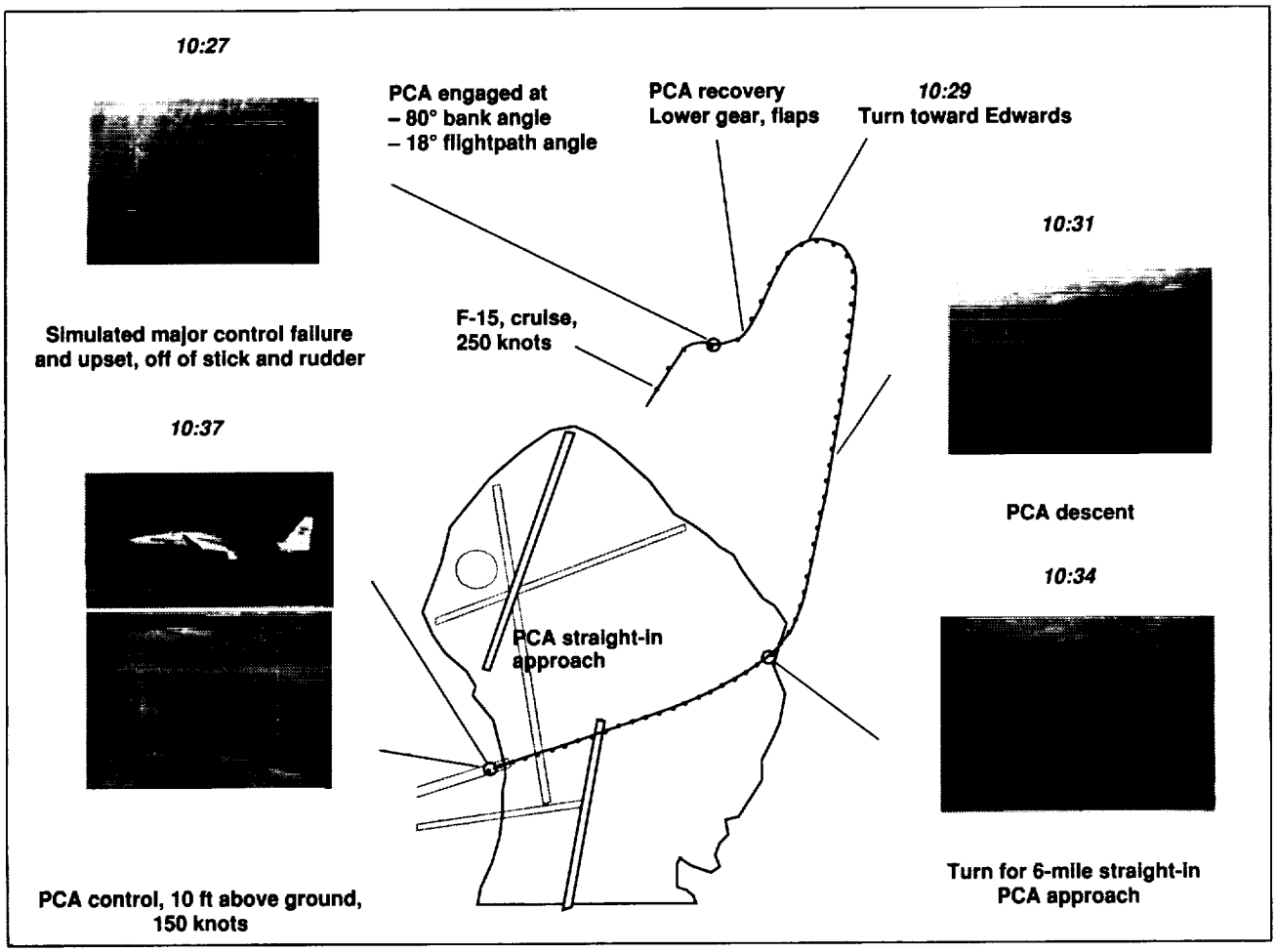


*Fig. 1. Ground track and HUD video pictures at several points.*

at McDonnell Douglas Aerospace (MDA) have duplicated the flight results. These simulators have also established the feasibility of a PCA mode, using feedback of parameters such as flightpath angle and bank angle to command the throttles to stabilize the airplane and follow the pilot's commands.

The NASA F-15 airplane has been used for this research. It incorporates digital engine controls and digital flight controls and has a general-purpose computer and data bus architecture to permit these digital systems to communicate with each other. The only equipment added to the airplane is a control panel containing two thumbwheels, one for the pilot's flightpath command, and the other for bank-angle command. All of the needed sensors and actuators are available from previous integrated flight/propulsion control research. Control computations are performed in the research computer. Flight PCA software was developed by MDA.

The NASA F-15 has recently completed 24 flights under PCA control. The pilot first simulated locked flight controls by selecting a backup flight-control mode and not moving the stick or rudder. He then engaged the PCA system with a switch and used the thumbwheels for control. Initial flights tested the PCA system at altitude: after several changes to the control laws, control was good. In later flights, approaches to a landing were made, including ones in which a PCA-controlled go-around was initiated 100 feet above the ground, and others in which PCA control was maintained to the runway. Four NASA pilots and several guest pilots from the USAF, Navy, and MDA flew the PCA. Each pilot flew the simulated flight-control failure upset, recovery, and approach shown in the figure. Beginning at 250 knots, the airplane was maneuvered to a 90-degree bank and a 20-degree dive; the flight controls were then not used. The PCA system was engaged; it rolled the airplane to wings level and damped the pitch oscillations. The pilot lowered the gear and flaps and used the PCA system for the descent, lineup, and final approach to within 10 feet of the runway.

This technology also has application to transport airplanes. It appears that a PCA system could be installed on future transport airplanes with little or no hardware changes, just additional software.

**Ames-Dryden contact: T. Maine**
**(805) 258-3794**
**Headquarters program office: OA**

## Final Flight-Test Results of Performance-Seeking Control

**John Orme**

Performance-seeking control (PSC) is a model-referenced adaptive control law that performs real-time optimization of the propulsion system during quasi-steady-state maneuvers. The original objectives of PSC were to maximize thrust during accelerations, to minimize specific fuel consumption while maintaining thrust during cruise, and, by operating the engine at cooler turbine temperatures, to extend engine life. The flexibility of the PSC algorithm allows for additional optimization objectives, and during the program, logic was added that decreases aircraft supersonic deceleration time. All program objectives were successfully demonstrated in the flight testing of PSC onboard the NASA F-15.

The PSC software, partitioned for multiprocessing on three CPUs (Motorola 88000 RISC architecture) of the Vehicle Management System computer, has separate models for the left and right propulsion systems and includes inlets, engines, and nozzles. One noteworthy feature of the PSC algorithm is its ability to adjust its onboard models to more accurately reflect the flight article. This function is accomplished primarily with the use of an extended Kalman filter, which estimates off-nominal engine performance. The PSC-derived models of the propulsion system are optimized in real time with basic linear programming techniques. The resulting model-based

optimal trims are applied to the propulsion system in an open-loop manner. Since there are no feedbacks of system performance, steady state may be reached, but PSC continuously optimizes and applies trims. The process of taking measurements, updating the models, optimizing the models, and applying trims continues until the pilot disengages PSC.

Demonstrations in flight indicate the PSC control law is capable of providing substantial improvements to the propulsion system and the aircraft's performance. Subsonically, PSC produces thrust increases of up to 15%, turbine temperature reductions exceeding 100°F, and as much as 2% savings in fuel consumption. Supersonic flight results also show significant performance benefits: 10% decreases in fuel consumption, 10% increases in thrust, and as much as 85° reductions in turbine temperature. In addition, deceleration time is reduced by as much as 50%.

The PSC thrust improvements for a subsonic acceleration from Mach 0.5 to 0.95 are shown in the first figure. The model-determined thrust estimate increases by 10% for either engine when being optimized by PSC. Optimal trims that increase thrust also reduce the amount of remaining temperature

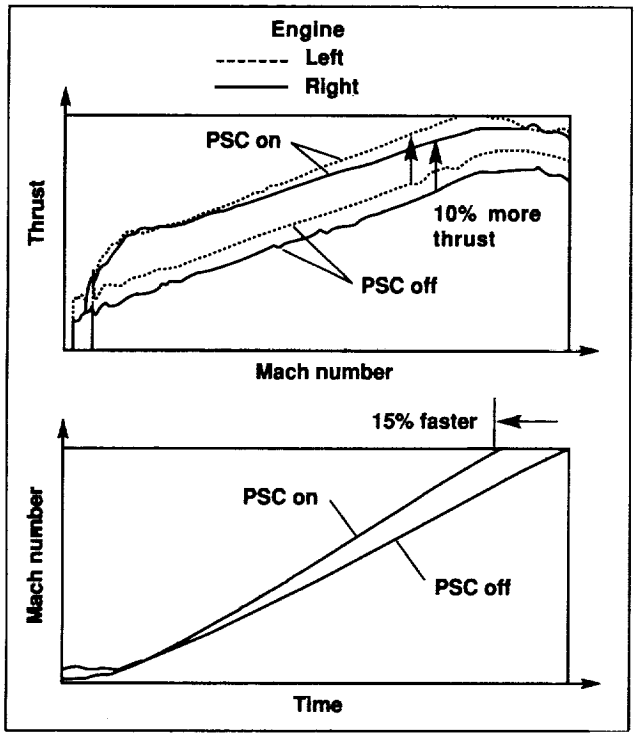


*Fig. 1. Performance-seeking control (PSC) maximum-thrust mode.*

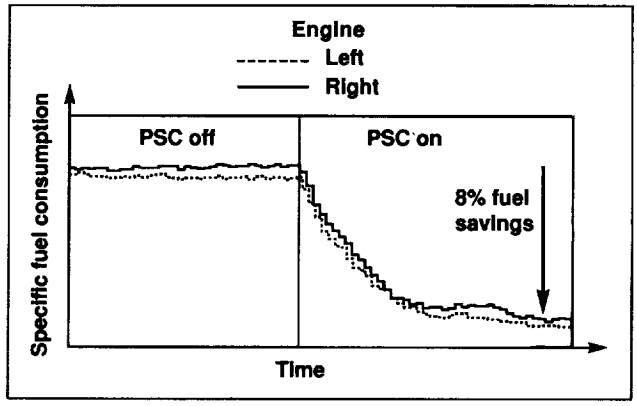


*Fig. 2. PSC minimum-fuel mode.*

and fan stall margins. Similar thrust increases have been obtained supersonically. The second part of the first figure is the corresponding Mach-number time history, which correlates the estimated thrust increase with aircraft acceleration. The increases in thrust result in the aircraft acceleration time being reduced by 15%. Such thrust improvements could clearly give an acceleration performance advantage to fighters.

The second figure illustrates the fuel savings available with the application of the PSC minimum-fuel mode. During a cruise at Mach 1.50 and 30,000 feet, the PSC algorithm trims the propulsion system to a more fuel-efficient operating condition, resulting in 8% fuel savings in both the left and right engines. The large fuel savings derive from the reduction of total engine fuel flow, while maintaining thrust. At supersonic cruise conditions the F-15 requires afterburner usage; engine operation with the afterburner is approximately three times less efficient than without the afterburner. As seen in the figure, the potential for fuel savings in supersonic cruise is significant. Subsonically, the standard engine without the afterburner operates close to its most fuel-efficient condition. As a result, the PSC minimum-fuel mode achieves only modest fuel savings subsonically: 1% to 2% savings have been demonstrated. Implications of such fuel savings are clear for both military and commercial aircraft; increased fuel efficiency may result in lower operating costs, extended range or endurance, or increased payload capability.

**Ames-Dryden contact: J. Orme**
**(805) 258-3683**
**Headquarters program office: OA**

# Handling-Qualities and Agility Research on the F-18 HARV

**Joseph W. Pahle, Keith Wichman, R. Joe Wilson**

The F-18 High-Angle-of-Attack Research Vehicle (HARV) project is evaluating advanced control laws, handling qualities criteria, and agility in the high-angle-of-attack flight regime. The HARV was modified to include thrust vectoring and a research flight-control system. The thrust-vectoring system allows the HARV to maneuver up to 65° angle of attack, and to trim (steady state) to 70° angle of attack.

Until recently, high-angle-of-attack investigations were mainly concerned with preventing post-stall departure, providing spin resistance, or developing spin-recovery procedures. With the advent of aircraft equipped with thrust-vectoring systems, post-stall departure is controlled, and aggressive maneuvering at elevated angle of attack is a reality. The flight-test objectives for the F-18 HARV include qualitative and quantitative evaluation of advanced control laws, and improved maneuvering capability (agility) and handling qualities in the high-angle-of-attack flight regime.

Flight-validated handling-qualities guidelines do not exist for the high-angle-of-attack range being explored with the F-18 HARV. Previously, aircraft have not been able to investigate the high-angle-of-attack regime in a safe, methodical manner to gather the required information. Using the capabilities of the F-18 HARV, flight-test techniques and maneuvers are being developed to help validate in flight some of the proposed high-angle-of-attack handling-qualities criteria.

The examples below illustrate two flight maneuvers, unique to post-stall maneuvering, that were flown at the Ames-Dryden Flight Research Facility during the handling-qualities evaluation. These maneuvers were flown in November and December 1992. The first figure is a reconstruction, from flight data, of a post-stall reversal (also known as a Herbst turn or J-turn). The target vehicle is a NASA chase F/A-18. The velocity vector of the HARV vehicle clearly shows the rapid onset of angle of attack

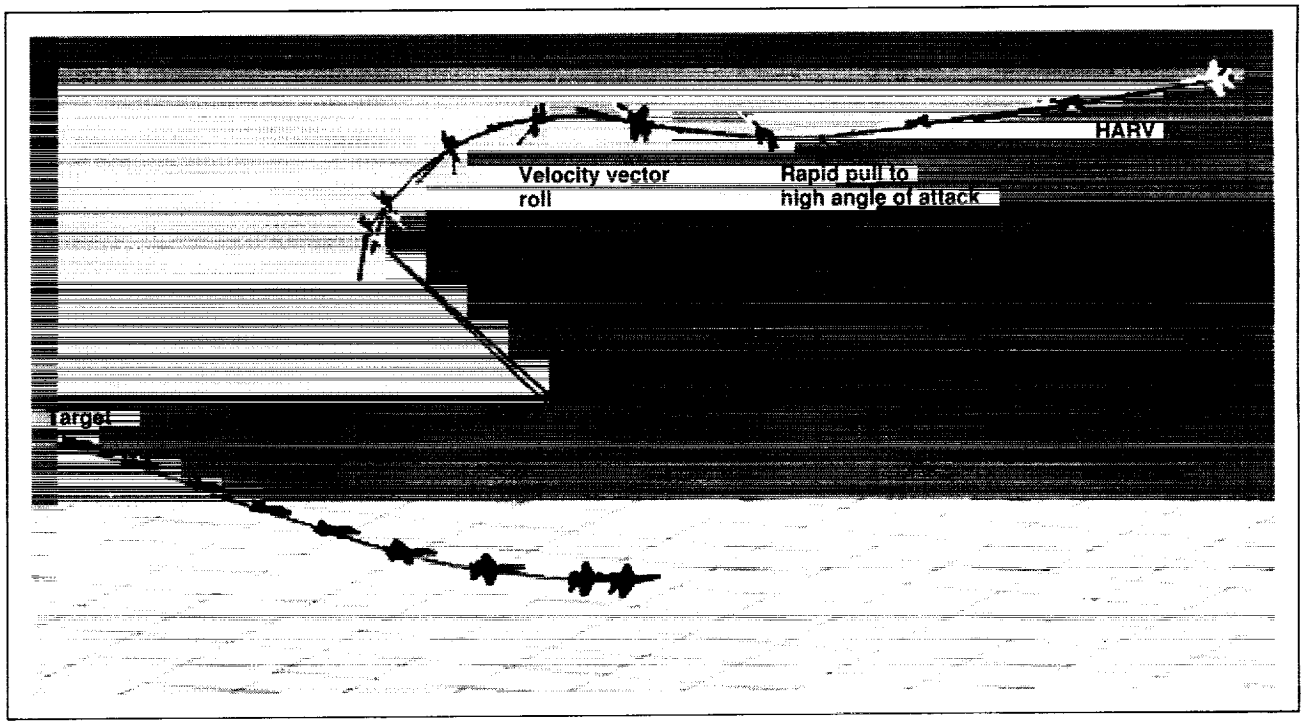


*Fig. 1. Post-stall reversal.*

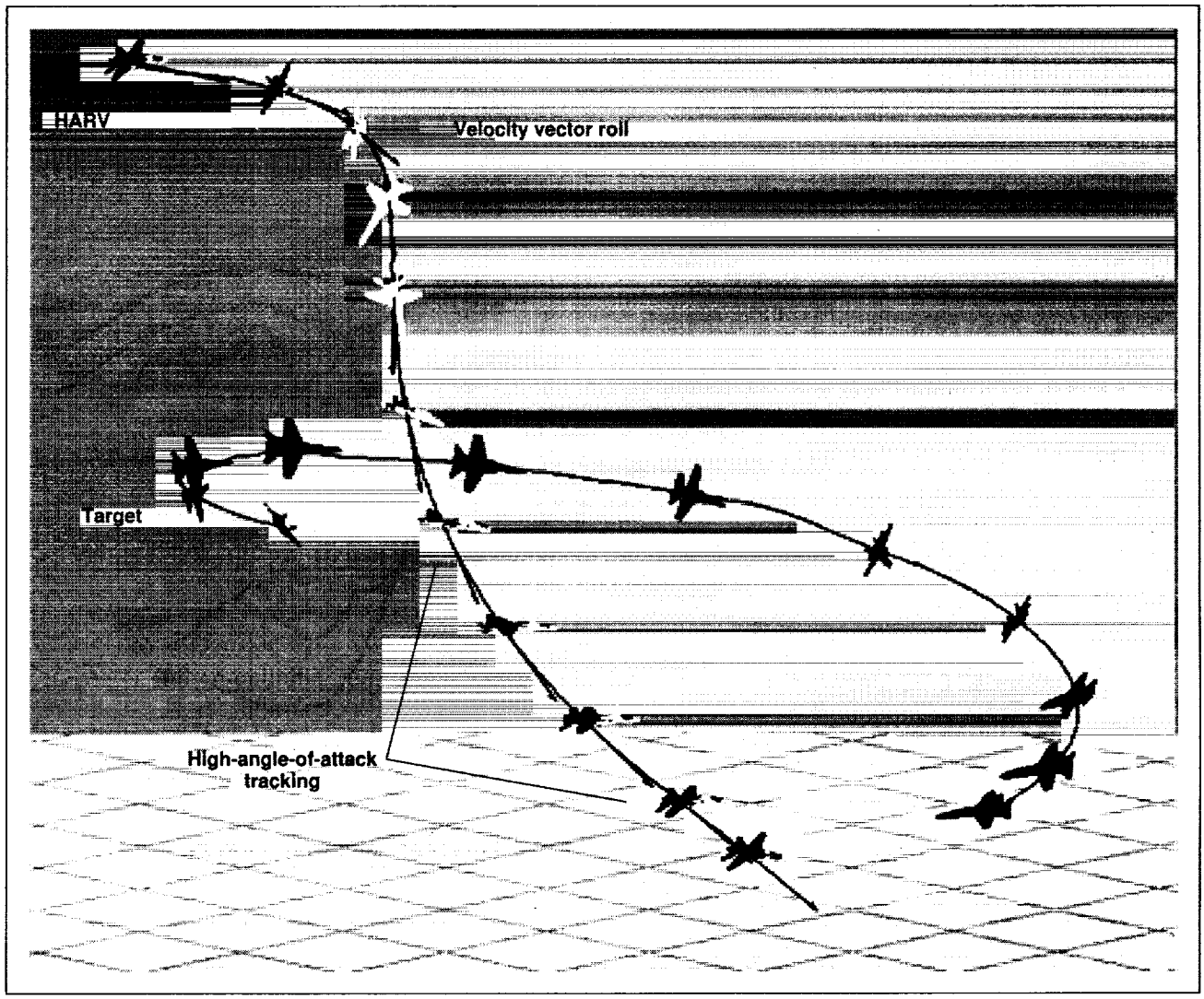


*Fig. 2. Offensive spiral.*

(maximum alpha is approximately 60°) just before the velocity vector roll and target acquisition (shown by the projected square). The overall maneuver takes about 17 seconds.

The second figure is a flight reconstruction of an offensive spiral (also known as a helicopter gun attack) where the HARV acquired the target at the end of a high-angle-of-attack reversal and continued to track the target for about 10 seconds in the 50°–60° angle-of-attack range. Although the HARV began the maneuver with an altitude advantage of about 5,000 feet, it is actually below the target by the end of the maneuver, illustrating the significant energy loss associated with sustained high-angle-of-attack flight.

**Ames-Dryden contact: J. Pahle**
**(805) 258-3185**
**Headquarters program office: OA**

# A Correction Technique for Strain Gages Exposed to Transient Temperature Environments

W. Lance Richards

Ground tests that simulate the aerodynamic heating of hypersonic vehicles often require test components instrumented with strain gages to be exposed to extremely severe heating rates. Such heating rates produce temperature gradients through the thickness of strain-gage installations, as shown in the first figure. These temperature gradients introduce errors in the strain measurement that are neglected in conventional strain-correction methods. The objectives of this investigation were to demonstrate the significance of these errors for a variety of radiantly heated, transient temperature profiles; to develop a new correction technique to account for these errors; and to demonstrate the technique by comparing analytical and experimental results.

Conventional strain-correction theory was first modified to allow a temperature difference to exist between the strain-gage sensing element and the substrate material. This temperature difference led to the definition of a new strain error called the *transient heating error.* Heating conditions ranging from 0.3°F/second to over 100°F/second were then applied to a test coupon, and the transient heating errors for a specific strain-gage installation were evaluated. The second figure shows that for heating rates between 10 and 100°F/second, transient heating errors were as significant as apparent strain—the most significant strain error that occurs in extreme temperature environments. For heating rates less than 10°F/second, transient heating errors were not as significant.

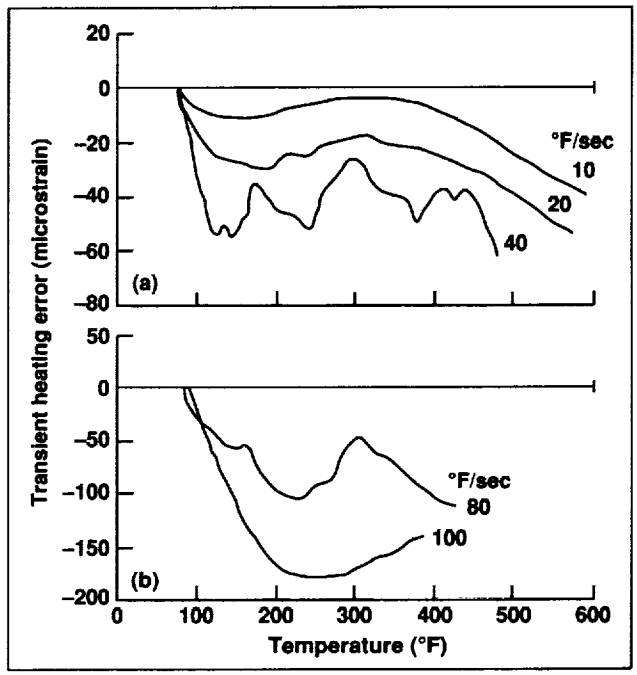


*Fig. 2. Transient heating error results.*

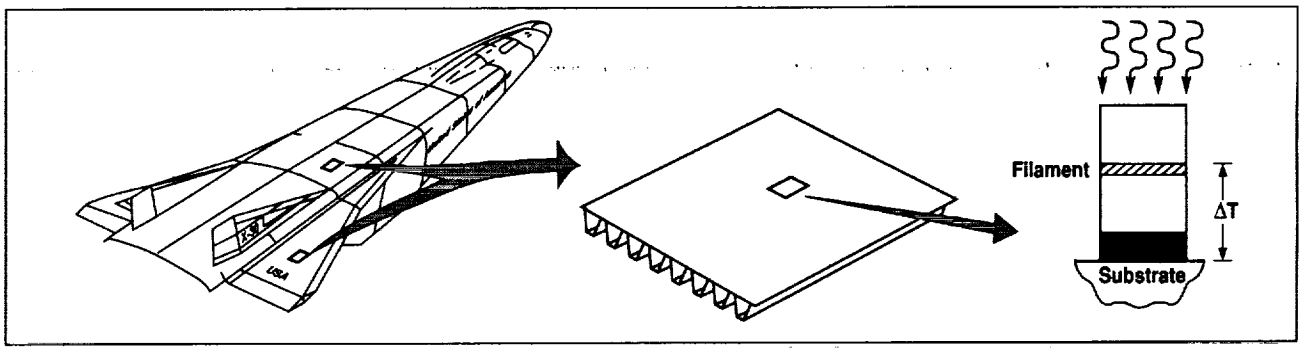


*Fig. 1. Temperature difference between the strain-gage filament and substrate produced during the transient heating of test components.*

A new strain-correction technique was then developed to correct strain-gage measurements for errors produced in transient heating environments. The third figure shows strain results from a 100°F/second heating profile corrected with both new and conventional strain-correction techniques and then compared to analytically determined strains. At this heating rate, conventional methods resulted in errors of 30%, whereas the new correction technique yielded results within a few percent of the true value. For all heating rates greater than 10°F/second, the indicated strain data corrected with the new technique correlated much better with analytical results than did the same data corrected with the conventional technique.

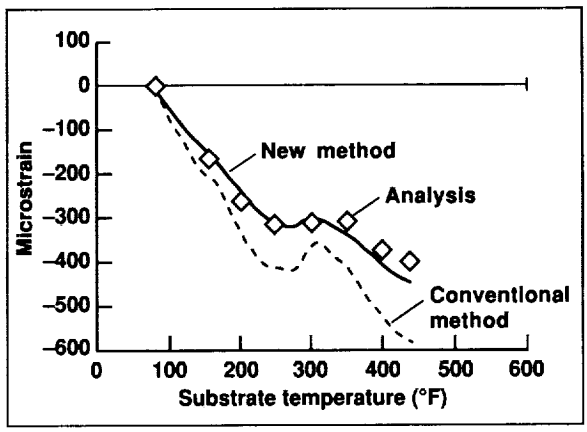


*Fig. 3. Comparison of new and conventional methods with analysis.*

**Ames-Dryden contact: W. Richards**
**(805) 258-3562**
**Headquarters program office: OA**

## Flight-Test Results of a Feasibility Study of Adaptive Aircraft Performance Technology

**Gerard Schkolnik**

Adaptive aircraft performance technology (AdAPT) is an adaptive, measurement-based algorithm that optimizes the aircraft and propulsion system in real time during quasi-steady-state operation. The primary advantage of a measurement-based approach is that virtually no models are required for its implementation. All of the required information is extracted in flight. Secondly, the algorithm is generic, and therefore easily and quickly portable to another fighter, a subsonic transport, or a supersonic transport. AdAPT makes mainstream performance optimization possible.

Optimal trims determined by AdAPT are sent to as many as eight aircraft and engine controls. These controls include stabilator, canard, flaperon, and inlet ramps. Additionally, the following engine nozzle controls are optimized: throat area, area ratio, and pitch and yaw vector angles. The algorithm simultaneously sends a small-amplitude sinusoidal excitation of a unique frequency to each control to identify the sensitivity or gradient of each control to the measured performance index. The identification algorithm uses a Fast Fourier Transform (FFT) that separates the response of the performance index to each control as a function of its unique frequency. The AdAPT optimization algorithm solves the Hamiltonian using the gradients to determine the optimum control trims to maximize performance. The structure of the AdAPT algorithm is generic and flexible, allowing for various performance measurements to be optimized. Both specific excess power and range factor have been identified as optimization modes for the program.

To establish the feasibility of a measurement-based approach, a study was performed on the NASA F-15 highly integrated digital engine control (HIDEC) aircraft. An excitation mode was created in performance seeking control (PSC), a model-based performance-optimization program now being flight-tested. This excitation mode allowed sinusoidal trims to be sent to the inlet first ramp and nozzle throat area, either separately or together. Aircraft controls and acceleration data from three longitudinal accelerometers were recorded on the instrumentation system for postflight analysis. The most important technical challenge for the measurement-based approach was identifying the performance gradients without excessively disturbing the aircraft's flightpath. Other issues with this approach include the effects of noise or other extraneous inputs on the identification and the threshold sensitivity of the sensors.

Maneuvers were flown across the subsonic and supersonic envelope of the F-15. Eleven test maneuvers were flown at nine flight conditions ranging from 0.7 Mach at 10,000 feet to 2.0 Mach at 45,000 feet. An amplitude parametric test, a frequency parametric test, and nine standard tests comprised the eleven test maneuvers. The standard tests included an inlet-excitation test, a nozzle-area excitation test, and a test during which both controls were excited simultaneously.

Overall, AdAPT successfully identified gradients at all conditions. As expected at low dynamic pressures where the inlet ramp is ineffective, the inlet ramp gradient was within the noise level. At higher dynamic pressures, the inlet ramp gradient was easily identified. The nozzle-throat area gradient was identifiable at all conditions. Simultaneous excitations of both controls produced gradients that were nearly identical to those produced when excitations were separate. Pilot comments with respect to disturbance to flightpath indicated that the excitation was generally not perceptible, and when perceptible, it was insignificant.

Time histories are shown in the first figure for simultaneous cowl (inlet ramp) and throat area excitations at a flight condition of 45,000 feet and 0.95 Mach. The first time history shows the excitations of the two controls, cowl and nozzle area; the

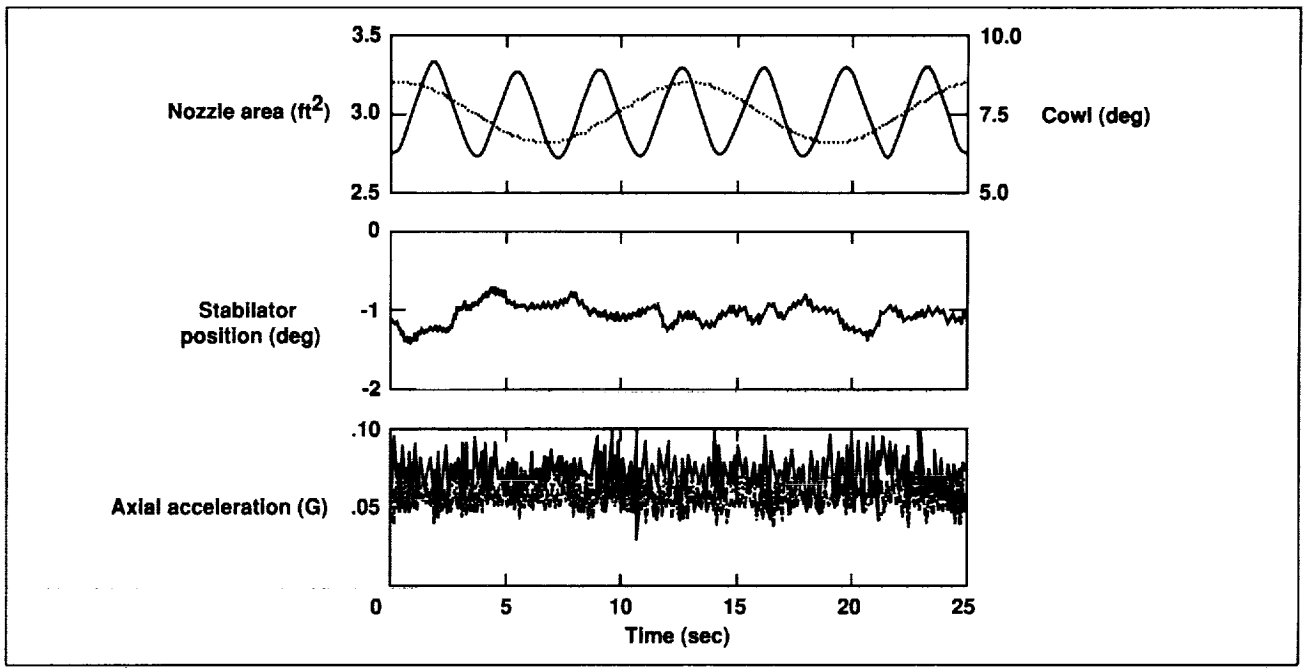


*Fig. 1. AdAPT feasibility-study time histories.*

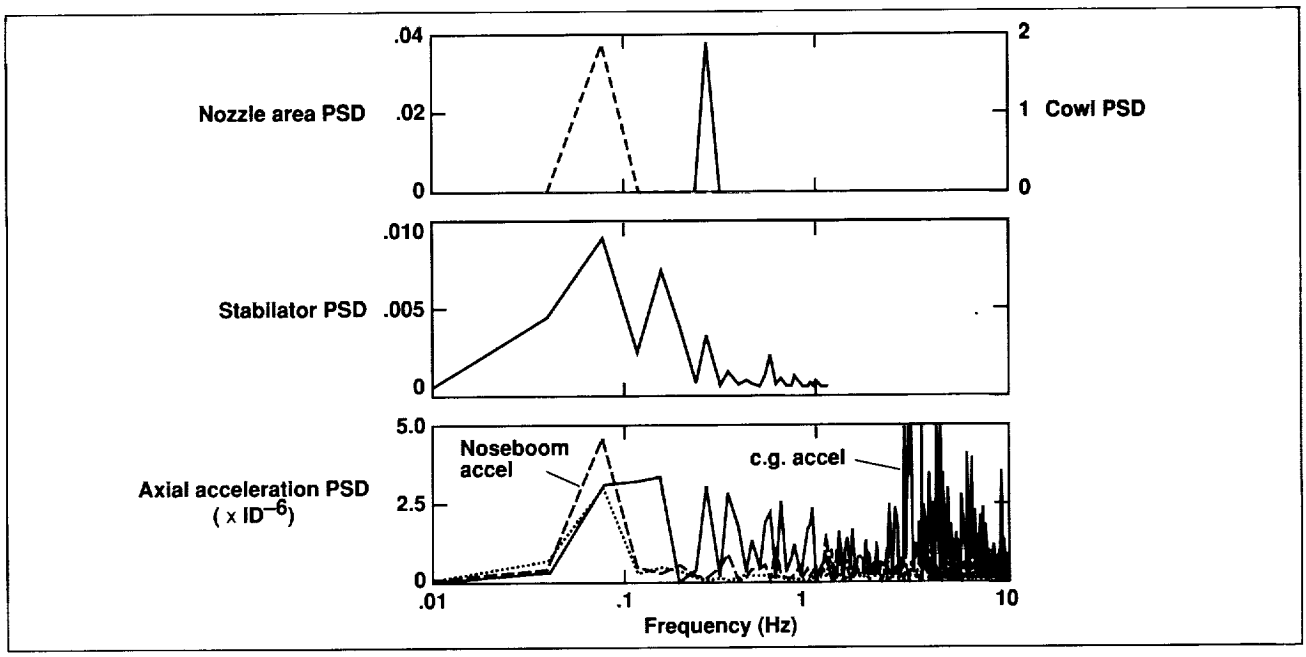


*Fig. 2. AdAPT feasibility-study power spectral densities.*

maneuver lasted 25 seconds. The nozzle area was excited with a period of 12 seconds and an amplitude of ±0.2 square feet. The cowl was excited at a shorter period of 3.7 seconds and an amplitude of ±2°. The second time history is of the stabilator position, which indicated how the controls were affecting stabilator position and, in turn, drag. The last time history shows the three longitudinal accelerometer traces for the same time period. One accelerometer had a much lower signal-to-noise ratio than the other two. Power spectral densities (PSD, plots of amplitude of the FFT squared versus frequency) for the corresponding signals are presented in the second figure. The first PSD shows the distinct peaks of the two controls with no interference between the two. The second PSD indicates that at this condition the nozzle area had a greater effect on the stabilator drag than did the cowl. The third PSD indicates that the two noseboom accelerometers clearly sensed the nozzle area excitation, but did not sense the cowl excitation. Also, noise levels were very low to approximately 5 hertz (well beyond any planned excitation frequency). By comparison, the c.g. accelerometer had an unacceptable performance: high noise levels started at very low frequencies, making the identification difficult. Overall, the results show that the identification is readily possible, virtually imperceptible to the pilot, and not affected by simultaneous excitations.

The development of measurement-based performance optimization promises to produce significant benefits with little additional cost. This flexible approach allows all aircraft, commercial and military, subsonic and supersonic, to attain an optimum configuration.

**Ames-Dryden contact: G. Schkolnik**
**(805) 258-3055**
**Headquarters program office: OA**

# Design and Development of the F/A-18 HARV Inlet Rake

**Andrew Yuhas, Ronald J. Ray**

A new inlet rake design has been developed for measuring distortion and pressure recovery levels on the F/A-18 High-Angle-of-Attack Research Vehicle (HARV) during extreme maneuvers. The new rake design was required to meet significant cost and time constraints of the program. NASA engineers conceived a new design concept and tasked General Electric Aircraft Engines (Evendale, Ohio) to conduct the design, fabrication, and validation tests. The rake is part of a joint effort by the Ames-Dryden Flight Research Facility and Lewis Research Center to develop and validate better ways to design engine inlets. The rake data will be used to improve computer codes and wind-tunnel test techniques. Lewis leads the high-angle-of-attack inlet research study.

The new design approach is centered around replacing the standard eight-leg, cantilevered design typically used in the past with one that connects all the legs together with a center hub, greatly simplifying the structural requirements. The result is a one-piece, wagon-wheel design (see first figure) that simplifies rake installation and aircraft modification requirements, thus greatly reducing cost and aircraft down time. The rake is more compact and requires significantly less changes to the aircraft than those used in the past. This simpler approach also reduces the required installation time from many months to only a few hours. A significant cost-savings was achieved using the new rake concept.

The rake features eight (8) equiangularly spaced radial legs with five (5) probes per leg location at the centroids of equal areas. Each probe contains a low- and high-response pressure-sensing port with the high-response transducer at the port. The rake is lightweight (less than 15 pounds) and incorporates a metal/composite body. The use of composite material provides resistance to structural vibrations and reduced weight.

The new inlet rake design has completed all laboratory structural qualification testing and will soon complete flight qualification. Further development of this rake design should lead to the capability for supersonic operation (Mach 2.5) and scaling to larger inlet diameters. Due to the low cost and reduced installation time of the rake, it should allow for greater accessibility for inlet research and development efforts in the future.

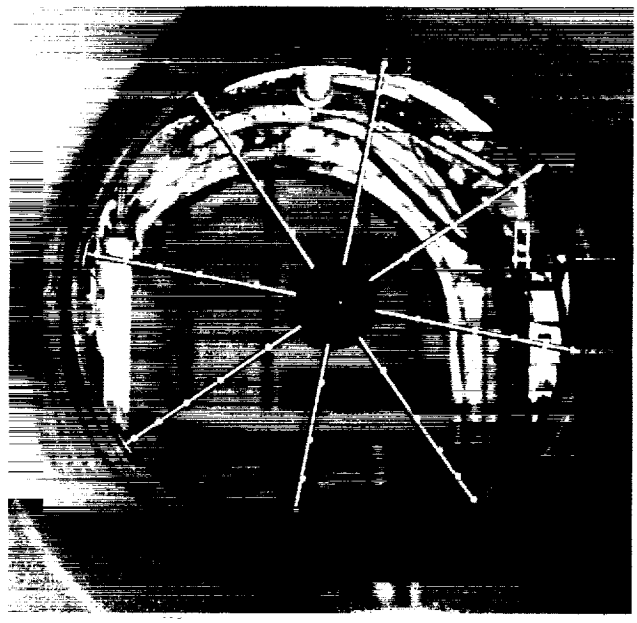

*Fig. 1. Wagon-wheel inlet rake installed in the F/A-18 HARV.*

NASA's high-angle-of-attack (or high alpha) technology program studies what occurs when a modern fighter-like aircraft, such as the F/A-18, flies with its nose tilted up at sharp angles to its flightpath. This high-alpha flight profile adversely affects engine performance. Early computer predictions have shown a greater thrust loss than anticipated. Improving the inlet design will increase the power and handling qualities of highly maneuverable aircraft. The new inlet rake will be a vital tool in this effort.

**Ames-Dryden contact: A. Yuhas**
**(805) 258-2312**
**Headquarters program office: OA**

# Evaluation of the Smart Actuator™ on the F-18 Systems Research Aircraft

**Eddie Zavala**

Current fly-by-wire servoactuators used in military and commercial aircraft do not contain control electronics. Generally, electronic control and monitoring of servoactuators is contained in a separate flight-control computer. As a result, a large amount of wiring is required to operate all the actuators on an aircraft. This fly-by-wire system configuration has a number of disadvantages. Especially in a large commercial aircraft, wire weight is significant. High maintenance costs and vulnerability to electromagnetic interference/electromagnetic pulse are additional disadvantages. Finally, this configuration requires unique flight-control interfaces for each actuator on the aircraft.

The Smart Actuator™, manufactured by HR Textron, contains two independent electronic channels that perform actuator control, fault monitoring, and redundancy management. Communication with the actuator has been simplified by using standard serial data buses. Other improvements include the use of fiber optics as the communications medium. The Smart Actuator™ was designed to fit in the F-18's left-aileron actuator bay.

Installation of the Smart Actuator™ on the aircraft required two interface units (see first figure). These interface units, manufactured by Dynamic Controls Inc., not only provide the electrical-to-optical interface between the Smart Actuator™ and the F-18 flight-control computers, but also provide data to the aircraft's instrumentation system. The use of the interface units also prevents the modification of the flight-control computers.

The performance of the smart actuation system throughout the flight-test program has been exceptional.

*Fig. 1. Smart Actuator™ and interface units.*

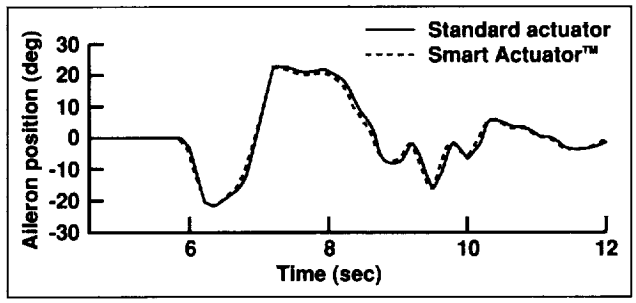


*Fig. 2. Performance of Smart Actuator™ versus standard actuator.*

As the second figure shows, the Smart Actuator™ performance is identical to that of the standard F-18 aileron actuator. The Smart Actuator™ is virtually transparent to the flight-control system. Likewise, the fiber-optic data buses in the smart actuation system have performed well throughout flight testing. Although environmental tests revealed that the fiber-optic buses were thermally sensitive, a maintenance/calibration procedure for the flight-test program was developed to account for these sensitivities. The reliability of the fiber optics was satisfactory and maintenance was easily performed. It should be noted that no in-flight anomalies have occurred in the flight-test program.

The development and flight test of the Smart Actuator™ has proved that local control and monitoring of servoactuators is possible. Flight-test results indicate that the performance of the Smart Actuator™ is identical to that of the standard F-18 aileron actuator. Although fiber-optic sensitivities were discovered, these issues can be factored into future system designs. The use of fiber optics and serial data buses simplifies system integration and provides valuable information regarding reliability and maintainability of fiber optics on aircraft. In addition, the use of fiber optics may translate to increased weight savings, lower maintenance costs, and decreased electromagnetic susceptibility for future aircraft.

**Ames-Dryden contact: E. Zavala**
**(805) 258-2198**
**Headquarters program office: OA**



C-4

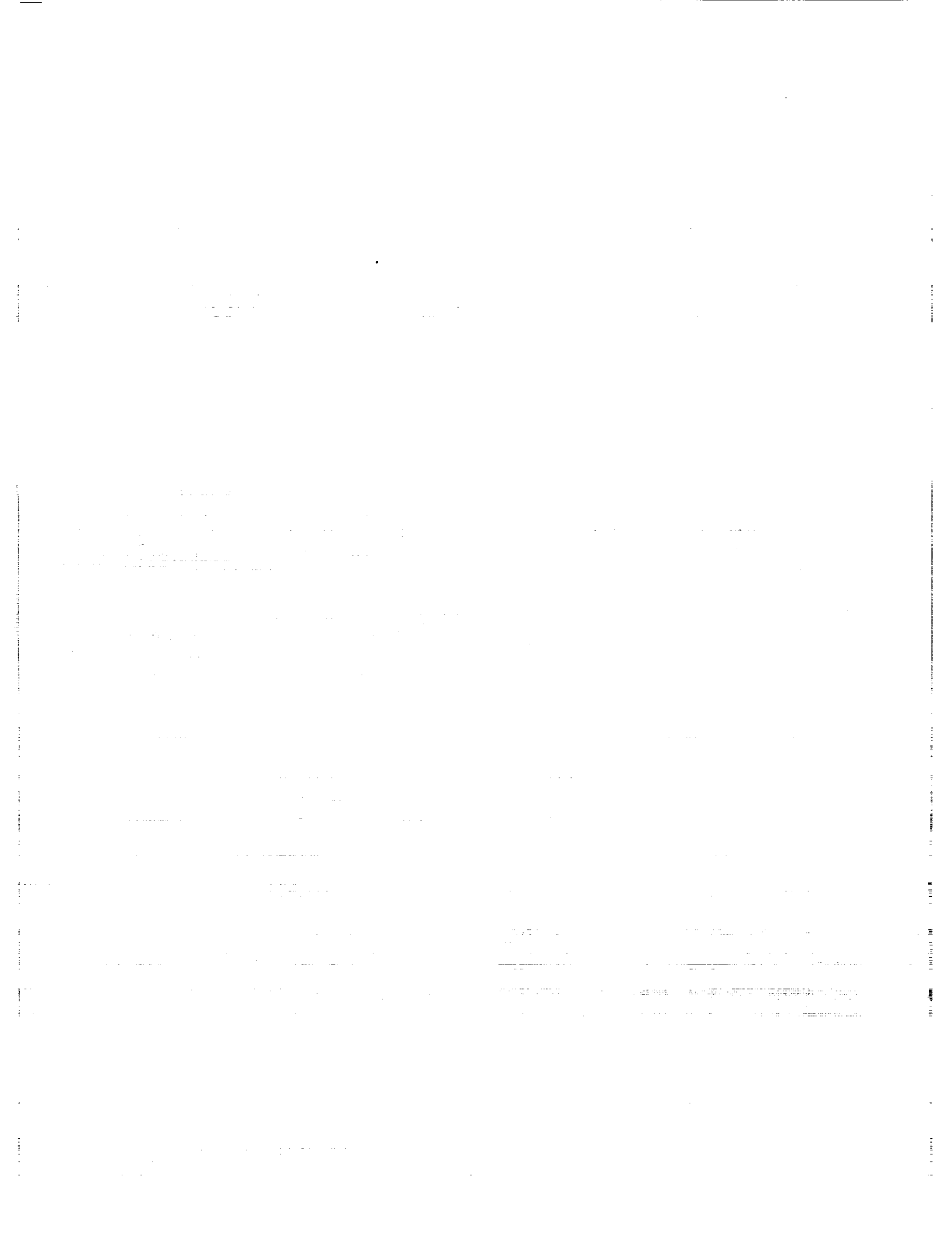

# Appendix

The color plates in this appendix correspond to black and white photographs in the text. Each caption provides the location of the corresponding photograph.

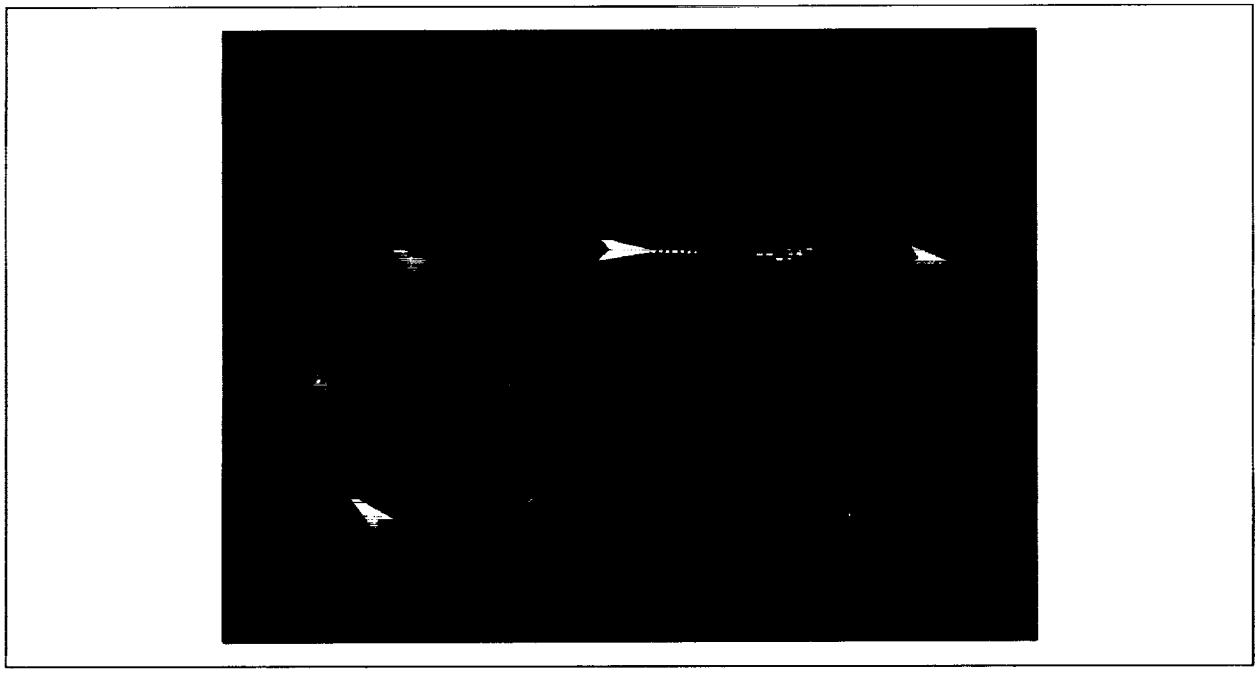

*Color plate 1. Advanced ATC display using integrated aircraft icons to perceptually code altitude (color), track vector (dotted line), altitude change (color of dotted line), and speed (length of dotted line). (fig. 1, page 65)*

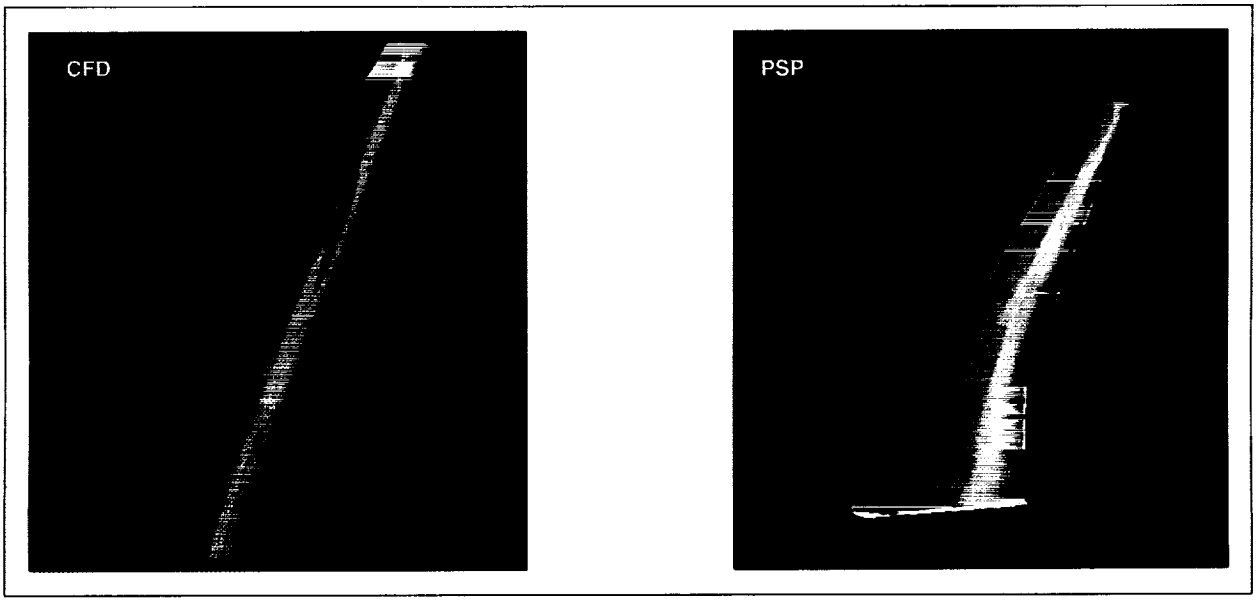


*Color plate 2. I_of_Newt real-time display of CFD and pressure-sensitive paint data. (fig. 1, page 107)*

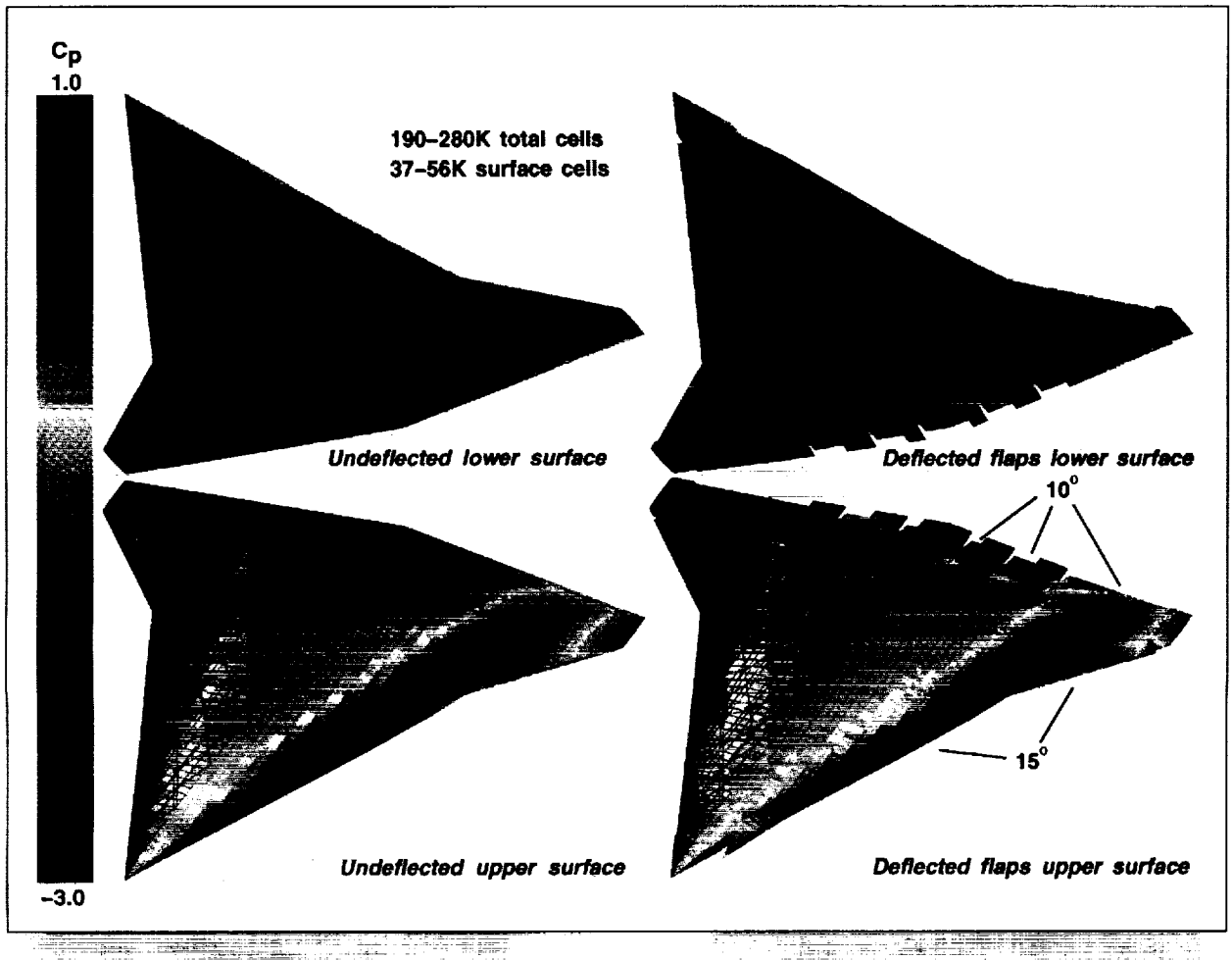


*Color plate 3. Grid and surface pressure coefficient distributions for two cranked-delta-wing configurations.* *(fig. 1, page 108)*

*Color plate 4. Visualization of vortex breakdown at –5 degrees of roll. (fig. 1, page 113)*

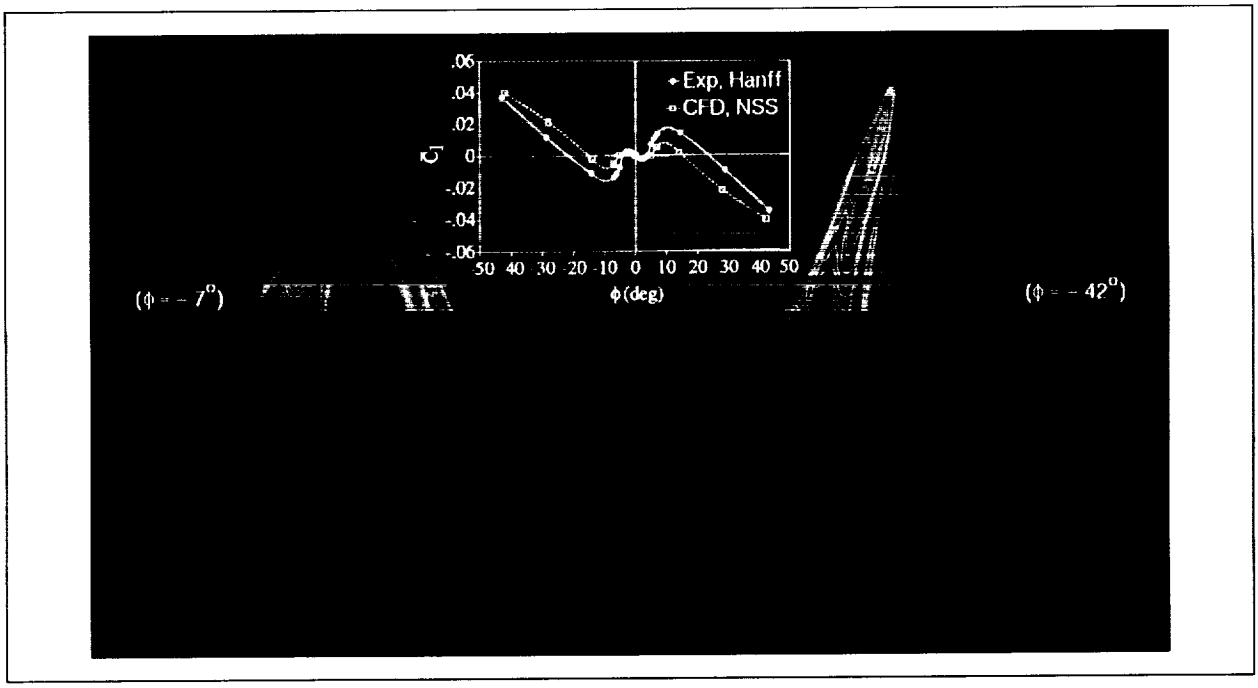


*Color plate 5. Comparison of computational and experimental $C_l$, and visualization of leeward-side surface pressures. (fig. 2, page 113)*

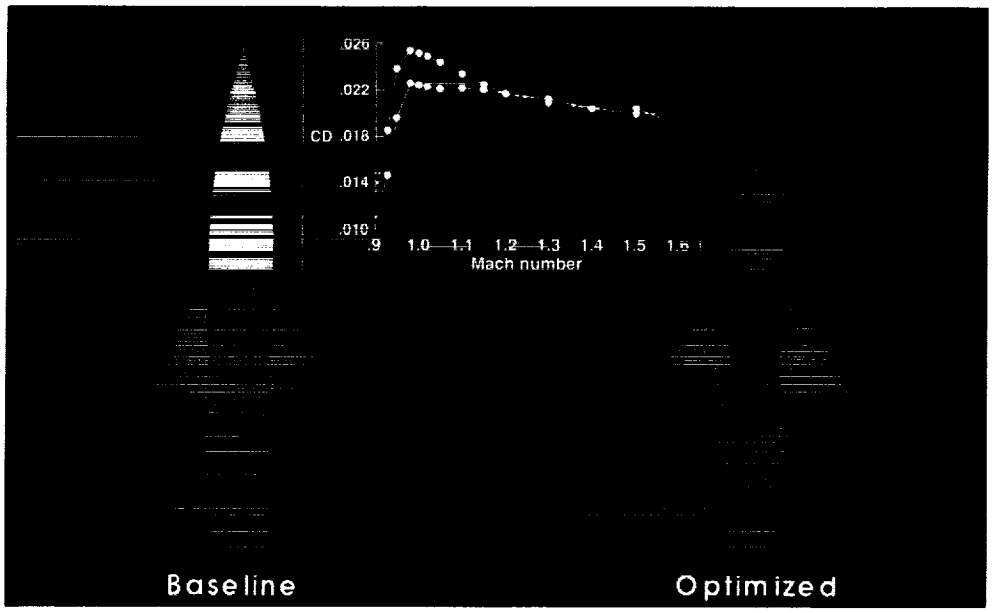


*Color plate 6. Comparison of baseline and optimized wing-body configurations. (fig. 1, page 114)*

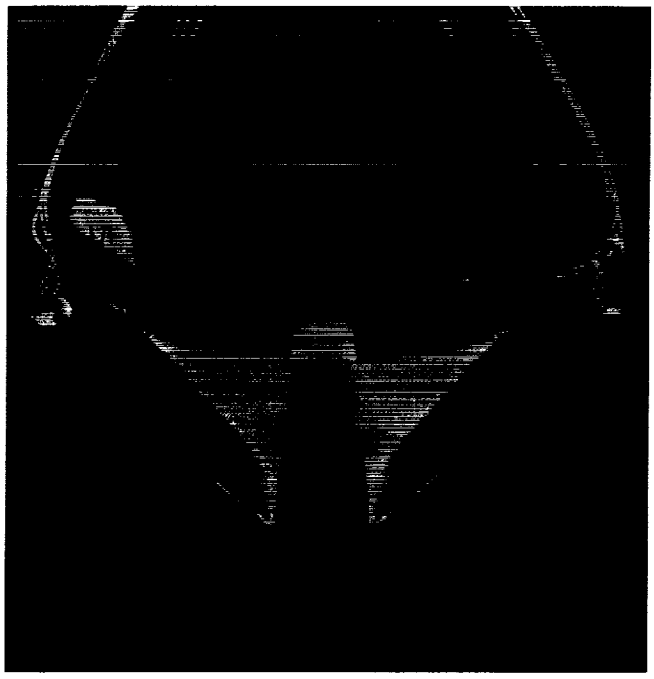

*Color plate 7. Unsteady flows over a wing-body configuration with oscillating control surfaces. (fig. 1, page 121)*

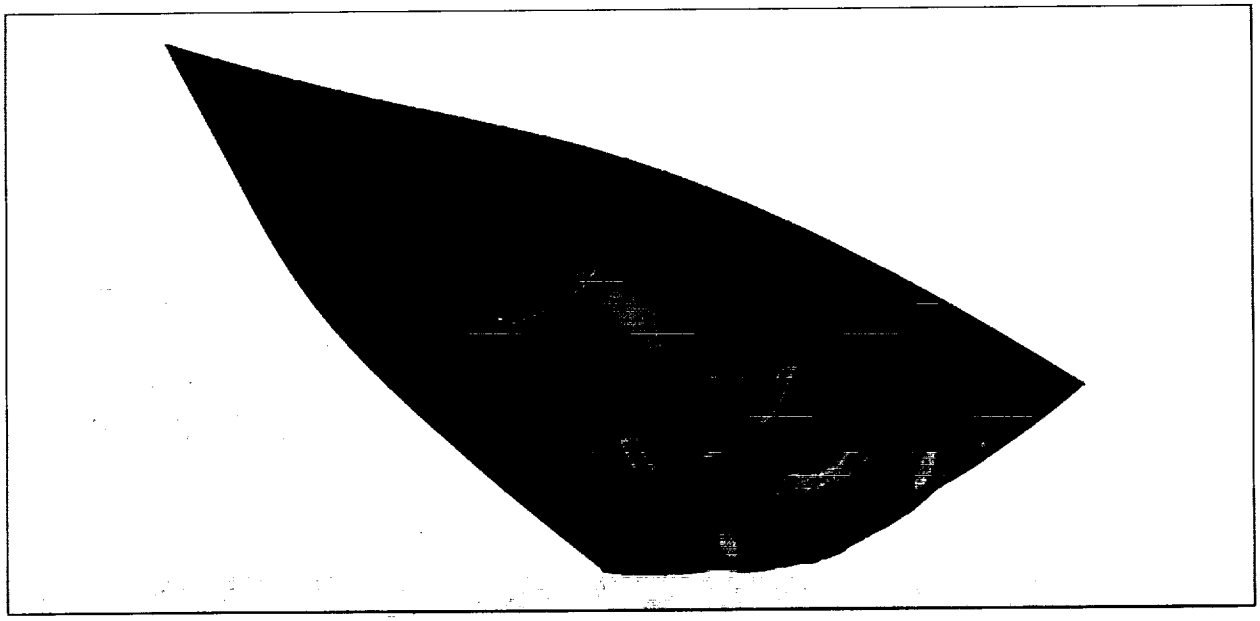

*Color plate 8. Current HRV design, with pressure contours shown. (fig. 1, page 126)*

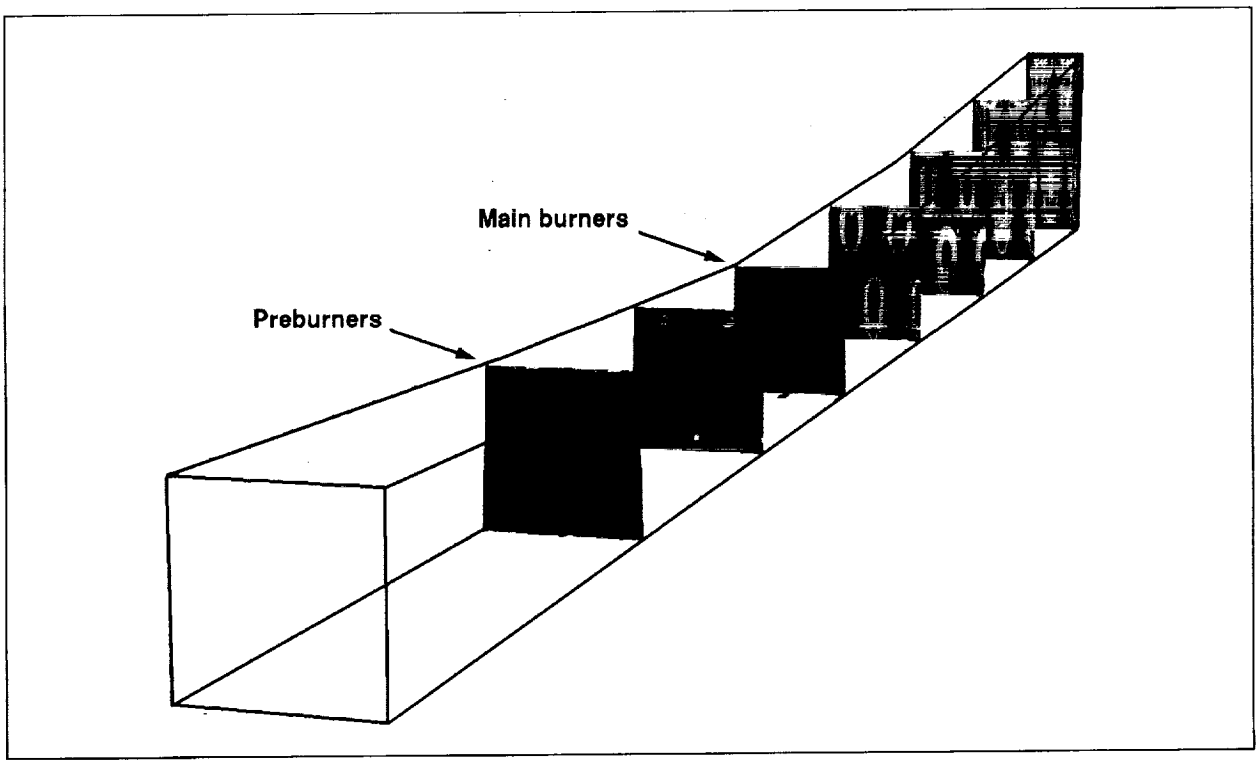


*Color plate 9. Current hydrocarbon scramjet concept, with water contours shown. (fig. 2, page 127)*

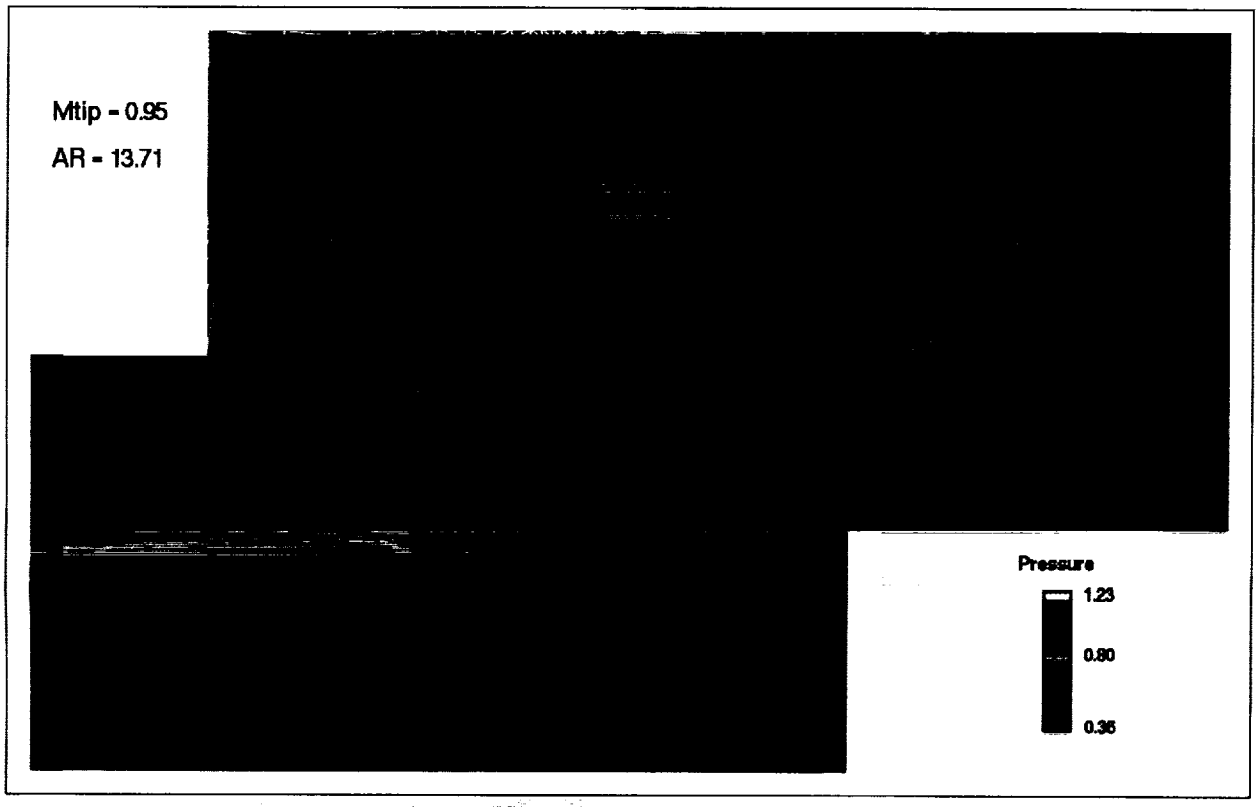


*Color plate 10. Solution-adaptive mesh and pressure contours for modeling high-speed impulsive noise from a three-dimensional helicopter rotor blade. (fig. 1, page 134)*

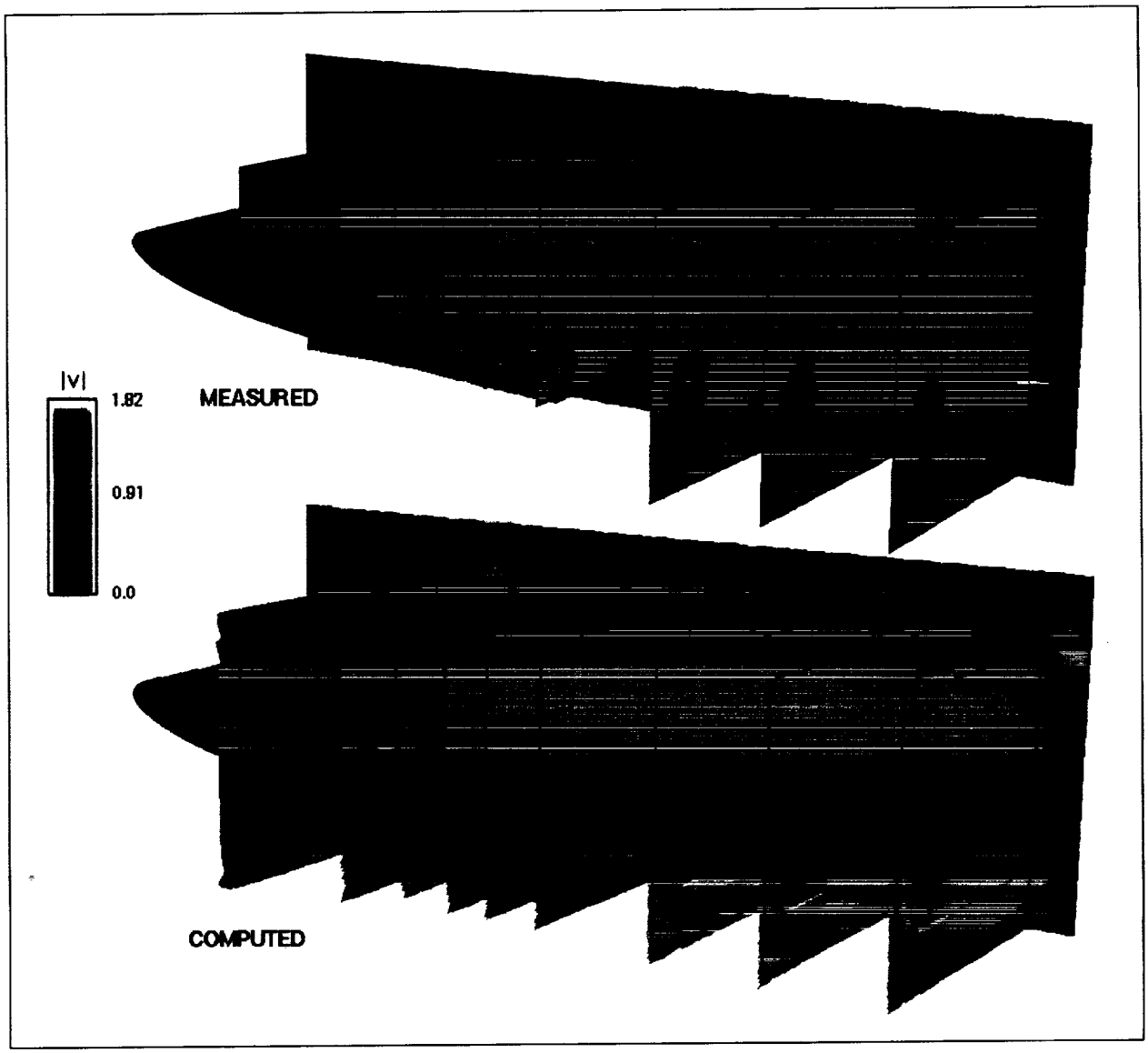


*Color plate 11. Comparison of measured and computed mean velocity. (fig. 1, page 139)*

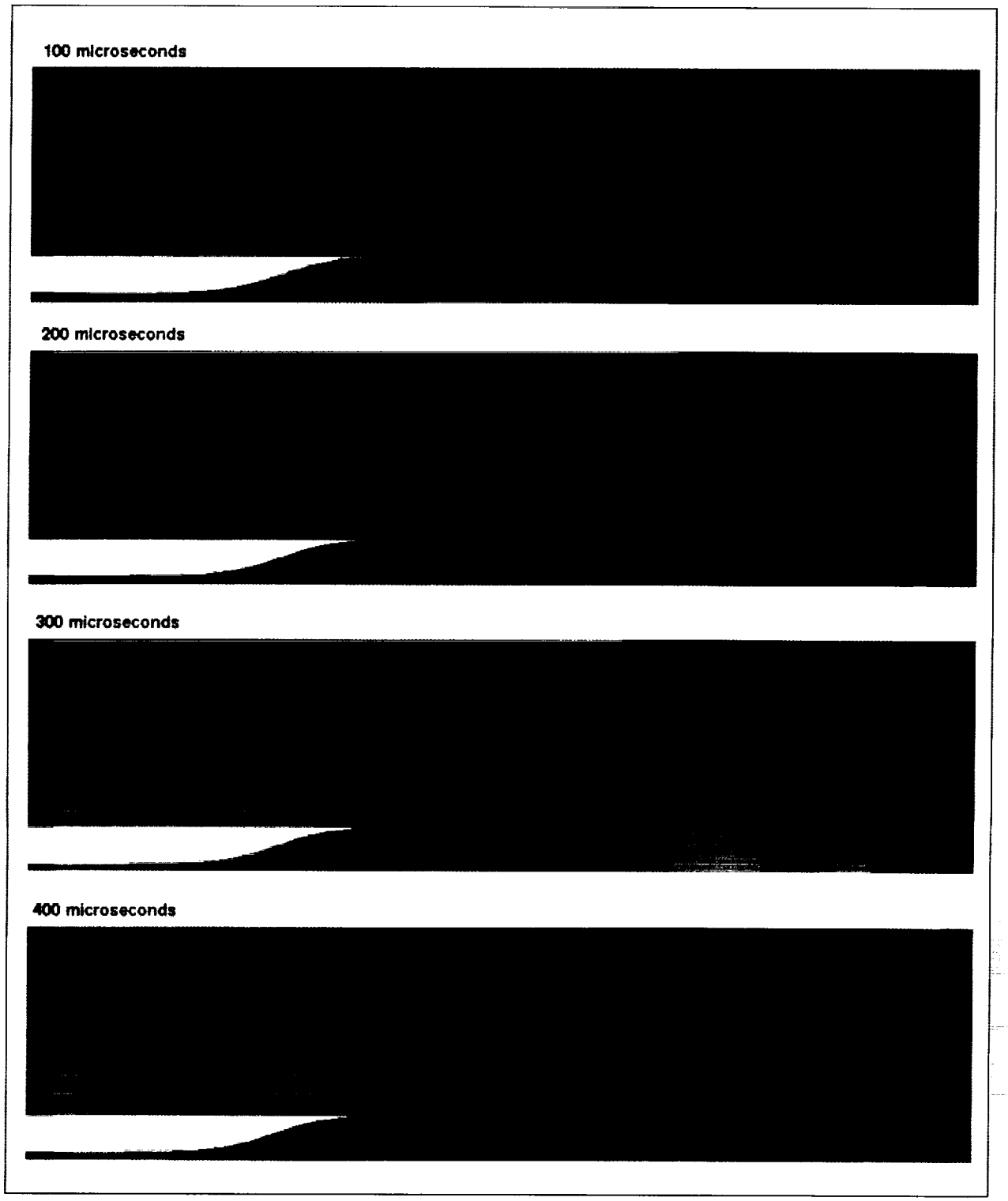


*Color plate 12. Time sequence for the transverse coupling case. Blast waves propagate into the supersonic combustor through two holes in the side of the detonation tube. The fuel layer can be seen in the center of the combustor. (fig. 1, page 140)*

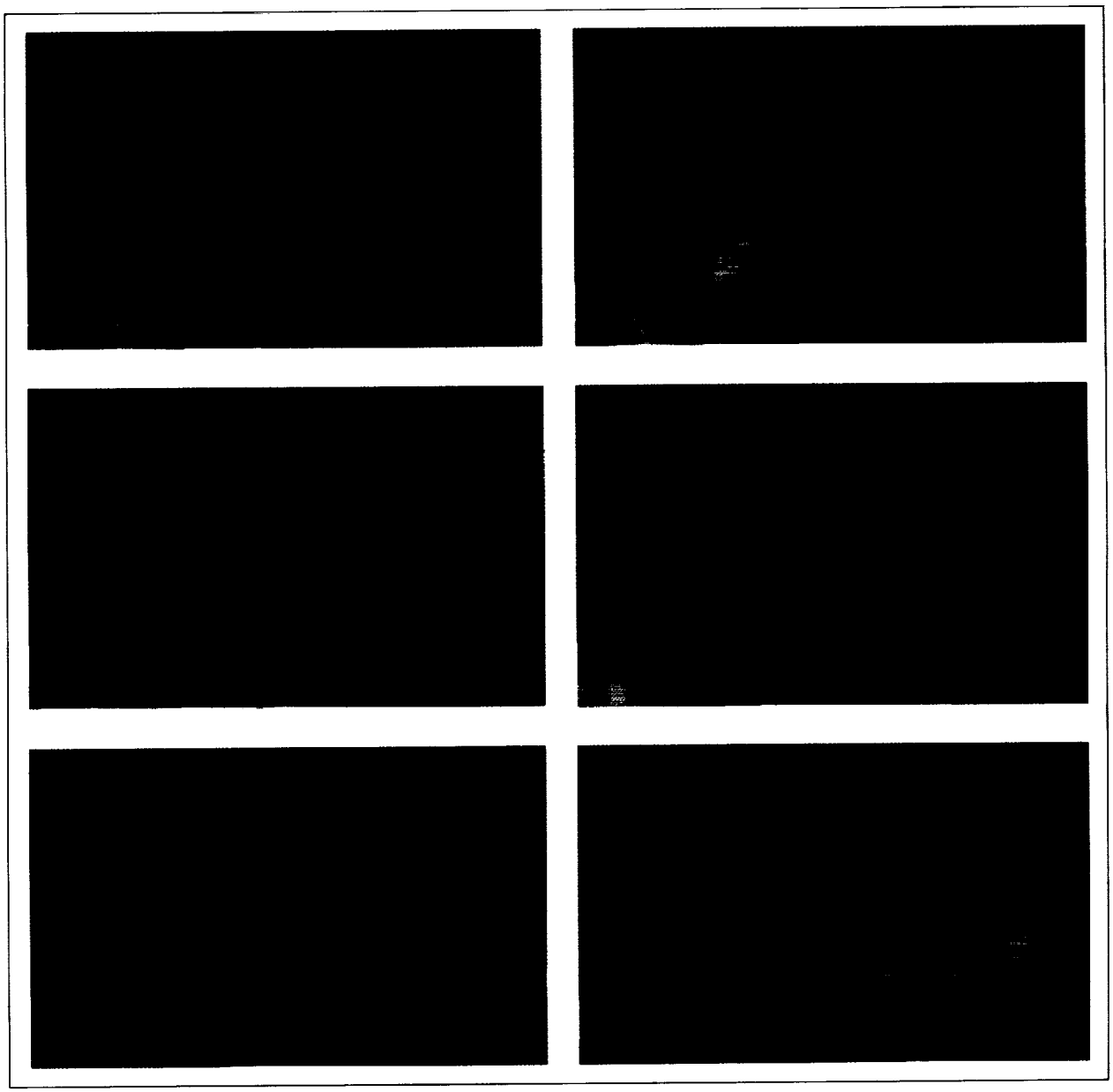

*Color plate 13. Time sequence of temperature contours, PDWA operation. Rapid combustion is seen in frame 2 (75 microseconds). The fuel layer (green contours) is seen to roll up and break up. Strong mixing vortices are generated. (fig. 2, page 141)*

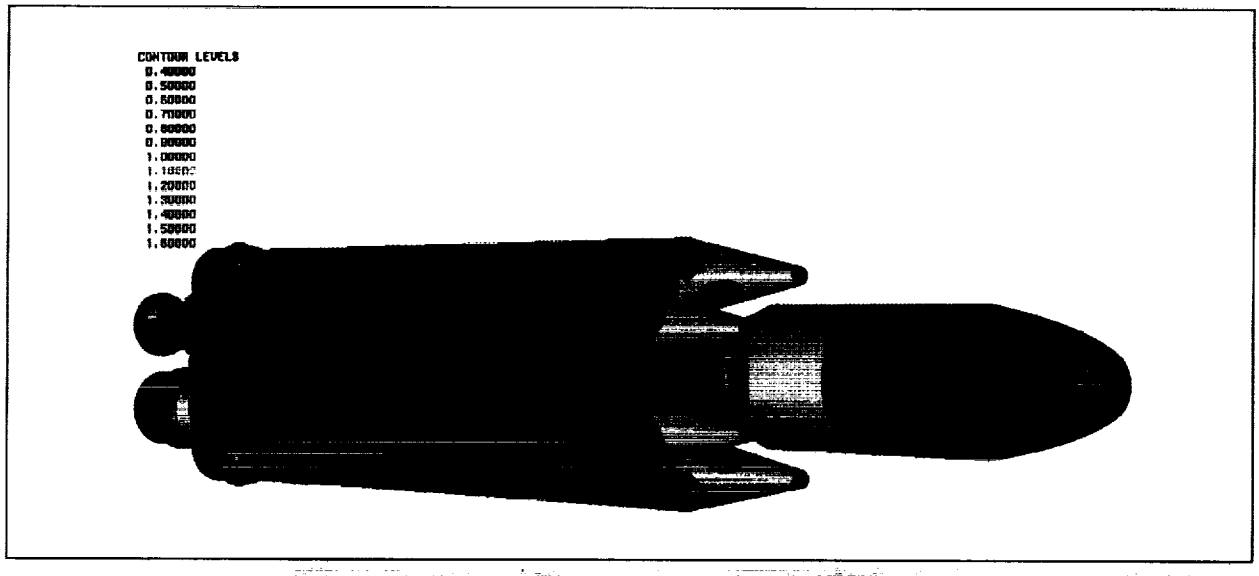


*Color plate 14. Normalized surface pressure over the Conestoga launch vehicle. (fig. 1, page 146)*

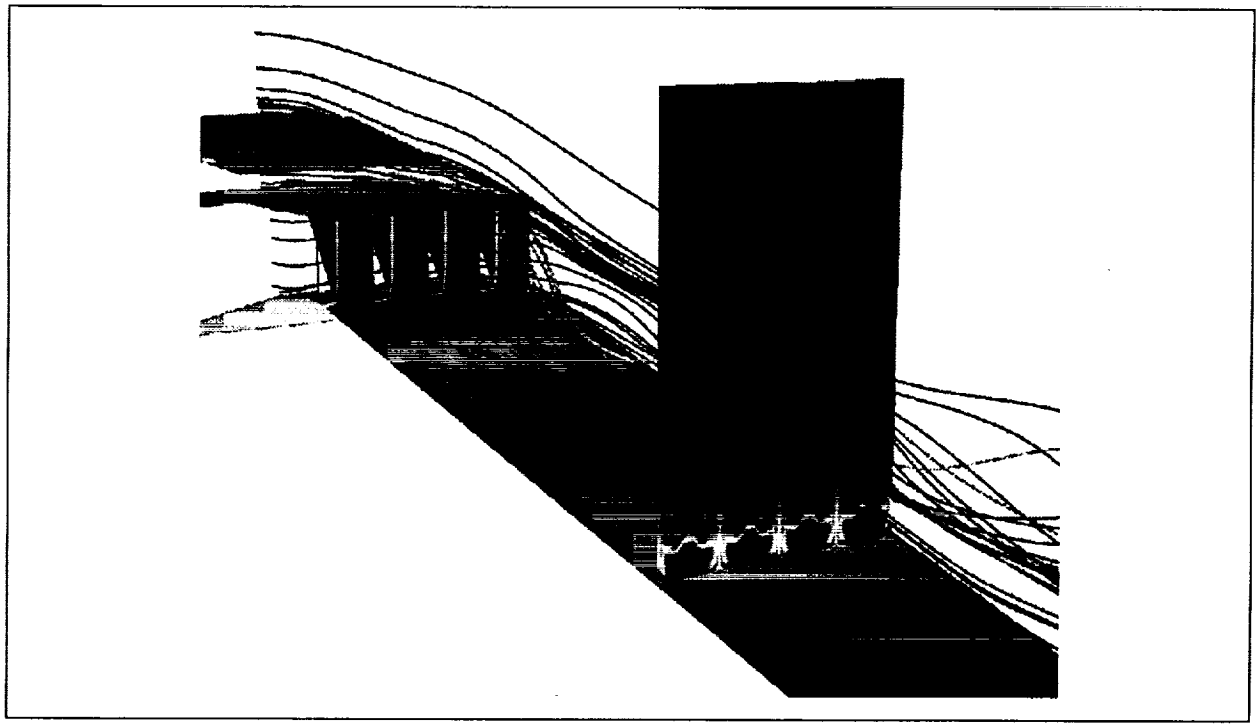

*Color plate 15. Surface pressure, total temperature, and particle traces. (fig. 1, page 153)*

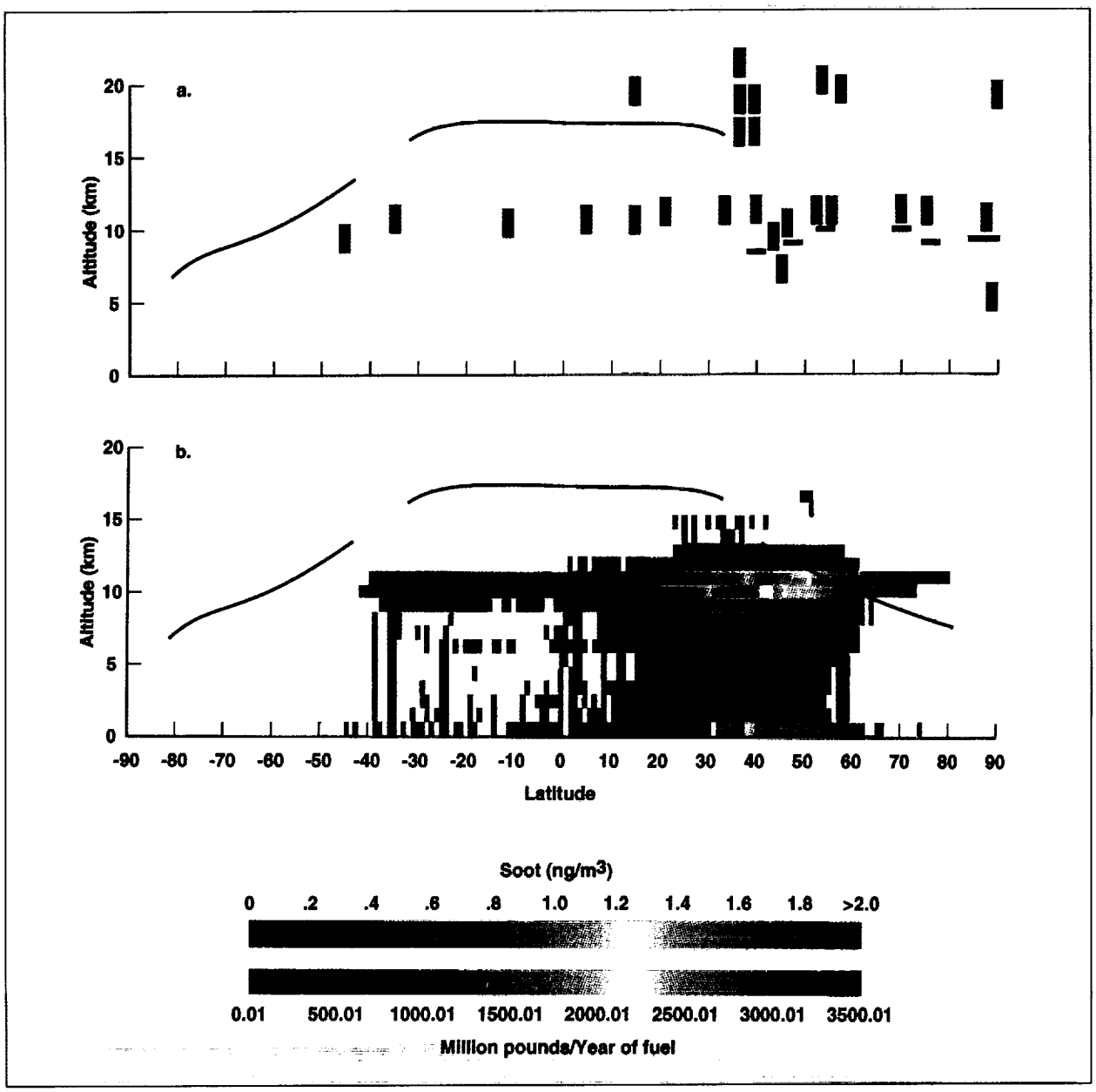


*Color plate 16. Comparison of observed upper-troposphere soot concentration and calculated aircraft fuel burning. (a) Observed soot concentrations in the upper troposphere and lower stratosphere. Tropopause height from 90 degrees south to about 35 degrees north, drawn as an idealized curve, as obtained from a reference publication. Tropopause heights from about 38 degrees north to 90 degrees north, drawn as discrete line segments on the plot, were measured during the flight in which the soot data at the same latitude were taken. (b) Fuel consumption by commercial aircraft during 1992. Idealized tropopause height drawn from a reference publication as in (a) above. Northern and southern hemisphere tropopause height is shown for wintertime. (fig. 1, page 206)*

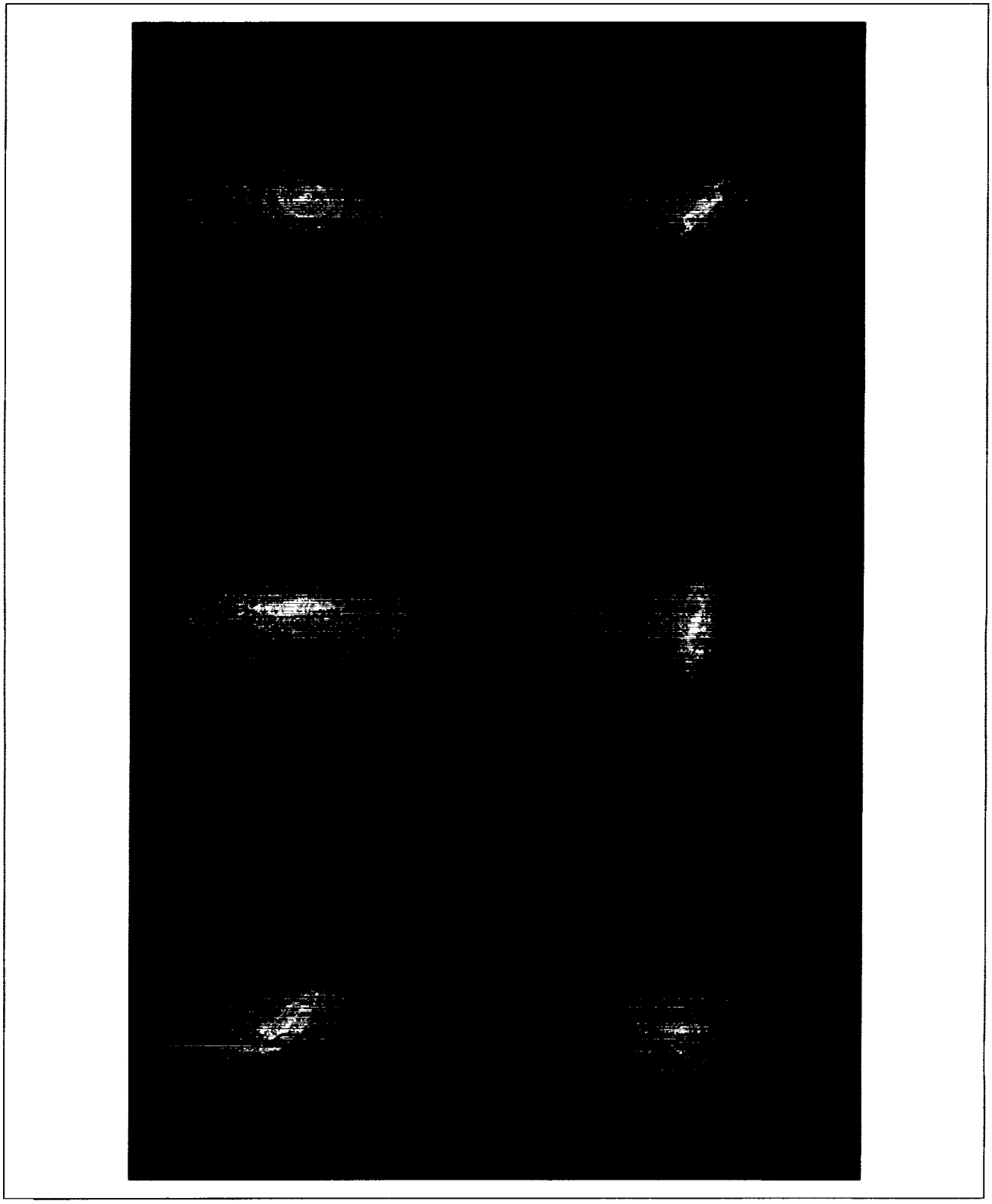

*Color plate 17. The warping of a disk galaxy (yellow particles) after it has been captured by a larger, nearby galaxy (blue particles). (fig. 1, page 246)*

# REPORT DOCUMENTATION PAGE

Form Approved
OMB No. 0704-0188



| 1. AGENCY USE ONLY *(Leave blank)* | 2. REPORT DATE | 3. REPORT TYPE AND DATES COVERED |
|---|---|---|
| | May 1994 | Technical Memorandum |

**4. TITLE AND SUBTITLE**

Research and Technology 1993

**5. FUNDING NUMBERS**

**6. AUTHOR(S)**

Ames-Moffett and Ames-Dryden Investigators

**7. PERFORMING ORGANIZATION NAME(S) AND ADDRESS(ES)**

Ames Research Center
Moffett Field, CA 94035-1000

**8. PERFORMING ORGANIZATION REPORT NUMBER**

A-94041

**9. SPONSORING/MONITORING AGENCY NAME(S) AND ADDRESS(ES)**

National Aeronautics and Space Administration
Washington, DC 20546-0001

**10. SPONSORING/MONITORING AGENCY REPORT NUMBER**

NASA TM-108816

**11. SUPPLEMENTARY NOTES**

Point of Contact: John T. Howe, Chief Scientist, Ames Research Center, MS 200-16, Moffett Field, CA 94035-1000; (415) 604-5500 or the contact person(s) at the end of each article

**12a. DISTRIBUTION/AVAILABILITY STATEMENT**

Unclassified — Unlimited
Subject Category 99

**12b. DISTRIBUTION CODE**

**13. ABSTRACT** ***(Maximum 200 words)***

Selected research and technology activities at Ames Research Center, including the Moffett Field site and the Dryden Flight Research Facility, are summarized. These activities exemplify the Center's varied and productive research efforts for 1993.

**14. SUBJECT TERMS**

Aeronautics, Space technology, Space sciences, Earth sciences, Life sciences, Computer science, Research and technology

**15. NUMBER OF PAGES**

306

**16. PRICE CODE**

A14

| 17. SECURITY CLASSIFICATION OF REPORT | 18. SECURITY CLASSIFICATION OF THIS PAGE | 19. SECURITY CLASSIFICATION OF ABSTRACT | 20. LIMITATION OF ABSTRACT |
|---|---|---|---|
| Unclassified | Unclassified | | |

NSN 7540-01-280-5500
☆US Government Printing Office 1994-585-521

Standard Form 298 (Rev. 2-89)
Prescribed by ANSI Std. Z39-18
298-102